Next Generation Biomaterials Discovery for Regenerative Medicine

Submitted by

Jordan Thorpe BSc MSc

School of Medicine

Department of Cancer & Stem Cells

The University of Nottingham

September 2019

Thesis submitted to The University of Nottingham for the degree of Doctor of Philosophy

Acknowledgements

I would like to thank both of my supervisors, Professor Chris Denning & Professor Morgan Alexander for their guidance and input throughout this PhD. Additionally, I would like to extend my gratitude to Associate Professor Cathy Merry, for much needed advice during this process.

I am also hugely grateful to Dr. Laurence Burroughs, whom without this project would have been impossible. His patience and dedication within the materials and analysis side of this project was invaluable, however it was the moral support through difficult times I appreciated the most.

The collaborative nature of this project has meant I have met so many amazing people, with the opportunity to work with great colleagues such as Dr. Sara Pijaun-Galito & Dr. Aishah Nasir, Joris Meurs, who have all been a pleasure to work & collaborate with.

I will never forget Dr. James Smith & Dr. Elizabeth Scott, my science 'Mum' & 'Dad', through the frustrating early years of being a dozy MSc & 1st year PhD student, to becoming something that resembles competent & eventually forming friendships which will be maintained for life.

Everyone within the lab has played a positive role throughout my PhD experience, Dr. Diogo Mosqueira for years of inappropriate jokes & puns, Dr. Jamie Bhagwan & team always there to brighten the mood.

Finally, I should give a huge thank you to my parents who have always believed in me and pushed me to fulfil my goals, and close friends outside the lab (special mentions to, Christopher Carroll, Jordan Thomas, Ben Purvis, Alex Reading, and Sian Green) for putting up with the complaining throughout the years!

Declaration

I declare work carried out in this thesis has been produced by myself, unless stated otherwise, and has not been submitted for any previous degree.

Jordan Thorpe

Abstract

Human pluripotent stem cells (hPSCs) have the capability to provide a limitless source of physiologically relevant human tissue for drug screening and therapeutic applications. Differentiated cell types can possess an immature phenotype limiting their scope of use, with hPSC-derived cardiomyocytes a prominent example. To truly realise the potential of hPSCs, fully defined and xeno-free culture systems must be in place, that are economically viable for industrial scale application. Additionally, the system must be capable of inducing relevant maturation of states of cell types cultured.

In this thesis a readily available and economical polymer library primarily composed of 281 acrylates & acrylamides were screened using polymer microarray technology, totalling 37,103 cell-surface interactions.

Serially passaged hPSCs were examined by RT-qPCR, flow cytometry, immunostaining, trilineage differentiation, integrin blocking, and phosphokinase protein arrays. hPSCs maintained trilineage differentiation capability, with inter-cell line differences discovered for expression of SOX2, SOX1, PAX6, and the phosphorylated state of protein kinases – compared to a Matrigel control.

Polymers that supported ≥7-day hPSC-CM attachment underwent studies into the contraction and electrophysiology properties of hPSC-CMs on primary amine polymeric surfaces compared to the Matrigel. Minor changes to the maturation state were observed, with further examination required for a definitive conclusion.

Table of Contents

Contents

List of Figures

List of Tables

Abbreviations

Abbreviation	Description
2D	Two Dimensional
3D	Three Dimensional
AA 2-P	L-Ascorbic Acid 2 Phosphate
ADP	Adenosine Diphosphate
ADP	Action Potential Duration
AEMA.C	N-(2-Aminoethyl) Methacrylate Hydrochloride
AEMAm.C	N-(2-Aminoethyl) Methacrylamide Hydrochloride
AFP	Alpha-Fetoprotein
AKT	Protein Kinase B
AP	Action Potential
APMAm.C	N-(3-Aminopropyl) Methacrylamide Hydrochloride
ATP	Adenosine Triphosphate
AVN	Atrioventricular Node
BA	Butyl Acrylate
BMP4	Bone Morphogenic Protein 4
BRG1	Brahma-Related Gene-1
BTS	N-Benzyl-p-Toluenesulphonamide
CASQ2	Calsequestrin 2
CDX2	Caudal-Related Homeobox-2
CER1	Cerberus 1
CICR	Calcium Induced Calcium Release

c-MYC	MYC Proto-Oncogene, BHLH Transcription Factor
CoV	Coefficient of Variation
CREB	cAMP Response Element-Binding Protein
CX43	Connexin-43
DAPI	4', 6-Diamidino-2-Phenylindole
DEPTOR	DEP-Domain-Containing mTOR-Interacting Protein
DFHA	Dodecafluoroheptyl Acrylate
DKK1	Dickkopf Homolog 1
DMAPA	Dimethylamino-Propyl Acrylate
DMEMAm	N-[2-(N,N-Dimethylamine)Ethyl) Methacrylate
DMF	N,N-Dimethylformamide
DMPMAm	N-(3-(Dimethylamino)Propyl) Methacrylamide
DN90	Time to Reach 90% of Relaxation State
DNA	Deoxyribonucleic Acid
DNMT3B	DNA Methyltransferase 3 Beta
DPBS	Dulbecco's Phosphate Buffered Saline
DRA	Disperse Red 1 Acrylate
DVAd	Divinyl Adipate
E3GDA	Triethylene Glycol Diacrylate
E8	Essential 8
EB	Embryoid Body
ECM	Extracellular Matrix
EHS	Engelbreth-Holm-Swarm
EHT	Engineered Heart Tissue
EMT	Epithelial to Mesenchymal Transition
END-2	Mouse Visceral Endoderm-Like
ERK	Extracellular-Signal-Regulated Kinase
FA	Fatty Acids
FAK	Integrin-Associated Focal Adhesion Kinase
FBS	Fetal Bovine Serum
FGF	Fibroblast Growth Factor
FHF	First Heart Field
FOXA2	Forkhead Box A2
FOXO1	Forkhead Box Protein O1
FOXO3a	Forkhead Box Protein O3a
GABRB3	Gamma-Aminobutyric Acid Type A Recptor Beta3
GATA4	GATA Binding Protein 4
GATA6	GATA Binding Protein 6
GDF3	Growth Differentiation Factor 3
GPCRs	G-Protein-Coupled Receptors
GSK-3	Glycogen Synthase Kinase 3
HA	Hyaluronic Acid
HAT	Acetyltransferases
HHEX	Haematopoietically-Expressed Homeobox Protein

hiPSC	Human Induced Pluripotent Stem Cell
HPhMA	Poly(N-(4-Hydroxyphenyl)Methacrylamide
hPSC	Human Pluripotent Stem Cell
hPSC-CM	Human Pluripotent Stem Cell Derived Cardiomyocyte
HSP60	Heat Shock Protein 60
hvCOC	Human Ventricle-Like Cardiac Organoid Chamber
Hz	Hertz
ICM	Inner Cell Mass
iDMA	Isodecyl Methacrylate
IPA	Isopropanol
JCNT	Junctin
JNK	Jun Amino-Terminal Kinase
KCNJ2	Potassium Voltage-Gated Channel Subfamily J Member 2
KLF4	Kruppel Like Factor 4
LA	Left Atria
LaA	Lauryl Acrylate
LMA	Lauryl Methacrylate
LN511	Biolaminin 511
MAPK	Mitogen-Activated Protein Kinase
MT	Matrigel
mBAM	N, N'-Methylenebisacrylamide
MEF	Mouse Embryonic Feeder
MEK	Mitogen-Activated Protein Kinase Kinase
MLC2a	Myosin Light Chain 2a
MLC2v	Myosin Light Chain 2v
mLST8	Mammalian Lethal with Sec12 Protein 8
mRNA	Messenger Ribonucleic Acid
mTOR	Mammalian Target of Rapamycin
NANOG	Homeobox Protein NANOG
NCX	Sodium-Calcium Exchanger Pump
NEAA	Non-Essential Amino Acids
NIH	National Institutes of Health
OCT3/4	Octamer-Binding Transcription Factor 3/4
OT	Outflow Tract
OTX2	Orthodenticle Homeobox 2
Pa	Pascal
PAX6	Paired Box 6
PCL	Poly-ϵ-Caprolactone
PCR	Polymerase Chain Reaction
PDK1	Phosphoinositide-Dependent Protein Kinase 1
PDMS	Poly(Dimethylsiloxane)
PEG	Poly(Ethylene Glycol)
PEGDA	Poly(Ethylene Glycol) Diacrylate
PETrA	Pentaerythritol Triacrylate

PFA	Paraformaldehyde
PGRN	Pluripotency Gene Regulatory Network
pHEMA	Poly(Hydroxyethyl Methacrylate)
PI3K	Phosphoinositide 3-Kinase
PIP3	Phosphatidylinositol (3,4,5)-Triphosphate
PKA	Protein Kinase A
PLB	Phospholamban
PMVE-alt-MA	Poly(Methyl Vinyl Ether-alt-Maleic Anhydride)
PPARGC1A	PPARG Coactivator 1 Alpha
PRAS40	Proline-Rich AKT Substrate 40kDA
PTEN	Tensin Homolog Deleted on Chromosome Ten
RA	Right Atria
RAi	Retinoic Acid Receptor Inhibitor
RAPTOR	Regulatory-Associated Protein of mTOR
REX-1	Reduced Expression-1
Rh	Human Recombinant
RNA	Ribonucleic Acid
ROCKi	Rho-Kinase Inhibitor
RPMI	Roswell Park Memorial Institute
RSK1	p90 Ribosomal S6 Kinase 1
RTK	Receptor Tyrosine Kinase
RT-qPCR	Reverse Transcriptase Quantitative Polymerase Chain Reaction
RYR2	Ryanodine-2 Receptor
SAN	Sinoatrial Node
SAPK	Stress Activated Protein Kinase
SCID	Severe Combined Immunodeficiency
SCN5A	Sodium Voltage-Gated Channel Alpha Subunit 5
SEMA	2-Sulfoethyl Methacrylate
SERCA2	Sarco/Endoplasmic Reticulum Ca2+ ATPase
SHF	Second Heart Field
SOX1	SYR-Box 1
SOX17	SRY-Box 17
SOX2	Sex Determining Region Y - Box2
SR	Sarcoplasmic Reticulum
SSEA-3	Stage Specific Embryonic Antigen 3
SSEA-4	Stage Specific Embryonic Antigen 4
SV	Sinus Venosus
T3	Tri-Iodo-L-Thyronine
TCDMDA	Tricyclodecane Dimethanol Diacrylate
TDGF1	Teratocarcinoma-Derived Growth Factor 1
TNNI	Slow Skeletal Troponin Inhibitor
TNNI3	Cardiac Troponin Inhibitor
TNNT2	Cardiac Troponin T

ToF-SIMS	Time of Flight Secondary Ion Mass Spectrometry
TRDN	Triadin
TSC	Tuberous Sclerosis Complex
T-Tubules	Transverse Tubules
UP90	Time to Reach 90% of Contraction Peak
US	United States of America
V	Volts
VEGF	Vascular Endothelial Growth Factor
Vitronectin	VN
Vmax	Depolarisation Velocity
WNT	Wingless Type
ZrCEA	Zirconium Carboxyethyl Acrylate
α-MHC	α-Myosin Heavy Chain Isoform
β-MHC	β-Myosin Heavy Chain Isoform

Thesis Rationale

Human pluripotent stem cells (hPSCs) offer the opportunity to revolutionise modern medicine. This is likely to be by introducing more biologically relevant drug toxicity testing platforms for industry, allowing the creation of disease harbouring cell lines directly from patients to investigate disease phenotype, or their emerging use as cellular therapies in a clinical setting.

To fulfil their promise monolayer cultures of hPSCs rely on optimal culture conditions, which critically influence hPSC biology. In 2D culture, the culture surface plays an important role in attachment, survival and signalling (Shafaie et al., 2017)(Stevens and George, 2005)(Sun et al., 2012).

Currently hPSCs are commonly cultured on Matrigel™, an ECM protein rich hydrogel secreted from Engelbreth-Holm-Swarm (EHS) mouse sarcoma cells, containing approximately; 60% laminin, 30% collagen IV and 8% entactin. Matrigel™

also contains undefined factors, demonstrates batch-to-batch variability and is xenogenic, limiting its clinical application. Recombinant adhesion proteins such as Biolaminin™ or Vitronectin XF™ are xeno-free, fully defined alternatives to Matrigel™ however their cost is prohibitive for industrial scale use.

Synthetic materials have the potential to provide a fully defined & reproducible hPSC culture surface that combines industrial scalability at a fraction of the cost of a biological coating – without the requirement of a coating step.

Previous polymer screening campaigns have discovered materials that fulfil these parameters, however they relied on previous iterations of culture medium, that were either xenogenic or undefined, or both. With the introduction of the simplified, xeno-free & defined Essential 8 medium, a synthetic material can be uncovered that may truly support a 'clean' culture system.

The work presented in this thesis is part of a large collaborative Biomaterials Discovery project grant, that seeks to screen polymeric materials in a high-throughput manner to solve issues including bacterial attachment, drug delivery, mesenchymal stem cell culture and the culture of hPSCs & their derived cardiomyocytes. Materials discovered in 2D here will be translated to topographical surfaces and 3D particle-based cultures in interdisciplinary collaborations.

Using polymer microarrays previously developed in laboratories at the University of Nottingham, this thesis will focus on creating a synthetic surface that is capable of culturing hPSCs in the fully defined, xeno-free Essential 8 medium in chapters 3 & 4.

In chapter 5, the same style of high content screening campaign will aim to discover synthetic materials that allow hPSC-CM attachment and promote their maturation for improved biological relevance both clinically and for toxicity testing.

1 Introduction

1.1 Stem Cells

Stem cells have the potential to play a transformative role in the field of regenerative medicine over the next 20 years, below, there is an overview of stem cells, their discovery, potency, and how pluripotency is maintained and differentiation to the mesoderm lineage, specifically to cardiomyocytes.

1.1.1 What Are Stem Cells?

'Stem cell' is an umbrella term for a range of cell types that demonstrate a potency to undergo self-renewal and differentiate into at least one sub-cell type. Stem cells were first discovered and rigorously characterised by Ernest McCulloch

and James Till in 1963, where the transplantation of what was to be termed haematopoietic stem cells could repopulate an irradiated spleen, it was demonstrated that these cells were self-renewing and capable of producing, erythrocytic, granulocytic and megakaryocytic cell types (Becker, Mcculloch and Till, 1963)(Siminovitch, McCulloch and Till, 1963).

Previous authors had made the conclusion that haematopoietic stem cells existed and could be damaged by irradiation (Sabin et al., 1936).

Stem cells of several tiers of potency have been identified; from totipotency, pluripotency, multipotency, to unipotency. Chapters 3 & 4 in this thesis focus on the culture of pluripotent stem cells, therefore these will be discussed in greater depth.

1.2 Stem Cell Potency during Development

1.2.1 Totipotency

During zygote formation, and the subsequent stages up to the 8-cell, stem cells can form all the cell-types within the adult body and extraembryonic tissues such as the placenta (Mitalipov and Wolf, 2009). Crucially these cells can orchestrate the formation of an entire organism in an organised spatial and temporal manner – this is the highest form of potency, totipotency (Mitalipov and Wolf, 2009).

1.2.2 Pluripotency

Blastocyst development by day 5 leads to the formation of the inner cell mass (ICM), where pluripotent embryonic stem cells can be derived. These cells are defined as pluripotent for their ability to form any cell type from the three germ layers that comprise the endoderm, mesoderm & ectoderm but lack the capacity to

organise into a full organism or derive extraembryonic cell types (Mitalipov and Wolf, 2009).

1.2.3 Adult Stem Cells (Multipotency & Unipotency)

Pluripotent stem cells exist during the early developmental stages; however, cells need to be continually replenished during adult life as ageing, disease and trauma occur. The gut, skin & gonads are examples where adult stem cells exist within the tissue to facilitate cellular turnover (Spradling, Drummond-Barbosa and Kai, 2001). Not all adult tissues contain stem cells directly, haematopoietic stem cells are found in the endosteal and perivascular regions of the bone marrow, which acts as a stem cell reservoirs from which they can be activated (Tweedell, 2017). Adult stem cells are either multipotent or unipotent, meaning they lack the flexibility in differentiation potential of the embryonic & induced stem cells (Wang et al., 2015)(Bond, Ming and Song, 2015)(Woo, Hwang and Shim, 2016).

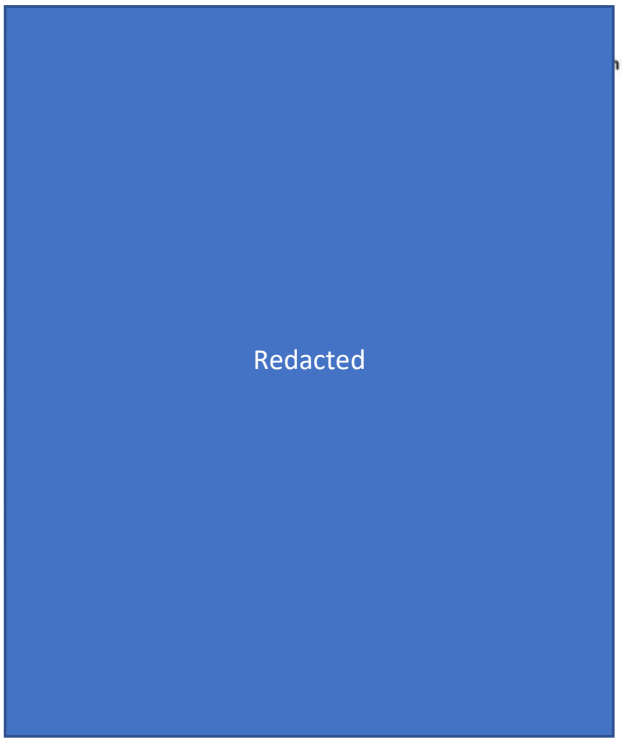

Figure 1.1 Developmental Potential of Differing Stem cell Potencies. Functional assays such as chimaera and teratoma formation determine the potency of a stem cell. Taken from Angeles *et al.,* 2015.

1.2.4 Derivation of Pluripotent Stem Cells for Research

Human embryonic stem cells are isolated from the ICM of between day 5-8 blastocytes, generated from in vitro fertilisation, with informed consent from the donor (Stojkovic et al., 2004).

The trophectoderm layer of the blastocyst is selectively removed with the use of specific antibodies in a technique called immunosurgery, or through manual dissection and cultured through mechanical passaging for expansion (Reubinoff et al., 2000)(Ludwig et al., 2006).

The pluripotency of a newly derived line must then be assessed, indicative markers such as GTCM-2, TG343, TRA-1-60, TRA-1-81, SSEA-3, SSEA-4 and alkaline phosphatase must be present (Stojkovic et al., 2004). The expression of key pluripotency genes, OCT-4, NANOG, SOX2, TDGF1, DNMT3B, GABRB3, GDF3 and REX-1 must also be demonstrated (Stojkovic et al., 2004)(Hoffman and Carpenter, 2005)(Initiative et al., 2007).

hESCs have the capacity to form all three germ layers in the human body, endoderm, ectoderm & mesoderm. hESCs must retain their tri-lineage differentiation potential, which can be proven by teratoma formation assays in severely combined immunodeficient mice & in vitro spontaneous differentiation (Thomson et al., 1998)(Stojkovic et al., 2004).

Despite the promising therapeutic capability of human embryonic stem cells, the requirement to use an in vitro fertilised embryo – which has the potential to form a full viable child, presents considerable ethical concerns. Due to these ethical

concerns, regulation prevents the derivation of hESCs in Germany, and historically impeded NIH funding for hESC research in the US (Robertson, 2010)(Stafford, 2008).

1.2.5 Induced Pluripotent Stem Cells

Ethical issues with hESCs were overcome through the invention of induced pluripotent stem cells (hiPSCs), where adult dermal fibroblasts were transduced with retroviruses containing human OCT3/4, SOX2, KLF4 and c-MYC, reverting to a pluripotent state (Takahashi et al., 2007).

The oncogenic c-MYC retrovirus was later found to be dispensable for iPSC formation, however this method still relied on integrating viral vectors (Nakagawa et al., 2008).

Methods requiring integrating viruses to induce pluripotency can alter the host genome, which are undesirable from a regulatory standpoint, for example retroviral integration during gene therapy for severe combined immunodeficiency (SCID) resulted in leukaemia for some individuals (Lundstrom, 2018).

The introduction of an RNA Sendai virus, which is incapable of integrating with the human genome, overcomes this issue (Fusaki et al., 2009). Further development of Sendai viral methods has led to replication-deficient strains which are 'auto-erasable' in response to microRNA-303 which is uniquely expressed in pluripotent stem cells, improving the safety of iPSC lines generated for clinical applications (Nishimura et al., 2017).

1.3 Regulation of Pluripotency & Differentiation

1.3.1 Maintaining Pluripotency

To unleash the therapeutic & pharmaceutical potential of pluripotent stem cells, an in-depth understand of the molecular mechanisms behind maintenance & loss of pluripotency is required.

At the therapeutic stage, contaminant hPSCs pose a tumorigenic risk to the patient, efficient directed differentiation protocols have been developed through greater understanding of pluripotency & development (Neofytou et al., 2015)(Xia et al., 2013)(Lian et al., 2013)(Buchholz et al., 2013).

Pluripotency is maintained and controlled through a pluripotency gene regulatory network (PGRN). At the core of the PGRN, the transcriptional triad, (octamer-binding transcription factor 4) OCT4, ((sex determining region Y)-box 2) SOX2 and homeobox transcription factor NANOG act to stabilise pluripotency through cooperatively binding at least 353 genes & regulatory elements within the wider interconnected pluripotency network (Boyer et al., 2005)(Li and Belmonte, 2017)(Li and Izpisua Belmonte, 2018).

OCT4, SOX2 & NANOG bind to each other's regulatory sequences for auto-regulation (Rodda et al., 2005). Chromatin immunoprecipitation data indicates OCT4, SOX2 & NANOG form feedforward loops, a system where a regulator controls a second regulator, where both can bind a common target, and it was identified that OCT4, SOX2 & NANOG form a autoregulatory loop (Boyer et al., 2005).

The ability of the OCT4/SOX2/NANOG triad to enable the input of activators, repressors, regulatory RNAs and alternations to the epigenetic landscape allow for redundancy in pluripotency maintenance, during fluctuations in concentration of the core triad, termed 'bistability' (Boyer et al., 2005)(Chen et al., 2008)(Masui et al., 2007)(Nichols et al., 1998)(Bilodeau et al., 2009)(Chia et al., 2010)(van den Berg et al., 2010)(Li and Belmonte, 2017).

For example, the function of chromatin modifiers such as Brahma-related gene-1 (BRG1) has been shown to maintain chromatin openness at OCT4 bound sites to recruit further pluripotency regulators, suppressing lineage specification (Xiaoli Zhang et al., 2014)(King and Klose, 2017).

1.3.2 Post-Translation Modification & Pluripotency Maintenance

Post-translational modifications such as protein glycosylation, phosphorylation & acetylation have been studied for their role in maintaining the pluripotent state (Wang, Peterson and Loring, 2014). Glycosylation of Thr228 of Pou5f1 specifically by O-linked-N-acetylglucosamine (O-GlcNAc), has been linked to maintenance of pluripotency in mouse ESCs by enhancing its transcriptional activity (Jang et al., 2012).

Phosphorylation of proteins regulates a broad range of signalling within the cell, PI3K/AKT/mTOR & MAPK pathways discussed in more detail in Chapter 4. Phosphorylation is linked to either the activation or deactivation of a proteins signalling capability, the activation of ERK1/2, AKT and SMAD2/3 pathways by phosphorylation upon stimulus of upstream FGFR, IGF-1R & TGF-βR respectively

leads to the broad expression of pluripotency and self-renewal genes (Armstrong et al., 2006)(A. M. Singh et al., 2012). Over 10,000 non-redundant phosphorylation sites exist in hPSCs, out of the scope of this thesis, however phosphorylation sites with functional consequences are present on OCT3/4, NANOG, SOX2, KLF4 and MYC, directly affecting the pluripotency state (Swaney et al., 2009)(Cai et al., 2012).

1.3.3 Metabolic State Influences Pluripotency

hPSCs are high proliferative which means they have demanding metabolic requirements. Whilst mammalian somatic cells primarily meet metabolic demand through oxidative phosphorylation, pluripotent stem cells rely on glycolysis. Glycolysis produces reduced ATP per glucose; however, it leads to increased biosynthesis of nucleotides and lipids, required for proliferation. Furthermore, glycolysis produces less metabolic induce stress via reactive oxygen species, aiding in the preservation of genomic/embryonic integrity (Dahan et al., 2019)(Spyrou, Gardner and Harvey, 2019). A summary of metabolic differences between pluripotent and somatic cells can be found in figure 1.2.

Figure 1.2 Summary of Metabolic Differences Between Pluripotent & Somatic Cells
Maintenance of pluripotency requires increases in glycolysis and reductions in mitochondrial stress. Increased lipid and nucleotide biosynthesis related to glycolysis aids in the rapid proliferation of hPSCs. Taken from Dahan *et al.,* 2018.

1.4 Differentiation of hPSCs Towards Specific Lineages

Development of directed differentiation methods has relied on the study of in vivo cues for all three lineages. In this thesis, an emphasis is placed on the mesoderm lineage, specifically the derivation of cardiomyocytes from hPSCs. Endoderm & ectoderm differentiations will be explored in more detail in chapter 4.

1.4.1 Differentiating hPSCs into Cardiomyocytes

The ability to differentiate hPSCs through the mesoderm lineage into cardiomyocytes has opened new avenues of scientific research. Currently, pluripotent stem cell derived cardiomyocytes (hPSC-CMs) are used to study a variety of diseases, such as inherited cardiomyopathies (Mordwinkin, Burridge and Wu, 2013)(Jung and Bernstein, 2015) and are increasing in their utility for drug discovery & drug toxicity testing (Sharma et al., 2018).

Efficient differentiation methods have taken time to develop, and the field is mired by a lack of maturation in hPSC-CMs that can be produced. To fulfil the potential of cardiomyocytes created in the laboratory, numerous publications have described the use embryoid body formation, co-culture and cues identified from vertebrate development, including Wnt modulation to drive directed differentiation (Kehat et al., 2001)(Mummery, 2003)(Burridge et al., 2007)(Kattman et al., 2011)(Zhang et al., 2011)(Burridge et al., 2014).

Chapter 5 will seek to develop novel biomaterial surfaces that can both support attachment of hPSC-CMs but also induce a greater level of maturation, as previously demonstrated to be possible by Patel et al., 2015.

1.5 In Vivo Mesoderm Formation & Cardiac Specification

The adult heart is formed of several different cell types with specialised roles, including; cardiomyocytes (contractile cells), cardiac conduction cells (found in the sinoatrial node, atrioventricular node, HIS bundle, left/right bundle branches & Purkinje fibres), cardiac fibroblasts, vascular smooth muscle cells and endothelial cells (Anderson et al., 2009)(Zhou and Pu, 2016)(Pinto et al., 2016).

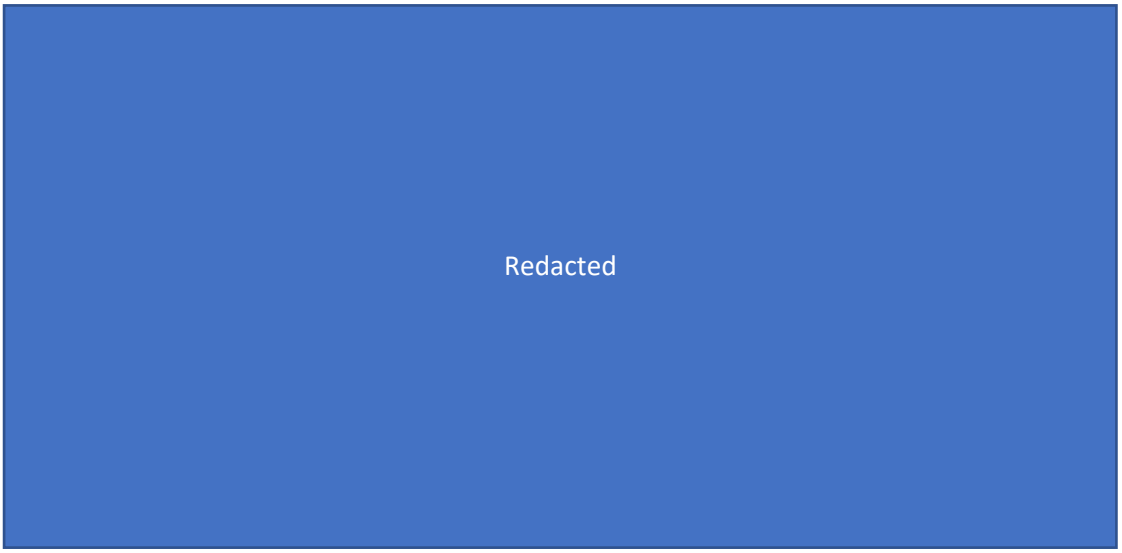

Figure 1.3 Summary of the key steps of early heart formation during embryo development. Formation of the First Heart Field (FHF) and Second Heart Field (SHF) lead on to contribute to the left-ventricle & right-ventricle respectively, the SHF also forms part of the outflow tract (ot), sinus venosus (sv) and both left/right atria (la/ra) during looping & chamber formation. Image taken from (Bruneau, 2013)

To form these cells types, which are organised into a functioning heart, requires an intricate sequence of events occurring during early embryo development, some of which are shown in figure 1.3.

Mesoderm is formed during gastrulation, where the three germ layers, endoderm, mesoderm, ectoderm, are organised within the inner cell mass. Mesoderm is situated between the endoderm & ectoderm.

During gastrulation, cells undergo epithelial to mesenchymal transition (EMT), which facilitates the migration of cells from each layer to gradually form more complex structures, whose roles are determined by complex chemical gradients of growth factors.

For early mesoderm formation, mouse Wnt3a (Wingless Type 3a), (Bone morphogenic protein 4) Bmp4, Activin-a & (fibroblast growth factor 2) Fgf2 (and human WNT3a, BMP4, ACTIVIN-A & FGF2) have been demonstrated as important for directing mouse PSCs & hPSCs (Yang et al., 2008)(Münsterberg and Hoppler, 2016)(Spater et al., 2014)(Bruneau, 2013).

Whilst canonical Wnt activation is essential during the early stages of cardiac mesoderm formation, these signals must be inhibited to allow the continuation to cardiac progenitors (Gessert and Kühl, 2010)(Ueno et al., 2007)(Lian et al., 2012).

To inhibit Wnt, neighbouring endoderm cells generate dickkopf homolog 1 (DKK1) & Crescent (Gessert and Kühl, 2010). Further progression to the cardiac sub-types in vivo is then dependent on the reactivation of cannonical Wnt signalling & FGF signalling for second heart field (SHF) progression or BMP dependent Wnt signalling for first heart field (FHF) progression (Cohen et al., 2007)(Ai et al., 2007), as shown in Figure 1.4.

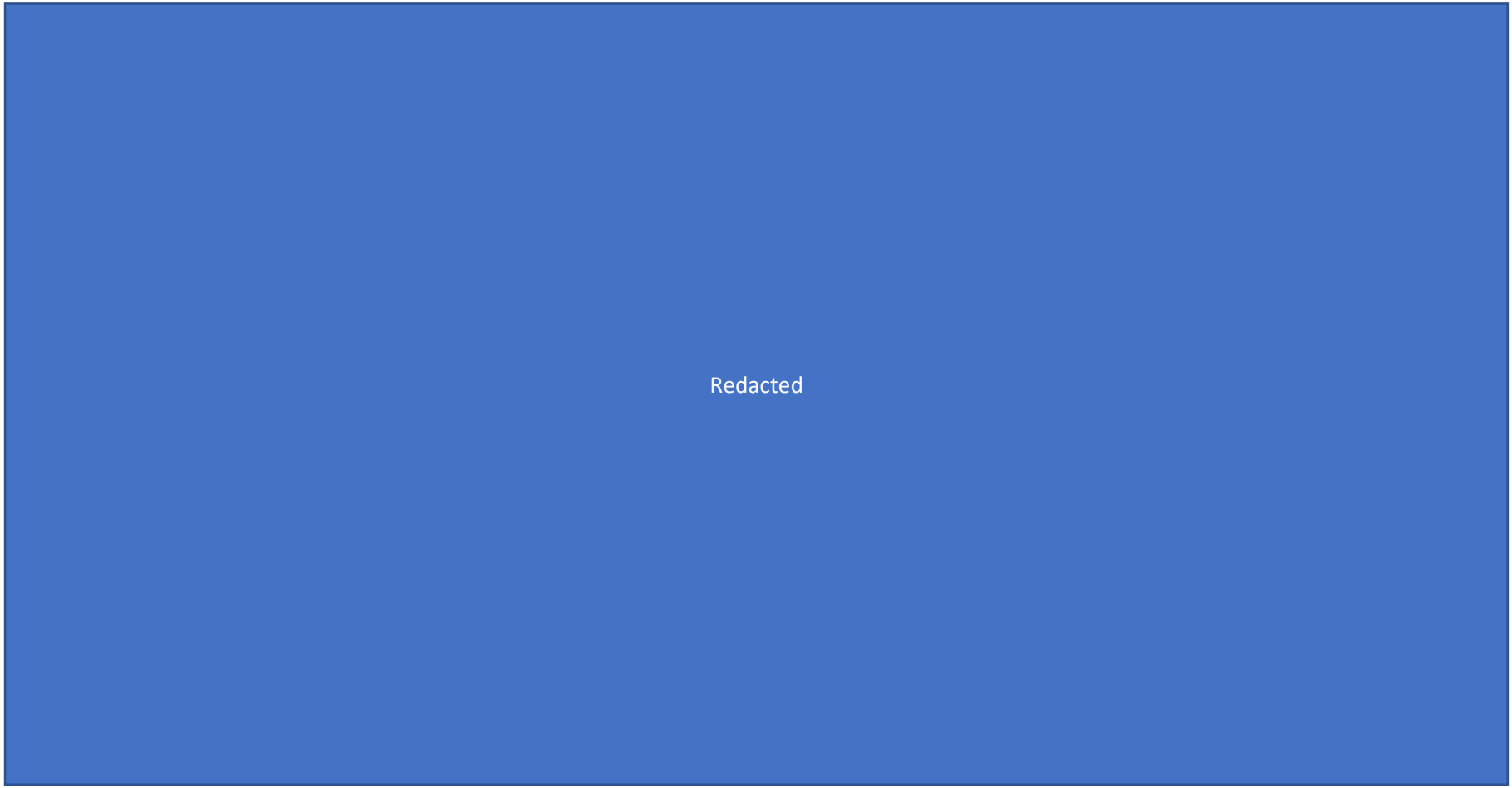

Figure 1.4 Overview of Signalling Involved in the Progression from Pluripotent Stem Cell to Cardiac Progenitors.
Intermediate stages shown, marked with known molecular markers. FHF: First Heart Field. SHF: Second Heart Field. EPDCs: Epicardium-Derived Cells. EMT: Epithelial to Mesenchymal Transition. Taken from Später *et al.,* 2014.

1.6 In Vitro Cardiomyocyte Derivation Using Human Pluripotent Stem Cells

1.6.1 Early Embryoid Body & Co-Culture Methods

Cardiomyocytes generated through differentiation methods must be mature to recapitulate the drug responses expected in adult tissue & for non-arrhythmic integration in therapeutic application (Goversen et al., 2018)(Liu et al., 2018).

Additionally, the differentiation of cardiomyocytes must firstly be efficient, if the number of cardiomyocytes required for screening and therapeutic applications are to be met economically (Chen et al., 2016).

Progress has been made in the optimisation of cardiomyocyte differentiation protocols. Early methods relied on mouse embryonic feeder (MEF) layer co-culture, the presence of serum and suspension culture to form embryoid body (EB) aggregates, with a differentiation efficiency lower than 1% (Kehat et al., 2001).

Cardiac differentiations were improved upon by mimicking the developmental process, studying the activation and repression of key signalling pathways during mesoderm formation.

The discovery that mouse visceral endoderm-like (END-2) cells co-cultured with hPSCs could provide the required signals for directed cardiac differentiation, improved efficiency (~30% of wells contained beating cells) and did not require the use of serum within the medium, additionally activin A was suggested to be

important for driving cardiac mesoderm formation (Mummery, 2003)(Passier et al., 2005).

By 2007 directed embryoid body-based differentiation methods were improved through the use of forced aggregation, involving centrifugation, in V-bottomed 96-well plates, with the addition of activin A & FGF2 in defined medium, resulting in 23.6% +/- 3.6% beating EBs (Burridge et al., 2007).

Another EB method was developed, in which Wnt modulation through the early use of BMP4, FGF2 & activin-a. This was followed by Wnt inhibition – on the basis this would allow for cardiac specification – using dickkopf homolog 1 & vascular endothelial growth factor (VEGF) (Yang et al., 2008). This protocol allowed for 40-50% cardiac troponin T (cTNT) positive cells, and was later improved upon through the addition of SB431542 & dorsomorphin (Kattman et al., 2011).

To improve embryoid body-based differentiations further, over 45 cardiogenic & medium components were systematically optimised to improve the differentiation efficiency. This resulted in a universal, cost-effective chemically defined method based on the forced aggregation method from Burridge et al., 2007, achieving 94.7% +/- 2.4% efficiency across 11 hPSC lines (Burridge et al., 2011).

It's important to note that previous work by a PhD student, Asha Patel, used this method in the previous hPSC-CM attachment/maturation polymer microarray screen (Patel et al., 2015).

1.6.2 Monolayer-Based Cardiomyocyte Derivation

Embryoid body techniques may have progressed in their capability to generate cardiomyocytes, however this technique historically proved difficult to achieve high purities & until recently lacked the necessary scale-up methods to produce cells at scale.

To conveniently produce high purity differentiations at the scale required for in vitro studies monolayer-based differentiation methods were developed.

An initial monolayer-based protocol cultured hPSCs was performed in three steps; change to RPMI-B27 medium with 100 ng/mL activin A for 24 hours, followed by four days with 10 ng/mL BMP4 supplementation, during which the medium was not exchanged, allowing the build-up of signalling factors produced by the cells. Afterwards cells were fed every 2-3 days with RPMI-B27 for a further 2-3 weeks to obtain ~30% cardiomyocyte yield (Laflamme et al., 2007).

The protocol from Laflamme et al., 2007 was a start in producing directed monolayer-based differentiations but only focused on one aspect of Wnt modulation, early activation.

By utilising early Wnt activation followed by Wnt inhibition with inhibitors; Noggin, DKK-1, Zhang et al., 2011 was able to increase cardiomyocyte yield to ~64% and experimented with the addition of retinoid compounds as an early example of influencing cardiomyocyte sub-type fate, where the addition of pan-retinoic acid receptor antagonist BMS-189453 (RAi) shifted cells to the ventricular phenotype.

1.6.3 A Fully Defined, Xeno-Free Protocol

Previous methods for deriving cardiomyocytes mentioned relied on undefined medium components and/or MEF conditioned medium during hPSC culture. More modern methods have worked to improve reproducibility and clinical translation potential through improved defined and animal free protocols.

A truly defined cardiomyocyte differentiation protocol emerged in 2014, when a combinatorial screen identified the precise media components essential and optimal for differentiation (Burridge et al., 2014). A simple medium of RPMI 1640 basal, L-ascorbic acid 2 phosphate (AA 2-P) and rice-derived recombinant human albumin was found to be more effective than previously used StemPro & RPMI-B27 (-ins) media. Supplementation in this protocol solely consisted of small molecules, with 6 µm CHIR99021 from day 0 to day 2, and 2 µm WNT-C59 from day 2 to day 4, and resulted in extremely high cardiomyocyte yields and purity, with 95% of cells positive for cardiac troponin T (TNNT2) (Burridge et al., 2014).

1.6.4 A Practical Compromise

The protocol by Burridge et al., 2014 provides a fully defined, xeno-free system, which was expected to result in differentiations containing up to 95% TNNT2+ beating sheets. Specifically noted, it was claimed the repeated differentiations across 11 cell lines all demonstrated between 80-95% efficiency (TNNT2+ cells), yielding on average greater than 3 x 10^5 cardiomyocytes per cm^2.

Experimentation using the Burridge protocol from all members within the Denning group failed to reproduce these results, with differentiations variably failing 2 out of 3 times.

In-house development has led to a more robust and reproducible differentiation protocol, which has reverted to the use of xenogenic and undefined components. The protocol, detailed in the methods chapter, induces mesoderm specification with StemPro Serum Free medium supplemented with BMP4 and a Matrigel overlay, followed 12-16 hours later with BMP4/Activin-a canonical Wnt activation. Cardiac specification is carried out in two steps using small molecule Wnt inhibitors XAV939 & KY0211, initially in RPMI-B27 (-ins), and two days later with RPMI-B27 containing insulin, followed by 4-6 days culture solely in RPMI-B27 (+ins), during which 80-95% TNNT2+ cultures are commonly obtained (Mosqueira et al., 2018)(Smith et al., 2018).

1.7 Cardiomyocyte Physiology & the Maturation Problem

1.7.1 A Key Summary

The differentiation protocols of hPSCs to cardiomyocytes have improved from 1% differentiation efficiency from early protocols in 2001 (Kehat et al., 2001), to regularly reaching 85-95% with modern methods (Smith et al., 2018). Whilst hPSC-CMs can be produced efficiently, the maturity of cardiomyocytes produced resembles cardiomyocytes of the 1st or 2nd trimester, with functional consequences for their physiological state (Van den Berg et al., 2016)(M. C. Ribeiro et al., 2015)(Sun and Nunes, 2017).

The maturation problem is well defined, differences between cells that can be generated within the laboratory using hPSCs range across every aspect, from, structure, sarcoplasmic reticulum, gene expression, metabolism, force conduction, electrophysiology, and calcium handling.

1.7.2 Cardiomyocyte Structure

The size and structure of cardiomyocytes play an important role in their functionality, during foetal development cardiomyocytes will undergo rapid proliferation, however postnatally, physiological hypertrophy of cardiomyocytes serves to increase their performance to match the requirements of the developing body (Jonker et al., 2007)(Li et al., 1996).

Compared to the hPSC-CM area of ~600 μm^2, adult cardiomyocytes can reach 30-40 times this size, a factor that is important for effective signal propagation throughout the heart (Laflamme and Murry, 2011)(Spach et al., 2004).

1.7.3 Contractile Apparatus

hPSC-CMs are not just smaller, but their structure is rounded and their contractile subunits, sarcomeres, are disorganised and shorter (1.6 μm vs 2.2 μm), reducing their ability to produce force (Lundy et al., 2013).

Proteins involved within the contractile machinery of the cardiomyocyte are currently expressed in their foetal isoform when derived from hPSCs. Such examples are, α-myosin heavy chain isoform (α-MHC) a faster cycling motor predominantly found in hPSC-CMs (Scuderi and Butcher, 2017). Myosin light chain 2a (MLC-2a) vs the ventricular form MLC-2v is another example, where the latter is solely expressed in adult ventricular myocytes (De Sousa Lopes et al., 2006).

The slow skeletal troponin inhibitor (TNNI) to cardiac troponin inhibitor (TNNI3) (adult form) switch has been demonstrated during development to be in an irreversible manner, even during stress or disease. The ratio of cTnI: ssTnI protein

isoforms a particularly suitable target to track maturation within this chapter (Bedada et al., 2014).

The switch is important for cardiac maturation because ssTnI isoform lacks a unique 32-residue N-terminal extension, which is present on cTnI, this region contains a phosphorylation site for protein kinase A (PKA). This cTnI additional phosphorylation site makes it responsive to adrenergic stimulation, this is linked to an increased possible rate of force relaxation (Gomes, Potter and Szczesna-cordary, 2002).

1.7.4 T-Tubules

T-Tubules are invaginations of the membrane that are critically important structures for propagating contraction throughout a cardiac tissue. T-Tubules are regularly spaced every 2 μm along an adult cardiomyocyte and align with the z-disks of sarcomeres (Yang et al., 2014).

T-tubules ensure rapid synchronised contraction by placing a high concentration of L-type calcium channels, responsible for the initial calcium influx, in close proximity to the sarcoplasmic reticulum (SR). This allows an initial calcium spark to induce further intracellular calcium release in a process known as (CICR) via ryanodine-2 receptors (RYR2), which is essential for mature calcium and contraction kinetics (Yang, Pabon and Murry, 2014).

1.7.5 Metabolism

In the fetal heart oxygen levels are low and fetal cardiomyocytes (and hPSC-CMs) rely heavily on glycolysis and lactate oxidation to fuel relatively low energy needs, when compared to adult cardiomyocytes (Ellen Kreipke et al., 2016).

After birth cardiomyocytes undergo physiological hypertrophy with increasing levels of stress and workload (Ellen Kreipke et al., 2016). During this period of growth and increased stress, the levels of free fatty acids in blood increase and the cardiomyocytes adapt a new energy profile based primarily from fatty acid oxidation to meet increased demands (Ellen Kreipke et al., 2016).

Changes in metabolic demands are also reflected on a structural level where fetal cardiomyocytes or hPSC-CMs have a relatively low number of mitochondria centred on the perinuclear area, adult cardiomyocytes have significantly more mitochondria than can occupy up to 40% of the cell area and contain more developed and organised cristae (Keung, Boheler and Li, 2014).

1.7.6 Gene Expression

It is suggested that hPSC-CMs closely resemble the cardiomyocytes found at the fetal stage of development. Berg et al., 2015 compared the transcriptome of human fetal cardiomyocytes in the first and second trimester to hPSC-CMs.

Without a maturation approach, current hPSC-CMs align closely to foetal cardiomyocytes in the first trimester, but with available maturation media the transcriptome aligns closer with foetal cardiomyocytes from the second trimester. The results from Berg et al., 2015 could now be used as a benchmark for maturation approaches attempted during this project.

Differences in gene expression between adult human cardiomyocytes and foetal / hPSC-CMs can result in either greatly reduced expression, or differing isoforms of key proteins being expressed. Relating to contraction, differing isoforms such as, TNNI1/TNNI3 & MYH6/MYH7 have been discussed above.

Detection of an I_{K1} current in hPSC-CMs is difficult due to the low expression of *KCNJ2*, this leads to an increased funny current I_f, a lesser polarised resting membrane potential of -20 to -60 mV and automaticity of contraction in culture (Dhamoon and Jalife, 2005)(Li et al., 2017).

Differences in gene expression relating to calcium handling in hPSC-CMs vs adult cardiomyocytes translates to reduced contractile force and a diminished plateau phase in the action potential. The hPSC-CMs currently show a reduced level of sarcoplasmic reticulum calcium handling proteins such as SERCA2, calsequestrin and phospholamban (Denning et al., 2016)(Yang, Pabon and Murry, 2014). This creates an important difference between hPSC-CMs and their mature counterparts, hPSC-CMs demonstrate a negative force-frequency relationship, however mature cardiomyocytes retain a positive force-frequency relationship utilising their high levels of stored intra-cellular calcium (Ruan et al., 2016).

1.8 Current Approaches to Maturation

To overcome the maturation barrier to hPSC-CMs, to allow their effective implementation for drug screening and cellular therapies, many approaches have been explored to induce further cardiomyocyte maturation.

These include, prolonged culture times, force cell alignment, electrical stimulation, mechanical stimulation, altering the substrate stiffness, medium additives, co-culture, matrix materials, 3D-culture and the use of biomaterials (figure 1.5).

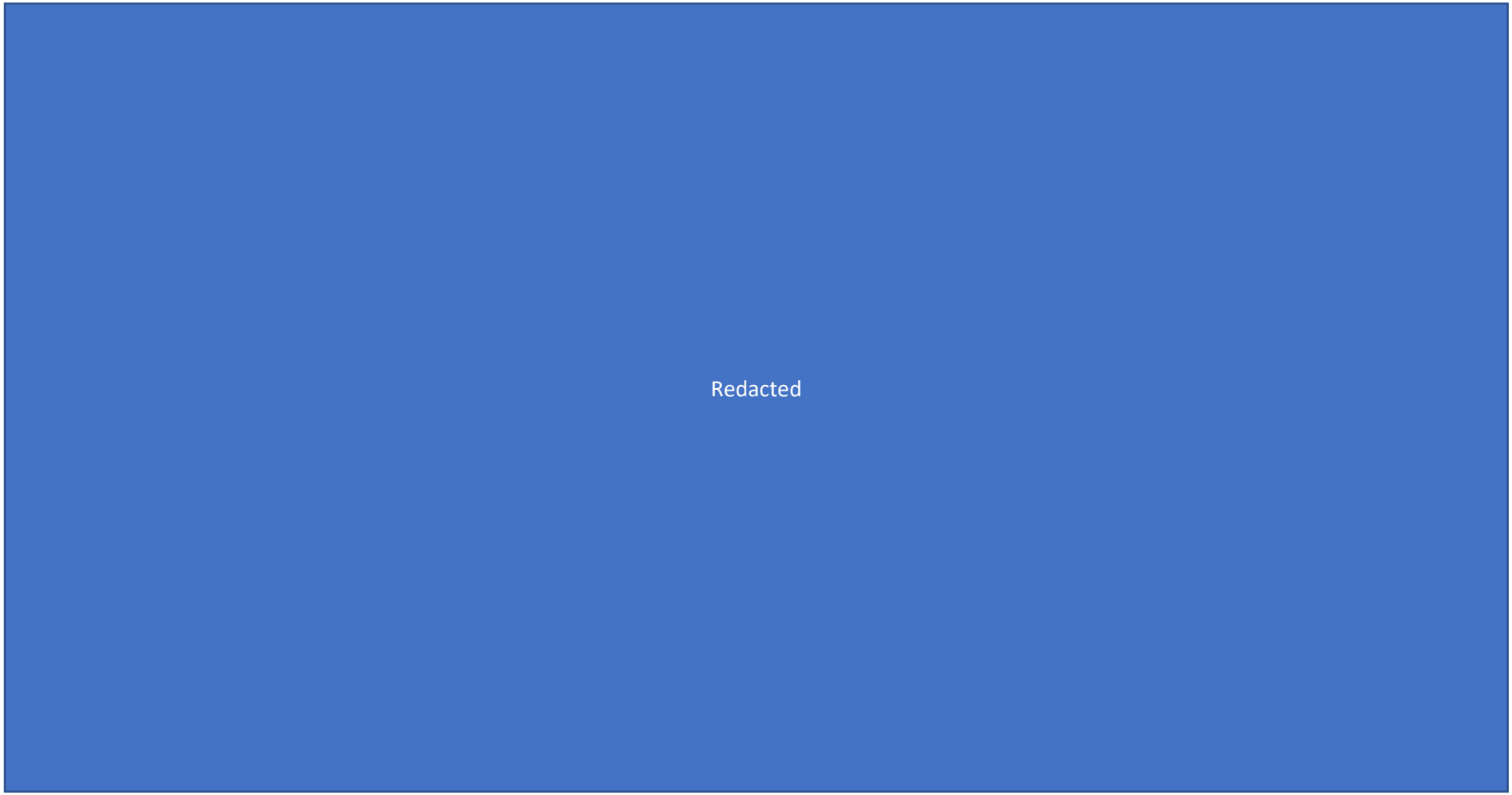

Figure 1.5 Summary of Maturation States & Strategies
Taken from Schwach & Passier 2019.

1.8.1 Prolonged Culture

Lundy et al., 2013 & Kamakura et al., 2013 studied hPSC-CM maturation in prolonged culture. 'Early' cardiomyocytes, 20-40 days and 'late' cardiomyocytes, 80-120 days were analysed. Prolonged culture increased cell area from 480 +/- 32 μm^2 to 1716 +/- 150 μm^2, decreases in circularity and an increase in sarcomeric length from 1.65 +/- 0.02 µm to 1.81 +/- 0.01 µm (vs 2.2 µm in mature cardiomyocytes) with greater visible sarcomeric organisation.

Further ultrastructure analysis revealed mitochondria contained more prominent cristae and were co-localised with myofibril bundles, multi-nucleation in 'late' hPSC-CMs drastically increased (>30% vs >5%). 'Late' stage hPSC-CMs also demonstrate improved action potentials and contraction characteristics (Dai et al., 2017)(Lundy et al., 2013).

These findings were mirrored in a study using embryoid bodies instead of monolayer culture (Kamakura et al., 2013). The levels of maturation achieved by both authors do not represent full maturation, calcium handling was modestly improved.

1.8.2 Cell alignment

It has been well characterised that cardiomyocytes form structures with anisotropic alignment to facilitate electrical propagation and contraction of the heart muscle. Electrospun fibrous aligned nanofiber structures can successfully induce cardiomyocyte alignment in culture (Khan et al., 2015)(Han et al., 2016). Alignment in 2D by Khan et al., 2015, resulted few demonstrable markers of maturation aside from modestly improved calcium handling.

Experimentation utilising a 3D aligned environment improved sarcomeric organisation, expression of key genes such as KCNJ2, MYH6 & CASQ2 and demonstrated appropriate pharmacological responses to isoproterenol and phenylephrine (Han et al., 2016).

Overall alignment on electrospun anisotropic fibrous scaffolds induces a limited maturation effect on hPSC-CMs.

1.8.3 Electrical Stimulation

In vivo embryonic cardiomyocytes are exposed to electrical fields during their development, which are believed to be involved in spatial patterning and tissue morphogenesis. One platform attempting to replicate this in vivo effect involves a type I collagen-based gel placed into a PDMS template where cardiomyocytes were co-cultured in 3D with fibroblasts and electrically stimulated through platinum wires – termed Biowire II (Zhao et al., 2019).

Biowires II stimulated with the 6-Hz regimen exhibited; physiological hypertrophy, greater sarcomeric organisation, improved calcium & electrophysiological properties. Specifically, pacing with 6 Hz increased contraction force 21-fold higher than pacing at 1 Hz ($p = < 0.0001$), and demonstrate a positive force frequency relationship, a hallmark of maturation. Beyond maturation, Biowires II also allows for defined atrial and ventricular zones to probe drug response in a chamber-specific manner (Zhao et al., 2019).

1.8.4 Mechanical Stimulation

The human heart experiences increasing mechanical load during development, shortly after birth increased mechanical load leads to physiological

hypertrophy and a dramatic shift from glucose/lactate oxidation to fatty acid oxidation (Ellen Kreipke et al., 2016).

It has been hypothesised that mechanical stimulation in vitro could mimic this natural process and induce greater maturation. Cyclic stress was compared to static stress and no stress of cardiomyocytes in 3D collagen type I structures. During cyclic stress β-MHC increased 550%-800% with a concomitant reduction in α-MHC 62%-50% - suggesting contractile maturation (Ruan et al., 2016).

Calcium dynamics were significantly improved with cyclic mechanical stress, peak calcium flux & departing velocity increased by greater than 100% (Ruan et al., 2016).

hESC-CMs in 3D gelatin scaffolds that underwent cyclic stress developed a more mature ultrastructure, greater elongation, and connexin-43 expression. Both studies confirm cyclic stress induces limited maturation in hPSC-CMs (Mihic et al., 2014). Note that a summary of physical stress & electrical induced maturation strategies are summarised in table 1.2.

1.8.5 Substrate Stiffness

During development the myocardial extracellular matrix alters and stiffens. Starting as a relatively soft mesoderm with a stiffness less than 500 Pa, changes in the extracellular matrix cause stiffening up to 10 kPa by embryonic day 14 (Young et al., 2014).

The altering stiffness was thought to allow the matching of intra/extracellular strains for prolonged rhythmic contraction required in vivo (Young et al., 2014).

A measurement of cell and substrate strains during contraction demonstrated that intermediate 11 kPa – 17 kPa substrates had a near balance of intracellular-substrate strain allowing for efficient contraction, and overly stiff substrates mimicking scar tissue resulted in loss of contraction over-time (Engler et al., 2008).

Young et al., 2014 utilised a thiolated hyaluronic acid/poly(ethylene glycol) diacrylate (PEGDA) hydrogel, which stiffens from ~2 kPa to 9 kPa. Substrates with a biologically relevant dynamic stiffness may increase maturation through improved myofibrillar assembly.

1.8.6 Media supplementation

Investigators have sought to discover soluble factors to induce maturation, by mimicking factors seen during development, such as Tri-iodo-L-thyronine (T3), or through high-throughput screening of compound libraries.

T3 has been found to induce maturation. hiPSC-CMs treated with T3 supplemented media for 1 week and reported; increased cell size, increases sarcomeric length, increased force generation, enhanced calcium handling & increased maximal mitochondrial respiration (Yang, Pabon and Murry, 2014).

It has been demonstrated that the synthetic glucocorticoid Dexamethasone increases force contraction, sarcomeric length and provides some improvements to calcium handling in hESC-CMs (Kosmidis et al., 2015).

1.8.7 3D Culture Environments

2D culture environments fail to recapitulate the tissue architecture of the human heart. Cardiomyocytes exhibit cell shape dependent functions, namely their contractile properties and cell-to-cell linkages (A. J. S. Ribeiro et al., 2015).

Engineered heart tissues (EHTs) present a promising 3D environment where contractile forces can be measured (Zimmermann, Melnychenko and Eschenhagen, 2004). Each EHT is formed of a fibrin gel encapsulating 0.5-1 million cardiomyocytes between two silicone posts.

The silicone posts are flexible with known mechanical properties, their displacement by cardiomyocyte contraction can be monitored and quantified using video-optics. EHTs are in the centimetre range and can be sustained for longer periods of time allowing for chronic drug interaction studies.

Maturation observed in EHTs include; an aspect ratio near 7:1, larger cell size compared to 2D methods, improved alignment, increased gene expression of key adult isoforms such as β-MHC and increased ion channel expression (Hirt et al., 2014).

These findings were mirrored in a more recent study, where the physical resistance to contraction was increased through modification to the silicone posts (Leonard et al., 2018).

More recent developments have shown EHTs can be used to also increase metabolic maturation, with a similarity of mitochondrial proteomes to adult cardiomyocytes (Ulmer et al., 2018). Despite these significant advances in

maturation, 3D culture environments have yet to fully recapitulate the adult phenotype.

1.8.8 Surface Chemistry

A relatively new and unexplored approach to inducing cardiomyocyte maturation is the adoption of novel surface chemistries. A combinatorial discovery approach utilising polymers formed of poly-e-caprolactone (PCL), polyethylene glycol (PEG) and carboxylated PCL (cPCL) to induce greater hPSC-CM maturation (Chun et al., 2015).

Results from culturing hPSC-CMs on an electrospun scaffolds of 4%PEG-96%PCL, coated with vitronectin, increased the ratio of adult cTnI to foetal ssTnI, and showed an increased percentage of cells expressing the myosin light chain-2a (MLC-2a). The 4%PEG-96%PCL polymer surface relied on a FBS containing medium for attachment, where it is known that the use of serum in otherwise defined conditions is sufficient to induce pathological hypertrophy, confounding drug & safety studies performed on cardiomyocytes exposed to it (Dambrot et al., 2014). Therefore, it is important to find surface chemistries that can support hPSC-CM attachment and maturation, when cultured in the absence of serum.

More relevant to the work being carried out in this PhD project would be the work by Patel et al., 2015, at the University of Nottingham, to identify hit polymers/co-polymers for cardiomyocyte attachment and maturation. In this study polymer spots were dispensed onto epoxy glass slides coated with 4% pHEMA to prevent random attachment. The ability of nearly 700 polymers was analysed for attachment and cell spreading, with and without serum. A significantly greater

number of polymers were adhesion ‘hits’ comparable to a gelatin control when serum was introduced, 48/116 homopolymers compared to 7/116 without serum.

The 3 most promising polymers without the need for serum were studied in more detail for their maturation properties. Results demonstrated a 2-fold and a 6-fold increase in upstroke velocity. hPSC-CMs on the best performing polymers had sarcomeric lengths of 1.97 µm, 1.80 µm & 1.70 µm respectively, less than the 2.20µm in mature cells but greater than 1.50 µm shown in gelatin controls. This increased sarcomeric length was translated functionally, to up to a 10-fold increased sensitivity to the cardiotoxic drug doxorubicin, proving the potential worth of synthetic biomaterial driven maturation for functional applications (Patel et al., 2015).

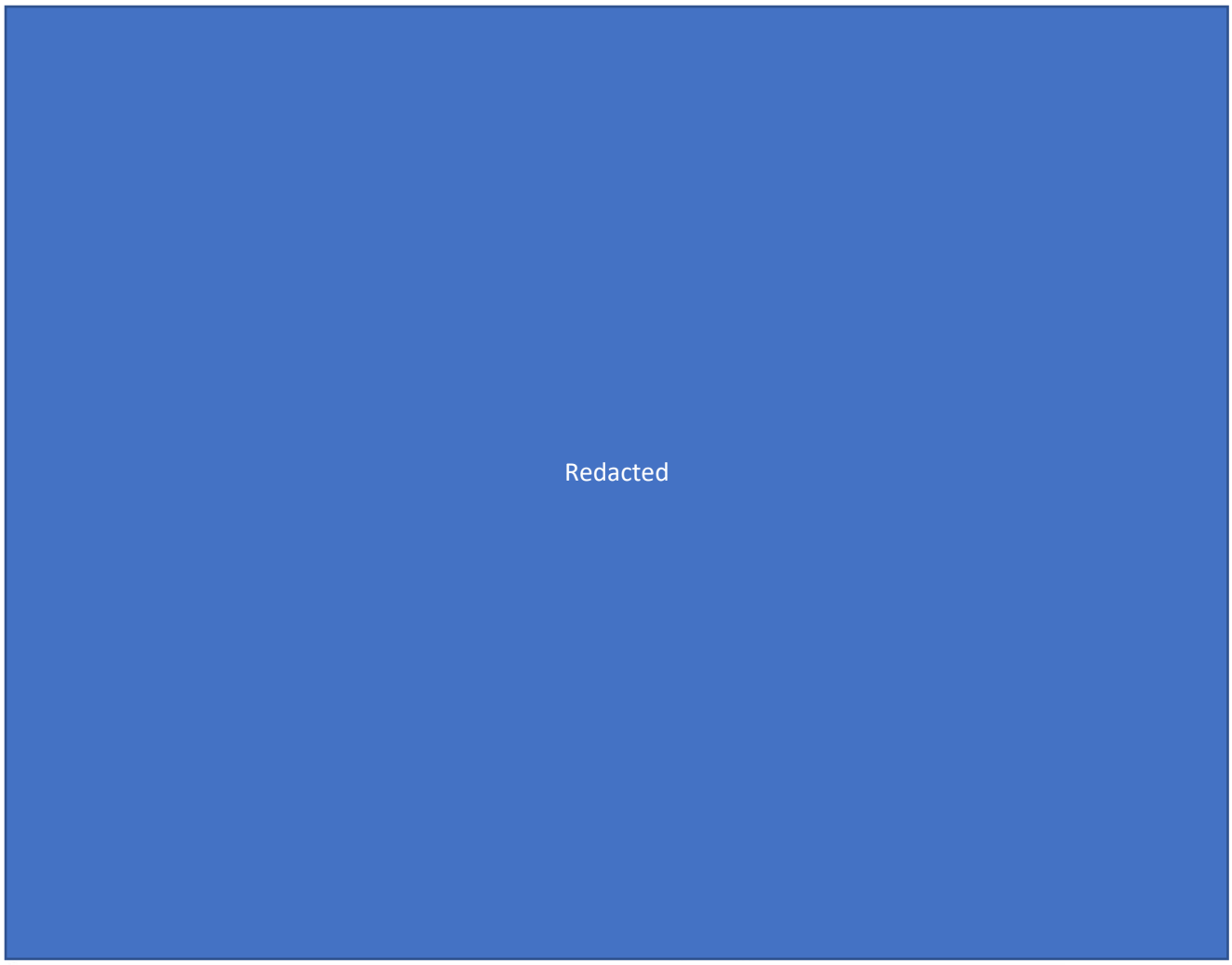

Table 1.1 Summary of Physical & Electrical Maturation Approaches Previously Taken.
Taken from Scuderi & Butcher 2017.

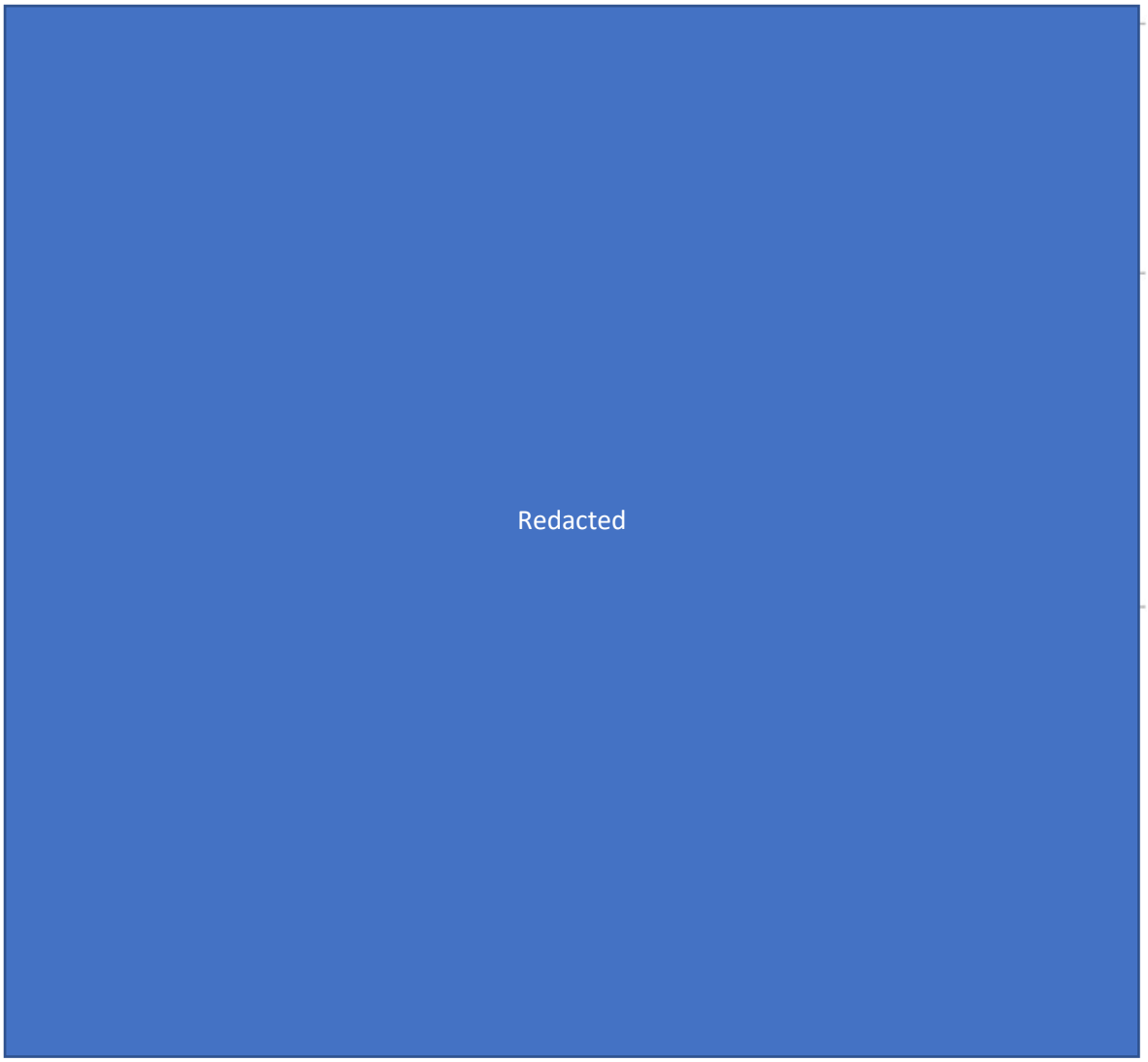
Redacted

1.8.9 Biomaterials – The Solution?

Undifferentiated hPSCs have unparalleled therapeutic potential, in a wide range of applications, from diabetes, to spinal injuries, stroke or heart disease, and many more. Yet the culture surfaces hPSCs are commonly grown on are either undefined & xenogenic, Matrigel™, or prohibitively expensive for industrial scale application, vitronectin & laminin-511. hPSC-CMs have therapeutic potential to replace lost & damaged cardiac tissue after cardiac ischemia.

Biomaterials present an opportunity to develop synthetic, fully defined, xeno-free culture surfaces, which are economically viable compared to existing recombinant protein-based surfaces. For example, Biolaminin 511 LN (LN511) (Biolamina) costs 43 p/cm^2 at the recommended concentration of 0.5 μg/cm^2, by comparison a top performing co-polymer in this thesis TCDMDA:BA (2:1) costs ~0.9 p/cm^2, when considering the cost of the monomer components in isolation.

Aside from fully defined, synthetic, reproducible surfaces, with great affordability, biomaterials also provide an opportunity to improve the function of hPSC-CMs, therefore clinical & pharmaceutical relevance (Patel et al., 2015).

As previously discussed, increasing the maturation state of hPSC-CM will increase their usefulness in disease models, provide better tools for toxicity testing & take the field one step closer toward therapeutic application (Veerman et al., 2015)(Koivumäki et al., 2018).

1.9 Biomaterials

1.9.1 What defines a Biomaterial?

The exact definition of what constitutes a biomaterial has been attempted multiple times during the fields development, one such definition that was 'endorsed by a consensus of experts' reads – 'A biomaterial is a nonviable material used in a medical device, intended to interact with biological systems.' (Donaruma, 1988)(Ratner, 2004).

Another attempt at defining biomaterials more broadly includes a wider range of uses; 'materials of synthetic as well as of natural origin in contact with tissue, blood, and biological fluids, and intended for use for prosthetic, diagnostic, therapeutic and storage applications without adversely affecting living organism and its components.' (Parida, Behera and Chandra Mishra, 2012). A broader attempt at defining biomaterials, 'A biomaterial is any matter, surface, or construct that interacts with biological systems.' (Pavlovic, 2015)

These definitions are now dated, with biomaterials being functionalised with living cells (viable material), and biomaterials approaches being utilised in vitro, outside of prosthetics, therapeutics & biological systems. This thesis is an example of such, where biomaterials are being used to induce maturation of human pluripotent stem cell (hPSC) derived cardiomyocytes, or continuous undifferentiated hPSC culture, where the application is both in vitro, drug screening, toxicity screening, disease modelling and in vivo, for therapeutics.

1.9.2 History of Biomaterials

Biomaterials are not a new concept, throughout history biomaterials have existed, some of the earliest records of biomaterials take form in a bitumen & vegetal fibre tooth filling ~13,000 years ago (Oxilia et al., 2017), and surgical sutures made from plant fibres, hair and wool threads used in ancient Egypt 3000BC (Muffly, Tizzano and Walters, 2011). Within the last 50-60 years of history, that the field of biomaterials has started to mature, where considerations for the selection and detailed characterisation of materials started to be considered (Stupp, 2001).

At its origins as a formal field of science, biomaterials have always been highly interdisciplinary, combining the expertise of; engineers, physical scientists, pathologists & clinicians – however with the rapid development technology to investigate cellular biology, cell biologists are probing the cellular mechanisms and interactions which govern the biological response to a given biomaterial.

The rapid expansion of technology in cell biology, including the derivation & culture of stem cells, has resulted in the highly interdisciplinary collaboration that has resulted in the production of this thesis.

1.9.3 Types of Materials used as Biomaterials

No two biomaterials are the same, each biomaterial has their own advantages and disadvantages which tailors them for a subset of applications. Where soft silicone-acrylate hydrogels are suitable for the contact lens, they lack the mechanical properties for bone replacement.

Biomaterials can broadly be separated into four main groups, metallic, naturally derived, ceramics, & polymeric - with the caveat that members of each grouping will possess their own material specific features.

1.9.4 Metallic Biomaterials

Metallic biomaterials are primarily used for joint replacements, stents, dental and orthopaedic implants. Metallic biomaterials provide good ductility, high strength and are inert which has made them ideal for load-bearing applications, however their relatively high elastic modulus compared to bone can result in 'stress shielding' leading to the eventual loss of bone material (Prasad et al., 2017).

Metallic materials such as stainless steel, cobalt-chromium and titanium have low corrosion properties however eventually undergo corrosion and wear over an extended period in an aggressive in vivo environment, potentially leading to the undesirable release of metallic ions which can lead to inflammatory responses (Saini et al., 2015). Metallic biomaterials will continue to play a vital role for joint replacements, with 3D printing & ceramic or polymeric coatings potentially enhancing their capabilities in the future (Mulford, Babazadeh and Mackay, 2016).

1.9.5 Naturally Derived

Nature presents us a diverse catalogue of biomaterials, including; collagen (Sumanasinghe, Bernacki and Loboa, 2006), fibrin (Gurevich et al., 2002), silk (Mauney et al., 2007), agarose (Zarrintaj et al., 2018), alginate (Sun and Tan, 2013), hyaluronan (Prestwich, 2011) and chitosan (Ahsan et al., 2018). Naturally derived biomaterials confer the advantages of being biocompatible, non-toxic, renewable and many have built-in sites for interactions with cells or biological factors, which can

greatly aid in the regeneration process. However, most natural biomaterials (silk excluded) suffer from poor mechanical properties, often from rapid degradation - failing to maintain a desired structure (Vehoff et al., 2007)(Mano et al., 2007).

1.9.6 Ceramics

Bioceramics are materials with high compressive strength, ideal for orthopaedic or dental implants. Bioceramics are relatively flexible in their application for these purposes because they consist of a range of materials that can be bioinert – stable (alumina & zirconia), bioactive – capable of interacting with biological tissue (hydroxyapatite & bioactive glass) or bioresorbable – degraded safely by the body in a controlled manner (tricalcium phosphate) (Hench, 2005). Bioinert ceramics are commonly used within joint replacements for their stability and load bearing properties (Piconi et al., 2018). Bioactive ceramics are capable of inducing releasing factors or inducing cell responses such as angiogenesis and can have tissue bonding capabilities (Gerhardt et al., 2011)(Miguez-Pacheco, Hench and Boccaccini, 2015).

Bioresorbable ceramics allow natural tissue to replace the implant over time, although the balance between porosity and structural integrity and the pace of the ceramic degradation are challenges researchers face. Disadvantages of bioceramics includes their brittle nature, and difficulty in the manufacturing process (Baino, Novajra and Vitale-Brovarone, 2015).

1.9.7 Synthetic Polymers

Synthetic Polymeric biomaterials (excluding natural polymers such as collagen & chitosan) are a modern era man-made creation and the focus of this thesis. Synthetic polymers are easy to manufacture, reproducible when

manufactured, and have flexibility in their structure & design. Alterations to the polymer composition can affect their physical mechanical, chemical, electrical and thermal properties, making synthetic polymeric materials extremely versatile (Teo et al., 2016). A wide range of synthetic polymers exist that are also biocompatible.

Synthetic polymers serve a wide field of biomaterial applications such as, poly(hydroxyethyl methacrylate) (pHEMA) and poly(lactic-co-glycolic) acid (PLGA) for contact lenses, poly(glycolic acid) for degradable sutures, poly(vinyl siloxane) for dental impressions, and poly(methyl methacrylate) as bone cement (Seal, Otero and Panitch, 2001). Synthetic polymers can also serve as anti-bacterial surfaces on medical devices, as microcarriers for drug delivery, and scaffolds/surfaces that are capable of supporting protein/cellular attachment for both in vivo and in vitro purposes (Liang et al., 2017).

Polymeric biomaterials have disadvantages, of primary concern for implants are toxic leachable compounds, which may have deleterious effects on the patient (Yin and Luan, 2016). Polymeric biomaterials also absorb water and proteins, which can be advantageous or disadvantageous dependent on the intended use.

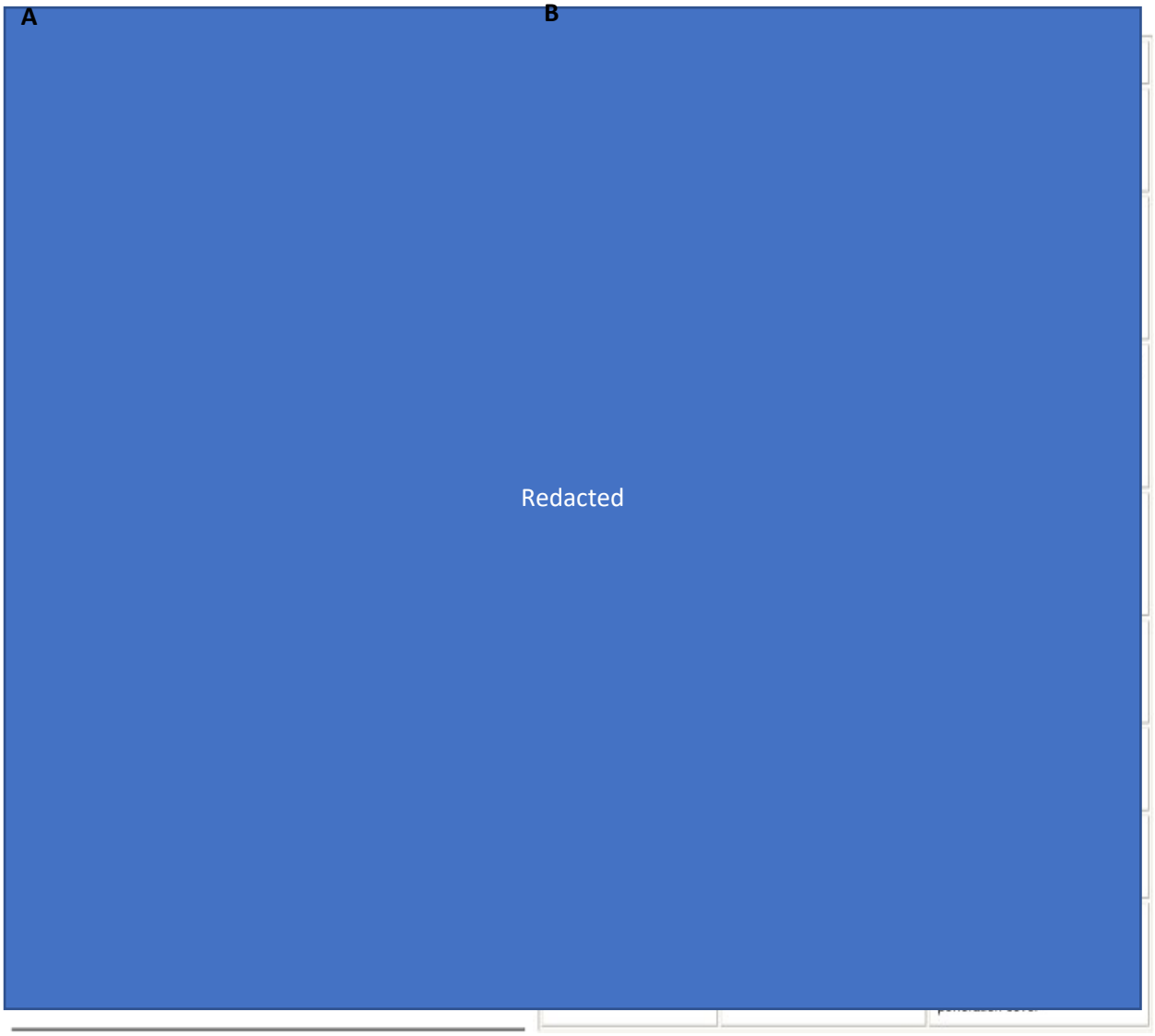

Table 1.2 Examples of biomaterial applications and the materials used to create them.

(A) Taken from Rater, 2004. (B) Taken from Yin & Lun, 2016.

1.10 The Development of High-Throughput Biomaterial Discovery

1.10.1 Polymer Microarray Development

To discover new biomaterials, polymer microarray screening techniques were first developed in 2004, a system that allowed the printing of thousands of materials on a nanolitre scale into a format resistant to aqueous culture (Anderson, Levenberg and Langer, 2004). Critically, this system utilised a pHEMA background to ensure the space between printed polymer spots prevented cellular and protein attachment, allowing independent assessment of each material and allowed for the analysis of multiple biological markers in a systematic manner, when combined with automated position-based microscopy.

Initially this screening method tested 1728 unique polymer – stem cell interactions, with an acrylate, diacrylate, triacrylate & methacrylate library. The results identified that high-throughput polymer library screens could identify biomaterials with differing capacities for hPSC attachment & influence their ability to differentiate into cytokeratin positive cells.

The utility of polymer microarray screening for biomaterials discovery was further evidenced when an array with 3456 polymers was shown to demonstrate differential attachment and marker expression for, mesenchymal stem cells, chondrocytes & neural stem cells (Anderson et al., 2005).

Since then other groups have expanded the search for biomaterials capable of supporting long-term hPSC culture. Brafman et al., 2010, utilised polymer microarrays to screen 1280 acrylamide gels to discover poly(methyl vinyl ether-alt-maleic anhydride) (PMVE-alt-MA), which they demonstrated was capable of long-

term (5 passage+) culture of three hPSC lines. This study demonstrated the capability of polymer microarrays to produce biomaterials that can support hPSC culture without serum. Culture conditions for PMVE-alt-MA relied on the use of StemPro™ medium, which contains bovine serum albumin, known to potentially influence hPSC attachment to synthetic surfaces.

1.10.2 Polymer Microarrays & Surface Analysis for Prediction of Biological Response

Polymer microarray technology advanced with the addition of surface analysis techniques to identify parameters that can predict biological response. An array study that first discovered clonal growth on hPSCs on polymeric biomaterials, in the presence of vitronectin, with a xeno-free & fully defined media, was the first perform an in-depth investigation to determine if surface characteristics such as wettability, modulus or chemistry can be used to predict biological response (figure 1.6).

Data from the study identified that only Time of Flight Secondary Ion Mass Spectrometry (ToF-SIMS) could predict biological response, with an R^2 value of 0.78.

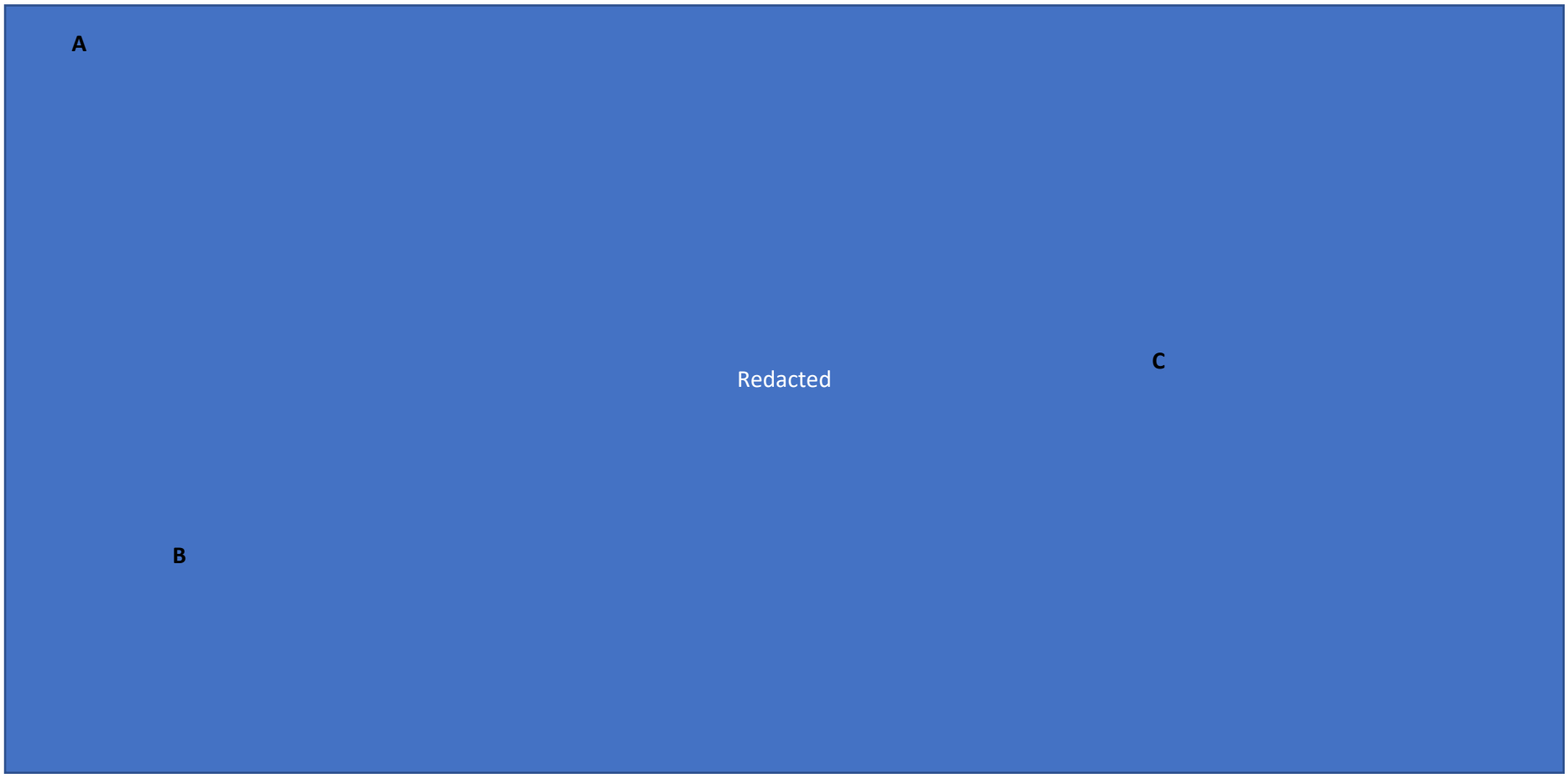

Figure 1.6 Overview of polymer microarray screening with human embryonic stem cells (hESCs) with in-depth surface characterisation.
(A) Identification of OCT4 positive hESCs cultured on polymer microarrays through high-content imaging. (B) Surface analysis techniques, atomic force microscopy, wettability & ToF-SIMS. (C) Identification of surface parameters that correlate to hESC attachment. Taken from Mei et al., 2010.

1.10.3 Polymer Microarrays for hPSC Culture in Defined Conditions

The development of culture medium for hPSCs has resulted in the need to perform new polymer microarray screens. Polymeric biomaterials that supported hESC attachment in the presence of serum containing medium, failed to do so without it (Anderson, Levenberg and Langer, 2004).

Polymeric biomaterials from Mei et al., 2010 required a coating of vitronectin adhesion protein, hESCs were cultured on MEF layers.

More recent work used polymer microarray screening to discover that poly(N-(4-hydroxyphenyl)methacrylamide)-co-HEMA, poly(HPhMA-co-HEMA), could support long-term culture in a 6-well scaled up format, retaining their capability to form all three germ layers (Celiz et al., 2015). Poly(HPhMA-co-HEMA) was proven to work with MEF-conditioned medium, the serum-free defined StemPro medium and mTeSR1 medium. HPhMA alone was capable of long-term culture with hPSCs. However, HPhMA demonstrated poor physical stability, with visible cracking at the surface in cell culture incubator conditions. Celiz et al., overcame this problem through the addition of 2-hydroxyethyl methacrylate (HEMA), in a 2:1 ratio of HPhMA:HEMA respectively.

Despite pHEMA forming the anti-cell attachment background of the microarray, in this co-polymer there was no negative effect on cell binding or proliferation observed. ToF-SIMS analysis of the third-generation array also indicated pHEMA was present at the surface of the array spot during the screening process, meaning it had inter-mixed with the polymer solutions deposited.

It was interesting to note that β_1 & $\alpha_V\beta_5$ integrins were identified as being the most important for cell attachment. $\alpha_V\beta_5$ was also highlighted by Mei et al., 2010 as being important for their own hPSC attachment studies to a synthetic material (Celiz et al., 2015). These findings could have implications for work carried out in this thesis.

1.10.4 Towards a Defined Medium

Further development of hPSC culture medium sought to primarily remove the albumin content. Serum albumin is the primary component of blood plasma, capable of binding fatty acids, hormones, and growth factors (Garcia-Gonzalo and Izpisúa Belmonte, 2008). In the context of cell culture albumin can be used to stabilise growth factors but batch-to-batch variations are linked to inconsistencies on hPSC culture.

A systematic individual and pair-wise screen, removing the 18 components from the previous medium mTeSR-1 resulted a fully-defined, albumin-free, xeno-free medium with just 8 components in addition to DMEM/F12 (Chen et al., 2011). This medium was termed Essential 8™ medium, a comparison of the components in Essential 8™ (E8) medium and mTeSR® medium are found in table 1.3.

Components	mTeSR® Medium	Essential 8™ Medium
DMEM F-12	X	X
L-scorbic acid	X	X
Selenium	X	X
Transferrin	X	X
$NaHCO_3$	X	X
Glutathione	X	
L-Glutamine	X	
Defined lipids	X	
Thiamine	X	
Trace elements B	X	
Trace Elements C	X	
β-Mercaptoethanol	X	
Albumin (BSA)	X	
Insulin	X	X
FGF2	X	X
TGFβ1	X	X
Pipecolic acid	X	
LiCl	X	
GABA	X	
H_2O	X	

Table 1.3 Comparison of medium components between mTeSR-1 & Essential 8 Medium. Taken from ThermoFisher Scientific Essential 8 FAQ.

Unpublished work by Celiz et al., 2015, and work in this thesis will demonstrate that Poly(HPhMA-co-HEMA) is not capable of supporting hPSC survival and culture in Essential 8 medium. Hence, the need to perform further polymer microarray screening in this thesis to find a biomaterial capable of long-term hPSC culture in what is often termed as a 'stripped-down' medium.

1.10.5 Extracellular Matrix & Biomaterials

For hPSCs or hPSC-CMs to adhere to a synthetic surface, a mechanism of attachment must exist. To facilitate adhesion to a given surface, cells express integrin receptors, which are type I transmembrane glycoproteins (Iwamoto and Calderwood, 2015). Integrins receptors are heterodimers of α & β subunits, where

humans express 18 types of the α subunit & 8 types of the β subunit, forming a total of 24 different combinations (Iwamoto and Calderwood, 2015).

Each subunit combination of integrins binds to specific ECM components, cell surface components or proteins present in the environment. For example, α5β1 binds to fibronectin, α6β1 laminin, and αVβ5/αVβ3 to vitronectin (Schaffner, Ray and Dontenwill, 2013)(Takizawa et al., 2017)(Michael A. Horton, 1997).

Integrins support attachment to the ECM through a process of activation, followed by clustering. Activation is a result of conformational changes to the extracellular domains of the heterodimer, where Kindlin & Talin are proposed to aid in the initial activation process (Iwamoto and Calderwood, 2015). To increase the strength of cellular adhesions, clustering of integrin-ECM interactions is required (Miyamoto, Akiyama and Yamada, 1995)(Karimi et al., 2018).

In the case of undifferentiated hPSCs, the integrins α3, α5, α6, α7, α11, αV, αE and β1, β2, β3, β5, have been identified as present in at least some culture conditions, with, α5, α6, αV, β1 & β5 specifically prevalent in hiPSCs (Meng et al., 2010)(Xu et al., 2001)(Meng et al., 2010).

Figure 1.7 Simplified summary of mechanisms involved in integrin activation & clustering.

Talin-based activation increases the affinity of integrins for the substrate and promotes clustering. Talin bound to cytoskeletal components such as F-Actin reveals Vinculin binding sites, reinforcing clustering interaction. Active or inactive integrins may be targeted for endocytoic recycling via short or long loop trafficking. Figure taken from: Iwamoto and Calderwood, 2015.

Integrin activation can result in intra-cellular signalling & structural changes affecting, migration, spreading, adhesion & survival (Vachon, 2011)(Hansen et al., 1994)(Huttenlocher and Horwitz, 2011). Specifically, in hPSCs integrins are linked to PI3K-AKT & MEK/ERK signalling, where PI3K-AKT signalling is linked to hPSC survival & dissociation-induced apoptosis & high levels of MEK/ERK signalling known to maintain pluripotency (Armstrong et al., 2006)(Li et al., 2007)(Ohgushi et al., 2010).

Integrin-associated focal adhesion kinases (FAK) have also been shown to affect the pluripotency state of hPSCs. In hPSCs, pluripotency is in part maintained through the expression and activation of integrin α6β1, which has been shown to

maintain FAK in the non-phosphorylated form at Y397, keeping in inactivate. A loss of integrin α6β1, results in activation of FAK via Y397 phosphorylation & loss of pluripotency (Villa-Diaz et al., 2016).

For these reasons, it will be important to identify, 1.) the mechanism of attachment to biomaterials discovered in this thesis, and 2.) how intracellular signalling of hPSCs are affected by the mechanism of attachment & degree of attachment they employ.

1.11 Hypothesis & Thesis Aims:

This thesis hypothesizes that polymeric biomaterials of an acrylate & acrylamide nature can support the culture of hPSCs in full-defined xeno-free Essential 8™ medium, to replace xenogenic Matrigel™ & provide an economical alternative to commercially available fully defined substrates such as, Vitronectin XF™ & Laminin-511 LN. This thesis also predicts that polymeric biomaterials of the same nature will be capable of supporting the attachment of hPSC-CMs in serum-free conditions and inducing levels of maturation beyond that of Matrigel™ culture.

To test both of the hypothesis above, work presented here will achieve the following objectives:

1) Screen a homopolymer microarray containing 284 unique polymer spots, for the attachment of hPSCs or hPSC-CMs, at 24/48 hours, or 7-day culture, respectively.

2) Perform two independent co-polymer screens, containing mixtures of 24 homopolymers relevant to each separate cell type, forming a co-polymer microarray containing 599 unique materials.

3) Investigate the ability of chosen co-polymer biomaterials to serial passage culture of hPSCs & maintain pluripotency after >15 days, 5 passages, on the synthetic surface.

4) Identify mechanisms of hPSC attachment to chosen co-polymer biomaterials, analyse changes to, gene expression & phosphokinase protein expression, compared to equivalent Matrigel™-based hPSC culture.

5) Detect maturation improvements on scaled-up hPSC-CM homopolymer & co-polymer attachment hits, through the assessment of functional contraction & electrophysiological properties using the CellOPTIQ®, gene expression, and immunostaining for structural maturation markers.

2 Chapter 2 - Materials & Methods

2.1 Cell Culture

2.1.1 Culture of Human Pluripotent Stem Cells

Human pluripotent stem cells were cultured on Matrigel™ coated tissue culture plastic surfaces, using Essential 8™ medium (E8).

Matrigel™ coating of glass or tissue culture plastic surfaces were performed by diluting Matrigel™ (Corning – 354234) 1:100 in Dulbecco's Modified Eagle Media (DMEM), adding 0.16 mL/cm^2 to the surface. Matrigel™ was left to polymerisation on the surface for 45 minutes at room temperature, or overnight at 4°C. Coated surfaces were kept for a maximum of two weeks.

Essential 8™ medium used in this thesis was either, Gibco-E8 (ThermoFisher - A1517001), TeSR™-E8™ (STEMCELL Technologies - #05990), or E8 produced in-house following the previously described formulation, with the addition of 100ng/mL Heparin sodium salt (Sigma-Aldrich – H3393) (Chen et al., 2011).

A subset of culture in this thesis was also performed in NutriStem® V9 XF medium (Biological Industries – 05-105-1), which notably contains 10% recombinant human albumin.

To passage hPSCs, they were first cultured to 70-90% confluence, then washed with Dulbecco's Phosphate Buffered Saline (DPBS) without Ca^{2+} or Mg^{2+} (ThermoFisher: 14190250), dissociation was performed by incubating hPSCs in TrypLE Select X1 (ThermoFisher: 12563029) for 2-3 minutes at 37°C & 5% CO_2 (timing was cell line dependent).

Counting of cells was performed through manual counting using a haemocytometer or the CEDEX HiRes Analyser (Roche), which combines trypan blue staining with automated cell counting.

Matrigel™ coated surfaces were seeded at a density of 20,000 cells/cm^2 with the addition of 10 µM Y-27632 Rho-kinase inhibitor (ROCKi) (Tocris – 1254), during the first 24 hours of culture.

2.1.2 Cardiac Differentiation & Dissociation

Differentiation of hPSCs to cardiomyocytes was carried out using an in-house monolayer-based protocol (Mosqueira et al., 2018)(Smith et al., 2018). Cells were passaged as described with TrypLE Select and seeded at a density of 30,000 – 50,000 cells/cm^2. hPSCs were fed with E8 medium the following day.

The next day hPSCs were fed with E8 medium (morning), this medium was exchanged 8 hours later to pre-conditioning medium, containing a 1:100 Matrigel™ diluted in StemPro™-34 (ThermoFisher – 10639011), medium was supplemented with 1 ng/mL rh BMP4 (R&D – 314-BP-050). Between 12-20 hours later, medium was exchanged to StemPro™-34 supplemented with 10 ng/mL rh BMP4 and 8ng/mL rh Activin A (ThermoFisher – PHC9564), this stage is termed day 0 of differentiation.

48 hours later medium was exchanged to RPMI 1640 basal medium (ThermoFisher – 21875034) supplemented with B27 minus insulin (ThermoFisher – A1895601), 10 µM KY02111 (R&D – 4732) & 10 µM XAV939 (R&D – 3748), day 2 of differentiation. An additional 48 hours later, medium was exchanged to the same medium, except for the addition of insulin within the B27 supplement (ThermoFisher – 17504-044), day 4 of differentiation.

From day 6 of differentiation onwards, medium was exchanged for RPMI-B27 (+ Insulin), with no additional supplements. Cardiac differentiations were typically ready for dissociation between day 13-15. Dissociation of hPSC-CMs was performed following the protocol found in (Breckwoldt et al., 2017).

hPSC-CM cultures were washed in Ca^{2+} & Mg^{2+} free Hank's Balanced Salt Solution (HBSS) (ThermoFisher – 14170112), then dissociated in 200 units/mL collagenase II solution (Worthington – LS004176), with 10 µM Y-27632 ROCKi, 1 mM HEPES (Sigma – H4034) & 30 nM N-Benzyl-p-toluenesulphonamide (BTS) (TCI chemicals: B3082), dissolved in Ca^{2+} & Mg^{2+} free HBSS.

Dissociation occurred over a 2.5-3.5-hour period, where cultures were kept at 37°C in 5% CO_2. Dissociated cells were collected, and the collagenase enzyme quenched in RPMI 1640 supplied with 24 µg/mL DNase II (Sigma – D8764). Cells were centrifuged at 100 xg for 15 minutes and resuspended in RPMI-B27, counted & seeded at the appropriate density.

2.1.3 HUES7 Fibroblast Culture

HUES7-Fibroblasts were maintained in a 'fibroblast' medium containing a DMEM basal medium supplemented with 20% FBS (ThermoFisher), 1% non-essential amino acids (NEAA) (ThermoFisher - 11140035), 1% GlutaMA (ThermoFisher - 35050061) & 100 µM β-mercaptoethanol (Sigma - M3148). hESC-HUES7 fibroblasts were dissociated using 0.05% trypsin for 3 minutes after which trypsin was inactivated with the fibroblast medium & centrifuged at 200 xg for 5 minutes. Cells were resuspended and counted for re-plating.

2.1.4 Polymer Microarray Preparation for Cell Culture

To prepare polymer microarrays for cell seeding, each side was UV sterilised inside a type II biological safety cabinet for 15 minutes per side. To avoid damaging polymer spots on the safety cabinet surface, arrays were balanced between two petri dishes & handled with sterile tweezers.

Polymer microarrays were placed into 4-well plates, washed three times with DPBS & then conditioned with the appropriate medium for one hour before being replaced with fresh medium, ready for cell seeding.

2.2 Cell Characterisation

2.2.1 Growth Curves

Growth curves were performed using hPSC culture technique previous described. Cell counting for growth curves was performed using the CEDEX HiRes Analyser to keep counting consistent between passages, where hPSCs were passaged every 72 hours. The following formula were used to calculating cumulative population doubling & the population doubling time:

$$Cumulative\ population\ doubling = Sum\ \frac{Log_{10}(fold\ increase\ in\ cell\ number\ per\ passage)}{Log_{10}(2)}$$

$$Population\ doubling\ time\ (hours) = \frac{Cumulative\ time\ in\ culture}{Cumulative\ population\ doubling}$$

2.2.2 Karyotyping

To determine the karyotype of hPSCs, cells were cultured as previously described to the 48-hour culture point. Cells were then incubated with 0.1 µg/mL KaryoMAX® Colcemid™ (ThermoFisher – 15212012) in E8 medium for 1 hour.

KaryoMAX® Colcemid™ containing medium and subsequent washing steps were all collected and kept. Cells were harvested with TrypLE as previously described and centrifuged at 160 xg for 4 minutes.

Cells were re-suspended dropwise in a 0.6% sodium citrate (Sigma – W302600) and incubated for 20 minutes at room temperature.

Cells were centrifuged again at 160 xg for 4 minutes & re-suspended dropwise in a fixative solution containing glacial acetic acid and methanol (1:6). The fixation step was repeated twice more and re-suspended in 1 mL fixative solution and stored at -20°C until ready for analysis.

Analysis was carried out by Dr. Nigel Smith (Nottingham City Hospital, UK) in accordance with the International System for Human Cytogenetic Nomenclature International Guidelines (ISCN, 2005).

2.2.3 Immunocytochemistry

hPSCs or hPSC-CMs were prepared for immunocytochemistry by initially performing a fixation step, followed by primary antibody staining against the desired epitope, and then labelling with a secondary antibody containing a fluorescent tag.

Cells were twice washed with DPBS and fixed with 4% paraformaldehyde (PFA) solution for 15 minutes at room temperature. PFA was subsequently removed and cells washed twice more with DPBS, for storage cells were kept at 4°C.

The staining procedure was initiated by washing cells with DPBS for 5 minutes. To stain for intracellular/nuclear markers, cells were permeabilised with

0.1% Triton-X for 15-60 minutes (longer incubation times were required for dense hPSC colonies) at room temperature.

Permeabilised cells were washed once with DPBS before a 1-hour incubation in blocking solution (DPBS + 4% of a species appropriate serum), to prevent non-specific epitope binding.

Primary antibody solutions were prepared in DPBS with 4% serum, full antibody list provided in Table 2.1, primary staining occurred through incubation overnight at 4°C.

The next day, cells were washed three times in DPBS containing 0.1% Tween. Secondary antibodies were diluted in DPBS + 4% serum and incubated with cells for 1-hour at room temperature, followed by three further washes with DPBS + 0.1% Tween. To stain the nuclei, cells were incubated with a 500 µg/mL DAPI nuclear stain (Sigma – D9542) for 15 minutes at room temperature. A final wash with DPBS was performed and then cells were stored in DPBS at 4°C.

Target	Primary Antibody	Primary Antibody Dilution	Secondary Antibody	Secondary Antibody Dilution
OCT4	Monoclonal Mouse IgG, Santa Cruz sc-5279	1:200	Goat anti-Mouse IgG Alexa Fluor Plus 555, ThermoFisher A32727	1:1000
NANOG	Monoclonal Mouse IgG, Millipore MABD24	1:500	Goat anti-Rabbit IgG Alexa Fluor Plus 647, ThermoFisher A32733	1:1000
SOX2	Polyclonal Rabbit IgG, Abcam ab97959	1:500	Goat anti-Mouse IgG Alexa Fluor 488, ThermoFisher A-11001	1:400
TRA-1-81	Monoclonal Mouse IgM, Millipore MAB4381	1:200		
SSEA4	Monoclonal Mouse IgG, Sigma MAB4304	1:100		
SOX17	Polyclonal Goat IgG, R&D Systems AF1924	1:100		
FOXA2	Polyclonal Rabbit IgG, Sigma 07-633	1:500		
SOX1	Polyclonal Goat IgG, R&D	1:100		

	Systems AF3369			
PAX6	Polyclonal Sheep IgG, R&D Systems AF8150	1:100		
Cardiac α-actinin	Monoclonal Mouse IgG, Sigma A7811	1:800		
Connexin-43	Polyclonal Rabbit IgG, Abcam ab11370	1:1000		
Cardiac Troponin T	Polyclonal Rabbit IgG, Abcam ab45932	1:500		
Kir2.1	Polyclonal Rabbit IgG, Abcam ab65796	1:100		
Caveolin-3	Polyclonal Rabbit IgG Abcam ab2912	1:50		
Calsequestrin	Polyclonal Rabbit IgG Abcam ab3516	1:50		

Table 2.1 Summary of Antibodies Used for Immunostaining.

2.2.4 Flow Cytometry

Flow cytometry was carried out to identify the % hPSCs positive for pluripotency markers, OCT4, NANOG, SOX2, TRA-1-81 & SSEA4. Cells were prepared by dissociating 70-90% confluent cultures with TrypLE as described above. Cells were counted with the CEDEX HighRes Analyser and aliquoted to 1million/tube.

Cells were centrifuged at 160 xg for 4 minutes at 4°C, before being re-suspended in a 200 µL DPBS solution with 4% serum. An 800 µL 4% PFA DPBS solution was added and incubated at room temperature for 15 minutes.

A further centrifugation step 160 xg for 4 minutes at 4°C was carried out, if cellular markers were intracellular an additional permeabilization step, where cells were incubated in 500 µL DPBS + 0.1% tween, for 15 minutes at room temperature, was performed. Permeabilised cells were centrifuged at 3500 xg for 7 minutes at 4°C.

Conjugated antibody solutions were prepared by dilution (Table 2.2) in DPBS with 4% serum, to a total volume of 100 µL. Cells were re-suspended in the antibody solution and incubated at room temperature for 60 minutes, before a final centrifugation/washing step & re-suspension in 500 µL DPBS with 4% serum.

Flow cytometry measurements were carried out using a FC500 Flow Cytometer (Beckman Coulter). Analysis was carried out with Kaluza Analysis (Beckman Coulter), non-stained controls were gated so <2% cells were classified as positive for a given marker, batch analysis was performed on all measurements to determine % marker positivity.

Classification	Product Name	Company/Code	Function
Conjugated Antibody	Human Oct-4A APC-conjugated Antibody	R&D Systems IC6344A	Binds to OCT3/4 antigen, conjugated to APC.
Conjugated Antibody			
Conjugated Antibody	Human/Mouse/Rat SOX2 Alexa Fluor® 647-conjugated Antibody	R&D Systems IC2018R	Binds to SOX2 antigen, conjugated to Alexa Fluor® 647.
Conjugated Antibody	TRA-1-81 (Podocalyxin) Monoclonal Antibody, PE-conjugated	Invitrogen 12-8883-82	Binds to TRA-1-81 antigen, conjugate to PE.
Conjugated Antibody	Human/Mouse SSEA-4 Fluorescein-conjugated Antibody	R&D Systems FAB1435F	Binds to SSEA-4 antigen, conjugated to Fluorescein.

Table 2.2 Summary of Antibodies used for Flow Cytometry

2.2.5 RNA Extraction, cDNA Synthesis & RT-qPCR

RNA extraction was performed using the NucleoSpin® RNA kit (Machery-Nagel – 740955) as per manufacturer's instructions, including DNase treatment. RNA purity and quantification were performed using the NanoDrop-1000 spectrophotometer (ThermoFisher).

Synthesis of cDNA was performed using SuperScript™ III Reverse Transcriptase (ThermoFisher – 18080093) to manufacturer's instructions. Control

samples were carried out minus the addition of reverse transcriptase enzyme, to ensure amplification is not due to contaminating genomic DNA.

Set-up of qPCR experiments were performed with either TaqMan™ Fast Advanced Master Mix (Thermofisher – 4444556) or GoTaq® qPCR Master Mix (Promega – A6001). MicroAmp™ Fast Optical 96-Well Reaction Plate, 0.1 mL (ThermoFisher – 4346907) which were sealed with MicroAmp™ Optical Adhesive Film (ThermoFisher – 4360954). qPCR experiments were run on the Applied Biosystems 7500 Fast Real-Time PCR System for 40 cycles & analysed with the ΔΔCt method using 7500 Fast System SDS V2.0 software (Applied Biosystems).

Primer Name/Target	Primer Sequence/TaqMan Code
hHPRT-F	TGACACTGGCAAAACAATGCA
hHPRT-R	GGTCCTTTTCACCAGCAAGCT
hOCT4-F	GCTCGAGAAGGATGTGGTCC
hOCT4-R	CGTTGTGCATAGTCGCTGCT
hNANOG-F	GCAGAAGGCCTCAGCACCTA
hNANOG-R	AGGTTCCCAGTCGGGTTCA
hSOX2-F	CACTGCCCCTCTCACACATG
hSOX2-R	TCCCATTTCCCTCGTTTTTCT
hKLF4-F	GATGGGGTCTGTGACTGGAT
hKLF4-R	CCCCCAACTCACGGATATAA
hZIC1-F	GCGCTCCGAGAATTTAAAGA
hZIC1-R	GTCGCTGCTGTTAGCGAAG
GATA6-F	Gcaaaaatacttcccccaca
GATA6-R	Tctcccgcaccagtcatc
SOX17-F	acgccgagttgagcaaga
SOX17-R	tctgcctcctccacgaag
hHAND1-F	AACTCAAGAAGGCGGATGG
hHAND1-R	CGGTGCGTCCTTTAATCCT
hEOMES-F	CGCCACCAAACTGAGATGAT
hEOMES-R	CACATTGTAGTGGGCAGTGG
hPAX6-F	CTTTGCTTGGGAAATCCGAG
hPAX6-R	AGCCAGGTTGCGAAGAACTC
hSOX1-F	GGAATGGGAGGACAGGATTT
hSOX1-R	AACAGCCGGAGCAGAAGATA
TaqMan™ Probe TNNI3	(Assay ID) Hs00165957_m1
TaqMan™ Probe TNNI1	(Assay ID) Hs00913333_m1
TaqMan™ Probe Casq2	(Assay ID) Hs00154286_m1
TaqMan™ Probe RYR2	(Assay ID) Hs00181461_m1
TaqMan™ Probe TNNT2	(Assay ID) Hs00165960_m1
TaqMan™ Probe PPARGC1a	(Assay ID) Hs00173304_m1

Table 2.3 Summary of RT-qPCR Primers used.

2.2.6 Integrin Blocking

To determine which integrins play an important role for initial hPSC attachment to polymeric surfaces discovered in this PhD, hPSCs were incubated with antibodies or RGD-blocking peptides directed against specific integrins (Table 2.4), therefore blocking their action.

Integrin blocking antibodies were used at a concentration of 10 µg/mL & RGD-blocking peptides at 15 µg/mL for the first 24 hours of culture in E8 medium. Cells were washed twice in DPBS, fixed in 4% PFA & stained with DAPI before a quantitative cell count was performed using the Operetta high content image analysis system (Perkin Elmer) & analysed with Columbus™ software (Perkin Elmer).

Classification	Product Name	Company/Code	Function
Antibody	Human Integrin alpha 2/CD49b Antibody	R&D Systems MAB1233	Binds to α2 integrin.
Antibody	Human Integrin alpha 5/CD49e Antibody	R&D Systems MAB1864	Binds to α5 integrin.
Antibody	Human Integrin alpha 6/CD49f Antibody	R&D Systems MAB1350	Binds to α6 integrin.
Antibody	Human Integrin alpha V beta 3 Antibody	R&D Systems MAB3050	Binds to αVβ3 integrin.
Antibody	Human Integrin alpha V beta 5 Antibody	R&D Systems MAB2528	Binds to αVβ5 integrin.
Antibody	Human Integrin beta 1/CD29 Antibody	R&D Systems MAB17782	Binds to β1 integrin.
RGD-Blocking Peptide	H-1830	BACHEM 4009173	Linear peptide, inhibits fibronectin binding.

RGD-Blocking Peptide	H-4088	BACHEM 4027886	Control peptide for H-2574.
RGD-Blocking Peptide	H-2574	BACHEM 4026200	Binds $\alpha_V\beta_5$ integrin.
RGD-Blocking Peptide	H-7232	BACHEM 4070810	Control peptide for H-7226
RGD-Blocking Peptide	H-7226	BACHEM 4069272	Binds $\alpha_V\beta_3$ integrin.
RGD-Blocking Peptide	H-3164	BACHEM 4030598	Inhibits binding to fibronectin.

Table 2.4 Summary of Antibodies & RGD-Blocking Peptides used to Block Integrin Mediated Attachment to Polymeric Surfaces.

2.2.7 Phosphokinase Proteome Array Kit

Phosphorylated proteins expression was semi-quantitatively analysed, comparing Matrigel™ cultured hPSCs to TCDMDA:BA cultured hPSCS using the human phospho-kinase array (R&D Systems - ARY003B). Protein lysates were collected, quantified using a Bradford assay, repeated 6 times. Total protein of 400 µg was used to incubate array membranes.

The Part A and B arrays were blocked in Array Buffer, followed by overnight incubation with protein lysates in separated wells at 4 °C. Detection was performed by incubation with biotinylated detection antibody. For visualization, the enhanced chemiluminescence (ECL) reagent was added, images taken using ImageQuant LAS-4000 (Fujitsu Life Sciences).

Analysis performed in Microsoft Excel, where background signal was first deducted from spot intensities before comparisons of phospho-protein expression were made.

2.3 Materials Preparation

2.3.1 Glass Slide Silanisation

Glass microscope slides (25 mm x 75mm) (Sigma) were activated using O_2 plasma (p_i=0.3 mbar, 100 W, 1 minute). Oxygen activated slides were transferred into dry (4 Å molecular sieves) toluene under an argon atmosphere. 3-Glycidyloxypropyl)trimethoxysilane was then added to the solution, and the reaction mixture heated to 50°C for 16 hours. The slides were then cooled to room temperature and washed twice by sonication with fresh toluene. The slides were then dried under vacuum in a silicone-free Heraeus Vacuum Oven (50°C, 0.325 mbar) for 24 hours.

Alternatively, glass slides to be used for methacrylate-based arrays or for the scale-up attempts with hPSC-CM hit materials, a 3-(trimethoxysilyl)propyl methacrylate was used in place of 3-Glycidyloxypropyl)trimethoxysilane.

2.3.2 Microarray Fabrication

For the coating of glass slides with the pHEMA anti cell adhesion background, a 4% (w/v) pHEMA (Sigma, P3932 BioReagent Grade) in 95% (v/v) ethanol/water solution was created and sonicated for 24 hours at room temperature.

A Holmarc HO-TH-01 dip-coater was used at a dip speed of 9mm/s, retraction speed of 2mm/s and dip duration of 2 seconds, to coat epoxy functionalised slides with pHEMA solution; slides were dipped a total of x4 times, with a 5-minute drying stage between dips.

The slides were dried for 16 hours at room temperature, before further drying occurred within a Heraeus Vacuum Oven (50°C, 0.85 mbar) for 48 hours.

Polymer microarrays were printed on to the pHEMA coated array slides using the XYZ3200 dispensing station (Biodot) using quilled metal pins (Arrayit, 946MP6B).

Microarray printing was carried out under an argon atmosphere of O_2 < 2000 ppm, with temperature maintained at 25°C and 30-35% humidity. An atmosphere purged of oxygen was important to prevent early termination of the free radical driven reactions.

Monomer solutions were prepared for printing by diluting them (50% v/v for oils, 50% w/v for solids) with either a mixture of N,N'-dimethylformamide, 1:1 N,N'-dimethylformamide:water or 1:1 N,N'-dimethylformamide:toluene, solubility

dependent. Photoinitiator 2,2-dimethoxy-2-phenyl acetophenone (1% w/v) was added to all solutions.

Four replicates were printed onto array 8.0 & 8.2, all other arrays had three printed replicates per slide. Monomers were purchased from Sigma, Scientific Polymers, Acros and Polysciences. Arrays were dried in a Heraeus Vacuum Oven (20°C, 0.325 mbar) for 7 days.

2.3.3 Preparation of Scaled-Up Polymer Surfaces on TCP

Tissue culture plastic surfaces were activated using O_2 plasma (p_i=0.7 mbar, 100 W, 10 minutes). Activated tissue culture plastic surfaces were placed in an argon atmosphere of O_2 < 500 ppm, where monomer mixtures containing 1% w/v 2,2-dimethoxy-2-phenyl acetophenone were added.

Monomer solutions were prepared by mixing undiluted monomers at the desired ratio. Separately, a 10% w/v solution of photoinitiator 2,2-dimethoxy-2-phenyl acetophenone was prepared in isopropanol. The 10% photoinitiator solution was added in a 1:10 ratio to the monomer mixture, resulting in a final concentration of 1% w/v photoinitiator, in the polymerisation mixture.

The polymerisation mixture was degassed at 35°C via sonication, for 20 minutes, to reduce O_2 present in the polymerisation mixture and mild heating to reduce viscosity for even spreading on TCP surfaces.

Coated TCP surfaces were exposed to UV irradiation at 365 nm for 1 hour, before being washed three times in isopropanol to remove unreacted monomer from the surface.

Polymerised surfaces were incubated at 37°C in dH_20 for 48 hours to allow the leeching of potentially toxic components.

Sterilisation of surfaces was carried out by incubating surfaces in 70% IMS for 20 minutes at room temperature, followed by two washes with dH_20.

2.4 Microscopy

2.4.1 Operetta™

Immunostained and live samples were imaged using the Operetta™ high content image analysis system (Perkin Elmer). Live samples were maintained at 37°C & 5% CO_2 & images were acquired every 30 minutes. Image analysis was carried out using the Columbus™ software (Perkin Elmer).

2.4.2 IMSTAR

Array imaging was carried out using the IMSTAR microscope (IMSTAR SA), utilising automated stage movement, combined with an array grid map. 'Landmark' locations allowed for manual focussing points across the array. Image analysis was carried out with CellProfiler™ software (CellProfiler™), where descriptions for each analysis pipeline are explained in results chapters 3 & 5.

2.4.3 CellOPTIQ®

Assessment of hPSC-CM contraction, electrophysiology & calcium handling was carried out using the CellOPTIQ® (Clyde Biosciences).

To assess contraction hPSC-CMs were kept in RPMI-B27 (+ins) medium & transferred to the live cell chamber, 37°C & 5% CO_2, where cells were kept for 10 minutes before measurements began, to allow for climatisation.

A high-speed camera captured 100 images/second for 10 seconds of contracting hPSC-CMs. Image sets were compiled into single files using an ImageJ plugin & analysed using Contractility Tool (Clyde Biosciences). Data for contraction amplitude, interval, upstroke & relaxation were assessed.

To assess the electrophysiological properties of hPSC-CMs, FluroVolt™ Membrane Potential Kit (ThermoFisher – F10488) was prepared by mixing 5µL/mL part B with 0.5 µL/mL part A and then added to RPMI B27 (+ins). Cells were incubated in FluroVolt™ containing medium for 20 minutes at 37°C & 5% CO_2. Medium was exchanged for fresh RPMI B27 (+ins) and cells were placed into the CellOPTIQ® live chamber to acclimatise for 10 minutes before measurements were taken.

2.5 Statistical Analysis & Repeat Number

Throughout this thesis biological replicates are represented 'N' & technical replicates are represented 'n'.

The use of standard deviation (SD), standard error of the mean (SEM) and coefficient of variation (CoV) are indicated in their use throughout this thesis. With the exception of array data 8.0/8.2, data is presented with the standard deviation shown, the coefficient of variation is used where data is presented as heat maps, or when individual polymer data is presented.

Statistics has been performed in GraphPad Prism, where $P > 0.05$ is classified as not significant. P-values of < 0.05, < 0.01, < 0.001, < 0.0001, are represented as *, **, ***, ****, respectively.

When comparing 3 or more data sets, One-Way Anova analysis has been employed, or Multiple T-tests with/without corrections where appropriate. Direct comparisons between two sets of data have been made using two-tailed t tests.

3 Chapter 3 – Pluripotent Stem Cell Polymer Array Screening

3.1 Introduction

This chapter aimed to discover polymers or heteropolymers, starting from a commercially available library, capable of supporting the attachment, survival, expression of the pluripotency marker OCT4 of human pluripotent stem cells (hPSCs) and proliferation over a 24-72-hour culture.

The final system will consist of a synthetic surface, which will, A) be reproducible in large-scale production, B) eliminate the need for any protein surface coating steps, C) allow for long term culture in a serum-free, xeno-free, defined medium, D) retain the full repertoire of human pluripotent stem cell properties.

Three biological questions will be addressed in this chapter;

1.) Can hPSCs, in Essential 8 Medium, demonstrate attachment to homopolymer/co-polymer surfaces and survive 24 hours post-seeding, in the presence of Rho Associated Kinase Inhibitor (ROCKi) (Y-27632).

2.) Can hPSCs undergo successful mitosis, including temporary detachment, even division and reattachment to polymer surfaces, whilst maintaining viability & undergoing colony formation?

3.) Can a homopolymer, or co-polymer, surface support culture for 72 hours reproducibly, reaching a confluent state similar to Matrigel cultures?

To investigate the above questions 12,503 cell-surface interactions were tested, with 1,155 unique homopolymers and heteropolymers (including all ratio mixtures) printed at the micro-scale and UV polymerised to form five generations of polymer microarrays.

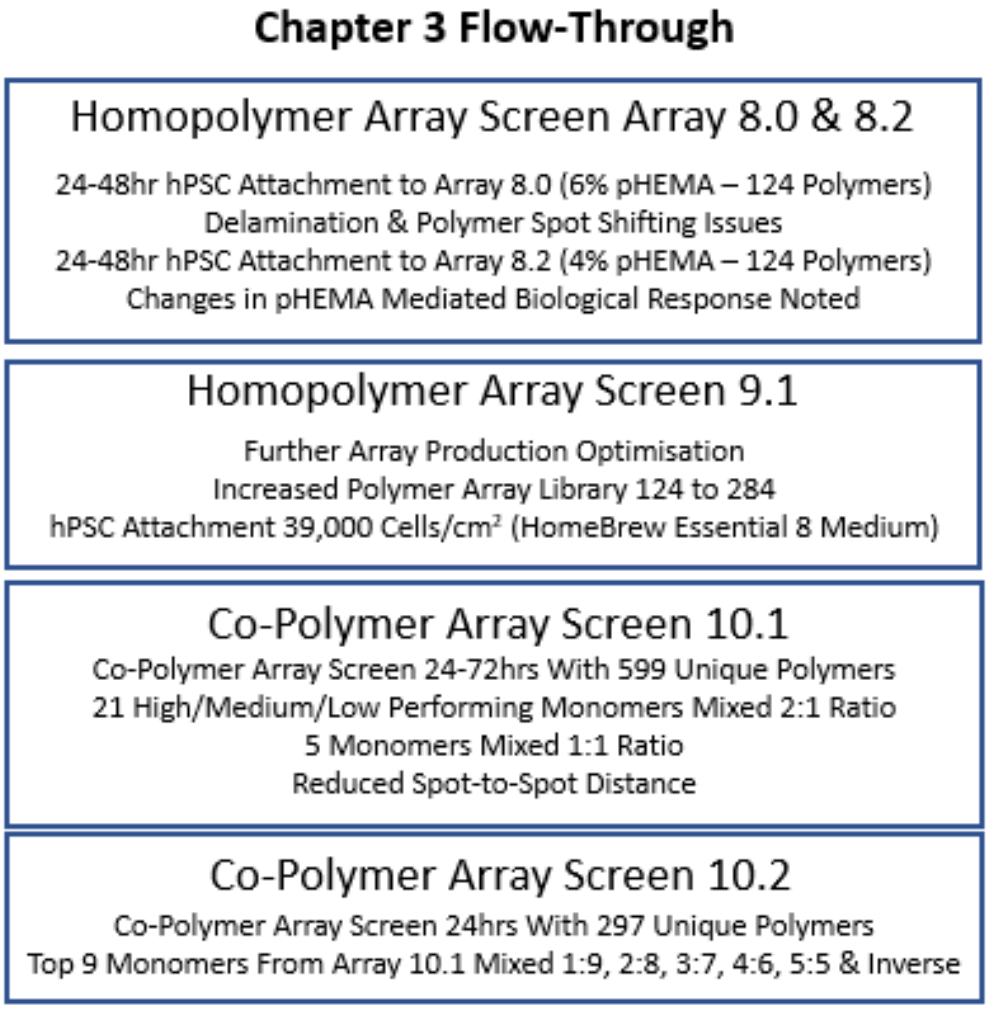

CellProfiler™ pipelines were created to analyse large image sets generated from array screens to identify if objects are not only positive for the DAPI nuclear stain, but also for the pluripotency marker OCT4.

Polymer surfaces with the potential to answer all three biological questions posed above; were taken forward to chapter 4, where scale-up and functional analysis was investigated.

3.2 Array fabrication

To discover novel biomaterials capable of supporting the culture of hESCs in Essential 8™ medium, polymer microarrays were fabricated. The process of polymer microarray fabrication started with the functionalisation of a glass microscope slide in order to maintain a stable pHEMA coating.

Oxygen plasma activation of a glass microscope slide followed by epoxy silanisation provided the chemical basis for the pHEMA layer to bind during a dip coating process (Figure 3.1 (A/B)).

pHEMA is resistant to cell attachment and protein binding, ensuring observed cell attachment is specific to hit materials. However, pHEMA also acts as a matrix allowing for physical integration and entanglement of printed monomer spots, improving array stability (Hook et al., 2010). Addition of pHEMA was performed with a dip coating technique (Figure 3.1 (C)).

Monomers to be printed onto pHEMA coated slides were prepared in 384-well polypropylene plates, where the monomer (or monomer mixture) was mixed at 50/50 v/v ratio with N,N-dimethylformamide (DMF) and 1%, 2,2-dimethoxy-2-phenylacetophenone photoinitiator (Figure 3.1 (D)).

DMF was chosen for array fabrication due to its aprotic nature, high boiling point and its low volatility. These properties allowed DMF to act as a solvent for a

wide range of materials, which was essential when using a diverse acrylate, methacrylate, diacrylate, triacrylate, acrylamide monomer library.

The low volatility of DMF was required to minimise evaporation during the extended printing process, this also allowed for overnight storage when sealed with parafilm.

Two types of printing method are typically used to generate polymer microarrays; contact printing & ink-jet printing. These printing techniques are universally used due to their ability to deposit thousands of materials in a time-efficient manner, and their flexibility when altering array layout or composition (Hook et al., 2010).

Contact printing involves physically dipping a metallic or ceramic pin directly into the monomer solution and transferring monomer to the array surface. Pins used in contact printing can contain a small groove which draws up monomer solution through capillary forces, allowing for; multiple, reproducible and controlled spot deposition from a single dip into the monomer solution (Hook et al., 2010).

Ink-jet printing is an alternative to contact printing that avoids contact with the surface and allows for greater control over deposition, however it can be prone to blockages and have difficulty with solutions of varying viscosities; for example, acrylates and triacrylates. For these reasons contact printing was chosen.

Printed monomers were exposed to a 10 second UV polymerisation step, after every individual monomer deposition (Figure 3.1 (E)). Printed arrays were

stored in a vacuum oven for 7-days to ensure residual DMF and monomer were removed.

Whilst the array creation process is largely the same as work performed by Celiz et al., 2015, an increase in pHEMA concentration from 4% to 6%, was carried out before the start of this project, this change was intended to improve the stability of printed polymer microarrays.

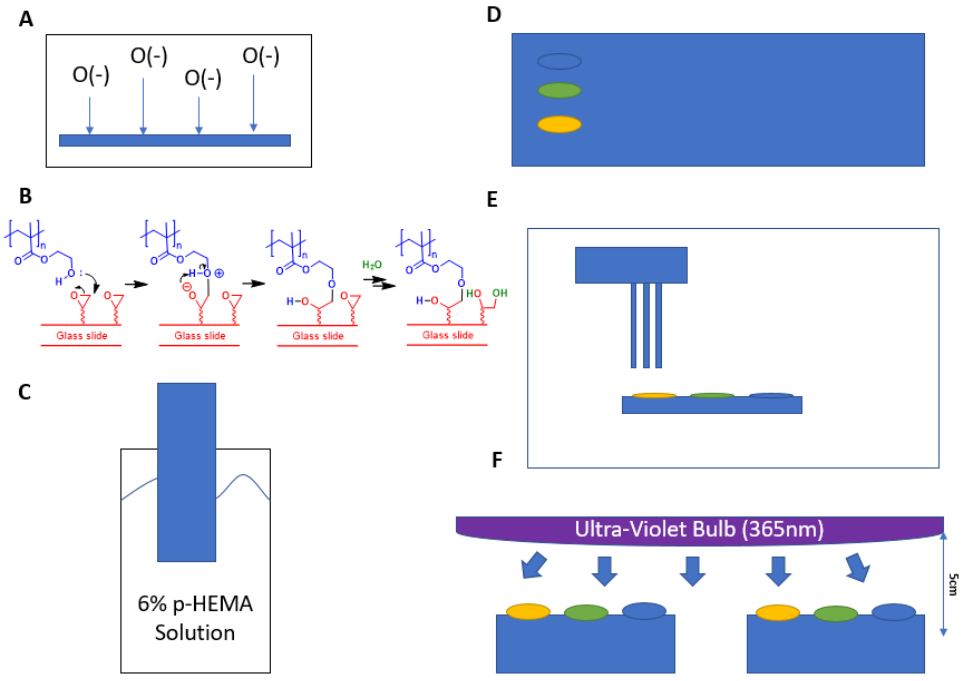

Figure 3.1 Assembly of Polymer Microarrays.

(A) Glass slides are exposed to a 100 W oxygen plasma at 0.3 mBAR for 1 minute. (B) Glass slides activated by oxygen plasma are coated with a 2% epoxy silane in dry toluene for 3hrs (Sigma Aldrich). (C) A 4% or 6% pHEMA coating is applied through dip coating. (D) Monomer solutions prepared in polypropylene plates, 50/50 v/v Monomer: N,N Dimethylformamide (DMF) (Sigma Aldrich), with 1% ,2-dimethoxy-2-phenylacetophenone photoinitiator. (E) Monomers applied to the array through pin contact printer (Biodot). (F) UV polymerisation (Blak-Ray XX-15L UV Bench Lamp, 230 V, 50 Hz, 15-Watt, 365 nm).

3.3 Results

3.3.1 Characterisation of ReBl-PAT Human Induced Pluripotent Stem Cells (hiPSCs)

To ensure the pluripotency of cells used in this chapter, the cells were characterised in their; expression of pluripotency markers, ability to maintain stable long-term growth (< 5 passages), whilst maintaining a stable (46) XY karyotype.

After at least five passages in culture, the expression of pluripotency markers; OCT4, SOX2, NANOG, SSEA4 and TRA-1-81 were determined by immunofluorescence, representative images – Figure 3.2 (A).

Imaging was carried out on the Operetta High Content Imaging System (PerkinElmer) and percentage positive expression calculated using Columbus software, as detailed in the methods section. This data is presented in Figure 3.2 (B).

ReBl-PAT hiPSCs were cultured for 72 hours per passage, reaching 70-90% confluence before TrypLE dissociation, representative image in Figure 3.2 (C).

ReBl-PAT hiPSCs were proven to have a stable karyotype after five passages, with an expected 46 (XY) spread confirmed across 30 metaphases by Dr. Nigel Smith. No spreads demonstrated deletions of irregularities, provided karyogram shown Figure 3.2 (D).

ReBl-PAT hiPSCs cultured for 8 passages demonstrated a stable growth pattern, with a doubling time of 21.5 hours +/- 1.9 hours, Figure 3.2 (E).

These results demonstrate the ReBl-PAT line used throughout this chapter has the expected pluripotent stem cell characteristics, with a stable human karyotype.

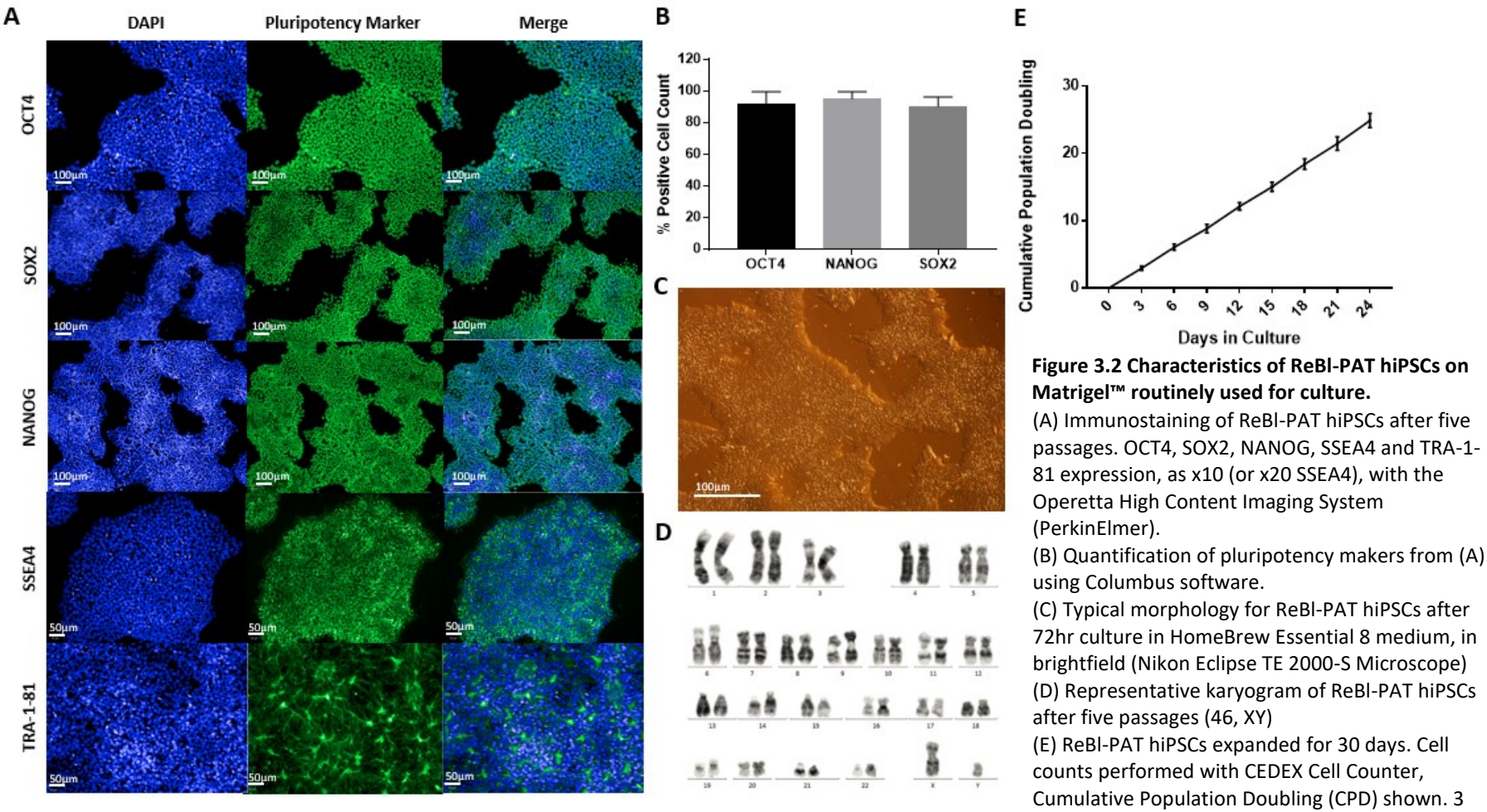

Figure 3.2 Characteristics of ReBl-PAT hiPSCs on Matrigel™ routinely used for culture.

(A) Immunostaining of ReBl-PAT hiPSCs after five passages. OCT4, SOX2, NANOG, SSEA4 and TRA-1-81 expression, as x10 (or x20 SSEA4), with the Operetta High Content Imaging System (PerkinElmer).

(B) Quantification of pluripotency makers from (A) using Columbus software.

(C) Typical morphology for ReBl-PAT hiPSCs after 72hr culture in HomeBrew Essential 8 medium, in brightfield (Nikon Eclipse TE 2000-S Microscope)

(D) Representative karyogram of ReBl-PAT hiPSCs after five passages (46, XY)

(E) ReBl-PAT hiPSCs expanded for 30 days. Cell counts performed with CEDEX Cell Counter, Cumulative Population Doubling (CPD) shown. 3 repeats shown, except day 27/30 where repeats = 1. Scale bars as shown.

3.3.2 Polymer Microarray Workflow-Through

With the ReBl-PAT line confirmed to be suitable for this work, a general flow-through of experimentation was laid out in Figure 3.3.

Polymer microarrays were sterilised by UV irradiation for 15 minutes per side, before a pre-incubation in the Essential 8™ medium. This step allowed for medium components to coat the surface, which may potentially act as an intermediary between the polymer surface and cell surface receptors (Figure 3.3 (A/B)).

Generation 8.0 & 8.2 homopolymer arrays were seeded with a cell density comparable to that used for tissue culture plastic (TCP) surfaces coated with Matrigel™, 25,000 cells/cm^2.

The expanded homopolymer arrays 9.0, 9.1, and the following co-polymer arrays were seeded with an increased density of 39,000 cells/cm^2. The inclusion of ROCKi (Y-27632) for the first 24 hours of culture was essential for cell survival (Figure 3.3(C)).

Arrays were cultured for either; 24 hours, 48 hours or 72 hours, and fixed in 4% paraformaldehyde. OCT4 and DAPI staining were performed. Images were collected with the High Content IMSTAR Microscope, this system allowed for programmed stage movement and automatic image acquisition (Figure 3.3(D)).

The open source software, CellProfiler™, was used to analyse the large number of images produced (Figure 3.3(E)).

This experimental flow-through allowed the for the culture of polymer microarrays and facilitated data collection to draw conclusions on the main aims of this chapter.

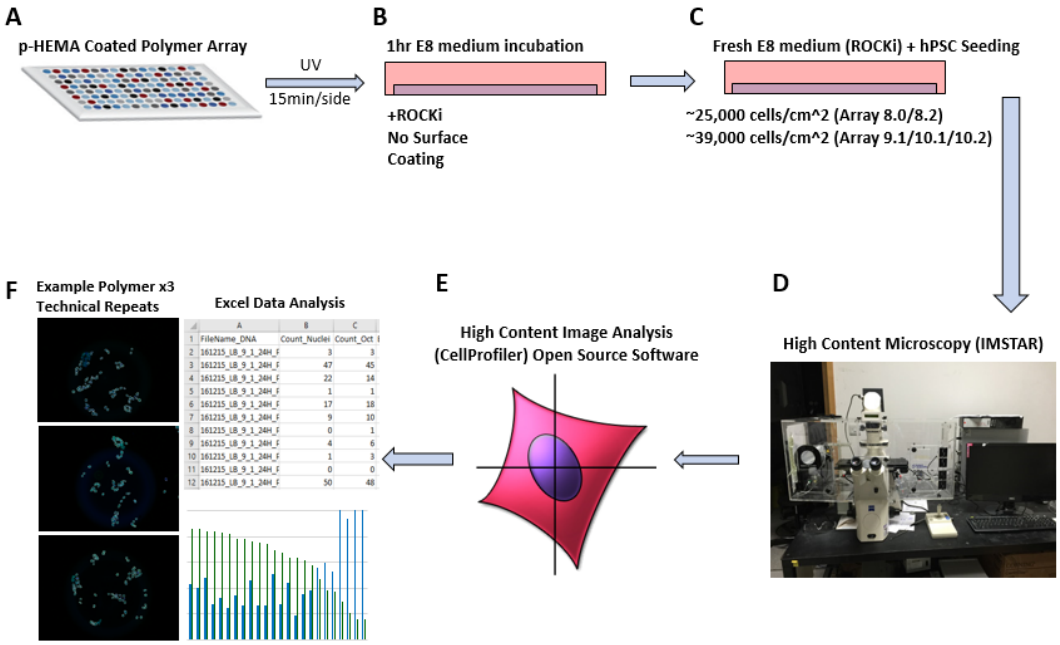

Figure 3.3 Workflow through of hPSC Array Screening.

(A) Poly-HEMA (pHEMA) coated polymer microarrays were sterilised with UV irradiation. (B) Incubation with medium 1hr prior to use, allowed for the attachment of proteins to the surface. (C) An exchange with fresh medium containing the pro-survival small molecule Rho-Associated Kinase Inhibitor (ROCKi) (Y-27632). (D) automated image acquisition with the IMSTAR microscope (IMSTAR SA). (E) Image processing with open source software (CellProfiler™). (F) Data analysis was performed in Microsoft Excel, identifying object counts and area.

3.3.3 Optimisation of CellProfiler™ Pipeline for Polymer Microarray Analysis

To ensure readouts generated were useful, the CellProfiler™ analysis pipeline had to be optimised. Initial attempts at adapting a basic cell count pipeline proved partially successful for identifying visibly spaced out nuclei, grown on a Matrigel™ surface, in Figure 3.4 (A)(I)/(II) 32 objects are accepted as positive.

This pipeline erroneously identified segments of auto-fluorescent polymer as positive objects. The basic parameters involving changes to the size filter and

automatic detection to be based on object shape, improved the number of accepted objects to 135, with a high fidelity to real nuclei shown in Figure 3.4 (B)(I)/(II).

This pipeline also eliminated the issue of identifying auto fluorescent polymers as positive objects.

A close correlation between the number of positive objects detected in the DAPI and OCT4 channel across several images is shown in Figure 3.4 (B)(III). This pipeline was unable to identify the number of nuclei in images generated from array 8.0 that became clustered after 24 hours culture.

To overcome the cell detection problem during colony formation & cell clustering, to provide a more reliable readout for array 8.0, the total image intensity of either DAPI or the OCT4 stain was quantified, Figure 3.4 (C)(II).

With the pipeline optimised, data could be interpreted in a useful manner, where best performing polymers could be separated from poorly performing polymers.

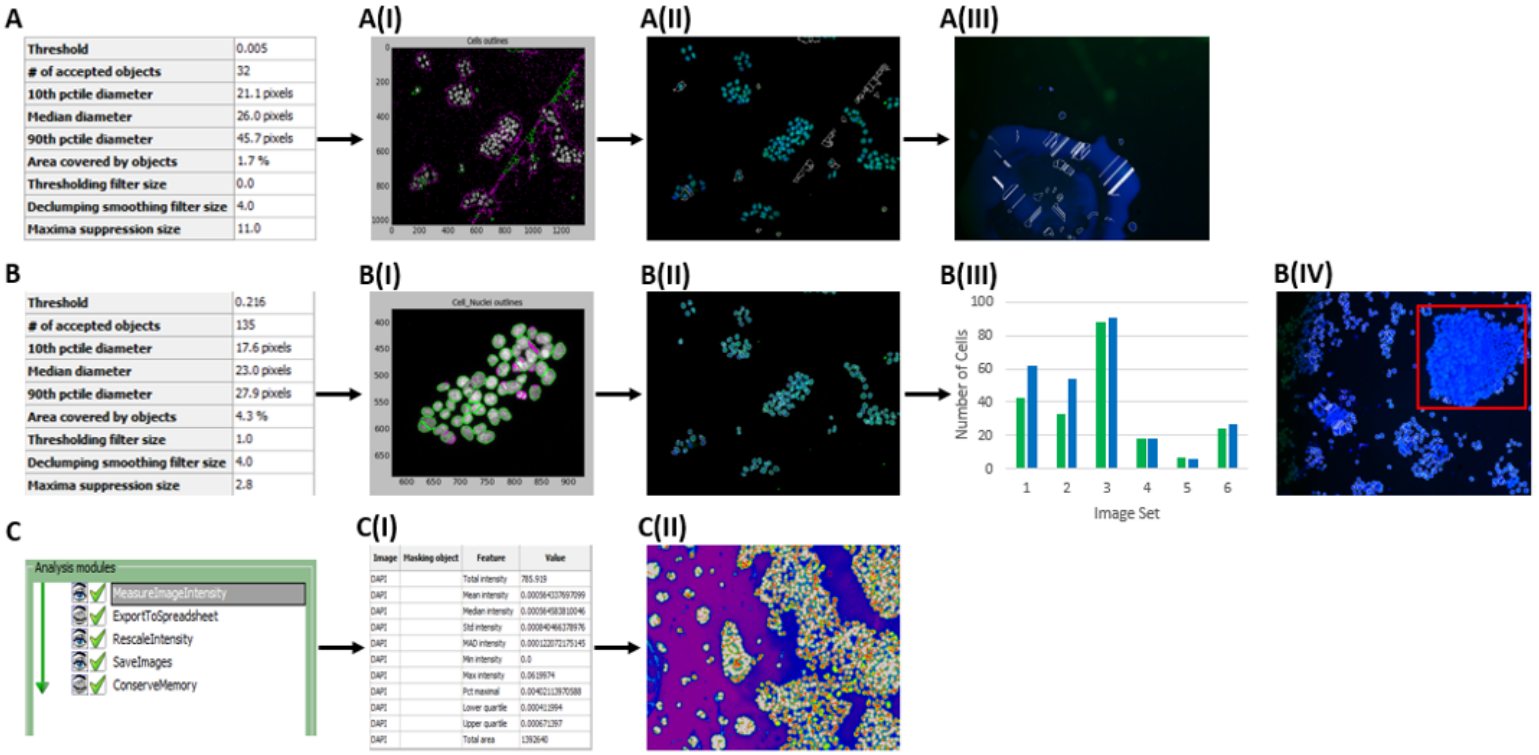

Figure 3.4 Optimisation of CellProfiler™ pipelines for polymer microarray analysis.

(A) Original cell count pipeline tested ReBl-PAT hiPSCs cultured for 24hrs, on a Matrigel™ surface. (A) Results summary table. (A)(I) Cell identification, green 'accepted', purple 'rejected'. (A)(II) Cell identification, white boarder 'positive' object. (A)(III) Polymer background being defined as 'positive' objects. (B) Optimised basic cell count pipeline tested. (B)(I) Cell identification, green 'accepted' object, purple 'rejected'. (B)(II) Cell identification, white 'positive' object. (B)(III) Pipeline tested across 6 images sets, OCT4 (green) & DAPI (blue) compared. (B)(IV) Optimised pipeline attempting to identify dense cell areas, highlighted in white 'positive' objects. (C) Image intensity pipeline to identify best performing polymers. (C)(I) Example of output results table. (C)(II) Image coloured based on fluorescent intensity.

3.3.4 Attachment of ReBl-PAT hiPSCs to polymer microarray '8.0' (6% pHEMA) & Array '8.2' (4% pHEMA)

Initial experiments used microarrays 8.0 & 8.2, which were created on a 6% and 4% pHEMA coating respectively. 4% pHEMA arrays were developed due to instability of 6% pHEMA, 8.0 arrays, this will be discussed in more depth within this chapter.

Both arrays contained 124 unique materials, all materials screened were homopolymers, except for five hand-selected heteropolymers based on previous interest, in array 8.0. The ability of polymers to support attachment at 24 hours, and survival/proliferation to 48 hours was assessed.

3.3.5 Array 8.0 (6% pHEMA)

To determine if any polymer(s) in the selected polymer library have the functionality of attaching human induced pluripotent stem cells for the first 24 hours of culture, and to support survival/proliferation to 48 hours, polymer microarrays 8.0 were seeded as described above.

The intensity pipeline developed in Figure 3.4 was used to successfully identify most attachment hits with accuracy. A limited number of spots were exceptions, such as N-[3-(Dimethylamino)propyl]methacrylamide (DMPMAm) in Figure 3.5 (A).

DMPMAm demonstrated cellular attachment and colony formation at 24 hours, however some of the fluorescence intensity is artefact, likely due to DAPI absorption and retention in DMPMAm/6% pHEMA hydrogel.

Polymer spots demonstrating autofluorescence were manually removed from the top performers list.

Array 8.0 revealed homopolymers that can support 24 hours attachment of hiPSCs, these are presented in Figure 3.5. The top 10 performing homopolymers, excluding DMPMAm, on average had a fluorescent signal of 21,246 +/- 21%, compared to the polymer array average of 11,966 +/- 60%.

Homopolymers that did not make the top 10 performing hits were still presenting attachment at 24 hours. 31/124 polymers spots were permissive to hPSC attachment and 24-hour survival.

Trimethylolpropane ethoxylate triacrylate (TMPETA) is one such homopolymer, where colony density observed at 24 hours qualitatively appeared less dense than the top 10 performing polymer spots, image fluorescent intensity was 11,881 +/- 23% vs 21,246 +/- 21% respectively.

Attachment on TMPETA by 24 hours culture continued to survival after the ROCKi was removed, up to 48 hours culture where average image DAPI fluorescent intensity was 9,211 +/- 28% – Figure 3.5 (B).

Names, structures and representative images of array 8.0 cell attachment hits, from the high-end, middle, and low-end of the top hits, are shown in Figure 3.6.

13/31 cell attachment hits are diacrylates. Only one chemistry containing fluorine was present in the attachment hits 12,524 +/- 18% relative fluorescent units, Hexafluoropent-1,5-diyl diacrylate (HFPDA).

These results demonstrated 31 polymer spots on array 8.0 can support hiPSC attachment for 24 hours culture, in commercial Essential 8™ medium, supplemented with ROCKi, at a seeding density of 25,000 cells/cm^2.

Further analysis as to which polymers can support hPSC survival beyond 24 hours, after the removal of ROCKi is required to identify polymeric biomaterials with the potential to address the questions proposed in this chapter.

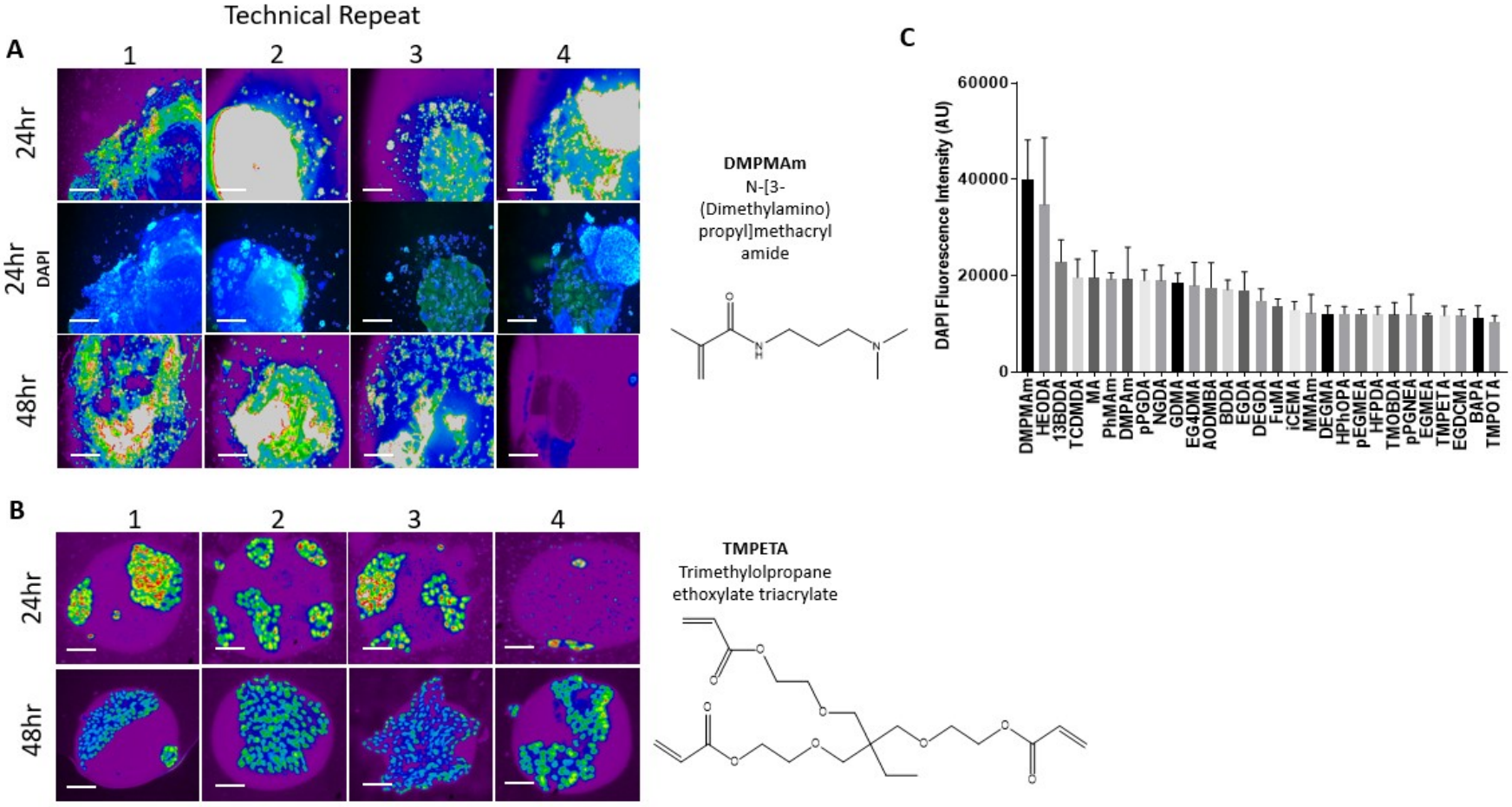

Figure 3.5 Analysis of '8.0' 6% pHEMA Polymer Microarrays Cultured for 24 Hours & 48 Hours with ReBl-PAT hiPSCs in Commercial Essential 8™ Medium.

Images assessed using CellProfiler™ fluorescence intensity pipeline. (A) Images of highest fluorescence intensity hit DMPMAm at 24-hour & 48-hour culture, with chemical structure shown. DAPI image included for 24-hour culture on DMPMAm shown for clarity. (B) Images of moderate fluorescent intensity, high cell attachment hit, TMPETA at 24 hours & 48 hours culture, with chemical structure shown. (C) Top monomer hits exceeding 15,000 (RU) fluorescent intensity, at 24 hrs culture, with standard error shown. Scale Bars = 100 µm

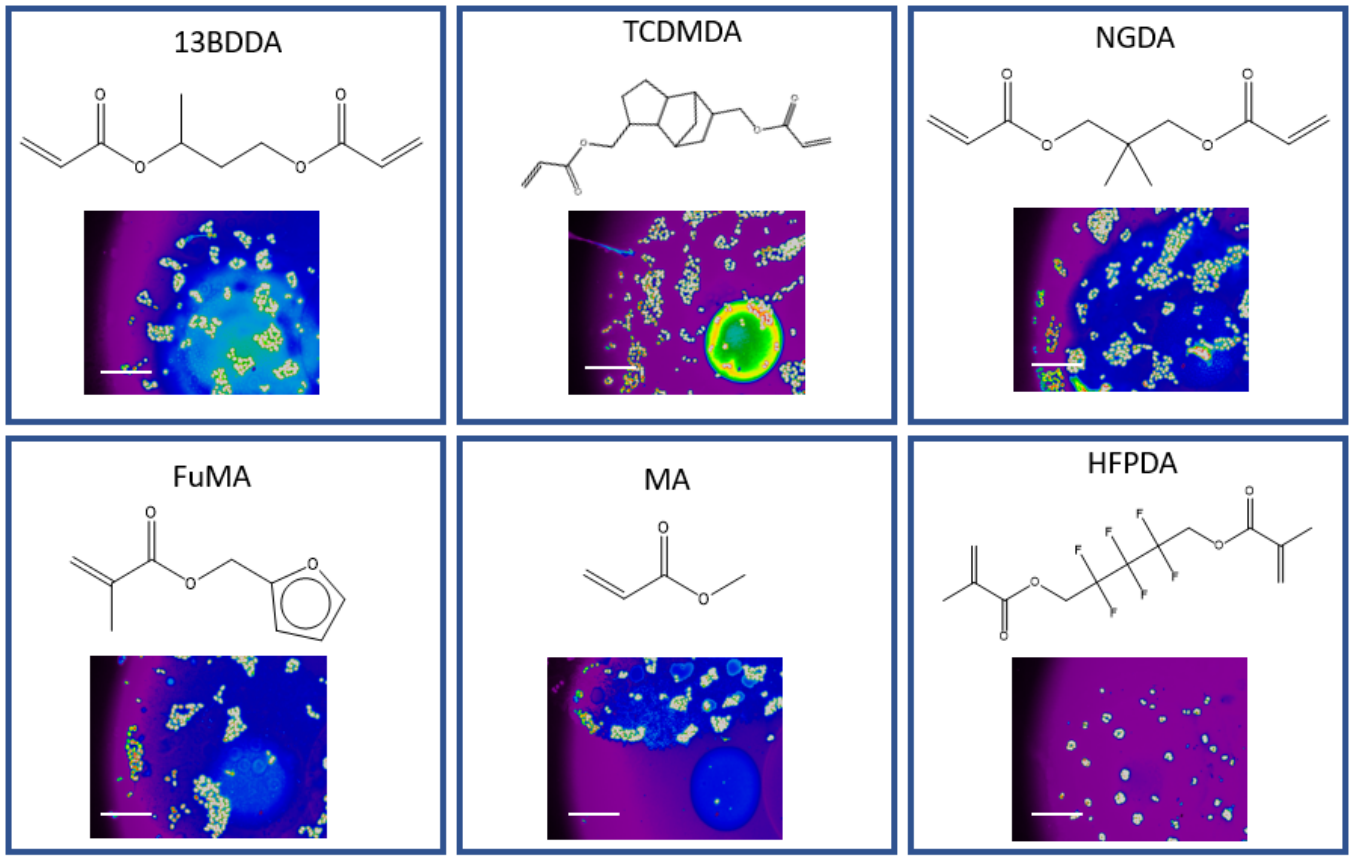

Figure 3.6 Selected Images of '8.0' 6% pHEMA Polymer Microarray Top Hits Cultured for 24 Hour with ReBl-PAT hiPSCs in Commercial Essential 8™ Medium.

Images assessed using CellProfiler™ fluorescence intensity pipeline. Selected hits taken from top/middle/low performing end of best performing polymer spots, that supported cell attachment. Chemical diversity presented. Full polymer identities can be found in table X. Scale Bars = 100 µm

3.3.6 Array 8.0 (6% pHEMA) at 48 hours Culture

This section sought to determine what proportion of the 31 polymer spots previously identified support 24 hours survival, could permit the continued survival of hiPSCs and proliferation, post-ROCKi removal, to 48 hours in culture.

To do this, 8.0 arrays created in the same batch were continued in culture for 48 hours before fixation. Results were analysed with the intensity Cellprofiler™ pipeline.

DMPMAm and N-[3-(Dimethylamino)propyl]acrylamide (DMPAm) were the top performing hits, however both present issues with suspected DAPI absorption, with fluorescence not localised to clear cell nuclei.

The top 10 performing hits, excluding DMPMAm & DMPAm, supported 16,593 +/- 14% DAPI fluorescent intensity, markedly less than the top 10 performing hits at 24-hour culture, 21,246 +/- 21%, representing a statistical decrease, P=0.01 (*), in performance by the 48-hour time period. Data for array 8.0 24-hour & 48-hour top hits for DAPI fluorescent intensity are shown in Figure 3.7 (A) & (C) respectively.

Images of a sub-selection of top hits are included in Figure 3.8, including DMPMAm & DMPAm, where visual clarity of cell nuclei are lacking. Tricyclodecane-dimethanol diacrylate (TCDMDA), Neopentyl glycol diacrylate (NGDA), and Glycerol dimethacrylate (GDMA), 19,337 +/- 9.9%, 18,888 +/- 37.5% & 18,337 +/- 32.6% average fluorescent units, are the following three best performers after DMPMAm & DMPAm.

Visually, colonies for TCDMDA do not appear to be directly attached to the polymer spot in Figure 3.8, however it should be noted that pHEMA background alone did not support cell attachment, as expected. GDMA presents the clearest visual correlation between cell colony positioning and the polymer spot position.

Together these results reveal 31/124 of polymers are capable of supporting attachment at 24 hours culture. 10 of these polymers are capable of continued survival and proliferation to 48 hours, maintaining ≥10,000 fluorescent units.

6 of the top performing hits were diacrylates, where two non-diacrylate structures DMPMAm & DMPAm are questionable in their ability to fulfil the aim of this section.

Results presented in this section are preliminary. Issues with array stability raise questions of reliability of data produced on array 8.0 and are discussed in the following section.

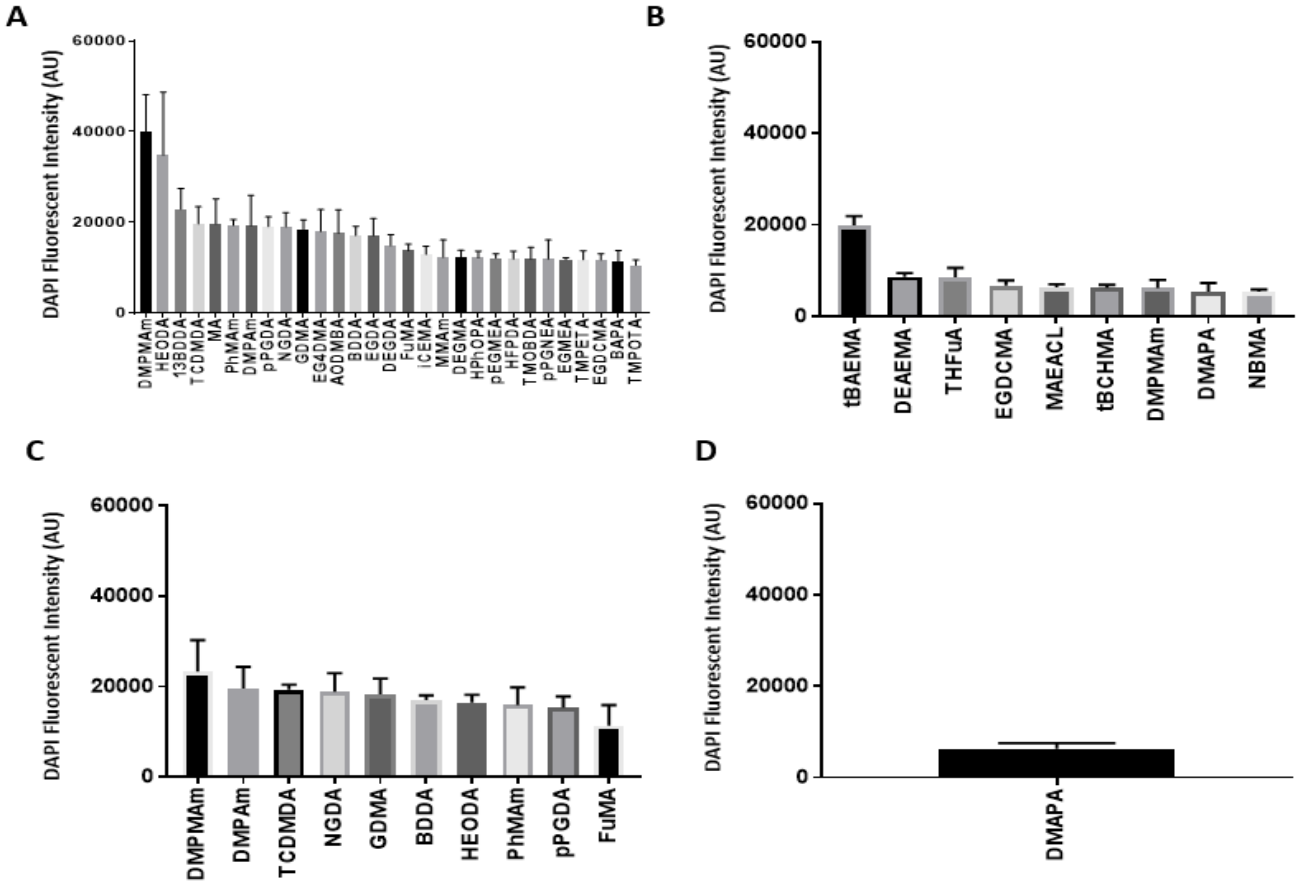

Figure 3.7 Comparison of '8.0' 6% pHEMA vs 4% pHEMA Polymer Microarrays, after 24 Hours or 48 Hours of ReBl-PAT hiPSC Culture in Commercial Essential 8™ Medium.

Images assessed using CellProfiler™ fluorescence intensity pipeline. (A) Top hits for DAPI fluorescent intensity on 6% pHEMA array '8.0' at 24 hours culture. (B) Top hits for DAPI fluorescent intensity on 4% pHEMA array '8.2' 24 hours culture. (C) Top hits for DAPI fluorescent intensity on 6% pHEMA array '8.0' 48 hours culture. (D) Top hits for DAPI fluorescent intensity on 4% pHEMA array '8.2' 48 hours culture. Arrays seeded at 26,000 cells/cm^2. All error bars displayed are standard error of the mean.

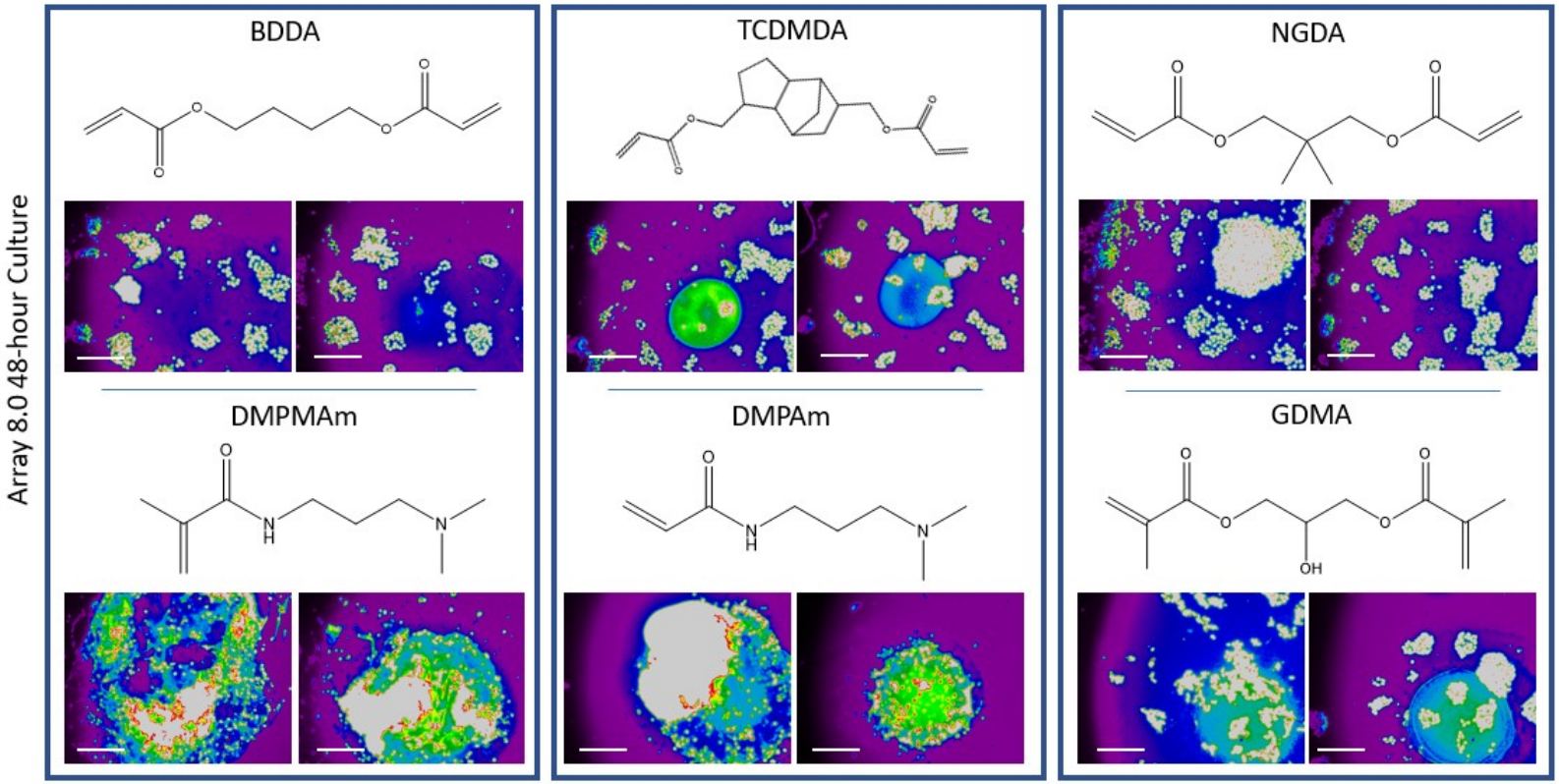

Figure 3.8 Selected Images of '8.0' 6% pHEMA Polymer Microarray Top Hits Cultured for 48 Hours with ReBl-PAT hiPSCs in Commercial Essential 8™ Medium.

Images assessed using CellProfiler™ fluorescence intensity pipeline. Selected hits taken from top 10 performing polymer spots. Full polymer identities can be found in Figure 8.1 & appendix section. Scale Bars = 100 µm

3.3.7 Fixing Array Fabrication Issues Array 8.0 (6% pHEMA) - Array 8.2 (4% pHEMA)

Data collected using array 8.0 (6% pHEMA) revealed a 31 polymer surfaces capable of supporting hiPSC culture at 24 hours with ROCKi. 10 polymer surfaces were shown to support up to 48 hours culture, ≥10,000 fluorescent units.

The 6% pHEMA layer introduced structural issues with the array fabrication, which compromised the integrity of the data shown so far. This section aims to highlight the faults associated with array 8.0, and how a reduction to 4% for the pHEMA coating alleviated the observed issues.

Arrays created with a 6% pHEMA coating demonstrated issues with delamination of both the pHEMA background itself and polymer spots. Control over spot size and reproducibility were lost when printing on 6% pHEMA coated arrays,

Time of Flight Secondary Ion Mass Spectrometry (ToF-SIMS) detected irregular spot sizes and spiking in Figure 3.9 (A) & (I), which allowed for potential cross-contamination between neighbouring polymer spots.

The ToF-SIMS analysis confirmed spots were printed in their expected array layout, however after exposure to the Essential 8™ medium and cell culture incubator conditions (37^{o}C & 5% CO^{2}) for 24 hours – 48 hours, polymer spots demonstrated a level of ‘drift’, this displaced them from their intended position in the array.

Drifting of polymer spots introduced problems with automated image acquisition on the IMSTAR, some polymer spots were only partially imaged, others have the potential to have been missed.

Issues with array fabrication were compounded with technical issues with the IMSTAR microscope itself, which would also shift between taking images, this is shown in Figure 3.9 (F), where the automated protocol to take an image of the DAPI staining, followed by the OCT4 staining resulted in images that didn't directly overlap. Separate brightfield image taken for clarity.

Movement back and forth, using the IMSTAR, between different but defined co-ordinates on the array also resulted in a shift from the original intended position, which may have contributed to the polymer spot drift problem on 6% pHEMA.

Reverting array production back to the previously used 4% pHEMA layer improved aspects of the array production process. A brightfield comparison of spot size and distribution of 6% pHEMA vs 4% pHEMA shown in Figure 3.9 (B) and (C) respectively showed an improvement on uniformity and reduced polymer spot spreading.

The presence of pHEMA related ions at the surface, using ToF-SIMS, showing the 6% and 4% pHEMA arrays respectively are compared in Figure 3.9 (H) and (I).

Spiking was eliminated, and polymer spot spreading reduced with the 4% pHEMA coating, importantly the presence of pHEMA ions visible at the surface of printed polymer spots also decreases from 6% to 4% pHEMA.

Inversely, the presence of polymer ions increases with the reduction of pHEMA concentration, DMPMAm was compared in Figure 3.9 (J), showing this effect.

The polymer Poly(ethylene glycol) methyl ether acrylate (pEGMEA) was imaged individually in Figure 3.9 (D & E) on 6% pHEMA (D) and 4% pHEMA (E), to highlight the correction of the spiking issue.

With these issues fixed or improved, greater confidence could be taken in the data produced from the arrays 8.2 onwards. Work on array improvement and printing was carried out by Dr. Laurence Burroughs.

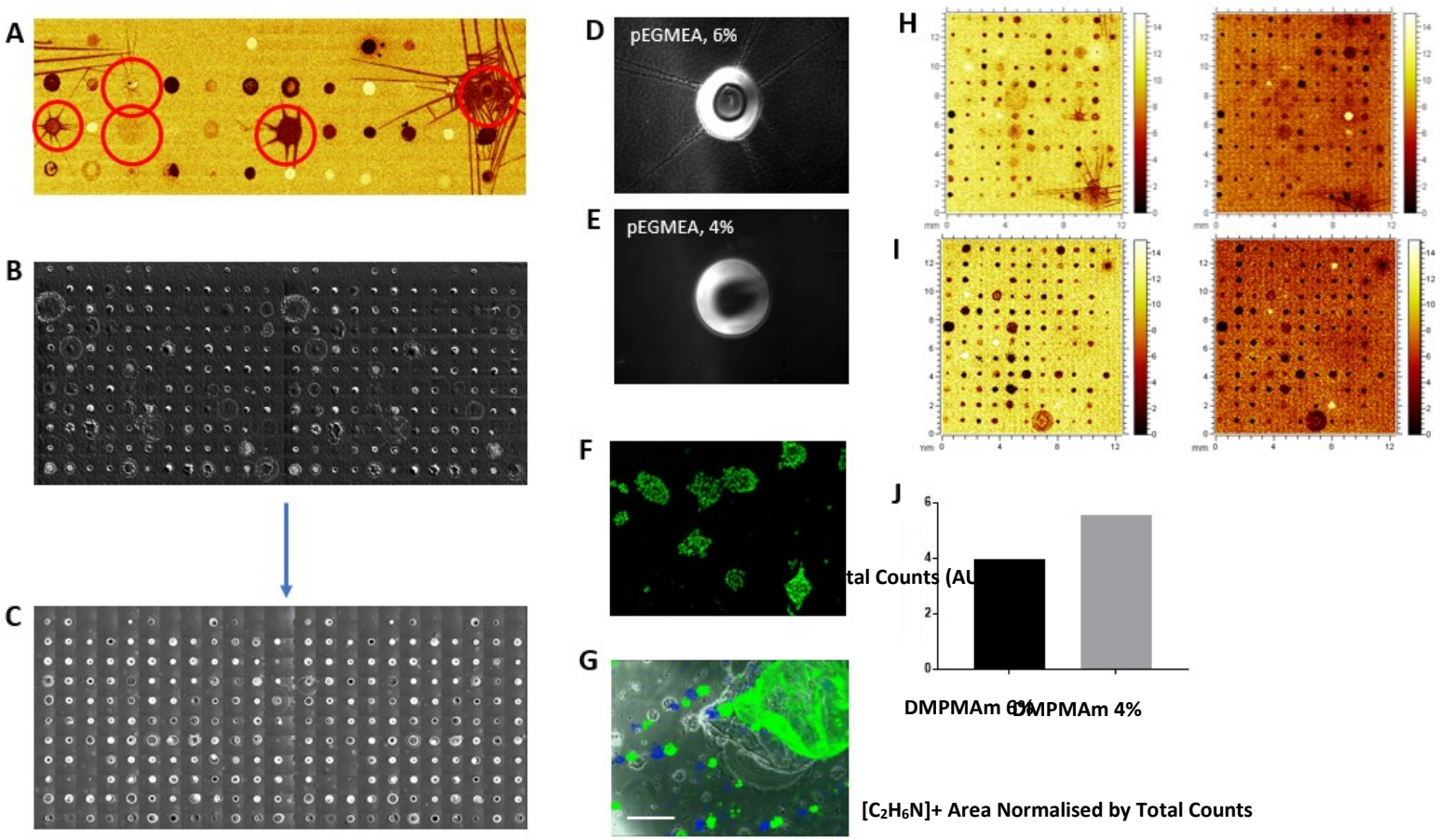

Figure 3.9 Optimisation of Array Production to Alleviate Issues of; Polymer Spot Spreading, Uneven Printing Size, pHEMA Delamination.

(A) Time of Flight Secondary Ion Mass Spectrometry (ToF-SIMS) analysis of a 6% pHEMA coated polymer microarray. (B) IMSTAR Brightfield microscopy of a 6% pHEMA coated polymer microarray. (C) IMSTAR Brightfield microscopy of a 4% pHEMA coated polymer microarray. (D-E) Brightfield imaging of pEGMEA printed on 4% & 6% pHEMA slides respectively. (F-G) IMSTAR microscopy of 6% pHEMA arrays cultured with hiPSCs for 24hrs, stained for DAPI & OCT4. (H) ToF-SIMS analysis 6% pHEMA coated polymer microarray, left: m/z = 45 $(C_2H_2O)^+$, right: m/z = 113 $[C_6H_9O_2]^+$ pHEMA ions. (I) ToF-SIMS analysis 4% pHEMA coated polymer microarray, left: m/z = 45 $(C_2H_2O)^+$, right: m/z = 113 $[C_6H_9O_2]^+$ pHEMA ions. (J) ToF-SIMS analysis 4% vs 6% pHEMA polymer microarrays for DMPMAm associated $[C_2H_6N]^+$ ion normalised. ToF-SIMS analysis by L. Burroughs.

3.3.8 Biological Response to Array 8.2 (4% pHEMA)

To test the biological response of the new array 8.2, the same seeding conditions and medium used for array 8.0 were replicated on new array 8.2 slides. Initially, array 8.2 was cultured for 24 hours before fixation.

The average DAPI fluorescent intensity data for the top 9 polymer spots was, 8,178 +/- 53%, shown in Figure 3.8. Top 9 polymer spots were selected due a limited number of polymers supporting cell attachment on array 8.2 (4% pHEMA).

Reductions in DAPI fluorescent intensity were observed when comparing the 6% pHEMA arrays (8.0) vs 4% pHEMA arrays (8.2). The average DAPI fluorescence intensity value across each array was 11,966 +/- 60%, vs 5489 +/- 70%, for 6% vs 4% pHEMA.

31/124 polymer spots on 6% pHEMA (8.0) supported cell attachment at 24 hours culture, only 9/124 polymer spots could support 24 hours cell survival on 4% pHEMA arrays (8.2).

At 48 hours culture, after the removal of ROCKi at 24 hours, array 8.2 (4% pHEMA) failed to support cell survival and colony formation, except for Dimethylamino-propyl acrylate (DMAPA), Figure 3.8 (B). With 6272 +/- 18.7% average DAPI fluorescence intensity, this value is lower than top performing polymer on the array 8.0 (6% pHEMA) at 48 hours, TCDMDA with a value of 19,337 +/- 9.9%. This is reflected in poor colony formation on DMAPA on 4% pHEMA (8.2).

Polymer spots on array 8.2 (4% pHEMA) are unable to support the high levels of attachment and colony formation needed, in a consistent manner, to be usable as a synthetic cell culture surface.

3.3.9 Array Expansion & Improvements

To generate a synthetic surface that meets the attachment, growth and reproducibility required for day-to-day cell culture, further improvements were made to array production, and the number of monomers tested increased from 124 to 281. 3 co-polymers were also included as positive controls for hiPSC-CM attachment, relevant for results chapter 3.

Improvements to array production and library expansion are shown in Figure 3.10 (A) Demonstrates how the increased number of monomers was accommodated, by printing two arrays staggered next to each other. This had the disadvantage of reducing the distance of each printed spot from each other, from 1500 µm in both X & Y axis, to 750 µm similarly.

To accommodate 284 spots, the number of technical repeats was reduced from 4 to 3. Delamination issues were reduced further through the introduction of a 50^{o}C 5-hour curing stage, to eliminate water from the epoxy silane – 4% pHEMA interface. Initial testing with the new array termed '9.0' had widespread fluorescence in the 488 nm channel, as shown in Figure 3.10 (C), this obscured detection of the OCT4 staining, and was found to be related to specific fluorescein monomers, which were removed to form the final '9.1' array.

Changes to the cell culture conditions were made in parallel to the introduction of array 9.1 (4% pHEMA). The cell seeding density was increased from 25,000 cells/cm^2 to 39,000 cells/cm^2 to increase the likelihood of finding polymers capable of cell attachment.

The culture medium was changed from commercially purchased Essential 8™ medium to HomeBrew Essential 8 medium, which was made in-house. HomeBrew Essential 8 medium contains the same ingredients as the commercially purchased medium, with the addition of 100 ng/mL heparin sodium salt from porcine intestinal mucosa, ~180 USP units/mg from Sigma Aldrich (H3149-10KU), this component improves the stability of growth factors (Chen et al., 2012), increasing the HomeBrew Essential 8 shelf-life.

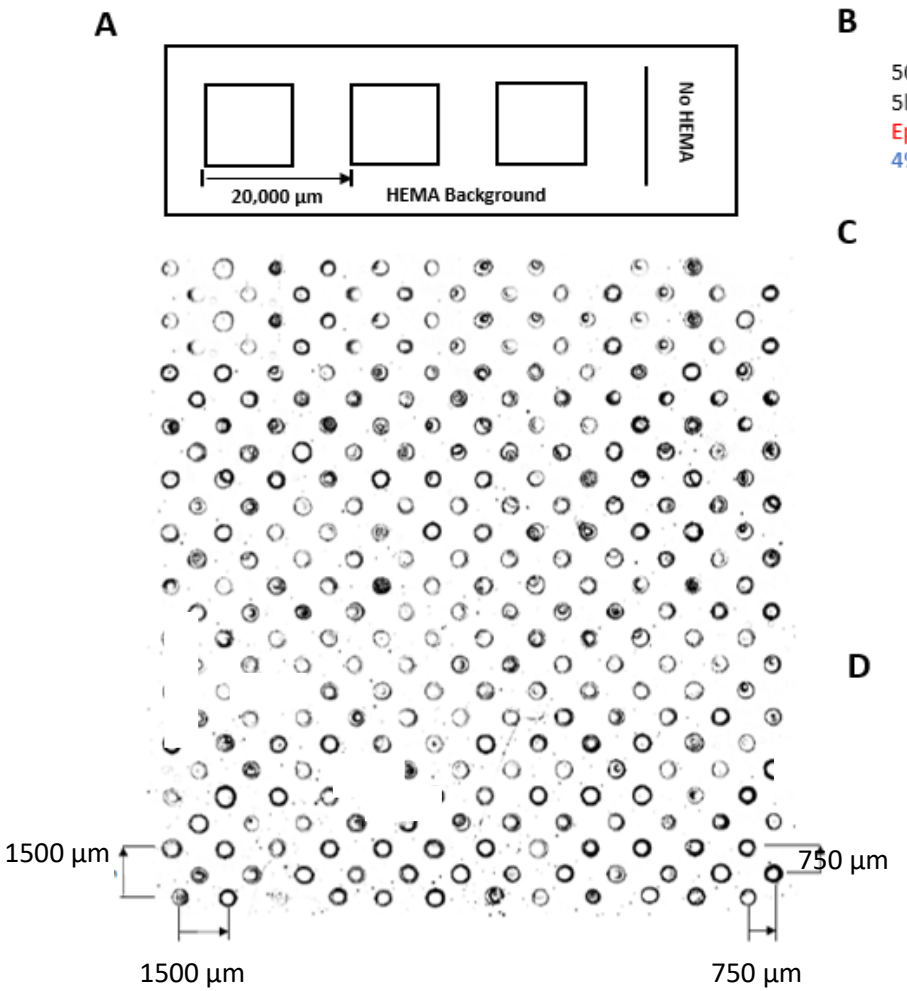

Figure 3.10 Changes made to Array '8.2' when Developing Array '9.0' & Array '9.1'.
(A) Accommodation of increased monomer selection, reduction from 4 technical repeats to 3 technical repeats. Introduction of staggered grids for ease of printing & analysis. (B) Introduction of 50°C heat curing step during array formation for increased structural stability. (C) Array '9.0' contained fluorescein monomers obscuring measurements at 488 nm. Array '9.1' fluorescein monomers were removed. (D) Summary of culture & array differences. Three co-polymers introduced from Patel et al., 2015, as positive controls for hiPSC-CM attachment.

3.3.10 Biological Response to Array 9.1 (4% pHEMA) at 24 hours

This section utilises a greater number of biological repeats (x3), to determine if the increased size of the polymer library and seeding density result in a higher number of polymer attachment hits at 24 hours culture, when compared to array 8.2.

The complete distribution of data for OCT4 positive objects and DAPI positive objects are shown in Figure 3.11 (A) & (B) respectively.

Due to the lower levels of cellular attachment, to array 9.1 (4% pHEMA) compared to the higher levels of attachment of 8.0 (6% pHEMA) arrays, a direct cell count pipeline for CellProfiler™ was favoured over the previously used fluorescent intensity pipeline. Accuracy of cell counts at 24 hours were deemed sufficient to produce reliable data.

This pipeline identified that on average polymers supported 13.4 +/- 78.5% DAPI positive cells & 8.1 +/- 93% OCT4 positive cells. An average of 73.9% of DAPI positive cells were also positive for OCT4 across array 9.1.

Positive object detection for the OCT4 channel was notably lower than that for the DAPI object detection. Some disparity may be due to a higher number of auto-fluorescent polymers in the DAPI channel, Figure 3.11 (C) & (D) show Tert-butylamino-ethyl methacrylate (tBAEMA) & N-[3-(Dimethylamino)propyl]methacrylamide (DMPMAm), these images confirmed the presence of non-polymer nuclei sized objects which are OCT4 negative after 24hr culture. Figure 3.11 (C)(I) and (D)(I) highlight a section of (C) and (D) for visual clarity.

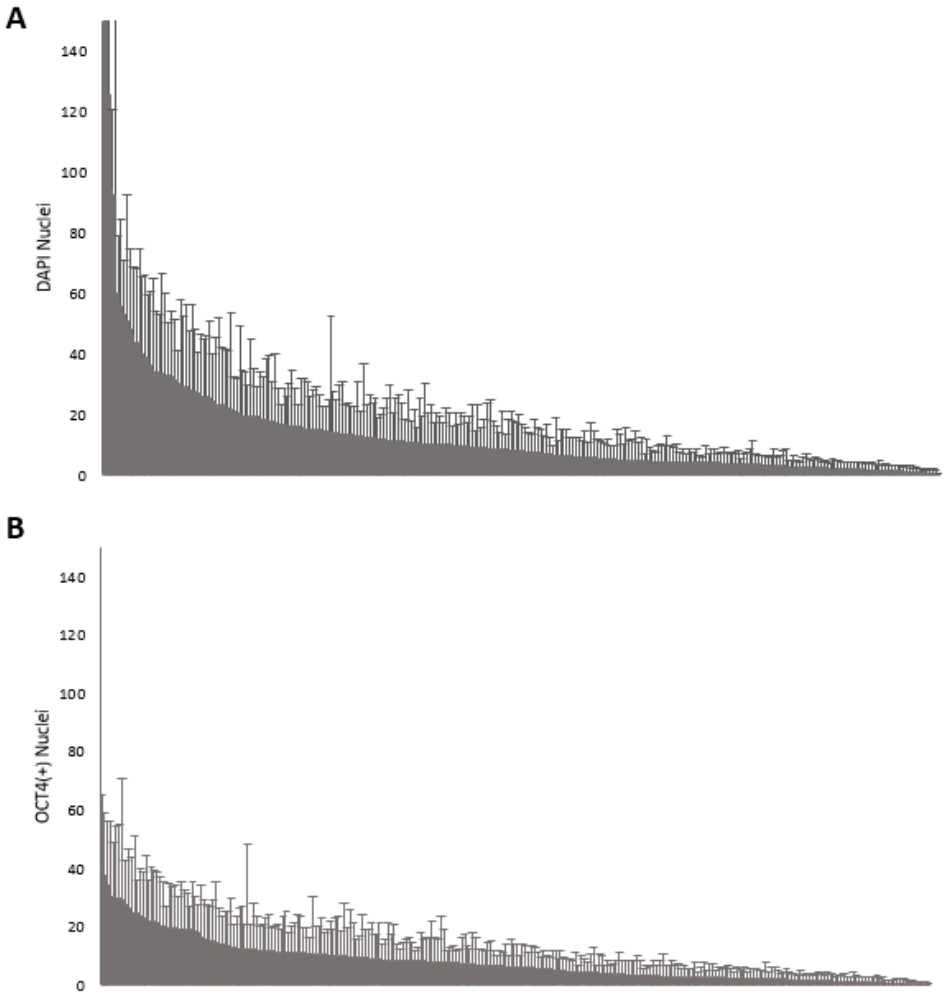

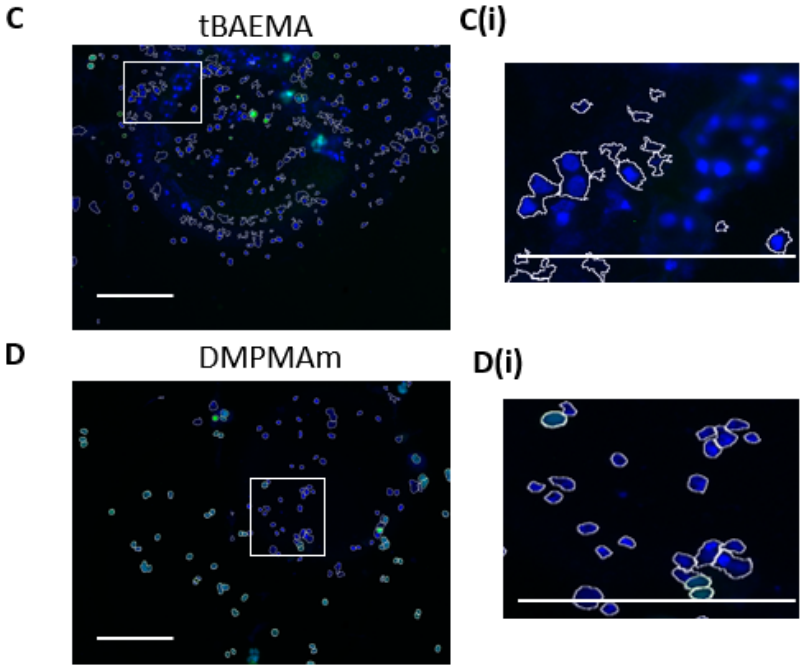

Figure 3.11 39,000 Cells/Cm^2 ReBl-PAT hiPSCs Seeded on Polymer Microarray '9.1' in HomeBrew Essential 8 Medium for 24 Hours.

Cells were stained for DAPI & OCT4, imaged using IMSTAR™ high content microscope, analysed with CellProfiler™ basic cell count pipeline. (A) Number of positive objects identified at the 461nm maximum emission wavelength, representing objects stained with DAPI. (B) Number of positive objects identified at the 488nm emission wavelength, representing OCT4 stained cell nuclei. (C),(C(i)),(D) & (D(i)) show examples of polymer spots on which objects are positive for the DAPI nuclear stain, with a majority of objects negative for the OCT4 pluripotency marker. Biological repeats = 3 Technical repeats = 9. Scale Bars = 100 µm

The top 10 performing polymer spots across three separate arrays, after 24 hours culture in HomeBrew Essential 8 medium, and the increased 39,000 cells/cm^2 seeding density, supported an average of 45.3 +/- 36% DAPI nuclei & 32 +/- 13.8% OCT4 nuclei, meaning polymer spots supported 70.6% OCT4 positive cells (Figure 3.12 (A)). Of the top 24 hits, 9 of the top hits were diacrylates, 5 contained cyclic ring structures, with considerable overlap with array 8.0 (6% pHEMA). Partial overlap was seen with the previous 8.2 (4% pHEMA) array, namely Tetrahydrofurfuryl acrylate (THFuA) and Norbornyl methacrylate (NBMA).

A comparison the % of DAPI objects positive for OCT4 staining on each polymer spot demonstrates that 22/24 top hits supported >70% OCT4 positive cells, with ethylene {glycol} diacrylate (EGDA) & zirconium bromonorbornanelactone carboxylate triacrylate (ZrBNCTA) as outliers, supporting 32% & 69.6% respectively (Figure 3.12 (B)). The variation in OCT4 positivity for DAPI positive objects is highlighted in Figure 3.12 (C) where two biological repeats are compared side by side, the first repeat demonstrated a lack of OCT4 expression after 24 hours culture.

Conversely, the structurally similar neopentyl glycol diacrylate (NGDA), structures shown in Figure 3.12 (E), was the best performer at maintaining OCT4 expression with 94% +/ -5.8%, however NGDA supported lesser attachment at the same time point than EGDA, 18 +/- 94% vs 92 +/- 83% respectively.

Top performing attachment polymer Tetrahydrofurfuryl acrylate (THFuA) which supported 48 +/- 50% DAPI positive cells with 86% +/- 6% of which being OCT4 positive, after 24 hours culture, is compared with the low attachment performing

polymer, Butyl Acrylate (BA), which supported 11 +/- 137% DAPI positive cells with 43% +/- 5% of which being OCT4 positive, in Figure 3.12 (C).

These results demonstrate a wide range of polymers can support cell attachment to the 24-hour time point, with ROCKi, when the monomer library size is increased, and cell seeding density heightened. To fulfil the aims of this chapter, polymer surfaces will have to continue to support hPSC survival and growth after the removal of ROCKi.

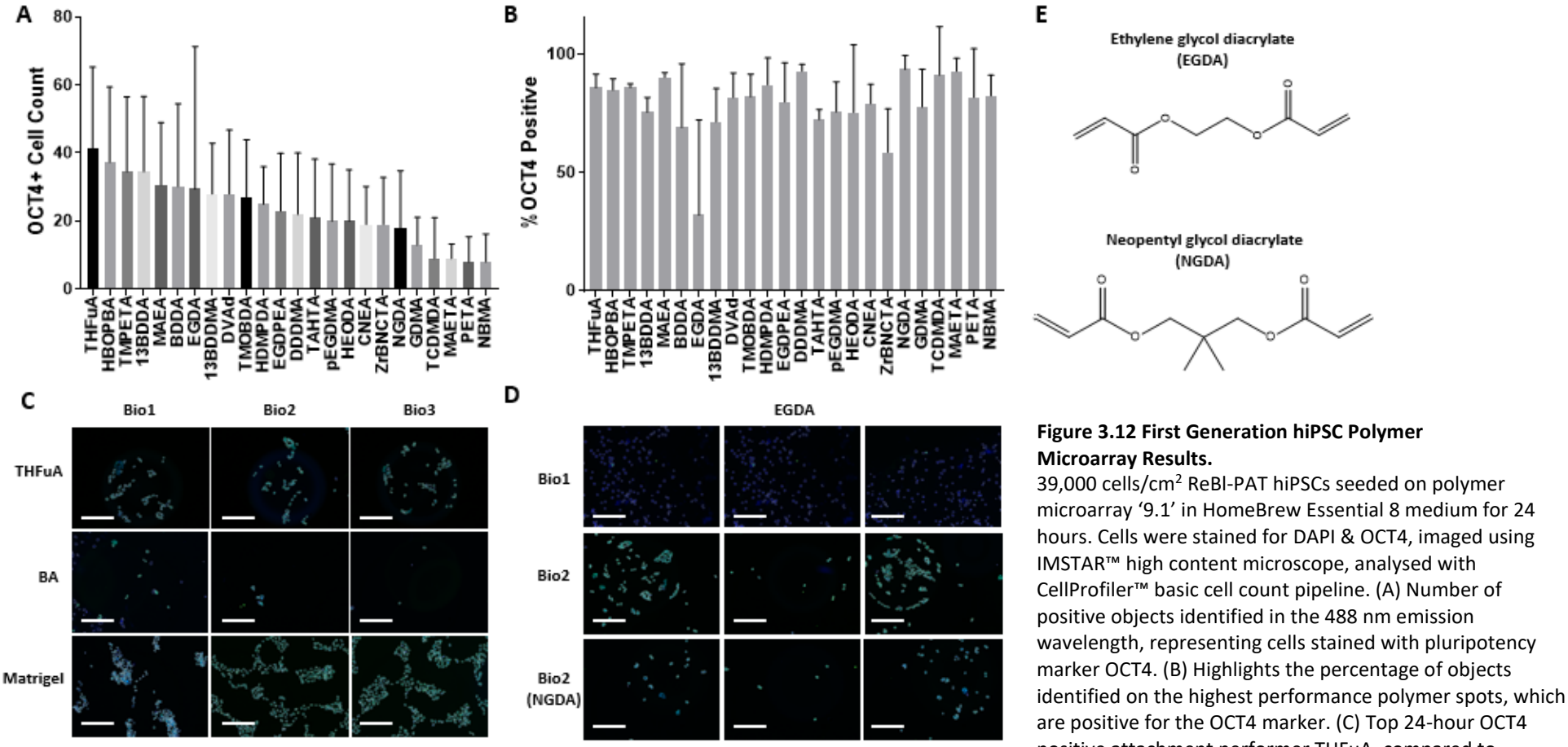

Figure 3.12 First Generation hiPSC Polymer Microarray Results.
39,000 cells/cm^2 ReBl-PAT hiPSCs seeded on polymer microarray '9.1' in HomeBrew Essential 8 medium for 24 hours. Cells were stained for DAPI & OCT4, imaged using IMSTAR™ high content microscope, analysed with CellProfiler™ basic cell count pipeline. (A) Number of positive objects identified in the 488 nm emission wavelength, representing cells stained with pluripotency marker OCT4. (B) Highlights the percentage of objects identified on the highest performance polymer spots, which are positive for the OCT4 marker. (C) Top 24-hour OCT4 positive attachment performer THFuA, compared to moderate attachment hit BA, and Matrigel™ control. (D) EGDA images compared to structurally similar polymer NGDA at 24-hour culture, highlighting EGDA's potential to induce rapid loss of OCT4 expression. (E) Chemical structure and name for EGDA & NGDA. Biological repeats = 3 Technical repeats = 9. Scale Bars = 100 µm

3.3.11 Biological Response to Array 9.1 (4% pHEMA) at 48 Hours Culture

Next it was determined which polymers can support cell survival post-ROCKi removal, and colony formation at 48 hours culture. An essential step towards creating a surface suitable for long-term culture. To do this hiPSCs were cultured on array 9.1 for 48 hours, with ROCKi being removed after 24 hours culture, before fixation and staining to determine which polymers can support 48-hour colony formation and survival.

6/284 polymers demonstrated limitd capability to fulfil the 2nd aim of this chapter, 48-hour survival and growth, the names, structures, and representative images are shown in Figure 3.13 (A-F). No homopolymer supported survival and colony formation reproducibly. Four of the six polymers capable of supporting hiPSCs to 48 hours culture matched with top hits from the 24 hours culture screen, o-Nitrobenzyl methacrylate (NBnMA) and N-[2-(N,N Dimethylamino)ethyl]methacrylamide (DMEMAm) were the exceptions.

At 24 hours culture NBnMA supported 3 +/- 100% DAPI positive objects, and DMEMAm supported 172 +/- 31.4% DAPI positive objects – however DMEMAm was omitted from the 24 hours top hits due to only 13% of DAPI objects being OCT4 positive. In conclusion, no homopolymers can fulfil the first two aims of this chapter, on array 9.1 (4% pHEMA), in a reproducibly manner.

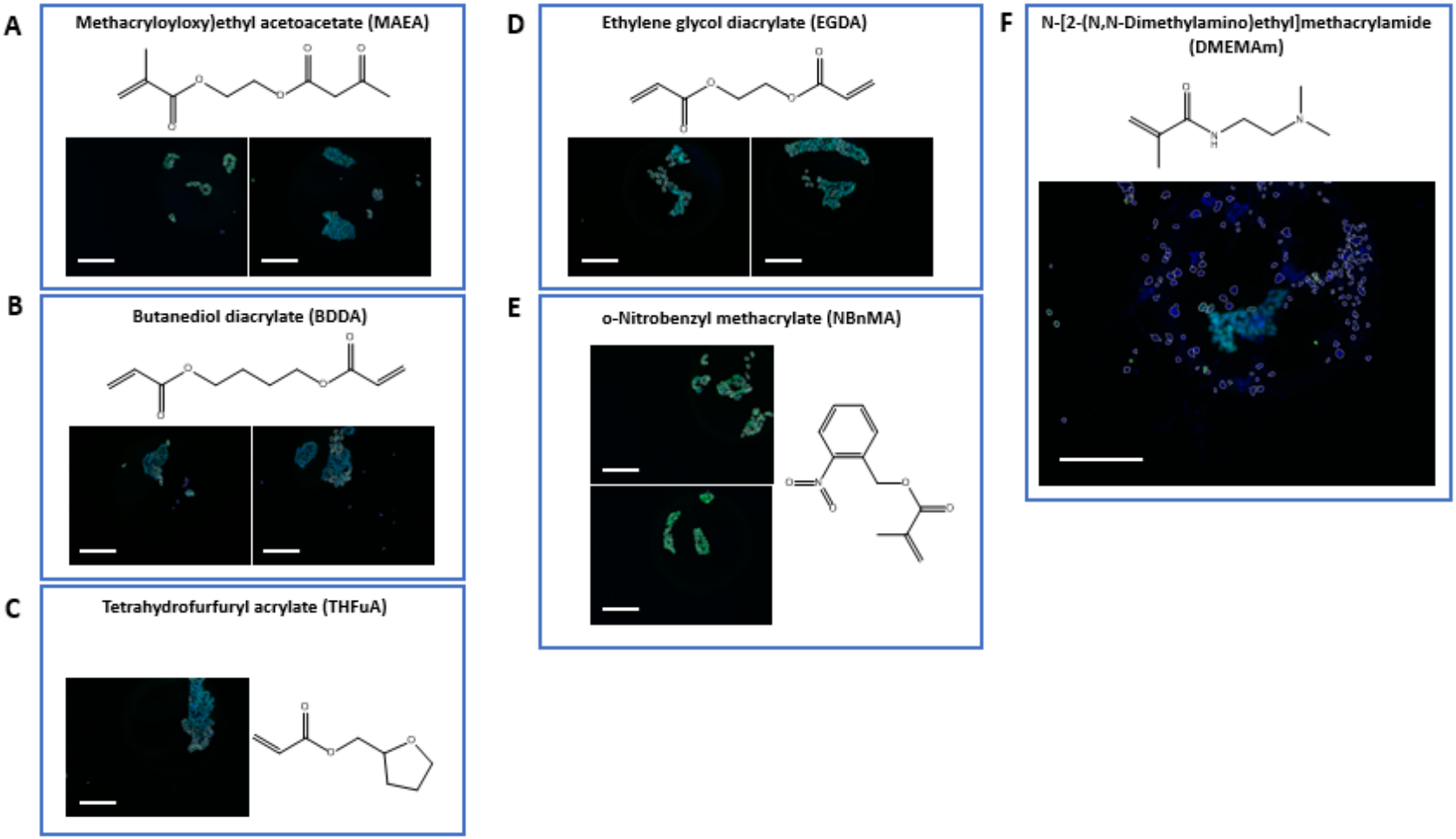

Figure 3.13 A Small Number of Polymer Spots Supported Cell Survival and Proliferation at 48 Hours Culture.
39,000 cells/cm^2 ReBl-PAT hiPSCs were seeded on polymer microarray '9.1' in HomeBrew Essential 8 medium for 48 hours. Cells were stained for DAPI & OCT4, imaged using IMSTAR™ high content microscope, analysed with CellProfiler™ basic cell count pipeline. (A-F) Immunofluorescent OCT4 & DAPI images, name and structures for polymer spots capable of supporting 48-hour culture. No individual polymer spots supported attachment reproducibly. Biological repeats = 3. Technical repeats = 9.
Scale Bars = 100 µm

3.3.12 Creation of hiPSC Polymer Microarray 10.1 (Co-polymers)

To create a synthetic surface capable of fulfilling the aims of this chapter; attachment at 24 hours culture with ROCKi, colony formation and survival after ROCKi has been removed at 48 hours, and the ability to support 72 hours culture reproducibly, co-polymer arrays were designed. The rationale behind heteropolymer arrays is present in previous work, where synergy between different monomers provided, polymer surface stability during long-term storage for Celiz et al., 2015, and generated an increase in hiPSC-CM maturation and attachment for Patel et al., 2015.

23 monomers were chosen to go forward considering; attachment data from 8.0/8.2/9.1 arrays at 24 hours and 48 hours culture, the ability to support OCT4 expression, chemical diversity, and diversity between top performers, moderate performers and low performing polymers. HEMA was specifically included due to the difference in biological response between 6% pHEMA and 4% pHEMA arrays, and the benefits of HEMA shown in Celiz et al., 2015 for hPSC synthetic culture surfaces.

Monomers selected are shown in Figure 3.15 and were combined in 2:1 ratio, however a subset were tested at 1:1 ratio, to form an array with 599 co-polymer / homopolymer combinations. To accommodate 599 polymer spots, the distance between each was reduced to 500 µm in both X & Y axis. Three technical repeats were maintained per array slide.

3.4 Biological Response to Array 10.1 (Co-polymers) at 24 hours Culture

3.4.1 CellProfiler™ Optimisation for Array 10.1

To assess the biological performance of array 10.1, the same seeding and medium conditions were used as per array 9.1. This section explores the data from 24 hours culture.

Further optimisation of the CellProfiler™ pipeline. Due to the reduced distance between each polymer spot (500 µm), images were cropped to ensure only cell attachment from the polymer spot of interest was considered (Figure 3.14 (A)). Detecting objects with a manually set threshold & detecting separations in objects through changes to fluorescent intensity allowed greater separation of single cells within colonies. A smoothing filter & suppression of local maxima was manually set to determine the minimum distance between individual cells (Figure 3.14 (B)).

Semi-dense clusters & colonies can have an accurate cell count applied to them, however denser colony formation particularly seen at 72-hour culture became too dense for accurate detection, even after several rounds of smoothing filter & suppression of local maxima optimisation (Figure 3.14 (C & D)).

The structures and abbreviations of the monomers taken forward to form array 10.1 can be found in Figure 3.15.

A

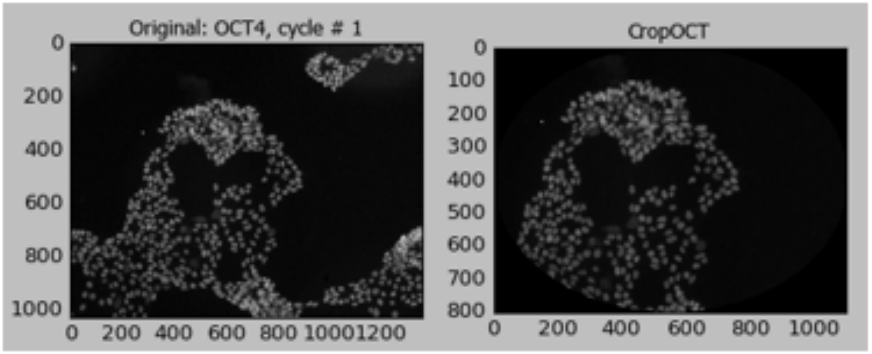

B

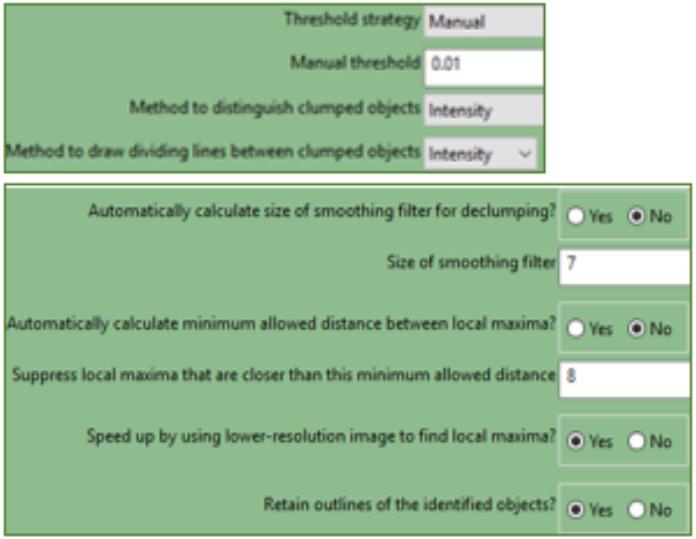

C

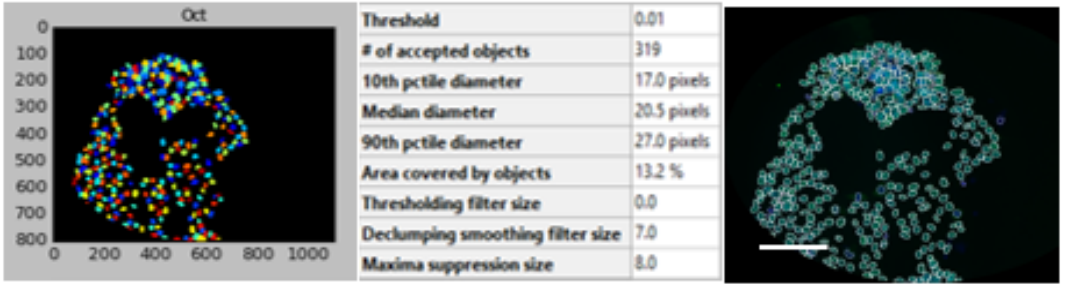

D

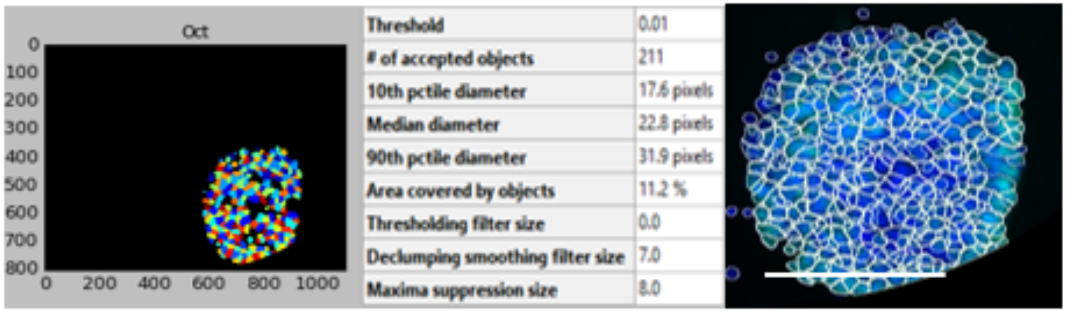

Figure 3.14 Improved Optimisation of CellProfiler™ Pipelines for Generation 2 Polymer Microarray Analysis.

(A) Images were cropped to avoid the inclusion of cells/objects from neighbouring polymer spots. (B) Manual thresholding was utilised to exclude polymer background. A combination of smoothing filters and suppress local maxima settings were optimised to maximise the number of detected cells in dense colonies. (C) Lightly clustered cells are readily identifiable with high accuracy on generation 2 arrays. (D) 72hr colonies form tight clusters that may also contain 3D stacking of cells, given the limited space for colony growth on microarray spots. Cell counts were not deemed usable for 72hr polymer array cultures. Scale bars = 200 pixels

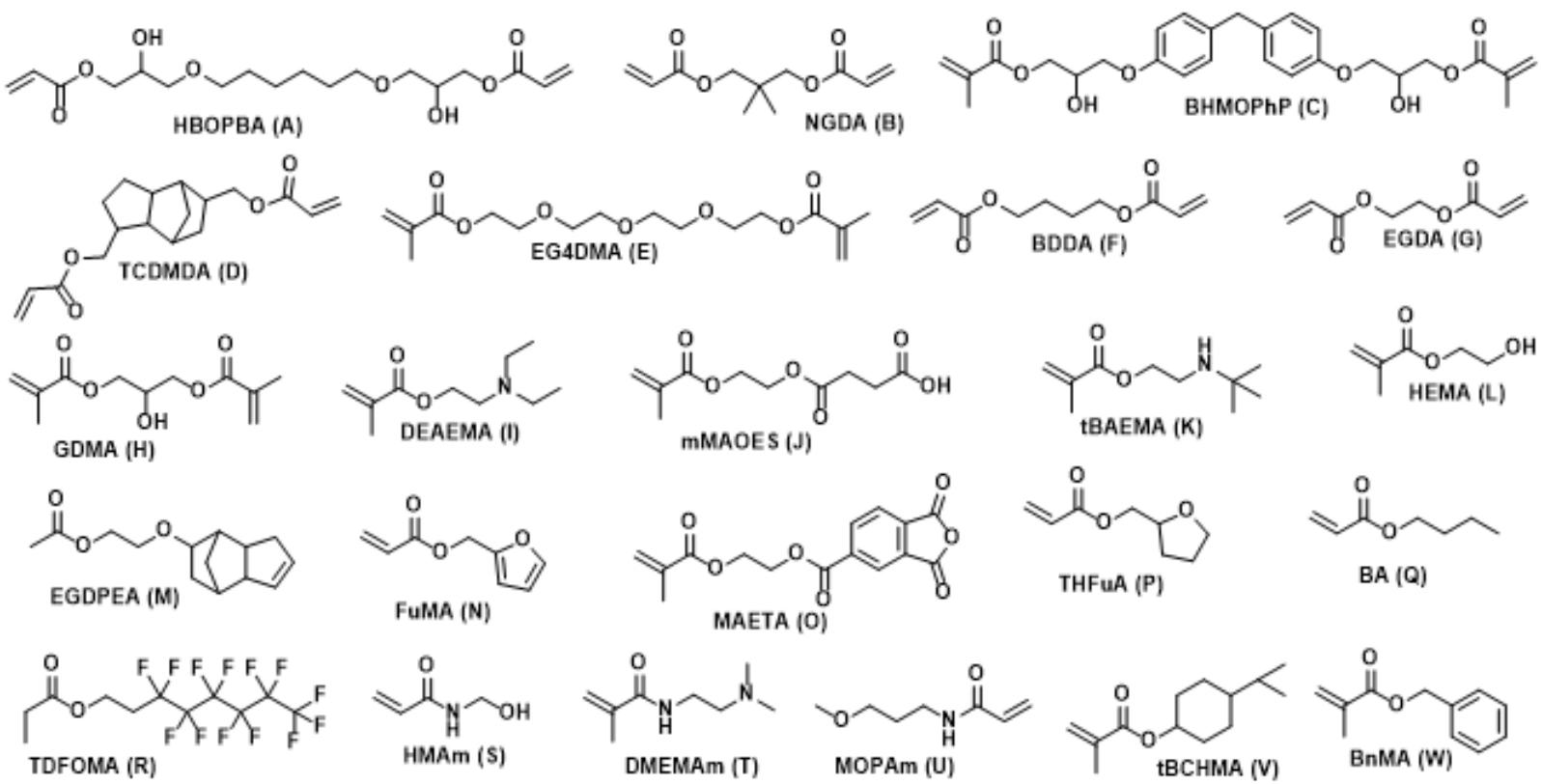

Figure 3.15 Monomer Hits Taken From 1st Generation Polymer Microarray Screen with ReBl-PAT hiPSCs, to be used in a 2nd Generation Array.

Selection was based on 24-hour and 48-hour data, 4% & 6% data, with a range of high, medium and low performing monomers selected, with chemical diversity considered. HEMA (L) included due to change in biological response between 4% & 6%, and work carried out by Celiz *et al.*, 2015.

3.4.2 Array 10.1 Cell Attachment Results (24-hour Culture)

The average DAPI cell attachment after 24 hours culture, increased on co-polymer array 10.1 when compared to homopolymer array 9.1, with array 10.1 supporting an average of 62 +/- 34.6% & array 9.1 supporting an average of 13.4 +/- 78.5% (Figure 3.16). Synergistic effects between homopolymers, a reduction in polymer spot-spot distance, or likely a combination of both led to an increase in cell attachment after 24 hours culture.

The average OCT4 positive cell count at 24 hours culture on array 10.1 was; 40 +/- 31%, versus 8 +/- 93% on array 9.1. Both the increase in DAPI count & OCT4 positive cells from array 9.1 to array 10.1 at 24 hours culture was deemed statistically significant, P=<0.0001 (****), in an unpaired t-test with Welch's correction.

Where monomers were combined in 2:1 ratio (major:minor), the top performing major monomers at 24 hours were TCDMDA, THFuA and EG4DMA, supporting on average 79 +/- 49%, 72 +/- 48.6% and 69 +/- 45% OCT4 positive cells respectively. The worst performing major monomers, MOPAm, HMAm and BnMA supported on average 27 +/- 66%, 20 +/- 45%, 19 +/- 42% OCT4 positive cells respectively.

DMEMAm as a homopolymer supported on average 175 +/- 38% DAPI positive cells, when used as the major monomer, however only 24 +/- 27% OCT4 positive cells on average, the poor OCT4 retention ability is consistent with the data for DMEMAm shown on array 9.1 as a homopolymer and was not improved through synergy with other monomers.

Taking major monomers BA, TDFOMA, HMAm, DMEMAm, MOPAm, tBCHMA & BnMA as examples, which were all relatively poor performing major monomers, with 141 (2:1) combinations attempted, only 5/141 heteropolymers provided above 80 OCT positive cell attachment. This suggests only minor monomers rarely rescue the performance of poor performing major monomers.

DMEMAm:MAETA (DMEMAm:4-Methacryloxyethyl trimellitic anhydride) (T:O) is the best performing example from the 5/141, supporting 87 +/- 72% OCT4 positive cells, however, DMEMAm as a homopolymer supported 66 +/- 27% OCT4. Due to the large increase in variation, an undesirable characteristic for a hPSC culture surface, combination of DMEMAm:MAETA doesn't present a clear advantage to using DMEMAm as a homopolymer, during the initial 24-hour culture period. Further evidence of minor monomers being incapable of rescuing poor major monomer performance can be demonstrated when looking at monomers S-W as a 50:50 ratio mixture by volume with monomers A-R.

Zero of the 90 50:50 ratio mixtures demonstrated OCT4 positive cell attachment capability ≥80. This evidence demonstrates that a strong performing major monomer likely forms the basis for cell survival at 24 hours culture, enhanced by minor monomers. To see clearly identify the top performing polymers, the 24 hits supporting ≥110 OCT4 positive cells were presented as a bar chart in Figure 3.17 (A). Top performing monomer TCDMDA was present in 10 of the 25 high OCT4 attachment hits, including TCDMDA as a homopolymer. THFuA was present 5 times, where EG4DMA appeared 3 times like other reoccurring components such as; GDMA, EGDA and MAETA.

It is important to note uncertainties with the data generated on array 10.1. Polymer spots exist in 500 μm proximity to one another, meaning hiPSCs attaching at one polymer could influence the local environment of spots surrounding it.

An example where hiPSCs have formed colonies, without extending across or growing on the pHEMA background is shown in Figure 3.17 (B).

The same situation is shown in a different area, where the proximity of the polymer spots to each other has allowed cells to migrate and connect between different polymer surfaces (Figure 3.17 (B)I)). This has the potential to generate false-positive hits or inflate the true cell attachment potential of a given polymer.

Despite these caveats, when taken together Figure 3.16 & Figure 3.17 provide a library of 181 homopolymers and heteropolymers that can support ≥50 OCT4 positive cells for 24 hours culture in ROCKi, which equates to 30% of unique polymer spots tested on array 10.1.

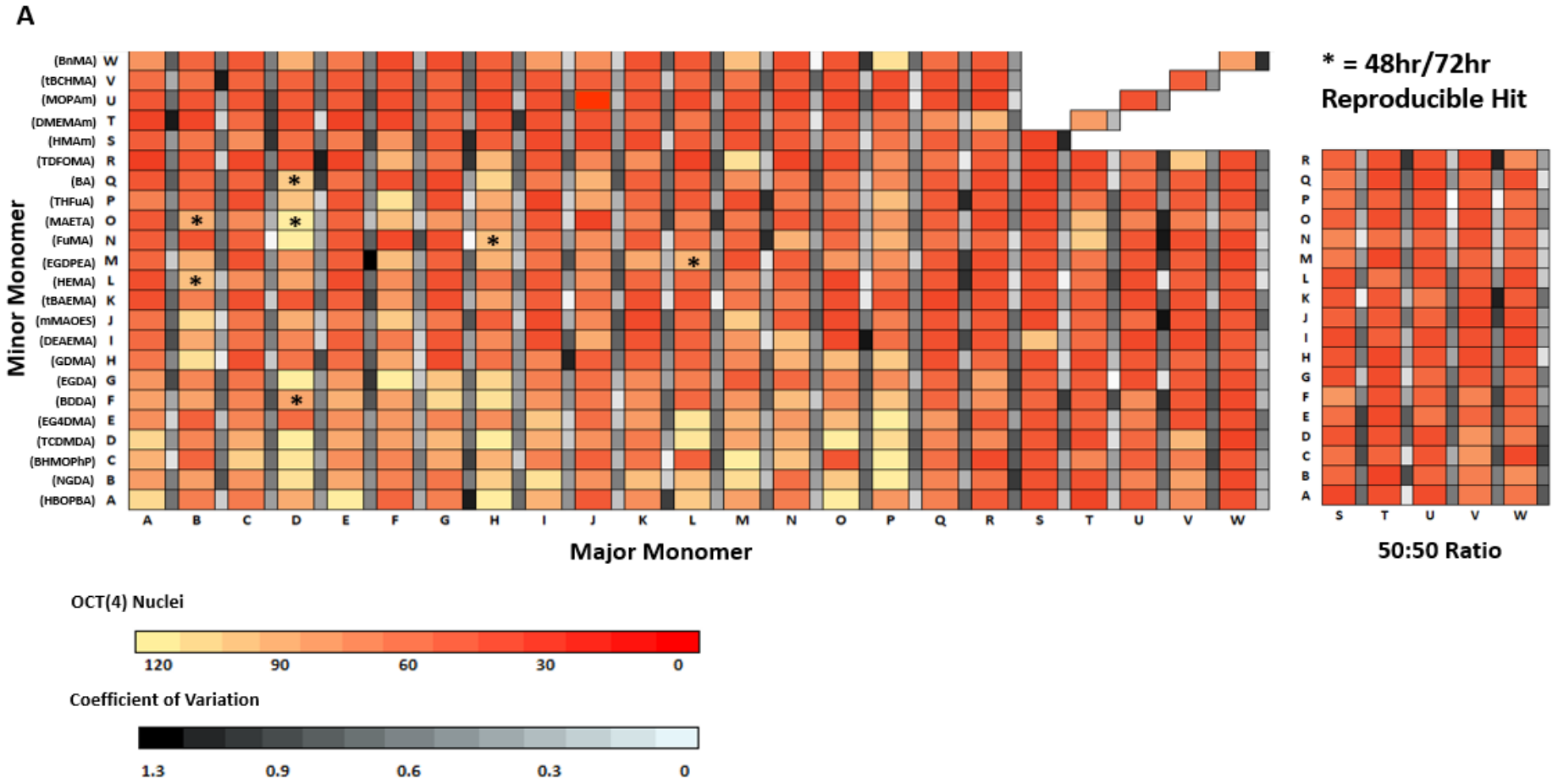

Figure 3.16 Generation 2 Polymer Microarray Results.

(A) Heatmap of OCT4 positive object detection using the improved cell count CellProfiler™ pipeline from Figure 3.14, after 24hrs of culture in HomeBrew Essential 8 Medium. Cells seeded 39,000 cells/cm^2. Monomers were mixed and combined in 2:1 ratio denoted major & minor respectively. Letting A to S refers to the monomers selected and labelled in figure X. Biological repeats = 3, Technical repeats = 9.

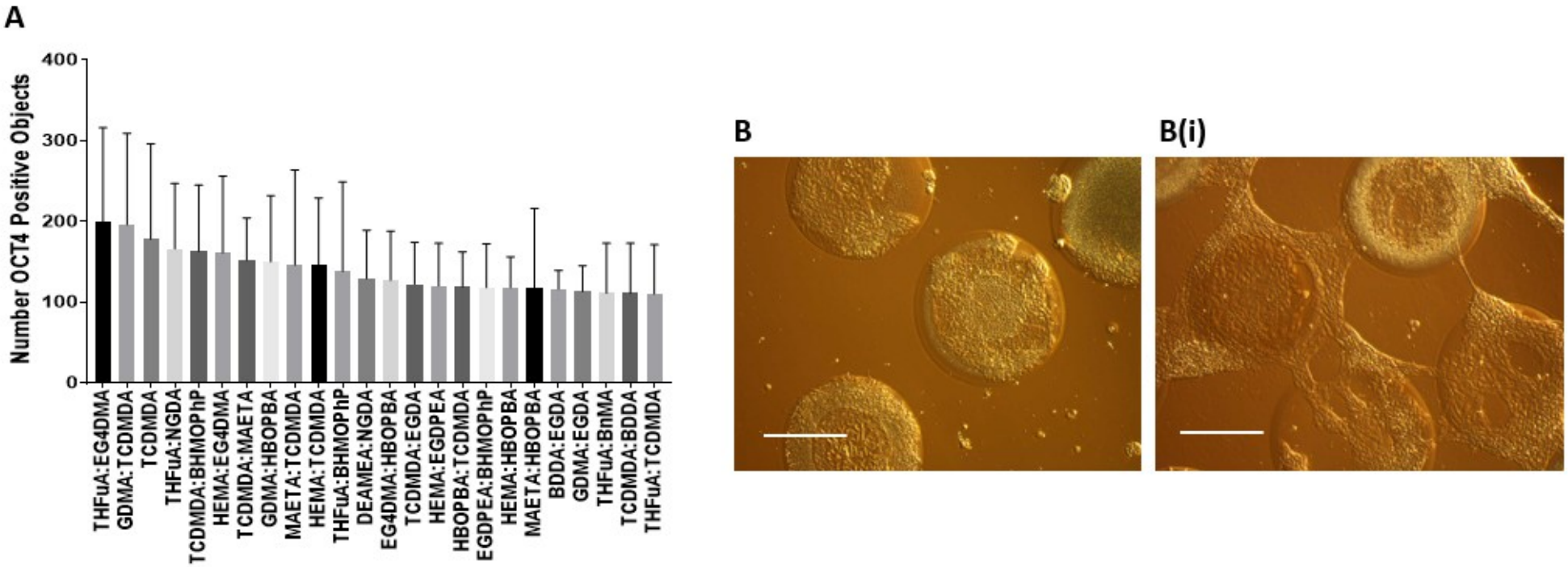

Figure 3.17 Generation 2 hPSC Polymer Microarray Results.

(A) Top performing co-polymers or homopolymers for 24hr attachment, ranked by number of OCT4 positive objects. Standard deviation shown. (B) Multiple attachment hit co-polymer spots in proximity with complete separation of hPSC colonies, after 24-hour culture. (B)(I) Multiple attachment hit co-polymer spots in proximity with overlapping attachment and cell spreading, obscuring true hits from false positives. Images taken with the Nikon Eclipse TE 2000-S Microscope, 10x magnification. Biological repeats = 3. Technical repeats = 9

3.4.3 Biological Response to Array 10.1 (Co-polymers) at 48- & 72-Hours Culture

181 polymers could support 24-hour culture on array 10.1, to determine what number of these polymers could fulfil all three of this chapters aims, arrays were left to reach the 48-hour and 72-hour culture time-points, with the removal of ROCKi after 24 hours. A complete list of polymers that were capable of culture for 48 hours or 72 hours, when colony formation was observed (Figure 3.18). At 48 hours culture, 7 heteropolymers were hits across multiple biological repeats, with TCDMDA & NGDA as the major component for 3 and 2 of the heteropolymers respectively.

At 72 hours only three polymers, two of which with MAETA as the minor component, supported robust colony formation across multiple biological repeats. Overlapping hits between 48-hour and 72-hour cultured arrays, revealed only heteropolymers features TCDMDA or NGDA to be consistent across the two time-points. Images of NGDA:MAETA and TCDMDA:MAETA stained for the pluripotency marker OCT4 and DAPI nuclear stain are shown in Figure 3.18 (B).

During culture of both the 48-hour and 72-hour cultured arrays, floating 'disk-shaped' colonies of cells were seen in the medium. Collecting the medium and re-seeding the floating colonies onto Matrigel™ demonstrated their viability for continued growth and survival. The presence of floating colonies hints that detachment from unspecified polymer spots may have occurred, which may have influenced the polymer hits shown in Figure 3.18 (A).

Despite the complication of floating colonies, these results demonstrate that heteropolymers consisting of TCDMDA or NGDA, with MAETA are capable of

supporting ReBl-PAT hiPSCs in Homebrew Essential 8 medium for 72 hours, with some reproducibility across multiple repeats.

So far only two ratios of monomer:monomer has been tested, to investigate if different ratios can increase biological performance, 9 top hits were selected to form a final array screen, these are shown in Figure 3.19.

A

Generation 2 hPSC Array 48hr Culture Hits (Multiple Biological Repeats)	Generation 2 hPSC Array 72hr Culture Hits (Multiple Biological Repeats)	Generation 2 hPSC Array 72hr/48hr Overlapping Hits
EG4DMA:EGDPEA	NGDA:MAETA	NGDA:MAETA
GDMA:FuMA	TCDMDA:MAETA	NGDA:HEMA
NGDA:HEMA	HEMA:EGDPEA	TCDMDA:MAETA
NGDA:MAETA		TCDMDA:BDDA
TCDMDA:BA		
TCDMDA:BDDA		
TCDMDA:MAETA		

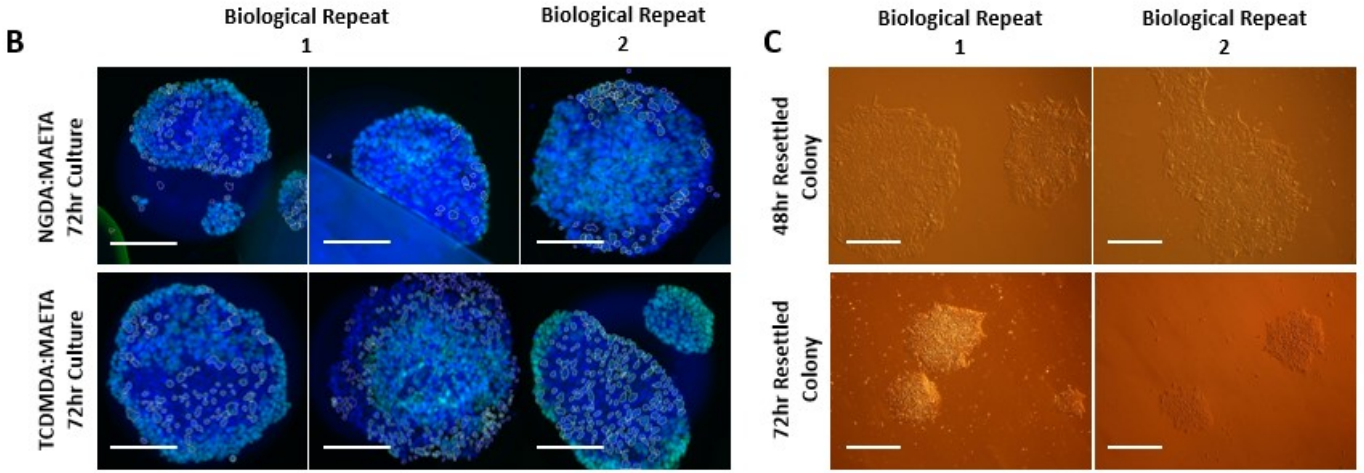

Figure 3.18 Generation 2 Co-Polymer Microarray (10.1) 48 Hour and 72 Hour Results.

(A) List of co-polymers that demonstrated attachment of ReBl-PAT hiPSCs after 48 hours culture, across multiple biological repeats. A list of co-polymers that supported 72-hour culture, across multiple biological repeats. A list of co-polymers that were represented with at least 1 biological hit across both 48-hour and 72-hour timepoints. (B) Immunofluorescent images of polymer microarray spots that supported 72-hour culture of ReBl-PAT hiPSCs in HomeBrew Essential 8 medium, across at least two biological repeats. Images captured on the IMSTAR™ Microscope (IMSTAR SA) (C) Floating colonies in the medium were observed at both 48-hour and 72-hour timepoints. Floating colonies resettled on Matrigel™ coated surfaces and allowed to attach and proliferate to determine viability. Brightfield images taken with the Nikon Eclipse TE 2000-S Microscope, at 10x magnification. Biological repeats = 3. Technical repeats = 9.

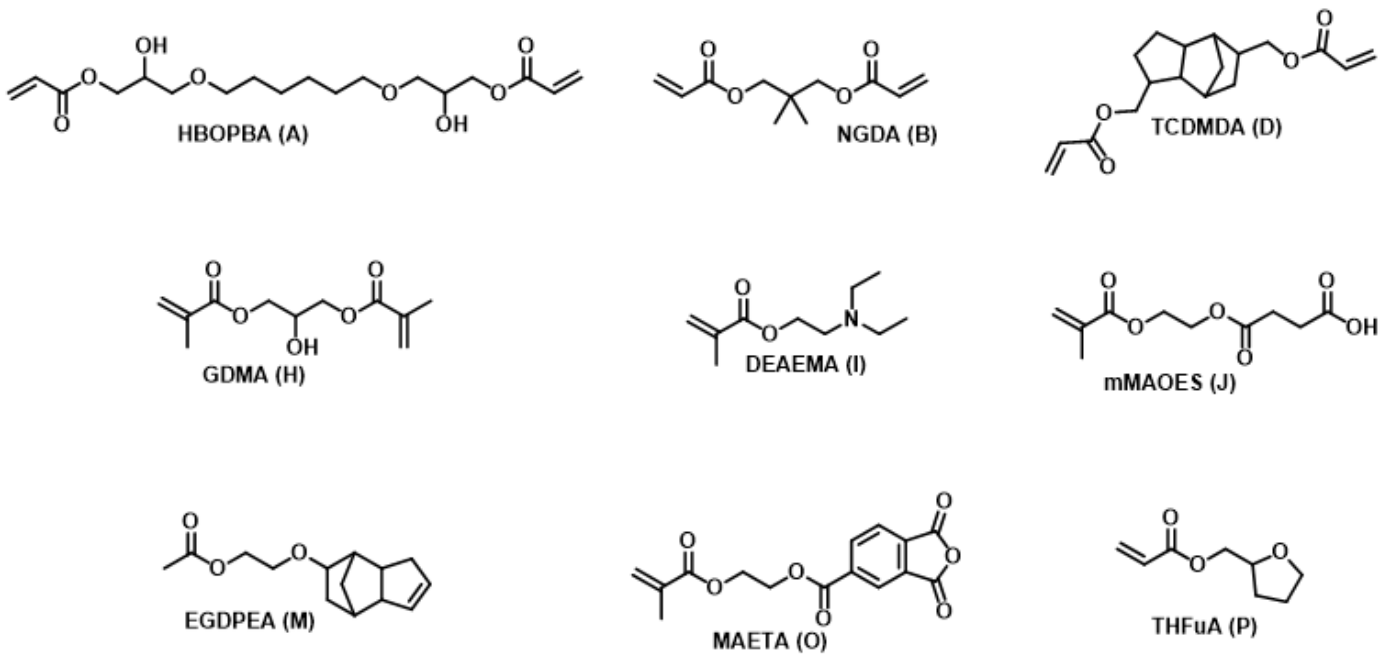

Figure 3.19 Monomer Hits Taken from 2nd Generation Polymer Microarray Screen with ReBl-PAT hiPSCs, to be used in 3rd Generation Array.

Selection was based on 24-hour, 48-hour & 72-hour data, strongest performers were selected with chemical diversity considered, resulting in the addition of DEAEMA, to retain an amine functionality.

3.4.4 Development and Response to Array 10.2 (Co-polymers at varying ratios) at 24 Hours Culture

To improve upon the performance of the hits found on array 10.1, and to determine if new hits can be found by mixing monomers at different volume-to-volume ratios, array 10.2 was developed. 9 hit monomers were selected for mixing at a 9:1, 8:2, 7:3, 6:4, 5:5 ratio and their inverse, forming an array with 297 unique spots, printed three times per pHEMA coated microscope slide.

The selection of monomers shown in Figure 3.19 was determined through the top hits identified in array 10.1, with DEAEMA included to maintain at least one nitrogen containing monomer. Due to the reduced number of spots compared to array 10.1, the inter-spot distance was increased to 1500 µm by 1500 µm (X & Y axis distance).

Seeding and culture conditions remained the same as array 10.1, except for the introduction of the embryonic human stem cell line, HUES7, which were tested alongside ReBl-PAT hiPSCs. The introduction of a 2nd cell line was to investigate if polymer-to-cell interactions were cell line specific, or applicable to multiple lines.

Data collated from both cell lines at the 24-hour array screen supported an average DAPI cell count of 14 +/- 121%, and an average OCT4 cell count of 14 +/- 121%, where the average % of DAPI nuclei, positive for OCT4, was 100%. The top 12 co-polymers, with ReBl-PAT & HUES7 combined data, supported an average of 42 +/- 24% DAPI & OCT4 positive nuclei.

Four top performing co-polymers are highlighted by their structure and chemical identity in Figure 3.20, where all of which are 1:9, X:MAETA. The combination of monomer hits are mostly in line with data from array 10.1, where MAETA demonstrated cell attachment at 24 hours with NGDA, HBOPBA and TCDMDA.

When broken down by the cell line used; ReBl-PAT or HUES7, the ReBl-PAT line has just a single MAETA containing polymer in the top ten, NGDA:MAETA (1:9), Figure 3.21 (A). THFuA as a homopolymer performed well on array 11.1, as previously shown with ReBl-PAT hiPSCs in generation 10.1 and 9.1 at 24 hours culture, supporting 38 +/- 68%, 88 +/- 40% & 41 +/- 59% respectively. However, DEAEMA as a homopolymer demonstrates equal cell attachment, 40 +/- 55%, which was not seen on previous array generations (Figure 3.21 (A)).

7 of the top 10 hits for ReBl-PATs contain NGDA or TCDMDA, reinforcing the pair as hit chemistries of great interest. The top 10 hits with ReBl-PAT hiPSCs supported an average of 45 +/- 60% DAPI & OCT4 positive nuclei, compared to the top 10 hits with the HUES7 hESC line which supported 66 +/- 23%. Considering 24-hour HUES7 attachment data on array 10.2 alone, MAETA was present in 8 of the 10 best performing polymers. 8 of the 10 also contained either TCDMDA or NGDA mimicking results seen with the ReBl-PAT line (Figure 3.21 (B)).

Images of both ReBl-PAT and HUES7 cells growing on Matrigel™ and polymer spots before fixation are shown in Figure 3.22 (A), where different polymers that supported cell attachment and spreading before fixation. Figure 3.22 (B) Highlights the delamination potential for some polymers present on the array. Figure 3.22 (C)

Compares images stained for the OCT4 pluripotency marker and DAPI nuclear stain, on both NGDA:MAETA (1:9) and TCDMDA:MAETA (1:9) across two biological repeats.

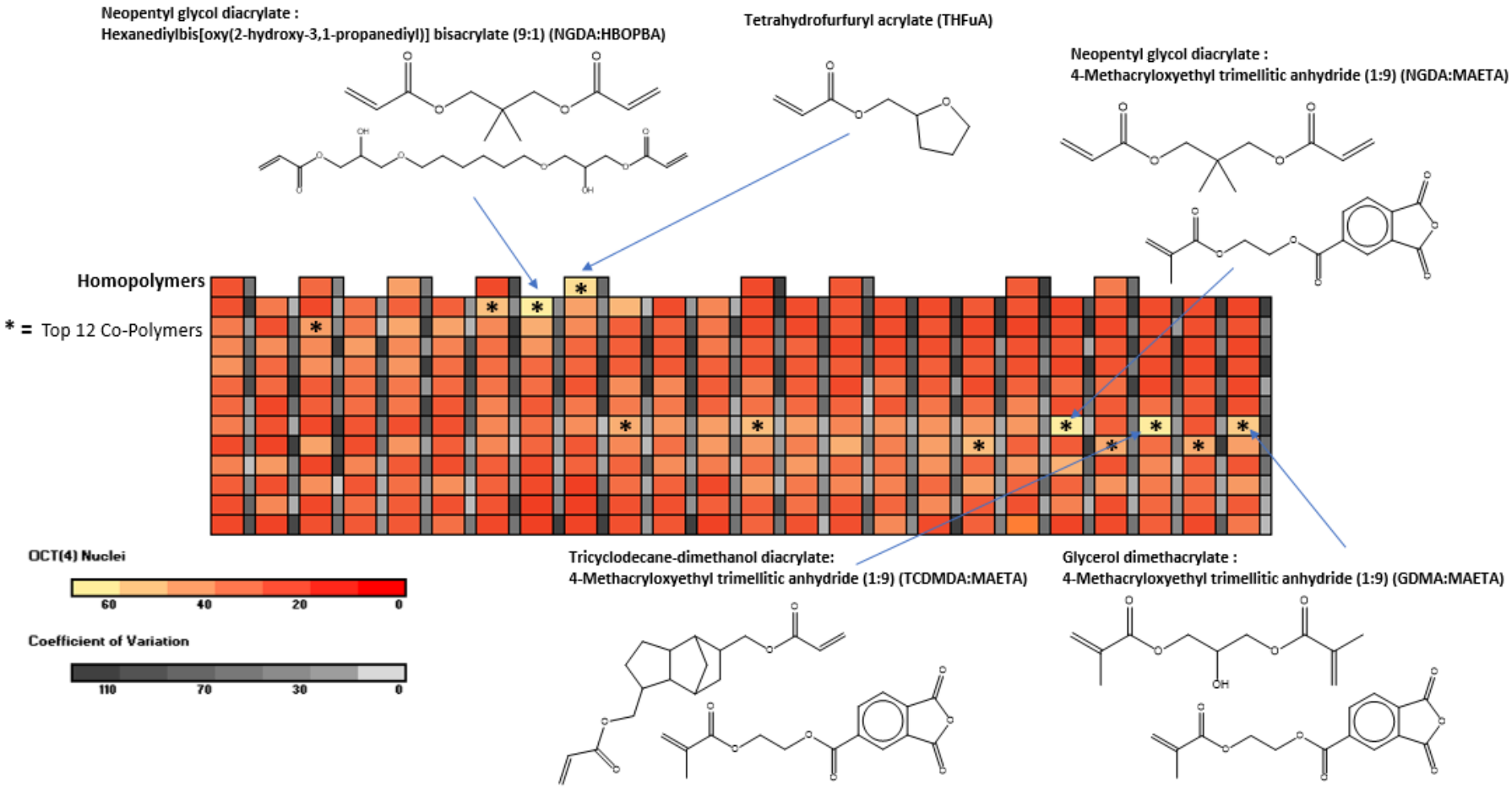

Figure 3.20 3rd Generation Polymer Microarrays Cultured with HUES7 and ReBl-PAT Pluripotent Stem Cells for 24 hours.

Heatmap representation of combined data, coefficient of variation is lower when lighter. Nine top performing monomers from 2nd Generation polymer microarrays were combined in; 1:9, 2:8, 3:7, 4:6, 5:5 ratios and their inverse, to form 297 unique polymers. Top five performing homopolymers/co-polymer combinations are highlighted. Cells were seeded at 39,000 cells/cm^2. Biological repeats = 4. Technical repeats = 12.

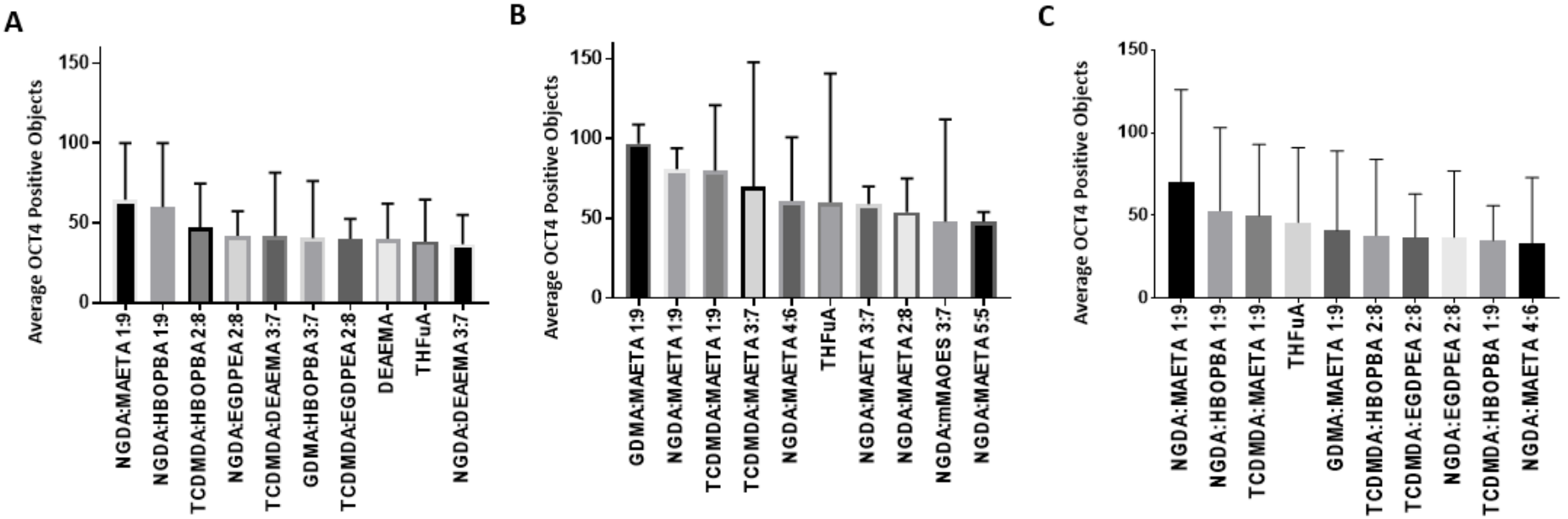

Figure 3.21 3rd Generation Polymer Microarrays Cultured with HUES7 and ReBl-PAT Pluripotent Stem Cells for 24 Hours.

Nine top performing monomers from 2nd Generation polymer microarrays were combined in; 1:9, 2:8, 3:7, 4:6, 5:5 ratios and their inverse, to form 297 unique polymers. (A) 24-hour top attachment hits for ReBl-PAT hiPSCs in HomeBrew E8 Medium. Biological Repeats = 2 Technical Repeats = 6. (B) 24-hour top attachment hits for HUES7 hESCs in HomeBrew E8 Medium. Biological Repeats = 2 Technical Repeats = 6 (C) Combined ReBl-PAT and HUES7 data for overall performance. Biological Repeats = 4. Technical Repeats = 12. Standard deviations shown.

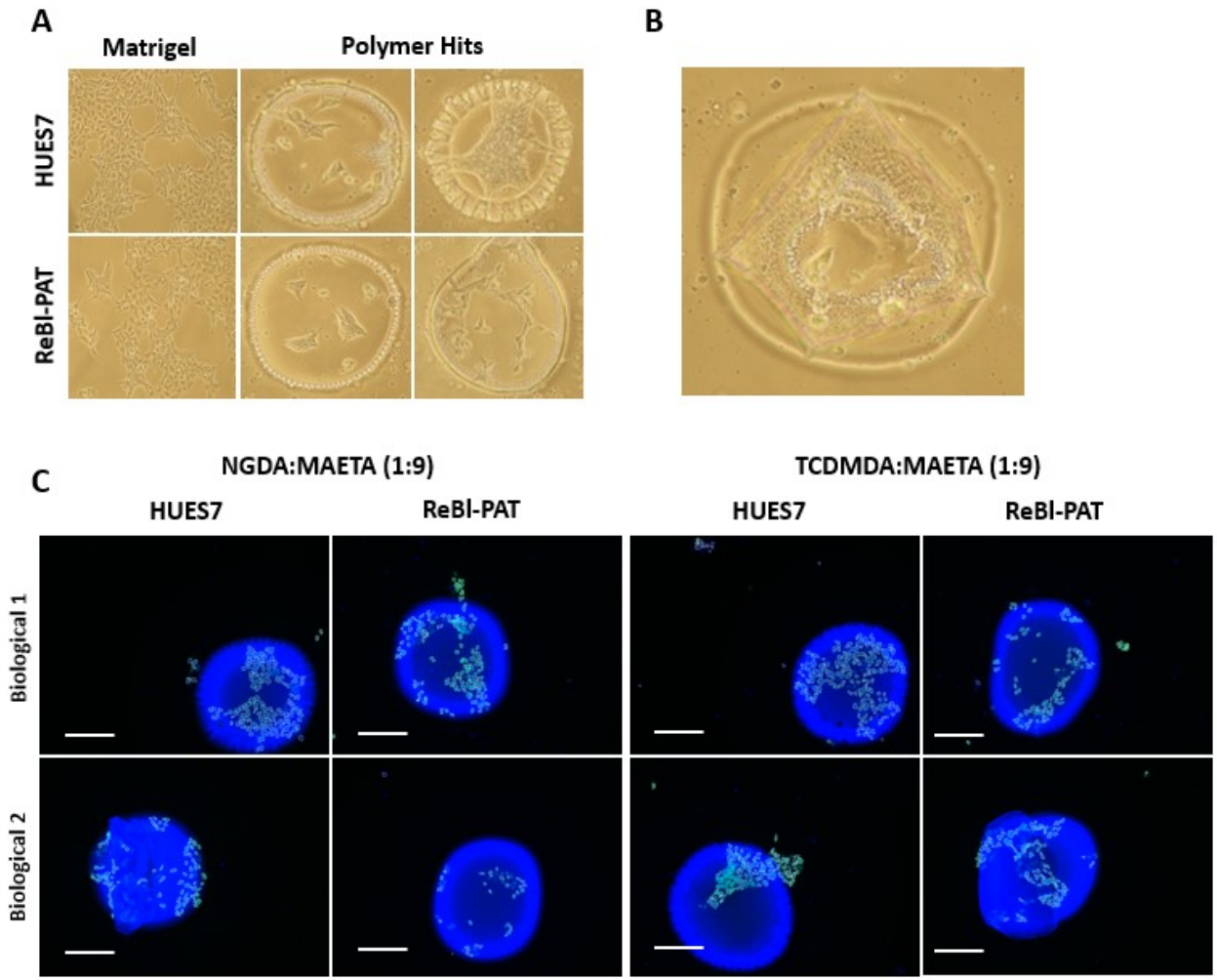

Figure 3.22 3rd Generation Polymer Microarrays Cultured with HUES7 and ReBl-PAT Pluripotent Stem Cells for 24 Hours.

Nine top performing monomers from 2nd Generation polymer microarrays were combined in; 1:9, 2:8, 3:7, 4:6, 5:5 ratios and their inverse, to form 297 unique polymers. (A) Matrigel™ and observed attachment hit polymers seen during culture at 24 hours. (B) Delamination of a polymer spot on the array. (C) DAPI and OCT4 stained high ranking hits shown across two cell lines; HUES7 & ReBl-PAT across two separate biological repeats. 24 hours culture.

3.4.5 Statistical Assessment of Array 10.2 Data (Regression Analysis)

To assess how useful the 24-hour culture data set from array 10.2 was at predicting polymer performance, Dr. Laurence Burroughs carried out statistical regression analysis with cell attachment data obtained and ToF-SIMs chemical fragmentation data, Figure 3.23 (A).

The resulting analysis presented an R^2 value of 0.64, which indicts a poor ability to predict hits correctly from this data set. However, top 24-hour performing homopolymer THFuA was correctly predicted. THFuA performance was relatively consistent across all three generations of array used, with a spike in 24-hour OCT4 positive cell attachment in array 10.1 (Generation 2) likely due to the reduced distance between polymer spots (Figure 3.23 (B)).

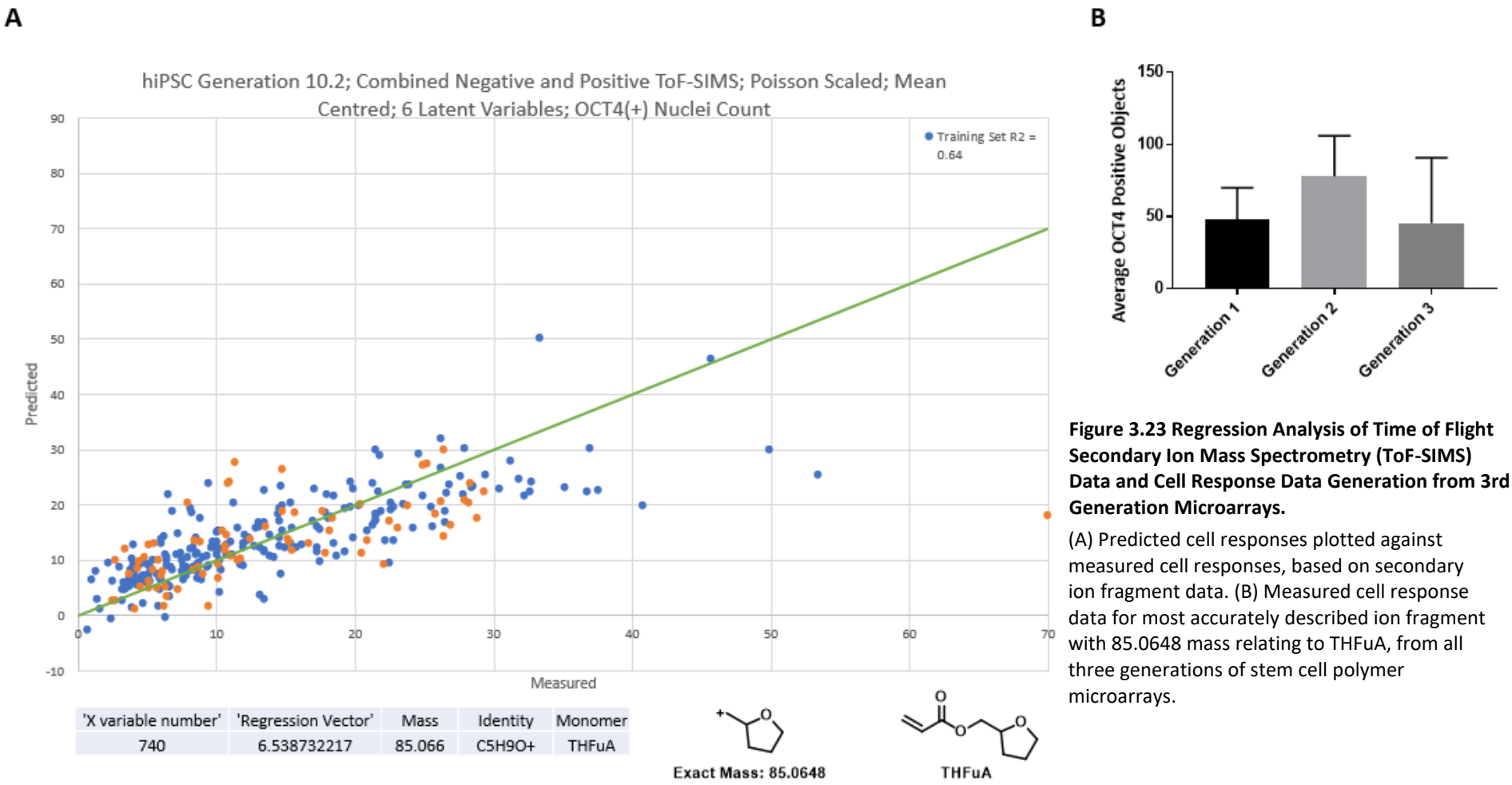

Figure 3.23 Regression Analysis of Time of Flight Secondary Ion Mass Spectrometry (ToF-SIMS) Data and Cell Response Data Generation from 3rd Generation Microarrays.

(A) Predicted cell responses plotted against measured cell responses, based on secondary ion fragment data. (B) Measured cell response data for most accurately described ion fragment with 85.0648 mass relating to THFuA, from all three generations of stem cell polymer microarrays.

3.5 Chapter Summary & Discussion

3.5.1 A comparison to previous polymer microarray work

Work performed by Celiz et al., 2015 cultured homopolymer microarrays (4% pHEMA), containing 141 unique polymers seeded with 51,800 cells/cm^2, in StemPro, mTeSR-1 and conditioned medium. Only 9/141 homopolymers demonstrated >30 OCT4 positive cell attachment at 24 hours culture.

The closest comparison that can be made in this chapter would be array 8.2, the 4% pHEMA homopolymer array containing 124 unique polymers, seeded at 25,000 cells/cm^2, cultured in LifeTech Essential 8™ medium. A comparable cell count was not performed, however only 1/124 homopolymers demonstrated any level of cell survival at 48 hours culture. The 25,000 cells/cm^2 was initially selected to reflect the culture density used in standard Matrigel™-based culture, but previous work had used over double this seeding density (51,800 cells/cm^2) for polymer discovery.

3.5.2 Media components play vital roles in hPSC attachment to polymers

The reduction in media components from StemPro & mTeSR-1 to the 'skinny' Essential 8™ medium, reduces that number of components that could potentially bind to polymer surfaces and act as attachment intermediaries between the polymer & cell.

The reduction in medium components has been demonstrated to have a critical effect on the capacity of some synthetic surfaces to support hPSC culture. An aminopropylmethacrylamide (known as APMAm.C & included on array 9.0 & beyond in this thesis) surface can culture hESCs in mTeSR-1 medium for 20 passages. Surface analysis and experimentation removing BSA, revealed BSA to be a critical component

for hESC attachment to the APMAm.C surface. Although the caveat that other components bound to BSA may also play a role in attachment is noted (Irwin et al., 2011).

3.5.3 Human dental pulp stem cells & hPSCs attach to identical or similar homopolymers

Overall data from array studies in this chapter highlighted the importance of three key monomers; TCDMDA, NGDA & MAETA for optimal biological performance.

A study using polymer microarrays to identify attachment hits for human dental pulp stem cells demonstrated a large cross-over in top performing monomeric hits, with hPSC 24-hour attachment hits in this thesis. In common the two array screens identified, 2-(Methacryloyloxy)ethyl acetoacetate (MAEA), 2,2,3,3,4,4-hexafluorobutyl methacrylate (F6BA), TCDMDA, 13BDDA, NGDA, trimethylolpropane ethoxylate triacrylate (TMPETA) & hexanediol ethoxylate diacrylate (HEODA), as top performing attachment hits (Rasi Ghaemi et al., 2018a).

For human dental pulp stem cells, tetrahydrofurfuryl methacrylate (THFuMA) was a top performing hit, where non-methacrylate version, tetrahydrofurfuryl acrylate (THFuA) was identified as the top performing 24-hour hit – but not the also tested THFuMA. This highlights how small changes to the functional group can have dramatic effects on the biological response, dependent on cell type (Rasi Ghaemi et al., 2018a).

Differentially this study used a poly(hydroxyethylmethacrylate) background, instead of pHEMA, as a means of inhibiting protein & cell attachment, removing the

hydrogel surface that pHEMA creates. This suggests that hits presented in this chapter should work effectively without the pHEMA layer upon scale-up.

Monomers printed onto arrays were also created at an increased concentration (75% vs 50% v/v), both with DMF solvent & identical photoinitiator (1% w/v). Which could influence cell response.

Similarly, both polymer microarray screens used 'skinny' medium. Essential 8™ in this screen, and DMEM supplemented with, penicillin, streptomycin & amphotericin for dental pulp stem cells. Assuming the addition of antibiotics has not played a significant role in attachment, either amino acids, vitamins, glucose or sodium pyruvate are facilitating attachment cellular attachment.

If the components of DMEM are not facilitating dental pulp stem cell attachment to the polymer, the mechanism of action could be, the carryover of adhesion proteins from the previous culture, absorption of ECM components produced by the cells, or a direct polymer-cell interaction.

The capability of a medium, DMEM, without the 8 essential components in E8 medium, to facilitate 24-hour attachment of a different type of human stem cell, to identical homopolymer surfaces, may have provided a valuable insight into the mechanism behind attachment of hPSCs to our polymer surfaces. This will be explored further in chapter 4.

3.5.4 Combinations with lesser performing monomers can have surprising results

MAETA & butyl acrylate (BA) are two homopolymers that were classified as low attachment, both supporting less than 8 OCT4 positive cells on average. When

combined with hit homopolymers TCDMDA and/or NGDA, the attachment performance was enhanced, and 48/72-hour culture enabled.

This presents a strong case for including a mixture of moderate & low performing monomers in future array co-polymer screens.

3.5.5 Third Generation Array 10.2 may have provided data with limited use

Data from array 10.2 suggests MAETA functions best as the major component, where up to 90% of the reaction mixture provided superior performance.

Two caveats exist for this conclusion, the first being that the top 10 performing polymers with ReBl-PATs only support this conclusion partially, where 1/10 hits contain MAETA.

The 2nd caveat relates to the lack of continuous mixing between monomers after addition, during the array preparation stage, in 384-well polypropylene plates, individual components may have separated out overtime.

This makes it difficult to determine what compositional differences exist for cell-surface interactions between the various monomer volume ratios, without in-depth ToF-SIMS analysis.

For this reason, and existing 72-hour hits, 48-hour and 72-hour experiments with array 10.2 were by-passed in favour of 96-well scale-up testing in chapter 4.

4 Chapter 4 – Scale-Up of Acrylate-Based Polymers for Human Pluripotent Stem Cell Culture

4.1 Introduction

In chapter 3, 12,503 polymer-to-cell interactions were tested in a microarray format and a selection of materials capable of supporting human pluripotent stem cell attachment, growth and survival for 24, 48, or 72-hours of culture was discovered.

To achieve one of the aims of this PhD project, namely, to develop a synthetic culture surface for hPSCs, the chosen hits from chapter 3 must be compatible with key requirements. These are to be scalable and be proven to retain key stem cell characteristics and chromosomal stability, even after serial passaging. Hit materials from chapter 3 were in the format of polymer microarray spots, approximately 0.03 cm^2 in size. In chapter 4 key hits had to be scaled initially to 0.32 cm^2, in a 96-well format. Synthetic surfaces were ultimately scaled to the 6-well plate format, with a surface area of 9.6 cm^2.

Successfully scaled-up hits were tested for their ability continuous culture across a minimum of five polymer plates and growth was tracked to show if cumulative population doubling times were comparable to the existing gold standard culture surface, Matrigel™. hPSCs were also tested to see if they retained a stable karyotype and a functional pluripotent state.

Aside from their ability to support pluripotency this chapter will uncover the molecular mechanisms behind the cell-surface interactions. Including integrin

blocking assays, which determined the integrins that are essential at the initial point of attachment. RT-qPCR was used to analyse integrin expression levels at 72 hours.

Finally, this chapter looked at the phosphorylated states of key signalling proteins within the cell with a phosphokinase-proteome array kit from R&D systems which looked at the comparison of 43 kinases and two total protein levels (β-catenin and Heat Shock Protein 60 (HSP60)) between hPSCs cultured on our best performing synthetic surface and Matrigel™.

Given the importance of trilineage differentiations in assessment of pluripotency, the role and value of these assays are introduced in the sections below. Similarly, the role of intracellular signalling play crucial roles in survival, growth and pluripotency and are also introduced below.

4.1.1 Trilineage Differentiation

A key part of this chapter is proving hPSCs, cultured on best performing polymer surfaces, are capable of supporting trilineage differentiation to mesoderm, endoderm & ectoderm lineages. To do this, directed differentiation protocols have been established by previous research. Since directed cardiomyocyte (mesoderm) formation was discussed in chapter 1, the sections here will focus on ectoderm (specifically neuroectoderm) and endoderm lineages and the protein markers that define the cell types produced.

4.1.2 Directed Neurectoderm Formation

In this chapter hPSCs grown for 5 passages on TCDMDA:BA will undergo a directed neuroectodermal differentiation protocol.

Neuroectoderm formation in vivo has been demonstrated to be under the control of BMP inhibitors and activin/nodal signalling (Hemmati-Brivanlou and Melton, 1994)(Lamb et al., 1993). This has led to the development of in vitro differentiation protocols based on the use of Noggin, Dorsomorphin and SB431542, where Noggin & Dorsomorphin inhibit BMP signalling and SB431542 antagonises activin/nodal signalling through ALK4, 5 & 7 kinases (Smith et al., 2008)(Zhou et al., 2010)(Surmacz et al., 2012).

In this chapter we focus on markers SOX1 and PAX6 for the identification of neuroectoderm formation.

4.1.3 SOX1

SOX1 is an HMG-box protein related to SRY and is one of the first transcription factors detected in ectoderm cells committed to neural fate. In mice, Sox1 has been shown to bind directly to the Hes1 promoter, supressing the transcription of Hes1, reducing Notch signalling, inducing neurogenesis (Kan et al., 2004). Furthermore, Sox1 binds β-catenin, suppressing its activity within TCF/LEF signalling, leading to a reduction in the Wnt signalling pathway (Kan et al., 2004). Continued expression of Sox1 in mice has been shown to maintain neural progenitor identity, preventing cell cycle exit and neurogenesis, knockdown of Sox1 results in gradual loss of the progenitor population (Elkouris et al., 2011).

4.1.4 PAX6

PAX6 is a crucial transcription factor for the development of the brain, eyes and olfactory system, heterozygous mutations to PAX6 have been demonstrated to cause ocular defects in humans (Chauhan et al., 2004)(Morrison et al., 2002)(Davis

and K.Cowell, 1993). PAX6 mutations have also been revealed to cause changes in the olfactory epithelium and cerebral malformation (Sisodiya et al., 2001).

A previous PhD student at the University of Nottingham, Luke Flatt, optimised a dual-SMAD inhibition protocol using small molecules, Dorsomorphin and SB431542, to generate 52.7 +/- 1.8% $SOX1^{+}PAX6^{+}$ by day 5 of differentiation. These experiments were carried out in E8 medium and with the ReBl-PAT hiPSC line. This protocol was used throughout this chapter.

4.1.5 Directed Definitive Endoderm Formation

Endoderm lineages in vivo form several crucial organs such as the intestines, lungs, liver, pancreas and thymus. During embryonic development endoderm lineages are specified through control of BMP, WNT/β-Catenin and Activin/NODAL signalling (Zorn and Wells, 2009)(Muñoz-Descalzo, Hadjantonakis and Arias, 2015)(Graham et al., 2014). In vitro differentiation methods have capitalised on this knowledge leading to the development of chemically defined definitive endoderm differentiation protocols.

A rapid screen for endodermal differential of hPSCs has been developed, which screened 1-12 µm CHIR99021 in either RPMI/B27 or RPMI/B27(-) (minus insulin). By day 2 of differentiation a petal/cobblestone morphology typical of definitive endoderm was noted, with RPMI/B27(-) + 4 µm CHIR99021 induced the highest upregulation of definitive endoderm markers, FOXA2, SRY-Box 17 (SOX17), Haematopoietically-Expressed Homeobox Protein (HHEX) and Cerberus 1 (CER1). Immunostaining identified ~85% of cells were SOX17+ by differentiation day 2 (Siller et al., 2016).

In this chapter we focus on FOXA2 and SOX17 as markers for definitive endoderm.

4.1.6 FOXA2

In mice, Foxa2 has been shown to specify endoderm in the posterior epiblast, which undergo epithelial-to-mesenchymal transition (EMT) to invade the primitive streak and differentiate into 'flattened' cells with apical-basal polarity, with Foxa2 regulating this cellular phenotype during early development (Burtscher, Lickert and Joyner, 2009). A conditional mutation to Foxa2 in developing mouse embryos resulted in head truncations, through disrupted axial mesendoderm formation, leading to poor specification of the anterior definitive endoderm (Hallonet et al., 2002).

SOX17

3D time-lapse imaging tracked presumptive definitive endoderm progenitors through the primitive streak to the mesoderm and subsequently to the embryo surface where they contact the visceral endoderm, Sox17 was shown to be a key orchestrator of this cellular migration. Sox17 was shown to be involved in gut endoderm morphogenesis and the assembly of the basement membrane, separating gut endoderm from mesoderm (Viotti, Nowotschin and Hadjantonakis, 2014). Sox17-null mice are deficient in gut endoderm (Kanai-Azuma et al., 2002).

Following on from the work of Siller et al., 2016, previous PhD student, Luke Flatt from the University of Nottingham, optimised the concentration of CHIR99021 on cell lines used within our laboratory, with 2 µM being the optimal concentration to support a high cell number in combination with 70% dual positive of SOX17/FOXA2

definitive endoderm markers. Hence this concentration of CHIR99021 in RPMI/B27(-) was used throughout this study.

4.2 Intracellular Signalling Pathways

To investigate functional differences at the phosphokinase proteome level between 15-day cultures on Matrigel or the best performing synthetic polymer, microarrays to detect phosphorylation changes were utilised. The phosphorylation state of kinases from key pathways relating to proliferation and survival (AKT, mTOR, MAPK/ERK), DNA damage response and apoptosis (P53) and proliferation/differentiation (Wnt) were probed.

4.2.1 PI3K-AKT Pathway

The PI3K-AKT pathway modules a plethora of functions within the cell, including metabolism, growth, proliferation and survival (Yu and Cui, 2016). In cellular metabolism Akt can regulate glucose uptake and lead to post-transcriptional modification of the glucose metabolism, resulting in Bax inhibition and long-term cellular survival even in the absence of growth factors (Rathmell et al., 2003)(Fan, Dickman and Zong, 2010). Additionally, by upregulating glucose uptake the PI3K-AKT-mTOR pathway is important in maintaining pluripotency by providing a steady source of acetyl-CoA, which maintains pluripotency by histone acetylation (Moussaieff et al., 2015)(Yu and Cui, 2016)(Moris et al., 2018).

4.2.2 mTOR Pathway

The mammalian target of rapamycin (mTOR) is an evolutionary conserved 289kDa serine/threonine kinase of the PI3K-related kinase family, mTOR acts as a central component of two separate complexes, mTORC1 & mTORC2.

4.2.3 mTORC1

mTORC1 is a 5-member complex including mTOR, regulatory-associated protein of mTOR (Raptor), mammalian lethal with Sec12 protein 8 (mLST8), proline-rich AKT substrate 40kDa (PRAS40) and DEP-domain-containing mTOR-interacting protein (Deptor) (Mathieu Laplante and Sabatini, 2009). mTORC1 activation is linked to AKT activation by growth factors, where AKT can phosphorylate PRAS40 leading to an increase in mTORC1 activation (Mathieu Laplante and Sabatini, 2009). Additionally, stimulation of the extracellular-signal-regulated kinase 1/2 (ERK1/2) and p90 ribosomal S6 kinase 1 (RSK1) can also lead to mTORC1 activation via tuberous sclerosis complex (TSC) 1/2 inhibition (Mathieu Laplante and Sabatini, 2009)(Roux et al., 2004).

mTORC1 is thought to be a master regulator of cell growth, proliferation and metabolism through the upregulation of anabolic processes increasing organelle, lipid and protein synthesis (Mathieu Laplante and Sabatini, 2009)(Porstmann et al., 2008).

In the context of pluripotent stem cells, rapamycin-mediated inhibition of mTORC1 leads to the loss of pluripotency in hESCs, additionally a CDK inhibitor failed to rescue pluripotency demonstrating the effect was not just due to growth inhibition (Zhou et al., 2009).

4.2.4 mTORC2

Relative to mTORC1 relatively little is known about the activity of mTORC2, like mTORC1, mTORC2 is formed of a complex of proteins with mTOR at the centre (Mathieu Laplante and Sabatini, 2009).

4.2.5 TOR Phosphorylation S2448

The phosphorylation site S2448 on mTOR is present on the phosphokinase proteome array used in this chapter, the function of S2448 has recently been linked to the activity of mTORC1 but not mTORC2, where phosphorylation increases activity of mTORC1 and inhibition of S2448 phosphorylation decreases mTORC1 activity (Rosner et al., 2010).

4.2.6 MAPK/ERK Pathway

Mitogen-activated protein kinase (MAPK) can respond to growth factors, cytokines and stress responses through extracellular signal related kinases (ERKs), jun amino-terminal kinases (JNKs) or stress activated protein kinases (p38/SAPKs). Whilst the MAPK pathways are extensive this thesis will focus on classical ERK1/2 specific signalling.

4.2.7 ERK1/2

ERK1/2 signalling is a response primarily to growth factors and mitogens that activate a wide range of transcription factors in the nucleus relating to cell growth, proliferation and differentiation (Morrison, 2012).

The Ras-Raf-MEK-ERK signalling cascade is well studied for its ability to control cellular proliferation and mediate apoptosis. MEK1/2 activation results in the phosphorylation of threonine and tyrosine residues on ERK1/2 on Thr-Glu-Tyr (TEY) recognition sites (Mebratu and Tesfaigzi, 2009). Inside the nucleus activated ERK1/2 phosphorylates factors such as TIF-IA, Sap-1a and Elk-1 leading to increased binding to the serum response factor, enhancing growth related transcription. ERK1/2 phosphorylates FOXO3a at S294, S344 and S425 leading to FOXO3a degradation by

the MDM2-depedendent ubiquitin-proteasome pathway, leading to increased cell survival (Mebratu and Tesfaigzi, 2009).

In human pluripotent stem cell culture the addition of 100 ng/mL bFGF promotes maintenance of pluripotency through MAPK and subsequent ERK1/2 activation, withdrawal of bFGF led to a fall in OCT4, SOX2 and NANOG protein levels, which was linked to a decrease in p-MAPK and p-ERK1/2 and differentiation (Haghighi et al., 2018). Conversely to mouse embryonic stem cells, high levels of ERK1/2 signalling for maintaining a pluripotent human embryonic stem cell state (Li et al., 2007).

4.2.8 P53 Signalling

P53 is a critical tumour suppressor through its ability to induce cell cycle arrest, DNA repair and apoptosis pathways in response to a multitude of stress signals, beyond these key functions p53 is also implicated in metabolic regulation and autophagy, although these are beyond the scope of this chapter (Laptenko and Prives, 2006)(Brady and Attardi, 2010). The activation of P53 is dependent on the stabilisation of a homotetrameric complex and post-translational modifications, P53 has a relatively short half-life of 5-20 minutes (Giaccia and Kastan, 1998)(Brady and Attardi, 2010). In this thesis three phosphorylation states of P53 are investigated, S15, S392, and S46.

4.2.9 Serine 15 Phosphorylation

Phosphorylation of p53 at S15 is thought to provide a universal role, with a basal level of S15 phosphorylation present in unstimulated cells (Loughery et al., 2014). When DNA damage occurs S15 is a primary target for phosphorylation by ATM

and ATR protein kinases leading to accumulation (Banin et al., 1998)(Cheng and Chen, 2010).

In the presence of metabolic stress or glucose deprivation, AMPK protein kinase will increase in activity and lead to increased S15 phosphorylation of P53, to induce cell cycle arrest and promote cellular survival (Jones et al., 2005).

4.2.10 Serine 392 Phosphorylation

Phosphorylation of p53 at S392 is a common and essential event in p53 activation by a range of stimuli, evidence shows that S392 phosphorylation causes a 10-fold increase in p53 stability and enhanced DNA binding (Du, Wu and Leng, 2016)(Cox and Meek, 2010)(Kazuyasu Sakaguchi et al., 1997).

4.2.11 Serine 46 Phosphorylation

P53 phosphorylation at S46 is linked to expression of apoptosis related genes such as p53AIP1 but is not linked to cycle cell arrest. During the induction of apoptosis S46 phosphorylation is increased, interesting it found S15 phosphorylation was largely unchanged (Smeenk et al., 2011).

Assessing the changes in the phosphorylation states of S392, S15 and S46 will be essential to determine if growth on polymeric surfaces cause extra cellular stress and apoptosis.

4.3 Summary of Chapter 4 Aims

1.) Scale-up of hits from Chapter 3 spotted as ~200 to 300 µm arrays to 0.32 cm^2 and 9 cm^2 on tissue culture plastic surfaces.

2.) To test key hits for, hPSC serial passaging for at least 5 passages, ability to maintain expression of pluripotency markers & differentiate to the three germ layers.

3.) To determine the mechanisms of cell attachment and survival of hPSCs cultured on the scaled hits in point (2).

4.4 Chapter Overview

Work carried out in this chapter initially sought to test a range of scaled-up materials in 96-well formats for their capability to support 72-hour culture of ReBl-PAT hiPSCs in E8 medium without further passaging.

Scale-up work began in a set-up, optimisation of the UV lamp heigh was required as the close distance (10 cm) of the UV-lamp induced heat & oxygen-related polymer surface deformations, when multiple batches of plates were created back-to-back. This was optimised through changing the height of the UV bulb, success was assessed by the continual production of optically transparent smooth surfaces.

Despite optimisation of the UV set-up & process, variability and toxicity remained a key issue with this project over the span of 1-year. The replacement of the UV glove box, for a system that allowed for greater control of the O_2 concentration in the argon atmosphere, resulted in a reduction in toxicity & variability. However, this means experimentation had to be repeated within this chapter.

Contamination of Gibco™ Essential 8 medium with albumin in some batches, has been suspected to cause variation in cell response to synthetic surfaces discovered in this thesis. However, with batch-to-batch albumin screening by mass

spectrometry, serial passaging was achieved with a chosen synthetic surface, allowing a detailed assessment of the pluripotency state and attachment mechanism.

Due to these difficulties, early scale-up was not quantified and some experiments had to be repeated after optimisation of the polymerisation process.

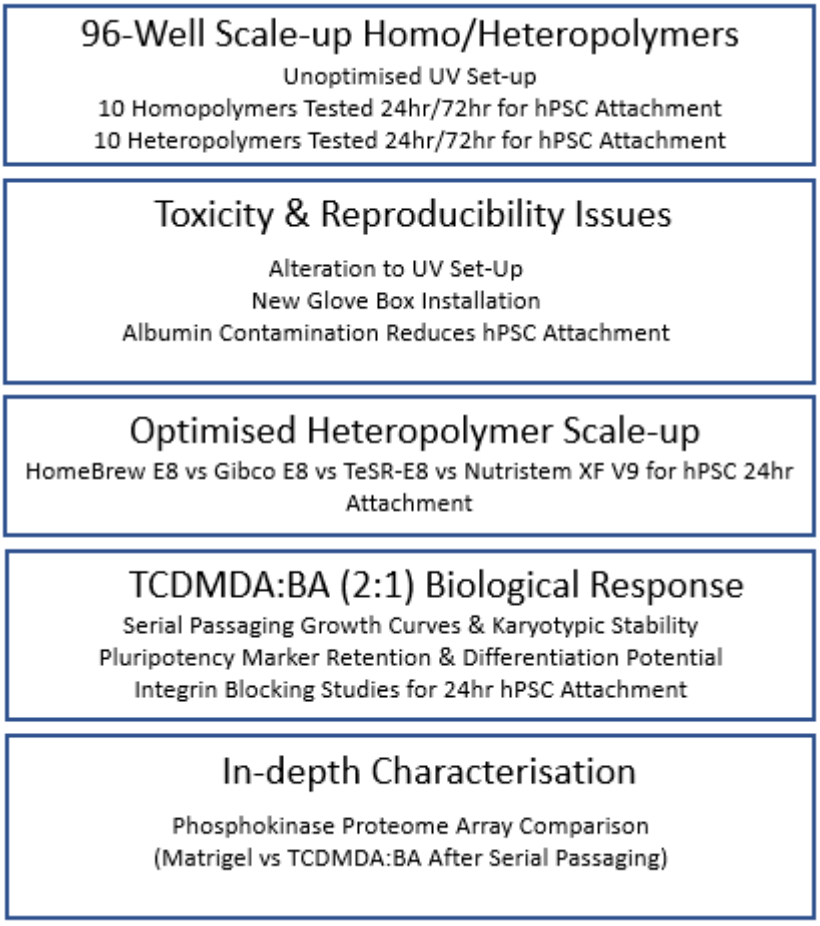

Figure 4.1 Chapter Summary of Key Experimentation Performed.

4.4.1 Preparation of Scaled-Up Materials

To assess the ability for hit materials to support a minimum of 5 serial passages whilst retaining pluripotency, they required scaling up from the array format. Scale-up of materials throughout this chapter consisted of UV initiated polymerised monomers.

Originally a 50/50 v/v mix of monomer to solvent was prepared with the addition of 2,2-dimethoxy-2-phenyl acetophenone (1% w/v) photo initiator, the UV bulb (365 nm) raised 10 cm above the surface (Figure 4.2 (A)). The 1hr UV polymerisation reaction took place in an argon atmosphere, where measured oxygen levels were below 2000 ppm.

During this time the UV light would breakdown the photo initiator into free radicals, which then caused the acrylate groups to react following the pathway shown in Figure 4.2 (B). To ensure sterility the surfaces were UV-sterilised in a class II cell culture cabinet for 25 minutes, followed by washing steps with either PBS or dH_20.

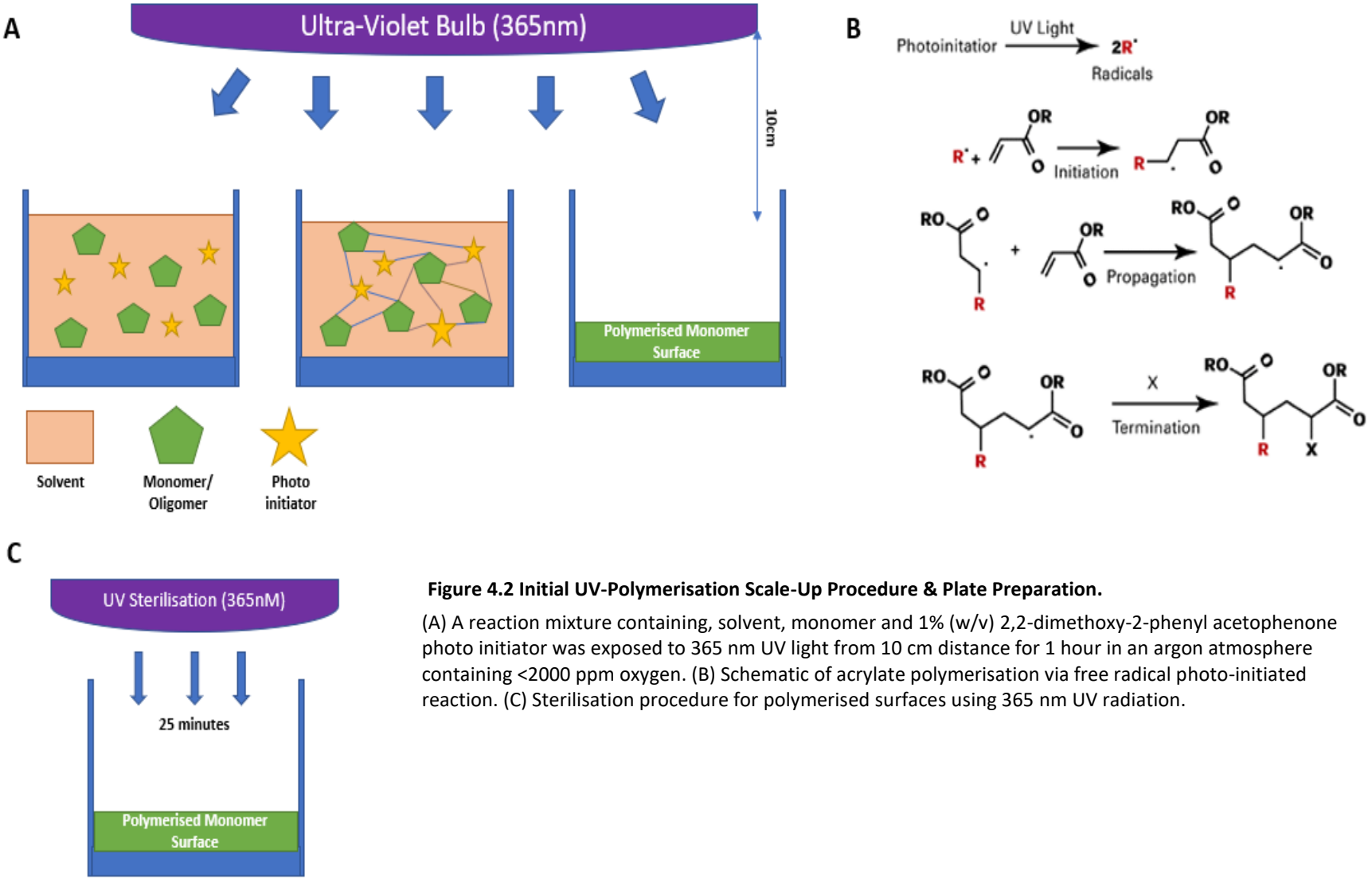

Figure 4.2 Initial UV-Polymerisation Scale-Up Procedure & Plate Preparation.

(A) A reaction mixture containing, solvent, monomer and 1% (w/v) 2,2-dimethoxy-2-phenyl acetophenone photo initiator was exposed to 365 nm UV light from 10 cm distance for 1 hour in an argon atmosphere containing <2000 ppm oxygen. (B) Schematic of acrylate polymerisation via free radical photo-initiated reaction. (C) Sterilisation procedure for polymerised surfaces using 365 nm UV radiation.

4.5 Results

4.5.1 Scale-up of Homopolymers for hPSC Culture

With a suitable method to prepare scaled-up materials for testing, 10 homopolymers previously selected for co-polymerisation in chapter 3 (hits shown Figure 4.3) were UV polymerised into a 96-well format.

Undifferentiated Rebl-PAT hiPSCs were seeded at ~57,100 cells/cm^2 in the presence of ROCKi and assessed for their 24-hour and 48-hour survival in Figure 4.4 (A). Initial scale-up testing was designed to be a quick litmus test, to determine which materials should be tested further, hence no quantification of attachment was performed. To ensure quality and health of the hiPSC ReBl-PATs used and to rule out toxicity related to production steps (e.g. plasma etching, prolonged UV exposure to TCP) a Matrigel™ control was also seeded on the same plate at a density of ~28,000 cells/cm^2.

Culture was carried out through to 72 hours, with ROCKi added for the first 24 hours. Representative images of hPSC cultured on synthetic substrates up to 48 hours can be found in Figure 4.4 (B). The continued addition of ROCKi up to the 48-hour time point was performed for top performing monomer tetrahydrofurfuryl acrylate (THFuA), in (C), whilst cells persisted – cell death was also apparent. Continued culture to 72 hours, without further ROCKi supplementation, resulted in a ~100 % loss of viability, like that observed if ROCKi was removed post-24-hour culture. Continually addition of ROCKi was shown not to be a viable strategy for continued hPSC survival on synthetic surfaces.

To meet the objectives of this chapter, namely to develop synthetic surfaces that support not only 72-hour culture but also serial passaging, co-polymers discovered in chapter 3 were scaled-up in the same manner for investigation.

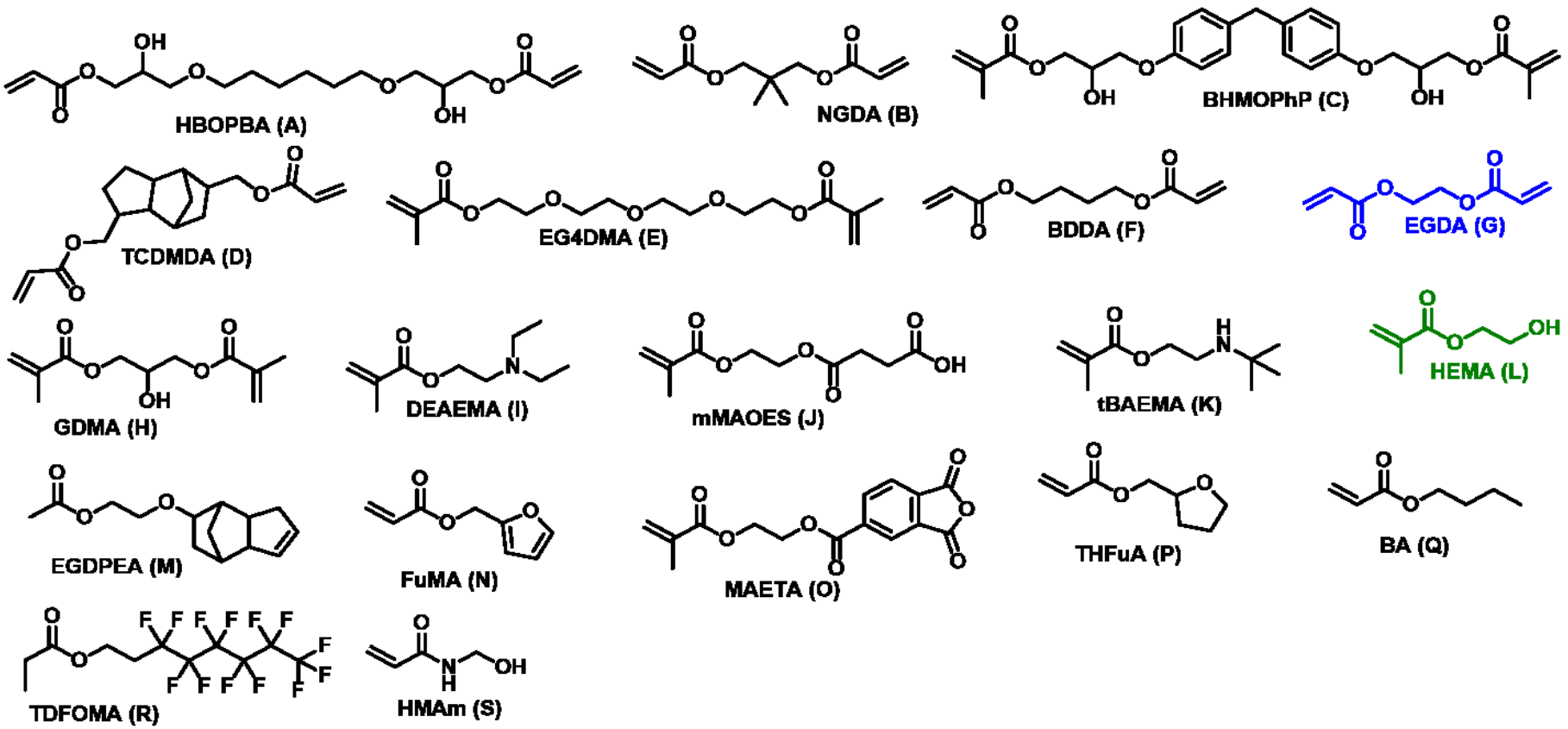

Figure 4.3 Monomer Hits Taken from 1st Generation Polymer Microarray Screen with ReBl-PAT hiPSCs, to be used in a 2nd Generation Array.

Selection was based on 24-hour and 48-hour data, 4% & 6% pHEMA data, with a range of high, medium and low performing monomers selected, with chemical diversity considered. HEMA (L) included due to change in biological response between 4% & 6%, and work carried out by Celiz *et al.,* 2015.

A

Polymer Identity	Concentration (% Total Volume)	Solvent Used	Experiment 1 – 57,000 cells/cm²Seed Density 24hr Survival	Experiment 1 – 57,000 cells/cm² Seed Density 48hr Survival	Experiment 2 – 57,000 cells/cm² Seed Density 24hr Survival	Experiment 2 – 57,000 cells/cm2 Seed Density 48hr Survival
HBOPBA	50	Isopropanol				
THFuA	50	Isopropanol				
NGDA	50	Isopropanol				
BDDA	50	Isopropanol				
TCDMDA	50	Isopropanol				
mMAOES	50	Isopropanol				
EGDA	50	Isopropanol				
EGDPEA	50	Isopropanol				
tBAEMA	50	Isopropanol				
DEAEMA	50	Isopropanol				

Alive

Dead

C

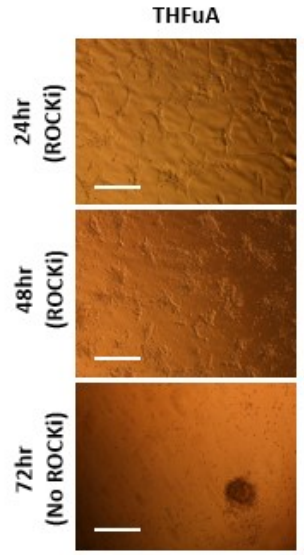

B

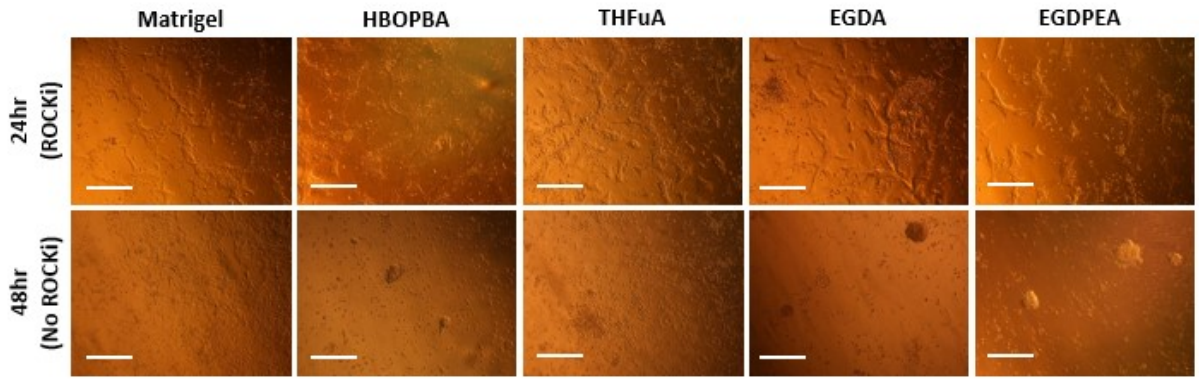

Figure 4.4 96-Well UV-Polymerisation Scale-Up of Ten Selected Hits Taken Forward from Homopolymer Array 9.1.
Polymers cultured with ReBl-PAT hiPSCs, in HomeBrew Essential 8 medium. (A) Summary table detailing; identity, concentration (v/v), solvent used and survival. (B) Representative images of a subset of scaled-up polymers at 24-hour culture with the addition of apoptosis inhibitor ROCKi, and 48-hour culture without ROCKi. (C) Culture of top performing 24-hour homopolymer THFuA, with continued ROCKi use for 48 hours. Scale bars = 100 µm

4.5.2 Scale-up of Hit 48-hour/72-hour Co-Polymer Hits for hPSC Culture

To discover if any of the co-polymer microarray hit materials can support culture of hPSCs, 10 selected co-polymers were scaled up as previously described into 96-wells (Figure 4.5). ReBl-PAT hiPSCs were cultured at either 57,000 cells/cm^2 or 114,000 cells/cm^2, co-polymers were tested if they supported 24-hour culture in the presence of ROCKi and continued culture to the 72-hour time-point. At the highest seeding density of 114,000 cells/cm^2, 5 of the 10 co-polymers supported 72-hour culture. This number was reduced to two co-polymers when the seeding density was reduced to 57,000 cells/cm^2, namely NGDA:THFuA & TCDMDA:BA. Three separate wells were imaged for both NGDA:THFuA & TCDMDA:BA (Figure 4.6 (B)).

Testing the ability of ReBl-PAT hiPSCs to survive on TCP treated with oxygen plasma determined that the addition of a polymer surface had an additive effect on the 72-hour survival and colony formation of hiPSCs, Figure 4.6 (B) vs (C). MAETA containing co-polymers could not be fully dissolved in isopropanol, whilst a 50/50 v/v mixture of isopropanol & acetone was an improvement, MAETA could not be entirely dissolved. In conclusion the co-polymers NGDA:THFuA & TCDMDA:BA were both of interest to investigate their 72-hour culture capabilities further.

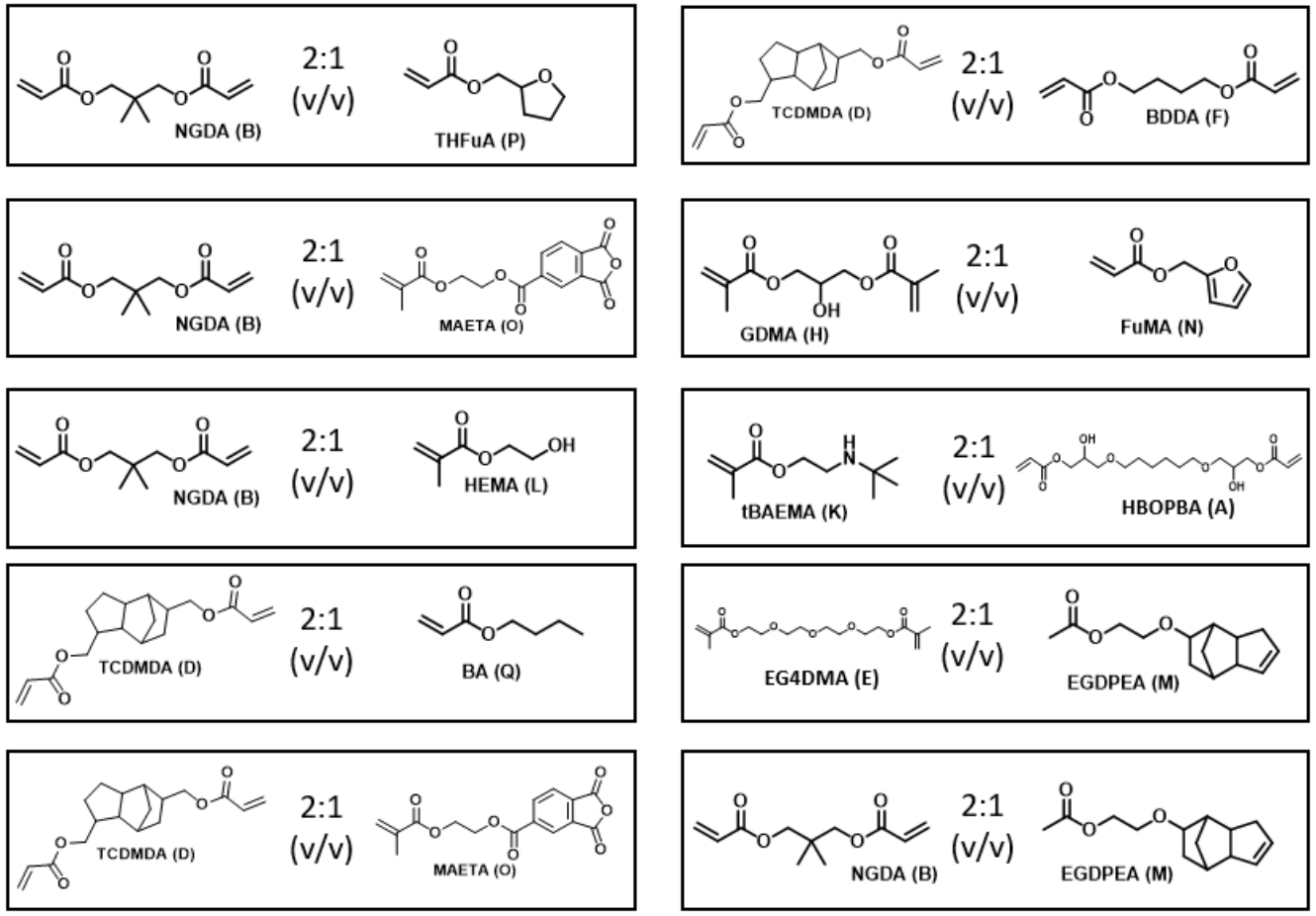

Figure 4.5 Co-Polymer Hits from 2nd Generation Polymer Microarray Screen with ReBl-PAT hiPSCs Selected for Scale-Up with UV-based Polymerisation.

A

Polymer Identity	Concentration (% Total Volume/Mass)	Solvent Used	Experiment 1 – 114,000 cells/cm² Seed Density 24hr Survival	Experiment 1 – 114,000 cells/cm² Seed Density 72hr Survival	Experiment 2 – 57,000 cells/cm² Seed Density 24hr Survival	Experiment 2 – 57,000 cells/cm² Seed Density 72hr Survival	Experiment 3 – 57,000 cells/cm² Seed Density 24hr Survival	Experiment 3 – 57,000 cells/cm² Seed Density 72hr Survival
NGDA:THFuA (2:1)	50	Isopropanol						
NGDA:MAETA (2:1)	50	IPA/Acetone						
NGDA:HEMA (2:1)	50	Isopropanol						
TCDMDA:BA (2:1)	50	Isopropanol						
TCDMDA:MAETA (2:1)	50	IPA/Acetone						
TCDMDA:BDDA (2:1)	50	Isopropanol						
GDMA:FUMA (2:1)	50	Isopropanol						
tBAEMA:HBOPBA (2:1)	50	Isopropanol						
EG4DMA:EGDPEA (2:1)	50	Isopropanol						
NGDA:EGDPEA (2:1)	50	Isopropanol						

Alive

Dead

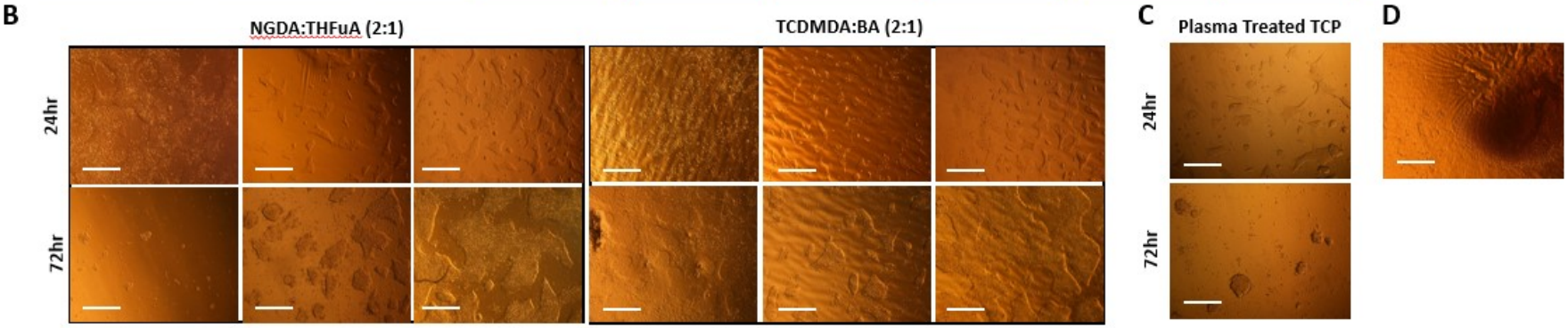

Figure 4.6 96-Well UV-Polymerisation Scale-Up of Ten Selected Co-Polymer Hits from Array 10.1.

Cultured with ReBl-PAT hiPSCs in HomeBrew Essential 8 medium. (A) Summary table detailing; identity, concentration (v/v), solvent used and survival. (B) Triplicate brightfield images of either NGDA:THFuA (2:1) or TCDMDA:BA (2:1) at 24-hour and 72-hour timepoints. (C) Culture onto oxygen plasma activated tissue culture plastic with the same conditions shown in (B). (D) Polymer aggregation after UV-polymerisation onto the surface, resulting in cell toxicity. Scale bars = 100 µm.

4.5.3 Serial Passaging

To demonstrate if NGDA:THFuA can support multiple polymer-to-polymer passages, hiPSC ReBl-PATs were dissociated after 72 hours culture from wells shown in Figure 4.7 (A), using TrypLE select and a 1:4 seeding ratio into unused 96-wells coated with NGDA:THFuA. Whilst cell coverage of the starting NGDA:THFuA reached monolayer in most areas, variation demonstrated in (B) highlights that areas with lower or no cell survival by 72 hours culture were present.

Culture of hiPSCs on NGDA:THFuA was demonstrated across three sets of polymer coated wells, passaging polymer-to-polymer, however 24-hour toxicity was observed but not quantified on plate 4. A second biological repeat using the same cell line was less successful, with rounded colony formation and colony detachment occurring as shown in Figure 4.7 (D).

Results shown here reveal that NGDA:THFuA is capable of supporting polymer-to-polymer passaging, an important step forward to meeting the goals of this thesis chapter. However, intra & inter-plate variation, including unpredictable complete cell death / toxicity at the 24-hour time point proved problematic, and variation in colony spreading & attachment strength to the surface was also evident.

Further improvements to polymer surface production & optimisation will be required to create a cell culture surface capable of reproducible polymer-to-polymer hPSC culture.

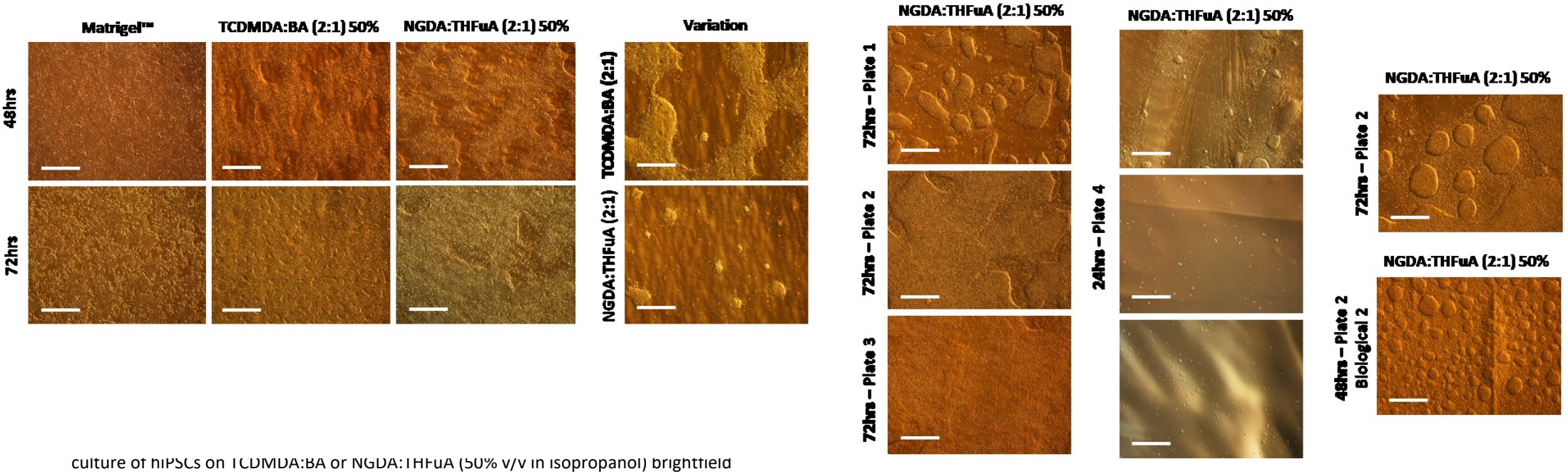

culture of hiPSCs on TCDMDA:BA or NGDA:THFuA (50% v/v in isopropanol) brightfield images of 24-hour and 72-hour culture. (B) Demonstration of variability of hiPSC survival and colony formation at 72-hour culture on polymer surfaces. (C) Brightfield images demonstrating the ability of hiPSCs to be passaged across three plates. Cells were passaged at a 1:4 ratio using TrypLE select. (D) Second biological repeat of multi-passage culture on NGDA:THFuA demonstrating rounded colony morphology. Scale bars = 100 μm.

4.5.4 6-Well Scale-Up

Production of scaled-up versions in 6-well plates was essential to meeting the aims of this chapter, to demonstrate synthetic surfaces can be fabricated at sizes regularly used for the maintenance of hPSC cultures. T25 and enclosed vessels were not selected due to the possibility that the flask walls would interfere with the UV radiation reaching the polymerisation reaction.

To produce a scaled-up version of a polymeric surface for hPSC culture, the surface size was increased from 0.32 cm^2 to 9.6 cm^2 by polymerising monomer solutions in 6-well plates. During which issues with the production of polymer plates became more evident, TCDMDA:BA polymerised plates produced a potent sweet smell when placed within incubator conditions (Figure 4.8 (A)), the production of multiple batches of plates in short succession caused visible deformations to the polymer surface, which induced cell toxicity during culture.

Over a range of optimisation experiments, the height of the UV bulb was increased from 10 cm to 20 cm, solvent use was reduced from 50% v/v to 10% v/v (10% v/v kept to dissolve the photo initiator), and an increase in cell seeding density by 10,400 cells/cm^2 to increase cell survival across the entire culture surface. Polymeric surfaces were washed once in isopropanol and three times in dH_20 for 1 minute each before being incubated in dH_20 for 48 hours in a 37^oC oven, surfaces were washed three further times after UV polymerisation with dH_20 and incubated at 37^oC until ready for use (Figure 4.8 (B)). Success was judged by the elimination of the potent sweet smell of TCDMDA:BA, likely generated from unpolymerized butyl acrylate, the presence of this odour suggested that full polymerisation was not taking

place. In hindsight, GPC or similar characterisation methodology would have determined the chemical state of the surface.

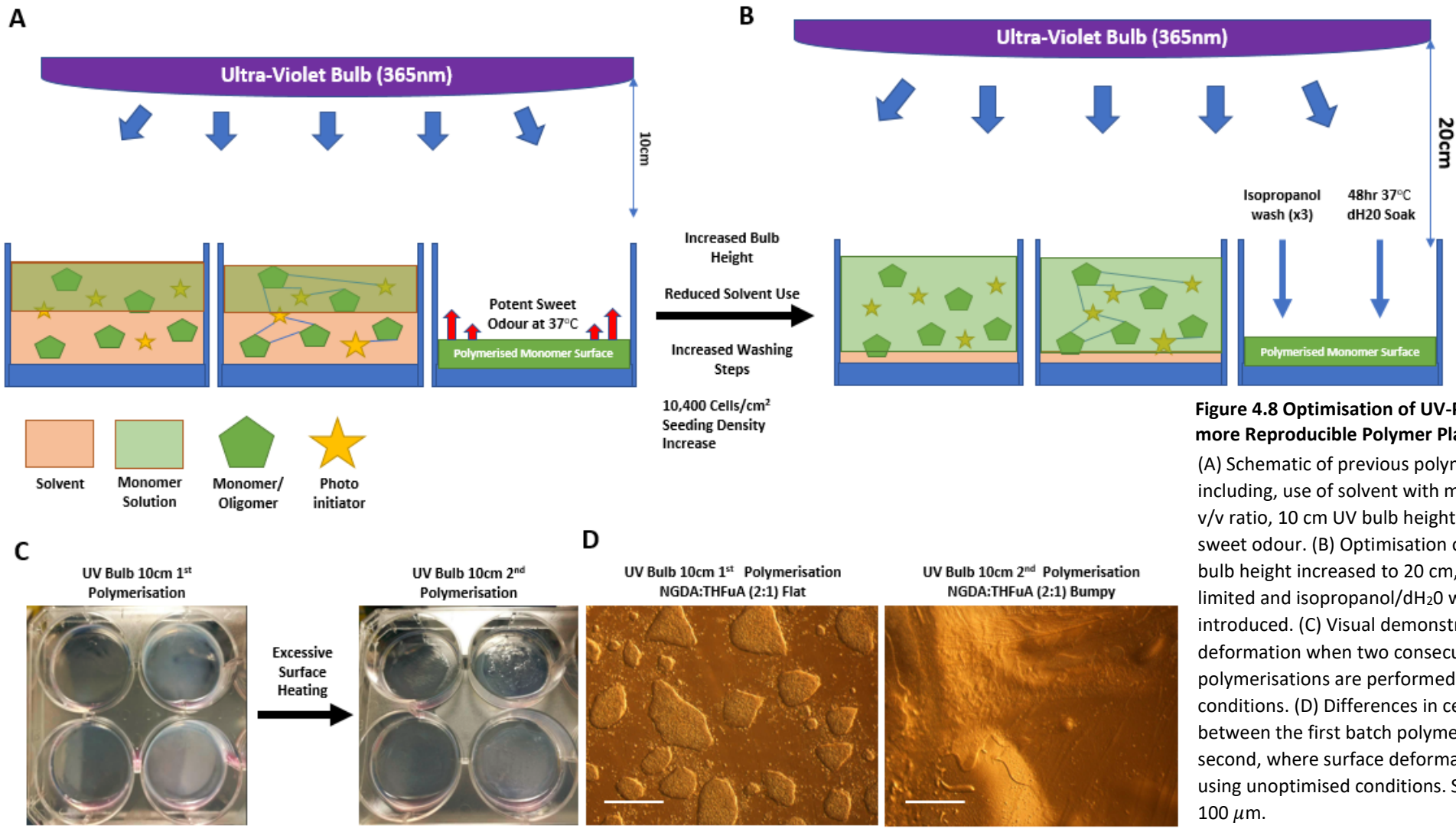

Figure 4.8 Optimisation of UV-Polymerisation for more Reproducible Polymer Plate Production.

(A) Schematic of previous polymerisation set-up including, use of solvent with monomer at 50/50 v/v ratio, 10 cm UV bulb height & characteristic sweet odour. (B) Optimisation of conditions, UV bulb height increased to 20 cm, solvent use limited and isopropanol/dH_20 washing steps introduced. (C) Visual demonstrate of surface deformation when two consecutive polymerisations are performed using unoptimised conditions. (D) Differences in cell response between the first batch polymerisation and the second, where surface deformation has occurred, using unoptimised conditions. Scale bars = 100 μm.

Continued work with NGDA:THFuA and TCDMDA:BA in LifeTech™ Essential 8 medium, whilst generally improved, continued to be problematic at the 6-well scale with variability at seemingly random points within polymer-to-polymer culture. Despite the ~10,400 cells/cm^2 seeding density increase to 73,000 cells/cm^2, it was observed that cell survival could be limited to the central area of the well. It was theorised that poor seeding technique or the creation of a convex architecture during polymer coating could be responsible for this seemingly random occurrence.

Both NGDA:THFuA and TCDMDA:BA proved problematic for variability, TCDMDA:BA was capable of culturing ReBl-PAT hiPSCs in LifeTech™ Essential 8 medium up to passage 10 or passage 8 in biological repeat 1 and 2, as shown in Figure 4.9 (A). During early stage of culture (first two passages) across both biological repeats the average cumulative population doubling on TCDMDA:BA was 64.8% of that compared to Matrigel™, passages 7 & 8 maintained on average 57% of the cumulative population doubling across the two repeats, the reduction in cumulative population was in-part due to seemingly random issues with cell attachment and spreading leading to less than a single population doubling during specific passages within culture shown in Figure 4.9.

Images demonstrating central monolayer culture, variation in cell coverage and 3D-like folding of cells during culture are shown in Figure 4.9 (B). At passage 6 samples for both Matrigel™ controls and TCDMDA:BA had their karyotype analysed, both samples maintained a healthy 46(XY) karyotype across 30 cells examined by Dr. Nigel Smith (Department of Cytogenetics at Nottingham University Hospital NHS Trust) (Figure 4.9 (C & D)).

Assessment of hPSC pluripotency and differentiation capabilities were performed after 5 serial passages on TCDMDA:BA. To assess if hPSCs cultured on TCDMDA:BA after serial passaging still possessed markers of pluripotency, three nuclear markers: OCT4, NANOG, SOX2, and one surface marker: TRA-1-81, were immunostained. hPSCs cultured after serial passaging on TCDMDA:BA demonstrated positivity for all four markers as shown in Figure 4.10. A comparison between Matrigel™ and TCDMDA:BA is shown with fluorescent gating kept the same between the two conditions, the loss of expression on Matrigel™ for OCT4 (69% +/- 19%), NANOG (58% +/- 19%) and SOX2 (36% +/- 27%) which suggested that the high seeding density, used to draw accurate growth comparisons, was too high to maintain pluripotency marker expression. Population doubling time on Matrigel™ was between 19-25 hours.

A second cell line, HUES7 (hESCs), was cultured on TCDMDA:BA to investigate how multiple cell lines perform after serial passaging. HUES7s were cultured in HomeBrew Essential 8 medium for this experiment. HomeBrew Essential 8 medium is an in-house equivalent of LifeTech Essential 8 medium, where the addition of 100 ng/mL heparin is thought to be the sole difference, heparin was added for growth factor stability. To maintain pluripotency on Matrigel™, the seeding densities on Matrigel™ was decreased from 73,000 to 41,700 cells/cm^2, however it was kept at 73,000 cells/cm^2 for TCDMDA:BA.

The average cumulative population doubling across both HUES7 repeats, shown in Figure 4.10 (B), was 81% compared to Matrigel™ culture. An average 23.4

+/- 3.2-hour doubling time was maintained on Matrigel™, consistent with experimentation with ReBl-PAT hiPSCs in LifeTech™ Essential 8 medium.

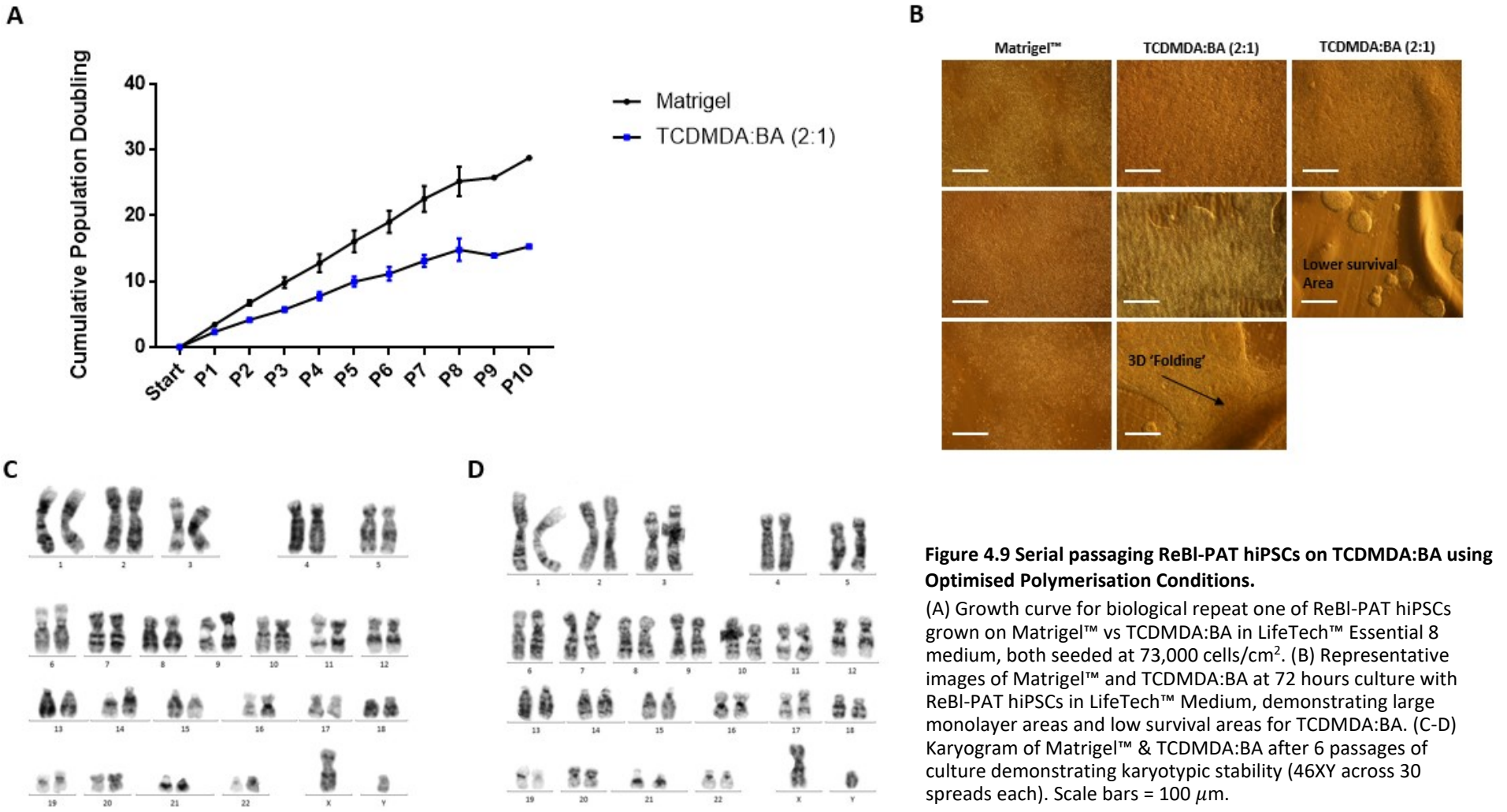

Figure 4.9 Serial passaging ReBl-PAT hiPSCs on TCDMDA:BA using Optimised Polymerisation Conditions.

(A) Growth curve for biological repeat one of ReBl-PAT hiPSCs grown on Matrigel™ vs TCDMDA:BA in LifeTech™ Essential 8 medium, both seeded at 73,000 cells/cm^2. (B) Representative images of Matrigel™ and TCDMDA:BA at 72 hours culture with ReBl-PAT hiPSCs in LifeTech™ Medium, demonstrating large monolayer areas and low survival areas for TCDMDA:BA. (C-D) Karyogram of Matrigel™ & TCDMDA:BA after 6 passages of culture demonstrating karyotypic stability (46XY across 30 spreads each). Scale bars = 100 μm.

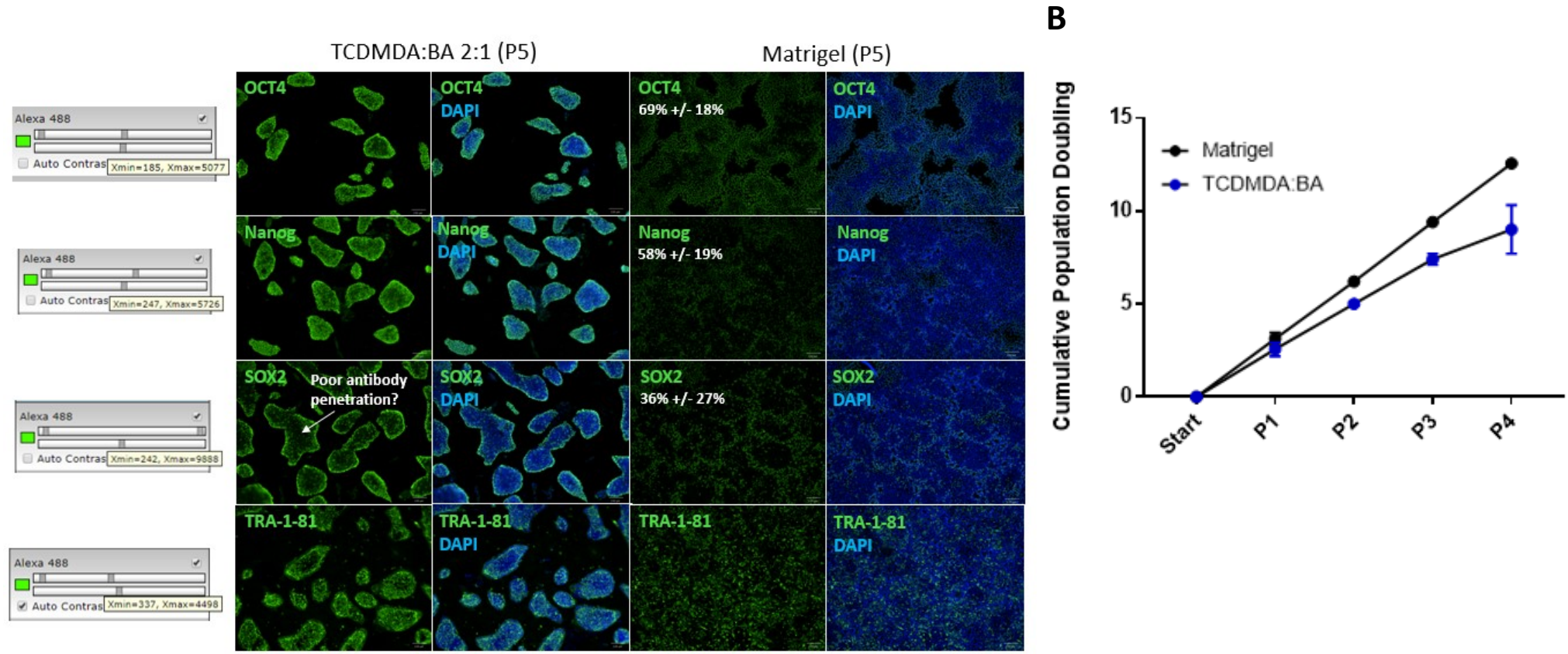

Figure 4.10 Pluripotency Staining of ReBl-PAT hiPSCs Grown on TCDMDA:BA for Five Passages.

(A) 72-hour growth of ReBl-PAT hiPSCs grown on Matrigel™ or TCDMDA:BA in LifeTech™ Essential 8 medium, both seeded at 73,000 cells/cm^2. Cells were immunostained for pluripotency markers: OCT4, NANOG, SOX2 & TRA-1-81. Images are displayed with the same intensity gating between Matrigel™ & TCDMDA:BA. (B) Cumulative population doubling of HUES7 hESCs cultured on Matrigel™ and TCDMDA:BA, seeding densities 41,700 cells/cm^2 & 73,000 cells/cm^2 respectively . Scale bars = 100 μm.

4.5.5 LifeTech Essential 8 Albumin Contamination

Observations that HomeBrew Essential 8 cultured cells appeared to perform better in terms of initial attachment and spreading by 24 hours in culture, on TCDMDA:BA, compared to LifeTech Essential 8 cultured cells prompted an investigation into the media compositions. HomeBrew Essential 8 medium is prepared in-house, with a known formulation, in theory HomeBrew Essential 8 is identical to LifeTech Essential 8 medium, bar the addition of 100 ng/mL porcine derived heparin sulphate, which is added to improve growth factor stability and therefore shelf life of HomeBrew Essential 8.

A mass spectrometry analysis of two commercial essential 8 media (LifeTech and TeSR) and the in-house prepared HomeBrew essential 8 medium by Joris Meurs revealed the suspected presence of albumin in LifeTech essential 8 medium, that was not present in either other two types of media (Figure 4.11 (A,B,C)). The presence of albumin was confirmed through protein digest experiments, where detected fragments were compared against the SwissProt and NCBIProt databases for known albumin fragment identities. MASCOT values are transformed p-values, where [Value=-10log(p)]. A calculator from MatrixScience.com (Mascot Search Results) determines that a protein score greater than 97 represents a p-value <0.0001. Two sets of digest results in Figure 4.11 (D) present values higher than 97, 127 & 116, compared to database fragment values for albumin.

ReBl-PAT hiPSCs from the same starting source were cultured for three passages (9 days) in Nutristem V9 XF, LifeTech Essential 8 or HomeBrew Essential 8 medium. ReBl-PATs from each media were seeded onto TCDMDA:BA at 73,000

cells/cm^2 onto the same polymer plate, after 24 hours culture brightfield images were taken to demonstrate comparative attachment (Figure 4.11 (E,F,G)). Nutristem V9 XF contains 10% human serum albumin and failed to support cell attachment and spreading. LifeTech Essential 8 medium claims to be an albumin-free medium, yet mass spectrometry results in Figure 4.11 (B) and digest experiments (D) evidenced albumin presence, LifeTech medium demonstrated greater attachment and spreading compared to Nutristem V9 XF but visibly lesser attachment and spreading in comparison to hiPSCs in HomeBrew Essential 8.

A different batch of LifeTech Essential 8 medium, which tested negative for the presence of albumin, was spiked with 0.1% - 10% human albumin as shown in Figure 4.11 (H). After 24 hours culture cells were fixed and stained with DAPI, imaged using Operetta high content microscope and quantified using Columbus software. With the addition of 0.1% human albumin the average DAPI count dropped from 16,113 +/- 2099 to 11,841 +/- 5830, the 277% increase in DAPI count standard deviation translated to no significant difference shown by One-Way ANOVA. When 1% human albumin was added to the medium, the average DAPI cell count was 4754 +/- 24 and One-Way ANOVA test produced a p-value of 0.005, when compared to the non-spiked control.

These results demonstrated that ≤1% concentrations of human albumin increased the variability of hiPSC attachment after 24 hours culture and 1% or greater concentrations of human albumin produced statistically significant reductions in cell number. It was important moving forward to screen batches of LifeTech Essential 8

medium using mass spectrometry for the presence of albumin, to ensure cell attachment was not hindered.

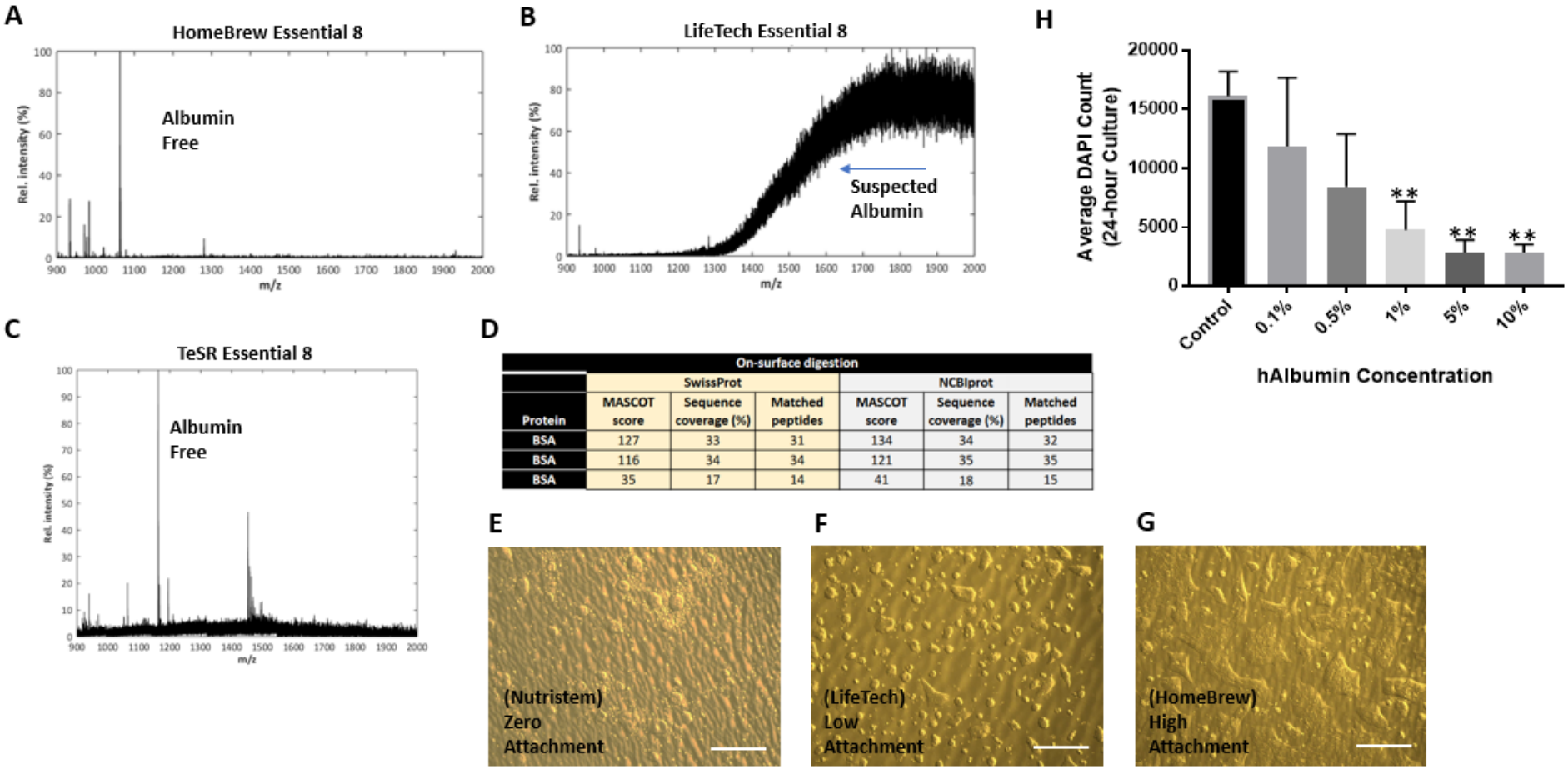

On-surface digestion						
	SwissProt			NCBIprot		
Protein	MASCOT score	Sequence coverage (%)	Matched peptides	MASCOT score	Sequence coverage (%)	Matched peptides
BSA	127	33	31	134	34	32
BSA	116	34	34	121	35	35
BSA	35	17	14	41	18	15

Figure 4.11 Analysis of Media Composition & the Effect of Albumin on hPSC Attachment to TCDMDA:BA

(A/B/C) Mass spectrometry analysis of LifeTech Essential 8, HomeBrew Essential 8 and TeSR Essential 8 media, respectively. (D) Protein digest experiments, fragments compared against SwissProt & NCBIProt databases. (E/F/G) Representative brightfield images of ReBl-PAT hiPSC attachment to TCDMDA:BA after 24 hours culture in Nutristem® V9 XF (E), LifeTech Essential 8 (F), or HomeBrew Essential 8 (G) media. Seeding densities all performed at 73,000 cells/cm^2. (H) Spiking of LifeTech Essential 8 medium (batch tested and confirmed albumin free via mass spectrometry) with human albumin, cell counts performed at 24-hour culture with ReBl-PAT hiPSCs. One-Way Anova performed using PRISM software, (**) P = <0.01. Scale bars = 100 μm. Three repeats performed.

4.5.6 UV Glove Box Installation

In order to improve the reproducibility of polymer plate production and reduce the chance of random cellular toxicity occurring, a glovebox capable of maintaining controlled atmospheric conditions was purchased.

The original system for polymerising polymer plates involved a UV lamp placed within a non-sealed box with an inlet attached for argon supply. This system relied on a constant flow of argon to displace the presence of other gases, such as oxygen, which prematurely terminates our free radical based polymerisation process. Whilst argon is heavier than oxygen with an atomic mass of 39.9 vs 15.9 respectively, meaning the lighter oxygen should be displaced, the lack of a sealed system meant air could leak back into the polymerisation chamber. Due to the poor atmospheric control of the original polymerisation chamber, an oxygen sensor would detect approximately 2000 ppm oxygen within the chamber (Figure 4.12 (A)).

The new glovebox polymerisation chamber consisted of an airtight central chamber, with a secure argon inlet and an outlet with a filter attached. Manipulation within the main chamber was performed using sealed gloves. To enter items into the main chamber, items would be placed into the sealed antechamber where a vacuum pump & argon inlet allowed the purging of oxygen from the atmosphere before items were moved into the main chamber. Improved control of atmospheric conditions within the polymerisation chamber were demonstrated by ≤200 ppm oxygen concentrations being detected with the same oxygen sensor previously used. Additionally, this new system required relatively low levels of argon use and did not release volatile acrylate monomers into the working environment (Figure 4.12 (B)).

Additionally, a new oxygen plasma etcher was sought, the original system was a custom-built plasma etcher utilising a high frequency generator. Tissue culture plastic was exposed to a 100 W plasma at $10x9^{-2}$ mbar pressure for 10 minutes and then used within 1-hour for UV-initiated polymerisation. The new oxygen plasma etcher was a commercially produced etcher, Nano plasma system produced by Diener Electronic. This system had a low-frequency plasma generator, advantageously the process was programmable and automated, ensuring consistency between runs, compared to the original system which required manual pressure and power optimisation every run.

Utilising the same pressure and power settings, the difference between the old system, high frequency generator, and the Nano plasma system, low frequency generator, was apparent after polymerisation of TCDMDA:BA was performed on oxygen plasma treated tissue culture plastic surfaces. Topographical patterns observed using the old system were not replicated when plasma etching was performed using the Nano plasma system (Figure 4.12 (C)). Despite this visual difference in the TCDMDA:BA surface using the Nano plasma system, polymerised surfaces produced in this manner were capable of supporting hPSC attachment and growth.

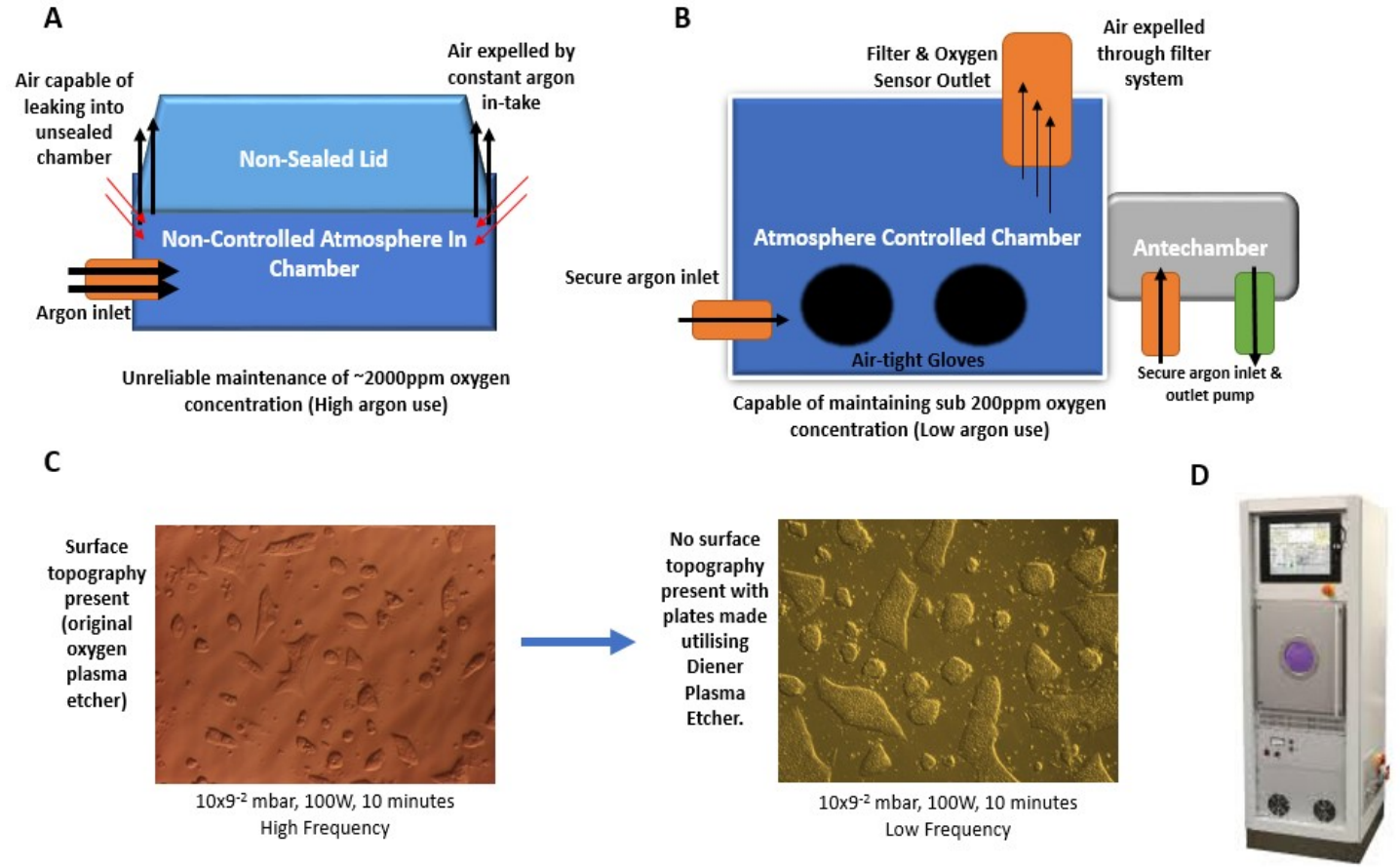

Figure 4.12 Comparison of Features and Polymer Production in Original UV-Box and New UV-Glove Box with a Controlled Atmosphere.
(A) Original UV-box for polymer plate production, argon pumped into an enclosed box, containing UV bulb, without a sealed lid or air filter. Air was capable of bi-directional travel, where rate of argon addition was relatively high to maintain outward airflow. (B) New atmosphere-controlled UV glovebox, airtight central chamber with secure valves for argon input and release of air through a chemical filter. Addition of items to the glovebox performed via an antechamber, with separate atmosphere controlled by argon inlet and vacuum pump. (C) Surface topography of TCDMDA:BA polymerised on tissue culture plastic plates plasma treated with either the original (custom build) high frequency plasma etcher or industrial Diener plasma etcher using low frequency settings. (D) Image of Nano plasma etcher.

4.5.7 Serial Passage Culture On TCDMDA:BA

Improved production of polymer surfaces through previously discussed optimisations to the polymerisation process and greater control of oxygen concentration within the polymerisation chamber allowed for the culture of hPSCs beyond 15 days, with culture up to 30 days demonstrated to be possible (Figure 4.13). Additionally, pre-screening of LifeTech Essential 8 medium to ensure the absence of albumin was vitally important.

Serial passaging beyond 15 days with the hiPSC AT1 line was performed in three types of medium, HomeBrew, LifeTech and TeSR E8, on TCDMDA:BA and Matrigel™, the gold standard culture surface, was used as a comparison. On Matrigel™ the HomeBrew medium produced the highest cumulative population doublings, 26.6 +/- 0.05 vs 24.2 +/- 1.2, against LifeTech medium. Culture with TeSR E8 was performed until day 24, where the cumulative population doubling was 18% lower than HomeBrew E8 at the same stage. Growth curves of AT1s cultured in HomeBrew, TeSR and LifeTech E8 can be found in Figure 4.13 (A), (B) and (C). A summary of all AT1 growth curves are contained within figure 4.13 (D). Multiple t-tests with the Holm-Sidak method determined no statistical significance between HomeBrew and LifeTech cumulative population doublings on Matrigel™.

Differences in the growth rate between type of media translated to culture on TCDMDA:BA, at day 24, 20 +/- 1.1 vs 16 +/- 2.0 cumulative population doublings had occurred in HomeBrew and LifeTech E8 respectively (Figure 4.13 (A) vs (C)). At the identical time point TeSR E8 demonstrated 26% lower cumulative population

doublings on TCDMDA:BA than HomeBrew E8. Despite differences being apparent, where three biological repeats existed, up to 24 days culture, adjusted p-values from multiple t-tests with the Holm-Sidak method did not determine the differences to be significant.

The ReBl-PAT hiPSC and HUES7 hESC line growth curves are shown in Figure 4.13 (E) & (F), all growth curves are summarised in (G). ReBl-PAT and HUES7 lines were cultured in LifeTech E8 medium. By day 24, on average, ReBl-PAT hiPSC populations cumulative doubled 14.8 +/- 1.7 times compared to 14.2 +/- 1.2 times with HUES7 hESCs, and 15.9 +/- 2.0 times AT1 hiPSCs. Multiple t-tests with the Holm-Sidak method produced p-values greater than 0.05 when comparing AT1 and HUES7 cumulative growth on TCDMDA:BA in LifeTech E8 medium. This demonstrates that growth between three different cell lines is consistent in the same type of medium.

A closer examination of growth differences between LifeTech and HomeBrew E8 was performed by considering the average non-cumulative population doubling at each individual passage, which coincides with each 72-hour time point. Values were averaged, made relative to the population doubling compared to growth in HomeBrew E8 medium on Matrigel, with the coefficient of variation shown (Figure 4.13 (H)). On average the individual population doublings per passage were 56.1% +/- 3.5% in LifeTech and 72.5% +/- 2.4% in HomBrew E8, when cultured on TCDMDA:BA, compared to population doublings from HomeBrew E8 culture on Matrigel™. Notably, culture in LifeTech E8 on TCDMDA:BA had an average of 18.5% +/- 9.9% coefficient of variance, higher than the average of 8.15% +/- 2% coefficient of variance from HomeBrew E8 equivalent cultures. T-tests adjusted for multiple

comparisons with the Holm-Sidaq method did not determine differences in individual population doublings to be significant between LifeTech and HomeBrew E8 culture on TCDMDA:BA.

These results show that culture in HomeBrew E8 on TCDMDA:BA may not induce a statistically important increase in population doublings however it may have an equally important role of reducing variation between passages.

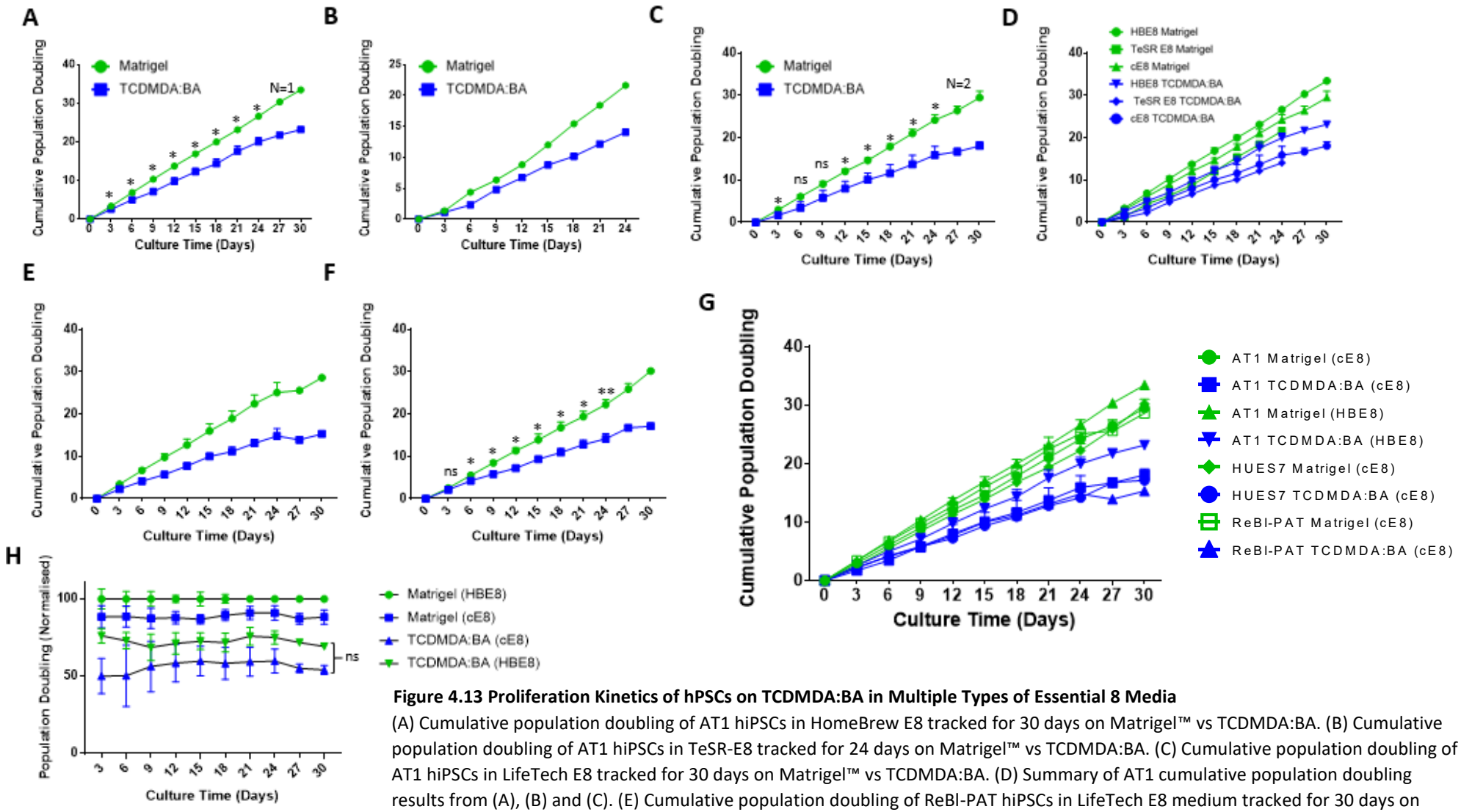

Figure 4.13 Proliferation Kinetics of hPSCs on TCDMDA:BA in Multiple Types of Essential 8 Media

(A) Cumulative population doubling of AT1 hiPSCs in HomeBrew E8 tracked for 30 days on Matrigel™ vs TCDMDA:BA. (B) Cumulative population doubling of AT1 hiPSCs in TeSR-E8 tracked for 24 days on Matrigel™ vs TCDMDA:BA. (C) Cumulative population doubling of AT1 hiPSCs in LifeTech E8 tracked for 30 days on Matrigel™ vs TCDMDA:BA. (D) Summary of AT1 cumulative population doubling results from (A), (B) and (C). (E) Cumulative population doubling of ReBI-PAT hiPSCs in LifeTech E8 medium tracked for 30 days on Matrigel™ vs TCDMDA:BA. (F) Cumulative population doubling of HUES7 hESCs in LifeTech E8 medium tracked for 30 days on Matrigel™ vs TCDMDA:BA. (G) Complete summary of growth curves presented for all cells lines and media types, Matrigel™ and TCDMDA:BA. (H) Individual passage population doubling averages normalised to Matrigel™ in HomeBrew E8 medium, coefficient of variations shown. (A-G) Standard deviations shown. Statistics performed; multiple t-tests corrected with the Holm-Sidaq correction.

4.5.8 RT-qPCR Analysis of Serially Passaged hPSCs on TCDMDA:BA

Having determined that ≥5 serial passages was possible with three cell lines on TCDMDA:BA, the next step was determining the ability of TCDMDA:BA to retain the pluripotent properties of the hPSCs. A quantitative PCR (qPCR) experiment analysed the expression of pluripotency markers OCT4, NANOG & SOX2, naïve potency markers KLF4 & ZIC1, early ectoderm markers SOX1 & PAX6, early endoderm markers SOX17 & GATA6 and early mesoderm markers HAND1 & EOMES. The 18S gene was used as a housekeeping gene in these experiments. Fold expression on TCDMDA:BA was normalised to that of the Matrigel™ counterpart. In AT1 hiPSCs cultured in LifeTech E8 for ≥5 passages, expression of all tested markers did not significantly increase, as determined by multiple t-tests, except for NANOG and EOMES which demonstrated a significant increase in gene expression, p=0.041 (*) & p=0.028 (*), Figure 4.14 (A).

ReBl-PAT hiPSCs on TCDMDA:BA maintained OCT4, NANOG and SOX2 pluripotency markers without statistical differences in expression to Matrigel™. An increase in the expression of naïve potency marker KLF4 (p=0.006) (**), which is an indicator of a more naïve state, and reduction of ZIC1 expression, also an indicator of naïve potency (p=0.001) (**) existed within ReBl-PAT hiPSCs cultured on TCDMDA:BA. An increase in the ectoderm marker PAX6 (p=0.003) (**) was shown, Figure 4.14 (B). These results were similarly shown in the HUES7 hESC line, no expression changes in pluripotency genes, but increased KLF4 (p=0.005) (**), decreased ZIC1 (p=0.002) (**) and an increased PAX6 (p=0.02) (*). Additionally, HUES7 hESCs also contained increased levels of SOX1 (p=0.04) (*), also an early ectoderm marker, Figure 4.14 (C).

Together these results show that expression of the pluripotency triad, OCT4, NANOG and SOX2 were unchanged (except for a significant NANOG increase in the hiPSC AT1 line). Yet across both a hiPSC (ReBl-PAT) and an hESC line (HUES7) early ectoderm markers were significantly upregulated and changes in naïve markers toward naïve potency was demonstrated. The extent that these gene expression changes affect cell function are not assessed here.

To assess if changes in naïve potency markers detected in this qPCR panel were stem cells like those demonstrated in pluripotent having undergone a directed transition protocol to naïve stem cells, a qPCR experiment was performed with an expanded list of Naïve markers: DMNT3L, NCA, STELLA, KLF4, ZIC1 & KLF17. Naïve stem cell samples were kindly provided by Dr. Sara Pijaun Galito. Expression values for both hiPSCs cultured on TCDMDA:BA & Naïve stem cells on vitronectin were normalised to Matrigel™ hiPSCs. Across two averaged repeats DMNT3L expression between Matrigel™ and TCDMDA:BA was markedly similar, 1.01 +/- 0.18, expression in naïve stem cells was 143 +/- 71. TCDMDA:BA demonstrated increases in expression of: NCA (2.7), STELLA (2.1), KLF4 (3.1) compared to Matrigel™ cultures however naïve stem cells presented a larger set of relative fold gene expression increases: NCA (1207), STELLA (10.9), KLF4 (24) (Figure 4.14 (D)).

Changes in naïve gene expression on TCDMDA:BA in comparison to Matrigel™ are unlikely to represent a true shift to the naïve state, due to the greatly increased relative fold changes shown in stem cells after being chemically directed to the naïve potent state. None of the samples (Matrigel™, TCDMDA:BA, Naïve stem cells) demonstrated KLF17 expression.

4.5.9 Flow Cytometry Analysis of hPSCs Serially Passaged on TCDMDA:BA

To determine if pluripotency markers NANOG, SOX2, TRA-1-81 and SSEA4 were maintained at the protein level, after ≥5 serial passages on TCDMDA:BA, at a comparable level to that of equivalent Matrigel™ cultures, flow cytometry experiments were performed. The percentage of cells positive for markers: NANOG, SOX2, TRA-1-81 and SSEA4 from Matrigel™ and TCDMDA:BA cultures for the AT1 hiPSC line were as follows: 98.6% +/- 0.92% & 95.7% +/- 3%, 92.6% +/- 3.3 & 86.3% +/- 6.1%, 81.7% +/- 10% & 86.8% +/- 12.7%, 98.4% +/- 1.88% & 97.6% +/-3%. Multiple T-tests without correction did not determine any significant differences between these values (Figure 4.14 (E)). HUES7 hESC line in the same format: 97.2% +/-0.2% & 94.7% +/-1.9%, 88.6% +/- 1.8% & 75.6% +/- 3%, 85.1% +/- 8.9% & 75.8% +/- 12%, 99.8% +/- 0.1% & 99.4% +/- 0.3%. Multiple T-tests without correction determined that the reduction of SOX2+ cells from cultures on TCDMDA:BA compared to Matrigel™ were significant with a p-value equalling 0.003 (**) (Figure 4.14(F)).

Together these data demonstrated that line-to-line variability exists at the gene & protein levels of expression. The AT1 hiPSC line retained closer similarity to Matrigel™ cultures in both tested gene expression and protein marker expression via flow cytometry. However, ReBl-PAT hiPSCs and HUES7 hESCs both demonstrated similar modifications to early ectoderm gene expression (PAX6) and alterations to naïve-linked gene expression (KLF4 & ZIC1), at the protein level a significant reduction in SOX2 was observed with the HUES7 line which could lead to dysregulation of pluripotency, despite SOX2 downregulation, ≥5 serial passages was still achievable with the HUES7 line on TCDMDA:BA.

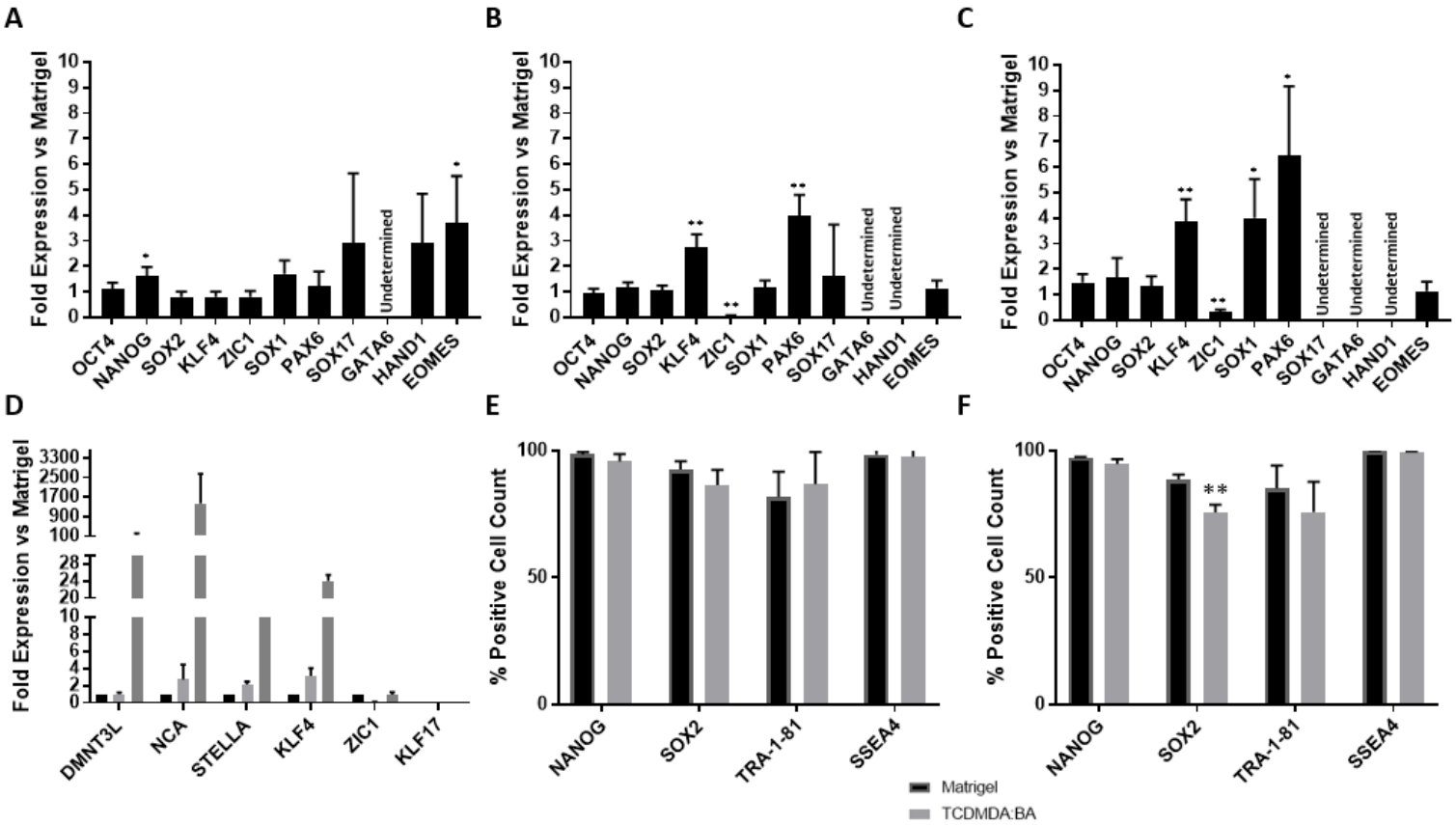

Figure 4.14 Assessment of Pluripotency Status Through Quantitative PCR (qPCR) & Flow Cytometry of hPSCs Cultured ≥5 Passages on TCDMDA:BA Compared to Matrigel™.

(A-C) RT-qPCR assessment of pluripotency, naïve and early tri-lineage differentiation markers after ≥5 passages on TCDMDA:BA or Matrigel™ on cell lines AT1 hiPSCs (A), ReBl-PAT hiPSCs (B) & HUES7 hESCs (C). (D) RT-qPCR assessment of an expanded naïve potency marker set for ReBl-PAT hiPSCs (n=1). (E-F) Flow cytometry experiments for pluripotency markers after ≥5 passages on TCDMDA:BA or Matrigel™ on AT1 hiPSCs or HUES7 hESCs respectively. SYBR Green mix used for RT-qPCR experiments, primer sequences can be found in the methods and materials chapter. N=3.

4.5.10 Immunostaining of hPSCs Serially Passaged on TCDMDA:BA

To confirm the presence of pluripotency markers OCT4, NANOG, SOX2, TRA-1-81 & SSEA4, immunostaining of hPSCs was performed TCDMDA:BA cultures of ≥5 serial passages. Previous issues with permeabilization with the dense colonies with individual cells visible on different focal planes (determining a level of 3D organisation exists), that form on TCDMDA:BA were solved by increasing 0.1% triton-X incubation to 1-hour. Operetta widefield microscopy highlighted that both AT1 hiPSCs and HUES7 hESCs cultured on TCDMDA:BA maintained the expression of OCT4, NANOG, SOX2 and TRA-1-81 throughout the entirety of colonies, as shown in Figure 4.15 (A) & (B) respectively. Quantification with Harmony software identified that 88% +/- 1.83% of cells were positive for OCT4, 95% +/- 0.5% were positive for NANOG and 91% +/- 2.45% were positive for SOX2 with the AT1 line, with reported values for NANOG and SOX2 aligning with previously discussed flow cytometry data for the AT1 hiPSC line. Quantification of markers with the HUES7 hESC line showed 97% +/- 0.4%, 98% +/- 0.7% and 97% +/- 0.8% positive expression for OCT4, NANOG and SOX2 respectively.

Confocal microscopy, performed by Dr. Aishah Nasir, revealed that OCT4 expression directly overlapped with the nuclear DAPI marker and confirmed the presence of TRA-1-81 and SSEA4 as surface markers in both AT1 and HUES7 cell lines (Figure 4.15 (C)).

Immunostaining results in Figure 4.15 demonstrate hPSCs cultured for ≥5 passages on TCDMDA:BA could retain key pluripotency markers, the next task was to determine if cultures maintained their ability to form all three germ-layer lineages:

endoderm, mesoderm, ectoderm. Protocols for definitive endoderm and neuroectoderm formation were appropriated from the work of Dr. Luke Flatt, a previous PhD student from within the laboratory. Mesoderm differentiation to cardiomyocytes was performed as described in the literature, with the full protocol described in Figure 4.16 (A) (Mosqueira et al., 2018). The definitive endoderm induction is the same of that reported in the literature, involving the addition of 2 µM GSK-3 inhibitor CHIR99021 to RPMI-B27 (minus insulin), with daily medium exchanges, after two days definitive endoderm has been reported to form, Figure 4.16 (B) (Siller et al., 2016).

The induction of neuroectoderm involved dual-smad inhibition with SB431542 (10 µM) & Dorsomorphin (1 µM) as reported in the literature (Morizane et al., 2011). However, the addition of tankrase 1 and 2 inhibitor XAV939 (2 µM), leading to WNT pathway inhibition was included, Figure 4.16 (C).

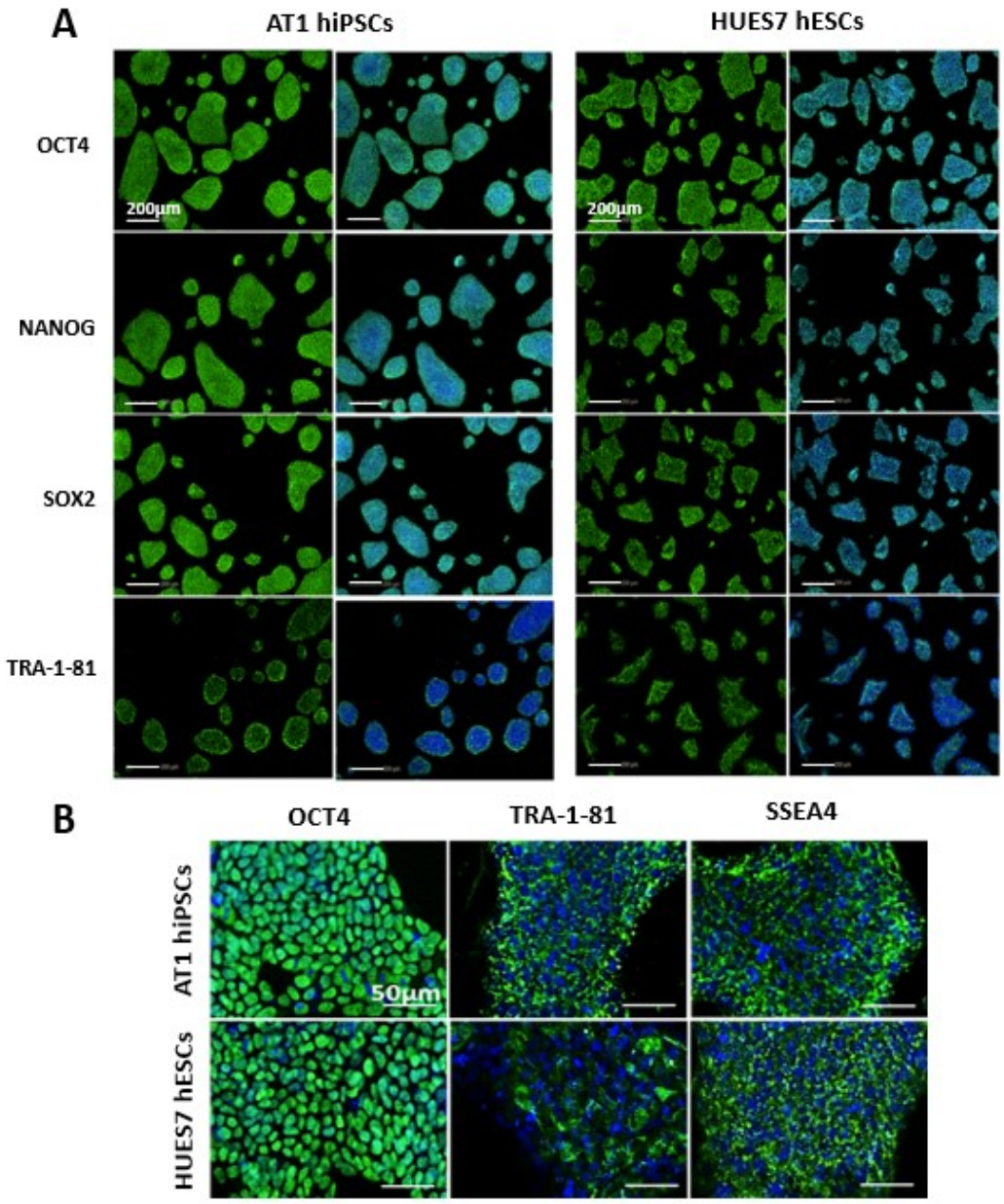

Figure 4.15 Immunostaining of hPSCs Cultured in LifeTech E8 on TCDMDA:BA for Pluripotency Markers

(A) Immunostaining of AT1 hiPSCs or HUES7 hESCs cultured in LifeTech E8 after serial passaging on TCDMDA:BA for pluripotency markers (x10 magnification). (B) Immunostaining of AT1 hiPSCs or HUES7 hESCs cultured in LifeTech E8 after serial passaging on TCDMDA:BA for pluripotency markers (x20 magnification). Scale bars as shown. N=3.

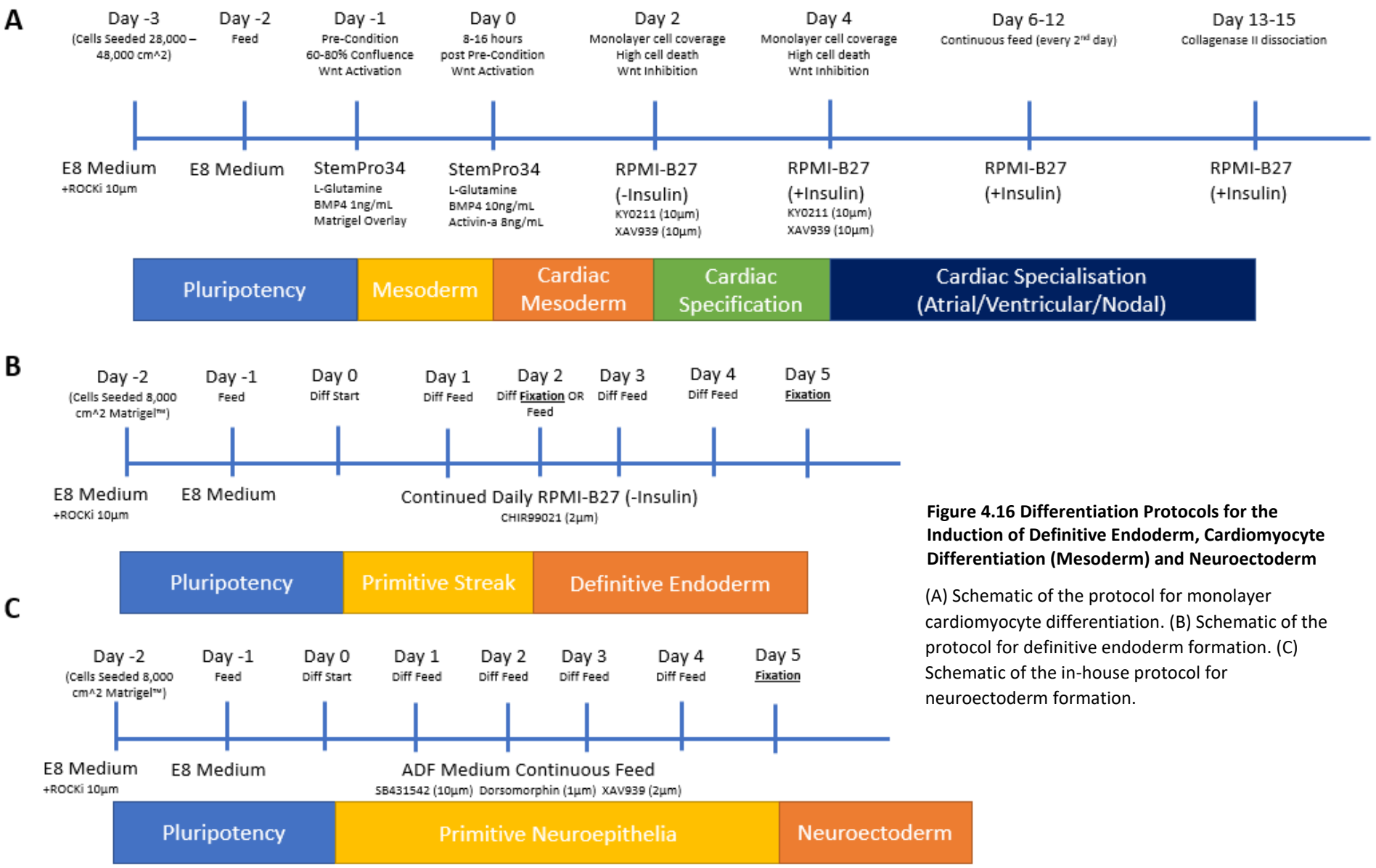

Figure 4.16 Differentiation Protocols for the Induction of Definitive Endoderm, Cardiomyocyte Differentiation (Mesoderm) and Neuroectoderm

(A) Schematic of the protocol for monolayer cardiomyocyte differentiation. (B) Schematic of the protocol for definitive endoderm formation. (C) Schematic of the in-house protocol for neuroectoderm formation.

4.5.11 Cardiomyocyte Differentiation of Serially Passaged hPSCs on TCDMDA:BA

Differentiation of hPSCs cultured for ≥5 passages on TCDMDA:BA surfaces in LifeTech E8 medium were successfully differentiated into contractile cardiomyocytes, following the protocol outlined in Figure 4.17 (A). By day 0 of differentiation, during mesoderm formation, Matrigel™ based cultures formed compact 2D colonies interspaced with cell-free areas. Differentially, TCDMDA:BA based cultures did not support 2D attachment, colonies compacted and rounded, by majority detached from the culture surface (Figure 4.17 (A)). By day 1 of differentiation, cultures had been exposed to a higher concentration of BMP4 (10 ng/mL), and activin-a (8 ng/mL) for 24 hours. Matrigel based cultures proliferated rapidly to form a dense monolayer of cells. Within TCDMDA:BA cultures, floating colonies had settled and proliferated outwards. From day 2 of differentiation until contraction, day 8, cultures on both surfaces presented a similar morphology. Day 8 onwards, TCDMDA:BA cultures varied from contractile monolayers (like Matrigel cultures) to the formation of large 3D contractile bodies.

Contractile analysis of day 8 in-situ cardiomyocyte differentiations on Matrigel and TCDMDA:BA confirmed the contractile nature of cardiomyocytes generated on TCDMDA:BA culture surfaces. Using the CellOPTIQ high speed imaging camera and contraction software, pixel displacement was analysed to provide surrogate measurements of contraction. Comparing Matrigel vs TCDMDA:BA respectively – contraction parameters were similar to Matrigel differentiations with too few repeats performed to draw statistically significant conclusions. This data proves that in-situ differentiation on TCDMDA:BA can form cardiomyocytes.

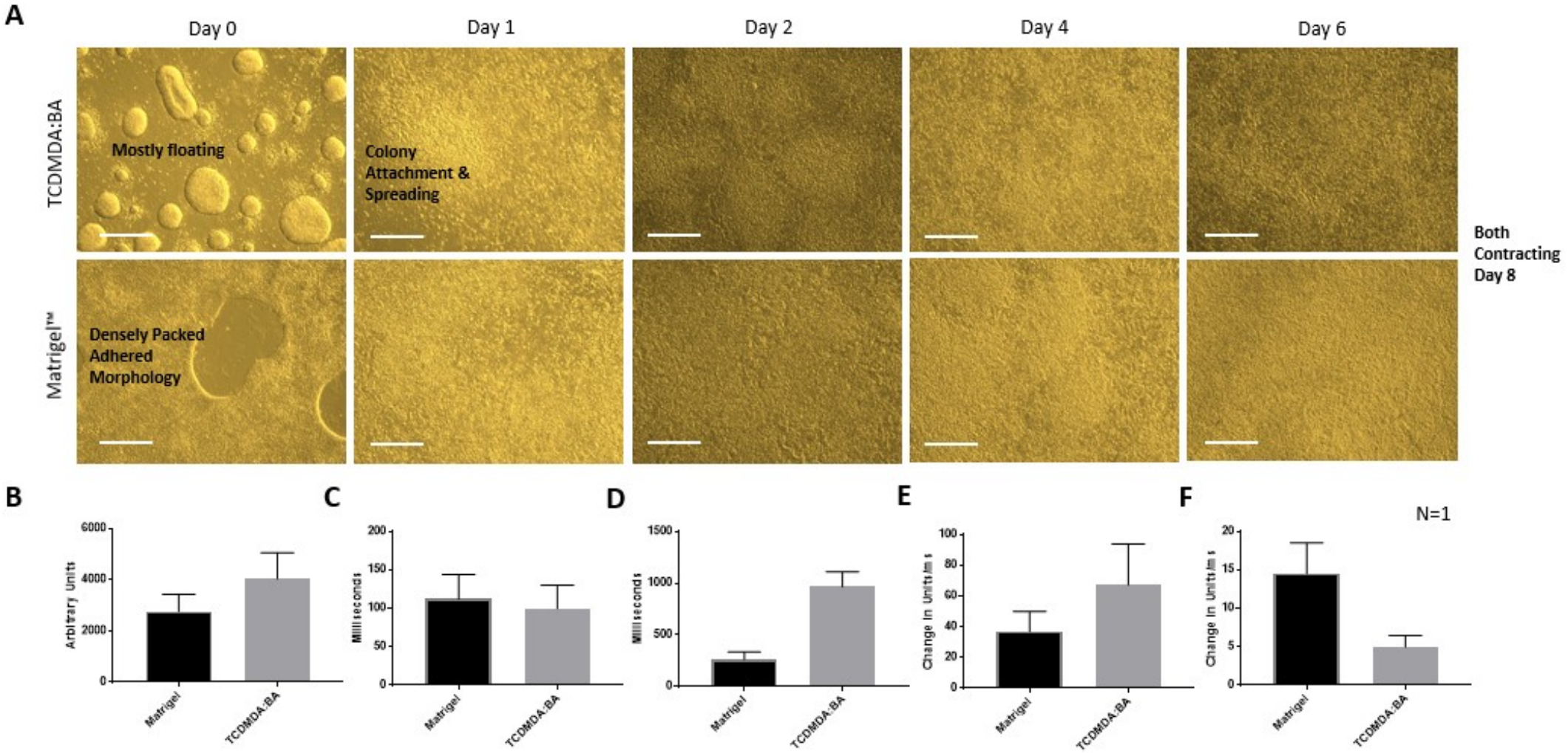

Figure 4.17 Differentiation of hPSCs on Matrigel and TCDMDA:BA to Cardiomyocytes.

(A) Representative brightfield images of cardiomyocyte differentiations of hPSCs cultured on Matrigel or TCDMDA:BA as labelled at specific time points. (B-F) CellOPTIQ contraction assessment at day 8 of cardiomyocyte differentiation. (B) Contraction Amplitude, (C) Upstroke 90% (UP90), (D) Downstroke 90% (DN90), (E) Contraction Rate, (F) Relaxation Rate. Recording were taken using the CellOPTIQ high speed camera and data analysed using the Contractility Tool (Clyde Biosciences). Scales bars = 100 µm.

4.5.12 Definitive Endoderm Formation from hPSCs Serially Passaged on TCDMDA:BA

To assess if hPSCs cultured on TCDMDA:BA for ≥5 passages can form endoderm and ectoderm lineages, differentiation protocols outlined in Figure 4.16 (B) & (C) were followed to generated definitive endoderm and neuroectoderm respectively. Definitive endoderm and neuroectoderm do not equate to a full differentiation, as performed with the mesoderm lineage to cardiomyocytes, but are proof of concept that hPSCs retain the capacity to form cells of each lineage.

Definitive endoderm was formed by day 2 of the previously outlined protocol, staining demonstrated that cultures with 63% +/- 19% FOXA2 and 71% +/- 19% SOX17 expression could be generated (Figure 4.18 (A)), confocal microscopy confirmed that expression of FOXA2 and SOX17 was confined to the nucleus, as expected for active transcription factors, also dual-staining confirmed cells produced using the outlined protocol were positive for both markers by differentiation day 2 (Figure 4.18 (B)). Originally it had been suggested to continue the definitive endoderm differentiation until day 5, by this timepoint cultures on TCDMDA:BA surfaces had formed large 3D clusters, approximately 1mm in diameter, still retaining expression of FOXA2 and SOX17, to the best extent to which that could be determined (Figure 4.18 (C)). Definitive endoderm cultures carried out on Matrigel surfaces until day 2 of differentiation demonstrated 64% +/- 10% & 68% +/- 16% expression of FOXA2 and SOX17 (Figure 4.18 (D)).

These results demonstrate that differentiation of hPSCs cultured on TCDMDA:BA in LifeTech E8 for ≥5 passages could retain their capacity to form definitive endoderm. Definitive endoderm formation on TCDMDA:BA results in more

3D-like structure compared to Matrigel by day 2, with large 3D structures (~1 mm) forming on TCDMDA:BA by day 5, whereas Matrigel retains monolayer surface coverage.

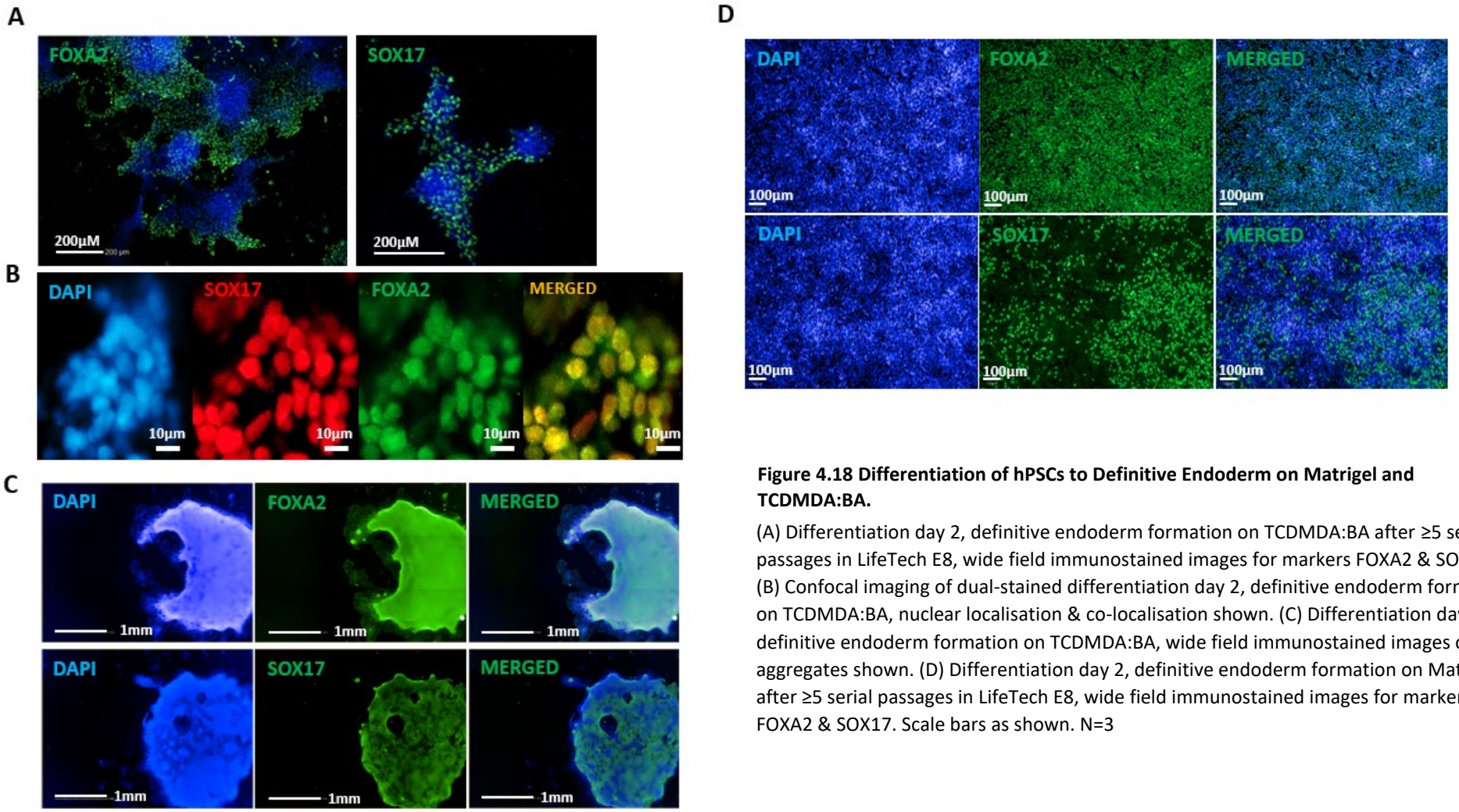

Figure 4.18 Differentiation of hPSCs to Definitive Endoderm on Matrigel and TCDMDA:BA.

(A) Differentiation day 2, definitive endoderm formation on TCDMDA:BA after ≥5 serial passages in LifeTech E8, wide field immunostained images for markers FOXA2 & SOX17. (B) Confocal imaging of dual-stained differentiation day 2, definitive endoderm formation on TCDMDA:BA, nuclear localisation & co-localisation shown. (C) Differentiation day 5, definitive endoderm formation on TCDMDA:BA, wide field immunostained images of 3D aggregates shown. (D) Differentiation day 2, definitive endoderm formation on Matrigel after ≥5 serial passages in LifeTech E8, wide field immunostained images for markers FOXA2 & SOX17. Scale bars as shown. N=3

4.5.13 Neuroectoderm Formation of hPSCs Serially Passaged on TCDMDA:BA

Differentiation of hPSCs cultured in LifeTech E8 on TCDMDA:BA and Matrigel for ≥5 passages to neuroectoderm was successfully performed, with Matrigel cultures positive for PAX6 (67% +/- 27%) and SOX1 (66% +/- 29%). Dual staining on Matrigel neuroectoderm cultures revealed co-localisation of PAX6 and SOX1 markers (Figure 4.19 (A)). PAX6 and SOX1 positivity was more difficult to determine on TCDMDA:BA surfaces due to the 3D-nature of the differentiation, single-stains for PAX6 & SOX1 determined estimated 64% +/- 16% & 75% +/- 18% positivity respectively (Figure 4.19 (B)). Neuroectoderm formation on TCDMDA:BA would often produce 3D structures, in some instances 3D structures would become macroscopic in appearance, ranging approximately 3 mm – 11 mm in length. Such structures still express PAX6 and SOX1 as demonstrated in Figure 4.19 (C), however due to their size it would not be appropriate to estimate percent marker positivity without sectioning or dispersing the clusters.

In summary, differentiation to the endoderm, mesoderm and ectoderm lineages were possible on TCDMDA:BA, after ≥5 passages in LifeTech E8 medium. A lack of 2D monolayer formation was evident in definitive endoderm differentiation, particularly by differentiation day 5, 3D structures also formed during neuroectoderm differentiation. The functional effect of these relatively large 3D structures, ranging from ~1 mm - ~11 mm in diameters (in extreme cases during neuroectoderm differentiation) has not been determined and is beyond the scope of this thesis.

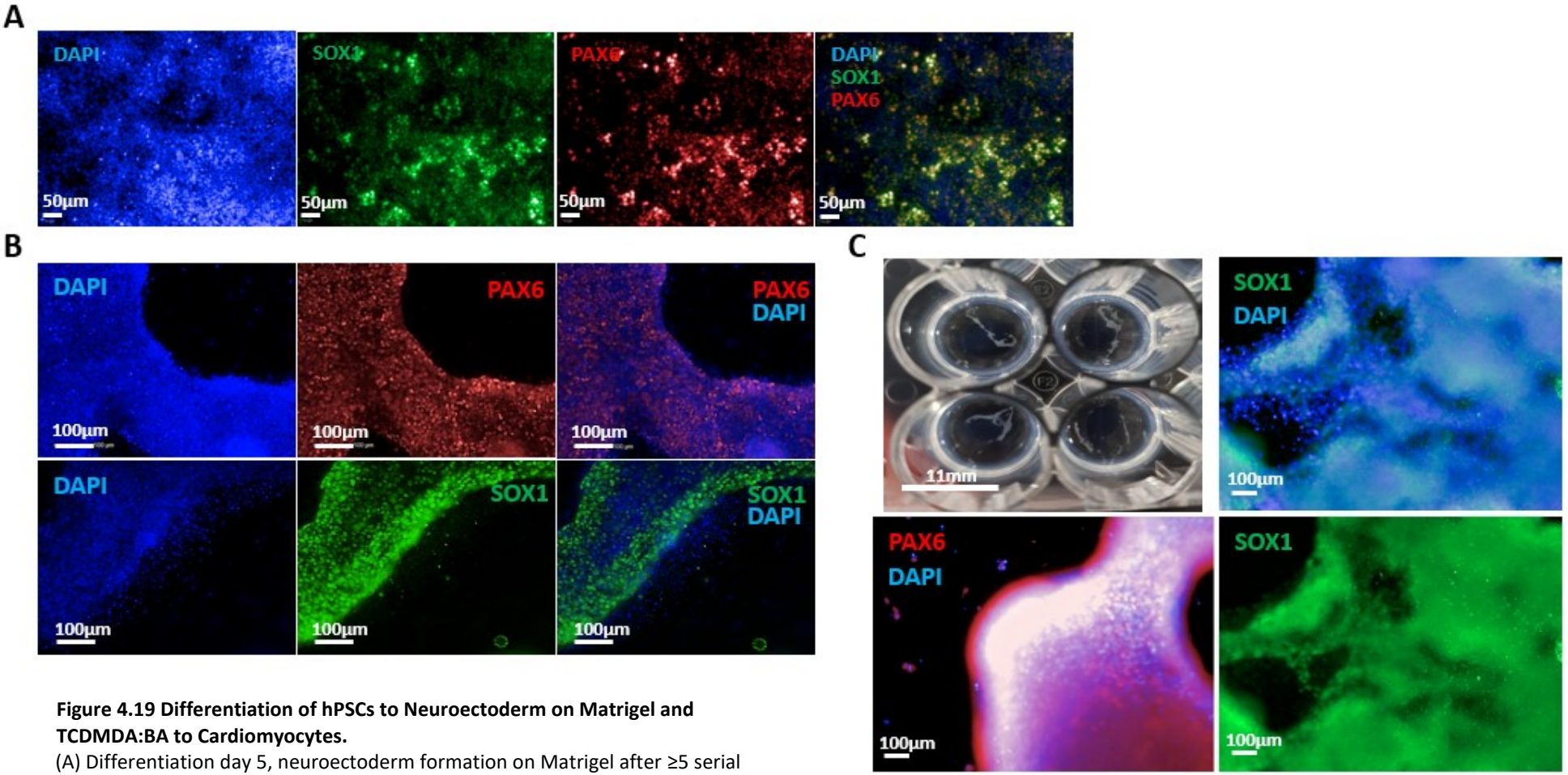

Figure 4.19 Differentiation of hPSCs to Neuroectoderm on Matrigel and TCDMDA:BA to Cardiomyocytes.

(A) Differentiation day 5, neuroectoderm formation on Matrigel after ≥5 serial passages in LifeTech E8, wide field immunostained images for markers SOX1 & PAX6. (B) Differentiation day 5, neuroectoderm formation on TCDMDA:BA after ≥5 serial passages in LifeTech E8, wide field immunostained images for markers SOX1 & PAX6. (C) Differentiation day 5, neuroectoderm formation on TCDMDA:BA, wide field immunostained images of 3D aggregates shown. Scale bars as shown. N=3

Having determined hPSC cultured for ≥5 passaged retained pluripotency markers and trilineage functional capacity, with the loss of cellular adhesion during specific cardiac differentiation timepoints and progressive adhesion loss during definitive endoderm and neuroectoderm differentiation, the attachment mechanism of hPSCs to TCDMDA:BA was explored.

4.5.14 Determination of Attachment Mechanism to TCDMDA:BA

An attachment mechanism was interrogated through integrin blocking assays. An antibody directed towards specific integrin subunits or an RGD-blocking peptide designed to inhibit specific integrin-related sites were incubated with hPSCs before seeding on to TCDMDA:BA, after 24 hours cell number was quantified through a DAPI count. Integrins β1, α2, α5, α6, αVβ3, αVβ5 were targeted covering a range of adhesion protein interactions such as, β1 for laminin & Matrigel, αVβ3 for vitronectin & fibronectin and αVβ5 specifically for vitronectin.

The AT1 hiPSC line demonstrated a statistically significant decrease in cell attachment at 24 hours when β1, αVβ3, αVβ5 were blocked, with 33.8%, 48.8% and 69.4% reduction in DAPI count compared to Matrigel respectively (Figure 4.20 (A)). A One-Way ANOVA statistical test corrected with Dunnett's test revealed DAPI reductions were significant, β1 ($p=0.02$), αVβ3 ($p=0.001$), αVβ5 ($p=0.0001$). Blocking with RGD-blocking peptides H7226 & H2574 reduced 24-hour DAPI counts by 88% ($p=0.0001$) and 85.2% ($p=0.0001$) respectively, statistical testing was performed using One-Way ANOVA corrected with Dunnett's test (Figure 4.20 (B)). RT-qPCR analysis of ITGB1 (β1), ITGB3 (β3), ITGB5 (β5), ITGA1 (α1), ITGAV (αV), revealed no

significant upward or downward trends of expression however variation between biological samples was high, averaging 48% across the tested genes (Figure 4.20 (C)).

Identical testing performed with the HUES7 hESC line produced results that closely aligned with those produced from the AT1 line. Blockade of β1 & αVβ5 reduced 24-hour DAPI count by 44.8% (p=0.008) & 92.8% (p=0.0001) respectively, however blocking with the αVβ3 antibody reduced DAPI count by 27.1%, which was deemed insignificant (Figure 4.20 (D)). Blocking with RGD-blocking peptides H7226 & H2574 reduced 24-hour DAPI counts by 96.2% (p=0.0001) and 87.9% (p=0.0001), where H7226 blocks αVβ3, a discrepancy in these results (Figure 4.20 (E)). RT-qPCR analysis of integrin expression with the HUES7 line revealed that a 2.44-fold increase in ITGB5 (β5) expression was statistically significant (p=0.02), whereas a 1.57-fold increase in ITGB3 (β3) was deemed insignificant by t-test comparisons (Figure 4.20 (F)).

Representative images of control cultures on TCDMDA:BA without integrin blocking, blocked with αVβ5 or H-2574 are shown in Figure 4.20 (G-I), with reduced DAPI cells visible across each condition. 48-hour culture of αVβ5 blocked hPSCs (upon seeding) was permissive for proliferation, however aggregation and folding of colonies was observed (Figure 4.20 (J)).

Results from both the AT1 and HUES7 cell lines were markedly similar, with β1 & αVβ5 integrin block causing a reduction in DAPI cell count by 24 hours culture. Whilst αVβ3 block by an antibody only significantly reduced DAPI cell count in the AT1 line, the αVβ3 integrin specific RGD-blocking peptide, H-7226, elicited an identical response across both cell lines. Together these results show that β1, αVβ3,

αVβ5 are mechanistically important for hPSC attachment to TCDMDA:BA in LifeTech E8 medium, αVβ3 & αVβ5 demonstrated the greatest reduction in DAPI cell count when blocked (RGD blockade only for HUES7s), both of which are involved in attachment to vitronectin peptides.

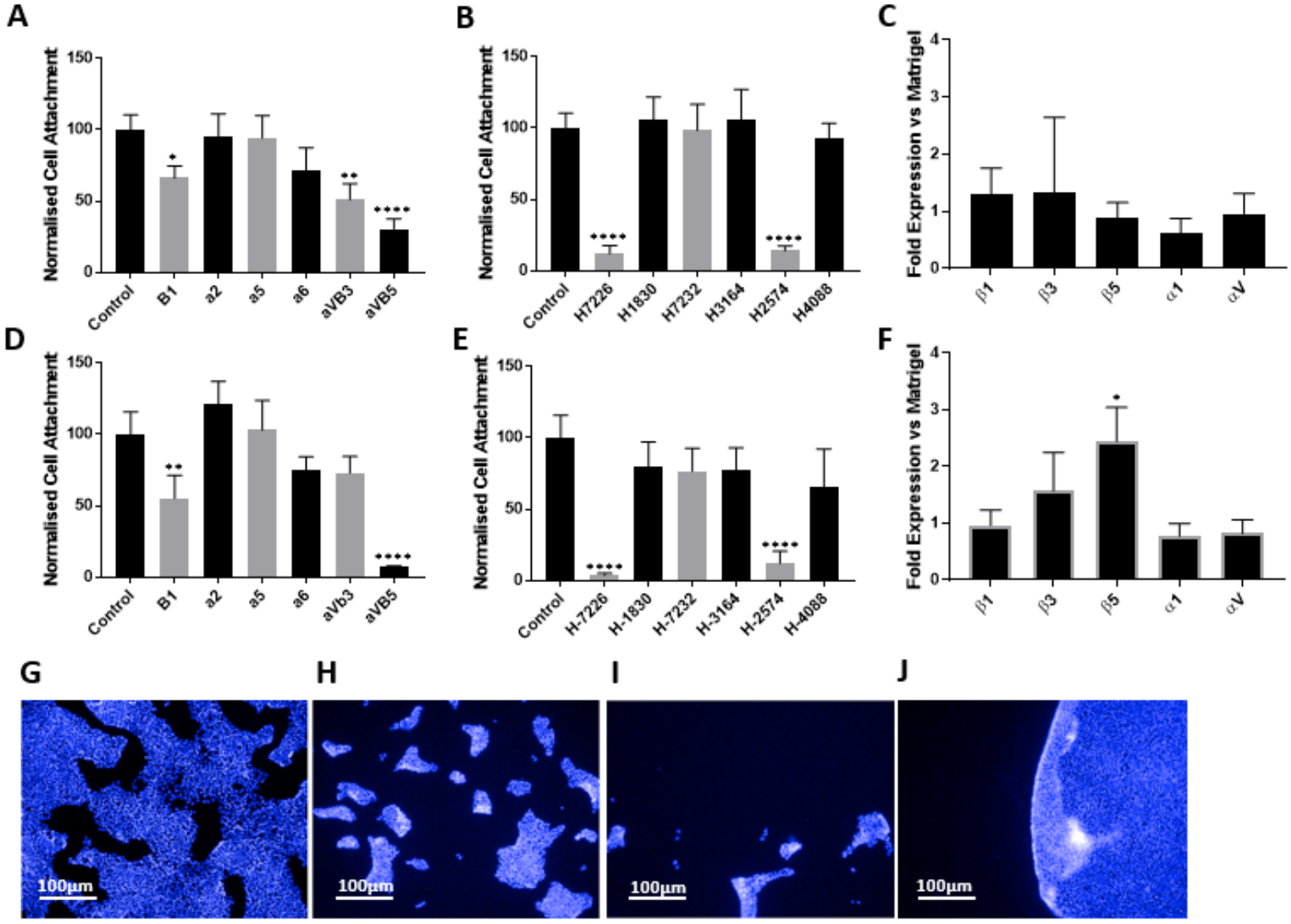

Figure 4.20 Determining Integrins Involved in Cellular Attachment of hPSCs to TCDMDA:BA.

(A) Integrin blockade assay of AT1 hiPSCs cultured in LifeTech E8 using integrin specific antibodies. (B) Integrin blockade assay of AT1 hiPSCs cultured in LifeTech E8 using specific RGD-blocking peptides. (C) SYBR Green RT-qPCR for integrin expression on TCDMDA:BA in comparison to Matrigel culture for AT1 hiPSCs. (D) Integrin blockade assay of HUES7 hESCs cultured in LifeTech E8 using integrin specific antibodies. (E) Integrin blockade assay of HUES7 hESCs cultured in LifeTech E8 using specific RGD peptides. (C) SYBR Green RT-qPCR for integrin expression on TCDMDA:BA in comparison to Matrigel culture for HUES7 hESCs. (G-I) Fluorescent images of TCDMDA:BA without integrin blocking, with αVβ5 blocking, or H-2574 blocking. (J) 48-hour culture of AT1 hiPSCs with αVβ5 blocked during seeding. Scales bars = 100 µm. N=3.

4.5.15 Examination of Protein Phosphorylation States on Signalling Kinases

Mechanisms beyond initial attachment to TCDMDA:BA should also be investigated to determine why population doubling on TCDMDA:BA is slower than that observed on Matrigel surfaces, these mechanisms could relate to changes in response to external stimuli (i.e. growth factors), or upregulation of pro-apoptosis pathways (i.e. P53 S46 phosphorylation). To look at these changes R&D phospho-proteome arrays were used to compare the phosphorylated state of 42 proteins in duplicate, and two total protein levels, Heat Shock Protein 60 (HSP60) and β-catenin.

Oversight and assistance within these experiments was provided by PhD student Christopher Carroll, however the experimentation and quantification were performed by myself.

The AT1 & HUES7 lines were both cultured for ≥5 passages on Matrigel and TCDMDA:BA, AT1 and HUES7 cultures were performed in parallel to eliminate differences due to medium batch or time-point changes. Cultures were harvested at the 48-hour time point to assess the phosphokinase proteome during the growth phase. Protein lysates were extracted on ice, in the presence of inhibitors to prevent phosphoprotein degradation. Protein quantification was performed using a Bradford Assay to ensure equal amounts were loaded between Matrigel and TCDMDA:BA samples. Arrays were prepared according to manufacturer's instructions, imaging performed simultaneously, and quantification performed using Image Studio Lite Version 5.2.

AT1 line on TCDMDA:BA presented a markedly similar phosphokinase proteome profile to Matrigel, visually a comparison can be drawn qualitatively by examining Figure 4.21 (A), where a small selection of important phosphorylation changes (P53 S46, FAK Y397 and TOR S2448) or phosphorylation changes common across both cell lines (Fyn Y420, Lyn Y397, EGFR S2448) are highlighted.

Across the entire array an average change in phosphorylation levels was 1.1, signalling that AT1 hiPSCs cultured on Matrigel and TCDMDA:BA are on average similar in their phospho-proteome. A full presentation of changes relative to Matrigel for both cell lines are presented in Figure 4.22. The largest fold-increase in protein phosphorylation were HCK Y411 (2.60), closely followed by c-Jun S63 (2.38), Lyn Y397 (1.76), EGFR Y1086 (1.74) and MSK1/2 S376/S360 (1.70). Master regulator mTOR S2448 was increased by 1.31-fold phosphorylation, with P53 S46 increased by 1.26-fold. FAK Y397 (0.85), P53 S392 (0.69), PDF Rb Y751 (0.50), Fyn Y420 (0.49) and Fgr Y412 (0.33) all demonstrated less phosphorylated states on TCDMDA:BA compared to Matrigel, as shown in Figure 4.21 (B).

Kinases were grouped to their related pathways PI3K/AKT/mTOR, MAPK and cell cycle. PI3K/AKT/mTOR pathway related kinases ranged from 0.9-1.3-fold difference on TCDMDA:BA compared to Matrigel. mTOR and P70 S6 Kinase demonstrated the highest relative increase in phosphorylation at 1.31, 1.30 (T421/S424) and 1.29 (T389) respectively (Figure 4.21 (C)). The MAPK pathway kinases present on the array also demonstrated great similarity with the level of phosphorylation on Matrigel ranging from 0.6-2.38-fold changes. Phosphorylation of c-Jun and MSK1/2 had the highest fold changes in phosphorylated state at 2.38 and

1.70. Of the proteins that were phosphorylated to a lesser extent relative to Matrigel, CREB and HSP27 relative signals were 0.78 and 0.60. Cell cycle related proteins were phosphorylated between 0.63-1.26-fold on TCDMDA:BA compared to Matrigel with pro-apoptosis P53 S46 the highest at 1.26-fold and P27 T198 at 0.63-fold. Other P53 phosphorylation states were 1.03-fold (S15) and 0.69-fold (S392).

Comparisons between HUES7s on Matrigel and TCDMDA:BA after ≥5 passages revealed wide ranging increases in relative phosphorylated states of the proteome analysed. A qualitative comparison can also be found for the HUES7 line, Figure 4.23 (A), where visual inspection shows a decrease in spot intensity on Matrigel compared to TCDMDA:BA. Quantification of intensity revealed that on average spot intensity on arrays incubated with TCDMDA:BA lysates were 3.63-fold higher intensity, confirming visual results (Figure 4.22).

Increased phosphorylation of EGFR Y1086 was the most prominent change at 13.3-fold higher than Matrigel, with Fyn Y420, p38a T180/Y182 and PDF Rb Y751 were phosphorylated 9.74, 7.69 and 6.64 times more respectively. A wide range of phosphorylation states were increased between 5 and 6-fold including, MSK1/2 S376/S360, c-Jun S63, ERK1/2 T202/Y204/T185/Y187, P27 T198 and AMPKa1 T183. Lyn Y397, TOR S2448, FAK Y397 were increased 3.62-fold, 3.40-fold, 2.71-fold (Figure 4.23 (B)).

Separated into pathway related groups it can be seen that all the tested kinases are more highly phosphorylated in TCDMDA:BA cultures (1.22-3.63-fold) compared to Matrigel cultures, AKT T308 demonstrated lowest increase in relative phosphorylation at a 1.22-fold increase, whilst AKT S473 was phosphorylated

relatively highly with a 3.60-fold increase. AKT S473, TOR S2448, GSK-3α/β S21/S9 and eNOS S1177 were all phosphorylated 3-fold or greater relative to Matrigel (Figure 4.23 (C)).

MAPK related phosphokinases present on the array were all upregulated by a minimum of 2.54-fold (JNK1/2/3 T183/Y185, T221/Y223) shortly followed by CREB S133 at 2.55-fold increase. ERK1/2 T202/Y204, T185/Y187, c-Jun S63 and MSK1/2 S376/S360 were all increased between 5-6-fold. P38α T180/Y182 phosphorylation sites were increased 7.69-fold with RSK1/2/3 S380/S386/S377 increased the most by a 13.28-fold relative increase.

Grouping cell cycle linked proteins together revealed a general increase in relative phosphorylation of P53, CHK-2 and p27 proteins. P27 and CHK-2 increased in their phosphorylated states the most at 5.3-fold and 3.4-fold each. Whilst P53 S293 and P35 S15 both demonstrated a ~2-fold increase interestingly P53 S46, key marker for induction of apoptosis, demonstrated 1.29-fold increase, a near identical increase of 1.26-fold increase observed with the AT1 line.

Increases in c-Jun S63, EGFR Y1086, TOR S2448 and Lyn Y397 were observed across both cell lines. Conversely, whilst AT1 line demonstrated a decrease in Fyn Y420 (0.49) within the HUES7 line Fyn Y420 was the 2nd most upregulated, 9.74-fold compared to Matrigel equivalents. PDF Rb Y751 demonstrated a 0.50-fold vs 6.64 phosphorylation state comparative to Matrigel on the AT1 line vs HUES7 line.

In summary the AT1 line demonstrated a phosphokinase proteome on TCDMDA:BA cultures closely aligned with its Matrigel counterpart, which may also be reflected in the RT-qPCR data, flow cytometry data and growth curves, where

analysis also confirmed fewer differences between Matrigel and TCDMDA:BA culture. The HUES7 line, which showed statistically significant perturbation in SOX2 positive cells in flow cytometry and increases in differentiation & naïve gene expression, displays an altered phosphokinase proteome profile.

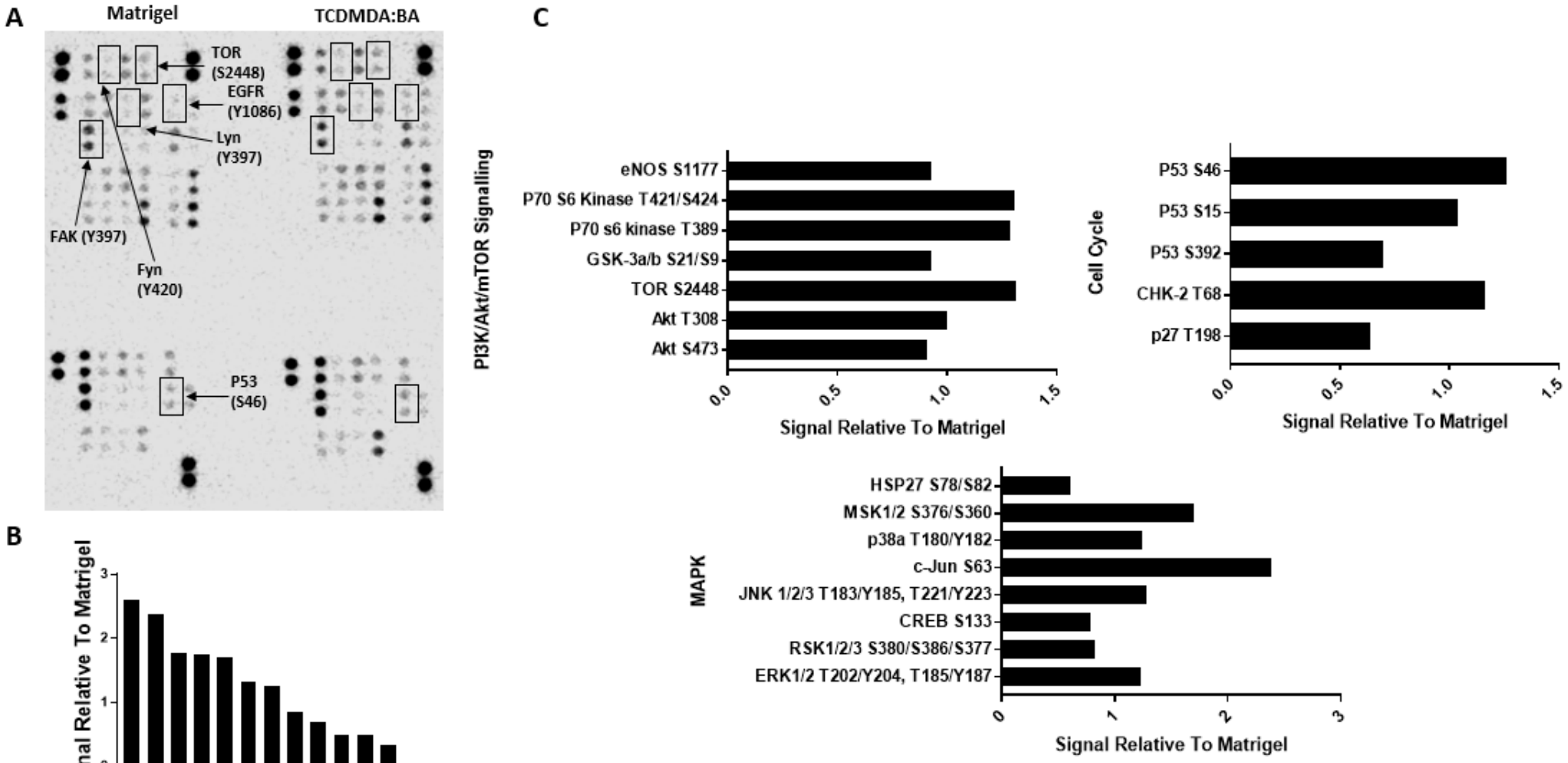

Figure 4.21 Comparison of Phosphokinase Proteome between AT1 hiPSCs on Matrigel vs TCDMDA:BA after ≥5 serial passages.

(A) Images of R&D Phospho-Kinase Proteome (left) Matrigel, (right) TCDMDA:BA after ≥5 serial passages in LifeTech Essential 8 medium. (B) Selected phosphorylated quantified relative to Matrigel. (C) Phosphorylation changes organised into PI3K/AKT/mTOR, MAPK and Cell Cycle related pathways.

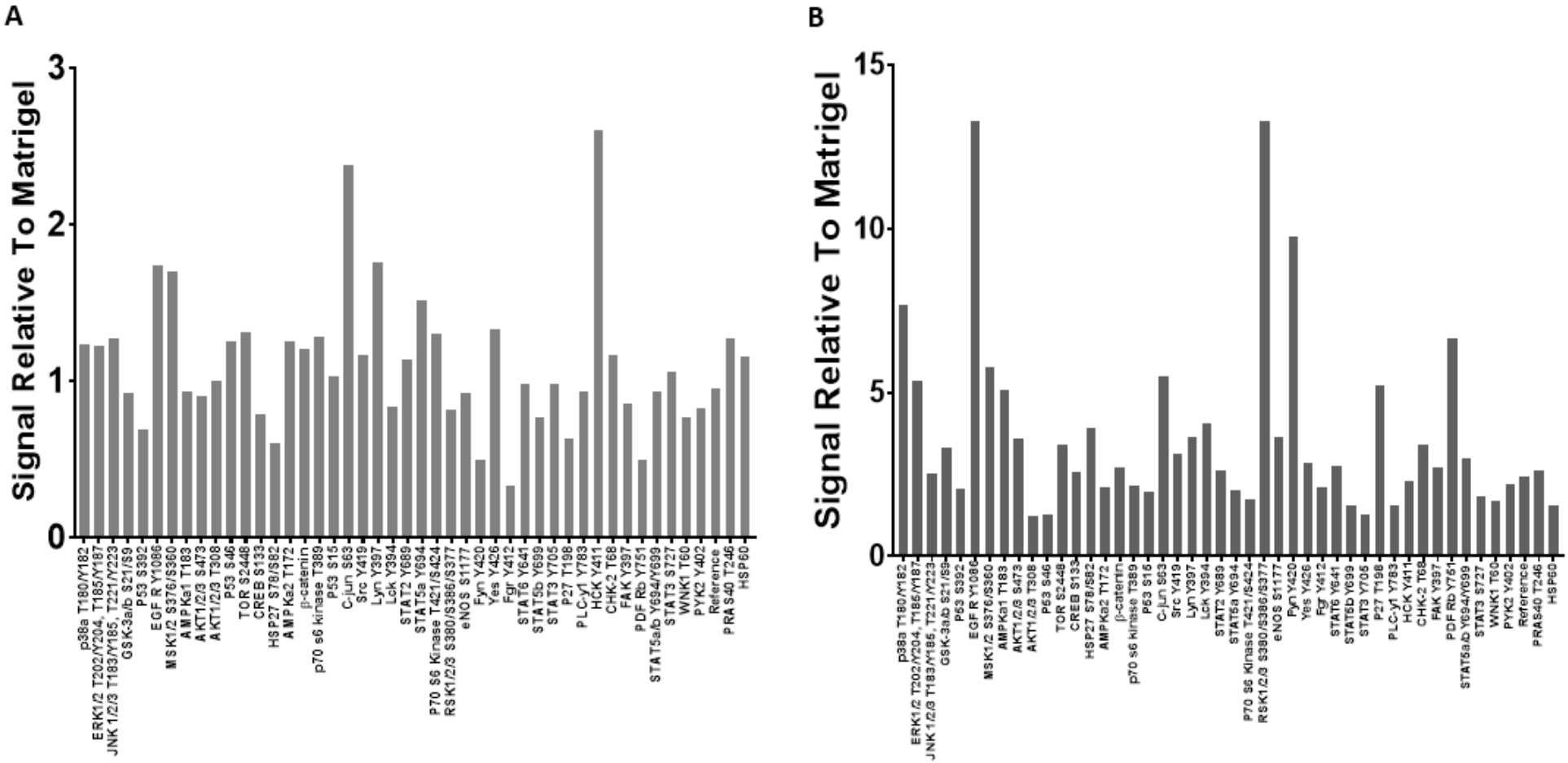

Figure 4.22 Comparison of Phosphokinase Proteome between hPSCs on Matrigel vs TCDMDA:BA after ≥5 Serial Passages.

(A) Quantification of full array for AT1 hiPSCs. (B) Quantification of full array for HUES7 hESCs.

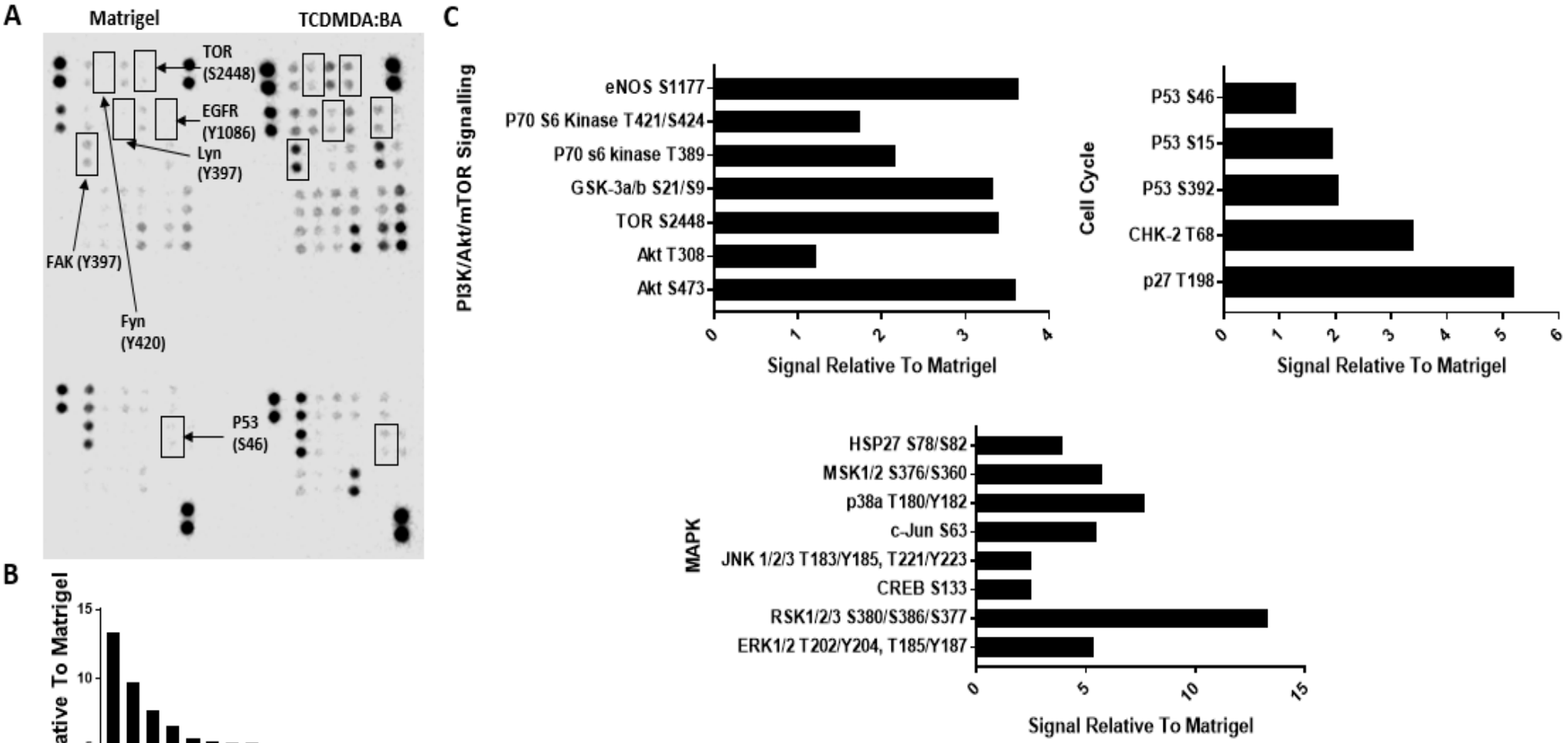

Figure 4.23 Comparison of Phosphokinase Proteome between HUES7 hESCs on Matrigel vs TCDMDA:BA after ≥5 Serial Passages.

(A) Images of R&D Phospho-Kinase Proteome (left) Matrigel, (right) TCDMDA:BA after ≥5 serial passages in LifeTech Essential 8 medium. (B) Selected phosphorylated quantified relative to Matrigel. (C) Phosphorylation changes organised into PI3K/AKT/mTOR, MAPK and Cell Cycle related pathways.

4.6 Chapter Discussion & Summary

4.6.1 Scale-Up Issues

Scaling up selected hits to the 96-well plate format involved a change in multiple parameters including, switching the background material, removal of the soft pHEMA hydrogel layer, utilising a non-toxic and TCP friendly solvent. Additionally, scale-up involved a greater volume of monomer solution and an increase in the thickness of the final polymer layer. All these combined, alongside technical issues presented a serious challenge to create scaled-up non-cytotoxic surfaces.

4.6.2 Surface Stiffness

The change in background material from glass to TCP could affect mechanotransduction responses of the cells. Focal adhesion assembly is mediated by the response integrins have to matrix stiffness, where it has been shown in epithelial cells that the β1 integrin expression declines in the presence of a soft matrix (~0.2 kPa) vs a stiffer matrix (>1GPa), resulting in a reduction of cellular spreading (Yeh et al., 2017). In bone marrow derived mesenchymal stem cells (BMMSCs) substrate stiffness has effects on morphology, adhesion, proliferation and the potential for cells to undergo osteogenic differentiation, with 62-68 kPa inducing an osteogenic phenotype compared to lower stiffness surfaces (13-16 kPa) (Sun et al., 2018). Studies on pluripotent stem cells offer inconsistent results regarding stiffness, with surface stiffnesses between 800 Pa and ~2.5 MPa being suggested as optimal for maintaining the pluripotent state (albeit ~2.5 MPa was the highest stiffness tested) (Fu et al., 2017)(Kim et al., 2018). Studies examining the

differentiation potential of pluripotent stem cells have found that soft substrates of ~13 Pa upregulated early endoderm markers Sox17 , ~100 Pa stiffness can promote neural ectoderm commitment, with stiffer substrates ~MPa potentially promoting mesodermal lineages (Jaramillo et al., 2015)(Keung et al., 2012)(Evans et al., 2009).

Atomic force microscopy experiments performed by Dr. Laurence Burroughs in this thesis found that TCDMDA:BA is presented as a 'phaseomer', meaning one homopolymer covers the surface, with the other interspersed as 'islands' across the surface. The background covering polymer is approximately ~30-60 MPa, whilst the interspersed 'islands' are below the MPa range, a stiffness not determined due to the limitations of the cantilever used. It is possible that the surface stiffness of these islands matches with the 800 Pa - ~2.5 MPa range discussed in the literature for maintaining pluripotency (Fu et al., 2017)(Kim et al., 2018).

The extent to which mechanotransduction changes occur in hPSCs within this thesis, due to the change of background substrate, underneath our polymeric coating is questionable without further study but not an effect to rule out. The effect of pHEMA-Polymer entanglement could also affect the surface stiffness that hPSCs are exposed to.

4.6.3 Polymerisation Conditions

The way in which acrylate-based monomers polymerise and attach to epoxy silane coated glass, and TCP could elicit changes in biological response to surface binding. Changes in concentration of monomers used, which were increased from 50% v/v on the microarrays to 90% v/v in the final scale-up, as well as the change in solvent, DMF-IPA, may elicit surface level changes in the final product, affecting the

biological response. An investigation into the effect of polymerisation conditions into hydrogel formation found that changes in both the initiator and acrylamide monomer concentration affected 'polymerisation kinetics, morphology and mechanical properties of the hydrogels' (Nigmatullin, Bencsik and Gao, 2014).

Furthermore, alterations to surface macro or nano topography have the potential to illicit changes to, proliferation, differentiation, migration and morphology (Lim and Donahue, 2007)(Unadkat et al., 2011)(Vasilevich et al., 2018).

4.6.4 Solvent Use & Concentration

Changing the solvent used from DMF to IPA was essential due to the toxic nature of DMF, with the volume used increasing from array fabrication to well plate polymerisation. DMF is also capable of dissolving TCP, altering the heteropolymer formulation and potentially disrupting the optics of the final product. IPA could dissolve most desire monomers, except for MAETA, and is compatible with TCP. The use of solvent has been explored within the literature, where a comparison of DMF vs toluene and 1-butanol found that DMF polymerised Butyl Acrylate (BA – used in the main polymer within this thesis chapter) 1.7 times faster than toluene and 5 times faster than 1-butanol, DMF also had a faster termination rate of 2.9 and 4.8 times faster than toluene and 1-butanol respectively (Xiao et al., 2011). It has also been noted that DMF has a high polarity which can increase radical formation. It should be noted these experiments were performed using atom transfer radical polymerisation (ATRP), not UV-initiated polymerisation (Grégory Chambard, Bert Klumperman and German, 2000).

Changing the concentration of the solvent used from 50% v/v with the array system to 10% v/v during scale-up preparations could have influenced the mechanical properties of the polymer surface. UV-based preparation of BisGMA-based adhesives with 0-40% ethanol content revealed differences in mechanical properties, with ultimate tensile strength and modulus of elasticity decreasing with increasing ethanol content (Ye et al., 2007). A comparison of ethylene glycol diacetate and hexanol solvents for acrylate preparation using thermal polymerisation demonstrated that solvent choice and solvent concentration affects the molecular weight and swelling properties of the final product (Jeannine E. Elliott† and Christopher N. Bowman*, 2002).

4.6.5 Atmospheric Oxygen Contamination

The presence of oxygen in the atmosphere where UV-initiated free radical polymerisation is taking place has been shown to cause early termination of methacrylate polymerisation (Andrzejewska et al., 2003). Excited photo initiator states are quenched by the presence of oxygen, and primary initiating radicals (R*) or propagating radicals (P-M*) may reaction with oxygen forming energetically unfavourable peroxyl radicals (POO*) which prefer to combine with other radicals forming peroxide bridges (POOP) – terminating the reaction early (Ligon et al., 2014). Reaction temperature is also an important consideration in relation to oxygen-linked early termination, at 80^{o}C in an open-air system, the UV polymerisation of a 5 µm polyurethane acrylate layer was inhibitory to polymerisation, where 20% polymerisation was achieved in 1 second at 6^{o}C, increases in temperature increase oxygen diffusion (Studer et al., 2003). The effect of temperature on the final product state in a semi-open-air system (open air with

argon pumped through) was demonstrated to cause surface deformations within this chapter. Similar deformations are noted and associated with oxygen-mediated reaction termination by Ligon et al., 2014.

In the original UV polymerisation set-up, a non-sealed container relied on the continuous inflow of argon gas to displace atmospheric oxygen from the on-going reaction, to prevent premature termination of the reaction. Poor control over the atmospheric conditions during polymerisation was identified as the main component of variation during this thesis. The introduction of an air-tight glove box, with antechamber, was found to stably reduce atmospheric oxygen greater than 10-fold compared to the previous system. A factor that was not considered during this thesis was the rate of reaction termination post-illumination, whilst the 1-hour UV exposure time will have most likely induced a high monomer-polymer conversation rate, atmospheric oxygen content post-illumination was found to have a greater effect on termination, than during UV-illumination (Andrzejewska et al., 2003). In the first polymerisation set-up, oxygen was freely reintroduced to the reaction atmosphere post-illumination, with argon flow stopped, a pitfall not experienced in a sealed reaction system.

Alternatives to prevent oxygen contamination exist aside from purging and controlling oxygen present in the reaction atmosphere, these alternatives were not explored within the chapter. One such alternative is to coat the reaction with a wax barrier, however this may risk introducing unwanted compounds to the surface of the final product, a cytotoxic and contamination risk (Bolon and Webb, 1978).

4.6.6 Culture on TCDMDA:BA

Culturing hPSCs on TCDMDA:BA presented challenges and differences to culture performed on Matrigel. The desired culture cycle for this thesis would be to passage every 3rd day at a 70-90% confluence, on TCDMDA:BA cultures ready for passaging every 3rd day could be produced and maintained for over 24 days. Regarding confluence, seeding technique was critical, unlike Matrigel where cells are mobile on an ECM coated surface, real-time imaging of hPSCs cultured on TCDMDA:BA (not shown) revealed their inability to migrate across the surface upon seeding. This led to uneven seeding and at times dense clustering of hPSCs and apoptosis of hPSC colonies if an undefined but critical size were not formed by 24 hours when ROCKi was removed during medium exchange. Repeated sub-optimal seeding technique upon passages was thought to be linked to loss of hPSC cultures through repeated high-density culture, where high-density culture has been previously linked to an increase in DNA and chromosomal damage, as well as diminished levels of total yes-associated-protein (YAP) leading to downregulation of pluripotency related genes NANOG, OCT4, & SOX2 (Hsiao et al., 2017)(Wu, Fan and Tzanakakis, 2015)(Jacobs et al., 2016). Sub-optimal seeding was aggravated due to the convex nature of polymer layer formation in TCP well plates, where polymerisation would form a thicker layer towards the well walls.

Colony formation on TCDMDA:BA was comparatively denser and '3D-like' than Matrigel. This evidenced by the extended 0.1% Triton-X100 incubation time required to allow antibody penetration throughout the colony (20 minutes vs 1 hour) and the requirement to focus on multiple fields to detect all the hPSCs on TCDMDA:BA. This could be due to the higher required seeding density on

TCDMDA:BA for survival, than Matrigel, but may also be influenced by the lack of motility on the polymer surface, leading to denser colonies.

4.6.7 Proliferation Kinetics

Proliferation over serial passages of TCDMDA:BA cultures produced fewer population doublings than their Matrigel equivalents in the same medium type. Culture of AT1 hiPSCs in homebrew E8 medium saw TCDMDA:BA with a cumulative population doubling 25% lower than Matrigel cultures, 25% lower relative cumulative population doublings was also consistent with LifeTech E8 medium also (both at day 24 culture, n=3). Part of this reduction in cumulative population doublings are explained by the failure to form critical sized colonies by 24 hours culture, leading to areas within the culture surface cell free by 72 hours culture.

More broadly it must be considered the starting conditions newly seeded hPSCs encounter upon both surfaces, where Matrigel contains 60% laminin, 30% collagen IV, and 8% entactin (Corning®), biological components to facilitate efficient integrin-based adhesion and migration. In contrast TCDMDA:BA consists of a neutrally charged cyclic ring and simple aliphatic carbon chains, of which the complexity could be equated to a polymerised chain of a single amino acid. Of the amino acids, only poly-L-lysine has been found to be capable of supporting cellular attachment, but not hPSC attachment, and since its discovery has been combined with RGD peptides or laminins for greater adhesion (Mazia, Schatten and Sale, 1975)(VandeVondele, Vörös and Hubbell, 2003)(Lam et al., 2015).

4.6.8 Synthemax® II-SC Comparison

Synthemax® II-SC is a 'fully synthetic, xeno-free, ready-to-use biomimetic surface' for the culture of hPSCs that is GMP compliant and readily purchasable from Corning® for £402.90 / 10 mg. Synthemax® II-SC is a peptide-copolymer containing the human vitronectin peptide KGGPQVTRGDVFTMP attached to a polymer that is readily dissolved in water and can be coated onto TCP or glass surfaces (Kelley et al., 2014).

Work performed in this thesis would have benefitted greatly with a direct comparison with Synthemax® II-SC and may still do so with the work performed here being intended for publication. Current knowledge of in-depth characterisation of hPSCs cultured on Synthemax® II-SC comes directly from Corning® or peer-reviewed publication where one or more authors are directly compensated by Corning®, creating a conflict of interest in the work discussed here.

A comparison of doubling times between Matrigel & Synthemax® II-SC was performed in mTeSR1 medium at a seeding density of 60,000 cells/cm^2 using dispase and gentle scraping as the passage technique. It is claimed that Synthemax® II-SC demonstrated a doubling time of 56 +/- 11 hours versus 66 +/- 19 hours for Matrigel (Kelley et al., 2014). Culture performed in this thesis, using the AT1 hiPSC line in Essential 8 medium and Trypsin passaging, where Matrigel was seeded at ~26,000 cells/cm^2 and TCDMDA:BA seeded at ~73,000 cells/cm^2, had the following average doubling times: 21.9 +/- 3.8 hours (HomeBrew E8 – Matrigel), 23.4 +/- 3 hours (LifeTech E8 – Matrigel), 30.7 +/- 6.5 hours (HomeBrew E8 – TCDMDA:BA) and 40.2 +/- 17 hours (LifeTech E8 – TCDMDA:BA). Differences will exist in the

population doubling time between different medium, however to assess the real population doubling of Matrigel in this thesis, it was found inappropriate to use the same high seeding density required for TCDMDA:BA culture (as done so by Kelley et al., 2014). Over-seeding Matrigel surfaces artificially made cumulative population doublings appear comparable between Matrigel and TCDMDA:BA, this could be the reason why the comparison between Matrigel and Synthemax® SC-II is favourable to Synthemax® SC-II, and why their Matrigel doubling time, 66 +/- 19 hours, is unusually high.

Assessment of OCT4 retention on Synthemax® SC-II was made in two separate publications, the first by Corning® which determined through flow cytometry that Synthemax® SC-II cultures were 85% +/- 7% positive for OCT4 expression versus 81% +/- 7% on Matrigel (Kelley et al., 2014). Immunostaining of OCT4 presented clear and fully segregated nuclei on Matrigel, an image which would unlikely have been obtainable with the size and density brightfield colonies after seeding at 60,000 cells/cm^2, unless the assessment was made before hPSCs were confluent. Assessment of Matrigel versus Synthemax® SC-II performed in a different study seeded 'similar number and size colonies' through manual dissection, by passage 3, flow cytometry for OCT4 expression on Matrigel was 96.6% versus 66.8% on Synthemax® SC-II, however OCT4 expression fluctuated between passages, by passage 9 Matrigel maintained OCT4 expression where Synthemax® SC-II supported 89.2% positive for OCT4 (Pennington et al., 2015). Comparatively in this thesis marker expression remain statistically comparable to Matrigel, except for SOX2 in the HUES7 line, which at 75.6% +/- 3% on TCDMDA:BA was reduced compared to Matrigel at 88.7% +/- 1.9% SOX2 positivity, after 5

passages. A ~30% loss of OCT4 marker expression compared to Matrigel on Synthemax® SC-II and a ~12% loss of SOX2 marker expression compared to Matrigel on TCDMDA:BA highlight the difficulties of replacing biological coatings with synthetic surfaces.

For a synthetic surface to be viable for large scale culture, it must be economically viable. Vitronectin coating for example has been assessed as being approximately x80 times more expensive than Matrigel, albeit this calculation was performed in 2012 and prices may have decreased since (Lam and Longaker, 2012). Synthemax® SC-II sold at £402.90 per 10mg, at the recommended concentration of 5 μg/cm^2, equates to 2000 cm^2 coating per 10 mg vial, or £0.20 per cm^2. For comparison, 100 mL of TCDMDA is £93.10 (Sigma) and 100 mL of BA is £19.20 (Sigma). Each cm^2 requires a coating of 13 uL of TCDMDA:BA (2:1), 8.7 uL of TCDMDA & 4.3 uL of BA, a total cost of £0.009 per cm^2, although this does not include the cost of production and mark-up value, it demonstrates the economical nature of the readily available acrylate library used within this thesis. Finally, Synthemax® SC-II requires a pre-coating step (which may be advantageous for application to 3D scaffolds), which is avoided with pre-UV polymerised TCDMDA:BA plates.

4.6.9 Reduction in Medium Components

The synthetic environment of TCDMDA:BA presents an additional challenge to cellular survival. Whilst past work with synthetic polymers with hPSCs has demonstrated the absorption of medium components to facilitate cellular attachment (Irwin et al., 2011). TCDMDA:BA and future synthetic hPSC culture

surfaces are statistically more likely to mediate attachment through direct binding of cells, or proteins produced by hPSCs immediately upon culture, due to the reduction of media components to just 8 within DMEM-F12 (Essential 8 medium).

4.6.10 Heparin

The increased cumulative population doublings and reduction in passage to passage variation observed in our Matrigel and TCDMDA:BA cultures using HomeBrew E8 vs LifeTech E8, is noteworthy. Theoretically the only difference is the addition of porcine derived heparin (100 ng/mL). Heparin has previously been studied for its effect on hPSC culture, in a custom medium formulation containing, ascorbic acid-2-phosphate (0.1 µg/mL), heparin sulphate sodium salt (100 ng/mL – 1000 ng/mL), transferrin (5 µg/mL), albumin conjugated with oleic acid (9.4 µg/mL), insulin (10 µg/mL), 2-mercaptoethanol (10 µM), sodium selenite (20 nM) and FGF-2 (10-100 ng/mL), in addition to basal medium (Furue et al., 2008). The study neglects to provide the company or source for the heparin used in both the main text and supplementary information, the source of heparin could be of importance.

It was found that 100 ng/mL heparin could support 6-day hPSC culture and growth in the absence of FGF-2, with the addition of 100 ng/mL heparin without FGF-2 inducing greater protein-level expression of cyclin D1 (Furue et al., 2008). Addition of 10 ng/mL FGF-2 increased the cell count further, this is a significant finding that suggests heparin has a direct role in the maintenance of self-renewal and proliferation in hPSCs, which could explain the higher cumulative population doublings observed in this thesis (Furue et al., 2008). Furue et al., 2008 also notes that 100 ng/mL of FGF-2 in the presence 100 ng/mL heparin induced lower growth

than 10 ng/mL of FGF-2 (~$2x10^6$ vs ~$4x10^6$ cells respectively). The highest concentration of heparin tested, 1000 ng/mL, was detrimental to hPSC culture.

Studies considering the role of heparin in hPSC culture highlight heparins capability to activate FGF-2 and FGF receptors, as well as stabilise FGF-2, where stabilisation was the logical reason for supplementing heparin into HomeBrew E8 medium (Loo et al., 2001)(Li et al., 2016)(Chillakuri, Jones and Mardon, 2010).

Future experiments and HomeBrew E8 formulations may want to consider the impact of different size heparins from defined sources, for medium optimisation and to define which fraction of heparins elicit the biological effects observed in this thesis.

4.6.11 Albumin Contamination

Within this thesis it was found that LifeTech E8, advertised as an albumin free medium, could be contaminated with unquantified but functionally significant concentration of albumin. Concentrations of human albumin as low as 0.1% decreased cell nuclei count and produced large variation in cell nuclei count after 24 hours culture on TCDMDA:BA. At 1% human albumin concentration cell nuclei count was reduced by 2/3rds. Albumin has previously been reported to inhibit cell attachment, one hypothesis is that absorbed albumin competes with proteins promoting cell adhesion for binding to the surface (Carré and Lacarrière, 2010). This hypothesis was confirmed with the discovery of inter-α-inhibitor (IαI), a novel hPSC surface adhesion peptide, where significantly lower cell adhesion was achieved in media containing albumin, or Essential 8 medium spiked with albumin, than in albumin free Essential 8 medium (Pijuan-Galitó et al., 2016).

Batches of LifeTech E8 were screened for the presence of albumin before use by mass spectrometry, the assumption was made that intra-batch supplements are consistent. If this assumption does not hold true, passage-to-passage variation with LifeTech E8 could be due to either low-level albumin contamination, or HomeBrew E8 could reduce variation with the addition of heparin.

4.6.12 Marker Expression on TCDMDA:BA

Flow cytometry assessment of AT1 hiPSCs and HUES7 hESCs on TCDMDA:BA and Matrigel revealed that the HUES7-line comparatively had a significantly reduced percentage of SOX2 positive cells on TCDMDA:BA, after ≥5 serial passages, 85% vs 76% (p=0.003 (**)). A study into the knockdown of SOX2 by short interfering RNA (siRNA) in hESCs demonstrated that a knockdown of SOX2 led to a decrease in SSEA4 (-16%), TRA-1-60 (-32%) and TRA-1-81 (-34%), with an increase in SSEA1 positive cells by 41% (Fong, Hohenstein and Donovan, 2008). Flow cytometry results with the HUES7-line did not result in a significant reduction in NANOG, TRA-1-81 or SSEA4 in this thesis, which is in line with the capability for prolonged culture and trilineage differentiation of the HUES7-line on TCDMDA:BA. Ideally the flow cytometry screen carried out in this thesis would have included SSEA1 as a control for differentiation (Draper et al., 2002).

RT-qPCR data on all three lines AT1, ReBl-PAT and HUES7 did not present a relative decrease in SOX2 expression or other pluripotency-triad genes NANOG & OCT4. Reduction of SOX2 at the protein level is linked to a reduction in NANOG & OCT4 expression (Fong, Hohenstein and Donovan, 2008). In the HUES7 and ReBl-PAT lines significant relative increases in early ectoderm markers PAX6 expression

were seen, additionally early ectoderm marker SOX1 in the HUES7-line. The partial loss of SOX2 positivity in the HUES7-line should trigger the expression of early mesodermal markers, which were not found to have increased in the RT-qPCR panel (Greber, Lehrach and Adjaye, 2007)(Wu et al., 2015). Conversely to the increase in early ectoderm markers and a decrease in % cell positivity for SOX2 seen here, directed differentiation to early neural ectoderm lineages increase SOX2 protein expression over 15 days, with PAX6 appearing at day 2 and SOX1 at day 6 (Pankratz et al., 2007).

Changes to fold-expression in RT-qPCR experiments shown in this thesis are up to 6-fold, it is unknown and beyond the scope of this chapter to determine the significance of these changes, however it did not impede the ability for hPSCs to be cultured for ≥5 passages and form all three lineages, therefore meeting the aims of this chapter.

4.6.13 Tri-lineage Differentiation

Tri-lineage differentiation after ≥5 serial passages was possible in both hPSC lines tested. Regarding mesoderm differentiation to cardiomyocytes, full beating sheets of cardiomyocytes was achieved at the same timepoint Matrigel controls reached the contraction stage. The addition of BMP4 (1 ng/mL) & Matrigel (1:100) in StemPro34 at day minus 1 of differentiation cause the rounding and lifting of colonies on TCDMDA:BA, instead of compaction seen on Matrigel. The cause for this was not determined within this thesis but may be due to a shift in integrin and cadherin expression, where the Matrigel overlay fails to provide adhesive molecules for the early mesoderm cell types. Reattachment and outgrowth from floating

colonies on TCDMDA:BA occurred after the addition of BMP4 (10 ng/mL) & activin-a (8 ng/mL) in StemPro34, by day 2 of differentiation cultures between Matrigel and TCDMDA:BA were visually comparable. Contraction data collected is not sufficient to draw any conclusions regarding functional changes between the two differentiations, without further repeats, RT-qPCR and electrophysiology data.

Differentiation to the endoderm lineage, specifically definitive endoderm, was capable with FOXA2 and SOX17 present at day 2 differentiation on TCDMDA:BA. Compared to Matrigel, surface area coverage was reduced, this could be due to non-optimal seeding for endoderm TCDMDA:BA differentiation, 3D clustering on TCDMDA:BA, or a reduced ability to support & retain the hPSCs going through the early differentiation stage. Continued exposure to CHIR99021 in RPMI/B27 (minus insulin) until differentiation day 5 resulted in monolayer cultures on Matrigel, but large ~1 mm 3D structures on TCDMDA:BA with positivity for FOXA2 and SOX17 markers. 2D areas of cells surrounding 3D constructs were positive for FOXA2 but not for SOX17 expression, which is consistent with the idea that SOX17 is a later marker for endoderm (Jaramillo et al., 2015).

The formation of ectoderm on TCDMDA:BA also resulted in the formation of large 3D structures in most differentiations by differentiation day 5 onwards, in a 48-well plate these structures were observed to approach ~11 mm in length, macroscopically visible. Expression of PAX6 and SOX1 was detected however for a true estimation of positivity in these structures, the cells would have needed dispersing or the constructs segmenting. It is feasible that such 3D structures could change biological response or differentiation outcome, if cells were taken further

toward neural lineages, however due to time constraints this type of analysis was beyond the scope of this thesis.

4.6.14 Integrin Mediated Binding to TCDMDA:BA

The primary mechanism for hPSC adherence to TCDMDA:BA was found to be αVβ3, αVβ5 and β1, where antibodies directed to block their engagement significantly reduced 24-hour DAPI cell count. αVβ5 most prominently reduced cellular count on both AT1 and HUES7 cells lines, with αVβ3 blockade by antibody not resulting in a significant decrease in cellular count for HUES7. However, β1 blockade on HUES7 hESCs had a more significant effect than on AT1 hiPSCs.

The β1 integrin mediates hPSC attachment to laminin when dimerised to α6 integrin, whereas αVβ5 and αVβ3 interact with vitronectin, with αVβ3 also interacting with fibronectin (Vacca et al., 2001)(M A Horton, 1997)(Braam et al., 2008)(Rodin et al., 2010). Furthermore, α6β1 integrin activation has been linked to the maintenance of pluripotency in hPSCs on Matrigel and the synthetic surface poly[2-(methacryloyloxy)ethyl dimethyl-(3 sulfopropyl) ammonium hydroxide] (PMEDSAH) (Villa-Diaz et al., 2016).

Integrin blockade was also performed with RGD-blocking peptides, where αVβ5 and αVβ3 blocking cyclic RGD-blocking peptides H-2574 and H-7226 but not their control peptides H-4088 and H-7232. The fibronectin blocking peptide H-3164 did not affect cell count after 24 hours culture. Results here showing a reduction in binding by blocking β1 and αVβ3 align with integrins found to be important for binding to the synthetic hPSC culture surface poly(HPhMA-co-HEMA) (Celiz et al., 2015). Whilst β1, αVβ3, αVβ5, confirmed by H-2574 & H-7226 (αVβ3 & αVβ5

blocking peptides) align with data which found these to be important for adhesion to IαI (Pijuan-Galitó et al., 2016). Previous polymer microarray work highlights that high acrylate containing polymers with ~70^{o} wettability also employ αVβ3 & αVβ5 engagements for hPSC adhesion with vitronectin absorption (Mei et al., 2010).

In summary previous work on integrin engagement for hPSCs on Matrigel, defined adhesion peptides and other acrylate-based synthetic surfaces align with the identification of β1, αVβ3 & αVβ5 as important cell adhesion integrins for TCDMDA:BA.

4.6.15 Intracellular Signalling Altered in HUES7 but not AT1 hPSCs on TCDMDA:BA

4.6.16 AT1 hiPSCs Intracellular Signalling

AT1 hiPSCs cultured for ≥5 passages on Matrigel and TCDMDA:BA displayed an almost identical phosphokinase proteome profile, PI3K/AKT/mTOR pathway did not vary beyond 0.9-1.3-fold compared to Matrigel. Within the MAPK pathway HSP27 phosphorylation at S78/S82 was relatively reduced by 40%, with HSP27 providing a protective role against a multitude of stress factors (Fan, 2012). A reduction in HSP27 activation by phosphorylation could either signal that AT1 hiPSCs on TCDMDA:BA are undergoing fewer stress signals, or they are failing to respond robustly to the induction of stress-related insult. It has been noted that HSP27 expression profile does not change during hPSC differentiation (Saretzki et al., 2008). The increased phosphorylation of c-Jun S63 (2.38-fold) is thought to be related to a protective response to DNA damage, inhibiting apoptosis, which signals that AT1 hiPSCs cultured on TCDMDA:BA are under higher duress (Vleugel et al., 2006)(Potapova et al., 2001). The hematopoietic cell kinase (HCK) demonstrated

the largest fold increase within AT1 hiPSCs cultured on TCDMDA:BA (2.6-fold), HCK expression is linked to cancer cell survival in leukaemia and enhances proliferation, whereas in mouse ESCs Hck has been shown to support self-renewal (Poh, O'Donoghue and Ernst, 2015)(Tamm, Böwer and Annerén, 2011). Whilst higher activation of c-Jun at S63 suggests higher rates of DNA damage are occurring, P53 S392 is less activated on TCDMDA:BA (0.69-fold signal), with P53 S15 and P53 S46 equal or marginally higher than Matrigel (1.03-fold and 1.26-fold respectively), furthermore CHK2 T68 phosphorylation is consistent with Matrigel cultures, which overall suggests TCDMDA:BA is comparable in the stress and DNA activation response.

4.6.17 HUES7 hESCs Intracellular Signalling

The phosphokinase proteome for HUES7 hESCs cultured on TCDMDA:BA was largely different from equivalent Matrigel cultures. The most notable change was a 13.3-fold increase of EGFR phosphorylation at Y1086, a key activating residue, leading to the induction of the PI3K/AKT pathway, triggering cellular proliferation & survival in cancer cells (Humtsoe and Kramer, 2010)(Humtsoe and Kramer, 2010). In mouse ESCs EGFR activation is related to the maintenance of self-renewal and pluripotency, in human adipose derived stem cells, EGFR was essential to maintain proliferation but also their ability to differentiate (Ai et al., 2017)(Yu et al., 2019).

Increased phosphorylation of Fyn Y420 was also greatly increased on TCDMDA:BA cultures (9.4-fold), Fyn is a Src-family kinase whose activation in hESCs has been linked to a differentiation state along with Src (3.1-fold) and Lyn (3.6-fold), whilst other Src-family kinases Lck (4.0-fold) & Yes (2.85-fold) decline in activity

upon differentiation (Xiong Zhang et al., 2014). The outcome of all Src-family kinases demonstrating an increase in their phosphorylated states on TCDMDA:BA appears counter-intuitive but could be due to either, a mixed population of cells with higher activation of pluripotency related pathways and a population of hPSCs undergoing differentiation, or the possibility that the activation of seemingly opposing phosphorylated kinases functions are determined by the balance and activation of multiple inter-linked pathways.

The relatively large increase in RSK1/2/3 activation (13.28-fold) matches with the increase in ERK1/2 activation (5.37-fold), which leads to RSK1/2/3 phosphorylation and activation (Roux, Richards and Blenis, 2003)(Tanimura and Takeda, 2017)(Cargnello and Roux, 2011). RSK1/2/3 and ERK1/2 activation are both linked to cell cycle progression, proliferation and survival (Cargnello and Roux, 2011)(Tanimura and Takeda, 2017)(Roux, Richards and Blenis, 2003). Meanwhile cell cycle related phosphorylated proteins P53 was between 1.29-2.05-fold increased, with the primary apoptotic related S46 at 1.29-fold higher. CHK2 T68 (3.40-fold) and p27 T198 (5.20-fold) are cell cycle inhibitors, to prevent the cellular division in the presence of DNA damage or anti-mitogenic signals, their upregulation could be in response to the rapid proliferation induced by high RSK1/2/3 and ERK1/2 signalling (Abbastabar et al., 2018)(Coqueret, 2003)(Zannini, Delia and Buscemi, 2014)(Yeh et al., 2009). Despite the presence of increased phosphorylation on kinases related to increase cell proliferation, HUES7 hESCs had fewer cumulative population doublings on TCDMDA:BA compared to Matrigel, a 36% reduction, given than P53 S46 phosphorylation was increased by 29% it is expected that a greater level of apoptosis is occurring on TCDMDA:BA, which could

account for the reduced 72-hour growth. To date, other synthetic surfaces have not performed an assessment of phosphokinase proteome states, making comparisons to other synthetic surfaces impossible.

4.7 Chapter Conclusion

The aims of this chapter, to scale-up polymeric surfaces, perform serial passaging, assess pluripotency and attachment mechanisms were achieved. TCDMDA:BA after an extensive optimisation period can be batch produced at a 6-well format, cultures retained high expression of pluripotency markers and the capability to form all three germ layers. Attachment to TCDMDA:BA was discovered to be reliant on β1, αVβ3 & αVβ5 in hPSCs, with changes in the phosphorylated states of 42 kinases found to be consistent to Matrigel cultures in the AT1 hiPSC line but altered in the HUES7 hESC line.

5 Chapter 5 – Next Generation Biomaterials for hPSC-Derived Cardiomyocyte Maturation

5.1 Chapter Overview

Due to the interdisciplinary nature of this project, challenges with both cell culture & materials production were met. A key step in this chapter is the introduction of a new glove box for performing UV-initiated polymerisation in an atmosphere where greater control of the oxygen content was possible. Therefore, analysis had to be repeated to assess the biological response of hPSC-CMs to hit homopolymer materials with greater control over the polymerisation process.

5.2 Introduction

To determine if synthetic culture substrates for hPSC-CMs discovered in this chapter induce changes to the maturation state, a CellOPTIQ system was used to measure the contractility and electrophysiology parameters of hPSC-CMs after 7 days culture.

5.2.1 Cardiomyocyte Contraction

Contraction in cardiomyocytes begins with the propagation of an action potential from one cell to the next, in vivo action potentials begin from the sinoatrial node where pacemaker cells demonstrate automaticity, spreading the action potential through the atrioventricular node, left & right bundles, terminating in the Purkinje fibres (Nerbonne and Kass, 2005). hPSC-CMs in this thesis are not reliant on pacemaker cells, due to their immature state ventricular-like and atrial-like

populations also demonstrate automaticity, propagating spontaneous action potentials in vitro (Veerman et al., 2015).

In mature cardiomyocytes gap junctions concentrated at the intercalated disks between adjacent cells, which allows the travel of ions, through channels such as Connexin-43, between cells (Kanno and Saffitz, 2001)(SÁEZ et al., 2003). When a threshold of Ca^{2+} concentration is reached, the opening of L-type Ca^{2+} channels occurs. L-type Ca^{2+} are concentrated along t-tubules membrane invaginations, placed into proximity of the sarcoplasmic reticulum (SR) and ryanodine receptor 2 (RYR2) channels, known as a 'dyad', where their dense concentration can lead to sparking (Guatimosim, Guatimosim and Song, 2011)(Hoang-Trong, Ullah and Jafri, 2015). Calcium influx from L-type channels induces calcium release from intracellular SR stores via RYR2, a process known as calcium induced calcium release (CICR) (Zhu, Santana and Laflamme, 2009)(Kane, Couch and Terracciano, 2015). Heightened concentrations of Ca^{2+} in the cytoplasm binds to troponin C (TnC), removing the inhibition of actomyosin ATPase caused by inhibitory troponin subunit (TnI) (Lehman et al., 2009)(Orzechowski et al., 2014). This causes a conformational change displacing tropomyosin from actin binding sites, myosin heads subsequently bind to actin filaments where hydrolysis of bound ATP causes crossbridge formation between the myosin head and actin active site, the myosin head pulls against the actin filament performing a 'power stroke', ADP is released and when new ATP binds the myosin head detaches from actin back to the original conformation (Málnási-Csizmadia and Kovács, 2010). After contraction Ca^{2+} levels in the cytoplasm are reduced through SERCA pumping Ca^{2+} back into the SR to be sequestered by calsequestrin 2 (CASQ2), which accounts for ~70% efflux, and out of the

cardiomyocyte via Na^{+}-Ca^{2+} exchanger (NCX) pumps which accounts for ~28% of Ca^{2+} efflux, the remaining Ca^{2+} is removed by a mitochondrial uniporter (Fearnley, Roderick and Bootman, 2011).

In immature hPSC-CMs cultured in 2D, t-tubules are not present meaning calcium influx via L-type channels are not in proximity to the SR, and RYR2 channels, preventing the large synchronised CICR burst that allows for efficient high amplitude contraction in adult cardiomyocytes (Figure 5.1). Additionally, immature hPSC-CMs lack the expression of CASQ2, junctin (JCTN), triadin (TRDN) and phospholamban (PLB), leading to ineffective calcium handling (Dolnikov et al., 2006)(Li, Chen and Li, 2013). JCTN & TRDN are modulators that interact with RYR2 and CASQ2, CASQ2 controls rate of SR Ca^{2+} store release and reuptake by modulating RYR2 (Györke et al., 2004)(Knollmann, 2009). Calcium-free CASQ2 deactivates RYR2 by binding to JCTN and TRDN and when bound by calcium, inhibition of RYR2 is relieved by the dissociation of CASQ2 (Györke et al., 2004)(Knollmann, 2009)(Li, Chen and Li, 2013). Without tight control over calcium release from the SR, hPSC-CMs are unable to sufficiently store high concentrations of Ca^{2+} in the SR, meaning repetitive contractions without exhaustion cannot occur (Li, Chen and Li, 2013).

PLB regulates Ca^{2+} reuptake by regulating SERCA, in presence of PLB, SERCA has a $K_{1/2}$ of ~0.9 µM, without PLB $K_{1/2}$ is ~0.4 µM (Fearnley, Roderick and Bootman, 2011).

The presence of t-tubules and modulators discussed above allow adult cardiomyocytes to exhibit uniform increases in calcium dynamics across the cell, however hPSC-CMs without t-tubules and modulators display U-shaped waves that

relate to the diffusion distance across the cytoplasm to Ca^{2+} stores at the centre of the cell (Brette and Orchard, 2003). A key aspect of cardiomyocyte contractile functionality that differs between adult CMs and hPSC-CMs is the ability to increase force produced when contraction frequency is increase, a positive force-frequency relationship, hPSC-CMs demonstrate a negative force-frequency relationship due to lack of mature calcium handling apparatus (Dolnikov et al., 2006).

Contraction within this thesis was assessed using the CellOPTIQ (Clyde Biosciences), equipped with a high-speed camera, 1000 images are taken over a period of 10 seconds, which are then compressed into a video file where the displacement of pixels between each frame is assessed with custom-built software (Clyde Biosciences). Pixel displacement represents a surrogate contraction amplitude, as the physical force produced is not being measured.

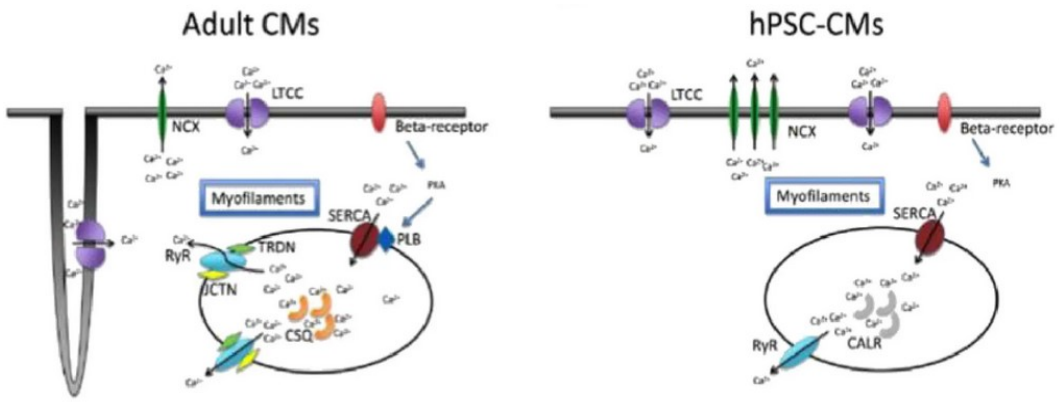

Figure 5.1 Comparison of Calcium Handling in Adult and hPSC-CMs.
(Left) T-tubules place L-type calcium channels in proximity to the SR, where RYR2 channels are modulated by TRDN & JCTN. (Right) Lack of T-tubules results in calcium diffusion dependent kinetics, lack of TRDN, JCTN, CASQ2 & PLB expression hinders calcium handling. Taken from Keung et al., 2014.

5.2.2 Cardiomyocyte Electrophysiology

The action potentials of cardiomyocyte cell types differ between pacemakers, atrial and ventricular cells. The ventricular action potential is divided into 5 phases, 0, 1, 2, 3 & 4 (Figure 5.2). Starting at phase 4, a true resting potential of ~-90 mV exists in ventricular cardiomyocyte. Due to the high concentration of K^+ inside the cell compared to the outside (150 mM vs 4 mM respectively), K^+ continues to diffuse out of the cell through towards the E_k of ~-96 mV (where K^+ would equal net zero) (Klabunde, 2017). Channels such as the potassium inward rectifier channel (Kir2.1) play a critical role in extruding K^+ ions to maintain the true resting potential, preventing gradual depolarisation and pacemaker-like currents (Miake, Marbán and Nuss, 2003)(Grant, 2009).

Neighbouring cells cause depolarisation to a threshold voltage of ~-70 mV, triggering rapid depolarisation of the cardiomyocyte through the opening of fast Na^+ channels (I_{Na}) in a transient manner (<1 ms) toward E_{Na} of +50 mV (phase 0) (Grant, 2009). When depolarised the first repolarisation step takes place, phase 1, where temporary opening of the transient outward K^+ channel (K_{to}) extrudes K^+ from the cell, causing the membrane potential to drop. However, at approximately -40 mV long-lasting L-type Ca^{2+} channels began taking in Ca^{2+} ions causing a large increase in intracellular Ca^{2+} levels (CICR previously discussed), offsetting transient I_{Kto} current. Ca^{2+} dynamics delay repolarisation creating a plateau of ~200ms (phase 2) (Klabunde, 2017)(Klabunde, 2012).

To initiate phase 3, repolarisation, the slowly activating delayed rectifier K^+ current (I_{Ks}) activates when membrane polarisation is more positive than -20 mV. I_{Ks}

rarely inactivates, accumulating over phase 2, to trigger the rapid delayed rectifier K^+ currents (I_{Kr}) when membrane potential becomes negative. This results in rapid activation and repolarisation of the membrane through K^+ efflux throughout phase 3 of the AP (Klabunde, 2012)(Grant, 2009)(Jeevaratnam et al., 2018). During final repolarisation I_{K1} activation increase the negative membrane potential and maintains the polarised state at the true resting membrane level (back to phase 4). A summary of the non-pacemaker AP can be found in figure 5.2, whilst the ventricular AP has been discussed here, I_{Kur} & I_{KACH} (atrial currents) are annotated at their respective phases (Jeevaratnam et al., 2018).

As previously discussed, the AP begins in the sinoatrial node (SAN), unlike ventricular and atrial cardiomyocytes, pacemaker cells have no phase 1 or phase 2 to their AP. Pacemakers have no true resting potential, with a maximum polarity of ~-60mV. Pacemakers are primarily reliant on Ca^{2+} currents for depolarisation, instead of fast Na^+ currents. Slow inward depolarising Na^+ currents 'funny currents' slowly depolarisation the pacemaker membrane until it reaches a threshold of -40 and -30 mV (phase 4 spontaneous depolarisation). At ~-50 mV T-type Ca^{2+} channels cause further depolarisation through opening L-type Ca^{2+} channels leading to phase 0 depolarisation. Repolarisation occurs during phase 3, with K^+ channels opening extruding K^+ from the pacemaker cell, with inward Ca^{2+} channels inactivating (Pinnell, Turner and Howell, 2007)(Mesirca, Torrente and Mangoni, 2015)(DiFrancesco, 2010).

hPSC-CMs are immature in their AP profile, due to lower expression of Kir2.1 (KCNJ2), the resting potential is less negative ~-50/-60 mV, hPSC-CMs also have a detectable funny current which is only present in pacemaker cells, not adult

ventricular/atrial CMs (Sartiani et al., 2007)(Zhang et al., 2009). hPSC-CMs also have a slower upstroke at phase 0, due to limited Na^+ channel expression (Ma et al., 2011). As discussed previously, the calcium handling machinery and t-tubules are either not expressed or reduced in their expression in hPSC-CMs vs adult CMs, leading to a shorter plateau phase.

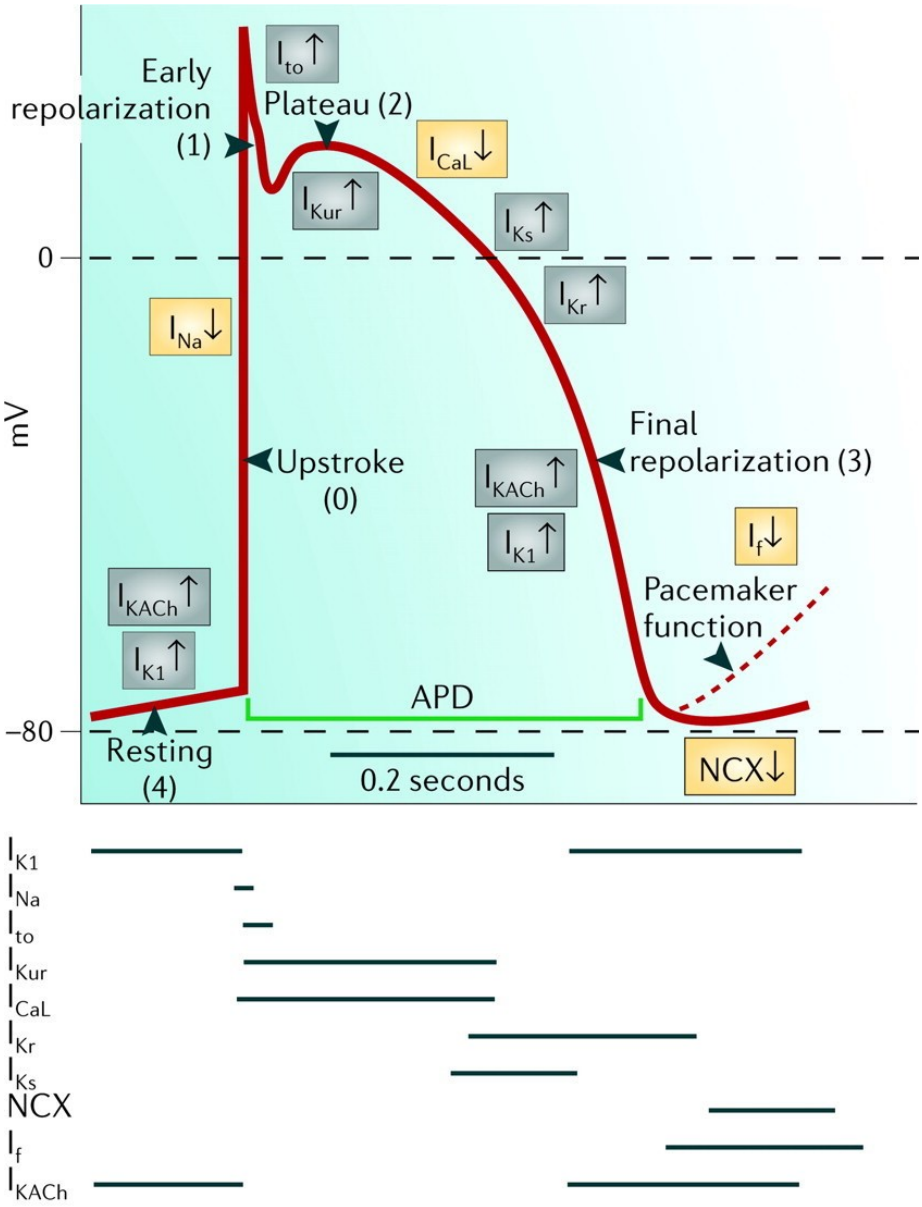

Figure 5.2 Summary of a Human Cardiac Action Potential.
Key ion currents are annotated to their phase of activation. Taken from Grant, 2009.

Within this thesis the AP will be measured using the CellOPTIQ, the use of a Fluovolt™ membrane potential kit will allow sub-millisecond changes to the membrane potential to be detected and assessed on Matrigel, compared to synthetic surfaces discovered within this chapter.

5.3 Chapter aims

1) To discover suitable homopolymers for hPSC-cardiomyocyte attachment & spreading, using homopolymer microarray 9.1.

2) To evaluate the maturation potential of top performing materials from homopolymer array 9.1 when cultured with hPSC-cardiomyocytes, including contractile & electrophysiological performance, sarcomeric organisation & gene expression.

3) To create and screen a co-polymer array based from the top hits found from homopolymer array 9.1, identify combinations with greater hPSC-cardiomyocyte attachment performance than the separate components.

4) To perform in-depth maturation characterisation of hPSC-CMs cultured on best performing co-polymers for cell attachment, in a scaled-up well plate format. This will include analysis of, contractile electrophysiological performance, calcium handling, sarcomeric organisation, expression of maturation-linked genes and metabolism.

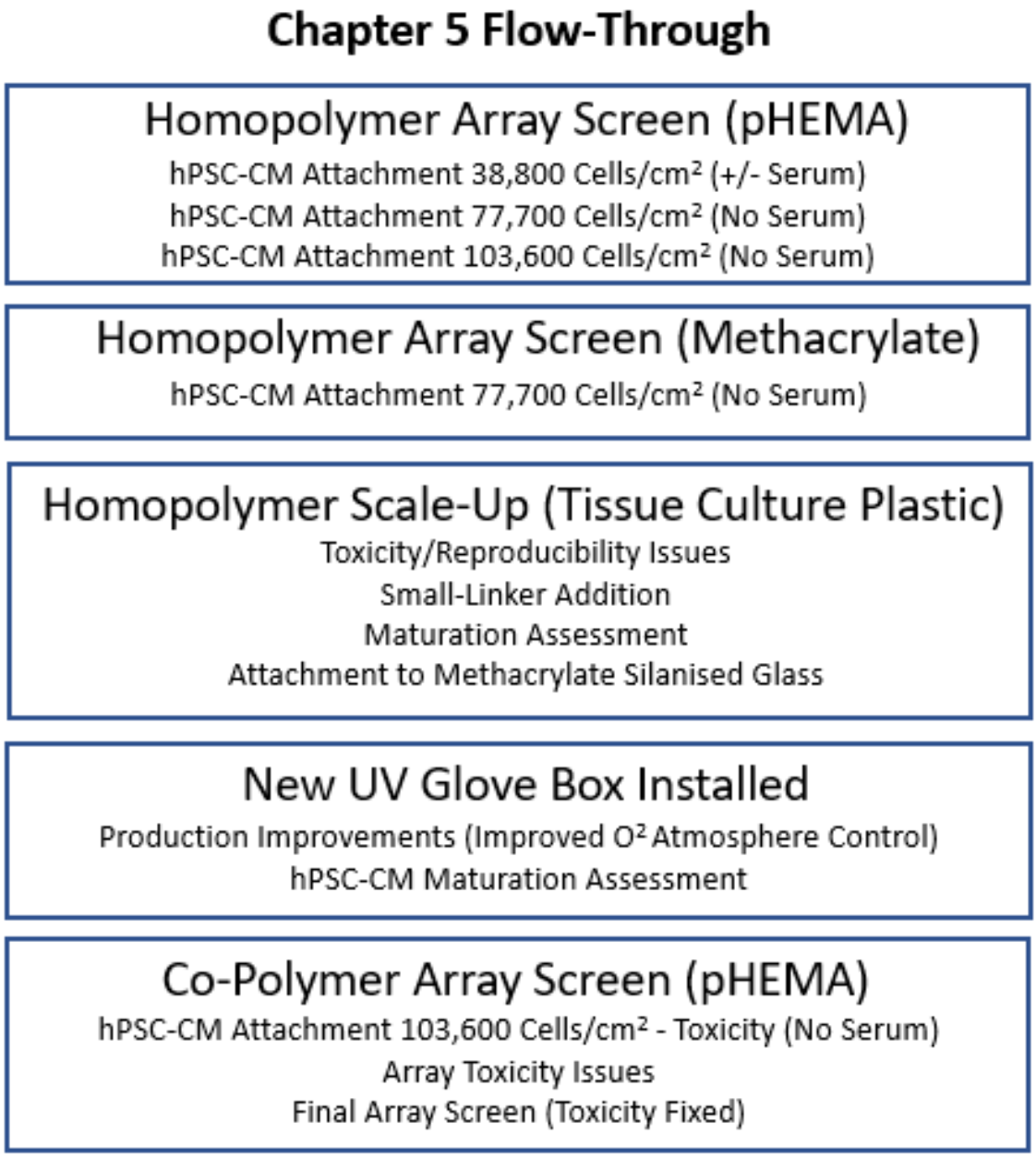

Figure 5.3 Chapter 5 Workflow-Through.

5.4 Results Section

5.4.1 Cardiomyocyte Differentiation & Purity Assessment

To generate cardiomyocytes for the polymer microarray screening process, a directed differentiation protocol for hPSCs was utilised, as shown in Figure 5.4. It was important to have high purity cultures for the array screening process, to ensure most of the attachment data produced relates to cardiomyocytes, not endothelial or other cell types present in the heterogenous differentiations.

All data used for the final microarray results were a minimum of 80% positive for the cardiac specific marker α-actinin, where purity analysis was conducted as shown in Figure 5.5 & Figure 5.6. Method M was selected due to the higher segmentation of objects in proximity, which more closely resembled true separation of nuclei, Figure 5.5 (A). Methods A-C were more prone to identifying multiple nuclei in proximity as singular objects.

The secondary antibody of choice, Alexa Fluor 488, at the used dilution (1:400) resulted in a small background signal typically less than 100 mean fluorescent intensity units (dependent on plate type/make), as shown in Figure 5.5. This ensured the concentration of secondary antibody used was not too high.

To determine purity, a cell-type negative immunostaining was performed with fibroblasts. These cells were stained with both the primary antibody for α-

actinin and the Alexa Fluor 488 secondary, to control for non-specific antibody staining.

Gating performed from the fibroblast staining was set to exclude a minimum of 99% stained fibroblasts, as shown in Figure 5.6 (B), however differentiations selected were above 80% purity for the array data shown in this chapter.

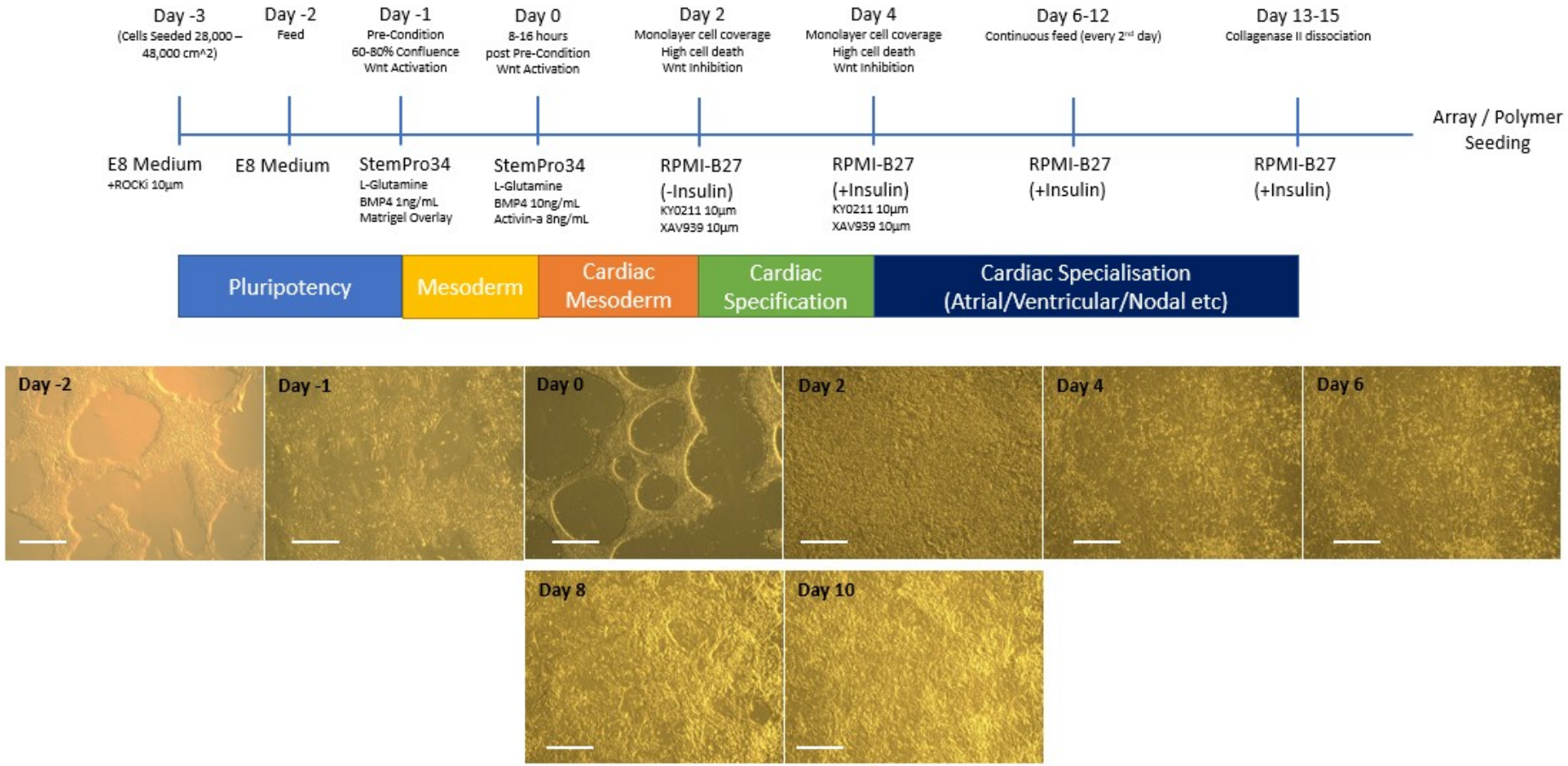

Figure 5.4 Directed Differentiation of Human Pluripotent Stem Cells to Cardiomyocytes through Bi-Phasic Wnt Modulation.

Monolayer differentiation of hPSCs to hPSC-CMs by Wnt modulation, day -3 relates to cell seeding, hPSCs are cultured for 48 hours before pre-conditioning begins. Matrigel overlay is optional but may improve reproducibility of differentiation. Contraction begins day ≤8. Scale bars = 100 µm.

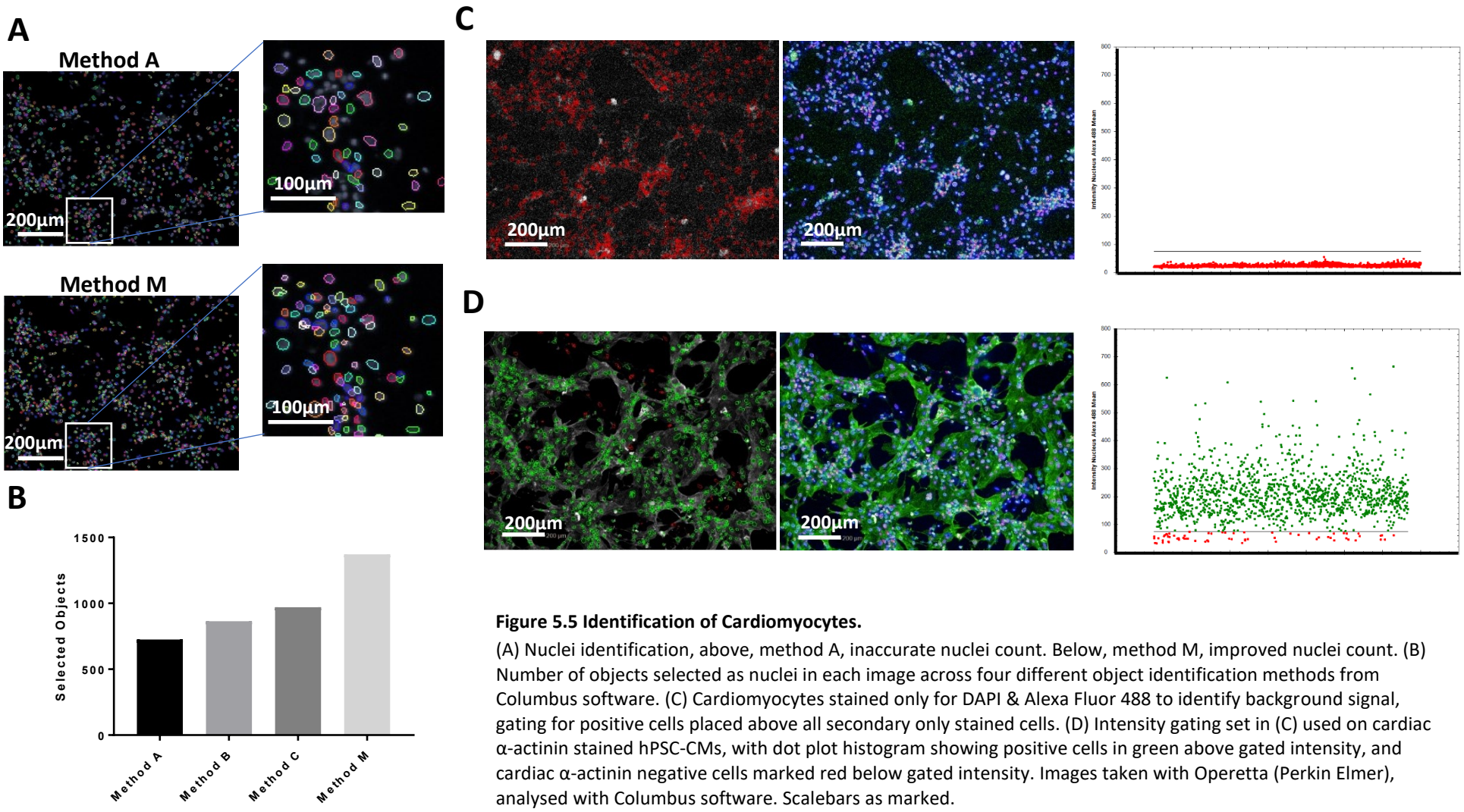

Figure 5.5 Identification of Cardiomyocytes.

(A) Nuclei identification, above, method A, inaccurate nuclei count. Below, method M, improved nuclei count. (B) Number of objects selected as nuclei in each image across four different object identification methods from Columbus software. (C) Cardiomyocytes stained only for DAPI & Alexa Fluor 488 to identify background signal, gating for positive cells placed above all secondary only stained cells. (D) Intensity gating set in (C) used on cardiac α-actinin stained hPSC-CMs, with dot plot histogram showing positive cells in green above gated intensity, and cardiac α-actinin negative cells marked red below gated intensity. Images taken with Operetta (Perkin Elmer), analysed with Columbus software. Scalebars as marked.

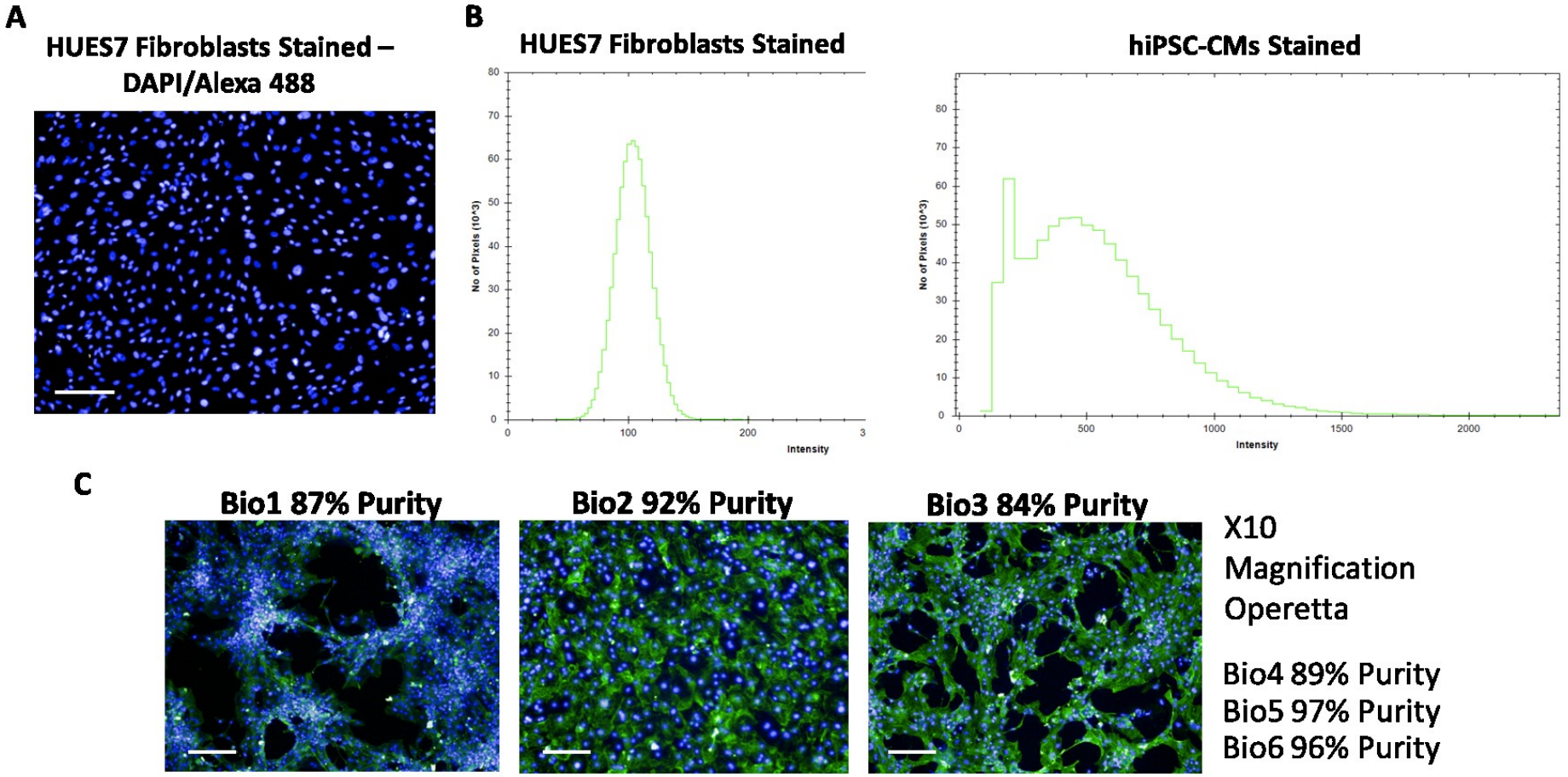

Figure 5.6 Columbus Analysis to Identify Cells Positive for Cardiac α-Actinin.

HUES7 fibroblast nuclei (negative cell type control) were identified with method M. (A) HUES7 fibroblasts stained only for DAPI & Cardiac α-Actinin to identify non-specific background staining. (B) Gating for positive cells placed above intensity signal for stained HUES7 fibroblasts. (C) Example images of purity staining with cardiac α-Actinin and purity values for 6 biological repeats used for generation 1 hPSC-CM array screening. Images taken with Operetta (Perkin Elmer), analysed with Columbus software. Scalebars = 200 µm.

5.5 Generation 1 Homopolymer Array for hPSC-CM Attachment

To discover novel biomaterials that support hPSC-CM attachment, and ideally maturation, a range of array experiments were designed. These parameters tested three different cell seeding densities; 38,800, 77,700 & 103,600 cells/cm^2.

All conditions were tested in a serum-free setting. The lowest seeding density 38,800 cells/cm^2 was additionally tested with 10% FBS preconditioning. This was performed for two key reasons, the first relates to past work by a former PhD student in the lab, Asha Patel, where hPSC-CMs cultured on serum-free arrays demonstrated that only 10% of polymers supported attachment, with average cell spreading equating to 274 +/- 75 μm^2 vs 2019 +/- 596 μm^2 on the gelatin control. The results from Patel et al., 2015 relied on combining homopolymers that demonstrated attachment after being serum preconditioned.

The second reason serum preconditioning was performed with 38,800 cells/cm^2 seeding density, was to reveal which homopolymers could support a greater level of cell spreading – if they were given a protein rich environment. These polymers could have a greater potential for synergy in co-polymer arrays by combining high attachment properties of one homopolymer with the greater cell spreading potential of another.

To ensure work was carried out reproducibly between polymer microarrays, a standardised workflow through was created to ensure sterilisation & medium incubation times were consistent. The protocol involved; x2 15-minute UV sterilisation steps, a 1-hour medium incubation step, fresh medium exchange & cell

seeding, followed by one-week culture, followed by analysis, graphically presented in Figure 5.7.

Analysis of object attachment to polymer spots was carried out using CellProfiler™, a basic pipeline was formulated that performed a cell count, through identifying 'primary' objects within a size & shape filter stained for 4', 6-diamidino-2-phenylindole (DAPI).

Secondary objects were detected based on 488 nm signal propagating from a primary object, the 488 nm signal was manually gated at 200 fluorescent intensity, above the background staining of fibroblasts stained for α-actinin.

Tertiary objects combine the α-actinin positive area identified in the secondary object module and include the primary object area to determine the entire object size. This is visually represented in Figure 5.8.

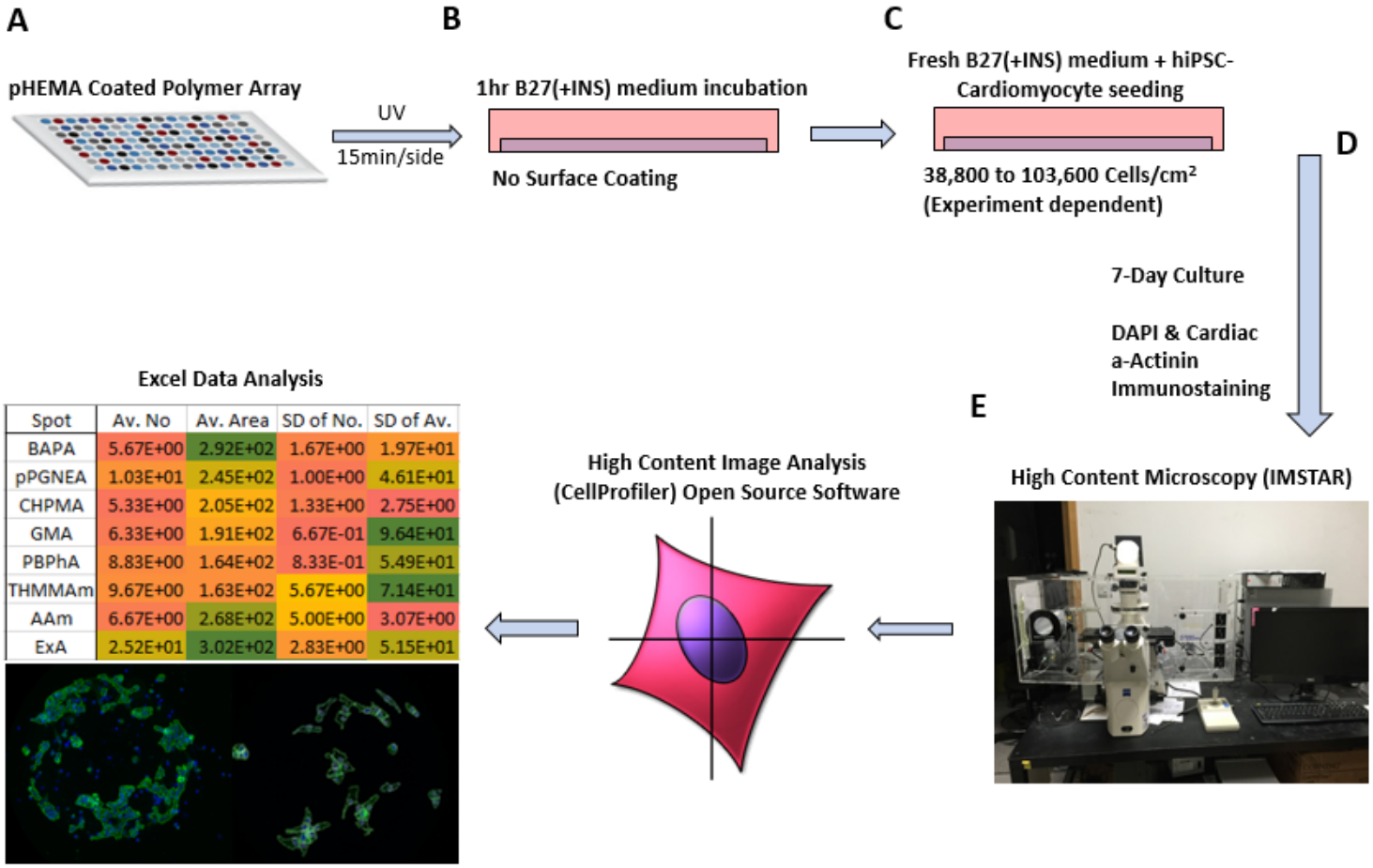

Figure 5.7 Workflow through of hPSC-derived Cardiomyocyte Polymer Microarray Screening.

(A) Sterilisation of polymer microarrays using UV irradiation for 15 minutes per side. (B) Medium incubation to allow proteins present in the medium to interact with polymer surfaces. (C) Seeding of hPSC-derived cardiomyocytes in fresh medium at varying densities (some experiments contained 10% FBS). (D) Cells cultured for 7 days and then immunostained with DAPI nuclear stain & cardiac a-Actinin. (E) Automated high content image collection with the IMSTAR microscope, followed by high content image analysis using open source software CellProfiler™. Data analysed in Microsoft Excel.

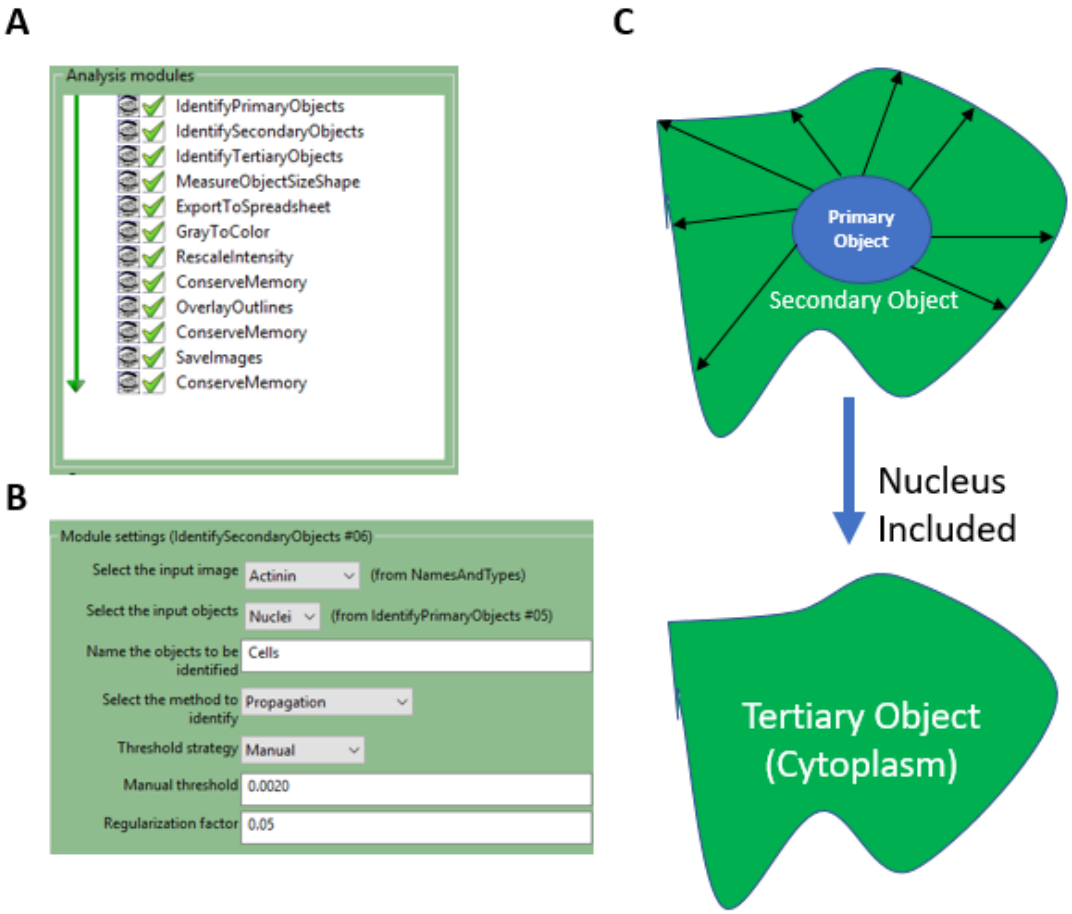

Figure 5.8 Basic CellProfiler™ Pipeline for Identifying the Nucleus and Cytoplasm of hPSC-derived Cardiomyocytes.

(A) List of analysis modules used to collect data from hPSC-CM polymer microarrays. (B) Example settings within a module, shown, the method and fluorescent threshold settings to identify the secondary object. (C) Visual representation of the primary, secondary and tertiary objects. (D) Example image produced with the CellProfiler™ pipeline. Scale bar = 100 µm.

5.5.1 Homopolymer Array '9.1' hPSC-CMs 38,800 Cells/Cm^2 Seeding Density, Attachment Results

To discover new biomaterials for hPSC-CM attachment, a provisional screening process was established. High purity hPSC-CMs were prepared as described in the methodology section to provide purities of ≥80%, as gauged by expression of α-actinin. These cells were seeded at a density of 38,800 cells/cm^2 onto a polymer array, termed 9.1. This cell density was selected because it would be sparse enough to induce cell spreading.

The arrays comprised 281 homopolymers contact printed as ~200 μm spots onto pHEMA coated epoxy silane treated slides, with three replicates of each polymer. In addition, 3 co-polymers were included which were identified in a previous study to facilitate partial maturation of hPSC-CMs (Patel et al., 2015).

The co-polymers included were mixed in 2:1 v/v ratio, their identities: 1.) N-(2-aminoethyl methacrylamide hydrochloride) : Tert-butylamino-ethyl methacrylate (iBMA:tBAEMA), 2.) Furfuryl methacrylate : Tert-butylaminoethyl methacrylate (FuMA:tBAEMA), 3.) Hexanediol ethoxylate diacrylate : Ethoxyethyl methacrylate (HEODA:EEMA).

After a culture period of 7 days on an array, hPSC-CMs were fixed and stained with DAPI & α-actinin to enable automated assessment using the approaches in Figure 5.7 and Figure 5.8. Three assessment criteria were used: 1) Attachment, 2) Coefficient of Variation (CoV), and 3) Reproducibility. Attachment was measured to ensure cells were capable of binding to the surface, the CoV determined the variation of attachment between all repeats (technical & biological). The assessment of

reproducibility was introduced to measure how well polymers performed across multiple biological repeats, where no. technical repeats * no. biological repeats supporting hPSC-CM attachment provided the value. This set out to identify polymers that supported very high attachment in one biological repeat with low variation, but not in other biological repeats, a false positive within the array screen.

Cell attachment was calculated by the number of DAPI stained objects between a gated size of 10-40 pixels, with a rounded shape. CoV was measured as the percentage standard deviation of the averaged attachment value. Reproducibility for each polymer spot was calculated by multiplying the number of technical repeats by the number of biological repeats, which supported attachment. Where only a single biological repeat supported attachment, this number was considered zero. Reproducibility was expressed as a percentage.

A key finding from these provisional experiments was only 7/284 polymers supported attachment of ≥100 nuclei, on average polymers supported 28 cells (Figure 5.9). The top 10 performers contained amine functional groups. For example, N-[2-(N,N-Dimethylamine)ethyl) methacrylate (DMEMAm), N-(3-(Dimethylamino)propyl) methacrylamide (DMPMAm) & Dimethylamino-propyl acrylate (DMAPA) contained a tertiary amine functional group. N-(3-aminopropyl) methacrylamide hydrochloride (APMAm.C) & N-(2-aminoethyl) methacrylamide hydrochloride (AEMAm.C) contain primary amine groups.

It was also observed that the 8th top performing homopolymer, DMAPA, was also a top performing homopolymer for hPSC-CM attachment in work carried out by previous PhD student Asha Patel (Patel et al., 2015).

The three partial maturation inducing co-polymers selected from Patel et al., 2015, iBMA:tBAEMA, FuMA:tBAEMA & HEODA:EEMA, supported 84 +/- 66%, 39 +/- 19%, 19 +/- 25% attachment respectively. None of the 'positive' controls were in the top 10 performing polymers for this experiment.

Nevertheless, the CoV was above 50% for 90/284 polymers, while the reproducibility score was less than 50% for 251/284 polymers. There were several possible reasons. Clumpy cells or algorithm failure, therefore an inaccurate assessment of pixel coverage. Absence of protein, hence an attempt with serum preconditioning, and low seeding density of 38,800 cells/cm^2, which was leading to uneven cell attachment. These explanations are explored in the following section.

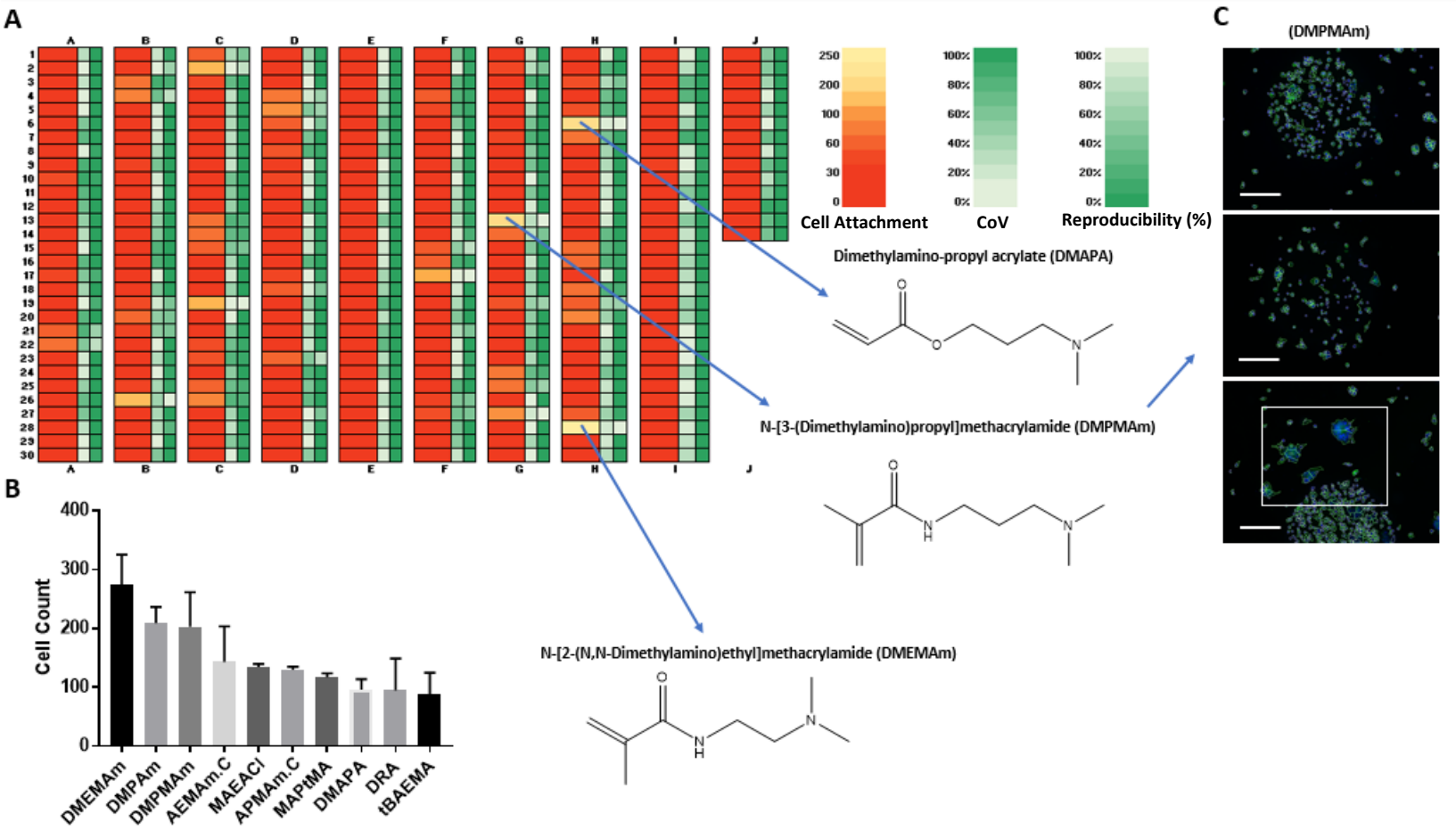

Figure 5.9 Attachment of hPSC-CMs on Homopolymer Array '9.1' Seeded at 38,800 Cells/Cm2 (Serum Free).

(A) Heatmap representation of hPSC-CM attachment, reproducibility indicated by coefficient of variation & a 'reproducibility' value, linked to the number of technical & biological repeats positive for attachment. (B) Top 10 homopolymer attachment hits. (C) Images specifically of DMPMAm across three technical repeats to demonstrating variation of attachment. Specifically highlighted an area of the DMPMAm – pHEMA interface with increased cell spreading. Image analysis performed in CellProfiler™, data analysis performed in Microsoft Excel.
Scale bars = 100 µm. N=2. n=6.

5.5.2 Homopolymer Array '9.1' hPSC-CMs 38,800 Cells/Cm^2 Seeding Density, Average Cell Area Results

With the aim of discovering homopolymer hits that support greater spreading of hPSC-CMs, the area of each cell was also measured with the CellProfiler™ pipeline (Figure 5.8).

Array 9.1 cultured with 38,800 cells/cm^2 for 1 week demonstrated that average cell area sizes ranged from 100-382.5 positive α-actinin pixels (Figure 5.10 (A)). On average polymers supported 224.3 +/- 41% positive α-actinin pixels.

The CellProfiler™ pipeline identifies tertiary objects for cell area, as previously described. The top performing homopolymers on array 9.1 cultured in the absence of serum ranged between 317.1-382.5 positive α-actinin pixels (Figure 5.10 (B)). 7% of polymers tested supported an average cell size of 300 or more positive α-actinin pixels.

A qualitative assessment the images for the three top performers, 2-Aminoethyl methacrylate hydrochloride (AEMA.C), Disperse red 1 acrylate (DRA) & N-(2-aminoethyl) methacrylamide hydrochloride (AEMAm.C) in (Figure 5.10 (C)) highlights that differences in measured average cell area are likely due to cell clumping, rather than improved spreading.

For this reason, the assessment of area for non-serum preconditioned arrays will be omitted for the remainder of this chapter. Assessment of hPSC-CM attachment for non-serum preconditioned arrays will be used to select top performing hits.

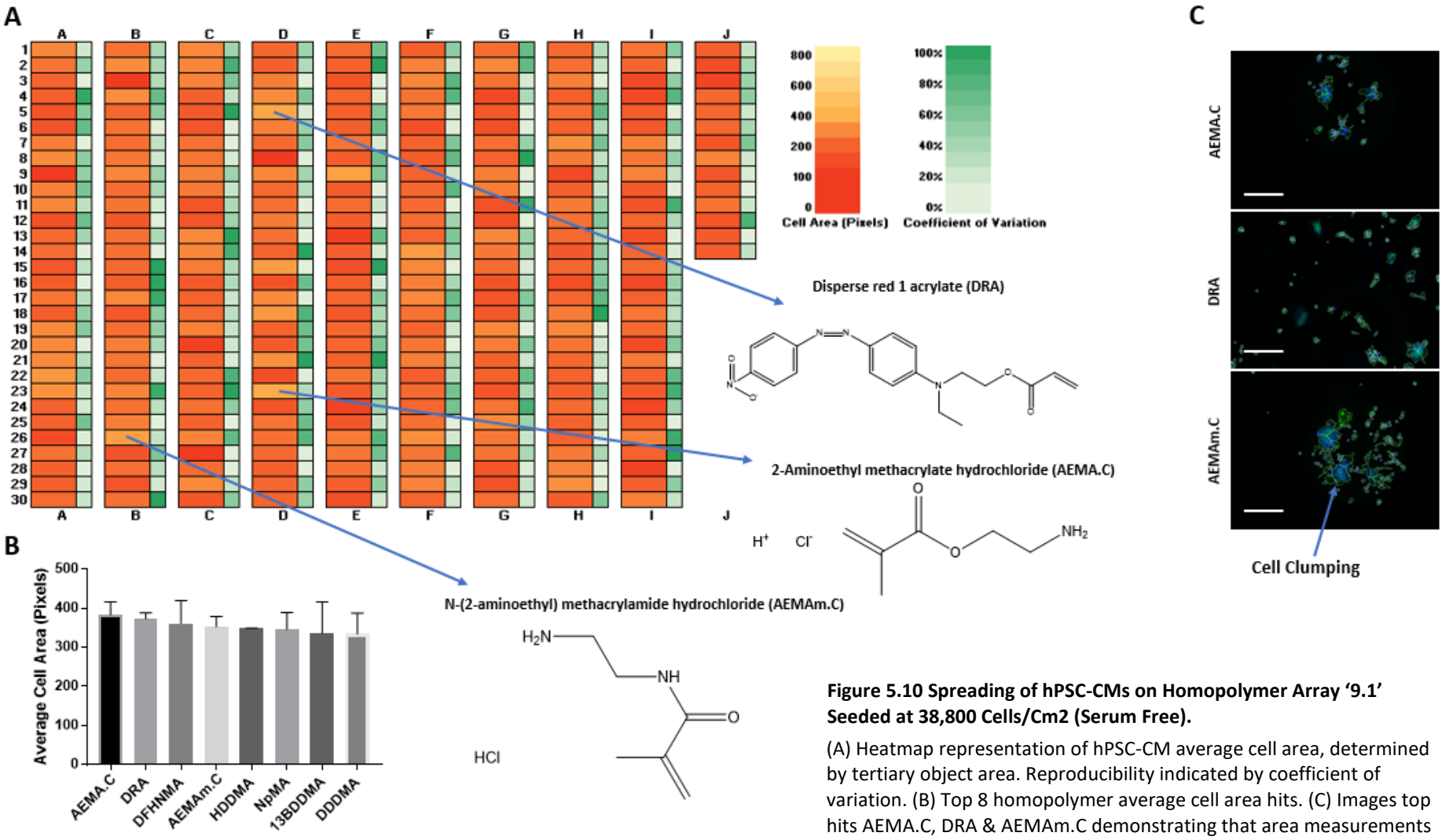

Figure 5.10 Spreading of hPSC-CMs on Homopolymer Array '9.1' Seeded at 38,800 Cells/Cm2 (Serum Free).

(A) Heatmap representation of hPSC-CM average cell area, determined by tertiary object area. Reproducibility indicated by coefficient of variation. (B) Top 8 homopolymer average cell area hits. (C) Images top hits AEMA.C, DRA & AEMAm.C demonstrating that area measurements have identified clumps of cells, rather than individual cells. Image analysis performed in CellProfiler™, data analysis performed in Microsoft Excel. Scale bars = 100 µm. N=2. n=6.

5.5.3 Homopolymer Array '9.1' hPSC-CMs (Serum Preconditioned) 38,800 cells/cm^2 Seeding Density, Attachment & Area Results

Preconditioning polymer microarrays with serum allows an undefined and diverse mixture of protein, including adhesion-related proteins to attach the polymer spots. Whilst this goes against the purpose of this chapter, to create synthetic fully defined systems, coating with a diverse mixture of proteins may allow the identification of homopolymers that can support protein binding but perhaps not facilitate initial hPSC-CM attachment. These monomers could have potential in co-polymer formats for synergistic effects.

Through the coating of polymer surfaces with adhesion proteins & extracellular matrix proteins, originating from the serum preconditioning step, it is hypothesised that greater cell attachment & cell spreading would be observed, compared to non-serum preconditioned arrays.

Average cell attachment to array 9.1 with serum preconditioning decreased but increased in CoV when compared to non-serum preconditioning, 20 +/- 53% vs 28 +/- 38% (Figure 5.11 & Figure 5.9 (A)). An unpaired t-test with Welch's correction found this difference to be significant, P=0.0006 (***).

Top hits for attachment to array 9.1, seeded at 38,800 cells/cm^2, after serum preconditioning were first ordered by highest reproducibility values, then presented again by highest attachment values (Figure 5.11 (B/B(i))).

All polymers that supported attachment with 100% reproducibility, 6/284, are represented in Figure 5.11 (B). None of these polymers supported ≥100 cells after serum preconditioning, however the average attachment for polymers with 100%

reproducibility was 53 +/- 34%, higher & less variable than the array average, 20 +/- 53%.

Highlighted in Figure 5.11 (B)I are the two homopolymer hits, DMAPA & APMAm.C, which supported 118 +/- 54% & 107 +/- 24% respectively, with 83% reproducibility.

Serum preconditioning had a positive effect on cell spreading. Figure 5.12 (A) & (B) showed a significant increase in the average cell area compared to the arrays seeded without serum preconditioning, 248 +/- 38% vs 224.3 +/- 41%, P=0.0027 (**).

Unlike the average cell area without serum preconditioning, the addition of serum does not suffer from the same cell clumping issue – a qualitative analysis through representative images in Figure 5.12 (C) demonstrates that homopolymers, Zirconium carboxyethyl acrylate (ZrCEA), Divinyl Adipate (DVAd) & Triethylene glycol diacrylate (E3GDA) are supporting true cell spreading. Quantitatively ZrCEA, DVAd & E3GDA, demonstrated an average cell size of 744 +/- 3%, 687 +/- 19% & 801 +/- 66% positive α-actinin pixels respectively.

Going forward with co-polymer arrays these homopolymers could be important for inducing attachment – spreading synergy.

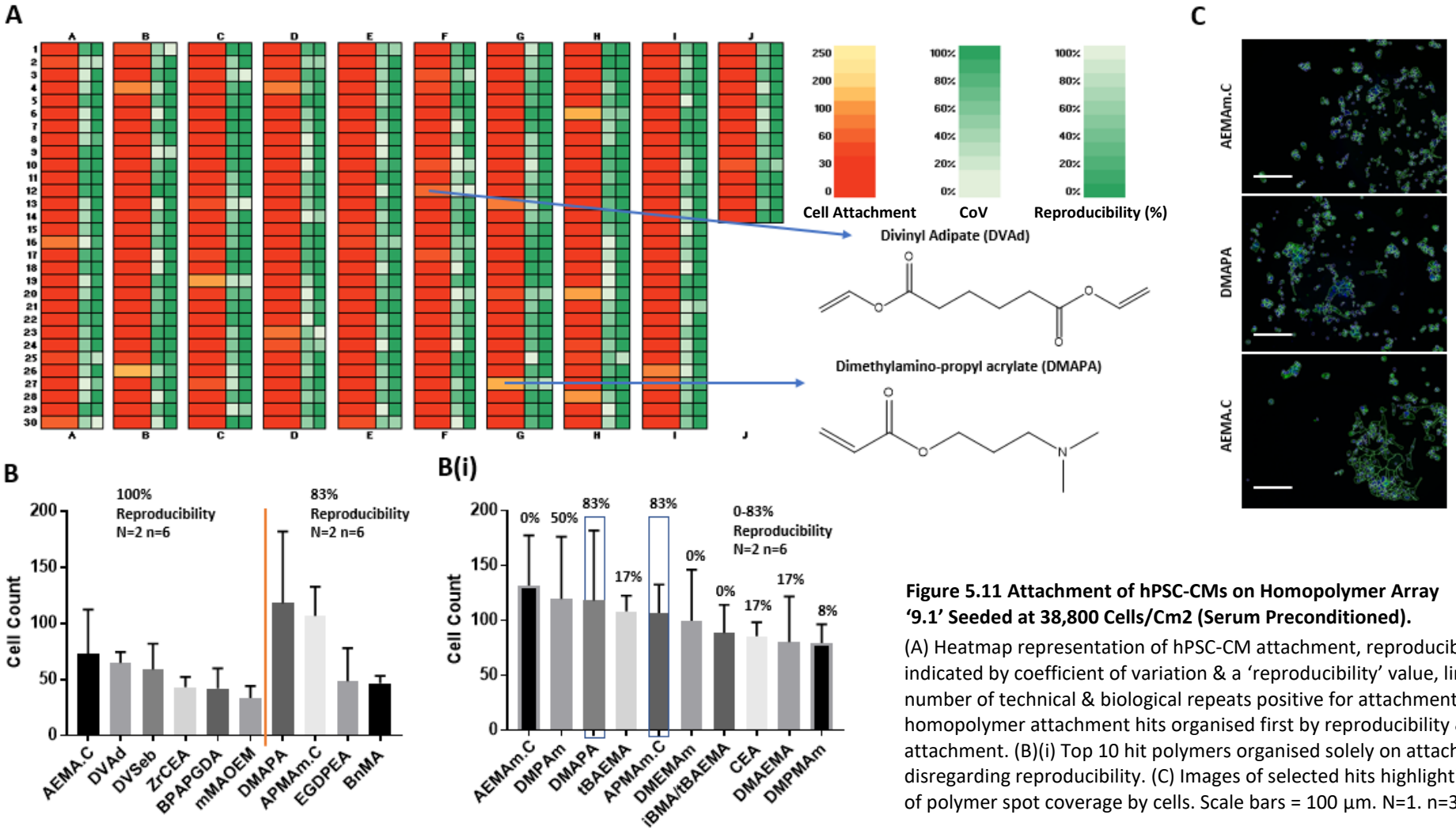

Figure 5.11 Attachment of hPSC-CMs on Homopolymer Array '9.1' Seeded at 38,800 Cells/Cm2 (Serum Preconditioned).

(A) Heatmap representation of hPSC-CM attachment, reproducibility indicated by coefficient of variation & a 'reproducibility' value, linked to the number of technical & biological repeats positive for attachment. (B) Top 10 homopolymer attachment hits organised first by reproducibility & then by attachment. (B)(i) Top 10 hit polymers organised solely on attachment, disregarding reproducibility. (C) Images of selected hits highlighting the level of polymer spot coverage by cells. Scale bars = 100 µm. N=1. n=3.

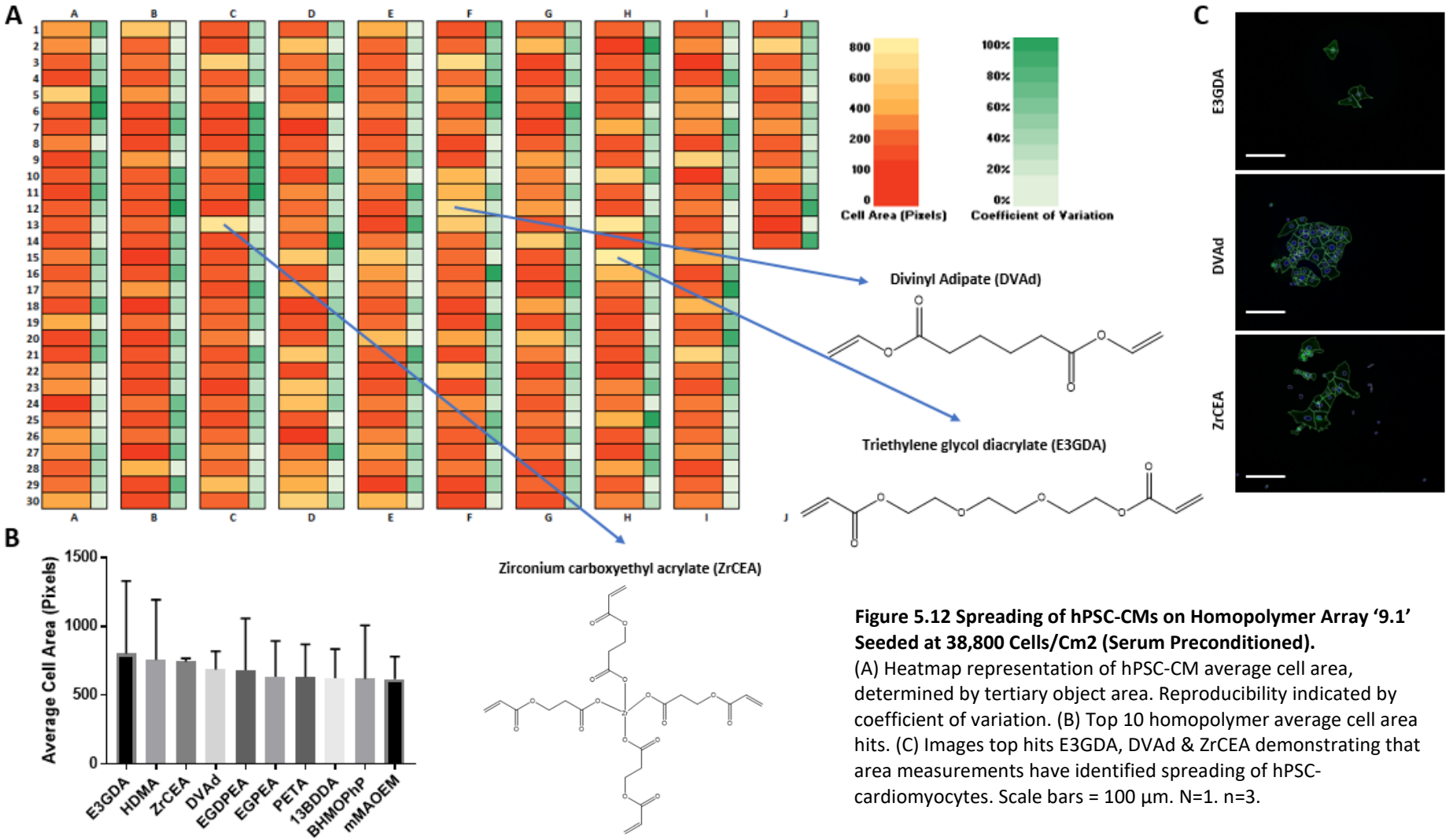

Figure 5.12 Spreading of hPSC-CMs on Homopolymer Array '9.1' Seeded at 38,800 Cells/Cm2 (Serum Preconditioned).
(A) Heatmap representation of hPSC-CM average cell area, determined by tertiary object area. Reproducibility indicated by coefficient of variation. (B) Top 10 homopolymer average cell area hits. (C) Images top hits E3GDA, DVAd & ZrCEA demonstrating that area measurements have identified spreading of hPSC-cardiomyocytes. Scale bars = 100 µm. N=1. n=3.

5.5.4 Homopolymer Array '9.1' hPSC-CMs (No Serum) 77,700 – 103,600 Cell/Cm^2 Seeding Density Results

Polymer microarray screening with a seeding density of 38,800 cells/cm^2 did not provide an adequate number of attachment hits to be taken forward for co-polymer microarray screening.

To identify more potential hit homopolymers, two further seeding densities were screened; 77,700 cells/cm^2 & 103,600 cells/cm^2. These densities similar to the range used on a Matrigel™ surface for monolayer attachment – 85,000 to 100,000 cells/cm^2.

At the highest seeding density, 85/284 of polymer spots supported over 100 DAPI nuclei. The top 10 performing homopolymers, first arranged by reproducibility (7/284 = 100%) & then by attachment performance where hits supported ≥230 nuclei / spot, are shown in Figure 5.13.

A high seeding density 103,600 cells/cm^2 vs 38,800 cells/cm^2 resulted in an increase in average cell attachment to spot, 95 +/- 59% vs 28 +/- 38%. An unpaired t-test with Welch's correction found this difference to be significant, P=<0.0001 (****).

The trend for amine chemistry containing homopolymers to perform well for attachment is evident, with 8 of the top 10 containing either a primary, tertiary or quaternary amine functionality.

The CoV across repeats at the highest density, 103,600 cells/cm^2 was on average 24% for the top 10 hits (ranked on reproducibility), primary amine containing chemistries APMAm.C, AEMAm.C & AEMA.C exhibited the greatest variation of top

performers, 33%, 51% & 53% respectively. AEMA.C failed to support cell attachment at the 103,600 cells/cm^2 seeding density, however at 77,700 cells/cm^2 & 38,800 cells/cm^2 AEMA.C was within the top performing hits.

Combined, data from the low seeding density ~38,800 cells/cm^2, with & without serum preconditioning, and results shown here in Figure 5.13 provide a suitable list of 24 homopolymers to be taken forward based on their performance.

Due to the demonstrated effect of pHEMA on biological response in chapter 3, (4% vs 6% pHEMA comparison), an array screen was also performed with an alternative background coating, to ensure hits were not dependent on the pHEMA layer.

5.5.5 Methacrylate Homopolymer Array '9.1' hPSC-CMs (No Serum) 77,700 Cells/Cm^2 Seeding Density

The pHEMA background was previously thought to be without effect on the biological response on polymer microarrays, has been demonstrated to influence cell response in chapter 3.

To ensure polymer hits for hPSC-CM attachment are not pHEMA dependent, the same array layout was printed onto a methacrylate background.

A methacrylate silane should provide a single layer of chemistry for printed polymers to chemically bond to, instead of the ~1-2-micron thick hydrogel formed by pHEMA dipping (4% pHEMA).

Top performing primary amines, APMAm.C, AEMAm.C & AEMA.C on pHEMA arrays, also form part of the top 10 hits on the methacrylate background (Figure 5.14).

The top 10 hits on the methacrylate background array, seeded at 77,700 cells/cm^2 supported an average of 378 +/- 20% cell attachment, 9 of which, with 100% reproducibility. Dodecafluoroheptyl acrylate (DFHA) was the exception, with 89% reproducibility.

Arrays coated with a methacrylate background outperformed pHEMA coated arrays, when both were seeded with 77,700 cells/cm^2, for cell attachment, 83 +/- 34% vs 50 +/- 34% DAPI nuclei respectively (P=<0.0001, ****).

Homopolymers ZrCEA & MAEAC, high performers on pHEMA also made the top 10 however top attachment hits on methacrylate coated arrays.

New hits solely present on methacrylate arrays such as 2-sulfoethyl methacrylate (SEMA) & isodecyl methacrylate (iDMA) also appear, supporting 366 +/- 8% & 325 +/- 15% nuclei, suggesting that the array background coating does play a role in determining the functional hits.

Due to undesirable background cell attachment on a methacrylate coated arrays and delamination of polymer spots observed in culture, the results presented here are confounded by these issues.

The array printing process does have the capacity to be optimised, specifically with humidity and temperature inside the array printer enclosure, which may improve the stability of methacrylate coated arrays, however that was beyond the

interest of this study – where sufficient data has informed the top performing hits going forward.

The selected homopolymers in Figure 5.15 to be taken forward for generation 2 co-polymer array screening was determined by examining the results from the three different seeding densities, results in the presence and absence of 10% FBS preconditioning, and finally by their translatability to a 2D methacrylate coated polymer array.

Hits are ranked in their overall performance and annotated with the letters (A-X) for cross-referencing with co-polymer array print locations.

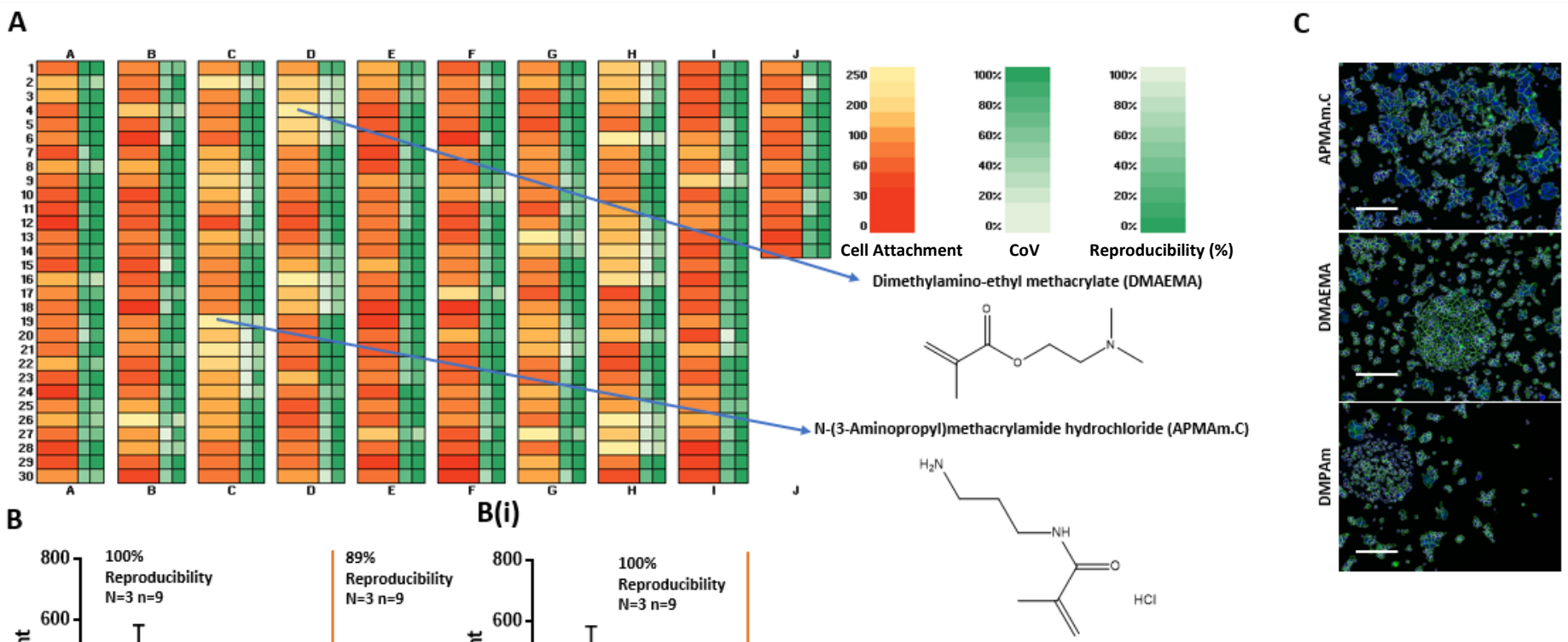

Figure 5.13 Attachment of hPSC-CMs on Homopolymer Array '9.1' Seeded at 103,800 Cells/Cm2 (Serum Free).
(A) Heatmap representation of hPSC-CM attachment, reproducibility indicated by coefficient of variation & a 'reproducibility' value, linked to the number of technical & biological repeats positive for attachment. (B) Top 10 homopolymer attachment hits organised first by reproducibility & then by attachment. (B)(i) Top 10 hit polymers organised solely on attachment, disregarding reproducibility. (C) Images of selected hits highlighting the level of polymer spot coverage by cells. Scale bars = 100 µm. N=3. n=9.

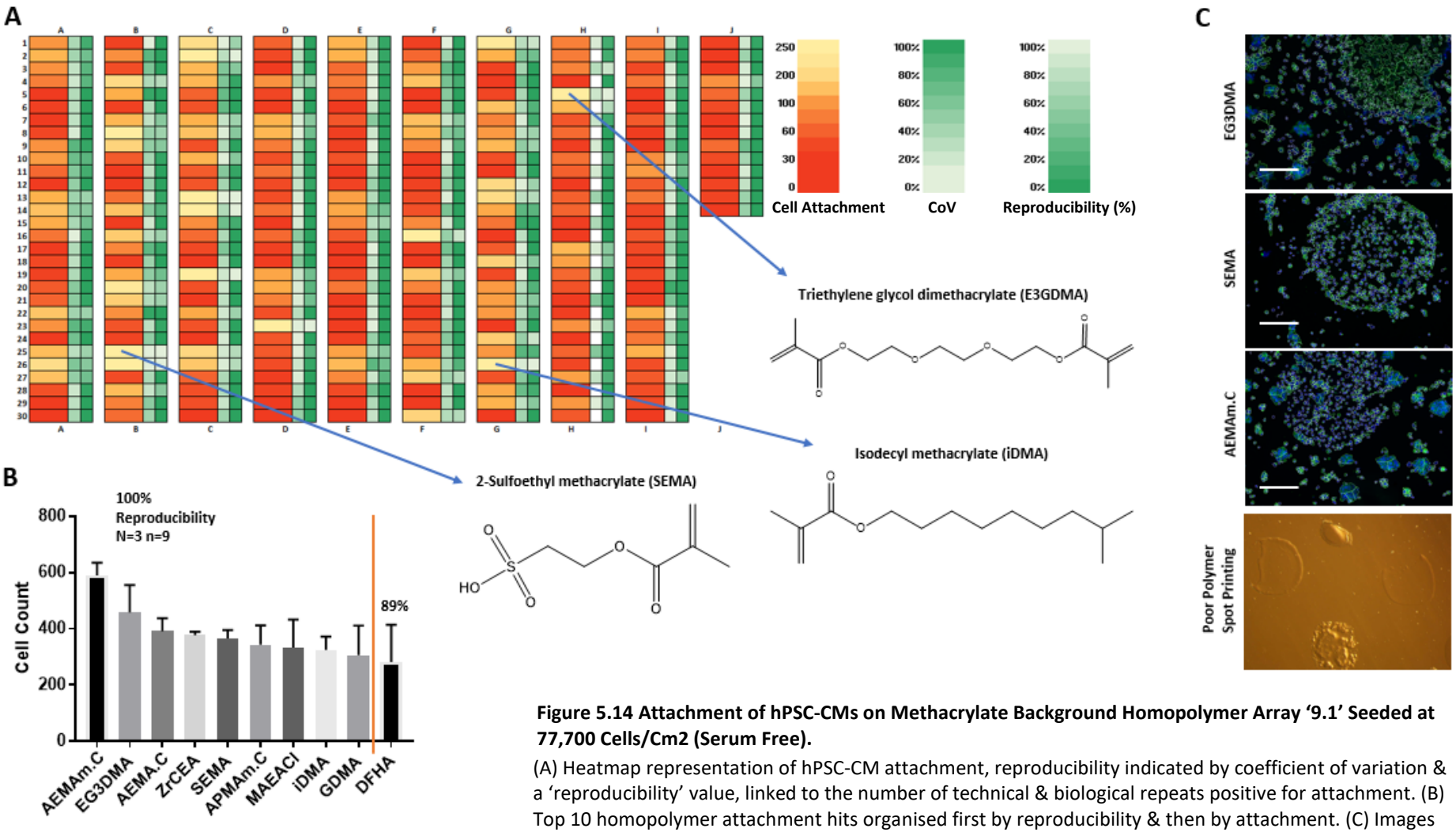

Figure 5.14 Attachment of hPSC-CMs on Methacrylate Background Homopolymer Array '9.1' Seeded at 77,700 Cells/Cm2 (Serum Free).

(A) Heatmap representation of hPSC-CM attachment, reproducibility indicated by coefficient of variation & a 'reproducibility' value, linked to the number of technical & biological repeats positive for attachment. (B) Top 10 homopolymer attachment hits organised first by reproducibility & then by attachment. (C) Images of selected hits highlighting the level of polymer spot coverage by cells. Also shown is a brightfield example of poorly printed polymer spots, deformed in size & shape. Scale bars = 100 µm. N=3. n=9.

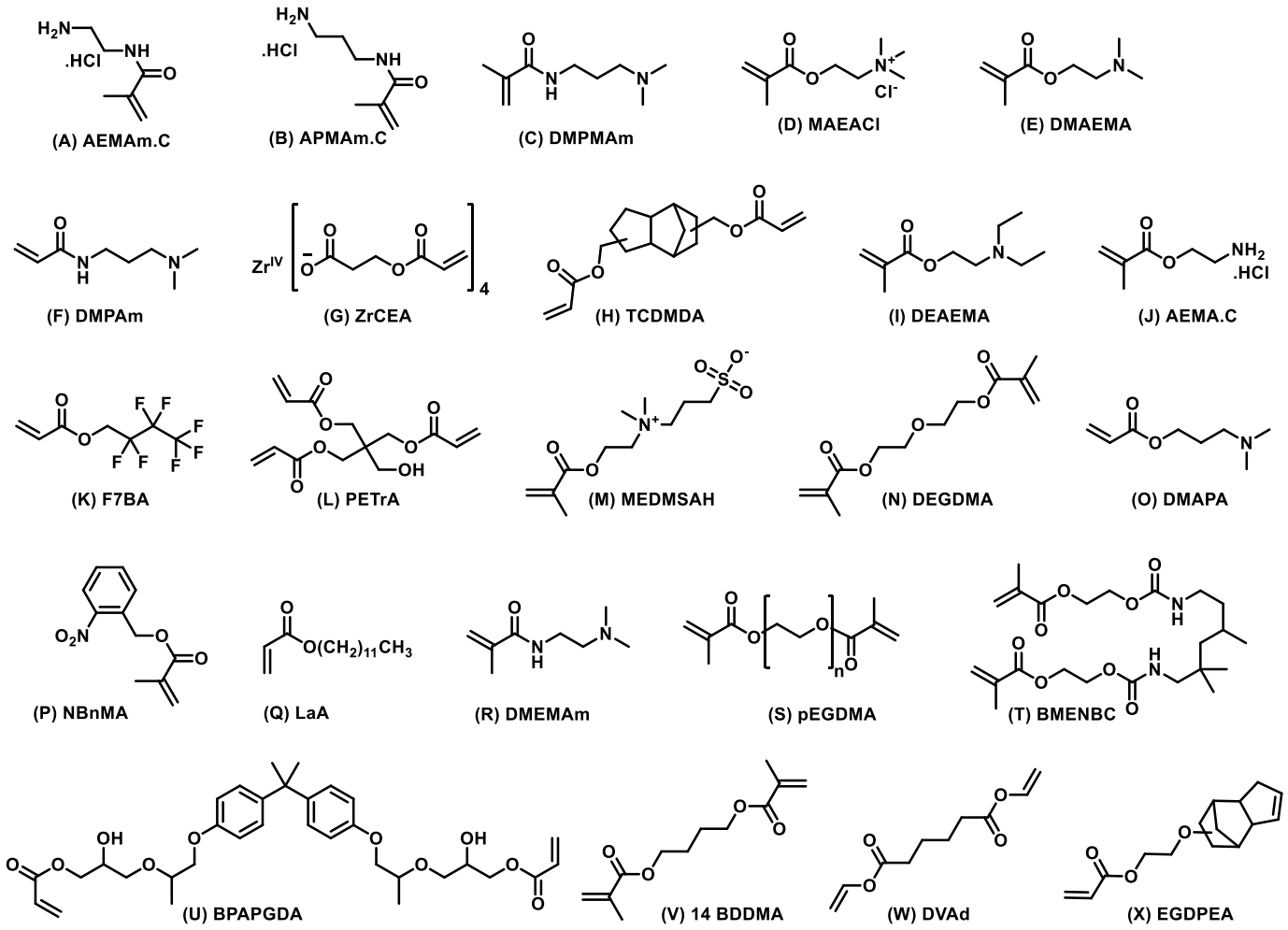

Figure 5.15 Selection of Top Performing Homopolymers for hPSC-CM Attachment & Spreading.
Hits from Generation 1 Homopolymer Array Screen '9.1'.
Data was considered from polymer microarray screening array 9.1, from three different densities; 38,800, 77,700 & 103,800 cells/cm^2, with & without 10% FBS preconditioning at the lowest seeding density, and when the traditional pHEMA array background was exchanged for a methacrylate background.
Hits are ordered in their overall ranked performance & labelled A-X for reference to generation 2 co-polymer array printing layouts.

5.6 Scale Up of Homopolymer Hits for Maturation Testing

With potential homopolymer attachment hits discovered through the polymer microarray screen, it was to be determined if any of them could influence the maturation status of hPSC-CMs.

To determine maturation status, larger culture surfaces are required than the microarray printed spots, which measure approximately 0.03 cm^2, to allow the efficient gathering of mRNA/protein for downstream analysis & great enough covered area to perform CellOPTIQ-based recordings.

Scale-up was performed using convenient well plate formats; 96-well (0.32 cm^2), 48-well (0.95 cm^2) to 12-well formats (3.8 cm^2). These formats are based on tissue culture plastic surfaces, which differ greatly in background stiffness from the glass substrate used for the polymer microarray screening, therefore scale-up to glass slides was also attempted.

Controls used as comparisons for attachment & maturation status included, Matrigel™; the gold standard ECM matrix, Poly-L-Lysine; structurally similar to APMAm.C/AEMAm.C/AEMA.C & a primary amine used in other cell culture systems.

Oxygen plasma activated TCP was also tested, plasma etching is one step of the process of creating polymer-coated surfaces. Due to the functionalisation of the surface with charged oxygen species, this could affect protein and/or cell binding.

Representative images of each control surface are shown in Figure 5.16 (A), hPSC-CMs demonstrate monolayer surface coverage with Matrigel™, poor

attachment & cell clumping with Poly-L-Lysine, and very low cell attachment on oxygen plasma treated TCP.

Scale-up of the primary amine homopolymers APMAm.C & AEMAm.C proved difficult, in Figure 5.16 (B) excessive hydrogel swelling (up to 230 times the original volume, 30 µl to 6.9 mL) can be observed after polymerisation with a 50/50 v/v concentration (monomer/isopropanol & dH_20 – in equal measures), and a 25/50 v/v concentration, when exposed to dH_20.

This swelling also occurs with cell culture medium and has been reported by another group who previously used APMAm.C as a biomaterial for human pluripotent stem cells (Irwin et al., 2011).

Before culture with cells, excess hydrogel was removed from the surface by additional washing stages. Cell attachment to hits can be seen in Figure 5.16 (C) where brightfield images were taken 7 days after culture on the surfaces of AEMAm.C, APMAm.C & DMPMAm. AEMAm.C provided the best cell coverage, comparable to Matrigel™, whilst APMAm.C formed more clustered areas of attachment, both materials supported hPSC-CMs that exhibited spontaneous contraction.

DMPMAm presented a high surface coverage but non-contractile cells. Whilst images in Figure 5.16 (C) show cell attachment, these results were not consistently reproducible.

Within a single well plate & between well plates, up to 40% of wells failed to support any cellular attachment, other attempts resulted in a lesser level of cell attachment. Scale-up optimisation for consistent attachment was required.

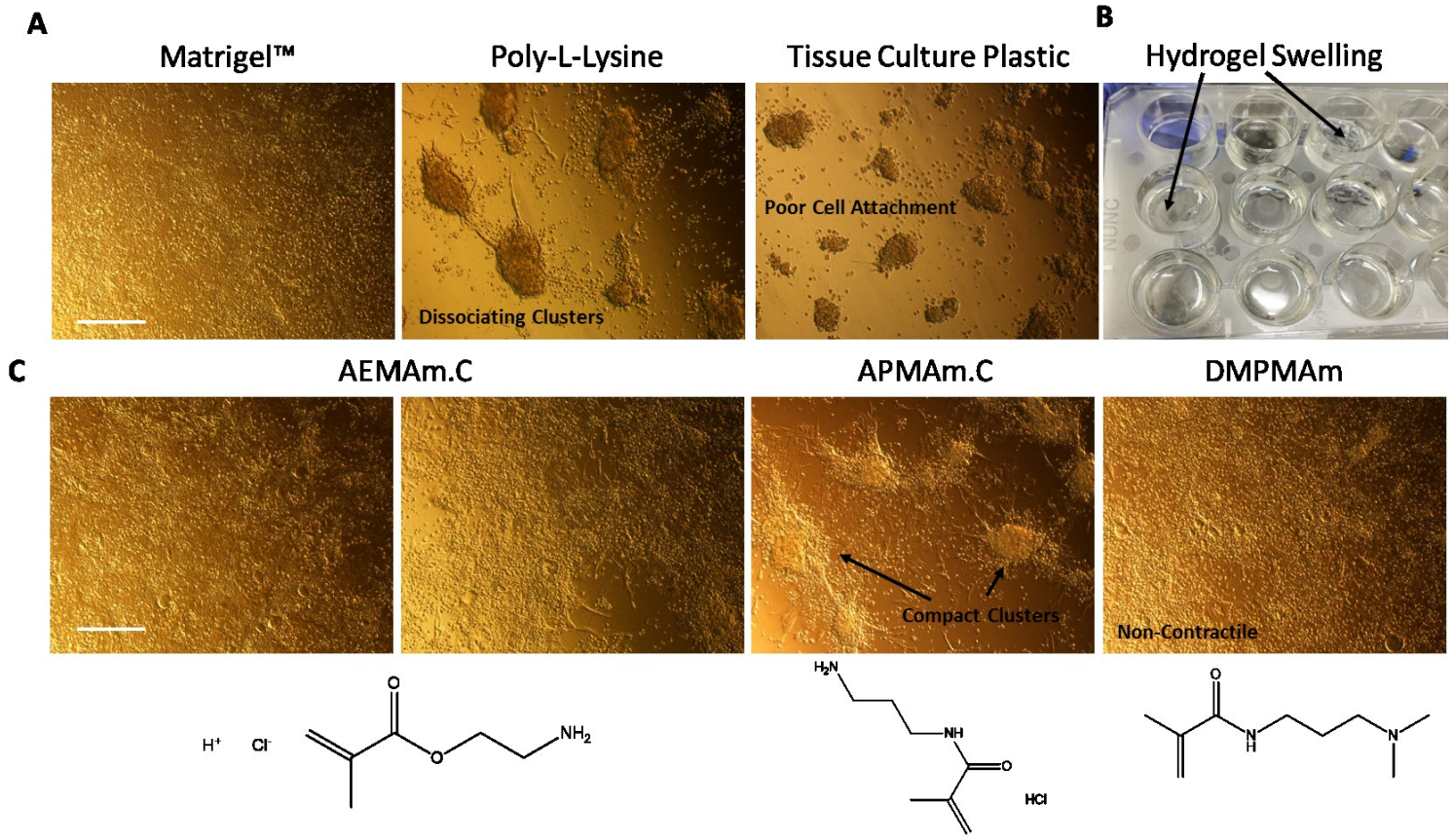

Figure 5.16 UV initiated Polymerisation of Best Performing Monomers onto Tissue Culture Plastic.
(A) Brightfield images of hPSC-derived cardiomyocytes on experimental controls; Matrigel™, Poly-L-Lysine & Tissue Culture Plastic (TCP) treated with identical oxygen plasma treatment used for UV polymerisation. (B) Post-UV polymerisation plate demonstrating excessive hydrogel swelling when soaked with dH_20. (C) UV polymerised hit indicated chemistry (chemical structure shown) to TCP, hPSC-CMs are 20 days old, seeded on the polymer surface for 7 days in shown images. Scale bars = 100 µm. N=3. n=6.

5.6.1 APMAm.C & AEMAm.C Scale-Up Reproducibility Issues

Array data indicates that both APMAm.C & AEMAm.C are capable of culturing hPSC-CMs in reproducibly. Across 6 biological repeats & 18 technical repeats, at the higher 77,700/103,600 cells/cm^2 seeding densities, both homopolymers demonstrated 100% reproducibility.

The failure for up to 40% of scaled-up APMAm.C & AEMAm.C surfaces to support zero cell attachment indicated an issue in the production process, or differences in the surface's physical properties.

Issues with the production process could have stemmed from the changes between the preparation for the array format & the well plate format.

APMAm.C/AEMAm.C monomers were dissolved in DMF, a highly effective aprotic polar solvent during array production. DMF is toxic to humans.

The array printing process had the advantage of depositing nanolitre volumes of monomer/solvent/photoinitiator. For scale-up purposes DMF presents a human health hazard, and was capable of partially dissolving TCP, for these reasons an alternative solvent was used.

Scale-up on TCP was performed with a 50/50 v/v solvent mixture of isopropanol & dH_20. Both primary amines were soluble in dH_20, however the photoinitiator of choice 2,2-dimethoxy-2-phenyl acetophenone (1% w/v) demonstrated poor solubility in dH_20 alone. Isopropanol as a solvent was compatible with TCP and possess volatility properties that should lead to evaporation during the UV polymerisation process.

It is possible that solvent or unpolymerised material persisted after the 1-hour UV polymerisation period & washing steps.

On the physical aspect, it is an assumption that the monomer polymerisation produces the same result at the μm^2 scale, as the cm^2.

During the array screen APMAm.C & AEMAm.C were printed to a glass slide, coated with a pHEMA hydrogel layer, where polymer-pHEMA entanglement takes place. The pHEMA layer provided a relatively soft surface modulus compared to TCP for cellular attachment, where it is uncertain to what extent cells would mechanosense the stiffer glass surface underneath.

Results from the methacrylate coated array demonstrated cellular attachment to APMAm.C/AEMAm.C, in the absence of the pHEMA entanglement, or softer surface modulus. Therefore, issues experienced with reproducible attachment are unlikely to be related the pHEMA layer or background material stiffness. These issues are visually represented in Figure 5.17.

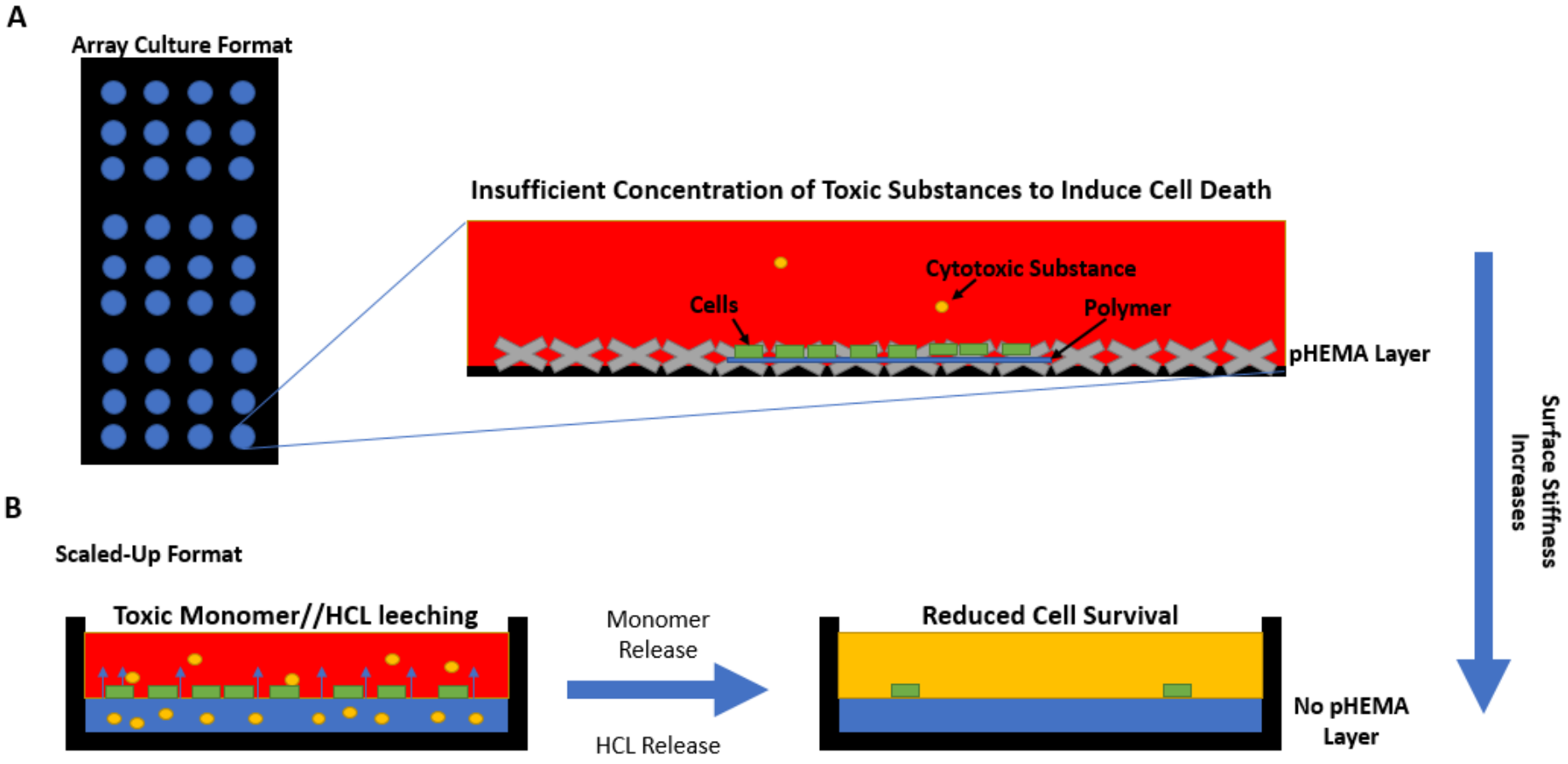

Figure 5.17 Toxic Unpolymerised Monomer, or Hydrochloric Acid Release is Potentially Greater During Scale-Up, Versus Array Format.
A.) Array format containing; nanolitre volumes of monomer, entangled in a pHEMA hydrogel. Trace amounts of toxic monomer & hydrochloric acid diluted in medium. B.) Well scale-up containing; a thicker layer of polymer, no pHEMA background. Greater concentrations of toxic monomer, or hydrochloric acid can build up at the surface, or within the medium. Surface stiffness will be altered without pHEMA layer presence.

5.6.2 Addition of Small Linker N, N'-Methylenebisacrylamide (mBAM) to Improve APMAm.C/AEMAm.C Stability & Induce Further hPSC-CM Maturation

APMAm.C has been previously used as a biomaterials for undifferentiated human pluripotent stem cells (Irwin et al., 2011).

No justification for the choice of APMAm.C is presented in the publication. However, they include 0.15% N, N'-Methylenebisacrylamide (mBAM) to a 12.5% concentration of APMAm.C, with a TCP background material, produces a functioning biomaterial, which assumedly is reproducible in production & biological response.

The addition of mBAM with 12.5% APMAm.C or AEMAm.C was tested for both attachment and functional maturation of hPSC-CMs. Whilst the attachment of cells still demonstrated variability, multiple repeats were permissible for 7-day cell attachment and could be analysed with the CELLOPTIQ platform for their contraction parameters. Furthermore, RT-qPCR data was also produced from these samples.

Figure 5.18 (A) highlights the structures of APMAm.C/AEMAm.C and the 'linker' mBAM. Contraction results measured using the high-speed camera & pixel displacement software from the CELLOPTIQ demonstrated a significant increase in contractile amplitude for all four polymers studied, when compared to Matrigel™.

AEMAm.C demonstrated greatest increase with a 111.4% +/- 2% increase in relative amplitude with a $P \leq 0.0001$ significance when a One-Way Anova comparison was performed. A non-parametric t-test between AEMAm.C with and without the mBAM linker revealed no significant difference in amplitude. APMAm.C demonstrated a 32% +/- 8.5% increase in relative amplitude and was assigned a significant difference of $P \leq 0.01$ through a One-Way Anova.

The addition of the mBAM linker to APMAm.C showed a greater statistic difference in relative contractile amplitude within the same test (P=≤ 0.0001), with a 56.5% +/- 4.8% increase in contractile amplitude. Comparing APMAm.C & APMAm.C with the mBAM linker, a non-parametric t-test detected a P-value of ≤ 0.05, indicating a modest improvement to contractile amplitude.

Measurements carried out were based on spontaneous contractions. Time for a single contraction interval to occur was equivalent between conditions (+/- 10%), with no significant changes relative to Matrigel™ control, Figure 5.18 (C). Improvements to the contraction rate relative to Matrigel™ for APMAm.C, APMAm.C+mBAM, AEMAm.C & AEMAm.C+mBAM were, 203% +/- 29%, 268.8% +/- 10.9%, 250% +/- 9.7% & 219% +/- 14% respectively.

Changes to contraction rate relative to Matrigel™ were statistically significant, a One-Way Anova with Dunnett's multiple comparisons identified P-values of, p=0.0074 (**), p=0.0002 (***), p=0.0004 (***) & p=0.0027 (**), as shown in Figure 5.18. The rate of relaxation relative to Matrigel™ for for APMAm.C, APMAm.C+mBAM, AEMAm.C & AEMAm.C+mBAM was, 155% +/-18.5%, 141.6% +/- 9.6%, 205% +/- 11% & 185% +/- 10.5% respectively.

Changes to relaxation rate relative to Matrigel™ were significant for APMAm.C, AEMAm.C & AEMAm.C+mBAM, p=0.0134 (*), p=0.0001 (***) & p=0.0007 (***). The P value for APMAm.C+mBAM was found to be insignificant, p=0.0644.

The contraction data presented here is not enough to conclusively demonstrate a maturation effect, further analysis into voltage parameters, gene

expression & structural properties are required. Improvements to the production process were still essential to the project at this stage.

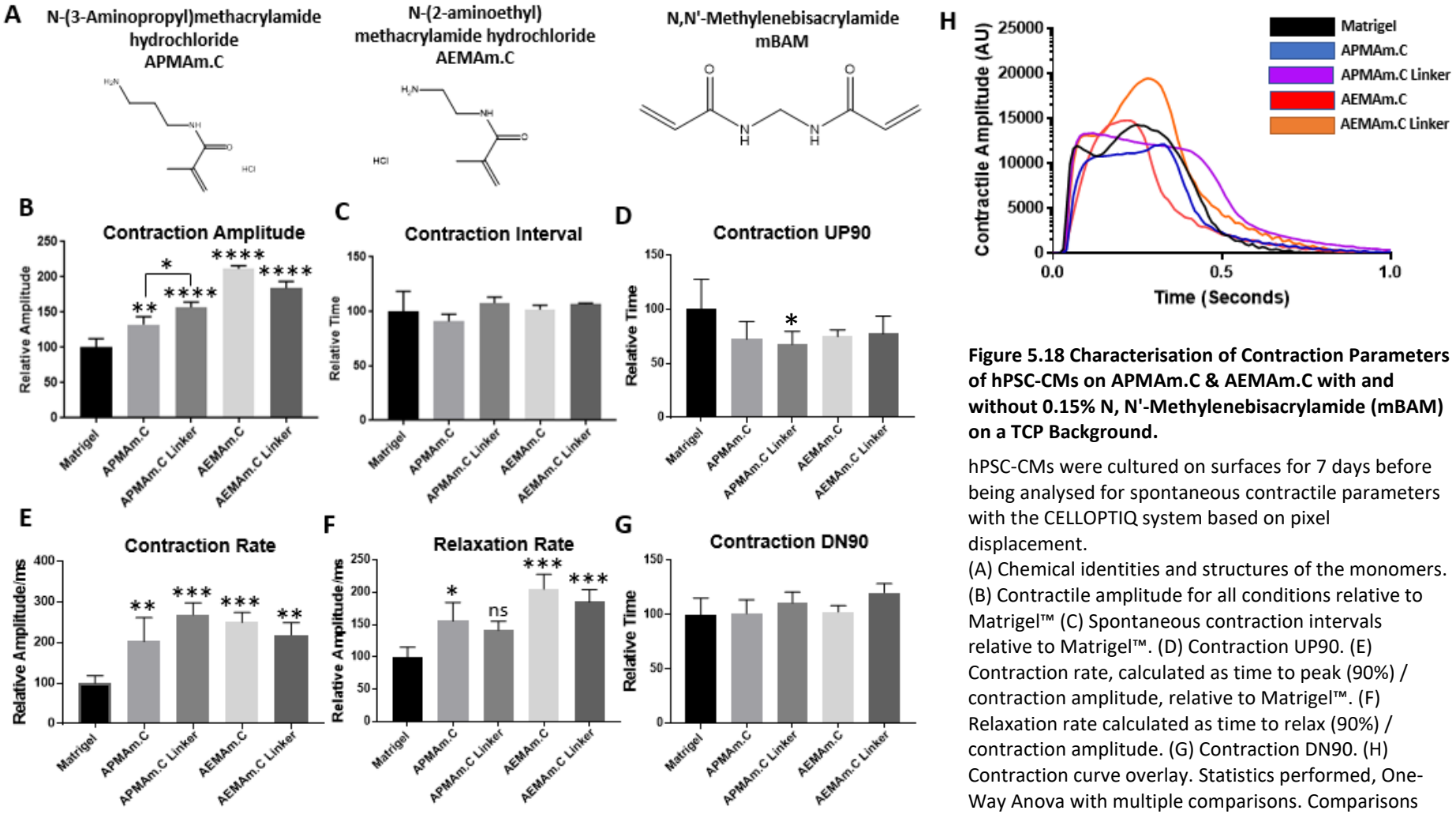

Figure 5.18 Characterisation of Contraction Parameters of hPSC-CMs on APMAm.C & AEMAm.C with and without 0.15% N, N'-Methylenebisacrylamide (mBAM) on a TCP Background.

hPSC-CMs were cultured on surfaces for 7 days before being analysed for spontaneous contractile parameters with the CELLOPTIQ system based on pixel displacement.
(A) Chemical identities and structures of the monomers. (B) Contractile amplitude for all conditions relative to Matrigel™ (C) Spontaneous contraction intervals relative to Matrigel™. (D) Contraction UP90. (E) Contraction rate, calculated as time to peak (90%) / contraction amplitude, relative to Matrigel™. (F) Relaxation rate calculated as time to relax (90%) / contraction amplitude. (G) Contraction DN90. (H) Contraction curve overlay. Statistics performed, One-Way Anova with multiple comparisons. Comparisons between two individual conditions, non-parametric T-test. N=3. n=15.

5.6.3 Investigation of Hydrochloric Acid Related Cytotoxicity

To investigate the role of HCL(-) in relation to the cytotoxicity and reproducibility issues encountered, APMAm.C & AEMAm.C were processed with a base, producing APMAm & AEMAm without the previously associated HCL(-) counter ion, this process was repeated three times and the pH was tested with universal indicator paper to confirm the loss of acidic nature. First APMAm, AEMAm and APMAm.C were tested on methacrylate silane functionalised glass slides, followed subsequent testing on TCP.

Testing on methacrylate silane functionalised glass with APMAm or AEMAm (25% v/v with dH_20 & IPA 50/50 v/v solvent) demonstrated hPSC-CM attachment for 7 days across two biological repeats, forming interspersed clusters of attachment or sparse single-cell attachment across areas of the surface. Matrigel on glass surfaces failed to maintain attachment hPSC-CM for 7 days within biological repeat 1, interspersed clusters of hPSC-CMs were attached on Matrigel for the second repeat (Figure 5.19 (A)). Attempts to polymerise APMAm.C (including the HCL(-) component) on methacrylate functionalised glass led to hydrogel swelling on the surface when dH_20 was added (as per washing steps), APMAm.C hydrogels proved to be cytotoxic for hPSC-CM culture. This suggested that processing of APMAm.C to remove HCL(-) affected properties related to UV polymerisation and swelling (Figure 5.19 (B)). A poly-L-lysine control on glass supported initial attachment of hPSC-CMs but failed to facilitate continued cell survival, as previously seen on TCP coated with poly-L-lysine (Figure 5.19 (C)).

Across two biological repeats, contraction measurements were obtained, measurements for Matrigel were limited to one data set (SEM of technical replicates used). Contraction interval and amplitude were reduced on both polymeric surfaces, APMAm and AEMAm in comparison to Matrigel, contraction amplitude on Matrigel was 3076 +/- 339 vs 1950 +/- 134 & 1891 +/- 93 (AU) respectively (Figure 5.19 (E)). Time to reach 90% of the contraction peak (UP90) was slower on APMAm (109 +/- 36 ms) vs Matrigel (73 +/- 8 ms), whilst time to reach 90% of the relaxation state (DN90) remained consistent across all three conditions (Figure 5.19 (F-G)).

On TCP three concentrations with APMAm were tested to assess if concentration would affect cytotoxicity and hPSC-CM attachment, 50%, 25% and 10% v/v with standard solvent mixture and photoinitiator concentration, the plate layout shown in Figure 5.20 (A). The same batch of APMAm starting material was used to create TCP coated plates.

Across three biological repeats, albeit on TCP-APMAm plates created within the same batch production, demonstrated 24-hour cytotoxicity across all three repeats (Figure 5.20 (B)). The lowest concentration (10%) APMAm supported sub-optimal hPSC-CM survival, with onset toxicity observed by 72 hours culture, however Matrigel coated wells within the same plate supported cellular survival and contractile monolayer formation as expected (Figure 5.20 (C)). This demonstrates that cytotoxicity observed was not due to oxygen plasma etching or UV exposure to the plates, and the viability of the hPSC-CMs upon seeding.

Combined these two experiments demonstrated that the removal of HCL(-) counter ions from the primary amine APMAm.C could support hPSC-CM attachment

and survival in specific instances (methacrylate silanised glass) but did not fix the reproducibility issues that were observed throughout the project to this stage.

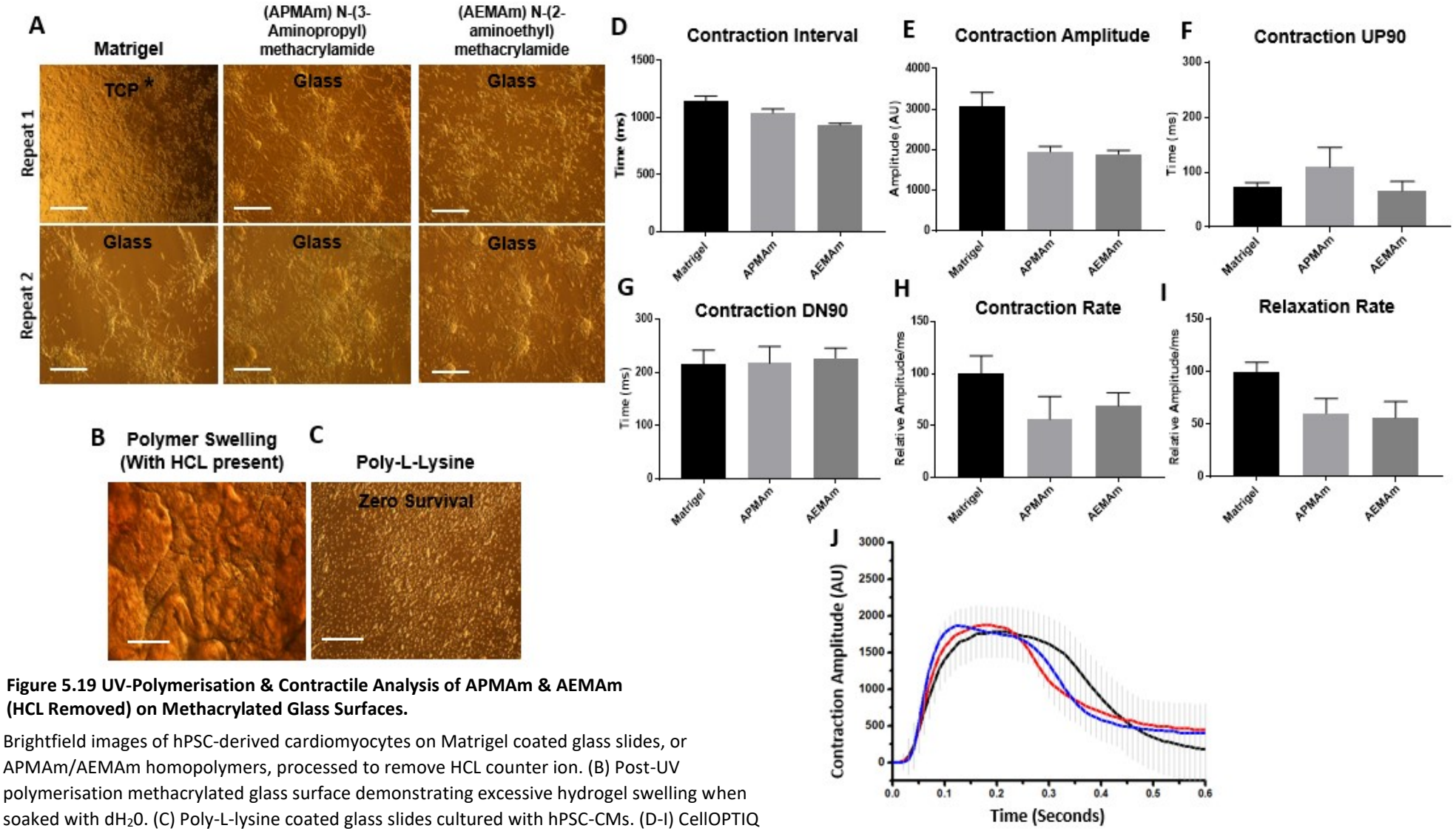

Figure 5.19 UV-Polymerisation & Contractile Analysis of APMAm & AEMAm (HCL Removed) on Methacrylated Glass Surfaces.

Brightfield images of hPSC-derived cardiomyocytes on Matrigel coated glass slides, or APMAm/AEMAm homopolymers, processed to remove HCL counter ion. (B) Post-UV polymerisation methacrylated glass surface demonstrating excessive hydrogel swelling when soaked with dH_20. (C) Poly-L-lysine coated glass slides cultured with hPSC-CMs. (D-I) CellOPTIQ contractile analysis. (J) Contraction curve overlay. Scale bars = 100 µm. N=2. n=10.

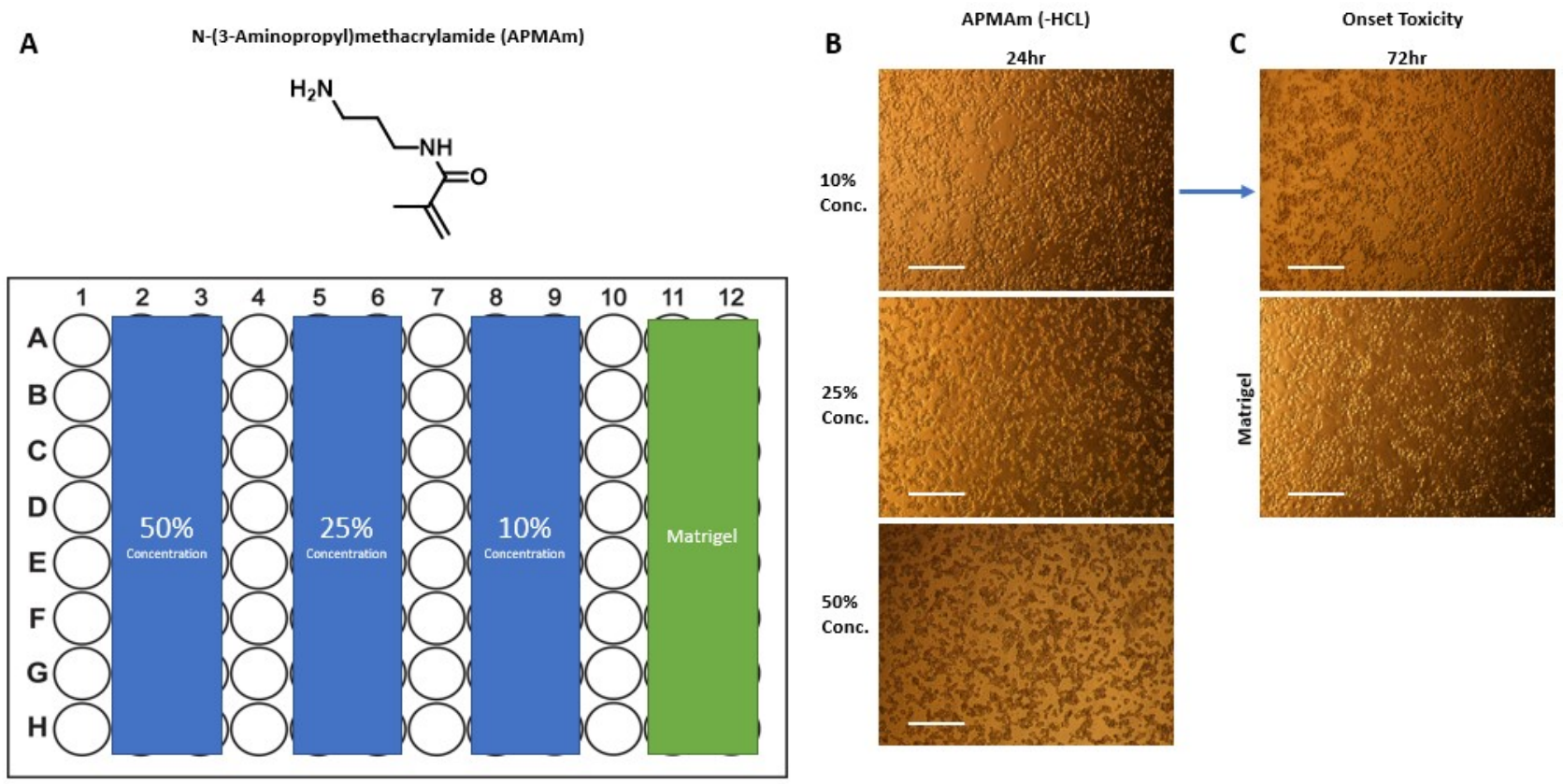

Figure 5.20 UV-Polymerisation of APMAm (HCL Removed) on Tissue Culture Plastic.

(A) Chemical structure of APMAm & plate layout for polymerisation. (B) Representative brightfield images of hPSC-derived cardiomyocytes cultured on APMAm TCP surfaces for 24 hours. (C) Representative images of 72-hour culture on 10% v/v APMAm and Matrigel control surface. Scale bars = 100 µm. N=3. n=48.

5.6.4 UV Glove Box Installation

To resolve the issue of reproducibility and cytotoxicity, the purchase of an air sealed glove box including antechamber was purchased. The differences between the original UV polymerisation box and the new glove box are detailed in chapter 4. In summary, the new glove box allowed for greater control of the atmospheric conditions in which UV polymerisation was carried out, the previous system unreliably support an oxygen concentration of ~2000 ppm, the new system could reliably maintain concentrations of below 200 ppm. This is highly advantageous for reproducibility in a UV polymerisation system because oxygen terminates the free radical based acrylate polymerisation reaction early, potentially leaving cytotoxic non-polymerised material on the polymeric culture surface.

5.7 Reproduction of Primary Amines with and without mBAM Linker

5.7.1 Contraction Analysis on Primary Amines

Contraction properties were assessed using the CellOPTIQ, values were normalised to the Matrigel control of each biological repeat, relative values were averaged to produce final values shown, statistics performed with an uncorrected Fisher's LSD One-Way ANOVA (Figure 5.21). APMAm.C produced the lowest relative contraction amplitude, 88% +/- 12% of Matrigel, with the addition of the short linker mBAM resulting in 102% +/- 9.4% amplitude (Figure 5.21 (A)). For contraction amplitude the trend was an increase in contraction amplitude the shorter the primary amine chain, with mBAM having an additive effect, however differences between primary amine or primary amine with mBAM did not result in statistical significance using a student's t-test. AEMAm.C + Linker, AEMA.C and AEMA.C + Linker

both elicited a significant increase in relative contractile strength, 124% +/- 8.2% (p=0.02), 130% +/- 7.7% (p=0.005), 136% +/- 13% (p=0.001) respectively. Except for APMAm.C all synthetic surfaces tested had a statistically significant improvement to relative upstroke 90%-time, p-values ranged between 0.034 to 0.014, with Matrigel exhibiting a wider variation in values (Figure 5.21 (B)). Time to reach 90% of relaxation, or the downward stroke (DN90) remained consistent compared to Matrigel between, 92% +/- 15% (APMAm.C) to 118% +/- 11% (AEMAm.C Linker), with a longer relaxation time a sign of maturation. The exception was AEMA.C + Linker, at 147% +/- 18% relative DN90, this increase in time to relax was significant, p=0.0032 (Figure 5.21 (C)).

AEMAm.C + Linker, AEMA.C and AEMA.C + Linker all had significantly faster relative contraction rates than Matrigel, 182% +/- 16%, 147% +/- 17% and 156% +/- 17%, where a faster rate of contraction is a sign of hPSC-CM maturation (Figure 5.21 (D)). Rate of relaxation on all synthetic surfaces were statistically unchanged from Matrigel (Figure 5.21 (E)). Contraction intervals for AEMAm.C (p=0.045) & AEMA.C Linker (p=0.0087) were significantly increased compared to Matrigel.

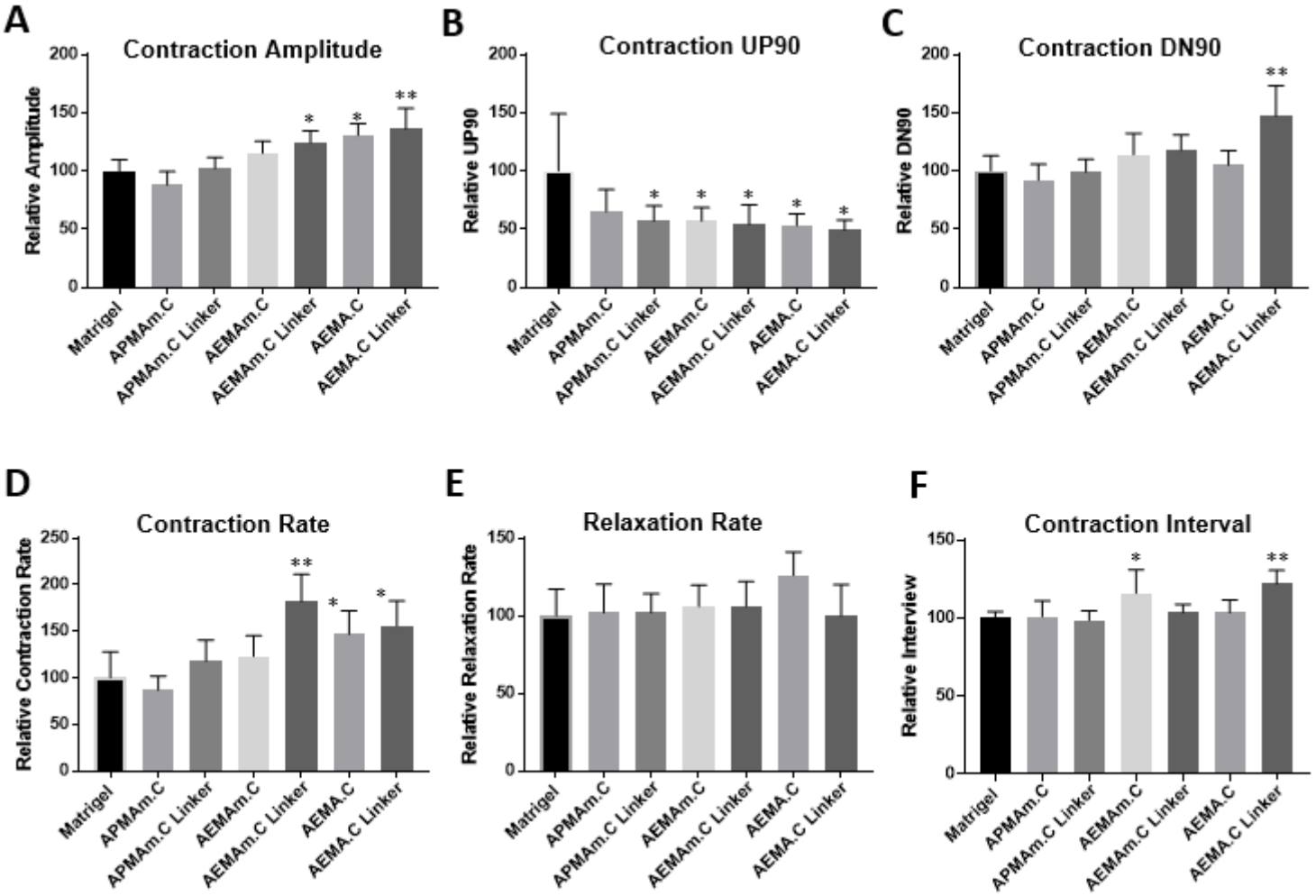

Figure 5.21 Characterisation of Contraction Parameters of hPSC-Derived Cardiomyocytes on Primary Amines +/- mBAM Linker After Polymerisation Optimisation.

(A) Contraction amplitude. (B) Time to reach 90% of contraction upstroke. (C) Time to reach 90% of relaxation state. (D) Rate of contraction. (E) Rate of relaxation. (F) Contraction interval (spontaneous). Statistics calculated using uncorrected Fisher's LSD One-Way ANOVA. N=3. n=15.

5.7.2 Assessment of Voltage Parameters on Primary Amines

Voltage assessments were made with FluoVolt™ dye and CellOPTIQ system on hPSC-CMs cultured on Matrigel and primary amine hits with and without short linker mBAM after 7 days of culture. The action potential interval, amplitude, T-rise, Action Potential Duration at 20%/50%/90% repolarisation (ADP20, ADP50, ADP90), triangularisation and ventricular index were recorded and calculated.

APMAm.C, and AEMAm.C + Linker both recorded statistically significant increases in the action potential interval compared to Matrigel, 118% +/- 11.9% (p=0.007) & 113% +/- 3.4% (p=0.04) respectively (Figure 5.22 (A)). Voltage amplitude was reduced for all primary amines tested, with or without the small linker (Figure 5.22 (B)). APMAm.C & APMAm.C + Linker had the greatest amplitude out of the primary amines, 80.5% +/- 12.7% (p=0.02)) & 84% +/- 12.9% (p=0.04). AEMA.C and AEMA.C + Linker demonstrated the greatest reductions in voltage amplitude, 66.6% +/- 12.3% (p=0.0004) & 60.1% +/- 6.9% (p=<0.0001). APMAm.C had a relative T-Rise of 125.3% +/- 8.8% (p=0.0004), whereas AEMAm.C (86.7% +/- 4.4%, p=0.03), AEMAm.C + Linker (85% +/- 5.2%, p=0.016) & AEMA.C (84.4% +/- 5.7%, p=0.013) all had shorter T-Rise values (Figure 5.22 (C)).

ADP20 and ADP50 were unchanged from Matrigel controls, with the exception of a reduction in ADP50 on APMAm.C + Linker, with a relative value of 90.7% +/- 3.9%, p=0.038 (Figure 5.22 (D & E)). AD90 was significantly reduced on APMAm.C + Linker (89.3% +/- 3.2%, p=0.0082), AEMA.C (94.1% +/- 4.7%, p=0.024) & AEMA.C + Linker (94.8% +/- 3.2%, p=0.0051) surfaces compared to Matrigel (Figure 5.22 (F)).

Triangularisation was determined by subtracting the ADP30 from ADP90, this measurement is a more reliable descriptor of repolarisation compared to reporting singular ADP values. Triangularisation was reduced on all synthetic surfaces tested, except for APMAm.C + Linker. APMAm.C (no linker) saw a relative value of 79% +/- 14.5% (p=0.032), AEMAm.C 77.9% +/- 9.4% (p=0.025), AEMAm.C + Linker 67.9% +/- 8.2% (p=0.0026), AEMA.C 68.8% +/- 11.6% (p=0.0032), AEMA.C + Linker 62.7% +/- 4.6% (p=0.0008) (Figure 5.22 (G)).

Ventricular index is a measure calculated by (ADP30-ADP40)/(ADP70-ADP80) which describes a relation between the early and late repolarisation time points, where a greater value is linked to an elongated repolarisation time and a ventricular action potential. The ventricular index did not significant differ on any of the surfaces tested compared to Matrigel (Figure 5.22 (H)).

In conclusion differences were seen in electrophysiological properties between primary amines and Matrigel. Mature CMs would exhibit a larger amplitude than demonstrated by the conditions here, with Matrigel performing best. Mature CMs should have an ADP90 of ~260 ms and a triangularisation of ~45 ms. Reduction in triangularisation and ADP90 on primary amine surfaces in this figure are signs of an improved maturation state, however triangularisation values on primary amines are still ≤125 ms and the ADP90 ≤360 ms, non-comparable to a mature phenotype. T-rise values reported in this thesis are considerably longer than those of mature cardiomyocytes (≤20 ms vs ~2.5 ms), whilst APMAm.C had prolonged T-rise measurements, significant decreases were seen for AEMAm.C, AEMAm.C Linker and AEMA.C, but all values exceeded 17 ms, ~7-fold higher than mature CMs. Despite

these changes the ventricular index was unchanged, meaning hPSC-CMs on our primary amine surfaces were just as ‘ventricular-like’ as Matrigel.

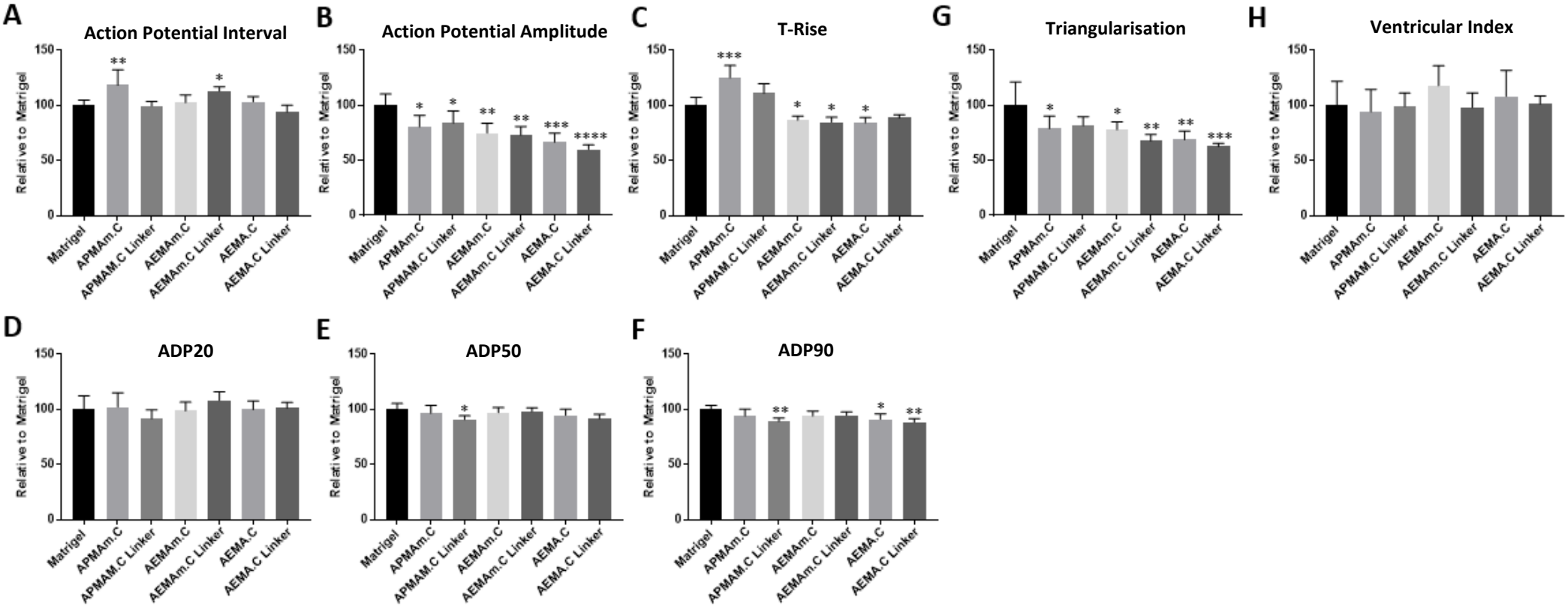

Figure 5.22 Characterisation of Voltage Parameters of hPSC-Derived Cardiomyocytes on Primary Amines +/- mBAM Linker After Polymerisation Optimisation.
(A) Action potential interval, (B) Action potential amplitude, (C) T-Rise, (D) ADP20, (E) ADP50, (F) ADP90, (G) Triangularisation, (H) Ventricular Index. Statistics calculated using uncorrected Fisher's LSD One-Way ANOVA. N=3. n=15.

5.7.3 Maturation Marker Gene Expression

To determine if maturation of hPSC-CMs was occurring on polymeric primary amine surfaces, a range of maturation markers were assessed by RT-qPCR. The range of selected genes cover, contraction machinery (TNNI1 & TNNI3), calcium handling (CASQ2 & RYR2), and metabolism (PPARGC1A). Due to time constraints only two biological samples could be prepared.

Expression of CASQ2 demonstrated an upward trend compared to Matrigel on the surfaces tested, with APMAm.C + Linker, AEMAm.C and AEMAm.C + Linker expressed a fold increase of 1.43 +/- 24%, 1.74 +/- 24% and 1.85 +/- 18% respectively (Figure 5.23 (A)). All surfaces except AEMA.C expressed RYR2 within the range of variation of the Matrigel control, AEMA.C expression was reduced to 0.74-fold +/- 12.6% (Figure 5.23 (B)). PPARGC1A controls the metabolic switch from glucose to fatty acid oxidation, all surfaces had a relative upward trend in expression versus the Matrigel control, APMAm.C had the highest fold increase of 1.54 +/- 15% (Figure 5.23 (C)).

Expression of foetal isoform TNNI1 was relatively trending upwards on all polymer surfaces, except for AEMA.C (0.99-fold +/- 18%) and AEMA.C + Linker (1.16-fold +/- 20.3%) where expression was matched with Matrigel (Figure 5.23 (D)). Adult isoform TNNI3 was also on an upward trend relative to Matrigel for all surfaces tested, however when the ratio of TNNI3-TNNI1 was assessed only AEMAm.C (1.45-

fold +/- 31.5%) & AEMA.C (1.68-fold +/- 40%) demonstrated a potential increase over Matrigel (Figure 5.23 (D & E)).

In conclusions changes to gene expression, if they remained consistent with the addition of a 3rd biological sample, would have demonstrated small fold-shifts in expression, mostly remaining consistent with Matrigel. The addition of small linker mBAM did not improve the expression of CASQ2, RYR2, PPARGC1A, TNNI1:TNNI3.

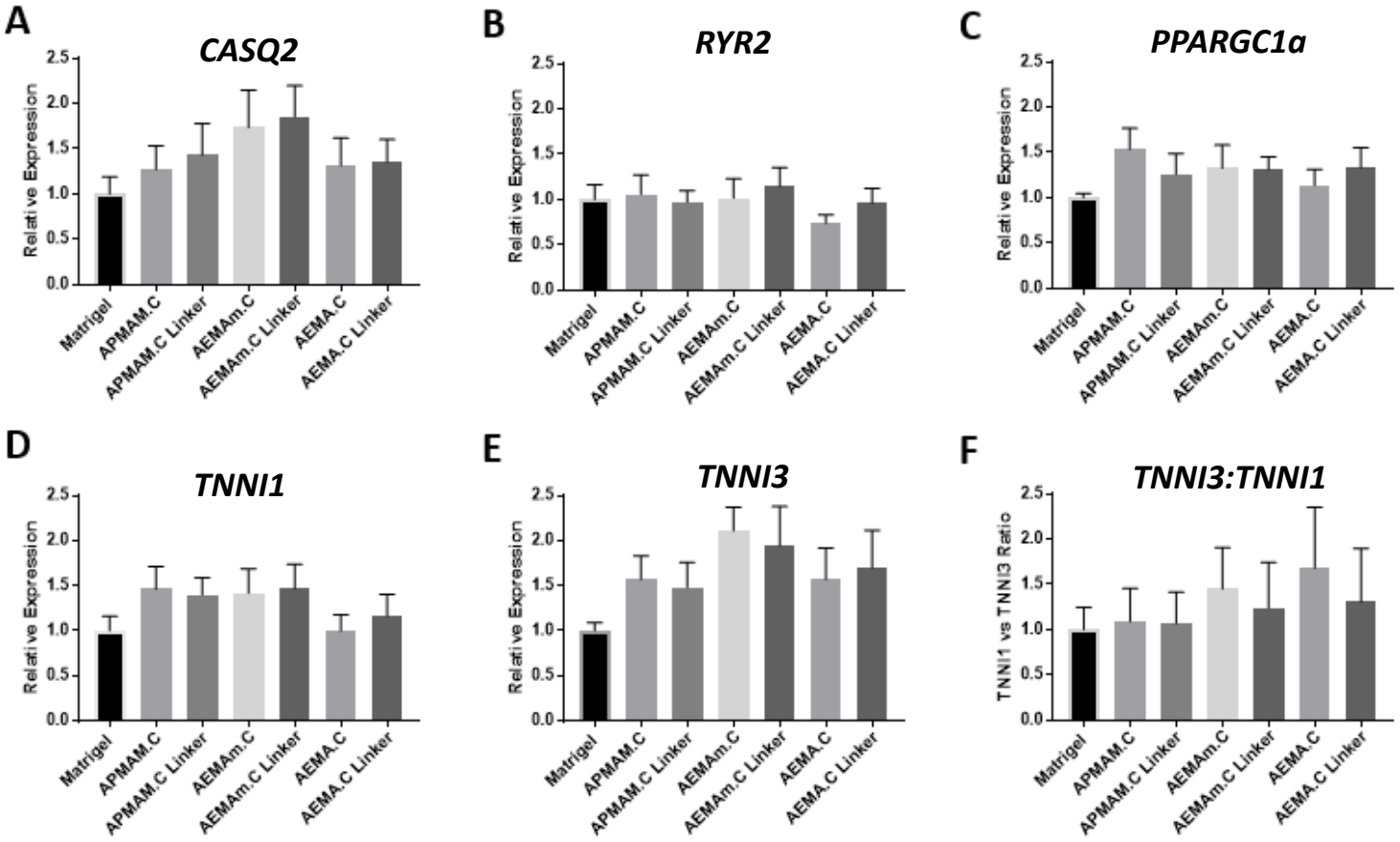

Figure 5.23 Characterisation of Maturation Gene Expression of hPSC-Derived Cardiomyocytes on Primary Amines +/- mBAM Linker After Polymerisation Optimisation.

(A) *CASQ2*, (B) *RYR2*, (C) *PPARGC1A*, (D) *TNNI1*, (E) *TNNI3*, (F) *TNNI1:TNNI3* Ratio. N=2. n=6.

5.8 Generation 2 Co-Polymer Microarray Screening

Monomers selected for their performance in the generation 1 homopolymer polymer microarray screen were mixed in 2:1 ratio to form a co-polymer microarray containing 599 unique materials, repeated three times on each full array slide.

Arrays were sterilised and preincubated with RPMI-B27 medium, in the absence of serum, as previously described for generation 1. A cell seeding density of 103,600 cells/cm^2 was used, culture carried out for a 7-day period before fixation & immunostaining with DAPI & cardiac α-actinin.

Changes to the CellProfiler™ pipeline were made, in the generation 1 screen, DAPI object attachment was used as cell attachment, this discounted data on cell spreading.

Originally the CellProfiler™ pipeline considered average cell area, however this was shown to be an ineffective way of selecting top performing materials – in the absence of serum preconditioning.

For generation 2 the pipeline was adapted to measure the total α-actinin positive area, within a cropped area. This will consider the combined impact of attachment & spreading, either of which warrant scale-up and maturation analysis.

Data was initially collated from 7 biological repeats, totalling 21 technical repeats to form a robust data set.

Data from biological repeats 1-7 reveals only one hits that supports ≥100,000 positive pixels, lauryl acrylate (LaA) mixed with TCDMDA (2:1 v/v ratio) – 103,530 +/- 63% average positive α-actinin pixels.

The average area of positive α-actinin pixels for repeats 1-7 was 10,680 +/- 30%. The top 10 performing co-polymers supported an average of 48,860 +/- 21% positive pixels. BMENBC (T) & DMEMAm (R) both appeared as the major monomer in 3/10 top hits.

The top three co-polymer hits have their representative images presented for biological repeats 1-3 in Figure 5.24 (B), demonstrating the variation between polymer technical repeats.

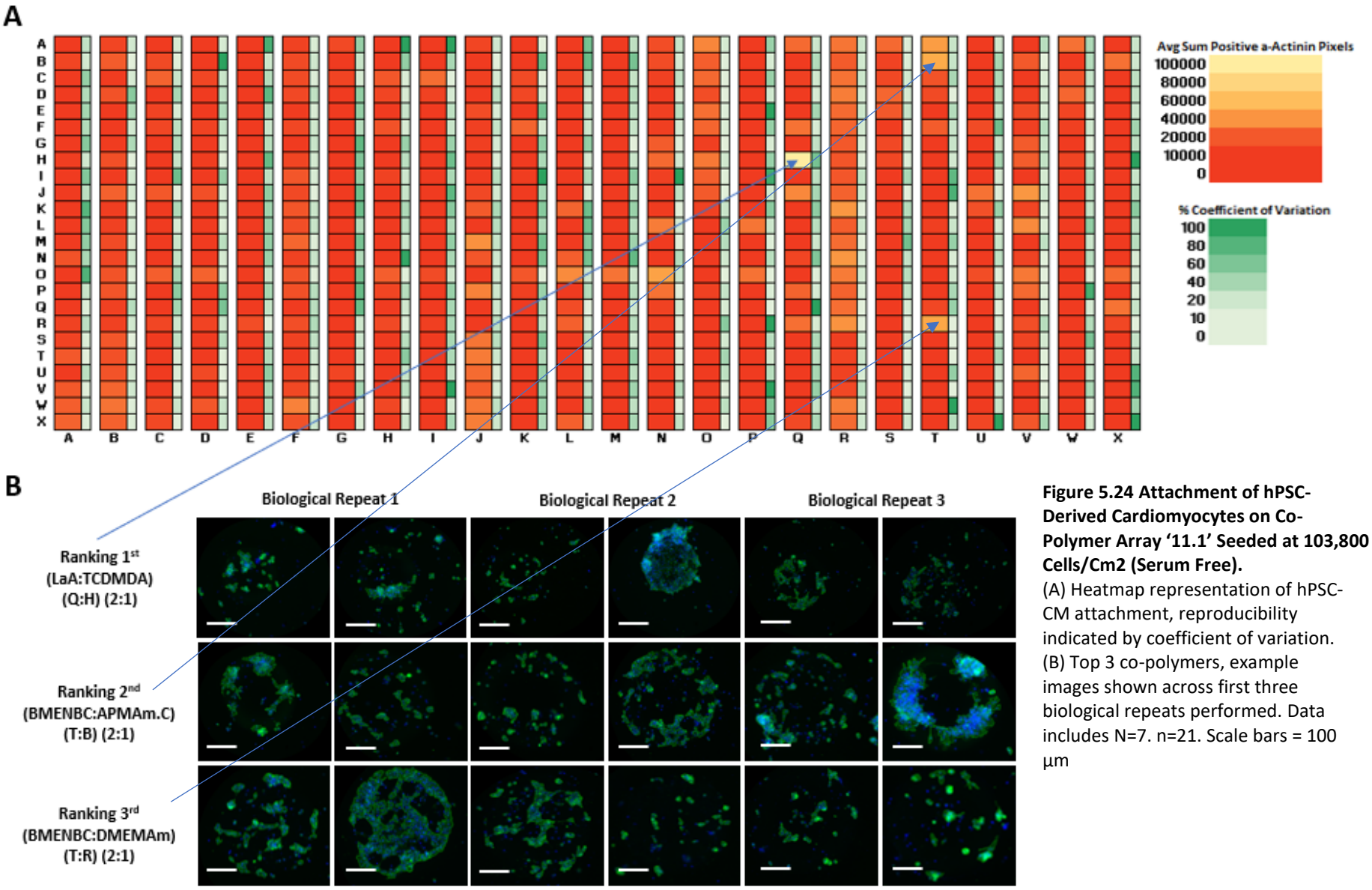

Figure 5.24 Attachment of hPSC-Derived Cardiomyocytes on Co-Polymer Array '11.1' Seeded at 103,800 Cells/Cm2 (Serum Free).
(A) Heatmap representation of hPSC-CM attachment, reproducibility indicated by coefficient of variation. (B) Top 3 co-polymers, example images shown across first three biological repeats performed. Data includes N=7. n=21. Scale bars = 100 µm

An expected result from combining hit homopolymers was synergy, to provide an increase in overall performance. Whilst additional value has been produced through the co-polymerisation process, a low number of high performing co-polymers – only 8/599 exceeded 40,000 average α-actinin positive pixels were discovered.

5.8.1 Array Contamination Reduced Polymer Performance on Generation 2 Arrays

Closer inspection of the data revealed the original top 24 homopolymers performance in the 2nd generation array did not match that of the 1st generation array. Data from the top homopolymer hits from the generation 1 array was reprocessed with the new CellProfiler™ pipeline used in the generation 2 arrays.

Homopolymer performance from biological repeats 1-7 from the 2nd generation co-polymer array screen was reduced, on average the top performing homopolymers supported 8477 +/- 36% on the 2nd generation array, versus 28754 +/- 24% on the 1st generation array. The differences between average homopolymer performance were deemed statistically significant (P=0.0005) (***) in an unpaired T-test with Welch's correction, performed in Prism. Key hits such as AEMA.C, a primary amine, supporting 115,239 +/- 64797 compared to 14,664 +/- 2624, on generation 1 & 2 respectively (Figure 5.25).

This indicated an issue with the array production process, either in the ability to faithfully print each material as previous, or contamination of the array with a toxic component. Reduced performance was not observed for hits such as DMPMAm & DMEMAm, both tertiary amines, however these are outliers to the trend as shown in Figure 5.25 (A).

Work carried out by Dr. Sara Pijuan-Galito used ToF-SIMS and revealed a contaminant across the array, after several washing stages with dH_20, including a 24-hour incubation at 37°C & 5% CO^2 in dH_20, two further repeats of the co-polymer array was performed. Comparison data for the homopolymers between co-polymer arrays biological repeats 8 & 9 and generation 1 arrays resulted in improvements for 15/24 homopolymers.

On average homopolymers supported 34,339 +/- 9% positive α-actinin pixels on generation 2 (repeats 8 & 9) compared to 28,754 +/- 24% on the 1st generation array. No significant difference (P=0.53) was shown for the average homopolymer performance across these data sets.

Performance for AEMA.C on biological repeats 8 & 9, 2nd generation co-polymer array, was 104,867 +/- 133, compared to 115,239 +/- 64797 for generation 1. APMAm.C, BPAPGDA, DMEMAm, DMPAm, DMPMAm, MAEACL, NBnMA, PETrA & TCDMDA had their performance increased beyond the values shown from the generation 1 arrays. PETrA saw a 4.94-fold increase in performance after washing steps had been performed for biological repeats 8 & 9, on the co-polymer array, as seen in Figure 5.25 (B).

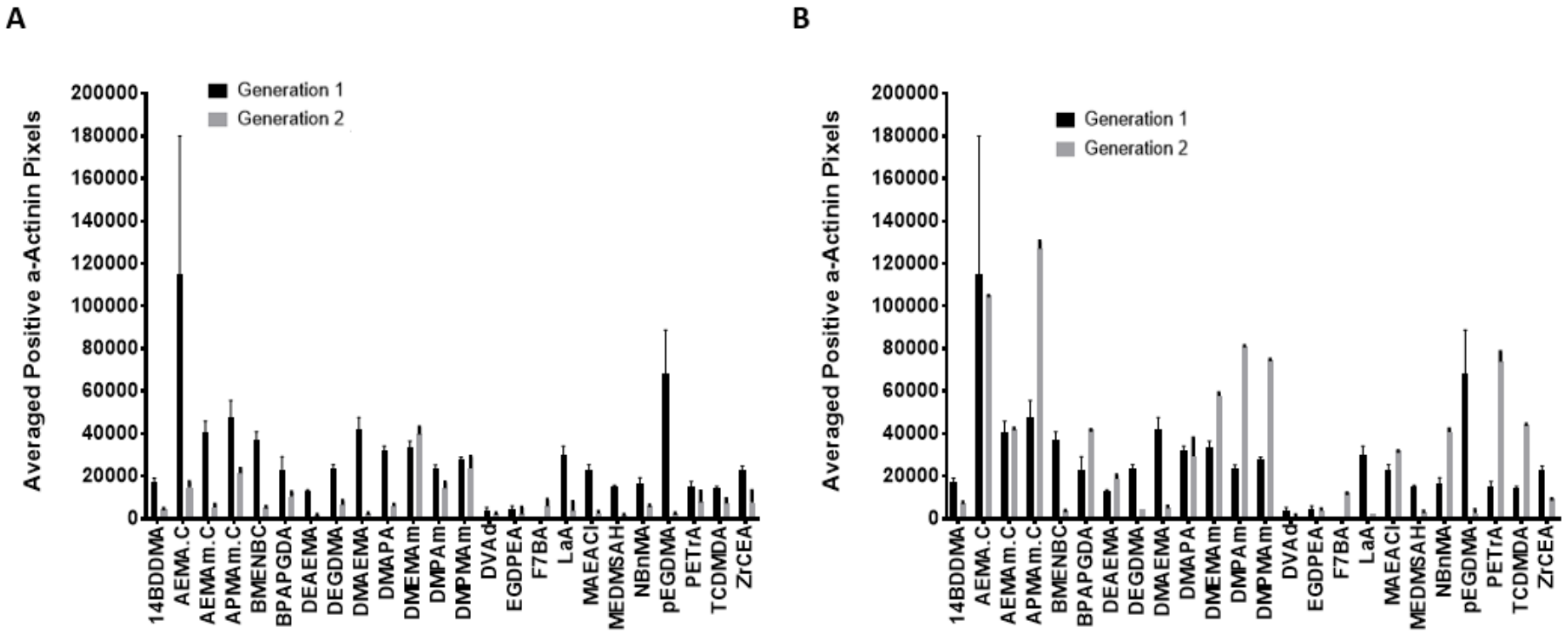

Figure 5.25 Comparison of Homopolymer Performance Selected for Co-Polymerisation on Generation 1 Homopolymer Microarrays vs Generation 2 Co-polymer Microarrays.

(A) Performance of homopolymers from biological samples 1-7 on generation 2 co-polymer microarrays, without array washing steps, compared to data of homopolymer performance from generation 1 homopolymer arrays. (B) Performance of homopolymers from biological samples 8-9 on generation 2 co-polymer microarrays, with array washing & soaking steps in dH_20, compared to data of homopolymer performance from generation 1 homopolymer arrays. Washing steps performed due to ToF-SIMS data collected by Dr. Sara Pijuan-Galito detected a contaminant across the polymer microarray surface.

5.8.2 Washing Stages Improved Homopolymer Performance on Generation 2 Co-Polymer Arrays

The improved performance of the homopolymers on the 2nd generation co-polymer arrays, biological repeats 8 & 9, resulted in an increase in performance for co-polymer hits. Whilst it would have been ideal to perform further repeats with the new dH_20 washing/soaking steps, this was not feasible due to technical constraints. Data from the biological samples 8-9 supported an average total α-actinin pixel coverage of 37,250 +/- 4% vs 10,680 +/- 44%, P=<0.0001 (****), Figure 5.24 and Figure 5.26.

The improvements to the reproducibility between technical repeats are clearly demonstrated in Figure 5.25 (B), where every image for the top performing hits are shown and are qualitatively similar, reflecting the quantitatively low coefficient of variation.

5.8.3 Best Synergising Monomers (Major & Minor)

Not all monomers were equal when comparing their performance after co-polymerisation. Four major monomers that consistently perform well, APMAm.C, AEMA.C, DMPAm & DMEMAm. APMAm.C & AEMA.C (letter codes B & J respectively) are structurally similar primary amines, where APMAm.C contains a propyl carbon chain & an acrylamide group, AEMA.C is an acrylate with a shorter ethyl chain.

AEMAm.C the acrylamide version of AEMA.C failed to synergise well as the major monomer, despite homopolymer performance being almost identical to the generation 1 homopolymer data (42,005 +/- 1.27% vs 40,732 +/- 13% respectively). DMPAm & DMEMAm (letter codes F & R) were also top performing major monomers,

and again structurally similar, both being tertiary amides with a single carbon difference in their R-group. Differentially, DMEMAm is a methacrylate, where DMPAm is an acrylate.

DMAPA (O) has been highlighted as a top performing minor monomer in Figure 5.26 (A), a cross-over monomer hit from the work of Patel et al., 2015. DMAPA is a tertiary amine, otherwise structurally identical to DMPAm, the amide version. The amide to amine switch with DMAPA reduced the synergistic properties, where 11/23 combinations failed to support high cell attachment when DMAPA was the major monomer. DMAPA does however form the major component of the top performing co-polymer, DMAPA:AEMAm.C, with an average of 285,625 +/- 23.5% pixels positive for α-actinin staining. More often, DMAPA appears in the top hits from generation 2 as a minor monomer, as can be seen in Figure 5.26 (B)

Co-polymerisation has generated 19 materials of interest that perform better than the top performing homopolymer APMAm.c for hPSC-CM attachment, when considering array data with dH_20 washing & soaking stages, Figure 5.27 (B).

Scale-up and optimisation of co-polymer production will be essential before probing which or any are inducing a maturation effect on the hPSC-CMs.

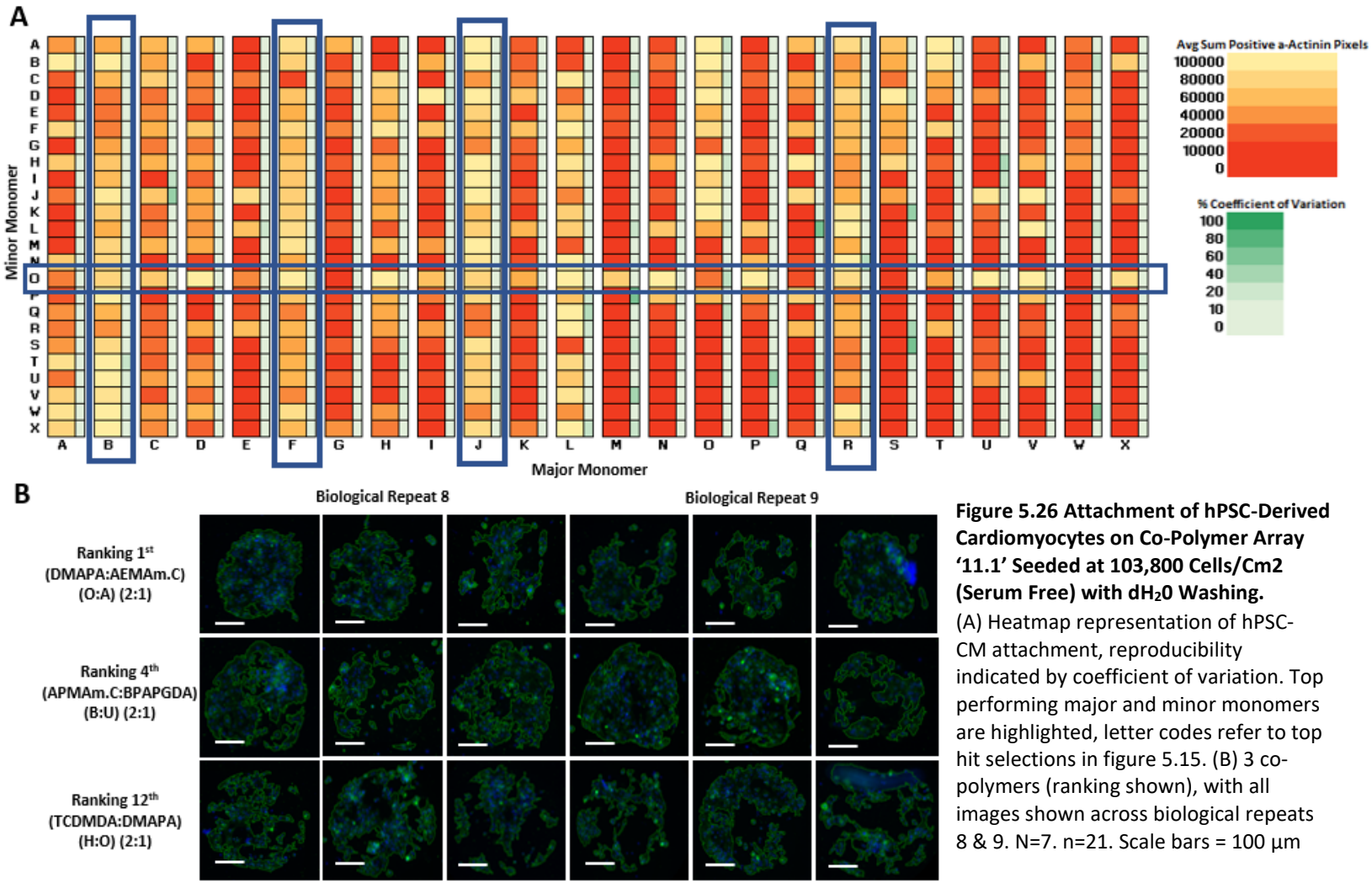

Figure 5.26 Attachment of hPSC-Derived Cardiomyocytes on Co-Polymer Array '11.1' Seeded at 103,800 Cells/Cm2 (Serum Free) with dH_20 Washing.
(A) Heatmap representation of hPSC-CM attachment, reproducibility indicated by coefficient of variation. Top performing major and minor monomers are highlighted, letter codes refer to top hit selections in figure 5.15. (B) 3 co-polymers (ranking shown), with all images shown across biological repeats 8 & 9. N=7. n=21. Scale bars = 100 µm

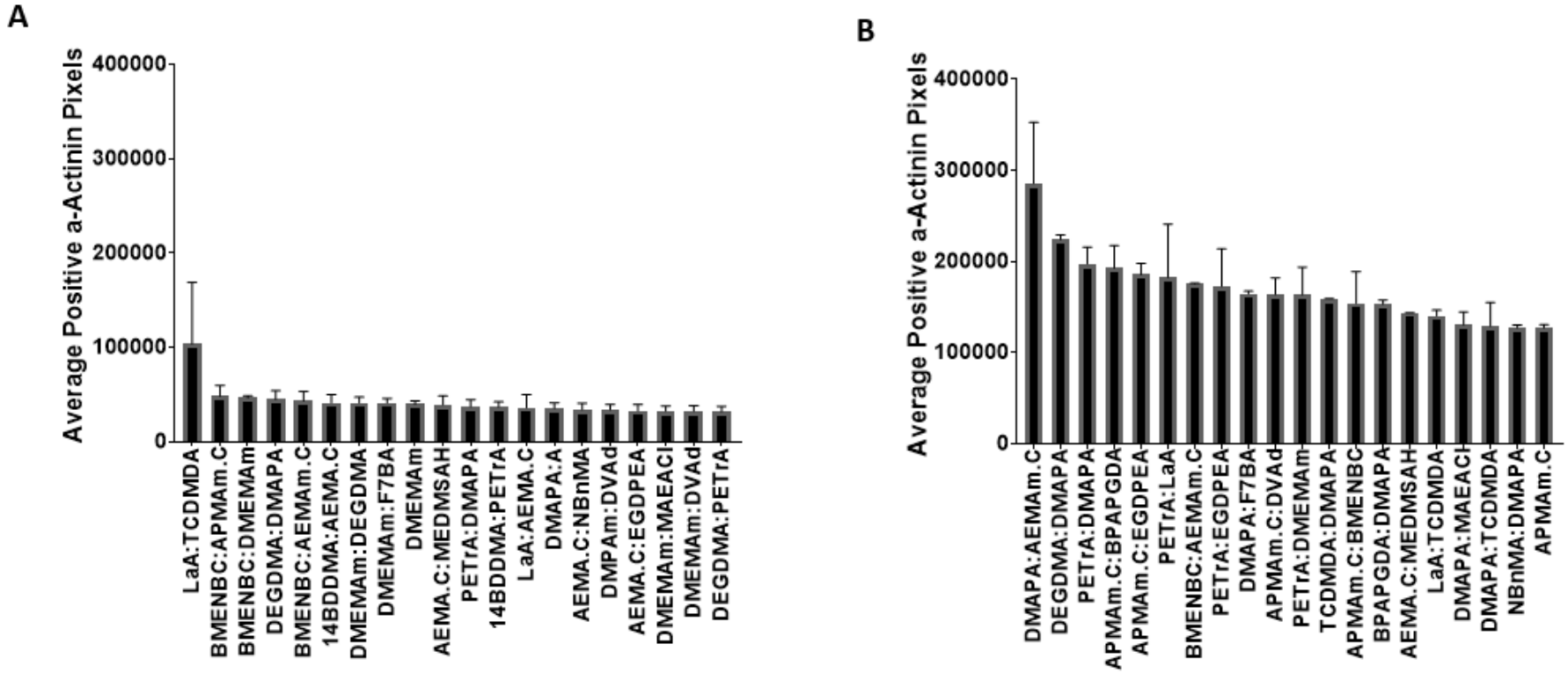

Figure 5.27 Comparison of Co-Polymer Performance for hPSC-Derived Cardiomyocyte Attachment & Spreading Between Biological Samples 1-7 (without array washing steps) vs Biological Samples 8 & 9 (with array washing steps).

(A) Performance of co-polymers from biological samples 1-7 on generation 2 co-polymer microarrays, without array washing steps. Top performing co-polymer LaA:TCDMDA highlighted. (B) Performance of co-polymers from biological samples 8 & 9 on generation 2 co-polymer microarrays, with array washing & soaking steps in dH_20. Top performing co-polymer from biological samples 1-7, LaA:TCDMDA, highlighted for comparison. Washing steps performed due to ToF-SIMS data collected by Dr. Sara Pijuan-Galito detected a contaminant across the polymer microarray surface.

5.9 Chapter Discussion & Summary

5.9.1 Synthetic Surfaces – A Challenging Environment

Screening of polymeric materials for hPSC-CM attachment resulted in 24 'top hits' from the 1st generation homopolymer array 9.1, few top hits supported near monolayer coverage, with others supporting sparse single cell attachment. Interestingly the major component of the undifferentiated stem cell scaled-up polymer, TCDMDA, was also a high ranking 1st generation array screen hit. Scale-up of best performing hits led to sporadic attachment of hPSC-CMs on non-primary amine top hits, including TCDMDA, which were difficult to reproduce. Another top hit PeTrA, supported a moderate level of hPSC-CM attachment but due to the triacrylate functionality was compatible with 2-photon 3D printing and was used as the base material for a publication, which even without the addition of electrical pacing or topographical grooves improved sarcomeric length (Vaithilingam et al., 2019).

The medium used to culture hPSC-CMs, RPMI + B27 (with insulin), has 27 components plus basal medium including the proteins, albumin, catalase, insulin, superoxide dismutase and transferrin (Brewer et al., 1993). This is over 4-times the number of components of E8 medium, providing high probability of medium components facilitating cell-surface adhesion. Albeit, the presence of albumin has been shown to be inhibitory for hPSC attachment in this thesis. Conversely, albumin has been demonstrated to facilitate cell-surface adhesion of undifferentiated hPSCs to APMAm.C, it is likely albumin performs an identical role in this thesis for hPSC-CM

adhesion to APMAm.C (Irwin et al., 2011). A polymeric screen utilising albumin-free medium may reveal addition attachment hits.

The additional challenge of developing synthetic surfaces, particularly 2D systems, for hPSC-CM adhesion are the spontaneous contractile forces generated. The force of adhesion of the hPSC-CM to the surface must be strong enough to prevent the force of contraction (which ideally increases as the surface induces greater maturation) from dissociating the hPSC-CM from the surface. Without the use of serum or other adhesion protein coatings, hPSC-CMs in this thesis are dependent on non-optimal adhesion scenarios until their own extracellular matrix and adhesion proteins can be established. In this thesis, hPSC-CMs cultured on polymer surfaces had 50% of their medium exchanged after the first three days of culture, to minimise disrupting caused by aspiration and pipetting. This aided in the continued attachment of hPSC-CMs on synthetic surfaces ≥7 days.

5.9.2 Primary Amines Supported Greater Attachment

In common between the best performing attachment hits was the primary amine functionality, with polymers similar in structure to poly-L-lysine, a substrate capable of supporting cell attachment (not hPSC-CMs as shown in this chapter) (Yavin and Yavin, 1974)(James et al., 2000). This suggests that the acrylate/acrylamide backbone may play an important role, be it structural or charge related, in supporting the attachment of hPSC-CMs. To note is the chain length of the primary amine, with the propyl chain of APMAm.C supporting more ‘cluster’ based attachment relative to the ethyl chains of AEMA.C of AEMAm.C, which more often supported near monolayer attachment.

Few synthetic materials exist in the literature that can support hPSC-CM adhesion. hPSC-CMs have been cultured on polystyrene, polyurethane, polyaniline, poly(lactic-co-glycolic acid) (PLGA) and poly(ε-caprolatone), however these previous publications have relied on the use of serum containing medium or the addition of a gelatin layer for improved adhesion (Wang et al., 2011)(Hsiao et al., 2013)(Kai et al., 2011). More recent work revealed serum and adhesion coating free synthetic surfaces for hPSC-CMs, however these materials were not scaled-up (Patel et al., 2016).

The only previously reported synthetic material to support serum-free cardiomyocyte attachment, in a scaled-up format is N-1(3-(trimethoxysilyl)propyl) diethylenetriamine (DETA), a primary amine, which could support rat embryonic cardiomyocytes for 8 weeks whilst retaining contraction properties (Das et al., 2004). Despite using a high seeding density of 70,000 – 100,000 cells/cm^2, comments on surface coverage as 'beating islands', in comparison to primary amines described in this chapter that support monolayer – to near monolayer coverage with a seeding density of 40,000 – 60,000 cells/cm^2 although hPSC-CMs and rat embryonic CMs will have different attachment and survival efficiencies.

5.9.3 Uncertain Functionality of Primary Amines

Initial work using primary amines discovered on the 1st generation polymer microarray, before improvements the fabrication process took place, demonstrated significant improvements in contractile properties, amplitude, contraction rate and relaxation time. When experimentation was repeated with improved polymer plate production only, AEMAm.C + Linker, AEMA.C and AEMA.C + Linker demonstrated

enhanced contractile amplitude and contraction rate. Analysis of voltage conditions saw reduced amplitudes and slower T-Rise for primary amines compared to Matrigel, however the ventricular index indicated no significant change. RT-qPCR analysis also indicated it was like, with additional replicates, that key maturation-linked genes were equivalent or slightly improved compared to Matrigel. To determine the true functional state of primary amines discovered here, further repeats would be required.

5.9.4 2nd Generation Array Hits Offer Attachment Improvements

The secondary array screen with 599 unique materials was met with its own toxicity issue, biological repeats 1-7 whilst mostly discounted did revealed TCDMDA:LaA as the top performing combination, with greater attachment than homopolymer alone. TCDMDA:BA, the undifferentiated hPSC polymer, and TCDMDA:LaA are identical in structure except LaA has an extended hydrocarbon chain (with the methacrylated version, LMA, a hPSC-CM attachment hit for previous PhD student Asha Patel). Additional washing steps for the 2nd generation arrays improved homopolymer performance to be more in-line with their 1st generation array performance. Some homopolymers such as APMAm.C demonstrated over a 2-fold improvement in attachment performance, however even with this increase in APMAm.C performance 19 co-polymer materials were recorded as having superior attachment capabilities compared to APMAm.C. Optimisation of the scale-up for these co-polymer hits was not achievable within the timeframe of this PhD project, however given the improved attachment properties it is entirely possible that one of the 19 materials also enhances the maturation state of hPSC-CMs, and are therefore important to investigate further.

5.9.5 Methods for Scaling hPSC-CMs for Industrial & Therapeutic Use

One factor to consider when seeking novel synthetic surfaces for the culture and maturation of hPSC-CMs is scalability. Work performed in this chapter using UV-polymerisation was most amendable to scale-out culture, however with the field heading towards 3D-culture, which is proven to increase maturation state, alternative fabrication methods should be considered for synthetic surfaces in this chapter to make them amendable to 3D culture (Correia et al., 2018)(Jiang et al., 2018)(Branco et al., 2019)(Schwach and Passier, 2019). Thermal polymerisation or hyperbranching have the ability to produce dissolvable pre-polymerised polymers, which could be drop casted onto 3D scaffolds, alternatively primary amines discussed in this chapter have the ability to form large hydrogel structures which could be optimised and amendable to 3D hydrogel culture.

Expansion of hPSC-CM generation for industrial and clinical uses could theoretically be done in two ways, scale-out or scale-up. Scale-out is comparatively simple, where matrix (or polymer) coated 2D dishes can be increased in number and/or surface area per culture vessel. Being an established culture technique, the main advantage to scale-out is the ease of use, where the capability to evenly distribute growth factors and small molecules to monolayers of cells could support greater reproducibility (Kempf, Andree and Zweigerdt, 2016). The downside to scale-out is the space & labour-intensive nature of supporting large number of culture vessels, at the scale required for therapeutics, where experimentation in a small mammal required $1x10^9$ cells to induce a therapeutic effect, a number that will be higher in an adult human heart (Chong et al., 2014)(Liu et al., 2018). Economic cost is a limiting factor for scale-out culture.

A modern form of scale-out culture involves 3D printing of microgrooves, used to align hPSC-CMs for maturation. The homopolymer PeTrA, a triacrylate amenable to 3D printing, was discovered to be capable of supporting hPSC-CM attachment within this chapter, through collaboration this material was 3D printed into microgroove but also impregnated with conductive carbon nanotubes. The combination of conductance and patterning significantly increase sarcomeric length to 1.86µm, compared to a 1.64µm control (Vaithilingam et al., 2019). Combined in the future with, medium improvements, surface modulus, and perhaps even nanotopograhy, this form of scale-out could provide a suitably mature source of hPSC-CMs amendable to relatively simply high-throughput analysis, compared to large 3D engineered tissues.

A transition to modern 3D cell culture is allowing for scale-up of hPSC-CM production, where large numbers of cells can potentially be produced through by using microcarriers, self-aggregation or micropatterned surfaces in combination with; spinner flasks, bioreactors, wave bioreactors & hydrogel systems (Figure 5.28) – at a cheaper cost to scale-out (Kempf, Andree and Zweigerdt, 2016). One such system can produce 1.5 to $2x10^9$ cardiomyocytes/litre, with ≥90% purity, using a spinner flask system (Chen et al., 2016). It has also been demonstrated that metabolic purification of cardiomyocyte differentiations in a suspension culture system can eliminate the possibility of teratoma formation due to residual stem cell populations (Hemmi et al., 2014).

With regard to improving maturation the production of 3D cardiac aggregates has been explored and demonstrated to induce metabolic maturation of hPSC-CMs

through transcriptomic profiling, x3-4 fold improvement on contraction kinetics and significantly improved electrophysiology in the ADP50/ADP90 and upstroke velocity, over 2D cultures (Correia et al., 2018). Within this thesis project, top performing homopolymer APMAm.C was functionalised onto poly(lactic acid) (PLA) microparticles, whilst no in-depth maturation analysis was conducted, the number and size of cell containing aggregates were increased compared to the control with x2-3-fold improvements to contractile parameters such as amplitude, relaxation time and contraction rate (Alvarez-Paino et al., 2019).

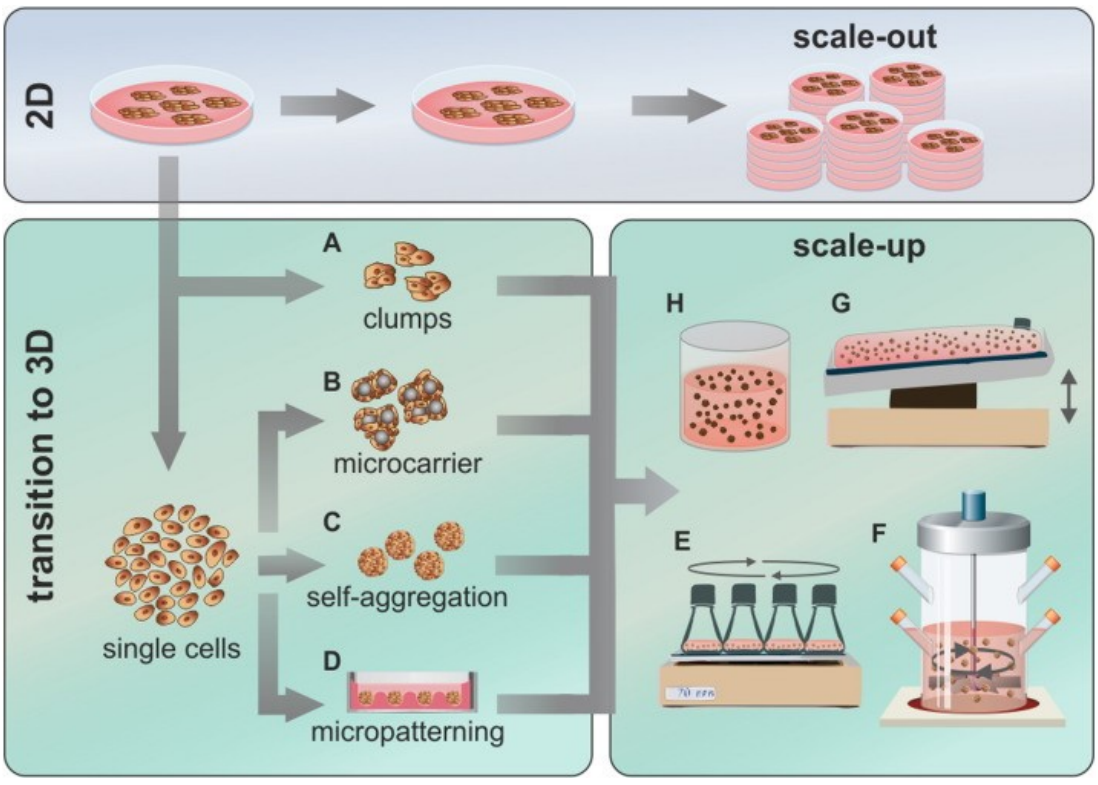

Figure 5.28 Strategies for Up-Scaling hPSC-Derived Cardiomyocyte Production.
Scale-out versus scale-up. Homogenous culture conditions for 3D scale-up are maintained by, spinning, stirring, agitation, or rocking Adapted from Kempf, Andree, and Zweigerdt, 2016.

5.9.6 3D Models to Improve Maturation Can Lack Scalability

The cutting edge of hPSC-CM work has begun to consider the cardiac geometry, to replicate chamber formation or chamber functionality of the heart. One such model combined fibroblasts and hPSC-CMs in a Matrigel and collagen I mixture around a mold containing an inflatable balloon, which allowed for the assessment of hPSC-CMs as a 'pump', termed miniature human ventricle-like cardiac organoid chambers (hvCOCs). HvCOCs had increased expression of calcium handling and ion channel genes compared to 3D microtissues and 2D cultures and demonstrated a positive force frequency relationship (Li et al., 2018).

Another study uses polycaprolactone (PCL) and gelatin with pull spinning fabrication to generate 'ventricle-like' tubes, with fibronectin coating. Ventricle-like tubes were responsive to pharmacological intervention and allowed for the measurements of ejection fraction, with a chamber volume of ~500 uL. Ejection fractions were reported to be 10^4 - 10^8 smaller than human ventricles (MacQueen et al., 2018). The application of synthetic materials discovered in this chapter could be utilised to replace PCL and the fibronectin coating, if the attachment co-polymers from the 2nd generation array screen support enhanced maturation parameters upon scale-up, such adaptions could reduce cost (removal of fibronectin) and enhance functionality.

Whilst more modern 3D models make important advancements on maturation and functionality, compared to lower tier 3D systems, they lack the scalability required for both large scale drug screening and therapeutic intervention, limiting their use to the academic or a low throughput setting.

Whereas well-plate format engineered heart tissues and cardiac organoids, situated between two flexible posts allow for relatively simplified high-throughput contraction analysis and have the potential for further maturation improvements through, co-cultures, media optimisation and compound addition (Mills et al., 2017)(Mills et al., 2019)(Mannhardt et al., 2016).

6 Chapter 6 – General Discussion & Conclusions

The aim of this thesis was to discover novel synthetic materials that could support the attachment and serial passaging of hPSCs whilst retaining their pluripotent state, and separately, synthetic materials that the attachment of hPSC-CMs for ≥7 days with improvements to their maturation state. To do this polymer microarray technology was utilised to initially screen 284 unique materials in a 1st generation array. 24 materials of interest were taken for each cell type (hPSCs and hPSC-CMs) to perform 2:1 pairwise mixing to form two independent 2nd generation arrays containing 599 & 576 unique materials for the hPSC & hPSC-CM 2nd generation array respectively. Additional co-polymers were created in the 2nd generation hPSC array by experimentation with 1:1 mixing for a subset of polymers. For undifferentiated hPSCs a 3rd generation array was created using 8 final hits mixed combinatorial with ratios 1:9, 2:8, 3:7, 6:4, 5:5 and the inverse, to form an array with 297 unique materials. In total 12,503 cell-material interactions for undifferentiated hPSCs, and 24,600 cell-materials interactions for hPSC-CMs were screened in this thesis.

The primary challenge within this project was to discover polymeric surfaces that could support hPSC attachment and survival in the E8 medium, containing just 8 components with basal medium. From a technical perspective the translation of polymer microarray spots of ~200 µm spots eventually to surface areas of 9.6 cm^2 proved difficult. This involved changes to the solvent used, monomer concentration, polymerisation surface, equipment set-up, new equipment (for greater control of the reaction atmosphere) and the introduction to washing & soaking stages to remove cytotoxic unpolymerised monomer and photo initiator. The time taken to overcome this challenge limited the biological characterisation possible of hPSCs and hPSC-CMs on synthetic surfaces.

6.1 Fulfilment of Thesis Objectives

Within this thesis there were five main objectives as outlined in hypothesis and thesis aims section of the introduction chapter, furthermore these main objectives were broken down further in each individual chapter.

Objective 1): Screen a homopolymer microarray containing 284 unique polymer spots, for the attachment of hPSCs or hPSC-CMs, at 24/48 hours, or 7-day culture respectively.

Array stability and imaging issues occurred with the alteration of the array production protocol to utilise a 6% pHEMA solution instead of a 4% pHEMA solution, two independent screening campaigns were successfully carried out for the undifferentiated hPSCs and hPSC-CMs once this issue was corrected. It was discovered that a 6% pHEMA background led to an increase in pHEMA layer thickness and increased cell attachment on homopolymers such as NGDA and

TCDMDA, compared to 4% pHEMA. In previous work performed on pHEMA coated arrays, the pHEMA layer was found to be critically important for scaled-up versions of polymers, large films prepared on an acrylate silane layer failed to reproduce the biological properties demonstrated with the array format (Mei et al., 2010). An increase in pHEMA ion intensity was discovered on the surface of polymers printed to arrays with 6% pHEMA but also detected on 4% pHEMA array with ToF-SIMs in this thesis. This phenomenon was also found within previous polymer microarray studies (Celiz et al., 2015)(Patel et al., 2015). Addition of HEMA to homopolymer HPhMA to improve surface stability and remove cracking issues (Celiz et al., 2015). The pHEMA layer was kept for 35mm dish for scale of hPSC-CM hit materials by Patel et al., 2015, where no comment was made on attempts without pHEMA. Attempts to replicate scale-up of hits from Patel et al., 2015 without pHEMA in this thesis created opaque surfaces.

With undifferentiated hPSCs, twenty homopolymers were discovered that could support ≥20 OCT4+ cells at 24-hour culture, however no homopolymers could support reproducible culture beyond the 24-hour time point, in the absence of ROCKi. In a previous polymer microarray screen, homopolymers of a similar chemical nature (acrylate, acrylamide library) were found to be capable of supporting long-term hPSC culture, albeit not in Essential 8 medium (Celiz et al., 2015). Despite increasing the monomer library from 141 (Celiz et al., 2015) to 281 (+3 co-polymers), it was not possible to produce 'hits' that could support reproducible 48-hour survival.

The hPSC-CM homopolymer array screen (with the addition of three hit copolymers for hPSC-CM attachment, Patel et al., 2015) uncovered 24 hits that supported hPSC-CM attachment after 7 days of culture. Arrays with three different seeding densities, 38,800 cells/cm^2, 77,700 cells/cm^2 and 103,800 cells/cm^2 were tested. Arrays where the pHEMA background was replaced with a methacrylate silane background were tested to ensure hit materials were not dependent on the presence of pHEMA as previously discussed. Finally a test comparing the incubation of serum vs no serum was performed, due to 5-10% FBS or horse serum a common component when seeding CMs & a previous study which found hPSC-CMs demonstrated attachment to a greater number of homopolymers & greater cellular spreading in the presence of serum (Patel et al., 2015)(Pandey et al., 2018)(Ikonen et al., 2013). Increased seeding densities was linked to an increase in the number of polymer attachment hits. Switching out pHEMA for methacrylate silane revealed that hits such as APMAm.C, AEMAm.C, DMAEMA, DMEMAm and DMPAm supported hPSC-CM attachment regardless of the presence of the pHEMA hydrogel layer. The addition of serum did not increase the number of attachment hits but induced greater cell spreading in hits DVAd & ZrCEA.

Co-polymers identified by a previous array screening campaign to be attachment and maturation hits for hPSC-CMs were present in the 1st generation array screen but their attachment performance was not replicated in this thesis (Patel et al., 2015). A direct comparison of iBMA:tBAEMA, FuMA:tBAEMA & HEODA:EEMA to a gelatin control was performed by Patel et al., 2015, where area coverage was 70% - 80% relative to a gelatin control. The co-polymers iBMA:tBAEMA, FuMA:tBAEMA & HEODA:EEMA, supported, 84 +/- 66%, 39 +/- 19%,

19 +/- 25 in this thesis respectively, with these values representing ≤50% coverage of polymer spots. These differences could be due to the change in medium composition used during the array screening process. RPMI-B27 used in this thesis contains 27 products plus basal medium including proteins such as albumin, however iBMA:tBAEMA, FuMA:tBAEMA & HEODA:EEMA were discovered by Patel et al., 2015 to attach hPSC-CMs in a relatively simple medium of RPMI supplemented with insulin, transferrin, selenium, chemically defined lipid and 1-thioglycerol.

In conclusion, homopolymer array screening campaigns were carried out for hPSCs and hPSC-CMs, identifying 24 materials to be combined into co-polymer arrays.

Objective 2): Perform two independent co-polymer screens, containing mixtures of 24 homopolymers relevant to each separate cell type, forming co-polymer microarrays containing 576/599 unique materials.

The formation of a co-polymer array for hPSC serially passaged culture successfully identified 10 co-polymers that could support reproducible hPSC growth and survival at 48- or 72-hours culture, with TCDMDA & NGDA as recurring major components. The proximity of polymer spots printed onto the hPSC co-polymer array was problematic for the highly proliferative nature of hPSCs. For accurate assessment of individual polymer performance, the array system relies on each printed spot acting as an independent island, without influence from adjacent printed polymers. In the first-generation array containing 284 polymer spots with

750 µm X & Y axis distance between adjacent polymers, this was reduced to 500 µm in the co-polymer array screen.

After 24-hour culture the co-polymer array screen supported hPSC colonies that branched between multiple adjacent polymer islands, overcoming the pHEMA protein and cell adhesion inhibition. This will have resulted in the identification of false positives. Even without direct branching from one polymer island to the next, the diffusion of ECM components could enhance the survival and growth of hPSCs on lesser hit materials. hPSCs produce autocrine and paracrine signals that affect self-renewal, growth and differentiation, with examples shown in Figure 6.1 (Peerani et al., 2007)(Mittal and Voldman, 2011)(Bendall et al., 2007)(ten Berge et al., 2011). Paracrine signals have been shown to be capable of reaching over 300 µm in distance with ~10,000 molecules being released, this is within the range that hPSC colonies may be capable of exerting effects on adjacent polymer islands (Handly, Pilko and Wollman, 2015).

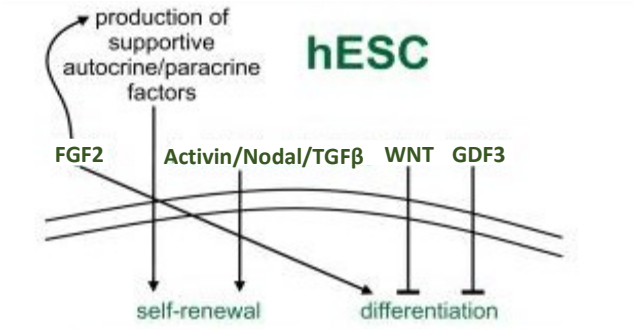

Autocrine factor	Function	Works through
FGF2/LGFLL (paracrine loop)	Differentiation to maintain self-renewal	ERK, others
TGFβ/Activin	Self-renewal	SMAD2/3
GDF3	Pluripotency, Inhibition of differentiation	BMP inhibition
WNT	Inhibition of differentiation	ß-catenin, potentially others

Figure 6.1 Examples of hESC autocrine signalling in self-renewal and differentiation.
Adapted from Pryzbyla *et al.,* 2012.

Co-polymer screening for hPSC-CM attachment hits proved problematic, the first 7 biological repeats performed on the arrays demonstrated reduced attachment on the homopolymer hits established from the 1st generation screen. Attachment to co-polymers was limited, with TCDMDA:LaA emerging as the top performer. Later it was discovered by ToF-SIMs that the arrays had a sulphur-containing contaminant uniformly present across the array surface. Extensive washing and soaking steps with dH_20 alleviated the cytotoxicity previously seen, allowing for 19 co-polymer hits with greater attachment than the best performing homopolymer, APMAm.C, to be identified. hPSC-CMs are non-proliferative cells and did not exhibit the same pHEMA invasion and spot-to-spot bridging as shown with the highly proliferative undifferentiated hPSCs.

Objective 3): Investigate the ability of chosen co-polymer biomaterials to support serial passaging of and maintain pluripotency after (≥15 days, 5+ passages) on the synthetic surface.

A single surface, TCDMDA:BA, was selected after initial testing to be the synthetic surface that supported serial passaging of hPSCs. Culture was demonstrated for up to 30 days with HUES7 hESCs, ReBl-PAT hiPSCs and AT1 hiPSCs (figure 4.13). Cumulative population doublings were not comparable with Matrigel, for example AT1s cultured in LifeTech E8 had 34% fewer population doublings by day 24 culture on TCDMDA:BA (figure 4.13). Although this difference was improved to 25% fewer population doublings with the use of HomeBrew E8 (figure 4.13). After 15 days of culture all three cell lines demonstrated stable karyotype.

Objective 4): Identify mechanisms of hPSC attachment to chosen co-polymer biomaterials, analyse changes to gene expression & phosphokinase proteome, compared to equivalent Matrigel™-based hPSC culture.

An in-depth assessment of AT1 and HUES7 hPSC cultures on TCDMDA:BA was carried out in this thesis. Overall it was identified that the β1, αVβ3, αVβ5 integrins were mechanistically important for the adhesion of hPSCs to TCDMDA:BA, closely aligning with previous work on synthetic hPSC culture surfaces (figure 4.20) (Villa-Diaz et al., 2010)(Celiz et al., 2015).

Comparison of gene expression determined that the AT1 and HUES7 lines have comparable expression of OCT4, NANOG & SOX2 to Matrigel, the AT1 line also had comparable expression of naïve potency and early differentiation markers (figure 4.14). The HUES7 line deviated with significant upregulation of early ectoderm makers SOX1 & PAX6, and changes in the regulation of ZIC1 & KLF4 indication a shift toward naïve potency (figure 4.14). It was revealed that whilst expression of naïve related makers increases with culture on TCDMDA:BA culture, the level of expression was drastically lower than that of cells chemically directed towards a naïve-like state (figure 4.14). The HUES7 hESC line demonstrated a 13% drop in SOX2 positivity as measured with flow cytometry versus Matrigel control, a decrease in pluripotency marker expression on synthetic surfaces have been reported previously with Synthemax™ SC-II, where OCT4 positivity was 30% lower than Matrigel cultures at passage 3 (Pennington et al., 2015). Both surfaces are capable of serial passaging and trilineage differentiation.

With regards to changes in the phosphokinase proteome, the AT1 phosphokinase proteome closely resembled that of the Matrigel equivalent on TCDMDA:BA, with the notable ~1.2-fold increase in apoptosis inducing S46 phosphorylation on p53 (figure 4.21). Aside from a similar ~1.3-fold increase in P53 S46, the HUES7 shifted its phosphokinase proteome towards increased activation of EGFR, RSK and the AKT pathway at 48-hour culture (figure 4.22 & 4.23). The HUES7 line did not exhibit improved population doublings compared to the AT1 line on TCDMDA:BA compared to Matrigel surfaces, suggesting that the increase in phosphorylation on cell cycle linked CHK2 and p27 and differentiation linked Fyn, Lyn and Src likely balances out these pro-proliferative signals (Fernandez-Alonso et al., 2017)(Reinhardt and Yaffe, 2009)(Craig et al., 1997).

Both cell lines still retained the ability to differentiate into, definitive endoderm, neuroectoderm and cardiomyocytes (mesoderm) after ≥5 serial passages on TCDMDA:BA (figures 4.16 – 4.19).

Objective 5): Detect maturation improvements on scaled-up hPSC-cardiomyocyte homopolymer & co-polymer attachment hits, through the assessment of functional contraction & electrophysiological properties using the CellOPTIQ® and gene expression.

Whilst scaled-up primary amines, APMAm.C, AEMAm.C and AEMA.C were tested for their functional capabilities with the CellOPTIQ compared to Matrigel, the enhanced contraction parameters initially assessed determined all three primary amines had significant improvements to contractile amplitude, contraction rate and relaxation rate (figure 5.18). These results were put into question, after the same

experiment repeated with optimised polymerisation revealed only AEMAm.C + Linker, AEMA.C and AEMA.C + Linker had significant improvements to contractile amplitude and contraction rate (figure 5.21). Furthermore, voltage parameter assessment on optimised surfaces of primary amine hits demonstrated that parameters such as amplitude and T-rise were significantly lesser than that of Matrigel, despite ventricular-index remaining constant (figure 5.22). Gene expression analysis may have presented an upward trend for CASQ2, PPARGC1A & TNNI3, however these fold increases were <2-fold and required further repeats to confirm significance (figure 5.23). An electrical stimulation maturation strategy similarly demonstrates 1.5-2-fold increases in gene expression MLC2V, SCN5A & SERCA, with decreases in the expression of RYR2, HCN4 & HCN3 (Chan et al., 2013). Where long-term culture (360 day) maturation strategy led to a 2-5-fold change in expression of cTNT, MYH6, MYH7 & MYL2 (Kamakura et al., 2013).

19 co-polymer attachment hits were identified in the 2nd generation array that supported greater cell attachment than the top performing homopolymer in the 2nd generation array, APMAm.C (figure 5.26 & 5.27). Due to technical issues and time constraints within the project, these best performing hits were not scaled-up and assessed for changes to the maturation state. It will be important moving forward that these materials undergo an intermediate scaled-up screen (96-well plates), to determine if any translate beyond the array format.

6.2 Future Work & Directions

The future of the work presented in this thesis must be considered from both the materials and cell culture aspects.

6.2.1 TCDMDA:BA Fabrication

The materials developed in this thesis are all amenable to UV-based polymerisation, however this has proven problematic with high degrees of variation in the polymerisation efficiency therefore leading to cytotoxic effects. Large improvements were made with the set-up optimisation and new equipment, however batch-to-batch production is susceptible to variation without a quantified quality control measure, such as NMR spectroscopy.

A switch to thermal polymerisation, which can be quality controlled in this manner would be preferable for fabrication, however some polymers of interest such as TCDMDA:BA were not amendable to this technique due to the rapid reactivity. As an alternative, hyperbranching polymerisation of TCDMDA:BA was attempted by PhD student Sophie Goodwin, a technique where polymerisation is halted mid-way and pre-polymerised material is purified from the final product (Sun et al., 2017)(Wang and Gao, 2017). pTCDMDA-co-pBA produced in this manner could be dissolved in IPA with applied heat and drop cast to TCP surfaces, and quality control checked with NMR spectroscopy. Future work would aim to optimise the hyperbranching process, the concentration of pTCDMDA-co-pBA dissolved in an optimal TCP-friendly solvent. Aside from enhanced quality control, hyperbranching (where thermal polymerisation isn't possible) creates a product that could be readily coated onto 2D and 3D structures alike, with rapid application of polymerised material (<30 seconds), adding flexibility for the end-user and simplification of the manufacturing process for a supplier.

A transition to 3D culture should also be investigated, the production of 3D microparticles formed of TCDMDA:BA at UoN, with a surfactant that is also a positive attachment hit for at least 24-hour culture. Combined with bioreactor culture it is envisioned that protein-free synthetic surfaces could provide the high cell number required for therapeutic or high-throughput screen purposes.

6.2.2 Addressing Reduced Growth Kinetics on TCDMDA:BA

Growth kinetics on TCDMDA:BA were ~25% lower than Matrigel, when cumulative population doublings were assessed over 24 days. Additionally, TCDMDA:BA requires a high cell seeding density (~73,000 cells/cm^2) to ensure post-24-hour survival, with real-time imaging demonstrating reduced cell movement on synthetic surfaces versus Matrigel. To address this issue wider polymer screens could identify new materials with improved hPSC attachment and growth kinetics, acrylates & acrylamides represent a small subsection of available materials.

Of the materials discovered in this thesis, 4-methacryloxyethyl trimellitic anhydride (MAETA) (acrylate) containing co-polymers NGDA:MAETA and TCDMDA:MAETA should be investigated further, utilising methanol with the application of heat for full solvation of MAETA (at concentrations of 25% - 50% for MAETA). MAETA has had previous use as a material for dental applications, where the combination of hydrophilic and hydrophobic groups promotes dental infiltration and strong adhesion (Nakabayashi et al., 1982)(Unemori et al., 2003). Homopolymers neopentyl glycol diacrylate (NGDA) & tricyclo[5.2.1.02,6]decanedimethanol diacrylate (TCDMDA) were also hit materials for human dental pulp stem cells (hDPSCs) (Rasi Ghaemi et al., 2018b). There's a

possibility that co-polymers demonstrated for hPSC proliferation and survival in this thesis have cross-over use for hDPSCs, and visa-versa with hits found within the hDPSC array screen. In addition to NGDA & TCDMDA, hits 2-(Methacryloyloxy)ethyl acetoacetate (MAEA), butane-1,3-diyl diacrylate (13BDDA) & trimethylolpropane ethoxylate triacrylate (TMPETA) were cross-over hits for hDPSCs, and hPSCs at 24 hours culture (Rasi Ghaemi et al., 2018b). Given the simplicity of the media used in both experiments, there could be common mechanism of that mediates attachment to synthetic surfaces. Given that hDPSCs were cultured in just DMEM basal medium for the initial 24-hour attachment period, this casts doubt on the prospect of medium components from E8 acting as essential mediators of cell-polymer attachment (Rasi Ghaemi et al., 2018b). Also of interest with hDPSCs is the ability of TMPETA (triacrylate) and PeTrA (triacrylate – found for hPSC-CMs) ability to support hDPSC proliferation in a scaled-up format in serum free conditions (Vining et al., 2018).

To improve growth kinetics existing hPSC hits could be further functionalised with growth factors, ECM components, or adhesion proteins, by physical immobilisation, covalent conjunctions or ECM-inspired immobilisation, with a review of polymer functionalisation provided by Z Wang et al., 2017 (Figure 6.2).

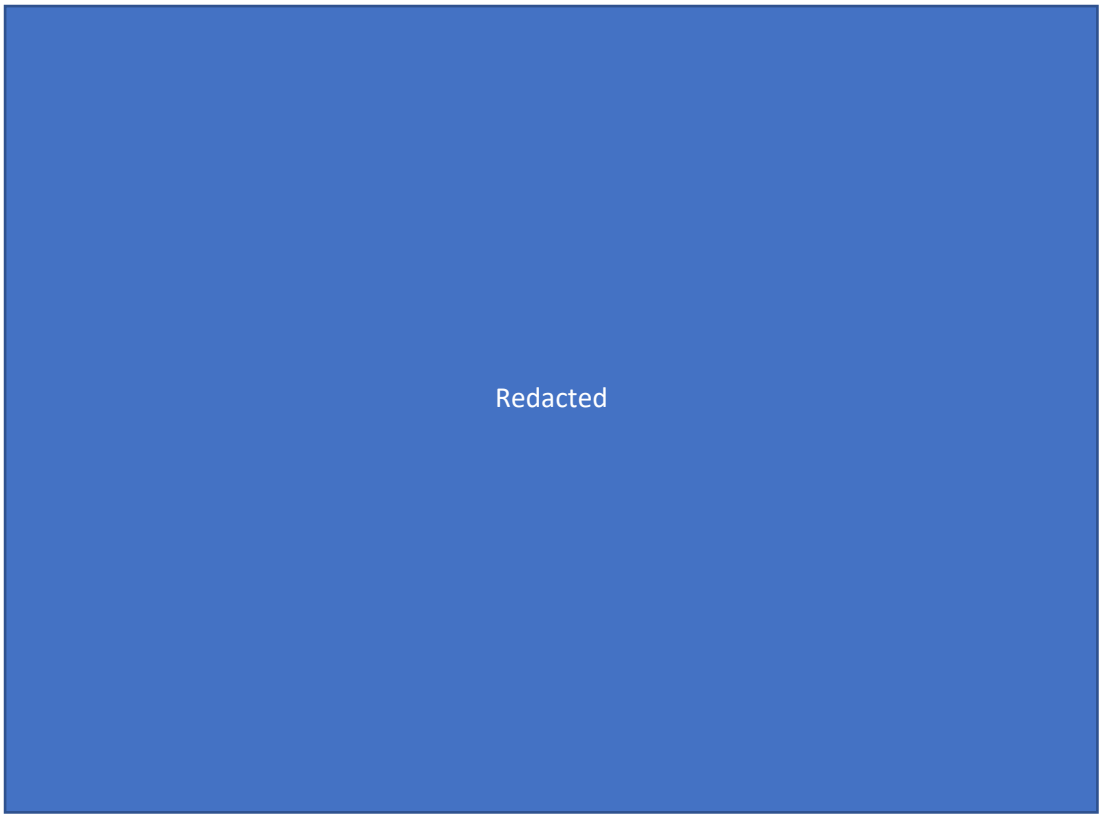

Figure 6.2 Methods for Functionalising Polymeric Surfaces.
Taken from Z Wang *et al.,* 2017.

However, this approach would detract from the scalability and the low-cost of the current approach which relies on economical widely available monomers and a simple polymerisation process.

Alternatively, the medium composition could be reworked to promote improved growth kinetics on TCDMDA:BA. Essential 8 medium is fully defined, with a minimal number of components, the addition of fully defined components to create 'Essential ≤9' medium could be a cost effective way of enhancing hPSC growth kinetics on synthetic surfaces, without the relatively complex functionalisation of the TCDMDA:BA surface. Recent developments in hPSC media optimisation have resulted in a novel 'B8' medium, that contains a thermally optimised form of FGF2, (FGF2-G3) and 'TGFβ3' which is claimed to be a more potent version of TGFβ (Kuo et al., 2019). Importantly, the FGF2-G3 and TGFβ3 are

created recombinantly using bacteria, altogether B8 eliminates up to 97% of the cost of commercially purchased medium, which makes the addition of further compounds more economically feasible (Kuo et al., 2019). Although it should be noted that the 97% cost reduction is not inclusive of labour/production costs. Furthermore, B8 medium supports reduced feeding schedules, which could prove valuable for a synthetic surface where hPSCs are potentially more exposed to sheer forces and must construct a full ECM matrix each passage, compared to ECM-laden Matrigel surfaces.

The addition of heparin in HomeBrew E8 medium presented proof of concept within this thesis. By day 24, 20 +/- 1.1 vs 16 +/- 2.0 cumulative population doublings had occurred in HomeBrew (containing 100 ng/mL heparin) and LifeTech E8 respectively on TCDMDA:BA (figure 4.13). The heparin used within the HomeBrew E8 in this thesis is of porcine origin and undefined in size. An investigation into heparin (and/or the more widely expressed heparan sulphate) addition utilising synthetically produced heparin peptides of differing sizes could identify defined component(s) that positively affect growth kinetics and reduce variation (Ling et al., 2016)(Furue et al., 2008)(Sasaki et al., 2008). The addition of other ECM components such as hyaluronans could also be investigated for their ability to improve growth kinetics on synthetic surfaces, due to their effects of proliferation and growth on hPSCs (Solis et al., 2012).

6.2.3 Utilising Primary Amines as 3D Hydrogels

APMAm.C, AEMAm.C and AEMA.C have the potential to form 3D hydrogels, with APMAm.C having been used to form 3D microparticles and 3D hydrogel

cultures in previous work (Peng, Tellier and Temenoff, 2016)(Gerges et al., 2016). To advance the maturation of hPSC-CMs, work should be undertaken to progress beyond the 2D fabrication of these materials, and their potential co-polymeric hits from the 2nd generation array, to fully formed 3D hydrogel cultures. Furthermore, impregnated hydrogels with hPSC-CMs could be situated around flexible silicone posts in the same manner of engineered heart tissues to allow for high-throughput analysis of contractile properties (Mannhardt et al., 2016). In addition to this, the addition of carbon nanofibers to a hydrogel mixture may allow for efficient flow of electrical current throughout the 3D hydrogel, where electrical pacing can induce further maturation (Shin et al., 2013)(Vaithilingam et al., 2019).

6.2.4 High-Throughput 3D Polymeric Array Screening

The development of 3D polymeric arrays is not a new concept. Alginate gel microwells, gelatin gel arrays, and peptide-functionalised thrombin hydrogels are just three examples of 3D polymeric arrays that have been developed previously (Ozawa et al., 2013)(Li et al., 2014)(Ranga et al., 2014). The stability of hydrogels printed to a traditional open-array format could present a challenge, as flow-stresses from medium exchange could sheer 3D printed gels from the surface, microwells would avoid this issue. Advanced printing technology may offer the ability to either print cells directly with the hydrogel materials, or accurately dispense a defined number of cells into pre-printed hydrogel spots (Choi et al., 2016)(Zhao et al., 2015). With published methodology already existing for the printing of mESCs and hPSCs into alginate 3D hydrogel arrays (Pascoal et al., 2018).

Whilst work has been performed to generate 3D microarrays, real-time monitoring of cellular behaviour inside 3D hydrogels in a high-throughput manner could prove invaluable. 3D capacitance sensors have been developed and tested in a hydrogel system, Figure 6.3 (Lee et al., 2016). The existence of the xCELLigence RTCA Cardio System, a system that utilises well plate formats with electrodes embedded into the surface is proof that capacitance sensors can be downscaled to the 384-well plate, which would make such a system compatible with high-throughput screening (Xi et al., 2011)(del Álamo et al., 2016). If a system was developed at the 384-well scale to have vertical capacitance sensors, 3D hydrogels could be tracked in real-time for their ability to support cell survival and growth. For hPSC-CMs capacitance measurements are also used as a surrogate for their contractile properties in 2D, which may be translatable to 3D sensors (Mulder et al., 2018). Furthermore, the functionalisation of selected hit 3D hydrogels could be screened for their effect, without relying on invasive or end-point assays.

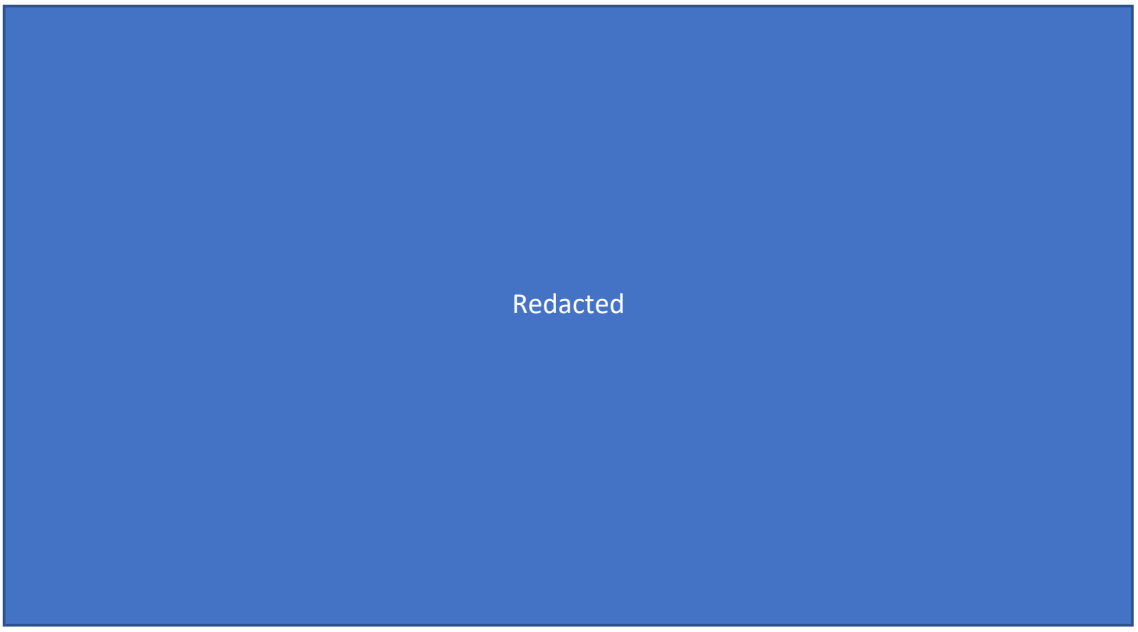

Figure 6.3 3D Capacitance Sensors Designed to Track Viability within an Alginate Hydrogel Containing Encapsulated Cells.
Taken from Lee *et al.,* 2016.

6.3 Limitations of this Thesis

Within this thesis several major improvements to the experimentation and data collected could have been made. The array screening process for hPSCs would have benefitted from an increase in repetition, from 3 biological repeats to 10+ biological repeats. Doing so would have provided an increase in the confidence of polymeric hits taken forward, as each polymer was subject to high attachment standard deviation. Regression analysis utilising generation 1 data failed to provide strong correlation between predicted & actual biological data based on ToF-SIMs ion fragments, further repeats may have fixed this issue.

The inclusion of multiple cell lines, perhaps x3-4, from the onset of the array screening project would have provided assurance from an early stage of

development, that the selected polymer for scale up (optimisation took ~1 year) would have use beyond the ReBl-PAT hiPSC line tested in this thesis.

Whilst the synergy of TCDMDA & BA, moderate and poorly performing homopolymers, created the top performing co-polymer (TCDMDA:BA), high performing homopolymers such as MAEA were not tested in the large-scale combinatorial array screen. Hit materials may have been overlooked in the development of lead hit materials from generation 2/3 hPSC arrays. Intermediate scale (96-well) screens could retrospectively look at the combination of a smaller selection of monomers that were not used in the 2nd generation array.

In a wider regard, the monomer library itself was limited to acrylates, acrylamides and their methylated versions. Polymeric array screening projects have also previously included polyurethanes and polyvinyl monomers, with a co-polymer of poly(butyleneglycol) & 4,4'-methylenediphenyldiisocyanate with a 3-(dimethylamino)-1,2-propanediol chain extender supporting 5 passages of hES-mesenchymal progenitor cells (Duffy et al., 2014).

Scaling-up materials proved to be challenging within this thesis. Batch-to-batch variation resulted in unpredictable toxicity problems, where complete cell death was observed. In experimentation with improved conditions, cell health & viability assays would have aided in the identification and improvement of toxicity and perhaps increased the rate at which optimisation occurred. Similarly, ramen spectroscopy, ToF-SIMs or NMR spectroscopy techniques may have been utilised to detect unreacted material within the polymerised surfaces during intermediate scale-up & 6-well scale-up investigations. A stringent quality control procedure

before polymeric plates were cultured with hPSCs/hPSC-CMs may have prevented catastrophic loss of passage ≤3 cultures saving, time, resources and energy. However, these types of assessments would have required the input and significant time commitment from an individual trained in relevant spectroscopy techniques on a constant basis throughout the project, which would have been impractical. Alternative fabrication protocols such as hyperbranching & thermal polymerisation have relatively simple NMR spectroscopy checks to determine product purity, hence have been discussed as future alternatives for fabrication of hit materials.

Time limitations due to array & scale-up optimisation limited the extent of biological investigation into hPSCs after serial passaging. Culture beyond 24 days was limited to 1-2 repeats per cell line, ideally three or more repeats would have been carried out up to 10 passages, with karyotyping repeated at this stage to ensure continued karyotype stability. RT-qPCR, flow cytometry and immunostaining experiments was successful in determining the expression of a limited number of pluripotency and differentiation markers. The phosphokinase proteome array also provided insights in proliferation, differentiation and cell cycle compared to Matrigel controls. If scale-up were achieved sooner in this project, ECM deposition, RNA sequencing and full proteomic experiments would have provided a wealth of information. Finally, the trilineage differentiations could have been repeated several more times to assess reproducibility and full ectoderm/endoderm differentiations performed into functional cell types such as neurons and liver cells. It is uncertain what affect the formation of large 3D structures has on the ability for hPSCs to form further differentiated cell types, and if their function is impaired or enhanced.

The attachment & maturation of hPSC-CMs were not investigated thoroughly at scale-up within this thesis. A high number of repeats, to assess average surface coverage, cell number, cell size, bi-nucleation rate and sarcomeric organisation would have greatly improved the quality of data produced. Polymer coatings reduced the optical quality for immunostaining of sarcomeric structures, with surfaces UV polymerised in clear plates (with poor optical properties) as to not interfere with the polymerisation process. Polymerisation to glass is an option for high quality immunofluorescent imaging required for sarcomeric analysis, however the surface stiffness would affect sarcomeric size and cell spreading. Further experimentation with black-walled TCP-based plates may have provided a suitable middle ground, if tested post-production optimisation.

The assessment of maturation with the CellOPTIQ provided functional read-outs however, the method of determining contractile properties relies on pixel displacement which could be affected by the strength of attachment to the surface. Confidence to contraction data in this thesis would have been provided with additional direct force measurements, perhaps based from micro posts coated with a thin polymer layer of interest (Rodriguez et al., 2014). Finally, the exploration of co-polymeric surfaces and their effect on the maturation state was not explored in this thesis, which limits the use of the 2nd generation array screen performed.

6.4 Final Remarks

This thesis has utilised powerful high-throughput polymeric array screening technology to identify economically and readily purchasable hit materials, that are capable of either maintaining prolonged culture of hPSCs for 30 days, or supporting

the attachment of hPSC-CMs for 7 days, with the later demonstrating a maturation state equivalent or near to that of xenogeneic Matrigel coatings.

Scale-up of materials identified at the microarray level, to a well plate format, in a reproducible manner was not as simple of a task as initially thought. Changes to the background substrate (glass/pHEMA – TCP), solvent used, and the scale of unreacted cytotoxic material to be removed as the area of polymerisation increased, led to an extended fabrication optimisation period. Hopefully work carried out during this thesis will aid future polymer microarray researchers translate from array to scale-up in a timely manner, should they opt for UV-based polymerisation.

Investigation into the biological changes of hPSCs on a synthetic surface compared to Matrigel revealed that cell line differences occur, with AT1 hiPSCs maintaining equivalent pluripotency and differentiation gene expression, cell positivity for pluripotency markers & phosphokinase proteome. Whilst the HUES7 hESC line had perturbations to differentiation gene expression, reduced SOX2 cell positivity and greatly altered phosphorylation state of PI3K/AKT/mTOR & MAPK pathway members, Src-family kinases and cell cycle kinases such as p27 & CHK2.

Assessment of hPSC-CMs on synthetic surfaces revolved around primary amine functionality, with other attachment homopolymer hits not demonstrating the level of attachment seen on APMAm.C, AEMAm.C and AEMA.C. Whilst a notable increase in hPSC-CM maturation was not demonstrated with these homopolymers, untested co-polymers with improved attachment properties still hold hope for identifying a synthetic surface that improves the maturation state of hPSC-CMs.

7 Bibliography

Abbastabar, M. et al. (2018) 'Multiple functions of p27 in cell cycle, apoptosis, epigenetic modification and transcriptional regulation for the control of cell growth: A double-edged sword protein', DNA Repair, 69, pp. 63–72. doi: 10.1016/j.dnarep.2018.07.008.

Ahsan, S. M. et al. (2018) 'Chitosan as biomaterial in drug delivery and tissue engineering', International Journal of Biological Macromolecules. Elsevier, 110, pp. 97–109. doi: 10.1016/J.IJBIOMAC.2017.08.140.

Ai, D. et al. (2007) 'Canonical Wnt signaling functions in second heart field to promote right ventricular growth', Proceedings of the National Academy of Sciences, 104(22), pp. 9319–9324. doi: 10.1073/pnas.0701212104.

Ai, G. et al. (2017) 'Epidermal growth factor promotes proliferation and maintains multipotency of continuous cultured adipose stem cells via activating STAT signal pathway in vitro.', Medicine. Wolters Kluwer Health, 96(30), p. e7607. doi: 10.1097/MD.0000000000007607.

del Álamo, J. C. et al. (2016) 'High throughput physiological screening of iPSC-derived cardiomyocytes for drug development', Biochimica et Biophysica Acta (BBA) - Molecular Cell Research. Elsevier, 1863(7), pp. 1717–1727. doi: 10.1016/J.BBAMCR.2016.03.003.

Alvarez-Paino, M. et al. (2019) 'Polymer microparticles with defined surface chemistry and topography mediate the formation of stem cell aggregates and cardiomyocyte function', ACS Applied Materials & Interfaces. American Chemical

Society, p. acsami.9b04769. doi: 10.1021/acsami.9b04769.

Amador-Arjona, A. et al. (2015) 'SOX2 primes the epigenetic landscape in neural precursors enabling proper gene activation during hippocampal neurogenesis.', Proceedings of the National Academy of Sciences of the United States of America. National Academy of Sciences, 112(15), pp. E1936-45. doi: 10.1073/pnas.1421480112.

Amura, C. R. et al. (2005) 'Inhibited neurogenesis in JNK1-deficient embryonic stem cells.', Molecular and cellular biology. American Society for Microbiology Journals, 25(24), pp. 10791–802. doi: 10.1128/MCB.25.24.10791-10802.2005.

Anderson, D. G. et al. (2005) 'Biomaterial microarrays: rapid, microscale screening of polymer–cell interaction', Biomaterials. Elsevier, 26(23), pp. 4892–4897. doi: 10.1016/J.BIOMATERIALS.2004.11.052.

Anderson, D. G., Levenberg, S. and Langer, R. (2004) 'Nanoliter-scale synthesis of arrayed biomaterials and application to human embryonic stem cells', Nature Biotechnology, 22(7), pp. 863–866. doi: 10.1038/nbt981.

Anderson, R. H. et al. (2009) 'The anatomy of the cardiac conduction system', Clinical Anatomy. John Wiley & Sons, Ltd, 22(1), pp. 99–113. doi: 10.1002/ca.20700.

Andrzejewska, E. et al. (2003) 'Termination mechanism during the photo-induced radical cross-linking polymerization in the presence and absence of oxygen', Physical Chemistry Chemical Physics. The Royal Society of Chemistry, 5(12), p. 2635. doi: 10.1039/b301849k.

Ang, S. L. et al. (2013) 'A targeted mouse Otx2 mutation leads to severe defects in

gastrulation and formation of axial mesoderm and to deletion of rostral brain', Development. Oxford University Press for The Company of Biologists Limited, 122(1), pp. 243–252. doi: 7588062.

Aouadi, M. et al. (2006) 'p38 Mitogen-Activated Protein Kinase Activity Commits Embryonic Stem Cells to Either Neurogenesis or Cardiomyogenesis', Stem Cells. John Wiley & Sons, Ltd, 24(5), pp. 1399–1406. doi: 10.1634/stemcells.2005-0398.

Armstrong, L. et al. (2006) 'The role of PI3K/AKT, MAPK/ERK and NFκβ signalling in the maintenance of human embryonic stem cell pluripotency and viability highlighted by transcriptional profiling and functional analysis', Human Molecular Genetics. Oxford University Press, 15(11), pp. 1894–1913. doi: 10.1093/hmg/ddl112.

Avilion, A. A. et al. (2003) 'Multipotent cell lineages in early mouse development depend on SOX2 function', Genes & Development, 17(1), pp. 126–140. doi: 10.1101/gad.224503.

Baino, F., Novajra, G. and Vitale-Brovarone, C. (2015) 'Bioceramics and Scaffolds: A Winning Combination for Tissue Engineering.', Frontiers in bioengineering and biotechnology. Frontiers Media SA, 3, p. 202. doi: 10.3389/fbioe.2015.00202.

Banin, S. et al. (1998) 'Enhanced Phosphorylation of p53 by ATM in Response to DNA Damage', Science, 281(5383), pp. 1674–1677. doi: 10.1126/science.281.5383.1674.

Becker, B. A. J., Mcculloch, E. A. and Till, J. E. (1963) 'SPLEEN COLONIES DERIVED FROM TRANSPLANTED MOUSE', 197, pp. 452–454.

Bedada, F. B. et al. (2014) ‘Acquisition of a quantitative, stoichiometrically conserved ratiometric marker of maturation status in stem cell-derived cardiac myocytes’, Stem Cell Reports. The Authors, 3(4), pp. 594–605. doi: 10.1016/j.stemcr.2014.07.012.

Bendall, S. C. et al. (2007) ‘IGF and FGF cooperatively establish the regulatory stem cell niche of pluripotent human cells in vitro’, Nature, 448(7157), pp. 1015–1021. doi: 10.1038/nature06027.

Van den Berg, C. et al. (2016) Differentiation of Human Pluripotent Stem Cells to Cardiomyocytes Under Defined Conditions. Available at: https://link.springer.com/content/pdf/10.1007%2F978-1-4939-3034-0.pdf.

van den Berg, D. L. C. et al. (2010) ‘An Oct4-Centered Protein Interaction Network in Embryonic Stem Cells’, Cell Stem Cell. Cell Press, 6(4), pp. 369–381. doi: 10.1016/J.STEM.2010.02.014.

ten Berge, D. et al. (2011) ‘Embryonic stem cells require Wnt proteins to prevent differentiation to epiblast stem cells’, Nature Cell Biology, 13(9), pp. 1070–1075. doi: 10.1038/ncb2314.

Bessonnard, S. et al. (2014) ‘Gata6, Nanog and Erk signaling control cell fate in the inner cell mass through a tristable regulatory network’, Development, 141(19), pp. 3637–3648. doi: 10.1242/dev.109678.

Betschinger, J. et al. (2013) ‘Exit from Pluripotency Is Gated by Intracellular Redistribution of the bHLH Transcription Factor Tfe3’, Cell. Cell Press, 153(2), pp. 335–347. doi: 10.1016/J.CELL.2013.03.012.

Bilodeau, S. et al. (2009) 'SetDB1 contributes to repression of genes encoding developmental regulators and maintenance of ES cell state.', Genes & development. Cold Spring Harbor Laboratory Press, 23(21), pp. 2484–9. doi: 10.1101/gad.1837309.

Binétruy, B. et al. (2007) 'Concise Review: Regulation of Embryonic Stem Cell Lineage Commitment by Mitogen-Activated Protein Kinases', Stem Cells. John Wiley & Sons, Ltd, 25(5), pp. 1090–1095. doi: 10.1634/stemcells.2006-0612.

Bolon, D. A. and Webb, K. K. (1978) 'Barrier coats versus inert atmospheres. The elimination of oxygen inhibition in free-radical polymerizations', Journal of Applied Polymer Science. John Wiley & Sons, Ltd, 22(9), pp. 2543–2551. doi: 10.1002/app.1978.070220913.

Bond, A. M., Ming, G. and Song, H. (2015) 'Adult Mammalian Neural Stem Cells and Neurogenesis: Five Decades Later', Cell Stem Cell. Cell Press, 17(4), pp. 385–395. doi: 10.1016/J.STEM.2015.09.003.

Bone, H. K. et al. (2011) 'A novel chemically directed route for the generation of definitive endoderm from human embryonic stem cells based on inhibition of GSK-3.', Journal of cell science. The Company of Biologists Ltd, 124(Pt 12), pp. 1992–2000. doi: 10.1242/jcs.081679.

Boyer, L. A. et al. (2005) 'Core Transcriptional Regulatory Circuitry in Human Embryonic Stem Cells', Cell. Cell Press, 122(6), pp. 947–956. doi: 10.1016/J.CELL.2005.08.020.

Braam, S. R. et al. (2008) 'Recombinant Vitronectin Is a Functionally Defined

Substrate That Supports Human Embryonic Stem Cell Self-Renewal via αVβ5 Integrin', Stem Cells. John Wiley & Sons, Ltd, 26(9), pp. 2257–2265. doi: 10.1634/stemcells.2008-0291.

Brady, C. A. and Attardi, L. D. (2010) 'p53 at a glance', Journal of Cell Science. The Company of Biologists Ltd, 123(15), pp. 2527–2532. doi: 10.1242/JCS.064501.

Branco, M. A. et al. (2019) 'Transcriptomic analysis of 3D Cardiac Differentiation of Human Induced Pluripotent Stem Cells Reveals Faster Cardiomyocyte Maturation Compared to 2D Culture', Scientific Reports. Nature Publishing Group, 9(1), p. 9229. doi: 10.1038/s41598-019-45047-9.

Brault, V. et al. (2001) 'Inactivation of the beta-catenin gene by Wnt1-Cre-mediated deletion results in dramatic brain malformation and failure of craniofacial development.', Development (Cambridge, England). Oxford University Press for The Company of Biologists Limited, 128(8), pp. 1253–64. doi: 10.1242/dev.088765.

Breckwoldt, K. et al. (2017) 'Differentiation of cardiomyocytes and generation of human engineered heart tissue', Nature Protocols. Nature Publishing Group, 12(6), pp. 1177–1197. doi: 10.1038/nprot.2017.033.

Brette, F. and Orchard, C. (2003) 'T-Tubule Function in Mammalian Cardiac Myocytes', Circulation Research, 92(11), pp. 1182–1192. doi: 10.1161/01.RES.0000074908.17214.FD.

Brewer, G. J. et al. (1993) 'Optimized survival of hippocampal neurons in B27-supplemented neurobasal?, a new serum-free medium combination', Journal of Neuroscience Research, 35(5), pp. 567–576. doi: 10.1002/jnr.490350513.

Bruneau, B. G. B. G. (2013) ‘Signaling and transcriptional networks in heart development and regeneration.’, Cold Spring Harbor Perspectives in Biology, 5(3). Available at: http://cshperspectives.cshlp.org/lookup/doi/10.1101/cshperspect.a008292%5Cnpapers3://publication/doi/10.1101/cshperspect.a008292.

Buchholz, D. E. et al. (2013) ‘Rapid and Efficient Directed Differentiation of Human Pluripotent Stem Cells Into Retinal Pigmented Epithelium’, STEM CELLS Translational Medicine. John Wiley & Sons, Ltd, 2(5), pp. 384–393. doi: 10.5966/sctm.2012-0163.

Burridge, P. W. et al. (2007) ‘Improved Human Embryonic Stem Cell Embryoid Body Homogeneity and Cardiomyocyte Differentiation from a Novel V-96 Plate Aggregation System Highlights Interline Variability’, Stem Cells, 25(4), pp. 929–938. doi: 10.1634/stemcells.2006-0598.

Burridge, P. W. et al. (2011) ‘A universal system for highly efficient cardiac differentiation of human induced pluripotent stem cells that eliminates interline variability’, PLoS ONE, 6(4). doi: 10.1371/journal.pone.0018293.

Burridge, P. W. et al. (2014) ‘Chemically defned generation of human cardiomyocytes’, Nature Methods, 11(8), pp. 855–860. doi: 10.1038/nMeth.2999.

Burtscher, I., Lickert, H. and Joyner, A. L. (2009) ‘Foxa2 regulates polarity and epithelialization in the endoderm germ layer of the mouse embryo.’, Development (Cambridge, England). The Company of Biologists Ltd, 136(6), pp. 1029–38. doi: 10.1242/dev.028415.

Cai, N. et al. (2012) ‘Post-translational modulation of pluripotency’, Journal of Molecular Cell Biology, 4(4), pp. 262–265. doi: 10.1093/jmcb/mjs031.

Calnan, D. R. and Brunet, A. (2008) ‘The FoxO code’, Oncogene. Nature Publishing Group, 27(16), pp. 2276–2288. doi: 10.1038/onc.2008.21.

Cargnello, M. and Roux, P. P. (2011) ‘Activation and function of the MAPKs and their substrates, the MAPK-activated protein kinases.’, Microbiology and molecular biology reviews : MMBR. American Society for Microbiology, 75(1), pp. 50–83. doi: 10.1128/MMBR.00031-10.

Carré, A. and Lacarrière, V. (2010) ‘How Substrate Properties Control Cell Adhesion. A Physical–Chemical Approach’, Journal of Adhesion Science and Technology. Taylor & Francis Group , 24(5), pp. 815–830. doi: 10.1163/016942409X12598231567862.

CATALDI, A. et al. (2006) ‘Cyclic Nucleotide Response Element Binding Protein (CREB) Activation Promotes Survival Signal in Human K562 Erythroleukemia Cells Exposed to Ionising Radiation/Etoposide Combined Treatment’, Journal of Radiation Research, 47(2), pp. 113–120. doi: 10.1269/jrr.47.113.

Celiz, A. D. et al. (2015) ‘Discovery of a Novel Polymer for Human Pluripotent Stem Cell Expansion and Multilineage Differentiation’, Advanced Materials, 27(27), pp. 4006–4012. doi: 10.1002/adma.201501351.

Chan, Y.-C. et al. (2013) ‘Electrical Stimulation Promotes Maturation of Cardiomyocytes Derived from Human Embryonic Stem Cells’, Journal of Cardiovascular Translational Research. Springer US, 6(6), pp. 989–999. doi:

10.1007/s12265-013-9510-z.

Chauhan, B. K. et al. (2004) 'Functional Properties of Natural Human PAX6 and PAX6(5a) Mutants', Investigative Ophthalmology & Visual Science. The Association for Research in Vision and Ophthalmology, 45(2), pp. 385–392. doi: 10.1167/iovs.03-0968.

Chen, G. et al. (2011) 'Chemically defined conditions for human iPSC derivation and culture', Nature Methods, 8(5), pp. 424–429. doi: 10.1038/nmeth.1593.

Chen, H. et al. (2015) 'Erk signaling is indispensable for genomic stability and self-renewal of mouse embryonic stem cells.', Proceedings of the National Academy of Sciences of the United States of America. National Academy of Sciences, 112(44), pp. E5936-43. doi: 10.1073/pnas.1516319112.

Chen, P.-H., Yao, H. and Huang, L. J.-S. (2017) 'Cytokine Receptor Endocytosis: New Kinase Activity-Dependent and -Independent Roles of PI3K.', Frontiers in endocrinology. Frontiers Media SA, 8, p. 78. doi: 10.3389/fendo.2017.00078.

Chen, W. C. W. et al. (2016) 'Development of a scalable suspension culture for cardiac differentiation from human pluripotent stem cells', 33(2), pp. 557–573. doi: 10.1002/stem.1868.Human.

Chen, X. et al. (2008) 'Zfp143 Regulates Nanog Through Modulation of Oct4 Binding', Stem Cells. John Wiley & Sons, Ltd, 26(11), pp. 2759–2767. doi: 10.1634/stemcells.2008-0398.

Cheng, Q. and Chen, J. (2010) 'Mechanism of p53 stabilization by ATM after DNA damage.', Cell cycle (Georgetown, Tex.). NIH Public Access, 9(3), pp. 472–8. doi:

10.4161/cc.9.3.10556.

Chia, N.-Y. et al. (2010) ‘A genome-wide RNAi screen reveals determinants of human embryonic stem cell identity’, Nature. Nature Publishing Group, 468(7321), pp. 316–320. doi: 10.1038/nature09531.

Chillakuri, C. R., Jones, C. and Mardon, H. J. (2010) ‘Heparin binding domain in vitronectin is required for oligomerization and thus enhances integrin mediated cell adhesion and spreading’, FEBS Letters, 584(15), pp. 3287–3291. doi: 10.1016/j.febslet.2010.06.023.

Choi, Y.-J. et al. (2016) ‘3D Cell Printing of Functional Skeletal Muscle Constructs Using Skeletal Muscle-Derived Bioink’, Advanced Healthcare Materials. John Wiley & Sons, Ltd, 5(20), pp. 2636–2645. doi: 10.1002/adhm.201600483.

Chong, J. J. H. et al. (2014) ‘Human embryonic-stem-cell-derived cardiomyocytes regenerate non-human primate hearts’, Nature. Nature Publishing Group, 510(7504), pp. 273–277. doi: 10.1038/nature13233.

Chun, Y. W. et al. (2015) ‘Combinatorial polymer matrices enhance in vitro maturation of human induced pluripotent stem cell-derived cardiomyocytes’, Biomaterials. Elsevier Ltd, 67, pp. 52–64. doi: 10.1016/j.biomaterials.2015.07.004.

Chung, C. et al. (2013) ‘Hippo-Foxa2 signaling pathway plays a role in peripheral lung maturation and surfactant homeostasis’, Proceedings of the National Academy of Sciences, 110(19), pp. 7732–7737. doi: 10.1073/pnas.1220603110.

Cohen, E. D. et al. (2007) ‘Wnt / b -catenin signaling promotes expansion of Isl-1 – positive cardiac progenitor cells through regulation of FGF signaling Find the latest

version : Wnt / β -catenin signaling promotes expansion of Isl-1 – positive cardiac progenitor cells through reg'. doi: 10.1172/JCI31731.1794.

Coqueret, O. (2003) 'New roles for p21 and p27 cell-cycle inhibitors: a function for each cell compartment?', Trends in cell biology, 13(2), pp. 65–70. Available at: http://www.ncbi.nlm.nih.gov/pubmed/12559756 (Accessed: 29 August 2019).

Correia, C. et al. (2018) '3D aggregate culture improves metabolic maturation of human pluripotent stem cell derived cardiomyocytes', Biotechnology and Bioengineering, 115(3), pp. 630–644. doi: 10.1002/bit.26504.

Cox, M. L. and Meek, D. W. (2010) 'Phosphorylation of serine 392 in p53 is a common and integral event during p53 induction by diverse stimuli', Cellular Signalling, 22(3), pp. 564–571. doi: 10.1016/j.cellsig.2009.11.014.

Craig, C. et al. (1997) 'A recombinant adenovirus expressing p27Kip1 induces cell cycle arrest and loss of cyclin-Cdk activity in human breast cancer cells', Oncogene. Nature Publishing Group, 14(19), pp. 2283–2289. doi: 10.1038/sj.onc.1201064.

Cuevas, B. D., Abell, A. N. and Johnson, G. L. (2007) 'Role of mitogen-activated protein kinase kinase kinases in signal integration', Oncogene. Nature Publishing Group, 26(22), pp. 3159–3171. doi: 10.1038/sj.onc.1210409.

Dahan, P. et al. (2019) 'Metabolism in pluripotency: Both driver and passenger?', The Journal of biological chemistry. American Society for Biochemistry and Molecular Biology, 294(14), pp. 5420–5429. doi: 10.1074/jbc.TM117.000832.

Dai, D.-F. et al. (2017) 'Mitochondrial Maturation in Human Pluripotent Stem Cell Derived Cardiomyocytes', Stem Cells International. Hindawi, 2017, pp. 1–10. doi:

10.1155/2017/5153625.

Dambrot, C. et al. (2014) ‘Serum supplemented culture medium masks hypertrophic phenotypes in human pluripotent stem cell derived cardiomyocytes’, Journal of Cellular and Molecular Medicine, 18(8), pp. 1509–1518. doi: 10.1111/jcmm.12356.

Das, M. et al. (2004) ‘Long-term culture of embryonic rat cardiomyocytes on an organosilane surface in a serum-free medium’, Biomaterials. Elsevier, 25(25), pp. 5643–5647. doi: 10.1016/J.BIOMATERIALS.2004.01.020.

Datan, E. et al. (2014) ‘mTOR/p70S6K signaling distinguishes routine, maintenance-level autophagy from autophagic cell death during influenza A infection.’, Virology. NIH Public Access, 452–453, pp. 175–190. doi: 10.1016/j.virol.2014.01.008.

Davis, A. and K.Cowell, J. (1993) ‘Mutations in the PAX6 gene in patients with hereditary aniridia’, Human Molecular Genetics. Narnia, 2(12), pp. 2093–2097. doi: 10.1093/hmg/2.12.2093.

Denning, C. et al. (2016) ‘Cardiomyocytes from human pluripotent stem cells: From laboratory curiosity to industrial biomedical platform’, Biochimica et Biophysica Acta - Molecular Cell Research. The Authors, 1863(7), pp. 1728–1748. doi: 10.1016/j.bbamcr.2015.10.014.

Dhamoon, A. S. and Jalife, J. (2005) ‘The inward rectifier current (IK1) controls cardiac excitability and is involved in arrhythmogenesis’, Heart Rhythm, 2(3), pp. 316–324. doi: 10.1016/j.hrthm.2004.11.012.

DiFrancesco, D. (2010) ‘The role of the funny current in pacemaker activity.’, Circulation research. Lippincott Williams & Wilkins, 106(3), pp. 434–46. doi:

10.1161/CIRCRESAHA.109.208041.

Dolnikov, K. et al. (2006) 'Functional Properties of Human Embryonic Stem Cell-Derived Cardiomyocytes: Intracellular Ca $^{2+}$ Handling and the Role of Sarcoplasmic Reticulum in the Contraction', Stem Cells, 24(2), pp. 236–245. doi: 10.1634/stemcells.2005-0036.

Donaruma, L. G. (1988) 'Definitions in biomaterials, D. F. Williams, Ed., Elsevier, Amsterdam, 1987, 72 pp.', Journal of Polymer Science: Polymer Letters Edition. John Wiley & Sons, Ltd, 26(9), pp. 414–414. doi: 10.1002/pol.1988.140260910.

Dowd, C. J., Cooney, C. L. and Nugent, M. A. (1999) 'Heparan Sulfate Mediates bFGF Transport through Basement Membrane by Diffusion with Rapid Reversible Binding', Journal of Biological Chemistry, 274(8), pp. 5236–5244. doi: 10.1074/jbc.274.8.5236.

Draper, J. S. et al. (2002) 'Surface antigens of human embryonic stem cells: changes upon differentiation in culture.', Journal of anatomy. Wiley-Blackwell, 200(Pt 3), pp. 249–58. doi: 10.1046/j.1469-7580.2002.00030.x.

Du, C., Wu, H. and Leng, R. (2016) 'UBE4B targets phosphorylated p53 at serines 15 and 392 for degradation', Oncotarget. Impact Journals, LLC, 7(3), pp. 2823–2836. doi: 10.18632/ONCOTARGET.6555.

Duffy, C. R. E. et al. (2014) 'A high-throughput polymer microarray approach for identifying defined substrates for mesenchymal stem cells', Biomater. Sci. Royal Society of Chemistry, 2(11), pp. 1683–1692. doi: 10.1039/C4BM00112E.

Elkouris, M. et al. (2011) 'Sox1 Maintains the Undifferentiated State of Cortical

Neural Progenitor Cells via the Suppression of Prox1-Mediated Cell Cycle Exit and Neurogenesis', STEM CELLS. John Wiley & Sons, Ltd, 29(1), pp. 89–98. doi: 10.1002/stem.554.

Ellen Kreipke, R. et al. (2016) 'Metabolic remodeling in early development and cardiomyocyte maturation', Seminars in Cell and Developmental Biology. Elsevier Ltd, 52, pp. 84–92. doi: 10.1016/j.semcdb.2016.02.004.

Engler, A. J. et al. (2008) 'Embryonic cardiomyocytes beat best on a matrix with heart-like elasticity: scar-like rigidity inhibits beating', Journal of Cell Science, 121(Pt 22), pp. 3794–3802. doi: 10.1242/jcs.029678.Embryonic.

Evans, N. D. et al. (2009) 'Substrate stiffness affects early differentiation events in embryonic stem cells.', European cells & materials, 18, pp. 1-13; discussion 13–4. Available at: http://www.ncbi.nlm.nih.gov/pubmed/19768669 (Accessed: 25 August 2019).

Fan, G.-C. (2012) 'Role of heat shock proteins in stem cell behavior.', Progress in molecular biology and translational science. NIH Public Access, 111, pp. 305–22. doi: 10.1016/B978-0-12-398459-3.00014-9.

Fan, Y., Dickman, K. G. and Zong, W.-X. (2010) 'Akt and c-Myc differentially activate cellular metabolic programs and prime cells to bioenergetic inhibition.', The Journal of biological chemistry. American Society for Biochemistry and Molecular Biology, 285(10), pp. 7324–33. doi: 10.1074/jbc.M109.035584.

Fearnley, C. J., Roderick, H. L. and Bootman, M. D. (2011) 'Calcium signaling in cardiac myocytes.', Cold Spring Harbor perspectives in biology. Cold Spring Harbor

Laboratory Press, 3(11), p. a004242. doi: 10.1101/cshperspect.a004242.

Feric, N. T. and Radisic, M. (2016) 'Maturing human pluripotent stem cell-derived cardiomyocytes in human engineered cardiac tissues', Advanced Drug Delivery Reviews. Elsevier B.V., 96, pp. 110–134. doi: 10.1016/j.addr.2015.04.019.

Fernandez-Alonso, R. et al. (2017) 'Protein Kinases in Pluripotency—Beyond the Usual Suspects', Journal of Molecular Biology. The Authors, 429(10), pp. 1504–1520. doi: 10.1016/j.jmb.2017.04.013.

Fong, H., Hohenstein, K. A. and Donovan, P. J. (2008) 'Regulation of Self-Renewal and Pluripotency by Sox2 in Human Embryonic Stem Cells', Stem Cells. John Wiley & Sons, Ltd, 26(8), pp. 1931–1938. doi: 10.1634/stemcells.2007-1002.

Fu, J. et al. (2017) 'Optimization of a polydopamine (PD)-based coating method and polydimethylsiloxane (PDMS) substrates for improved mouse embryonic stem cell (ESC) pluripotency maintenance and cardiac differentiation', Biomaterials Science. The Royal Society of Chemistry, 5(6), pp. 1156–1173. doi: 10.1039/C7BM00266A.

Furue, M. K. et al. (2008) 'Heparin promotes the growth of human embryonic stem cells in a defined serum-free medium.', Proceedings of the National Academy of Sciences of the United States of America. National Academy of Sciences, 105(36), pp. 13409–14. doi: 10.1073/pnas.0806136105.

Fusaki, N. et al. (2009) 'Efficient induction of transgene-free human pluripotent stem cells using a vector based on Sendai virus, an RNA virus that does not integrate into the host genome.', Proceedings of the Japan Academy. Series B, Physical and biological sciences. The Japan Academy, 85(8), pp. 348–62. doi:

10.2183/PJAB.85.348.

Garcia-Gonzalo, F. R. and Izpisúa Belmonte, J. C. (2008) 'Albumin-Associated Lipids Regulate Human Embryonic Stem Cell Self-Renewal', PLoS ONE. Edited by S. Rutherford, 3(1), p. e1384. doi: 10.1371/journal.pone.0001384.

Gerges, I. et al. (2016) 'A Tailor-Made Synthetic Polymer for Cell Encapsulation: Design Rationale, Synthesis, Chemical-Physics and Biological Characterizations', Macromolecular Bioscience. John Wiley & Sons, Ltd, 16(6), pp. 870–881. doi: 10.1002/mabi.201500386.

Gerhardt, L.-C. et al. (2011) 'The pro-angiogenic properties of multi-functional bioactive glass composite scaffolds', Biomaterials, 32(17), pp. 4096–4108. doi: 10.1016/j.biomaterials.2011.02.032.

Gessert, S. and Kühl, M. (2010) 'The Multiple Phases and Faces of Wnt Signaling During Cardiac Differentiation and Development', Circulation Research. Lippincott Williams & Wilkins, 107(2), pp. 186–199. doi: 10.1161/CIRCRESAHA.110.221531.

Giaccia, A. J. and Kastan, M. B. (1998) 'The complexity of p53 modulation: emerging patterns from divergent signals', Genes & Development. Cold Spring Harbor Laboratory Press, 12(19), pp. 2973–2983. doi: 10.1101/gad.12.19.2973.

Gomes, A. V, Potter, J. D. and Szczesna-cordary, D. (2002) 'Review Article', (10), pp. 323–333. doi: 10.1080/15216540290114676.

Goversen, B. et al. (2018) 'The immature electrophysiological phenotype of iPSC-CMs still hampers in vitro drug screening: Special focus on IK1', Pharmacology & Therapeutics. Pergamon, 183, pp. 127–136. doi:

10.1016/J.PHARMTHERA.2017.10.001.

Graham, S. J. L. et al. (2014) ‘BMP signalling regulates the pre-implantation development of extra-embryonic cell lineages in the mouse embryo’, Nature Communications. Nature Publishing Group, 5(1), p. 5667. doi: 10.1038/ncomms6667.

Grant, A. O. (2009) ‘Cardiac ion channels.’, Circulation. Arrhythmia and electrophysiology. Lippincott Williams & Wilkins, 2(2), pp. 185–94. doi: 10.1161/CIRCEP.108.789081.

Greber, B., Lehrach, H. and Adjaye, J. (2007) ‘Silencing of core transcription factors in human EC cells highlights the importance of autocrine FGF signaling for self-renewal’, BMC Developmental Biology. BioMed Central, 7(1), p. 46. doi: 10.1186/1471-213X-7-46.

Grégory Chambard, Bert Klumperman, * and and German, A. L. (2000) ‘Effect of Solvent on the Activation Rate Parameters for Polystyrene and Poly(butyl acrylate) Macroinitiators in Atom Transfer Radical Polymerization’. American Chemical Society . doi: 10.1021/MA992153G.

Guatimosim, S., Guatimosim, C. and Song, L.-S. (2011) ‘Imaging calcium sparks in cardiac myocytes.’, Methods in molecular biology (Clifton, N.J.). NIH Public Access, 689, pp. 205–14. doi: 10.1007/978-1-60761-950-5_12.

Gurevich, O. et al. (2002) ‘Fibrin Microbeads for Isolating and Growing Bone Marrow–Derived Progenitor Cells Capable of Forming Bone Tissue’, Tissue Engineering. Mary Ann Liebert, Inc. , 8(4), pp. 661–672. doi:

10.1089/107632702760240571.

Györke, I. et al. (2004) 'The Role of Calsequestrin, Triadin, and Junctin in Conferring Cardiac Ryanodine Receptor Responsiveness to Luminal Calcium', Biophysical Journal, 86(4), pp. 2121–2128. doi: 10.1016/S0006-3495(04)74271-X.

Haghighi, F. et al. (2018) 'bFGF-mediated pluripotency maintenance in human induced pluripotent stem cells is associated with NRAS-MAPK signaling', Cell Communication and Signaling. BioMed Central, 16(1), p. 96. doi: 10.1186/s12964-018-0307-1.

Hallonet, M. et al. (2002) 'Maintenance of the Specification of the Anterior Definitive Endoderm and Forebrain Depends on the Axial Mesendoderm: A Study Using HNF3β/Foxa2 Conditional Mutants', Developmental Biology. Academic Press, 243(1), pp. 20–33. doi: 10.1006/DBIO.2001.0536.

Han, J. et al. (2016) 'Cell alignment induced by anisotropic electrospun fibrous scaffolds alone has limited effect on cardiomyocyte maturation', Stem Cell Research. The Authors, 16(3), pp. 740–750. doi: 10.1002/stem.1868.Human.

Handly, L. N., Pilko, A. and Wollman, R. (2015) 'Paracrine communication maximizes cellular response fidelity in wound signaling', eLife. eLife Sciences Publications, Ltd, 4. doi: 10.7554/ELIFE.09652.

Hansen, L. K. et al. (1994) 'Integrin binding and cell spreading on extracellular matrix act at different points in the cell cycle to promote hepatocyte growth.', Molecular biology of the cell. American Society for Cell Biology, 5(9), pp. 967–75. Available at: http://www.ncbi.nlm.nih.gov/pubmed/7841524 (Accessed: 6 March

2019).

Hemmati-Brivanlou, A. and Melton, D. A. (1994) 'Inhibition of activin receptor signaling promotes neuralization in Xenopus', Cell. Cell Press, 77(2), pp. 273–281. doi: 10.1016/0092-8674(94)90319-0.

Hemmi, N. et al. (2014) 'A Massive Suspension Culture System With Metabolic Purification for Human Pluripotent Stem Cell-Derived Cardiomyocytes', Stem Cells Trans Med, 3, pp. 1–11. doi: 10.5966/sctm.2013-0118.

Hemmings, B. A. and Restuccia, D. F. (2012) 'PI3K-PKB/Akt pathway.', Cold Spring Harbor perspectives in biology. Cold Spring Harbor Laboratory Press, 4(9), p. a011189. doi: 10.1101/cshperspect.a011189.

Hench, L. L. (2005) 'Bioceramics', Journal of the American Ceramic Society. John Wiley & Sons, Ltd (10.1111), 81(7), pp. 1705–1728. doi: 10.1111/j.1151-2916.1998.tb02540.x.

Hirt, M. N. et al. (2014) 'Functional improvement and maturation of rat and human engineered heart tissue by chronic electrical stimulation', Journal of Molecular and Cellular Cardiology. Elsevier B.V., 74, pp. 151–161. doi: 10.1016/j.yjmcc.2014.05.009.

Hoang-Trong, T. M., Ullah, A. and Jafri, M. S. (2015) 'Calcium Sparks in the Heart: Dynamics and Regulation', Research and reports in biology. NIH Public Access, 6, p. 203. doi: 10.2147/RRB.S61495.

Hoffman, L. M. and Carpenter, M. K. (2005) 'Characterization and culture of human embryonic stem cells', Nature Biotechnology. Nature Publishing Group, 23(6), pp.

699–708. doi: 10.1038/nbt1102.

Horton, M. A. (1997) ‘The alpha v beta 3 integrin "vitronectin receptor".’, The international journal of biochemistry & cell biology, 29(5), pp. 721–5. Available at: http://www.ncbi.nlm.nih.gov/pubmed/9251239 (Accessed: 28 August 2019).

Horton, M. A. (1997) ‘The αvβ3 integrin “vitronectin receptor”’, The International Journal of Biochemistry & Cell Biology. Pergamon, 29(5), pp. 721–725. doi: 10.1016/S1357-2725(96)00155-0.

Hsiao, C.-W. et al. (2013) ‘Electrical coupling of isolated cardiomyocyte clusters grown on aligned conductive nanofibrous meshes for their synchronized beating’, Biomaterials. Elsevier, 34(4), pp. 1063–1072. doi: 10.1016/J.BIOMATERIALS.2012.10.065.

Hsiao, C. et al. (2017) ‘Human pluripotent stem cell culture density modulates YAP signaling’, Biotechnology journal. NIH Public Access, 11(5), pp. 662–675. doi: 10.1002/biot.201500374.Human.

Humtsoe, J. O. and Kramer, R. H. (2010) ‘Differential Epidermal Growth Factor Receptor Signaling Regulates Anchorage-Independent Growth by Modulation of the PI3K/AKT Pathway’, Oncogene. NIH Public Access, 29(8), p. 1214. doi: 10.1038/ONC.2009.419.

Huttenlocher, A. and Horwitz, A. R. (2011) ‘Integrins in cell migration.’, Cold Spring Harbor perspectives in biology. Cold Spring Harbor Laboratory Press, 3(9), p. a005074. doi: 10.1101/cshperspect.a005074.

Hyslop, L. et al. (2005) ‘Downregulation of NANOG Induces Differentiation of Human Embryonic Stem Cells to Extraembryonic Lineages’, Stem Cells. John Wiley & Sons, Ltd, 23(8), pp. 1035–1043. doi: 10.1634/stemcells.2005-0080.

Ikonen, L. et al. (2013) ‘2D and 3D self-assembling nanofiber hydrogels for cardiomyocyte culture.’, BioMed research international. Hindawi, 2013, p. 285678. doi: 10.1155/2013/285678.

Initiative, T. I. S. C. et al. (2007) ‘Characterization of human embryonic stem cell lines by the International Stem Cell Initiative’, Nature Biotechnology. Nature Publishing Group, 25(7), pp. 803–816. doi: 10.1038/nbt1318.

Irwin, E. F. et al. (2011) ‘Engineered polymer-media interfaces for the long-term self-renewal of human embryonic stem cells’, Biomaterials, 32(29), pp. 6912–6919. doi: 10.1016/j.biomaterials.2011.05.058.

Iwamoto, D. V and Calderwood, D. A. (2015) ‘Regulation of integrin-mediated adhesions’, Current Opinion in Cell Biology. Elsevier Current Trends, 36, pp. 41–47. doi: 10.1016/J.CEB.2015.06.009.

Jacobs, K. et al. (2016) ‘Higher-Density Culture in Human Embryonic Stem Cells Results in DNA Damage and Genome Instability.’, Stem cell reports. Elsevier, 6(3), pp. 330–41. doi: 10.1016/j.stemcr.2016.01.015.

James, C. D. et al. (2000) ‘Aligned microcontact printing of micrometer-scale poly-L-Lysine structures for controlled growth of cultured neurons on planar microelectrode arrays’, IEEE Transactions on Biomedical Engineering, 47(1), pp. 17–21. doi: 10.1109/10.817614.

Jang, H. et al. (2012) ‘O-GlcNAc Regulates Pluripotency and Reprogramming by Directly Acting on Core Components of the Pluripotency Network’, Cell Stem Cell, 11(1), pp. 62–74. doi: 10.1016/j.stem.2012.03.001.

Jaramillo, M. et al. (2015) ‘Inducing endoderm differentiation by modulating mechanical properties of soft substrates’, Journal of Tissue Engineering and Regenerative Medicine, 9(1), pp. 1–12. doi: 10.1002/term.1602.

Jeannine E. Elliott†, A. and Christopher N. Bowman*, † (2002) ‘Effects of Solvent Quality during Polymerization on Network Structure of Cross-Linked Methacrylate Copolymers’. American Chemical Society. doi: 10.1021/JP012845I.

Jeevaratnam, K. et al. (2018) ‘Cardiac Potassium Channels: Physiological Insights for Targeted Therapy.’, Journal of cardiovascular pharmacology and therapeutics. SAGE Publications, 23(2), pp. 119–129. doi: 10.1177/1074248417729880.

Jensen, C. J. et al. (1999) ‘90-kDa ribosomal S6 kinase is phosphorylated and activated by 3-phosphoinositide-dependent protein kinase-1.’, The Journal of biological chemistry. American Society for Biochemistry and Molecular Biology, 274(38), pp. 27168–76. doi: 10.1074/jbc.274.38.27168.

Jiang, Y. et al. (2018) ‘Maturation of Cardiomyocytes Derived from Human Pluripotent Stem Cells: Current Strategies and Limitations.’, Molecules and cells. Korean Society for Molecular and Cellular Biology, 41(7), pp. 613–621. doi: 10.14348/molcells.2018.0143.

Jones, R. G. et al. (2005) ‘AMP-Activated Protein Kinase Induces a p53-Dependent Metabolic Checkpoint’, Molecular Cell, 18(3), pp. 283–293. doi:

10.1016/j.molcel.2005.03.027.

Jonker, S. S. et al. (2007) 'Myocyte enlargement, differentiation, and proliferation kinetics in the fetal sheep heart', Journal of Applied Physiology. American Physiological Society, 102(3), pp. 1130–1142. doi: 10.1152/japplphysiol.00937.2006.

Jung, G. and Bernstein, D. (2015) 'hiPSC MODELING OF INHERITED CARDIOMYOPATHIES Opinion Statement', 16(7), pp. 1–15. doi: 10.1007/s11936-014-0320-7.

Kai, D. et al. (2011) 'Guided orientation of cardiomyocytes on electrospun aligned nanofibers for cardiac tissue engineering', Journal of Biomedical Materials Research - Part B Applied Biomaterials. John Wiley & Sons, Ltd, 98 B(2), pp. 379–386. doi: 10.1002/jbm.b.31862.

Kamakura, T. et al. (2013) 'Ultrastructural Maturation of Human-Induced Pluripotent Stem Cell-Derived Cardiomyocytes in a Long-Term Culture', Circulation Journal, 77(5), pp. 1307–1314. doi: 10.1253/circj.CJ-12-0987.

Kan, L. et al. (2004) 'Sox1 acts through multiple independent pathways to promote neurogenesis', Developmental Biology. Academic Press, 269(2), pp. 580–594. doi: 10.1016/J.YDBIO.2004.02.005.

Kanai-Azuma, M. et al. (2002) 'Depletion of definitive gut endoderm in Sox17-null mutant mice.', Development (Cambridge, England), 129(10), pp. 2367–79. Available at: http://www.ncbi.nlm.nih.gov/pubmed/11973269 (Accessed: 20 August 2019).

Kane, C., Couch, L. and Terracciano, C. M. N. (2015) 'Excitation–contraction coupling

of human induced pluripotent stem cell-derived cardiomyocytes', Frontiers in Cell and Developmental Biology. Frontiers, 3, p. 59. doi: 10.3389/fcell.2015.00059.

Kanno, S. and Saffitz, J. E. (2001) 'The role of myocardial gap junctions in electrical conduction and arrhythmogenesis', Cardiovascular Pathology. Elsevier, 10(4), pp. 169–177. doi: 10.1016/S1054-8807(01)00078-3.

Karimi, F. et al. (2018) 'Integrin Clustering Matters: A Review of Biomaterials Functionalized with Multivalent Integrin-Binding Ligands to Improve Cell Adhesion, Migration, Differentiation, Angiogenesis, and Biomedical Device Integration', Advanced Healthcare Materials. John Wiley & Sons, Ltd, 7(12), p. 1701324. doi: 10.1002/adhm.201701324.

Kattman, S. J. et al. (2011) 'Stage-specific optimization of activin/nodal and BMP signaling promotes cardiac differentiation of mouse and human pluripotent stem cell lines', Cell Stem Cell. Elsevier Inc., 8(2), pp. 228–240. doi: 10.1016/j.stem.2010.12.008.

Kazuyasu Sakaguchi, *,‡ et al. (1997) 'Phosphorylation of Serine 392 Stabilizes the Tetramer Formation of Tumor Suppressor Protein p53'. American Chemical Society . doi: 10.1021/BI970759W.

Kehat, I. et al. (2001) 'Human embryonic stem cells can differentiate into myocytes with structural and functional properties of cardiomyocytes', J. Clin. Invest, 108, pp. 407–414. doi: 10.1172/JCI200112131.Introduction.

Kelley, J. et al. (2014) 'Feeder-Free Expansion of Human Induced Pluripotent Stem Cells (hiPSC) on Corning Synthemax II-SC Substrate Coated Surface in Defined

Medium Sn APPS hots', (17), pp. 2–5. Available at: http://csmedia2.corning.com/LifeSciences/Media/pdf/snappshots_205_FeederFree_Expansion_of_hiPSC_on_SC_Substrate_Coated_Surface_in_Defined_Medium.pdf.

Kempf, H., Andree, B. and Zweigerdt, R. (2016) 'Large-scale production of human pluripotent stem cell derived cardiomyocytes', Advanced Drug Delivery Reviews. Elsevier, 96, pp. 18–30. Available at: http://www.ncbi.nlm.nih.gov/pubmed/26658242 (Accessed: 11 February 2019).

Keung, A. J. et al. (2012) 'Soft microenvironments promote the early neurogenic differentiation but not self-renewal of human pluripotent stem cells', Integrative Biology. Narnia, 4(9), pp. 1049–1058. doi: 10.1039/c2ib20083j.

Keung, W., Boheler, K. R. and Li, A. R. (2014) 'Developmental cues for the maturation of metabolic, electrophysiological and calcium handling properties of human pluripotent stem cell-derived cardiomyocytes', Stem cell research & therapy. doi: 10.1161/CIRCRESAHA.117.311920.

Khan, M. et al. (2015) 'Evaluation of changes in morphology and function of human induced pluripotent stem cell derived cardiomyocytes (hiPSC-CMs) cultured on an aligned-nanofiber cardiac patch', PLoS ONE. Edited by M. Pesce. Public Library of Science, 10(5), pp. 1–19. doi: 10.1371/journal.pone.0126338.

Kim, I. G. et al. (2018) 'Mechanotransduction of human pluripotent stem cells cultivated on tunable cell-derived extracellular matrix', Biomaterials. Elsevier, 150, pp. 100–111. doi: 10.1016/J.BIOMATERIALS.2017.10.016.

King, H. W. and Klose, R. J. (2017) 'The pioneer factor OCT4 requires the chromatin

remodeller BRG1 to support gene regulatory element function in mouse embryonic stem cells', eLife, 6. doi: 10.7554/eLife.22631.

Kishi, M. et al. (2000) 'Requirement of Sox2-mediated signaling for differentiation of early Xenopus neuroectoderm.', Development (Cambridge, England), 127(4), pp. 791–800. Available at: http://www.ncbi.nlm.nih.gov/pubmed/10648237 (Accessed: 11 March 2019).

Klabunde, R. E. (2012) Cardiovascular physiology concepts. Lippincott Williams & Wilkins/Wolters Kluwer. Available at: https://www.cvphysiology.com/textbook.htm (Accessed: 2 September 2019).

Klabunde, R. E. (2017) 'Cardiac electrophysiology: normal and ischemic ionic currents and the ECG', Advances in Physiology Education. American Physiological Society Bethesda, MD, 41(1), pp. 29–37. doi: 10.1152/advan.00105.2016.

Klajn, A. et al. (2014) 'SOX2 overexpression affects neural differentiation of human pluripotent NT2/D1 cells', Biochemistry (Moscow), 79(11), pp. 1172–1182. doi: 10.1134/S0006297914110042.

Knollmann, B. C. (2009) 'New roles of calsequestrin and triadin in cardiac muscle.', The Journal of physiology. Wiley-Blackwell, 587(Pt 13), pp. 3081–7. doi: 10.1113/jphysiol.2009.172098.

Koivumäki, J. T. et al. (2018) 'Structural Immaturity of Human iPSC-Derived Cardiomyocytes: In Silico Investigation of Effects on Function and Disease Modeling.', Frontiers in physiology. Frontiers Media SA, 9, p. 80. doi: 10.3389/fphys.2018.00080.

Kosmidis, G. et al. (2015) ‘Altered calcium handling and increased contraction force in human embryonic stem cell derived cardiomyocytes following short term dexamethasone exposure’, Biochemical and Biophysical Research Communications. Elsevier Ltd, 467(4), pp. 998–1005. doi: 10.1016/j.bbrc.2015.10.026.

Kunath, T. et al. (2007) ‘FGF stimulation of the Erk1/2 signalling cascade triggers transition of pluripotent embryonic stem cells from self-renewal to lineage commitment’, Development, 134(16), pp. 2895–2902. doi: 10.1242/dev.02880.

Kuo, H.-H. et al. (2019) ‘Negligible-Cost and Weekend-Free Chemically Defined Human iPSC Culture’, bioRxiv. Cold Spring Harbor Laboratory, p. 685503. doi: 10.1101/685503.

Laflamme, M. A. et al. (2007) ‘Cardiomyocytes derived from human embryonic stem cells in pro-survival factors enhance function of infarcted rat hearts’, Nature Biotechnology, 25(9), pp. 1015–1024. doi: 10.1038/nbt1327.

Laflamme, M. A. and Murry, C. E. (2011) ‘Heart regeneration’, Nature, pp. 326–335. doi: 10.1201/9781315120188.

LaJevic, M. D. et al. (2011) ‘Activation of p38 mitogen-activated protein kinase by norepinephrine in T-lineage cells’, Immunology. Wiley-Blackwell, 132(2), p. 197. doi: 10.1111/J.1365-2567.2010.03354.X.

Lam, A. T.-L. et al. (2015) ‘Improved Human Pluripotent Stem Cell Attachment and Spreading on Xeno-Free Laminin-521-Coated Microcarriers Results in Efficient Growth in Agitated Cultures.’, BioResearch open access. Mary Ann Liebert, Inc., 4(1), pp. 242–57. doi: 10.1089/biores.2015.0010.

Lam, M. T. and Longaker, M. T. (2012) 'Comparison of several attachment methods for human iPS, embryonic and adipose-derived stem cells for tissue engineering.', Journal of tissue engineering and regenerative medicine. NIH Public Access, 6 Suppl 3(0 3), pp. s80-6. doi: 10.1002/term.1499.

Lamb, T. M. et al. (1993) 'Neural induction by the secreted polypeptide noggin.', Science (New York, N.Y.), 262(5134), pp. 713–8. Available at: http://www.ncbi.nlm.nih.gov/pubmed/8235591 (Accessed: 11 March 2019).

Laplante, M. and Sabatini, D. M. (2009) 'mTOR signaling at a glance.', Journal of cell science. The Company of Biologists Ltd, 122(Pt 20), pp. 3589–94. doi: 10.1242/jcs.051011.

Laplante, M. and Sabatini, D. M. (2009) 'mTOR signaling at a glance', Journal of Cell Science, 122(20), pp. 3589–3594. doi: 10.1242/jcs.051011.

Laptenko, O. and Prives, C. (2006) 'Transcriptional regulation by p53: one protein, many possibilities', Cell Death & Differentiation. Nature Publishing Group, 13(6), pp. 951–961. doi: 10.1038/sj.cdd.4401916.

Law, N. C., White, M. F. and Hunzicker-Dunn, M. E. (2016) 'G protein-coupled receptors (GPCRs) That Signal via Protein Kinase A (PKA) Cross-talk at Insulin Receptor Substrate 1 (IRS1) to Activate the phosphatidylinositol 3-kinase (PI3K)/AKT Pathway.', The Journal of biological chemistry. American Society for Biochemistry and Molecular Biology, 291(53), pp. 27160–27169. doi: 10.1074/jbc.M116.763235.

Lee, C. S. et al. (2002) 'Foxa2 controls Pdx1 gene expression in pancreatic beta-cells in vivo.', Diabetes. American Diabetes Association, 51(8), pp. 2546–51. doi:

10.2337/diabetes.51.8.2546.

Lee, C. S. et al. (2005) 'Foxa2 is required for the differentiation of pancreatic α-cells', Developmental Biology. Academic Press, 278(2), pp. 484–495. doi: 10.1016/J.YDBIO.2004.10.012.

Lee, S.-M. et al. (2016) 'Real-time monitoring of 3D cell culture using a 3D capacitance biosensor', Biosensors and Bioelectronics. Elsevier, 77, pp. 56–61. doi: 10.1016/J.BIOS.2015.09.005.

Lehman, W. et al. (2009) 'Structural Basis for the Activation of Muscle Contraction by Troponin and Tropomyosin', Journal of molecular biology. NIH Public Access, 388(4), p. 673. doi: 10.1016/J.JMB.2009.03.060.

Leonard, A. et al. (2018) 'Afterload promotes maturation of human induced pluripotent stem cell derived cardiomyocytes in engineered heart tissues', Journal of Molecular and Cellular Cardiology. Academic Press, 118, pp. 147–158. doi: 10.1016/J.YJMCC.2018.03.016.

Li, F. et al. (1996) 'Rapid transition of cardiac myocytes from hyperplasia to hypertrophy during postnatal development.', Journal of molecular and cellular cardiology. Elsevier, 28(8), pp. 1737–46. doi: 10.1006/jmcc.1996.0163.

Li, H. L. et al. (1999) 'The tyrosine kinases Syk and Lyn exert opposing effects on the activation of protein kinase Akt/PKB in B lymphocytes.', Proceedings of the National Academy of Sciences of the United States of America. National Academy of Sciences, 96(12), pp. 6890–5. doi: 10.1073/pnas.96.12.6890.

Li, J. et al. (2007) 'MEK/ERK signaling contributes to the maintenance of human

embryonic stem cell self-renewal', Differentiation. Elsevier, 75(4), pp. 299–307. doi: 10.1111/J.1432-0436.2006.00143.X.

Li, M. et al. (2017) 'Overexpression of KCNJ2 in induced pluripotent stem cell-derived cardiomyocytes for the assessment of QT-prolonging drugs', Journal of Pharmacological Sciences. Elsevier Ltd, 134(2), pp. 75–85. doi: 10.1016/j.jphs.2017.05.004.

Li, M. and Belmonte, J. C. I. (2017) 'Ground rules of the pluripotency gene regulatory network', Nature Reviews Genetics. Nature Publishing Group, 18(3), pp. 180–191. doi: 10.1038/nrg.2016.156.

Li, M. and Izpisua Belmonte, J. C. (2018) 'Deconstructing the pluripotency gene regulatory network', Nature Cell Biology. Nature Publishing Group, 20(4), pp. 382–392. doi: 10.1038/s41556-018-0067-6.

Li, R. A. et al. (2018) 'Bioengineering an electro-mechanically functional miniature ventricular heart chamber from human pluripotent stem cells', Biomaterials. Elsevier, 163, pp. 116–127. doi: 10.1016/J.BIOMATERIALS.2018.02.024.

Li, S., Chen, G. and Li, R. A. (2013) 'Calcium signalling of human pluripotent stem cell-derived cardiomyocytes.', The Journal of physiology. Wiley-Blackwell, 591(21), pp. 5279–90. doi: 10.1113/jphysiol.2013.256495.

Li, X. et al. (2014) 'Micro-scaffold array chip for upgrading cell-based high-throughput drug testing to 3D using benchtop equipment', Lab Chip. Royal Society of Chemistry, 14(3), pp. 471–481. doi: 10.1039/C3LC51103K.

Li, Y. et al. (2016) 'Heparin binding preference and structures in the fibroblast

growth factor family parallel their evolutionary diversification', Open Biology. The Royal Society, 6(3), p. 150275. doi: 10.1098/rsob.150275.

Liagre, B. et al. (2007) 'MAP kinase subtypes and Akt regulate diosgenin-induced apoptosis of rheumatoid synovial cells in association with COX-2 expression and prostanoid production.', International journal of molecular medicine, 19(1), pp. 113–22. Available at: http://www.ncbi.nlm.nih.gov/pubmed/17143555 (Accessed: 24 August 2019).

Lian, X. et al. (2012) 'Robust cardiomyocyte differentiation from human pluripotent stem cells via temporal modulation of canonical Wnt signaling.', Proceedings of the National Academy of Sciences of the United States of America. National Academy of Sciences, 109(27), pp. E1848-57. doi: 10.1073/pnas.1200250109.

Lian, X. et al. (2013) 'Directed cardiomyocyte differentiation from human pluripotent stem cells by modulating Wnt/β-catenin signaling under fully defined conditions', Nature Protocols. Nature Publishing Group, 8(1), pp. 162–175. doi: 10.1038/nprot.2012.150.

Liang, Y. et al. (2017) 'Polymeric Biomaterials: Diverse Functions Enabled by Advances in Macromolecular Chemistry.', Macromolecules. NIH Public Access, 50(2), pp. 483–502. doi: 10.1021/acs.macromol.6b02389.

Lieu, D. K. et al. (2013) 'Mechanism-Based Facilitated Maturation of Human Pluripotent Stem Cell–Derived Cardiomyocytes', Circulation: Arrhythmia and Electrophysiology, 6(1), pp. 191–201. doi: 10.1161/CIRCEP.111.973420.

Ligon, S. C. et al. (2014) 'Strategies to Reduce Oxygen Inhibition in Photoinduced

Polymerization', Chemical Reviews. American Chemical Society, 114(1), pp. 557–589. doi: 10.1021/cr3005197.

Lim, J. Y. and Donahue, H. J. (2007) 'Cell Sensing and Response to Micro- and Nanostructured Surfaces Produced by Chemical and Topographic Patterning', Tissue Engineering. Mary Ann Liebert, Inc. 140 Huguenot Street, 3rd Floor New Rochelle, NY 10801 USA , 13(8), pp. 1879–1891. doi: 10.1089/ten.2006.0154.

Ling, L. et al. (2016) 'Effect of heparin on the biological properties and molecular signature of human mesenchymal stem cells.', Gene. NIH Public Access, 576(1 Pt 2), pp. 292–303. doi: 10.1016/j.gene.2015.10.039.

Liu, J. et al. (2014) 'p38 MAPK signaling mediates mitochondrial apoptosis in cancer cells induced by oleanolic acid.', Asian Pacific journal of cancer prevention : APJCP, 15(11), pp. 4519–25. doi: 10.7314/apjcp.2014.15.11.4519.

Liu, Y.-W. et al. (2018) 'Human embryonic stem cell–derived cardiomyocytes restore function in infarcted hearts of non-human primates', Nature Biotechnology. Nature Publishing Group, 36(7), pp. 597–605. doi: 10.1038/nbt.4162.

Loo, B. M. et al. (2001) 'Binding of heparin/heparan sulfate to fibroblast growth factor receptor 4.', The Journal of biological chemistry. American Society for Biochemistry and Molecular Biology, 276(20), pp. 16868–76. doi: 10.1074/jbc.M011226200.

Loughery, J. et al. (2014) 'Critical role for p53-serine 15 phosphorylation in stimulating transactivation at p53-responsive promoters.', Nucleic acids research. Oxford University Press, 42(12), pp. 7666–80. doi: 10.1093/nar/gku501.

Ludwig, T. E. et al. (2006) ‘Derivation of human embryonic stem cells in defined conditions’, Nature Biotechnology. Nature Publishing Group, 24(2), pp. 185–187. doi: 10.1038/nbt1177.

Lundstrom, K. (2018) ‘Viral Vectors in Gene Therapy.’, Diseases (Basel, Switzerland). Multidisciplinary Digital Publishing Institute (MDPI), 6(2). doi: 10.3390/diseases6020042.

Lundy, S. D. et al. (2013) ‘Structural and Functional Maturation of Cardiomyocytes Derived from Human Pluripotent Stem Cells’, Stem Cells and Development, 22(14), pp. 1991–2002. doi: 10.1089/scd.2012.0490.

Ma, J. et al. (2011) ‘High purity human-induced pluripotent stem cell-derived cardiomyocytes: electrophysiological properties of action potentials and ionic currents’, American Journal of Physiology-Heart and Circulatory Physiology, 301(5), pp. H2006–H2017. doi: 10.1152/ajpheart.00694.2011.

Ma, X., Chen, H. and Chen, L. (2016) ‘A dual role of Erk signaling in embryonic stem cells’, Experimental Hematology, 44(3), pp. 151–156. doi: 10.1016/j.exphem.2015.12.008.

MacQueen, L. A. et al. (2018) ‘A tissue-engineered scale model of the heart ventricle’, Nature Biomedical Engineering. Nature Publishing Group, 2(12), pp. 930–941. doi: 10.1038/s41551-018-0271-5.

Málnási-Csizmadia, A. and Kovács, M. (2010) ‘Emerging complex pathways of the actomyosin powerstroke.’, Trends in biochemical sciences. NIH Public Access, 35(12), pp. 684–90. doi: 10.1016/j.tibs.2010.07.012.

Mannhardt, I. et al. (2016) ‘Human Engineered Heart Tissue: Analysis of Contractile Force’, Stem Cell Reports. Elsevier, 7(1), p. 29. doi: 10.1016/J.STEMCR.2016.04.011.

Manning, B. D. and Toker, A. (2017) ‘AKT/PKB Signaling: Navigating the Network’, Cell, 169(3), pp. 381–405. doi: 10.1016/j.cell.2017.04.001.

Mano, J. F. et al. (2007) ‘Natural origin biodegradable systems in tissue engineering and regenerative medicine: present status and some moving trends.’, Journal of the Royal Society, Interface. The Royal Society, 4(17), pp. 999–1030. doi: 10.1098/rsif.2007.0220.

Masui, S. et al. (2007) ‘Pluripotency governed by Sox2 via regulation of Oct3/4 expression in mouse embryonic stem cells’, Nature Cell Biology. Nature Publishing Group, 9(6), pp. 625–635. doi: 10.1038/ncb1589.

Mattoon, D. R. et al. (2004) ‘The docking protein Gab1 is the primary mediator of EGF-stimulated activation of the PI-3K/Akt cell survival pathway’, BMC Biology. BioMed Central, 2(1), p. 24. doi: 10.1186/1741-7007-2-24.

Mauney, J. R. et al. (2007) ‘Engineering adipose-like tissue in vitro and in vivo utilizing human bone marrow and adipose-derived mesenchymal stem cells with silk fibroin 3D scaffolds’, Biomaterials, 28(35), pp. 5280–5290. doi: 10.1016/j.biomaterials.2007.08.017.

Mayo, L. D. et al. (2005) ‘Phosphorylation of human p53 at serine 46 determines promoter selection and whether apoptosis is attenuated or amplified.’, The Journal of biological chemistry. American Society for Biochemistry and Molecular Biology, 280(28), pp. 25953–9. doi: 10.1074/jbc.M503026200.

Mazia, D., Schatten, G. and Sale, W. (1975) 'Adhesion of cells to surfaces coated with polylysine. Applications to electron microscopy', The Journal of Cell Biology, 66(1), pp. 198–200. doi: 10.1083/jcb.66.1.198.

Mebratu, Y. and Tesfaigzi, Y. (2009) 'How ERK1/2 activation controls cell proliferation and cell death: Is subcellular localization the answer?', Cell cycle (Georgetown, Tex.). NIH Public Access, 8(8), pp. 1168–75. doi: 10.4161/cc.8.8.8147.

Mei, Y. et al. (2010) 'Combinatorial development of biomaterials for clonal growth of human pluripotent stem cells', Nature Materials. Nature Publishing Group, 9(9), pp. 768–778. doi: 10.1038/nmat2812.

Meng, Y. et al. (2010) 'Characterization of integrin engagement during defined human embryonic stem cell culture', The FASEB Journal, 24(4), pp. 1056–1065. doi: 10.1096/fj.08-126821.

Meng, Y. et al. (2018) 'GATA6 phosphorylation by Erk1/2 propels exit from pluripotency and commitment to primitive endoderm', Developmental Biology, 436(1), pp. 55–65. doi: 10.1016/j.ydbio.2018.02.007.

Mesirca, P., Torrente, A. G. and Mangoni, M. E. (2015) 'Functional role of voltage gated Ca(2+) channels in heart automaticity.', Frontiers in physiology. Frontiers Media SA, 6, p. 19. doi: 10.3389/fphys.2015.00019.

Miake, J., Marbán, E. and Nuss, H. B. (2003) 'Functional role of inward rectifier current in heart probed by Kir2.1 overexpression and dominant-negative suppression.', The Journal of clinical investigation. American Society for Clinical Investigation, 111(10), pp. 1529–36. doi: 10.1172/JCI17959.

Miguez-Pacheco, V., Hench, L. L. and Boccaccini, A. R. (2015) 'Bioactive glasses beyond bone and teeth: Emerging applications in contact with soft tissues', Acta Biomaterialia, 13, pp. 1–15. doi: 10.1016/j.actbio.2014.11.004.

Mihic, A. et al. (2014) 'The effect of cyclic stretch on maturation and 3D tissue formation of human embryonic stem cell-derived cardiomyocytes', Biomaterials. Elsevier Ltd, 35(9), pp. 2798–2808. doi: 10.1016/j.biomaterials.2013.12.052.

Mills, R. J. et al. (2017) 'Functional screening in human cardiac organoids reveals a metabolic mechanism for cardiomyocyte cell cycle arrest', Proceedings of the National Academy of Sciences. National Academy of Sciences, 114(40), p. 201707316. doi: 10.1073/pnas.1707316114.

Mills, R. J. et al. (2019) 'Drug Screening in Human PSC-Cardiac Organoids Identifies Pro-proliferative Compounds Acting via the Mevalonate Pathway', Cell Stem Cell, 24(6), p. 895–907.e6. doi: 10.1016/j.stem.2019.03.009.

Mitalipov, S. and Wolf, D. (2009) 'Totipotency, Pluripotency and Nuclear Reprogramming', Adv Biochem Eng Biotechnol, 114(1), pp. 185–199. doi: 10.1007/10.

Mittal, N. and Voldman, J. (2011) 'Nonmitogenic survival-enhancing autocrine factors including cyclophilin A contribute to density-dependent mouse embryonic stem cell growth', Stem Cell Research, 6(2), pp. 168–176. doi: 10.1016/j.scr.2010.10.001.

Mitton, B. et al. (2014) 'The Role of pp90rsk-Mediated CREB Phosphorylation in Acute Myelogenous Leukemia', Blood, 124(21). Available at:

http://www.bloodjournal.org/content/124/21/2229?sso-checked=true (Accessed: 23 August 2019).

Miyamoto, S., Akiyama, S. K. and Yamada, K. M. (1995) 'Synergistic roles for receptor occupancy and aggregation in integrin transmembrane function.', Science (New York, N.Y.), 267(5199), pp. 883–5. Available at: http://www.ncbi.nlm.nih.gov/pubmed/7846531 (Accessed: 5 March 2019).

Mordwinkin, N. M., Burridge, P. W. and Wu, J. C. (2013) 'A review of human pluripotent stem cell-derived cardiomyocytes for high-throughput drug discovery, cardiotoxicity screening, and publication standards', Journal of Cardiovascular Translational Research, 6(1), pp. 22–30. doi: 10.1007/s12265-012-9423-2.

Morey, L., Santanach, A. and Di Croce, L. (2015) 'Pluripotency and Epigenetic Factors in Mouse Embryonic Stem Cell Fate Regulation.', Molecular and cellular biology. American Society for Microbiology (ASM), 35(16), pp. 2716–28. doi: 10.1128/MCB.00266-15.

Moris, N. et al. (2018) 'Histone Acetyltransferase KAT2A Stabilizes Pluripotency with Control of Transcriptional Heterogeneity', STEM CELLS, 36(12), pp. 1828–1838. doi: 10.1002/stem.2919.

Morizane, A. et al. (2011) 'Small-molecule inhibitors of bone morphogenic protein and activin/nodal signals promote highly efficient neural induction from human pluripotent stem cells', Journal of Neuroscience Research. John Wiley & Sons, Ltd, 89(2), pp. 117–126. doi: 10.1002/jnr.22547.

Morrison, D. et al. (2002) 'National study of microphthalmia, anophthalmia, and

coloboma (MAC) in Scotland: investigation of genetic aetiology.', Journal of medical genetics. BMJ Publishing Group Ltd, 39(1), pp. 16–22. doi: 10.1136/jmg.39.1.16.

Morrison, D. K. (2012) 'MAP kinase pathways.', Cold Spring Harbor perspectives in biology. Cold Spring Harbor Laboratory Press, 4(11). doi: 10.1101/cshperspect.a011254.

Mosqueira, D. et al. (2018) 'CRISPR/Cas9 editing in human pluripotent stem cell-cardiomyocytes highlights arrhythmias, hypocontractility, and energy depletion as potential therapeutic targets for hypertrophic cardiomyopathy', European heart journal, 39(43), pp. 3879–3892. doi: 10.1093/eurheartj/ehy249.

Moussaieff, A. et al. (2015) 'Glycolysis-Mediated Changes in Acetyl-CoA and Histone Acetylation Control the Early Differentiation of Embryonic Stem Cells', Cell Metabolism. Cell Press, 21(3), pp. 392–402. doi: 10.1016/J.CMET.2015.02.002.

Muffly, T. M., Tizzano, A. P. and Walters, M. D. (2011) 'The history and evolution of sutures in pelvic surgery.', Journal of the Royal Society of Medicine. Royal Society of Medicine Press, 104(3), pp. 107–12. doi: 10.1258/jrsm.2010.100243.

Mulder, P. et al. (2018) 'Predicting cardiac safety using human induced pluripotent stem cell-derived cardiomyocytes combined with multi-electrode array (MEA) technology: A conference report', Journal of Pharmacological and Toxicological Methods. Elsevier, 91, pp. 36–42. doi: 10.1016/J.VASCN.2018.01.003.

Mulford, J. S., Babazadeh, S. and Mackay, N. (2016) 'Three-dimensional printing in orthopaedic surgery: review of current and future applications', ANZ Journal of Surgery, 86(9), pp. 648–653. doi: 10.1111/ans.13533.

Mummery, C. (2003) 'Differentiation of Human Embryonic Stem Cells to Cardiomyocytes: Role of Coculture With Visceral Endoderm-Like Cells', Circulation, 107(>21), pp. 2733–2740. doi: 10.1161/01.CIR.0000068356.38592.68.

Muñoz-Descalzo, S., Hadjantonakis, A.-K. and Arias, A. M. (2015) 'Wnt/ß-catenin signalling and the dynamics of fate decisions in early mouse embryos and embryonic stem (ES) cells.', Seminars in cell & developmental biology. NIH Public Access, 47–48, pp. 101–9. doi: 10.1016/j.semcdb.2015.08.011.

Münsterberg, A. and Hoppler, S. (2016) 'WNT and BMP regulate roadblocks toward cardiomyocyte differentiation: lessons learned from embryos inform human stem cell differentiation.', Stem cell investigation, 3, p. 33. doi: 10.21037/sci.2016.07.03.

Nakabayashi, N. et al. (1982) '[Studies on dental self-curing resins (20) - adhesion mechanism of 4-META/MMA-TBB resin to dentine (author's transl)].', Shika rikogaku zasshi. Journal of the Japan Society for Dental Apparatus and Materials, 23(61), pp. 34–9. Available at: http://www.ncbi.nlm.nih.gov/pubmed/7042865 (Accessed: 17 September 2019).

Nakagawa, M. et al. (2008) 'Generation of induced pluripotent stem cells without Myc from mouse and human fibroblasts', Nature Biotechnology. Nature Publishing Group, 26(1), pp. 101–106. doi: 10.1038/nbt1374.

Nakano, N. et al. (2017) 'PI3K/AKT signaling mediated by G protein-coupled receptors is involved in neurodegenerative Parkinson's disease (Review)', International Journal of Molecular Medicine. Spandidos Publications, 39(2), pp. 253–260. doi: 10.3892/ijmm.2016.2833.

Neofytou, E. et al. (2015) ‘Hurdles to clinical translation of human induced pluripotent stem cells’, The Journal of Clinical Investigation. American Society for Clinical Investigation, 125(7), pp. 2551–2557. doi: 10.1172/JCI80575.

Nerbonne, J. M. and Kass, R. S. (2005) ‘Molecular Physiology of Cardiac Repolarization’, Physiological Reviews. American Physiological Society, 85(4), pp. 1205–1253. doi: 10.1152/physrev.00002.2005.

Nichols, J. et al. (1998) ‘Formation of Pluripotent Stem Cells in the Mammalian Embryo Depends on the POU Transcription Factor Oct4’, Cell. Cell Press, 95(3), pp. 379–391. doi: 10.1016/S0092-8674(00)81769-9.

Nigmatullin, R., Bencsik, M. and Gao, F. (2014) ‘Influence of polymerisation conditions on the properties of polymer/clay nanocomposite hydrogels’, Soft Matter. Royal Society of Chemistry, 10(12), p. 2035. doi: 10.1039/c3sm52887a.

Nishimura, K. et al. (2017) ‘Simple and effective generation of transgene-free induced pluripotent stem cells using an auto-erasable Sendai virus vector responding to microRNA-302’, Stem Cell Research. Elsevier, 23, pp. 13–19. doi: 10.1016/J.SCR.2017.06.011.

Niwa, H. et al. (2005) ‘Interaction between Oct3/4 and Cdx2 Determines Trophectoderm Differentiation’, Cell. Cell Press, 123(5), pp. 917–929. doi: 10.1016/J.CELL.2005.08.040.

Ohgushi, M. et al. (2010) ‘Molecular Pathway and Cell State Responsible for Dissociation-Induced Apoptosis in Human Pluripotent Stem Cells’, Cell Stem Cell. Cell Press, 7(2), pp. 225–239. doi: 10.1016/J.STEM.2010.06.018.

Orzechowski, M. et al. (2014) ‘Tropomyosin movement on F-actin during muscle activation explained by energy landscapes’, Archives of Biochemistry and Biophysics. Academic Press, 545, pp. 63–68. doi: 10.1016/J.ABB.2014.01.001.

Oxilia, G. et al. (2017) ‘The dawn of dentistry in the late upper Paleolithic: An early case of pathological intervention at Riparo Fredian’, American Journal of Physical Anthropology. John Wiley & Sons, Ltd, 163(3), pp. 446–461. doi: 10.1002/ajpa.23216.

Ozawa, F. et al. (2013) ‘Alginate gel microwell arrays using electrodeposition for three-dimensional cell culture’, Lab on a Chip. The Royal Society of Chemistry, 13(15), p. 3128. doi: 10.1039/c3lc50455g.

Pandey, P. et al. (2018) ‘Cardiomyocytes Sense Matrix Rigidity through a Combination of Muscle and Non-muscle Myosin Contractions’, Developmental Cell, 44(3), p. 326–336.e3. doi: 10.1016/j.devcel.2017.12.024.

Pankov, R. et al. (2003) ‘Specific beta1 integrin site selectively regulates Akt/protein kinase B signaling via local activation of protein phosphatase 2A.’, The Journal of biological chemistry. American Society for Biochemistry and Molecular Biology, 278(20), pp. 18671–81. doi: 10.1074/jbc.M300879200.

Pankratz, M. T. et al. (2007) ‘Directed neural differentiation of human embryonic stem cells via an obligated primitive anterior stage.’, Stem cells (Dayton, Ohio). NIH Public Access, 25(6), pp. 1511–20. doi: 10.1634/stemcells.2006-0707.

Parida, P., Behera, A. and Chandra Mishra, S. (2012) ‘Classification of Biomaterials used in Medicine’, International Journal of Advances in Applied Sciences, 1(3), pp.

31–35. doi: 10.11591/ijaas.v1i3.882.

Pascoal, J. F. et al. (2018) ‘Three-Dimensional Cell-Based Microarrays: Printing Pluripotent Stem Cells into 3D Microenvironments’, in. Humana Press, New York, NY, pp. 69–81. doi: 10.1007/978-1-4939-7792-5_6.

Passier, R. et al. (2005) ‘Increased Cardiomyocyte Differentiation from Human Embryonic Stem Cells in Serum-Free Cultures’, Stem Cells. John Wiley & Sons, Ltd, 23(6), pp. 772–780. doi: 10.1634/stemcells.2004-0184.

Patel, A. K. et al. (2015) ‘A defined synthetic substrate for serum-free culture of human stem cell derived cardiomyocytes with improved functional maturity identified using combinatorial materials microarrays’, Biomaterials. Elsevier Ltd, 61, pp. 257–265. doi: 10.1016/j.biomaterials.2015.05.019.

Patel, A. K. et al. (2016) ‘High throughput screening for discovery of materials that control stem cell fate’, Current Opinion in Solid State and Materials Science. Elsevier, 20(4), pp. 202–211. doi: 10.1016/J.COSSMS.2016.02.002.

Pavlovic, M. (2015) ‘What Are Biomaterials?’, in Bioengineering. Cham: Springer International Publishing, pp. 229–244. doi: 10.1007/978-3-319-10798-1_18.

Peerani, R. et al. (2007) ‘Niche-mediated control of human embryonic stem cell self-renewal and differentiation’, The EMBO Journal, 26(22), pp. 4744–4755. doi: 10.1038/sj.emboj.7601896.

Peng, Y., Tellier, L. E. and Temenoff, J. S. (2016) ‘Heparin-based hydrogels with tunable sulfation & degradation for anti-inflammatory small molecule delivery.’, Biomaterials science. NIH Public Access, 4(9), pp. 1371–80. doi:

10.1039/c6bm00455e.

Pennington, B. O. et al. (2015) ‘Defined Culture of Human Embryonic Stem Cells and Xeno-Free Derivation of Retinal Pigmented Epithelial Cells on a Novel, Synthetic Substrate’, Stem Cells Translational Medicine. Wiley-Blackwell, 4(2), p. 165. doi: 10.5966/SCTM.2014-0179.

Peterson, T. R. et al. (2009) ‘DEPTOR Is an mTOR Inhibitor Frequently Overexpressed in Multiple Myeloma Cells and Required for Their Survival’, Cell. Cell Press, 137(5), pp. 873–886. doi: 10.1016/J.CELL.2009.03.046.

Pevny, L. H. et al. (1998) ‘A role for SOX1 in neural determination.’, Development (Cambridge, England), 125(10), pp. 1967–78. Available at: http://www.ncbi.nlm.nih.gov/pubmed/9550729 (Accessed: 11 March 2019).

Piconi, C. et al. (2018) ‘Alumina and Zirconia Ceramics in Joint Replacements’:, https://doi.org/10.1177/228080000300100103. SAGE PublicationsSage UK: London, England. doi: 10.1177/228080000300100103.

Pijuan-Galitó, S. et al. (2016) ‘Human serum-derived protein removes the need for coating in defined human pluripotent stem cell culture’, Nature Communications. Nature Publishing Group, 7(May 2015), p. 12170. doi: 10.1038/ncomms12170.

Pinnell, J., Turner, S. and Howell, S. (2007) ‘Cardiac muscle physiology’, Continuing Education in Anaesthesia Critical Care & Pain. Elsevier, 7(3), pp. 85–88. doi: 10.1093/BJACEACCP/MKM013.

Pinto, A. R. et al. (2016) ‘Revisiting cardiac cellular composition’, Circulation Research. Lippincott Williams & WilkinsHagerstown, MD, 118(3), pp. 400–409. doi:

10.1161/CIRCRESAHA.115.307778.

Poh, A. R., O'Donoghue, R. J. J. and Ernst, M. (2015) 'Hematopoietic cell kinase (HCK) as a therapeutic target in immune and cancer cells', Oncotarget. Impact Journals, LLC, 6(18), p. 15752. doi: 10.18632/ONCOTARGET.4199.

Porstmann, T. et al. (2008) 'SREBP Activity Is Regulated by mTORC1 and Contributes to Akt-Dependent Cell Growth', Cell Metabolism. Cell Press, 8(3), pp. 224–236. doi: 10.1016/J.CMET.2008.07.007.

Potapova, O. et al. (2001) 'Protective role for c-Jun in the cellular response to DNA damage.', The Journal of biological chemistry. American Society for Biochemistry and Molecular Biology, 276(30), pp. 28546–53. doi: 10.1074/jbc.M102075200.

Prasad, K. et al. (2017) 'Metallic Biomaterials: Current Challenges and Opportunities.', Materials (Basel, Switzerland). Multidisciplinary Digital Publishing Institute (MDPI), 10(8). doi: 10.3390/ma10080884.

Prestwich, G. D. (2011) 'Hyaluronic acid-based clinical biomaterials derived for cell and molecule delivery in regenerative medicine.', Journal of controlled release : official journal of the Controlled Release Society. NIH Public Access, 155(2), pp. 193–9. doi: 10.1016/j.jconrel.2011.04.007.

Ranga, A. et al. (2014) '3D niche microarrays for systems-level analyses of cell fate', Nature Communications. Nature Publishing Group, 5(1), p. 4324. doi: 10.1038/ncomms5324.

Rasi Ghaemi, S. et al. (2018a) 'High-Throughput Assessment and Modeling of a Polymer Library Regulating Human Dental Pulp-Derived Stem Cell Behavior', ACS

Applied Materials and Interfaces. American Chemical Society, 10(45), pp. 38739–38748. doi: 10.1021/acsami.8b12473.

Rasi Ghaemi, S. et al. (2018b) 'High-Throughput Assessment and Modeling of a Polymer Library Regulating Human Dental Pulp-Derived Stem Cell Behavior', ACS Applied Materials & Interfaces. American Chemical Society, 10(45), pp. 38739–38748. doi: 10.1021/acsami.8b12473.

Rathmell, J. C. et al. (2003) 'Akt-directed glucose metabolism can prevent Bax conformation change and promote growth factor-independent survival.', Molecular and cellular biology. American Society for Microbiology Journals, 23(20), pp. 7315–28. doi: 10.1128/mcb.23.20.7315-7328.2003.

Ratner, B. D. (Buddy D. . (2004) Biomaterials science : an introduction to materials in medicine. Elsevier Academic Press. Available at: https://books.google.co.uk/books?hl=en&lr=&id=9PMU1iYGe34C&oi=fnd&pg=PR5&dq=Biomaterials+Science:+A+Multidisciplinary+Endeavor&ots=gnV6remyBB&sig=yuFi34dUejSL99YIdBOUG_2zbqM#v=onepage&q=Biomaterials Science%3A A Multidisciplinary Endeavor&f=false (Accessed: 14 February 2019).

Reinhardt, H. C. and Yaffe, M. B. (2009) 'Kinases that control the cell cycle in response to DNA damage: Chk1, Chk2, and MK2', Current Opinion in Cell Biology. Elsevier Current Trends, 21(2), pp. 245–255. doi: 10.1016/J.CEB.2009.01.018.

Reubinoff, B. E. et al. (2000) 'Embryonic stem cell lines from human blastocysts: somatic differentiation in vitro', Nature Biotechnology. Nature Publishing Group, 18(4), pp. 399–404. doi: 10.1038/74447.

Ribeiro, A. J. S. et al. (2015) ‘Contractility of single cardiomyocytes differentiated from pluripotent stem cells depends on physiological shape and substrate stiffness’, Proceedings of the National Academy of Sciences, 112(41), pp. 12705–12710. doi: 10.1073/pnas.1508073112.

Ribeiro, M. C. et al. (2015) ‘Functional maturation of human pluripotent stem cell derived cardiomyocytes invitro - Correlation between contraction force andelectrophysiology’, Biomaterials. Elsevier Ltd, 51, pp. 138–150. doi: 10.1016/j.biomaterials.2015.01.067.

Robertson, J. A. (2010) ‘Embryo Stem Cell Research: Ten Years of Controversy’, The Journal of Law, Medicine & Ethics. John Wiley & Sons, Ltd (10.1111), 38(2), pp. 191–203. doi: 10.1111/j.1748-720X.2010.00479.x.

Rodda, D. J. et al. (2005) ‘Transcriptional regulation of nanog by OCT4 and SOX2.’, The Journal of biological chemistry. American Society for Biochemistry and Molecular Biology, 280(26), pp. 24731–7. doi: 10.1074/jbc.M502573200.

Rodin, S. et al. (2010) ‘Long-term self-renewal of human pluripotent stem cells on human recombinant laminin-511’, Nature Biotechnology. Nature Publishing Group, 28(6), pp. 611–615. doi: 10.1038/nbt.1620.

Rodriguez, M. L. et al. (2014) ‘Measuring the contractile forces of human induced pluripotent stem cell-derived cardiomyocytes with arrays of microposts.’, Journal of biomechanical engineering. American Society of Mechanical Engineers, 136(5), p. 051005. doi: 10.1115/1.4027145.

Rog-Zielinska, E. A. et al. (2014) ‘Glucocorticoids and foetal heart maturation;

implications for prematurity and foetal programming', Journal of Molecular Endocrinology, 52(2), pp. R125–R135. doi: 10.1530/JME-13-0204.

Ronaldson-bouchard, K. et al. (2018) 'Advanced maturation of human cardiac tissue grown from pluripotent stem cells'. doi: 10.1038/s41586-018-0016-3.

Rosner, M. et al. (2010) 'mTOR phosphorylated at S2448 binds to raptor and rictor', Amino Acids. Springer Vienna, 38(1), pp. 223–228. doi: 10.1007/s00726-008-0230-7.

Roux, L. N. et al. (2018) 'Modeling of Aniridia-Related Keratopathy by CRISPR/Cas9 Genome Editing of Human Limbal Epithelial Cells and Rescue by Recombinant PAX6 Protein', STEM CELLS. John Wiley & Sons, Ltd, 36(9), pp. 1421–1429. doi: 10.1002/stem.2858.

Roux, P. P. et al. (2004) 'Tumor-promoting phorbol esters and activated Ras inactivate the tuberous sclerosis tumor suppressor complex via p90 ribosomal S6 kinase.', Proceedings of the National Academy of Sciences of the United States of America. National Academy of Sciences, 101(37), pp. 13489–94. doi: 10.1073/pnas.0405659101.

Roux, P. P., Richards, S. A. and Blenis, J. (2003) 'Phosphorylation of p90 Ribosomal S6 Kinase (RSK) Regulates Extracellular Signal-Regulated Kinase Docking and RSK Activity', Molecular and Cellular Biology. American Society for Microbiology (ASM), 23(14), p. 4796. doi: 10.1128/MCB.23.14.4796-4804.2003.

Ruan, L.-J. et al. (2016) 'Mechanical Stress Conditioning and Electrical Stimulation Promote Contractility and Force Maturation of Induced Pluripotent Stem Cell-

Derived Human Cardiac Tissue', Circulation, 134(20), pp. 1557–1567. doi: 10.1586/14737175.2015.1028369.Focused.

Sabin, F. R. et al. (1936) 'Changes in the Bone Marrow and Blood Cells of Developing Rabbits.', The Journal of experimental medicine, 64(1), pp. 97–120. doi: 10.1084/jem.64.1.97.

SÁEZ, J. C. et al. (2003) 'Plasma Membrane Channels Formed by Connexins: Their Regulation and Functions', Physiological Reviews. American Physiological Society, 83(4), pp. 1359–1400. doi: 10.1152/physrev.00007.2003.

Saini, M. et al. (2015) 'Implant biomaterials: A comprehensive review', World Journal of Clinical Cases, 3(1), p. 52. doi: 10.12998/wjcc.v3.i1.52.

Sarbassov, D. D. et al. (2005) 'Phosphorylation and Regulation of Akt/PKB by the Rictor-mTOR Complex', Science, 307(5712), pp. 1098–1101. doi: 10.1126/science.1106148.

Saretzki, G. et al. (2008) 'Downregulation of Multiple Stress Defense Mechanisms During Differentiation of Human Embryonic Stem Cells', Stem Cells. John Wiley & Sons, Ltd, 26(2), pp. 455–464. doi: 10.1634/stemcells.2007-0628.

Sartiani, L. et al. (2007) 'Developmental Changes in Cardiomyocytes Differentiated from Human Embryonic Stem Cells: A Molecular and Electrophysiological Approach', Stem Cells, 25(5), pp. 1136–1144. doi: 10.1634/stemcells.2006-0466.

Sasaki, N. et al. (2008) 'Heparan Sulfate Regulates Self-renewal and Pluripotency of Embryonic Stem Cells', Journal of Biological Chemistry, 283(6), pp. 3594–3606. doi: 10.1074/jbc.M705621200.

Sawicka, K. et al. (2016) ‘Elevated ERK/p90 ribosomal S6 kinase activity underlies audiogenic seizure susceptibility in fragile X mice’, Proceedings of the National Academy of Sciences. National Academy of Sciences, 113(41), pp. E6290–E6297. doi: 10.1073/PNAS.1610812113.

Schaffner, F., Ray, A. M. and Dontenwill, M. (2013) ‘Integrin α5β1, the Fibronectin Receptor, as a Pertinent Therapeutic Target in Solid Tumors.’, Cancers. Multidisciplinary Digital Publishing Institute (MDPI), 5(1), pp. 27–47. doi: 10.3390/cancers5010027.

Schmelter, M. et al. (2006) ‘Embryonic stem cells utilize reactive oxygen species as transducers of mechanical strain-induced cardiovascular differentiation’, The FASEB Journal. Federation of American Societies for Experimental Biology, 20(8), pp. 1182–1184. doi: 10.1096/fj.05-4723fje.

Schwach, V. and Passier, R. (2019) ‘Native cardiac environment and its impact on engineering cardiac tissue’, Biomaterials Science. Royal Society of Chemistry, 7(9), pp. 3566–3580. doi: 10.1039/C8BM01348A.

Scuderi, G. J. and Butcher, J. (2017) ‘Naturally Engineered Maturation of Cardiomyocytes’, Frontiers in Cell and Developmental Biology, 5(May), pp. 1–28. doi: 10.3389/fcell.2017.00050.

Seal, B. ., Otero, T. . and Panitch, A. (2001) ‘Polymeric biomaterials for tissue and organ regeneration’, Materials Science and Engineering: R: Reports. Elsevier, 34(4–5), pp. 147–230. doi: 10.1016/S0927-796X(01)00035-3.

Shafaie, S. et al. (2017) ‘Influence of surface geometry on the culture of human cell

lines: A comparative study using flat, round-bottom and v-shaped 96 well plates', PLOS ONE. Edited by C. J. Connon. Public Library of Science, 12(10), p. e0186799. doi: 10.1371/journal.pone.0186799.

Shahar, O. D. et al. (2013) 'Acetylation of Lysine 382 and Phosphorylation of Serine 392 in p53 Modulate the Interaction between p53 and MDC1 In Vitro', PLoS ONE. Edited by B. D. Price. Public Library of Science, 8(10), p. e78472. doi: 10.1371/journal.pone.0078472.

Sharma, A. et al. (2018) 'Use of human induced pluripotent stem cell–derived cardiomyocytes to assess drug cardiotoxicity', Nature Protocols, 13(December). doi: 10.1038/s41596-018-0076-8.

Shin, S. R. et al. (2013) 'Carbon-nanotube-embedded hydrogel sheets for engineering cardiac constructs and bioactuators', ACS Nano, 7(3), pp. 2369–2380. doi: 10.1021/nn305559j.

Siller, R. et al. (2016) 'Development of a rapid screen for the endodermal differentiation potential of human pluripotent stem cell lines', Scientific Reports. Nature Publishing Group, 6(October 2015), pp. 1–14. doi: 10.1038/srep37178.

Siminovitch, L., McCulloch, E. A. and Till, J. E. (1963) 'The distribution of colony-forming cells among spleen colonies', Journal of Cellular and Comparative Physiology, 62(3), pp. 327–336. doi: 10.1002/jcp.1030620313.

Singh, A. M. et al. (2007) 'A Heterogeneous Expression Pattern for Nanog in Embryonic Stem Cells', Stem Cells, 25(10), pp. 2534–2542. doi: 10.1634/stemcells.2007-0126.

Singh, A. M. et al. (2012) ‘Signaling Network Crosstalk in Human Pluripotent Cells: A Smad2/3-Regulated Switch that Controls the Balance between Self-Renewal and Differentiation’, Cell Stem Cell, 10(3), pp. 312–326. doi: 10.1016/j.stem.2012.01.014.

Singh, A. M. M. et al. (2012) ‘Signaling network crosstalk in human pluripotent cells: A Smad2/3-regulated switch that controls the balance between self-renewal and differentiation’, Cell Stem Cell. Elsevier Inc., 10(3), pp. 312–326. doi: 10.1016/j.stem.2012.01.014.

Sinner, D. et al. (2004) ‘Sox17 and -catenin cooperate to regulate the transcription of endodermal genes’, Development, 131(13), pp. 3069–3080. doi: 10.1242/dev.01176.

Sisodiya, S. M. et al. (2001) ‘PAX6 haploinsufficiency causes cerebral malformation and olfactory dysfunction in humans’, Nature Genetics. Nature Publishing Group, 28(3), pp. 214–216. doi: 10.1038/90042.

Smeenk, L. et al. (2011) ‘Role of p53 Serine 46 in p53 target gene regulation’, PLoS ONE. Edited by A. Gartel, 6(3), p. e17574. doi: 10.1371/journal.pone.0017574.

Smith, J. G. W. et al. (2018) ‘Isogenic Pairs of hiPSC-CMs with Hypertrophic Cardiomyopathy/LVNC-Associated ACTC1 E99K Mutation Unveil Differential Functional Deficits’, Stem cell reports. ElsevierCompany., 11(5), pp. 1226–1243. doi: 10.1016/j.stemcr.2018.10.006.

Smith, J. R. et al. (2008) ‘Inhibition of Activin/Nodal signaling promotes specification of human embryonic stem cells into neuroectoderm’, Developmental Biology.

Academic Press, 313(1), pp. 107–117. doi: 10.1016/J.YDBIO.2007.10.003.

Solis, M. A. et al. (2012) 'Hyaluronan Regulates Cell Behavior: A Potential Niche Matrix for Stem Cells', Biochemistry Research International. Hindawi, 2012, pp. 1–11. doi: 10.1155/2012/346972.

Song, L. et al. (2016) 'SOX1 inhibits breast cancer cell growth and invasion through suppressing the Wnt/β-catenin signaling pathway', APMIS. John Wiley & Sons, Ltd (10.1111), 124(7), pp. 547–555. doi: 10.1111/apm.12543.

De Sousa Lopes, S. M. C. et al. (2006) 'Patterning the heart, a template for human cardiomyocyte development', Developmental Dynamics, 235(7), pp. 1994–2002. doi: 10.1002/dvdy.20830.

Spach, M. S. et al. (2004) 'Cell size and communication: Role in structural and electrical development and remodeling of the heart', Heart Rhythm, 1(4), pp. 500–515. doi: 10.1016/j.hrthm.2004.06.010.

Spater, D. et al. (2014) 'How to make a cardiomyocyte', Development, 141(23), pp. 4418–4431. doi: 10.1242/dev.091538.

Spradling, A., Drummond-Barbosa, D. and Kai, T. (2001) 'Stem cells find their niche', Nature, 414(6859), pp. 98–104. doi: 10.1038/35102160.

Spyrou, J., Gardner, D. K. and Harvey, A. J. (2019) 'Metabolism Is a Key Regulator of Induced Pluripotent Stem Cell Reprogramming', Stem Cells International. Hindawi, 2019, pp. 1–10. doi: 10.1155/2019/7360121.

Stafford, N. (2008) 'Germany liberalises law on stem cell research.', BMJ (Clinical research ed.). BMJ Publishing Group, 336(7649), p. 851. doi:

10.1136/bmj.39552.538356.DB.

Stevens, M. M. and George, J. H. (2005) ‘Exploring and engineering the cell surface interface.’, Science (New York, N.Y.). American Association for the Advancement of Science, 310(5751), pp. 1135–8. doi: 10.1126/science.1106587.

Stojkovic, M. et al. (2004) ‘Derivation of Human Embryonic Stem Cells from Day-8 Blastocysts Recovered after Three-Step In Vitro Culture’, Stem Cells. John Wiley & Sons, Ltd, 22(5), pp. 790–797. doi: 10.1634/stemcells.22-5-790.

Studer, K. et al. (2003) ‘Overcoming oxygen inhibition in UV-curing of acrylate coatings by carbon dioxide inerting, Part I’, Progress in Organic Coatings. Elsevier, 48(1), pp. 92–100. doi: 10.1016/S0300-9440(03)00120-6.

Stupp, S. I. (2001) ‘Biomaterials Introduction for Annual Review of Materials Research’, Annual Review of Materials Research. Annual Reviews 4139 El Camino Way, P.O. Box 10139, Palo Alto, CA 94303-0139, USA , 31(1), p. annurev.mr.31.010101.100002. doi: 10.1146/annurev.mr.31.010101.100002.

Sugiyama, M. G., Fairn, G. D. and Antonescu, C. N. (2019) ‘Akt-ing Up Just About Everywhere: Compartment-Specific Akt Activation and Function in Receptor Tyrosine Kinase Signaling’, Frontiers in Cell and Developmental Biology. Frontiers, 7, p. 70. doi: 10.3389/fcell.2019.00070.

Sumanasinghe, R. D., Bernacki, S. H. and Loboa, E. G. (2006) ‘Osteogenic Differentiation of Human Mesenchymal Stem Cells in Collagen Matrices: Effect of Uniaxial Cyclic Tensile Strain on Bone Morphogenetic Protein (BMP-2) mRNA Expression’, Tissue Engineering. Mary Ann Liebert, Inc. 2 Madison Avenue

Larchmont, NY 10538 USA , 12(12), pp. 3459–3465. doi: 10.1089/ten.2006.12.3459.

Sun, J. and Tan, H. (2013) 'Alginate-Based Biomaterials for Regenerative Medicine Applications.', Materials (Basel, Switzerland). Multidisciplinary Digital Publishing Institute (MDPI), 6(4), pp. 1285–1309. doi: 10.3390/ma6041285.

Sun, M. et al. (2017) 'Synthesis and characterization of hyperbranched poly(ester-amine) by Michael addition polymerization.', Designed monomers and polymers. Taylor & Francis, 20(1), pp. 458–467. doi: 10.1080/15685551.2017.1351728.

Sun, M. et al. (2018) 'Effects of Matrix Stiffness on the Morphology, Adhesion, Proliferation and Osteogenic Differentiation of Mesenchymal Stem Cells.', International journal of medical sciences. Ivyspring International Publisher, 15(3), pp. 257–268. doi: 10.7150/ijms.21620.

Sun, X. and Nunes, S. S. (2017) 'Bioengineering Approaches to Mature Human Pluripotent Stem Cell-Derived Cardiomyocytes.', Frontiers in cell and developmental biology. Frontiers Media SA, 5, p. 19. doi: 10.3389/fcell.2017.00019.

Sun, Y. et al. (2012) 'Surface Coating as a Key Parameter in Engineering Neuronal Network Structures In Vitro', Biointerphases. Springer Berlin Heidelberg, 7(1), p. 29. doi: 10.1007/s13758-012-0029-7.

Surmacz, B. et al. (2012) 'Directing Differentiation of Human Embryonic Stem Cells Toward Anterior Neural Ectoderm Using Small Molecules', STEM CELLS. John Wiley & Sons, Ltd, 30(9), pp. 1875–1884. doi: 10.1002/stem.1166.

Swaney, D. L. et al. (2009) 'Human embryonic stem cell phosphoproteome revealed by electron transfer dissociation tandem mass spectrometry', Proceedings of the

National Academy of Sciences, 106(4), pp. 995–1000. doi: 10.1073/pnas.0811964106.

Takahashi, K. et al. (2007) 'Induction of Pluripotent Stem Cells from Adult Human Fibroblasts by Defined Factors', Cell. Cell Press, 131(5), pp. 861–872. doi: 10.1016/J.CELL.2007.11.019.

Takemura, H. et al. (2005) 'Subtype Switching of L-Type Ca 2+ Channel From Ca', Investigations, Experimental, 69(November), pp. 1405–1411.

Takizawa, M. et al. (2017) 'Mechanistic basis for the recognition of laminin-511 by α6β1 integrin', Science Advances, 3(9), p. e1701497. doi: 10.1126/sciadv.1701497.

Tamm, C., Böwer, N. and Annerén, C. (2011) 'Regulation of mouse embryonic stem cell self-renewal by a Yes-YAP-TEAD2 signaling pathway downstream of LIF.', Journal of cell science. The Company of Biologists Ltd, 124(Pt 7), pp. 1136–44. doi: 10.1242/jcs.075796.

Tan, Y. et al. (2000) 'BAD Ser-155 phosphorylation regulates BAD/Bcl-XL interaction and cell survival.', The Journal of biological chemistry. American Society for Biochemistry and Molecular Biology, 275(33), pp. 25865–9. doi: 10.1074/jbc.M004199200.

Tanimura, S. and Takeda, K. (2017) 'ERK signalling as a regulator of cell motility', The Journal of Biochemistry. Narnia, 162(3), pp. 145–154. doi: 10.1093/jb/mvx048.

Teo, A. J. T. et al. (2016) 'Polymeric Biomaterials for Medical Implants and Devices', ACS Biomaterials Science & Engineering. American Chemical Society, 2(4), pp. 454–472. doi: 10.1021/acsbiomaterials.5b00429.

Thévenin, A. F. et al. (2011) ‘Activation by phosphorylation and purification of human c-Jun N-terminal kinase (JNK) isoforms in milligram amounts.’, Protein expression and purification. NIH Public Access, 75(2), pp. 138–46. doi: 10.1016/j.pep.2010.08.002.

Thomson, J. A. et al. (1998) ‘Embryonic stem cell lines derived from human blastocysts.’, Science (New York, N.Y.). American Association for the Advancement of Science, 282(5391), pp. 1145–7. doi: 10.1126/SCIENCE.282.5391.1145.

Tweedell, K. S. (2017) ‘The adaptability of somatic stem cells: A review’, Journal of Stem Cells and Regenerative Medicine, 13(1), pp. 3–13.

Ueno, S. et al. (2007) ‘Biphasic role for Wnt/beta-catenin signaling in cardiac specification in zebrafish and embryonic stem cells.’, Proceedings of the National Academy of Sciences of the United States of America. National Academy of Sciences, 104(23), pp. 9685–90. doi: 10.1073/pnas.0702859104.

Ulmer, B. M. et al. (2018) ‘Contractile Work Contributes to Maturation of Energy Metabolism in hiPSC-Derived Cardiomyocytes’, Stem Cell Reports, 10(3), pp. 834–847. doi: 10.1016/j.stemcr.2018.01.039.

Unadkat, H. V et al. (2011) ‘An algorithm-based topographical biomaterials library to instruct cell fate.’, Proceedings of the National Academy of Sciences of the United States of America. National Academy of Sciences, 108(40), pp. 16565–70. doi: 10.1073/pnas.1109861108.

Unemori, M. et al. (2003) ‘Water absorption of poly(methyl methacrylate) containing 4-methacryloxyethyl trimellitic anhydride’, Biomaterials. Elsevier, 24(8),

pp. 1381–1387. doi: 10.1016/S0142-9612(02)00521-5.

Vacca, A. et al. (2001) ‘alpha(v)beta(3) integrin engagement modulates cell adhesion, proliferation, and protease secretion in human lymphoid tumor cells.’, Experimental hematology, 29(8), pp. 993–1003. Available at: http://www.ncbi.nlm.nih.gov/pubmed/11495705 (Accessed: 28 August 2019).

Vachon, P. H. (2011) ‘Integrin signaling, cell survival, and anoikis: distinctions, differences, and differentiation.’, Journal of signal transduction. Hindawi Limited, 2011, p. 738137. doi: 10.1155/2011/738137.

Vadlakonda, L. et al. (2013) ‘The Paradox of Akt-mTOR Interactions’, Frontiers in Oncology. Frontiers, 3, p. 165. doi: 10.3389/fonc.2013.00165.

Vaithilingam, J. et al. (2019) ‘Multifunctional Bioinstructive 3D Architectures to Modulate Cellular Behavior’, Advanced Functional Materials. John Wiley & Sons, Ltd, p. 1902016. doi: 10.1002/adfm.201902016.

VandeVondele, S., Vörös, J. and Hubbell, J. A. (2003) ‘RGD-grafted poly-l-lysine-graft-(polyethylene glycol) copolymers block non-specific protein adsorption while promoting cell adhesion’, Biotechnology and Bioengineering. John Wiley & Sons, Ltd, 82(7), pp. 784–790. doi: 10.1002/bit.10625.

Vasilevich, A. S. et al. (2018) ‘Designed Surface Topographies Control ICAM-1 Expression in Tonsil-Derived Human Stromal Cells’, Frontiers in Bioengineering and Biotechnology. Frontiers, 6, p. 87. doi: 10.3389/fbioe.2018.00087.

Veerman, C. C. et al. (2015) ‘Immaturity of Human Stem-Cell-Derived Cardiomyocytes in Culture: Fatal Flaw or Soluble Problem?’, Stem Cells and

Development, 24(9), pp. 1035–1052. doi: 10.1089/scd.2014.0533.

Veerman, C. C. et al. (2017) ‘Switch from fetal to adult SCN5A isoform in human induced pluripotent stem cell-derived cardiomyocytes unmasks the cellular phenotype of a conduction disease-causing mutation’, Journal of the American Heart Association, 6(7). doi: 10.1161/JAHA.116.005135.

Vehoff, T. et al. (2007) ‘Mechanical properties of spider dragline silk: humidity, hysteresis, and relaxation.’, Biophysical journal. The Biophysical Society, 93(12), pp. 4425–32. doi: 10.1529/biophysj.106.099309.

Villa-Diaz, L. G. et al. (2010) ‘Synthetic polymer coatings for long-term growth of human embryonic stem cells’, Nature Biotechnology. Nature Publishing Group, 28(6), pp. 581–583. doi: 10.1038/nbt.1631.

Villa-Diaz, L. G. et al. (2016) ‘Inhibition of Focal Adhesion Kinase Signaling by Integrin α6β1 Supports Human Pluripotent Stem Cell Self-Renewal’, STEM CELLS. John Wiley & Sons, Ltd, 34(7), pp. 1753–1764. doi: 10.1002/stem.2349.

Vining, K. H. et al. (2018) ‘Synthetic Light-Curable Polymeric Materials Provide a Supportive Niche for Dental Pulp Stem Cells’, Advanced Materials. John Wiley & Sons, Ltd, 30(4), p. 1704486. doi: 10.1002/adma.201704486.

Viotti, M., Nowotschin, S. and Hadjantonakis, A.-K. (2014) ‘SOX17 links gut endoderm morphogenesis and germ layer segregation.’, Nature cell biology. NIH Public Access, 16(12), pp. 1146–56. doi: 10.1038/ncb3070.

Vleugel, M. M. et al. (2006) ‘c-Jun activation is associated with proliferation and angiogenesis in invasive breast cancer’, Human Pathology, 37(6), pp. 668–674. doi:

10.1016/j.humpath.2006.01.022.

Vousden, K. H. and Lu, X. (2002) 'Live or let die: the cell's response to p53', Nature Reviews Cancer. Nature Publishing Group, 2(8), pp. 594–604. doi: 10.1038/nrc864.

Wang, D. et al. (2015) 'Identification of multipotent mammary stem cells by protein C receptor expression', Nature. Nature Publishing Group, 517(7532), pp. 81–84. doi: 10.1038/nature13851.

Wang, L. et al. (2007) 'PRAS40 regulates mTORC1 kinase activity by functioning as a direct inhibitor of substrate binding.', The Journal of biological chemistry. American Society for Biochemistry and Molecular Biology, 282(27), pp. 20036–44. doi: 10.1074/jbc.M702376200.

Wang, L. et al. (2017) 'Akt3 is responsible for the survival and proliferation of embryonic stem cells.', Biology open. Company of Biologists, 6(6), pp. 850–861. doi: 10.1242/bio.024505.

Wang, P.-Y. Y. et al. (2011) 'Modulation of alignment, elongation and contraction of cardiomyocytes through a combination of nanotopography and rigidity of substrates', Acta Biomaterialia. Acta Materialia Inc., 7(9), pp. 3285–3293. doi: 10.1016/j.actbio.2011.05.021.

Wang, X. and Gao, H. (2017) 'Recent Progress on Hyperbranched Polymers Synthesized via Radical-Based Self-Condensing Vinyl Polymerization.', Polymers. Multidisciplinary Digital Publishing Institute (MDPI), 9(6). doi: 10.3390/polym9060188.

Wang, Y.-C., Peterson, S. E. and Loring, J. F. (2014) 'Protein post-translational

modifications and regulation of pluripotency in human stem cells', Cell Research. Nature Publishing Group, 24(2), pp. 143–160. doi: 10.1038/cr.2013.151.

Wang, Z. et al. (2012) 'Distinct Lineage Specification Roles for NANOG, OCT4, and SOX2 in Human Embryonic Stem Cells', Cell Stem Cell. Cell Press, 10(4), pp. 440–454. doi: 10.1016/J.STEM.2012.02.016.

Wolfrum, C. et al. (2004) 'Foxa2 regulates lipid metabolism and ketogenesis in the liver during fasting and in diabetes', Nature. Nature Publishing Group, 432(7020), pp. 1027–1032. doi: 10.1038/nature03047.

Woo, D.-H., Hwang, H. S. and Shim, J. H. (2016) 'Comparison of adult stem cells derived from multiple stem cell niches', Biotechnology Letters. Springer Netherlands, 38(5), pp. 751–759. doi: 10.1007/s10529-016-2050-2.

Wu, J., Fan, Y. and Tzanakakis, E. S. (2015) 'Increased culture density is linked to decelerated proliferation, prolonged G1 phase, and enhanced propensity for differentiation of self-renewing human pluripotent stem cells.', Stem cells and development. Mary Ann Liebert, Inc., 24(7), pp. 892–903. doi: 10.1089/scd.2014.0384.

Wu, Q. et al. (2015) 'MSX2 mediates entry of human pluripotent stem cells into mesendoderm by simultaneously suppressing SOX2 and activating NODAL signaling', Cell Research. Nature Publishing Group, 25(12), pp. 1314–1332. doi: 10.1038/cr.2015.118.

Xi, B. et al. (2011) 'Functional Cardiotoxicity Profiling and Screening Using the xCELLigence RTCA Cardio System', Journal of Laboratory Automation. SAGE

PublicationsSage CA: Los Angeles, CA, 16(6), pp. 415–421. doi: 10.1016/j.jala.2011.09.002.

Xia, Y. et al. (2013) 'Directed differentiation of human pluripotent cells to ureteric bud kidney progenitor-like cells', Nature Cell Biology. Nature Publishing Group, 15(12), pp. 1507–1515. doi: 10.1038/ncb2872.

Xiao, M. et al. (2011) 'Surface-initiated atom transfer radical polymerization of butyl acrylate on cellulose microfibrils', Carbohydrate Polymers. Elsevier, 83(2), pp. 512–519. doi: 10.1016/J.CARBPOL.2010.08.011.

Xu, C. et al. (2001) 'Feeder-free growth of undifferentiated human embryonic stem cells', Nature Biotechnology. Nature Publishing Group, 19(10), pp. 971–974. doi: 10.1038/nbt1001-971.

Xu, X. et al. (2013) 'Stress-mediated p38 activation promotes somatic cell reprogramming', Cell Research, 23(1), pp. 131–141. doi: 10.1038/cr.2012.143.

Yamamoto, T. et al. (2006) 'Continuous ERK Activation Downregulates Antiproliferative Genes throughout G1 Phase to Allow Cell-Cycle Progression', Current Biology, 16(12), pp. 1171–1182. doi: 10.1016/j.cub.2006.04.044.

Yang, L. et al. (2008) 'Human cardiovascular progenitor cells develop from a KDR+embryonic-stem-cell-derived population', Nature, 453(7194), pp. 524–528. doi: 10.1038/nature06894.

Yang, Pabon, L. and Murry, C. E. (2014) 'Engineering adolescence: Maturation of human pluripotent stem cell-derived cardiomyocytes', Circulation Research, 114(3), pp. 511–523. doi: 10.1161/CIRCRESAHA.114.300558.

Yang, X. et al. (2014) ‘Tri-iodo-l-thyronine promotes the maturation of human cardiomyocytes-derived from induced pluripotent stem cells’, Journal of Molecular and Cellular Cardiology. Elsevier Ltd, 72, pp. 296–304. doi: 10.1016/j.yjmcc.2014.04.005.

Yao, K. et al. (2014) ‘JNK1 and 2 play a negative role in reprogramming to pluripotent stem cells by suppressing Klf4 activity’, Stem Cell Research. Elsevier, 12(1), pp. 139–152. doi: 10.1016/J.SCR.2013.10.005.

Yavin, E. and Yavin, Z. (1974) ‘Attachment and culture of dissociated cells from rat embryo cerebral hemispheres on polylysine-coated surface.’, The Journal of cell biology. The Rockefeller University Press, 62(2), pp. 540–6. doi: 10.1083/jcb.62.2.540.

Yayon, A. et al. (1991) ‘Cell surface, heparin-like molecules are required for binding of basic fibroblast growth factor to its high affinity receptor’, Cell. Cell Press, 64(4), pp. 841–848. doi: 10.1016/0092-8674(91)90512-W.

Ye, Q. et al. (2007) ‘Relationship of solvent to the photopolymerization process, properties, and structure in model dentin adhesives.’, Journal of biomedical materials research. Part A. NIH Public Access, 80(2), pp. 342–50. doi: 10.1002/jbm.a.30890.

Yeh, Y.-C. et al. (2017) ‘Mechanotransduction of matrix stiffness in regulation of focal adhesion size and number: reciprocal regulation of caveolin-1 and β1 integrin’, Scientific Reports. Nature Publishing Group, 7(1), p. 15008. doi: 10.1038/s41598-017-14932-6.

Yeh, Y.-H. et al. (2009) ‘The cell cycle checkpoint kinase CHK2 mediates DNA damage-induced stabilization of TTK/hMps1’, Oncogene. Nature Publishing Group, 28(10), pp. 1366–1378. doi: 10.1038/onc.2008.477.

Yin, J. and Luan, S. (2016) ‘Opportunities and challenges for the development of polymer-based biomaterials and medical devices.’, Regenerative biomaterials. Oxford University Press, 3(2), pp. 129–35. doi: 10.1093/rb/rbw008.

Young, J. L. et al. (2014) ‘Mechanosensitive kinases regulate stiffness-induced cardiomyocyte maturation’, Scientific Reports, 4, pp. 1–11. doi: 10.1038/srep06425.

Yu, J. S. L. and Cui, W. (2016) ‘Proliferation, survival and metabolism: the role of PI3K/AKT/mTOR signalling in pluripotency and cell fate determination.’, Development (Cambridge, England). Oxford University Press for The Company of Biologists Limited, 143(17), pp. 3050–60. doi: 10.1242/dev.137075.

Yu, M. et al. (2019) ‘EGFR deficiency leads to impaired self-renewal and pluripotency of mouse embryonic stem cells.’, PeerJ. PeerJ, Inc, 7, p. e6314. doi: 10.7717/peerj.6314.

YU, X. et al. (2005) ‘Foxa1 and Foxa2 Interact with the Androgen Receptor to Regulate Prostate and Epididymal Genes Differentially’, Annals of the New York Academy of Sciences. John Wiley & Sons, Ltd (10.1111), 1061(1), pp. 77–93. doi: 10.1196/annals.1336.009.

Zannini, L., Delia, D. and Buscemi, G. (2014) ‘CHK2 kinase in the DNA damage response and beyond.’, Journal of molecular cell biology. Oxford University Press, 6(6), pp. 442–57. doi: 10.1093/jmcb/mju045.

Zarrintaj, P. et al. (2018) 'Agarose-based biomaterials for tissue engineering', Carbohydrate Polymers. Elsevier, 187, pp. 66–84. doi: 10.1016/J.CARBPOL.2018.01.060.

Zhang, J. et al. (2009) 'Functional Cardiomyocytes Derived From Human Induced Pluripotent Stem Cells', Circulation Research, 104(4), pp. e30-41. doi: 10.1161/CIRCRESAHA.108.192237.

Zhang, Q. et al. (2011) 'Direct differentiation of atrial and ventricular myocytes from human embryonic stem cells by alternating retinoid signals', Cell Research, 21(4), pp. 579–587. doi: 10.1038/cr.2010.163.

Zhang, S. and Cui, W. (2014) 'Sox2, a key factor in the regulation of pluripotency and neural differentiation.', World journal of stem cells. Baishideng Publishing Group Inc, 6(3), pp. 305–11. doi: 10.4252/wjsc.v6.i3.305.

Zhang, X. et al. (2010) 'Pax6 is a human neuroectoderm cell fate determinant.', Cell stem cell. NIH Public Access, 7(1), pp. 90–100. doi: 10.1016/j.stem.2010.04.017.

Zhang, X. et al. (2014) 'Src-family tyrosine kinase activities are essential for differentiation of human embryonic stem cells', Stem Cell Research. Elsevier, 13(3), pp. 379–389. doi: 10.1016/J.SCR.2014.09.007.

Zhang, X. et al. (2014) 'Transcriptional Repression by the BRG1-SWI/SNF Complex Affects the Pluripotency of Human Embryonic Stem Cells', Stem Cell Reports. Cell Press, 3(3), pp. 460–474. Available at: https://www.sciencedirect.com/science/article/pii/S2213671114002343?via%3Dihub (Accessed: 20 February 2019).

Zhao, Y. et al. (2015) ‘The influence of printing parameters on cell survival rate and printability in microextrusion-based 3D cell printing technology’, Biofabrication. IOP Publishing, 7(4), p. 045002. doi: 10.1088/1758-5090/7/4/045002.

Zhao, Y. et al. (2019) ‘A Platform for Generation of Chamber-Specific Cardiac Tissues and Disease Modeling.’, Cell. Elsevier, 176(4), p. 913–927.e18. doi: 10.1016/j.cell.2018.11.042.

Zhou, J. et al. (2009) ‘mTOR supports long-term self-renewal and suppresses mesoderm and endoderm activities of human embryonic stem cells.’, Proceedings of the National Academy of Sciences of the United States of America. National Academy of Sciences, 106(19), pp. 7840–5. doi: 10.1073/pnas.0901854106.

Zhou, J. et al. (2010) ‘High-Efficiency Induction of Neural Conversion in Human ESCs and Human Induced Pluripotent Stem Cells with a Single Chemical Inhibitor of Transforming Growth Factor Beta Superfamily Receptors’, STEM CELLS, 28(10), pp. 1741–1750. doi: 10.1002/stem.504.

Zhou, P. and Pu, W. T. (2016) ‘Recounting Cardiac Cellular Composition.’, Circulation research. NIH Public Access, 118(3), pp. 368–70. doi: 10.1161/CIRCRESAHA.116.308139.

Zhu, W.-Z., Santana, L. F. and Laflamme, M. A. (2009) ‘Local Control of Excitation-Contraction Coupling in Human Embryonic Stem Cell-Derived Cardiomyocytes’, PLoS ONE. Edited by A. Schwartz. Public Library of Science, 4(4), p. e5407. doi: 10.1371/journal.pone.0005407.

Zimmermann, W. H., Melnychenko, I. and Eschenhagen, T. (2004) ‘Engineered heart

tissue for regeneration of diseased hearts', Biomaterials, 25(9), pp. 1639–1647. doi: 10.1016/S0142-9612(03)00521-0.

Zorn, A. M. and Wells, J. M. (2009) 'Vertebrate endoderm development and organ formation.', Annual review of cell and developmental biology. NIH Public Access, 25, pp. 221–51. doi: 10.1146/annurev.cellbio.042308.113344.

8 Appendix

A

AD18	AM08	AM79	AM83	BM40	DM04	CM08	40BM36 60BM38	AD17	AM38	BM85
AD25	AM06	AT08	BM39	20BM36 80BM38	DM06	AD05	BM53	AM10	AM80	DM01
AM13	AM23	AT02	BM82	BM30	CM02	BD04	AD01	AM53	AM77	
AM12	AM45	BM35	BM13	BM56	AM78	BM11	BM34	CM07	AD02	
AD23	AD20	AM73	BM57	BM38	CM04	CD01	BM63	AD16	AM31	AM47
AM02	AM09	BD03	BM60	BM14	CM01	BM92	AD24	AM27	40BM36 60BM38	CM15
AM15	AM35	AM72	BM81	BM55	CD05	BD05	BM41	AM54	BM83	
AM19	AM46	BM22	BM18	BM31	CM16	BM08	BM42	AM55	AT07	
AD22	AD19	AT03	BM49	BM25	AM05	AD15	BM62	AD09	AM52	AD03
AM06	AM07	DM05	BM84	BM17	DM03	BM06	BM15	BM74	AM69	CM13
AM22	AM51	AM48	BM89	BM48	AM81	BM24	BM52	CM10	BM33	
AD04	AM70	BM36	AM29	CM15 CM13	CM06	BM23	AD10	80BM36 20BM38	BM09	

B

AM02	AM06	AM79	AM83	BM40	DM04	45102-52-1	16715-83-6	AD17	AM38	BM85
AM13	AM19	AT08	BM39	2997-88-8	DM06	AD05	BM53	2082-81-7	AM80	DM01
AM70	AM23	AT02	BM82	BM30	4986-89-4	BD04	AD01	AM53	AM77	
BM23	AM45	BM35	BM13	BM56	AM78	BM11	BM34	CM07	AD02	
AM07	AM08	AM73	BM57	BM38	CM04	CD01	BM63	AM22	AM31	AD20
AM15	AD19	BD03	BM60	BM14	CM01	6606-59-3	AD24	AM27	AM75	
AD16	AM35	AM72	BM81	BM55	CD05	BD05	BM41	AM54	BM83	
BM24	AM46	BM22	BM18	BM31	CM16	BM08	BM42	AM55	AT07	
AM10	AM09	AT03	BM49	BM25	AM05	AD15	71195-85-2	AD09	AM52	AD03
AM47	AD18	DM05	BM84	BM17	DM03	BM06	AM12	BM74	AM69	
BM15	AM51	AM48	BM89	BM48	AM81	AD23	BM52	CM10	BM33	
DM09	AD25	BM36	AM28	CM15	CM06	682-09-7	AD10	72607-53-5	BM09	

Figure 8.1 Layout of Polymer Microarrays within the 8.X Series.

(A) Array 8.0, 6% p-HEMA, containing five co-polymers. (B) Array 8.2 4% p-HEMA, with co-polymers removed and in-house synthesised additions, denoted with numerical coding. Full monomer identities and structures in the appendix.

Figure 8.2 Layout of Generation 1 Polymer Microarray (9.1).
Colour codes; blue = fluorine containing, red = nitrogen containing, gold = chlorine containing.

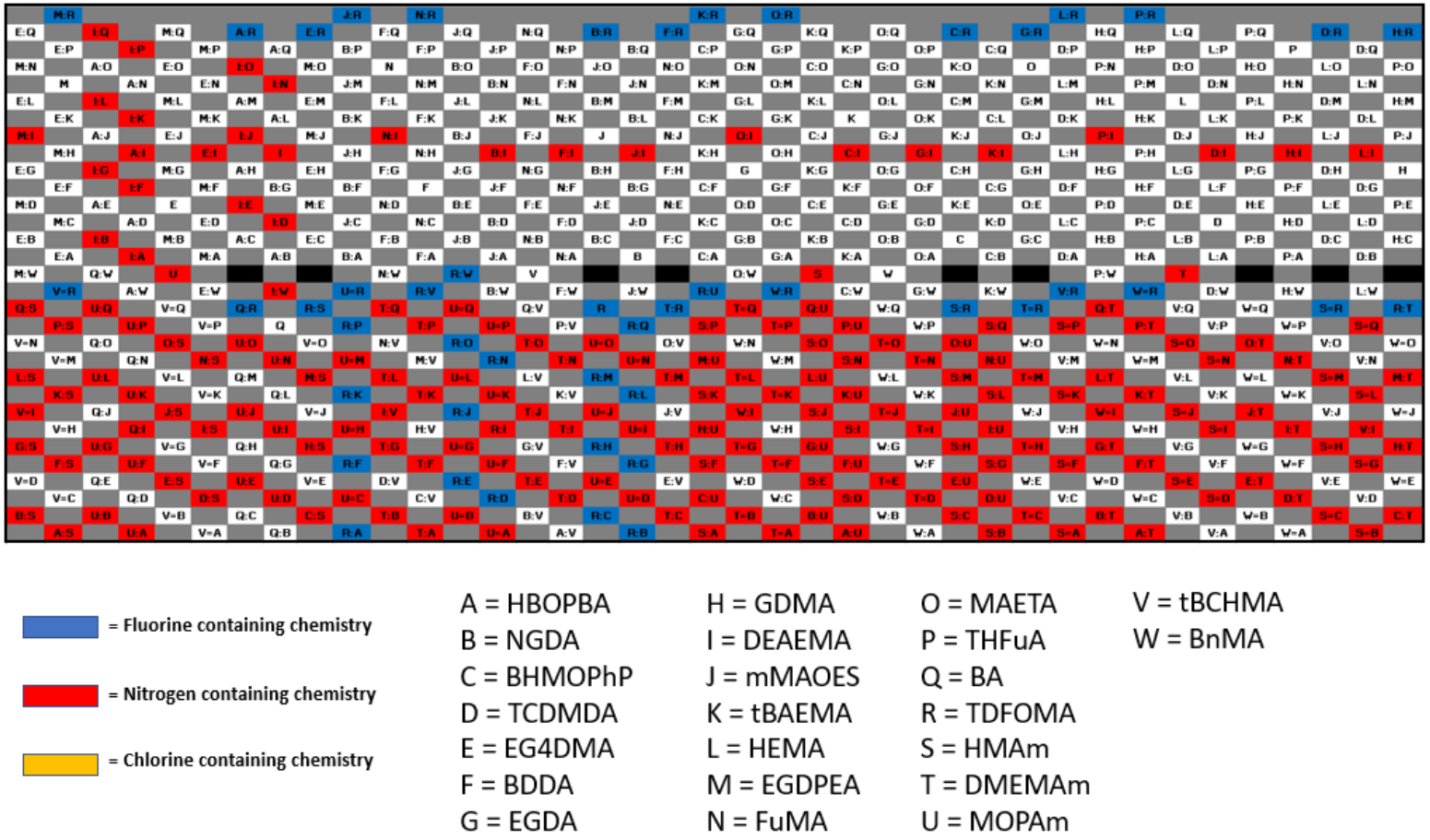

Figure 8.3 Layout of Generation 2 Polymer Microarray (10.1).

Monomers mixed in 2:1 ratio. Colour codes; blue = fluorine containing, red = nitrogen containing, gold = chlorine containing.

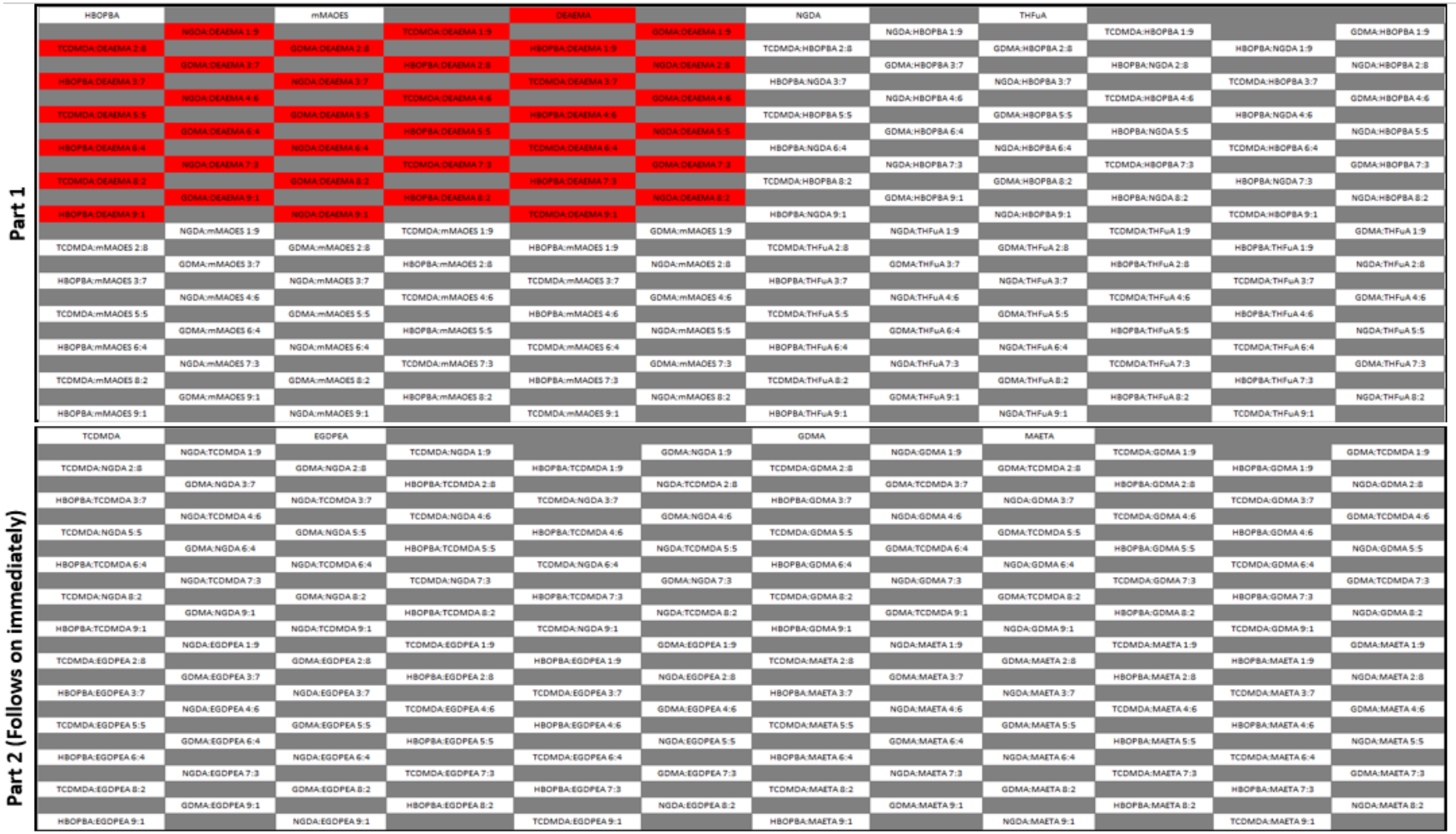

Figure 8.4 Layout of Generation 3 Polymer Microarray (10.2)

Full polymer identities available within the appendix section. Red = contains Nitrogen.

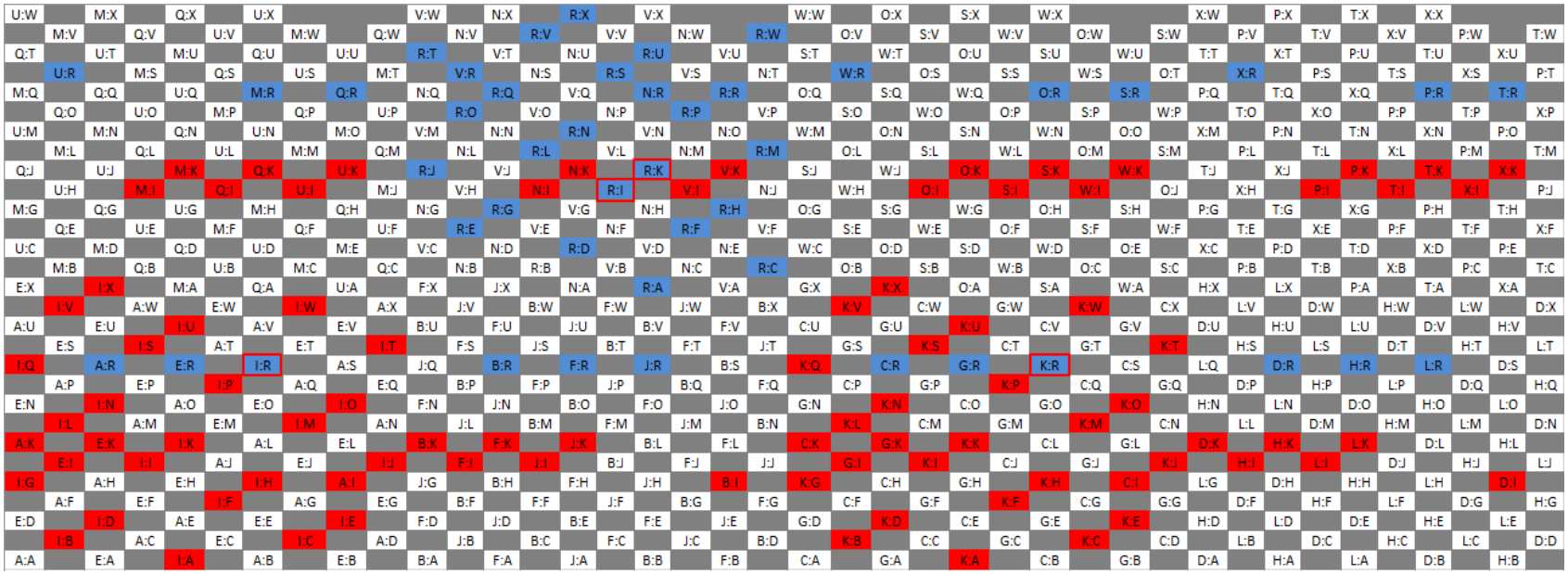

Figure 8.5 Layout of Generation 2 Polymer Microarray (11.1) (hPSC-CM)

Fluorine containing = Blue. Nitrogen containing = Red.

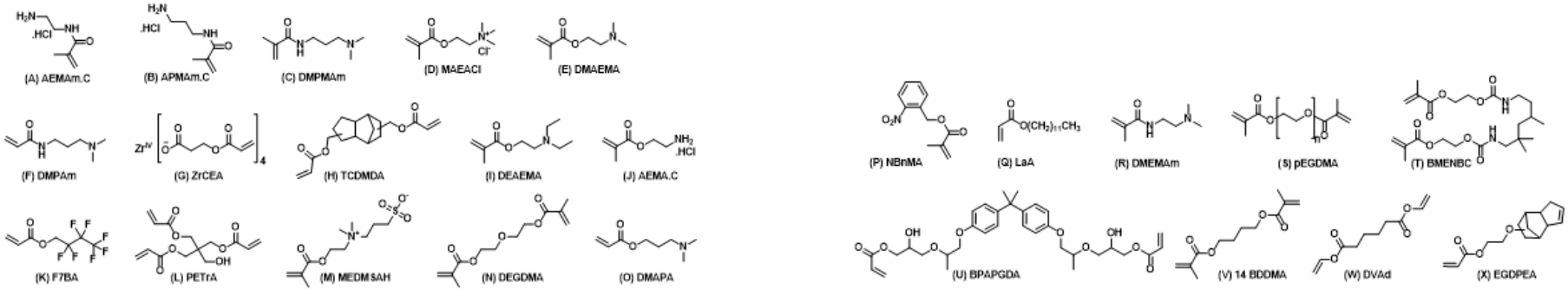

Acronym	Name	Code	Structure
13BDDA	Butanediol-1,3 diacrylate	AD02	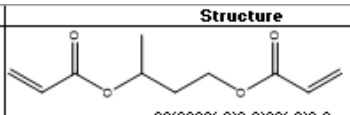 CC(CCOC(-O)C-C)OC(-O)C-C
AAcAm	Diacetone acrylamide	CM01	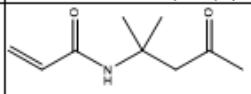 CC(-O)CC(C)(C)NC(-O)C-C
AcAPAm	N-[2-(Acryloylamino)phenyl]acrylamide	CD06	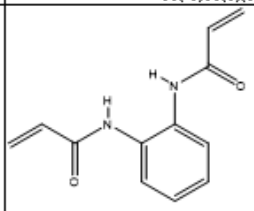 C12H12N2O2
ACl	Acryloyl Chloride	AM82	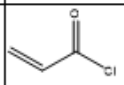 ClC(-O)C-C
AnMA	Anthracenylmethylacrylate	AM18	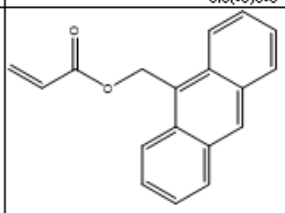 C18H14O2
BA	Butyl acrylate	AM02	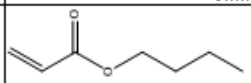 CCCCOC(-O)C-C
BAGDA	Bisphenol A glycerolate diacrylate	AD13	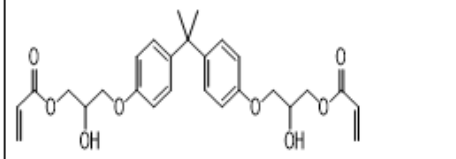 CC(C)(c1ccc(OCC(O)COC(-O)C-C)cc1)c2ccc(OCC(O)COC(-O)C-C)cc2
BMAM	N-Benzylmethacrylamide		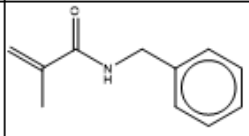 CC(-C)C(-O)NCc1ccccc1
BnA	Benzyl acrylate	AM83	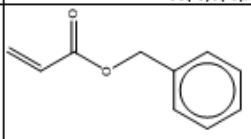 C-CC(-O)OCc1ccccc1

BPEODA	Bisphenol A ethoxylate diacrylate	AD20	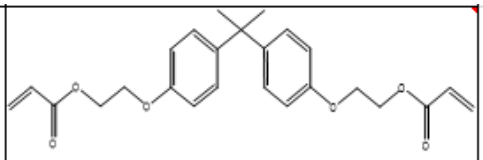 C25H28O6
BTHPhMA	Benzotriazol-2-yl)-4-hydroxyphenyl]ethyl methacrylate	BM78	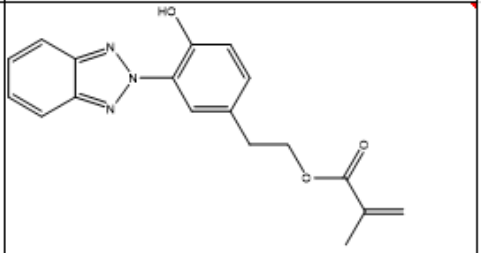 C18H17N3O3
BzHPEA	Benzoyl-3-hydroxy-phenoxy)ethyl acrylate	AM50	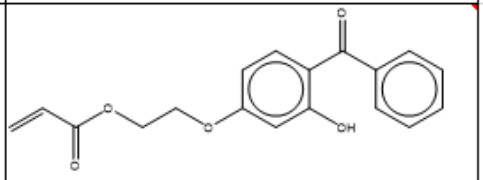 Oc1cc(OCCOC(=O)C=C)ccc1C(=O)c2ccccc2
CHMA	Cyclohexyl methacrylate	BM30	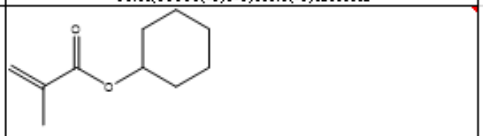 CC(=C)C(=O)OC1CCCCC1
CHPMA	Chloro-2-hydroxy-propyl methacrylate	BM60	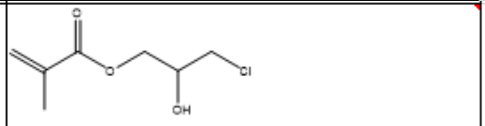 CC(=C)C(=O)OCC(O)CCl
CMAOE	Caprolactone 2-(methacryloyloxy)ethyl ester	BM09	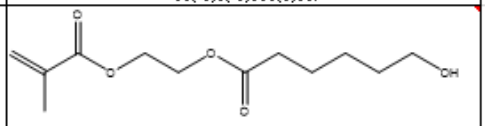 CC(=C)C(=O)OCCOC(=O)CCCCCO
CNEA	Cyanoethyl acrylate	AM81	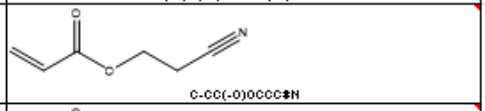 C=CC(=O)OCCC#N
NBMAm	N-(Butoxymethyl)acrylamide	CM14	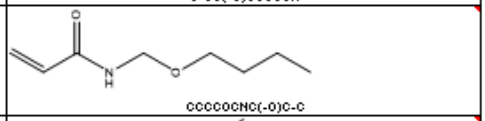 CCCCOCNC(=O)C=C
DEAEA	Diethylamino ethyl acrylate	AM36	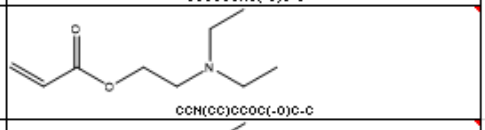 CCN(CC)CCOC(=O)C=C
DEAEMA	Diethylaminoethyl methacrylate	BM48	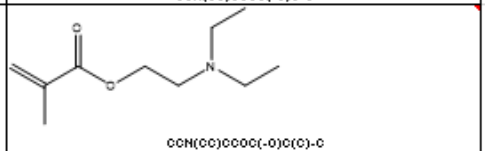 CCN(CC)CCOC(=O)C(C)=C

DEGDA	Di(ethylene glycol) diacrylate	AD15	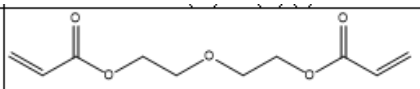 C=CC(=O)OCCOCCOC(=O)C=C
DEGDMA	Diethylene glycol dimethacrylate		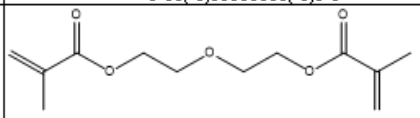 CC(=C)C(=O)OCCOCCOC(=O)C(C)=C
DEGEEA	Di(ethylene glycol) ethyl ether acrylate	AM45	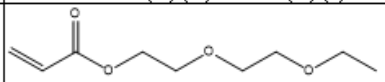 CCOCCOCCOC(=O)C=C
DEGEHA	Di(ethylene glycol) 2-ethylhexyl ether acrylate	AM72	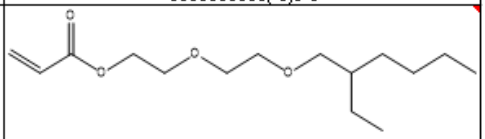 C15H28O4
DMCSPMA	Dimethylchlorosilylpropyl methacrylate	BM59	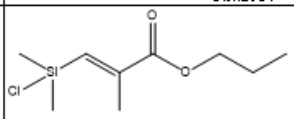 CCCOC(=O)C(/C)=C/[Si](C)(C)Cl
DPEPHA	Dipentaerythritol penta/hexa-acrylate	AH01	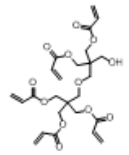
E3GDA	Triethylene glycol diacrylate		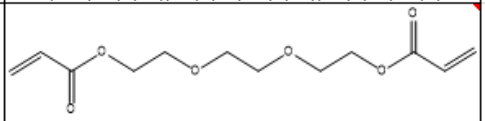 C=CC(=O)OCCOCCOCCOC(=O)C=C
EA	Ethyl acrylate	AM04	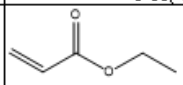 CCOC(=O)C=C
EaNIA	Ethyl trans-a-cyano-3-indole-acrylate	BM03	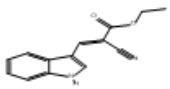 C14H12N2O2
EbCNA	Ethyl-cis-B-cyano-acrylate	BM02	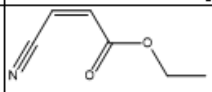 C6H7NO2
ECNTA	Ethyl-2-cyano-3-(2-thienyl)acrylate	BM75	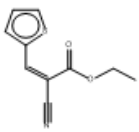 CCOC(=O)\C(=C/c1cccc1)C#N

EG3DMA	Tri(ethylene glycol) dimethacrylate	BD06	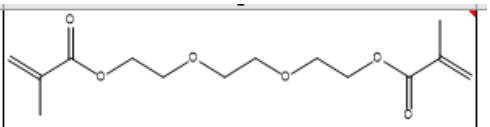 CC(=C)C(=O)OCCOCCOCCOC(=O)C(C)=C
EG4DMA	Tetraethylene glycol dimethacrylate	BD05	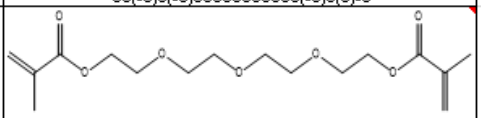 CC(=C)C(=O)OCCOCCOCCOCCOC(=O)C(C)=C
EGDPEA	Ethylene glycol dicyclopentenyl ether acrylate	AM49	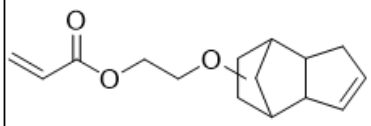 C=CC(=O)OCCOC1CC2CC1C3CC=CC23
EGDCMA	Ethylene glycol dicyclopentenyl ether methacrylate	BM56	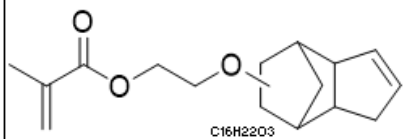 C16H22O3
EGDMA	Ethylene glycol dimethacrylate	BD03	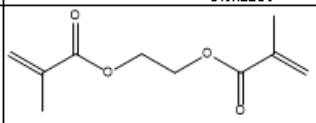 CC(=C)C(=O)OCCOC(=O)C(C)=C
EGMEA	Ethylene glycol methyl ether acrylate	AM47	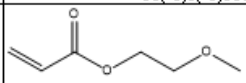 COCCOC(=O)C=C
EGMMA	Ethylene glycol methyl ether methacrylate	BM55	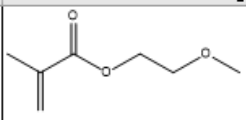 COCCOC(=O)C(C)=C
EGPEA	Ethylene glycol phenyl ether acrylate	AM51	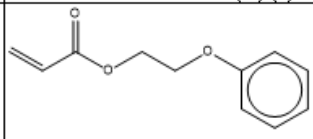 C=CC(=O)OCCOc1ccccc1
EGPhMA	Ethylene glycol phenyl ether methacrylate	BM57	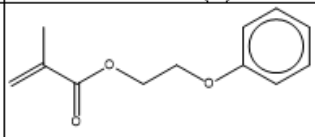 CC(=C)C(=O)OCCOc1ccccc1
EHA	Ethylhexyl acrylate	AM05	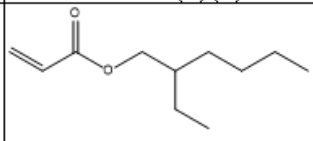 CCCCC(CC)COC(=O)C=C
EHMA	Ethylhexyl methacrylate	BM13	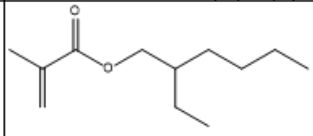 CCCCC(CC)COC(=O)C(C)=C
EOEA	Ethoxyethyl acrylate	AM46	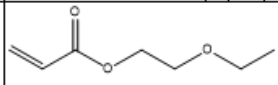 CCOCCOC(=O)C=C

ExA	Epoxidized acrylate	AM03	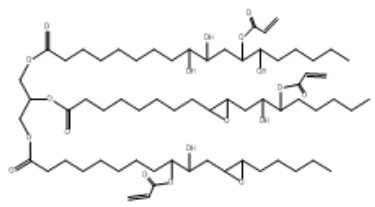 C66H112O19
GA	Glycidyl acrylate	AM21	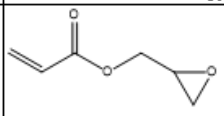 C=CC(=O)OCC1CO1
GPOTA	Glycerol propoxylate triacrylate	AT08	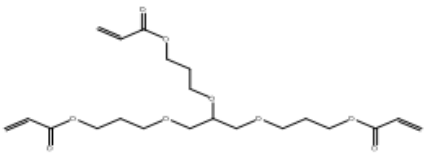 C=CC(=O)OCCCOCC(COCCCOC(=O)C=C)OCCCOC(=O)C=C
HA	Hexyl acrylate	AM06	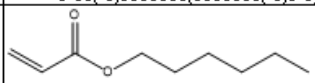 CCCCCCOC(=O)C=C
HDDMA	1,6-Hexanediol dimethacrylate,		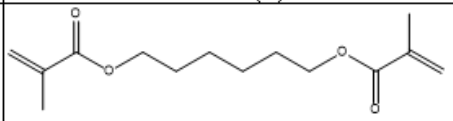 CC(=C)C(=O)OCCCCCCOC(=O)C(C)=C
HDMPDA	y-2,2-dimethylpropyl 3-hydroxy-2,2-dimethylpropionate di	AD25	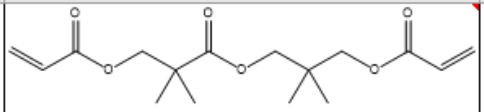 CC(C)(COC(=O)C=C)COC(=O)C(C)(C)COC(=O)C=C
HEA	Hydroxyethyl acrylate	AM76	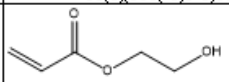 OCCOC(=O)C=C
HfCEA	Hafnium carboxyethyl acrylate	AM26	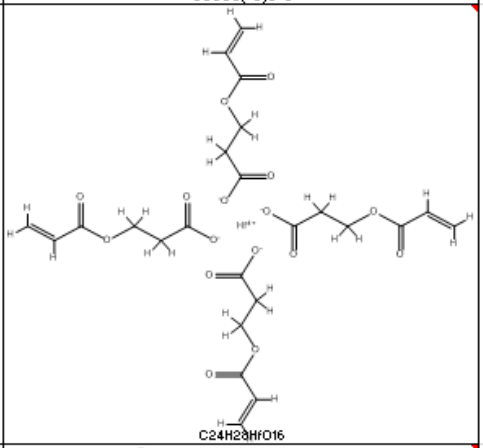 C24H28HfO16
HFiPA	Hexafluoroisopropyl acrylate	AM70	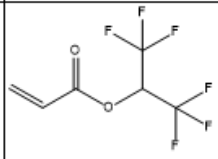 FC(F)(F)C(OC(=O)C=C)C(F)(F)F

HFiPMA	Hexafluoroisopropyl methacrylate	BM69	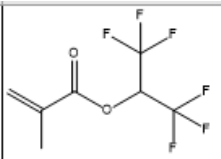 CC(=C)C(=O)OC(C(F)(F)F)C(F)(F)F
HMA	Hexyl methacrylate	BM14	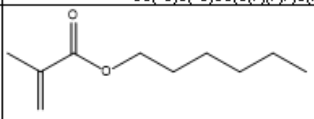 CCCCCCOC(=O)C(C)=C
HMDA	Hexamethylene diacrylate	AD04	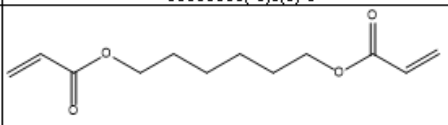 C=CC(=O)OCCCCCCOC(=O)C=C
HPA	Hydroxypropyl acrylate	AM28	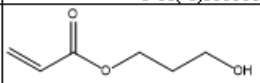 OCCCOC(=O)C=C
HPhMA	N-(4-Hydroxyphenyl)methacrylamide	DM03	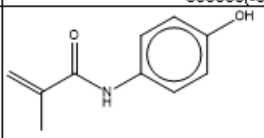 CC(=C)C(=O)Nc1ccc(O)cc1
iBA	Isobutyl acrylate	AM07	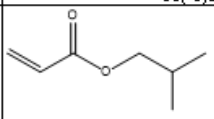 CC(C)COC(=O)C=C
iBMA	Isobornyl methacrylate	BM36	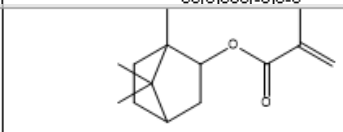 CC(=C)C(=O)OC1CC2CCC1(C)C2(C)C
iBOA	Isobornyl acrylate	AM23	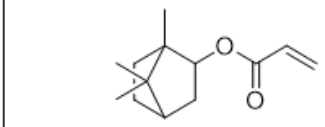 CC1(C)[C@H]2CC[C@]1(C)C(C2)OC(=O)C=C
iBOMAm	N-(Isobutoxymethyl)acrylamide	CM09	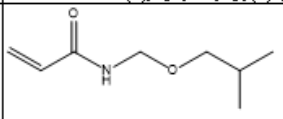 CC(C)COCNC(=O)C=C
iDA	Isodecyl acrylate	AM73	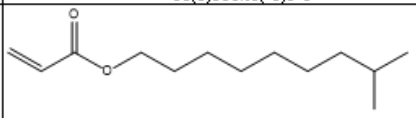 CC(C)CCCCCCCOC(=O)C=C
iDMA	Isodecyl methacrylate	BM17	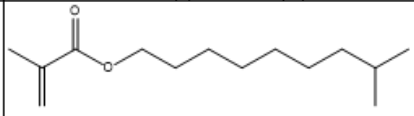 CC(C)CCCCCCCOC(=O)C(C)=C
iOA	Isooctyl acrylate	AM08	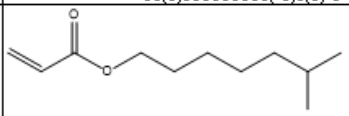 CC(C)CCCCCOC(=O)C=C

iPAm	N-Isopropylacrylamide	CM06	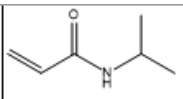 CC(C)NC(=O)C=C
LaA	Lauryl acrylate	AM09	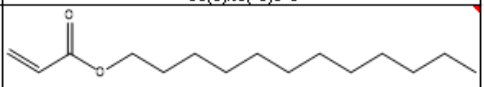 CCCCCCCCCCCCOC(=O)C=C
LMA	Lauryl methacrylate	BM18	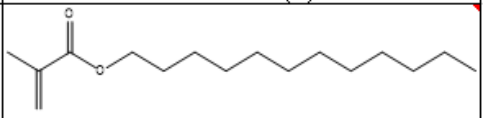 CCCCCCCCCCCCOC(=O)C(C)=C
MAA	Methyl 2-acetamidoacrylate	BM05	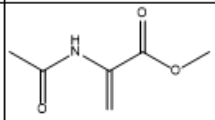 COC(=O)C(=C)NC(C)=O
MAAH	Methacrylic anhydride	BM92	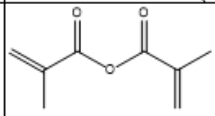 CC(=C)C(=O)OC(=O)C(C)=C
MAEA	Methacryloyloxy)ethyl acetoacetate	BM80	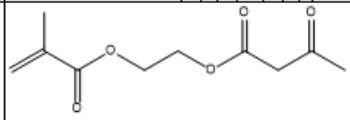 CC(=O)CC(=O)OCCOC(=O)C(C)=C
MAEACl	[2-(Methacryloyloxy)ethyl]trimethylammonium chloride solution	BM89	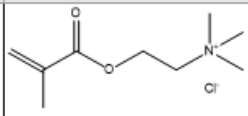 [Cl-].CC(=C)C(=O)OCC[N+](C)(C)C
MAL	Methacryloyl-L-Lysine		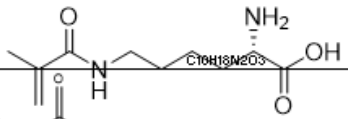 C10H18N2O3
Mam	Methacrylamide	DM04	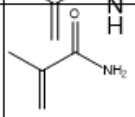 CC(=C)C(N)=O
MAPtMA	Methacrylamidopropyltrimethylammonium chloride,		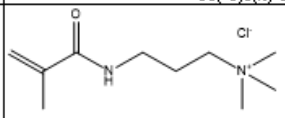 [Cl-].CC(=C)C(=O)NCCC[N+](C)(C)C
MBMAm	N,N'-Methylenebismethacrylamide	DD01	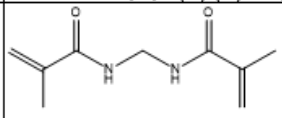 CC(=C)C(=O)NCNC(=O)C(C)=C
MEDMSAH	[2-(Methacryloyloxy)ethyl]dimethyl-(3-sulfopropyl) ammonium hydroxide	BM85	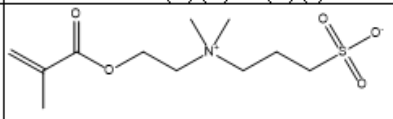 CC(=C)C(=O)OCC[N+](C)(C)CCC[S]([O-])(=O)=O

MMAm	N-Methylmethacrylamide	DM05	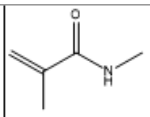 CNC(=O)C(C)=C
MTEMA	Methylthioethyl methacrylate	BM25	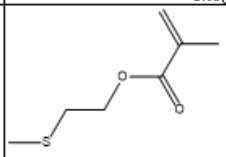 C7H12O2S
NaPhA	Sodium 3-phenyl-acrylate	BM72	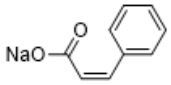 C9H7NaO2
NBMA	Norbornyl methacrylate	BM38	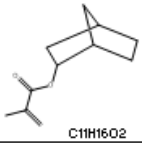 C11H16O2
NDMAm	N-Dodecylmethacrylamide		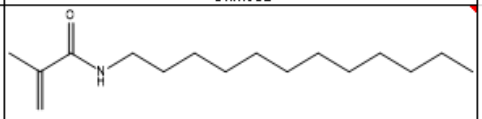 CCCCCCCCCCCCNC(=O)C(C)=C
NGDA	Neopentyl glycol diacrylate	AD05	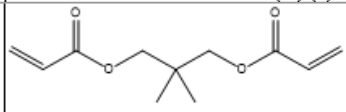 CC(C)(COC(=O)C=C)COC(=O)C=C
NGPDA	Neopentyl glycol propoxylate diacrylate	AD23	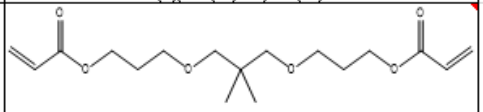 CC(C)(COCCCOC(=O)C=C)COCCCOC(=O)C=C
NMEMA	2-N-Morpholinoethyl methacrylate, 95%		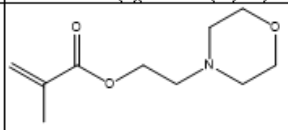 CC(=C)C(=O)OCCN1CCOCC1
NpA	Naphthyl acrylate	AM24	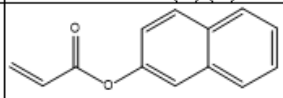 C13H10O2
NpMA	Naphthyl methacrylate	BM37	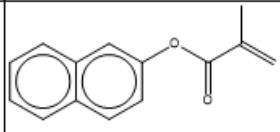 CC(=C)C(=O)Oc1ccc2ccccc2c1
ODA	Octadecyl acrylate	AM11	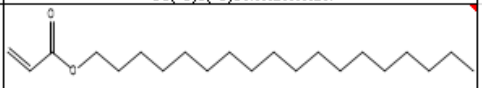 CCCCCCCCCCCCCCCCCCOC(=O)C=C

OFPMA	Octafluoropentyl methacrylate	BM71	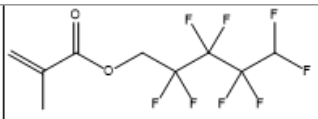 CC(=C)C(=O)OCC(F)(F)C(F)(F)C(F)(F)C(F)F
PA	Propargyl acrylate	AM12	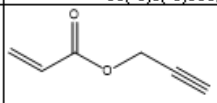 C=CC(=O)OCC#C
PEDAM	Pentaerythritol diacrylate monostearate	AD12	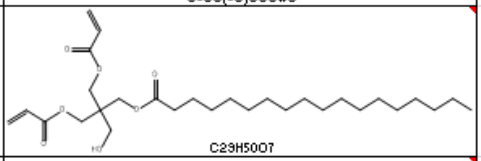 C23H50O7
pEGMA	Poly(ethylene glycol) methacrylate	BM81	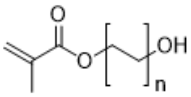 CC(=C)C(=O)OCCO
pEGMEMA	Poly(ethylene glycol) methyl ether methacrylate	BM82	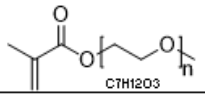 C7H12O3
PETA	Pentaerythritol tetraacrylate		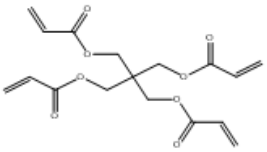 C=CC(=O)OCC(COC(=O)C=C)(COC(=O)C=C)COC(=O)C=C
PhMA	Phenyl methacrylate	BM40	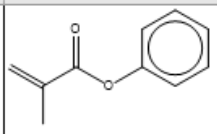 CC(=C)C(=O)Oc1ccccc1
PhMAm	N-Phenylmethacrylamide	DM06	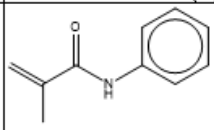 CC(=C)C(=O)Nc1ccccc1
PMAm	N-(Phthalimidomethyl)acrylamide		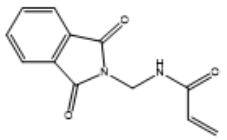 C12H10N2O3
pPGNEA	Poly(propylene glycol) 4-nonylphenyl ether acrylate	AM79	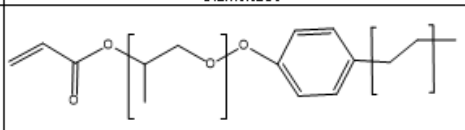 C15H20O4
SMA	Stearyl methacrylate	BM22	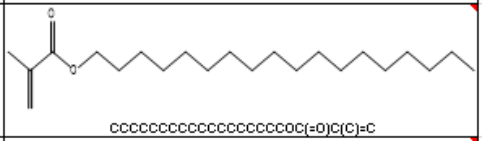 CCCCCCCCCCCCCCCCCCOC(=O)C(C)=C

SPAK	Sulfopropyl acrylate potassium salt	AM78	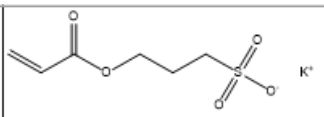 [K+].[O-][S](=O)(=O)CCCOC(=O)C=C
SPMAK	3-Sulfopropyl methacrylate potassium salt	BM86	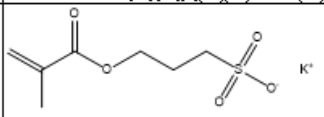 [K+].CC(=C)C(=O)OCCC[S]([O-])(=O)=O
TAHTA	1,3,5-Triacryloylhexahydro-1,3,5-triazine	CT01	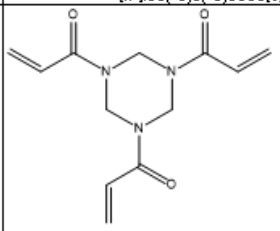 C=CC(=O)N1CN(CN(C1)C(=O)C=C)C(=O)C=C
TAIC	Tris[2-(acryloyloxy)ethyl] isocyanurate	AT09	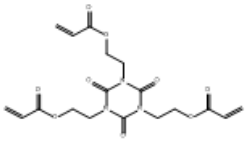 C=CC(=O)OCCN1C(=O)N(CCOC(=O)C=C)C(=O)N(CCOC(=O)C=C)C1=O
tBA	Tert-butyl acrylate	AM13	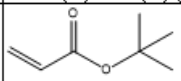 CC(C)(C)OC(=O)C=C
tBAEMA	Tert-butylamino-ethyl methacrylate	BM49	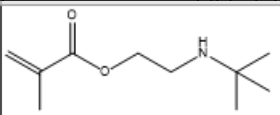 CC(=C)C(=O)OCCNC(C)(C)C
tBAm	N-tert-Butylacrylamide	CM03	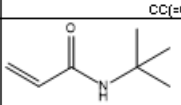 CC(C)(C)NC(=O)C=C
tBCHA	Tert-butylcyclohexylacrylate	AM19	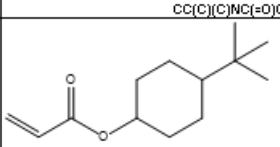 CC(C)(C)C1CCC(CC1)OC(=O)C=C
tBCHMA	Tertbutylcyclohexyl methacrylate	BM84	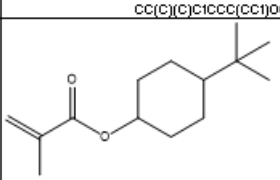 CC(=C)C(=O)OC1CCC(CC1)C(C)(C)C
tBMAm	N-tert-Butylmethacrylamide	DM02	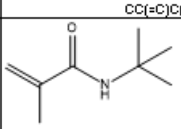 CC(=C)C(=O)NC(C)(C)C
TEGDA	Tetra(ethylene glycol) diacrylate	AD18	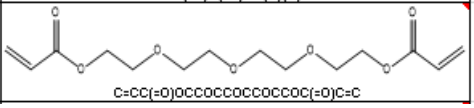 C=CC(=O)OCCOCCOCCOCCOC(=O)C=C

THFuA	Tetrahydrofurfuryl acrylate	AM22	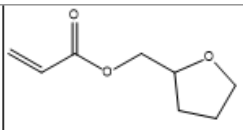 C=CC(=O)OCC1CCCO1
THFuMA	Tetrahydrofurfuryl methacrylate	BM35	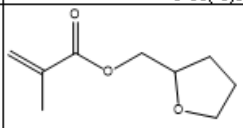 CC(=C)C(=O)OCC1CCCO1
TMBAm	N-(1,1,3,3-Tetramethylbutyl)acrylamide	CM16	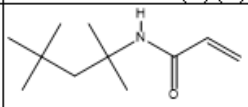 C11H21NO
TMCHMA	Trimethylcyclohexyl methacrylate	BM31	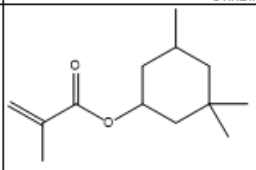 CC1CC(CC(C)(C)C1)OC(=O)C(C)=C
TMHA	Trimethylhexyl acrylate	AM15	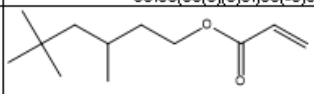 C12H22O2
TMOSPA	Trimethoxysilyl propyl acrylate	AM16	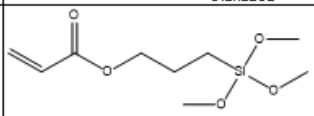 CO[Si](CCCOC(=O)C=C)(OC)OC
TMPDAE	Trimethyl propane diallyl ether		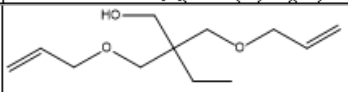 CCC(CO)(COCC=C)COCC=C
TMPETA	Trimethylolpropane ethoxylate triacrylate	AT07	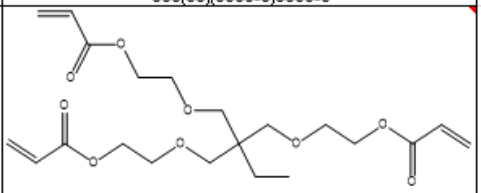 CCC(COCCOC(=O)C=C)(COCCOC(=O)C=C)COCCOC(=O)C=C
TMPOTA	Trimethylolpropane propoxylate triacrylate	AT02	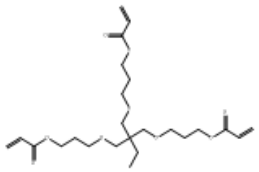 C24H38O9
TMPTA	Trimethylolpropane triacrylate	AT03	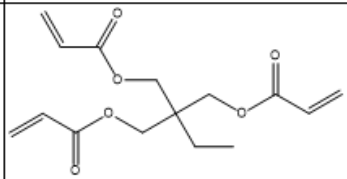 CCC(COC(=O)C=C)(COC(=O)C=C)COC(=O)C=C
TMSA	Trimethylsilylacrylate	AM17	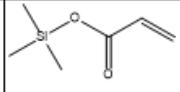 C6H12O2Si

TMSOEMA	Trimethylsilyloxy)ethyl methacrylate	BM10	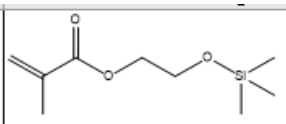 CC(=C)C(=O)OCCO[Si](C)(C)C
TMSOSMA	Tris(trimethylsilyloxy)-silyl propyl methacrylate	BM29	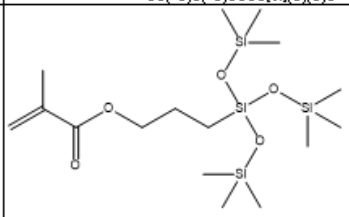 CC(=C)C(=O)OCCC[Si](O[Si](C)(C)C)(O[Si](C)(C)C)O[Si](C)(C)C
TPEMDA	Trimethylolpropane ethoxylate methyl ether diacrylate	AD19	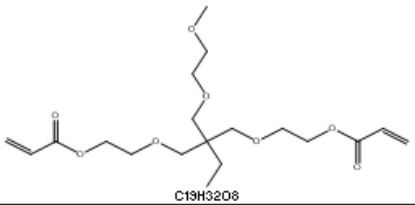 C19H32O8
TPGDA	Tri(propylene glycol) diacrylate	AD22	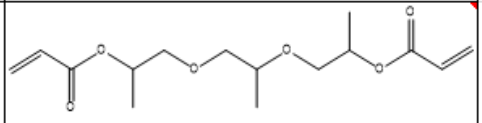 CC(COCC(C)OC(=O)C=C)OCC(C)OC(=O)C=C
ZnA	Zinc acrylate	AM33	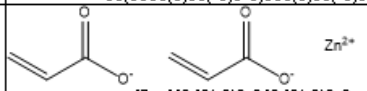 [Zn++].[O-]C(=O)C=C.[O-]C(=O)C=C
ZrA	Zirconium acrylate	AM34	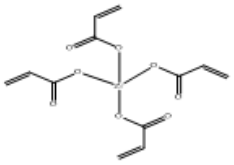 C12H12O8Zr
ZrBNCTA	Zirconium bromonorbornanelactone carboxylate triacrylate	AT10	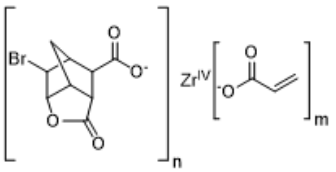 [C9H8BrO4-].[C2HO2-].CH2Zr4+
13BDDMA	1,3-Butanediol dimethacrylate, 98%		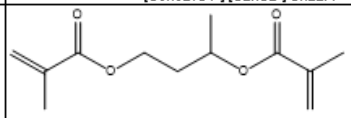 CC(CCOC(=O)C(C)=C)OC(=O)C(C)=C
14BDDMA	1,4-Butanediol dimethacrylate		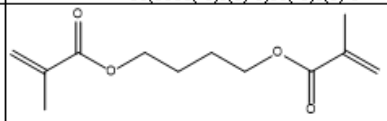 CC(=C)C(=O)OCCCCOC(=O)C(C)=C
AA	Allyl acrylate	AM01	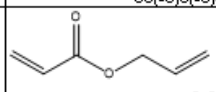 C=CCOC(=O)C=C
AAm	Acrylamide	CM08	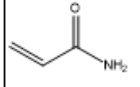 NC(=O)C=C

AEMA.C	2-Aminoethyl methacrylate hydrochloride,		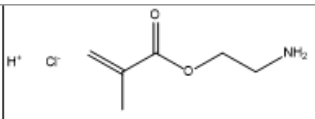 [H+].[Cl-].CC(=C)C(=O)OCCN
AEMAm.C	N-(2-aminoethyl) methacrylamide hydrochloride		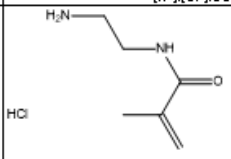 C6H13ClN2O
AMA	Allyl methacrylate	BM07	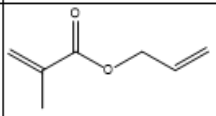 CC(=C)C(=O)OCC=C
AODMBA	(R)-α-Acryloyloxy-β,β-dimethyl-γ-butyrolactone	AM80	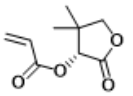 C8H12O4
AOHPMA	Acryloyloxy-2-hydroxypropyl methacrylate	BD01	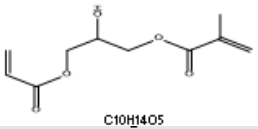 C10H14O5
APMAm.C	N-(3-Aminopropyl)methacrylamide hydrochloride	DM07	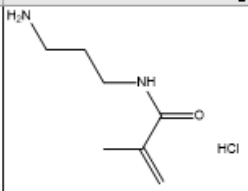 C7H15ClN2O
BAC	N,N'-Bis(acryloyl)cystamine	CD02	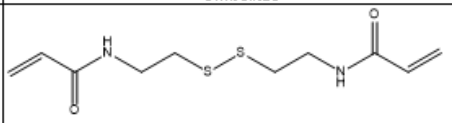 C=CC(=O)NCCSSCCNC(=O)C=C
BACOEA	Butylamino carbonyl oxy ethyl acrylate	AM53	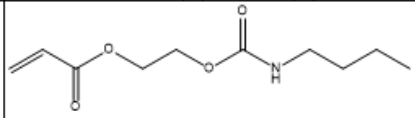 CCCCNC(=O)OCCOC(=O)C=C
BAPA	1,4-Bis(acryloyl)piperazine	CD05	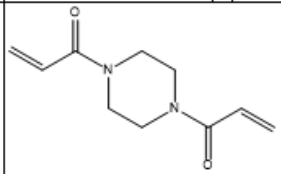 C=CC(=O)N1CCN(CC1)C(=O)C=C
BAPODA	Bisphenol A propoxylate diacrylate	AD26	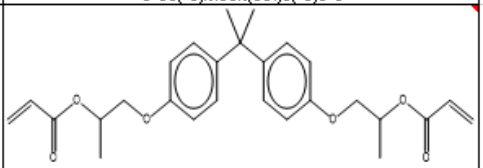 CC(COc1ccc(cc1)C(C)(C)c2ccc(OCC(C)OC(=O)C=C)cc2)OC(=O)C=C

BDDA	Butanediol diacrylate	AD01	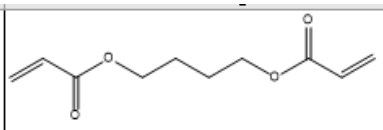 C=CC(=O)OCCCCOC(=O)C=C
BFEODA	Bisphenol F ethoxylate diacrylate	AD21	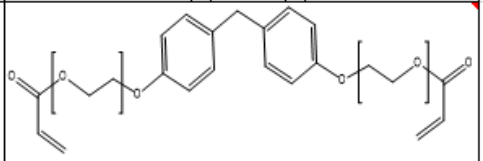 C23H24O6
BHMA	Benzhydryl methacrylate		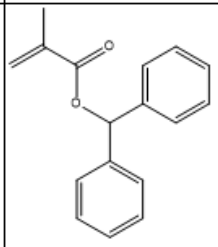 C17H16O2
BMA	Butyl methacrylate	BM08	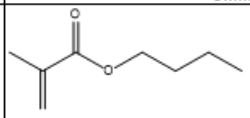 CCCCOC(=O)C(C)=C
BMAOEP	Bis[2-(methacryloyloxy)ethyl] phosphate	BD02	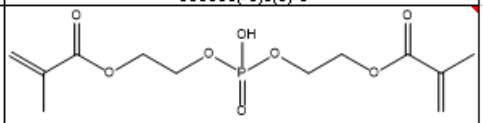 CC(=C)C(=O)OCCO[P](O)(=O)OCCOC(=O)C(C)=C
BMENBC	Bis(2-methacryloxyethyl) N,N'-1,9-nonylene biscarbamate		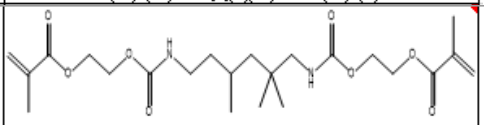 CC(CCNC(=O)OCCOC(=O)C(C)=C)CC(C)(C)CNC(=O)OCCOC(=O)C(C)=C
BnPA	Benzyl 2-n-propyl acrylate	BM74	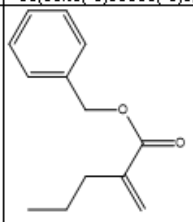 C13H16O2
BOEMA	Butoxyethyl methacrylate	BM52	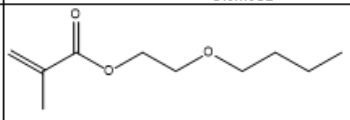 CCCCOCCOC(=O)C(C)=C
BOMAm	N-(Butoxymethyl)acrylamide	CM04	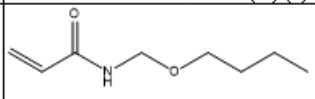 CCCCOCNC(=O)C=C

BPAPGDA	Bisphenol A propoxylate glycerolate diacrylate	AD08	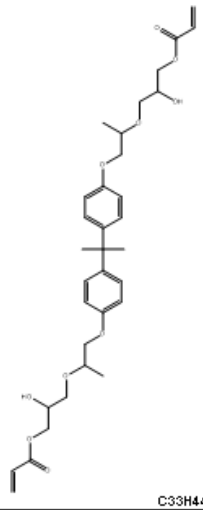 C33H44O10
BPDMA	Bisphenol A dimethacrylate	BD07	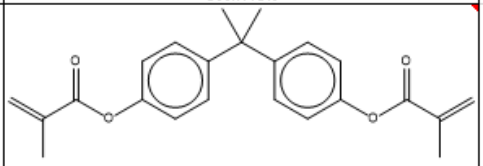 CC(=C)C(=O)Oc1ccc(cc1)C(C)(C)c2ccc(OC(=O)C(C)=C)cc2
CEA	Carboxyethyl acrylate	AM52	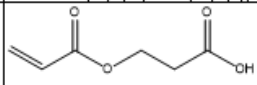 OC(=O)CCOC(=O)C=C
CHA	Cyclohexyl acrylate		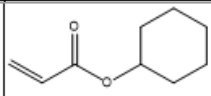 C=CC(=O)OC1CCCCC1
COEA	2-Cinnamoyloxyethyl acrylate		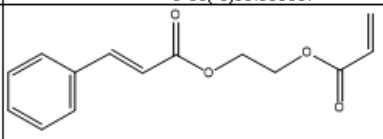 C14H14O4
CzEA	Carbazol-9-yl ethyl acrylate	AM42	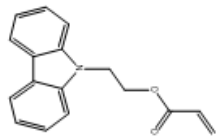 C17H15NO2
DAAM	N,N-Diallylacrylamide		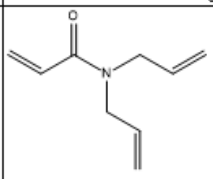 C=CCN(CC=C)C(=O)C=C
DDDMA	1,10-Decanediol dimethacrylate		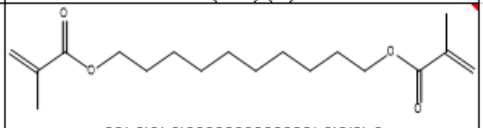 CC(=C)C(=O)OCCCCCCCCCCOC(=O)C(C)=C

DEGMA	Di(ethylene glycol) methyl ether methacrylate	BM53	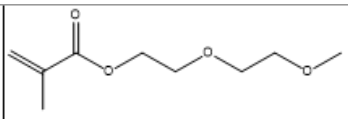 COCCOCCOC(=O)C(C)=C
DFFMOA	Dodecafluoro-7-(trifluoromethyl)-octyl acrylate	AM60	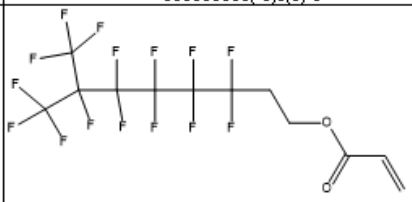 C12H7F15O2
DFHA	Dodecafluoroheptyl acrylate	AM57	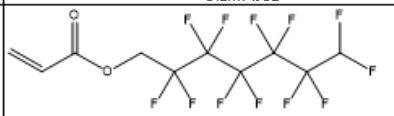 FC(F)C(F)(F)C(F)(F)C(F)(F)C(F)(F)C(F)(F)COC(=O)C=C
DFHNMA	Dodecafluoro-2-hydroxy-8-(trifluoromethyl)nonyl methacrylate	BM65	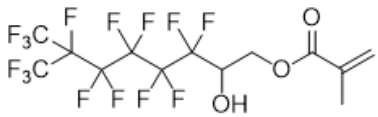 C14H11F15O3
DHEBAM	N,N'-(1,2-Dihydroxyethylene)bisacrylamide	CD03	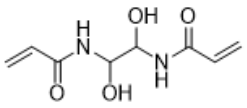 O[C@H](NC(=O)C=C)[C@@H](O)NC(=O)C=C
DiPEMA	2-Diisopropylaminoethyl methacrylate		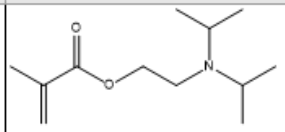 CC(C)N(CCOC(=O)C(C)=C)C(C)C
DMA	Decyl methacrylate	BM11	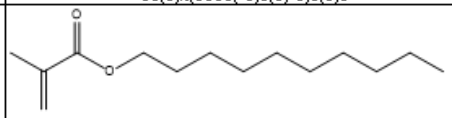 CCCCCCCCCCOC(=O)C(C)=C
DMAEA	Dimethylamino-ethyl acrylate	AM37	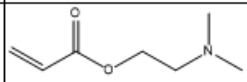 CN(C)CCOC(=O)C=C
DMAEMA	Dimethylamino-ethyl methacrylate	BM50	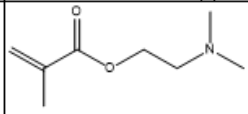 CN(C)CCOC(=O)C(C)=C
DMAm	N,N'-Dimethylacrylamide	CM05	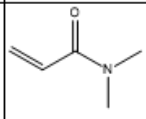 CN(C)C(=O)C=C
DMAPA	Dimethylamino-propyl acrylate	AM38	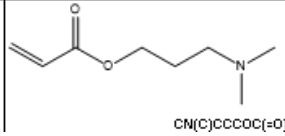 CN(C)CCCOC(=O)C=C

DMEMAm	N-[2-(N,N-Dimethylamino)ethyl]methacrylamide		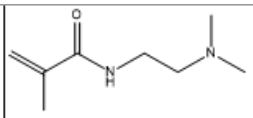 CN(C)CCNC(=O)C(C)=C
DMMAm	N,N-Dimethylmethacrylamide	DM09	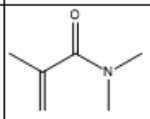 CN(C)C(=O)C(C)=C
DMPAm	N-[3-(Dimethylamino)propyl]acrylamide	CM13	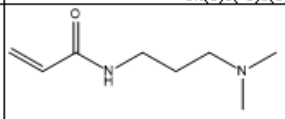 CN(C)CCCNC(=O)C=C
DMPMAm	N-[3-(Dimethylamino)propyl]methacrylamide	DM01	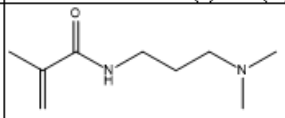 CN(C)CCCNC(=O)C(C)=C
DOAm	Disperse Orange 3 acrylamide	CM11	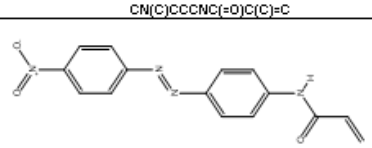 C15H12N4O3
DRA	Disperse red 1 acrylate	AM43	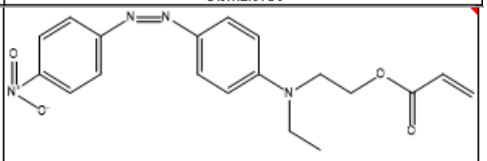 C19H20N4O4
DVAd	Divinyl Adipate		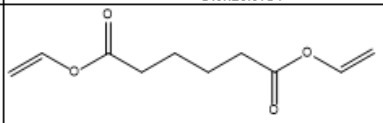 C=COC(=O)CCCCC(=O)OC=C
DVSeb	Divinyl sebacate		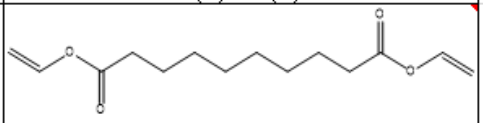 C14H22O4
DYA	Disperse yellow 7 acrylate	AM25	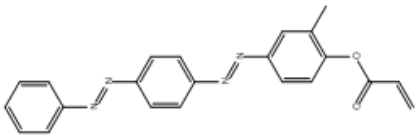 C22H18N4O2
EBAM	N,N'-Ethylenebisacrylamide	CD01	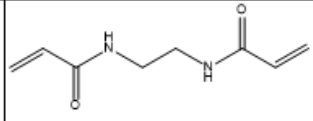 C=CC(=O)NCCNC(=O)C=C

EEA	Ethyl 2-ethylacrylate	BM04	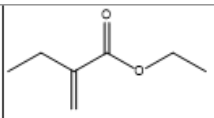 CCOC(=O)C(=C)CC
EEMA	Ethoxyethyl methacrylate	BM54	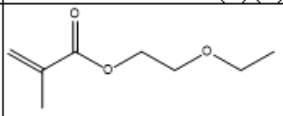 CCOCCOC(=O)C(C)=C
EGDA	Ethylene {glycol} diacrylate	AD16	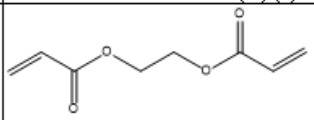 C=CC(=O)OCCOC(=O)C=C
EMA	Ethyl methacrylate	BM12	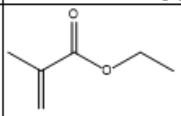 CCOC(=O)C(C)=C
EPA	Ethyl 2-propylacrylate	BM73	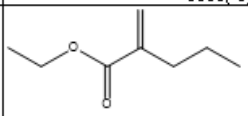 C8H14O2
ETMSA	Ethyl 2-(trimethylsilylmethyl)acrylate	BM76	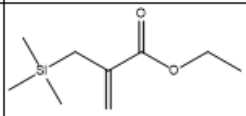 C9H18O2Si
F6BA	Hexafluorobutyl acrylate	AM69	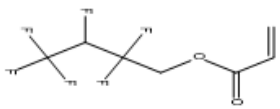 C7H6F6O2
F6BMA	Hexafluorobutyl methacrylate	BM68	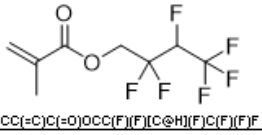 CC(=C)C(=O)OCC(F)(F)[C@H](F)C(F)(F)F
F7BA	Heptafluorobutyl acrylate	AM71	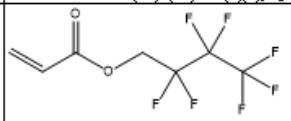 FC(F)(F)C(F)(F)C(F)(F)COC(=O)C=C
F7BMA	Heptafluorobutyl methacrylate	BM70	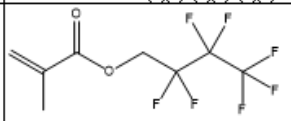 CC(=C)C(=O)OCC(F)(F)C(F)(F)C(F)(F)F

FDA	Fluorescein O,O'-diacrylate	AD07	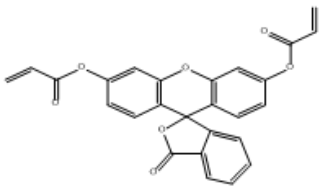 C26H16O7
FOA	Fluorescein O-acrylate	AM30	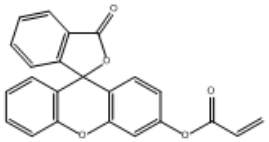 C23H14O5
FuMA	Furfuryl methacrylate	BM34	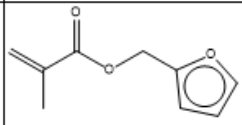 CC(=C)C(=O)OCc1occc1
GDGDA	Glycerol 1,3-diglycerolate diacrylate	AD11	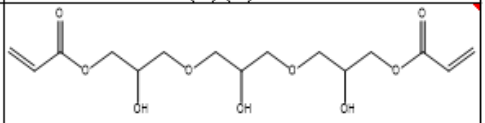 C15H24O9
GDMA	Glycerol dimethacrylate	BD04	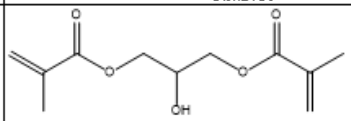 CC(=C)C(=O)OCC(O)COC(=O)C(C)=C
GMA	Glycidyl methacrylate	BM33	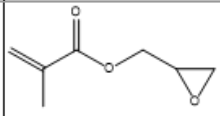 CC(=C)C(=O)OCC1CO1
HBA	Hydroxybutyl acrylate	AM27	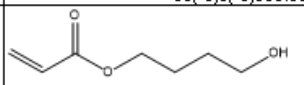 OCCCCOC(=O)C=C
HBMA	Hydroxybutyl methacrylate	BM43	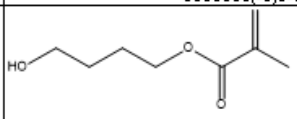 C8H14O3
HBOPBA	Hexanediylbis[oxy(2-hydroxy-3,1-propanediyl)] bisacrylate	AD27	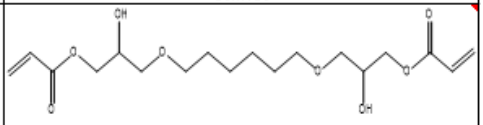 C18H30O8
HDFDA	Heptadecafluorodecyl acrylate	AM61	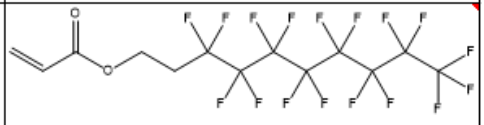 FC(F)(F)C(F)(F)C(F)(F)C(F)(F)C(F)(F)C(F)(F)C(F)(F)C(F)(F)COCC(=O)C=C
HDFDMA	Heptadecafluorodecyl methacrylate	BM66	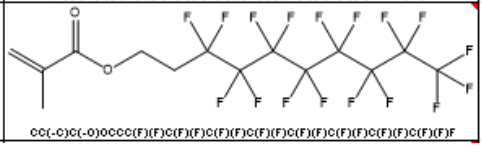 CC(=C)C(=O)OCCC(F)(F)C(F)(F)C(F)(F)C(F)(F)C(F)(F)C(F)(F)C(F)(F)C(F)(F)C(F)(F)F

HDMA	1-Hexadecyl methacrylate		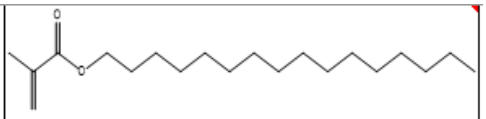 CCCCCCCCCCCCCCCCOC(=O)C(C)=C
HEAm	N-Hydroxyethyl acrylamide	CM10	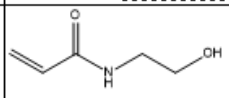 C5H9NO2
HEMA	Hydroxyethyl methacrylate	BM44	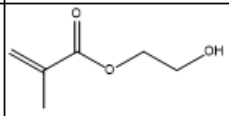 CC(=C)C(=O)OCCO
HEODA	Hexanediol ethoxylate diacrylate	AD17	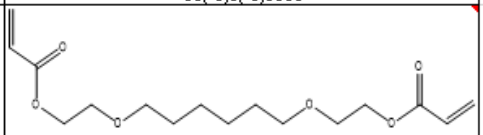 C16H26O6
HFDA	Heneicosafluorododecyl acrylate	AM65	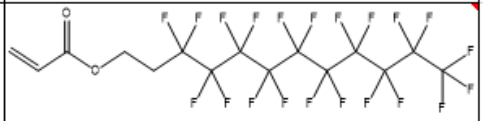 FC(F)(F)C(F)(F)C(F)(F)C(F)(F)C(F)(F)C(F)(F)C(F)(F)C(F)(F)C(F)(F)C(F)(F)C(F)(F)CCOC(=O)C=C
HFHUMA	Hexadecafluoro-2-hydroxy-10-(trifluoromethyl)undecyl methacrylate	BM64	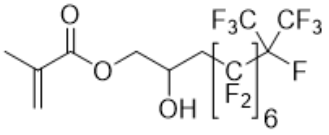 C16H11F13O3
HFPDA	Hexafluoropent-1,5-diyl diacrylate	AD03	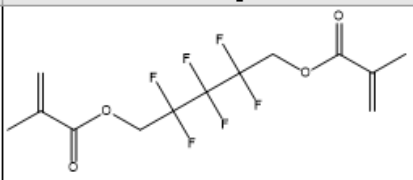 C13H14F6O4
HMAm	N-(Hydroxymethyl)acrylamide	CM15	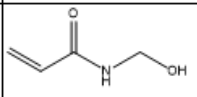 OCNC(=O)C=C
HMBAM	N,N'-Hexamethylenebisacrylamide		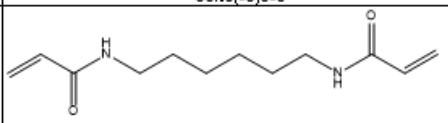 C=CC(=O)NCCCCCCNC(=O)C=C
HMBMAm	N,N'-Hexamethylenebis(methacrylamide)	DD02	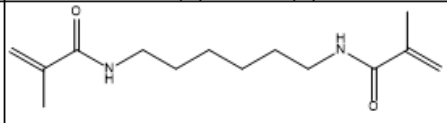 CC(=C)C(=O)NCCCCCCNC(=O)C(C)=C
HPhOPA	Hydroxy-3-phenoxypropyl acrylate	AM31	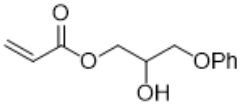 CCCOC(=O)C(/O)=C/Oc1ccccc1

HPHPBAH	Hydroxypivalyl hydroxypivalate bis[6-(acryloyloxy)hexanoate]	AD28	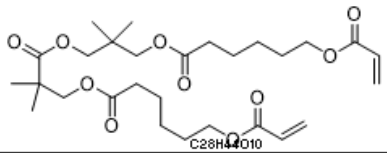 C28H44O10
HPMA	Hydroxypropyl methacrylate	BM45	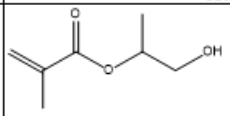 CC(CO)OC(=O)C(C)=C
HPMAm	N-(2-Hydroxypropyl)methacrylamide		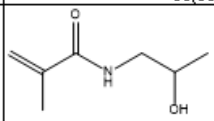 CC(O)CNC(=O)C(C)=C
HPMAP	Hydroxypropyl 2-(methacryloyloxy)ethyl phthalate	BM46	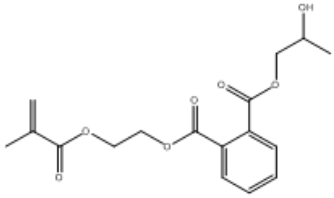 C17H20O7
HTFDA	Hexadecafluoro-9-(trifluoromethyl)decyl acrylate	AM64	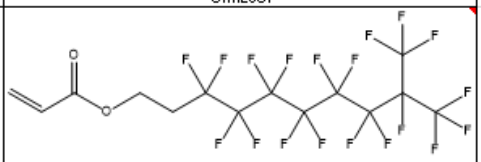 FC(F)(F)C(F)(C(F)(F)F)C(F)(F)C(F)(F)C(F)(F)C(F)(F)C(F)(F)C(F)(F)CCOC(=O)C=C
iBuMA	Isobutyl methacrylate	BM15	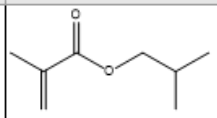 CC(C)COC(=O)C(C)=C
iCEMA	Isocyanatoethyl methacrylate	BM83	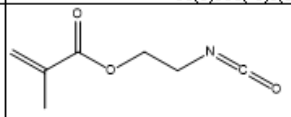 CC(=C)C(=O)OCCN=C=O
MA	Methyl acrylate	AM10	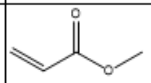 COC(=O)C=C
MAAHS	Methacrylic acid N-hydroxysuccinimide ester	BM88	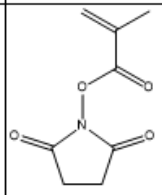 C8H9NO4
MAETA	4-Methacryloxyethyl trimellitic anhydride		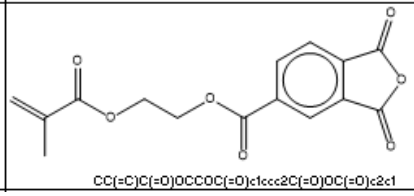 CC(=C)C(=O)OCCOC(=O)c1ccc2C(=O)OC(=O)c2c1

MAHBP	4-Methacryloxy-2-hydroxybenzophenone		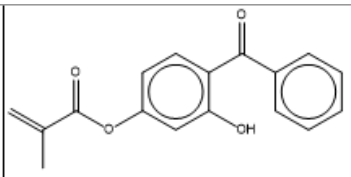 CC(=C)C(=O)Oc1ccc(c(O)c1)C(=O)c2ccccc2
MAPU	2-methacryloxyethyl phenyl urethane		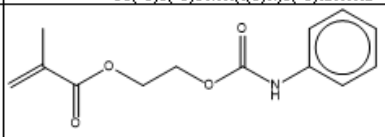 CC(=C)C(=O)OCCOC(=O)Nc1ccccc1
MBAm	N,N'-Methylenebisacrylamide	CD04	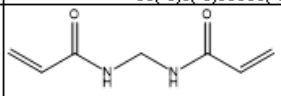 C=CC(=O)NCNC(=O)C=C
MHMB	Methyl 3-hydroxy-2-methylenebutyrate	BM06	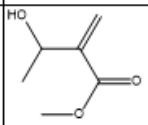 C6H10O3
MMA	Methyl methacrylate	BM20	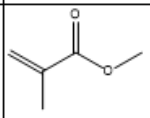 COC(=O)C(C)=C
mMAOEM	mono-2-(Methacryloyloxy)ethyl maleate	BM41	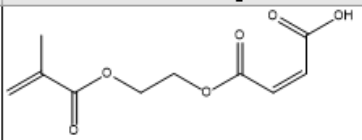 CC(=C)C(=O)OCCOC(=O)\C=C/C(O)=O
mMAOES	mono-2-(Methacryloyloxy)ethyl succinate	BM42	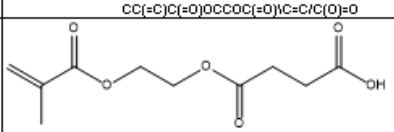 CC(=C)C(=O)OCCOC(=O)CCC(O)=O
MOPAm	N-(3-Methoxypropyl)acrylamide	CM07	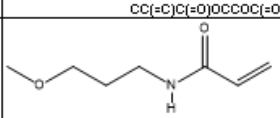 C7H13NO2
MSPMA	Methyldiethoxysilyl-propyl methacrylate	BM26	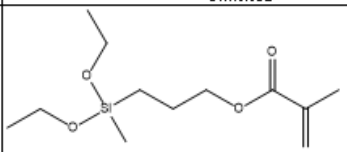 C12H24O4Si
NAM	N-Acryloylmorpholine		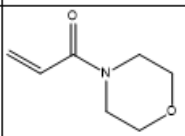 C=CC(=O)N1CCOCC1

NAS	N-Acryloxysuccinimide		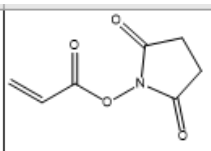 C=CC(=O)ON1C(=O)CCC1=O
NBnMA	o-Nitrobenzyl methacrylate, . 95%		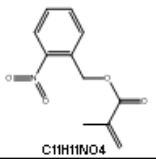 C11H11NO4
NDDMA	1,9-Nonanediol dimethacrylate		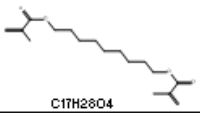 C17H28O4
nOcMA	n-Octyl methacrylate,		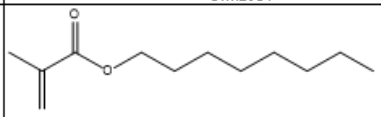 CCCCCCCCOC(=O)C(C)=C
NPhPMA	Nitrophenyl-2-pyrrolidonemethyl acrylate	AM44	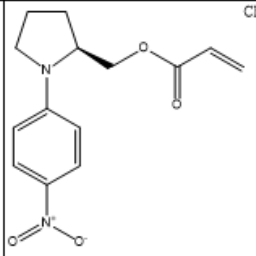 Chiral C14H16N2O4
OFHMA	Octafluoro-2-hydroxy-6-(trifluoromethyl)heptyl methacrylate	BM62	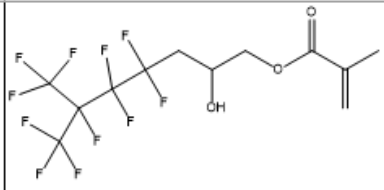 C12H11F11O3
OFPA	Octafluoropentyl acrylate	AM74	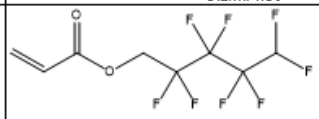 FC(F)C(F)(F)C(F)(F)C(F)(F)COC(=O)C=C
PAHEMA	Phosphoric acid 2-hydroxyethyl methacrylate ester	BM47	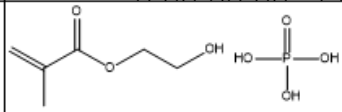 CC(=C)C(=O)OCCO.O[P](O)(O)=O
PBBA	Pentabromobenzyl acrylate	AM56	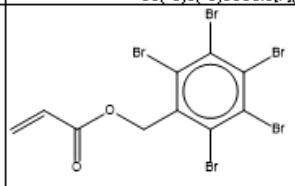 Brc1c(Br)c(Br)c(COC(=O)C=C)c(Br)c1Br
PDA	1,4-Phenylene diacrylate		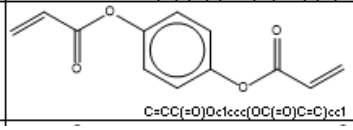 C=CC(=O)Oc1ccc(OC(=O)C=C)cc1

PDDMA	1,5-Pentanediol dimethacrylate		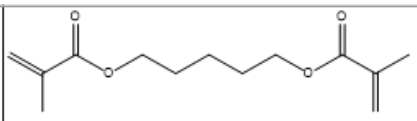 CC(=C)C(=O)OCCCCCOC(=O)C(C)=C
pEGDA	Polyethylene glycol diacrylate		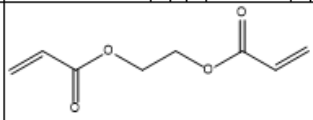 C=CC(=O)OCCOC(=O)C=C
pEGDMA	Poly(ethylene glycol) (600) dimethacrylate		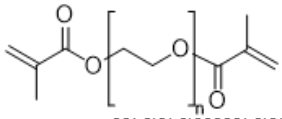 CC(=C)C(=O)OCCOC(=O)C(C)=C
pEGMEA	Poly(ethylene glycol) methyl ether acrylate	AM77	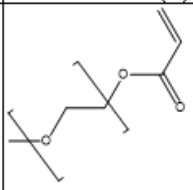 C6H10O3
pEGPhEA	Poly(ethylene glycol) phenyl ether acrylate	AM75	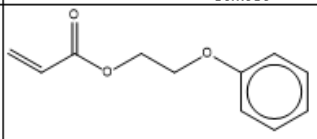 C=CC(=O)OCCOc1ccccc1
PhEMA	2-Phenylethyl methacrylate		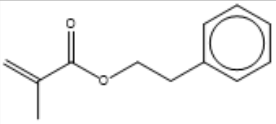 CC(=C)C(=O)OCCc1ccccc1
PETrA	Pentaerythritol triacrylate	AT06	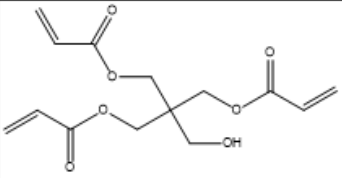 OCC(COC(=O)C=C)(COC(=O)C=C)COC(=O)C=C
pFDA	Perfluorodecyl acrylate	AM62	 FC(F)(F)C(F)(F)C(F)(F)C(F)(F)C(F)(F)C(F)(F)C(F)(F)C(F)(F)C(F)(F)COC(=O)C=C
PFPA	Pentafluoropropyl acrylate	AM68	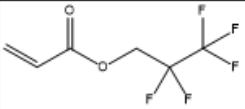 FC(F)(F)C(F)(F)COC(=O)C=C
PFPhA	Pentafluorophenyl acrylate		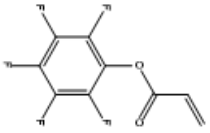 C9H3F5O2

PFPhMA	Pentafluorophenyl methacrylate, 95%		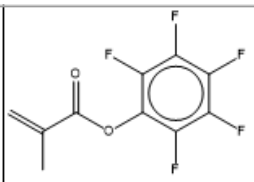 CC(=C)C(=O)Oc1c(F)c(F)c(F)c(F)c1F
PFPMA	Pentafluoropropyl methacrylate	BM67	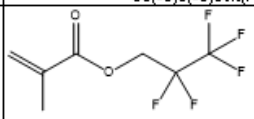 CC(=C)C(=O)OCC(F)(F)C(F)(F)F
PhA	Phenyl acrylate, 95%		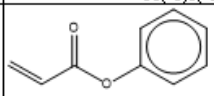 C=CC(=O)Oc1ccccc1
PhEA	2-Phenylethyl acrylate		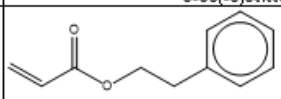 C=CC(=O)OCCc1ccccc1
PHPMA	3-Phenoxy 2 hydroxy propyl methacrylate		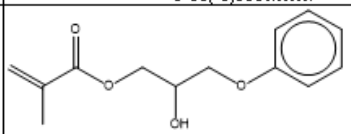 CC(=C)C(=O)OCC(O)COc1ccccc1
PMA	Propargyl methacrylate		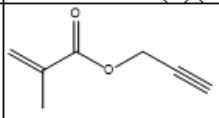 CC(=C)C(=O)OCC#C
PMMA	1-Pyrenylmethyl methacrylate		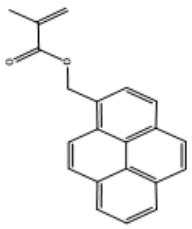 C21H16O2
pPGA	Poly(propylene glycol) acrylate	AM54	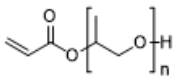 C[C@H](CO)OC(=O)C=C
pPGDA	Poly(propylene glycol) diacrylate	AD24	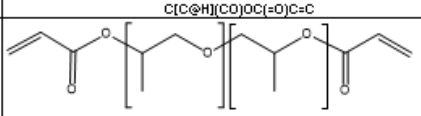 C12H18O5
pPGDMA	Poly(propylene glycol) (400) dimethacrylate		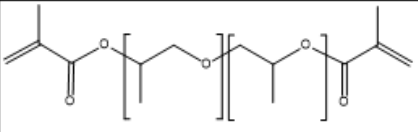 C14H22O5
pPGMEA	Poly(propylene glycol) methyl ether acrylate	AM55	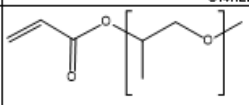 C7H12O3

pEGPhEA	Poly(ethylene glycol) phenyl ether acrylate	AM75	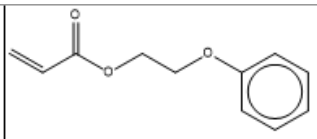 C=CC(=O)OCCOc1ccccc1
PhEMA	2-Phenylethyl methacrylate		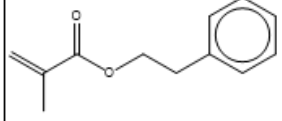 CC(=C)C(=O)OCCc1ccccc1
PETrA	Pentaerythritol triacrylate	AT06	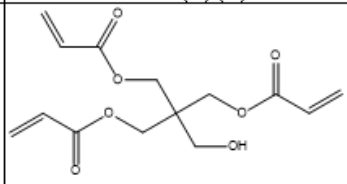 OCC(COC(=O)C=C)(COC(=O)C=C)COC(=O)C=C
pFDA	Perfluorodecyl acrylate	AM62	 FC(F)(F)C(F)(F)C(F)(F)C(F)(F)C(F)(F)C(F)(F)C(F)(F)C(F)(F)C(F)(F)CCOC(=O)C=C
PFPA	Pentafluoropropyl acrylate	AM68	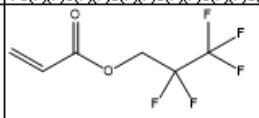 FC(F)(F)C(F)(F)COC(=O)C=C
SEMA	2-Sulfoethyl methacrylate		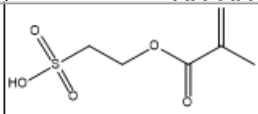 C6H10O5S
tBMA	Tert-butyl methacrylate	BM23	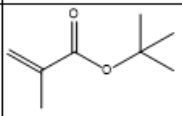 CC(=C)C(=O)OC(C)(C)C
TBNpMA	Tribromoneopentyl methacrylate		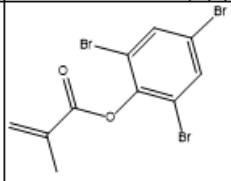 C10H7Br3O2
tBOCAPAm	N-(t-BOC-aminopropyl)methacrylamide		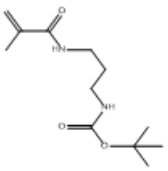 C12H22N2O3
TBPhA	2,4,6-Tribromophenyl acrylate		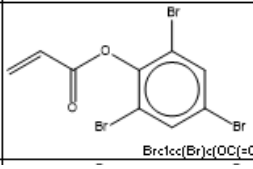 Brc1cc(Br)c(OC(=O)C=C)c(Br)c1

TBPMA	Tribromophenyl methacrylate	BM58	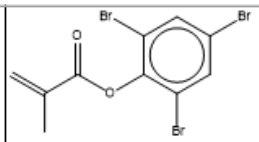 CC(=C)C(=O)Oc1c(Br)cc(Br)cc1Br
TCDMDA	Tricyclodecane-dimethanol diacrylate	AD10	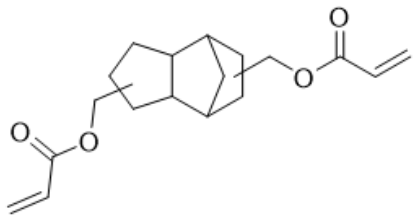 C=CC(=O)OCC1CCC2C3CC(CC3COC(=O)C=C)C12
TCSPMA	Trichlorosilyl propyl methacrylate	BM61	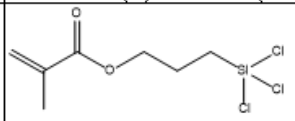 CC(=C)C(=O)OCCC[Si](Cl)(Cl)Cl
TDFOcA	Tridecafluorooctyl acrylate	AM58	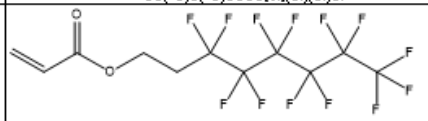 FC(F)(F)C(F)(F)C(F)(F)C(F)(F)C(F)(F)C(F)(F)COC(=O)C=C
TDFOMA	Tridecafluorooctyl methacrylate	BM63	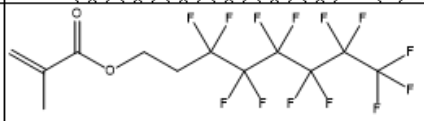 CC(=C)C(=O)OCCC(F)(F)C(F)(F)C(F)(F)C(F)(F)C(F)(F)C(F)(F)F
TEGMA	Tri(ethylene glycol) methyl ether methacrylate	BM90	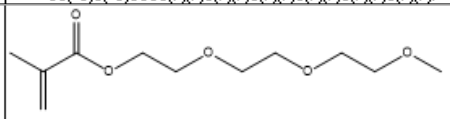 COCCOCCOCCOC(=O)C(C)=C
TFCAm	7-[4-(Trifluoromethyl)coumarin]acrylamide	CM12	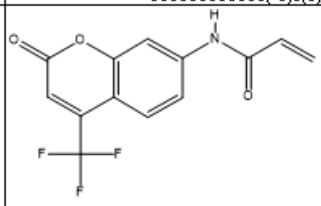 C13H8F3NO3
TFPMA	Tetrafluoropropyl methacrylate		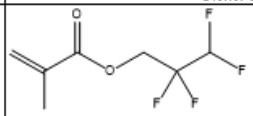 CC(=C)C(=O)OCC(F)(F)C(F)F
THMMAm	N-[Tris(hydroxymethyl)methyl]acrylamide	CM02	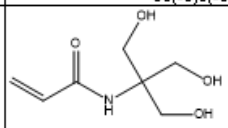 OCC(CO)(CO)NC(=O)C=C
TMOBDA	Trimethylolpropane benzoate diacrylate	AD09	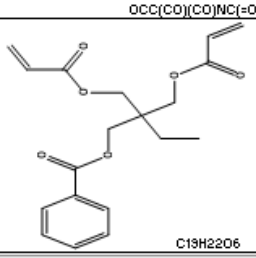 C19H22O6

TMOPTMA	1,1,1-Trimethylolpropane trimethacrylate		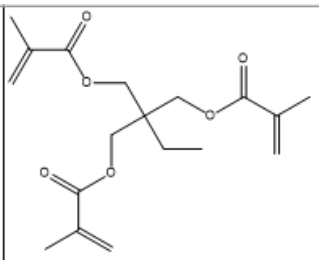 CCC(COC(=O)C(C)=C)(COC(=O)C(C)=C)COC(=O)C(C)=C
TMOSPMA	Trimethoxysilyl propyl methacrylate	BM27	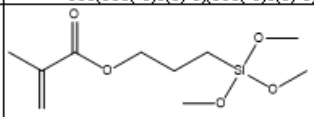 CO[Si](CCCOC(=O)C(C)=C)(OC)OC
tOcAm	N-tert-Octylacrylamide		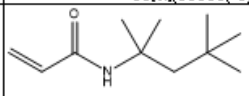 CC(C)(C)CC(C)(C)NC(=O)C=C
TPhMAm	N-(Triphenylmethyl)methacrylamide	DM08	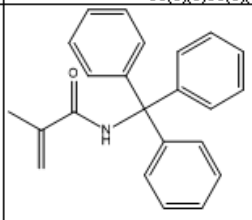 C23H21NO
VMA	Vinyl methacrylate	BM24	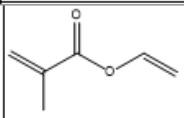 CC(=C)C(=O)OC=C
ZrCEA	Zirconium carboxyethyl acrylate	AM35	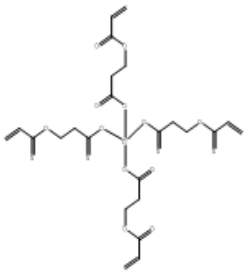 C24H28O16Zr
GMMA	Glycerol monomethacrylate		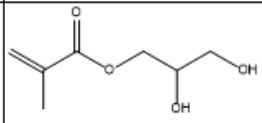 CC(=C)C(=O)OCC(O)CO
MAEP	Monoacryloxyethyl phosphate		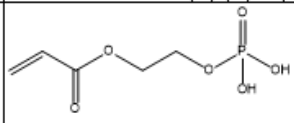 O[P](O)(=O)OCCOC(=O)C=C
MAEPC	2-Methacryloyloxyethyl phosphorylcholine	BM87	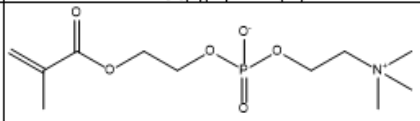 CC(=C)C(=O)OCCO[P]([O-])(=O)OCC[N+](C)(C)C

PBPhA	Pentabromophenyl acrylate		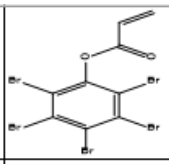 C9H3Br5O2
PBPhMA	Pentabromophenyl methacrylate		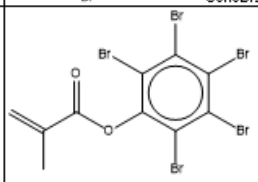 CC(=C)C(=O)Oc1c(Br)c(Br)c(Br)c(Br)c1Br
PPPDMA	PEO(5800)-b-PPO(3000)-b-PEO(5800) dimethacrylate		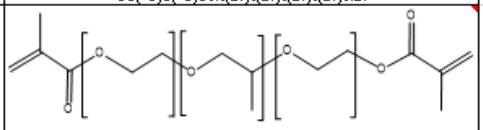 C15H24O6
ClEA	2-Chloroethyl acrylate		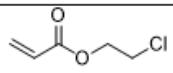
MClMA	Methyl 2-(chloromethyl)acrylate		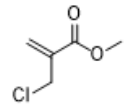
AEAm.C	N-(2-aminoethyl)acrylamide hydrochlide		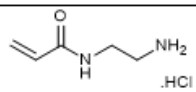 .HCl
SolA	Solketal acrylate		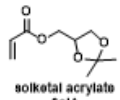 solketal acrylate SolA
DHPA	2,3-dihydroxypropyl acrylate		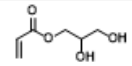 2,3-dihydroxypropyl acrylate DHPA
PPDDA	3-phenoxypropane-1,2-diyl diacrylate		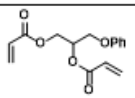 3-phenoxypropane-1,2-diyl diacrylate PPDDA

Table 8.1 Full Table of Chemical Identities & Structures